Vol. 197, June 15, 1987
Complete in one issue

ISSN 0003-2670

ANALYTICA CHIMICA ACTA

International journal devoted to all branches of analytical chemistry

ELSEVIER

ANALYTICA CHIMICA ACTA

International journal devoted to all branches of analytical chemistry
Revue internationale consacrée à tous les domaines de la chimie analytique
Internationale Zeitschrift für alle Gebiete der analytischen Chemie

PUBLICATION SCHEDULE FOR 1987

	J	F	M	A	M	J	J	A	S	O	N	D
Analytica Chimica Acta	192	193	194	195	196	197	198	199	200	201	202	203

Scope. *Analytica Chimica Acta* publishes original papers, short communications, and reviews dealing with every aspect of modern chemical analysis both fundamental and applied.

Submission of Papers. Manuscripts (three copies) should be submitted as designated below for rapid and efficient handling:

Papers from the Americas to: Professor Harry L. Pardue, Department of Chemistry, Purdue University, West Lafayette, IN 47907, U.S.A.

Papers from all other countries to: Dr. A. M. G. Macdonald, Department of Chemistry, The University, P.O. Box 363, Birmingham B15 2TT, England. Papers dealing particularly with computer techniques to: Professor J. T. Clerc, Universität Bern, Pharmazeutisches Institut, Baltzerstrasse 5, CH-3012 Bern, Switzerland.

Submission of an article is understood to imply that the article is original and unpublished and is not being considered for publication elsewhere. Upon acceptance of an article by the journal, authors will be asked to transfer the copyright of the article to the publisher. This transfer will ensure the widest possible dissemination of information.

Papers in English, French and German are published. There are no page charges. Manuscripts should conform in layout and style to the papers published in this Volume. See inside back cover for "Information for Authors".

Reprints. Fifty reprints will be supplied free of charge. Additional reprints (minimum 100) can be ordered. An order form containing price quotations will be sent to the authors together with the proofs of their article.

Publication. *Analytica Chimica Acta* appears in 12 volumes in 1987. The subscription for 1987 (Vols. 192–203) is Dfl. 2700.00 plus Dfl. 300.00 (p.p.h.) (total approx. US $1463.40). All earlier volumes (Vols. 1–191) except Vols. 23 and 28 are available at Dfl. 243.00 (US $118.54), plus Dfl. 18.00 (US $8.78) p.p.h., per volume.

Our p.p.h. (postage, packing and handling) charge includes surface delivery of all issues, except to subscribers in the U.S.A., Canada, Australia, New Zealand, P.R. China, India, Israel, South Africa, Malaysia, Thailand, Singapore, South Korea, Taiwan, Pakistan, Hong Kong, Brazil, Argentina and Mexico, who receive all issues by air delivery (S.A.L. — Surface Air Lifted) at no extra cost. For Japan, air delivery requires 50% additional charge; for all other countries airmail and S.A.L. charges are available upon request.

Subscription. Subscription should be sent to: Elsevier Science Publishers B.V., Journals Department, P.O. Box 211, 1000 AE Amsterdam, The Netherlands. Tel: 5803 911, Telex: 18582, to which requests for sample copies can also be sent.

Claims for issues not received should be made within three months of publication of the issues. If not they cannot be honoured free of charge.

Readers in the U.S.A. and Canada can contact the following address: Elsevier Science Publishing Co. Inc., Journal Information Center, 52 Vanderbilt Avenue, New York, NY 10017, U.S.A., Tel: (212) 916-1250, for further information, or a free sample copy of this or any other Elsevier Science Publishers journal.

Advertisements. Advertisement rates are available from the publisher on request.

0003-2670/87/$03.50

Printed in The Netherlands

ANALYTICA CHIMICA ACTA

Abstracted, Indexed in: Anal. Abstr.; Biol. Abstr.; Chem. Abstr.; Curr. Contents Phys. Chem. Earth Sci.; ife Sci.; Index Med.; Mass Spectrom. Bull.; Sci. Citation Index; Excerpta Med.)

OL. 197 **CONTENTS** **JUNE 15, 1987**

(Continued overleaf)

(Contents continued)

ANALYTICA CHIMICA ACTA
VOL. 197 (1987)

ANALYTICA CHIMICA ACTA

International journal devoted to all branches of analytical chemistry

ELSEVIER Amsterdam–Oxford–New York–Tokyo

Analytica Chimica Acta, 197 (1987) 1—42
Elsevier Science Publishers B.V., Amsterdam — Printed in The Netherlands

Review

SPECTROSCOPIC TECHNIQUES FOR THE ANALYSIS OF POLYMER SURFACES AND INTERFACES

F. GARBASSI* and E. OCCHIELLO

Istituto G. Donegani S.p.A., Novara Research Center, Via G. Fauser 4, 28100 Novara (Italy)

(Received 1st July 1986)

SUMMARY

The techniques considered are ion-scattering spectroscopy, secondary-ion mass spectrometry, x-ray photoelectron spectroscopy, internal reflection spectroscopy, diffuse reflectance spectroscopy, photoacoustic spectroscopy, other vibrational techniques, transmission spectroscopies and nuclear magnetic resonance spectroscopy. The methods are compared with respect to applicability, sensitivity, instrumentation and working conditions.

Polymeric materials have become increasingly important in technology, as have composite materials (polymeric matrices reinforced with fillers to improve mechanical properties) and blends (polymer mixtures). Applications of polymer films are now vital in various fields. As a consequence, adequate knowledge of surface and interfacial phenomena is crucial because a significant proportion of the properties of these materials depend on these phenomena. Examples are problems with adhesion and the dependence of the mechanical properties of fiber-reinforced plastics on matrix/filler interactions. Studying surfaces and interfaces is difficult for two main reasons: the first is the necessity to observe a layer of limited thickness, so that surface properties can be distinguished from bulk properties; the second is sensitivity because very often the species of interest is present in rather low amounts.

Numerous techniques have been developed to study surface phenomena in metals and inorganic solids, mainly in catalysis, metallurgy and electronics. Several of these techniques have been applied to the study of surfaces and/or interfaces in polymeric materials. In this review, spectroscopic techniques are considered. The presentation reflects the increasing usefulness of physical probes. First, ions are discussed (ISS, RBS, SIMS), then electrons (XPS) and finally photons (ultraviolet, visible, infrared, etc.). A list of the most commonly used acronyms for instrumental techniques is provided in Table 1. The number of papers written on the various topics is overwhelming, so that no attempt can sensibly be made to provide a complete coverage of the literature. Instead, some applications, chosen from recent work, will be cited to illustrate the possibilities of each technique.

0003-2670/87/$03.50

TABLE 1

List of acronyms for the commoner spectroscopic techniques

ISS	Ion-scattering spectroscopy
RBS	Rutherford back-scattering spectroscopy
SIMS	Secondary-ion mass spectrometry
LEIS	Low-energy ion scattering
XPS	X-ray photoelectron spectroscopy
IRS	Internal reflection spectroscopy
ATR	Attenuated total reflectance
DRS	Diffuse reflectance spectroscopy
PAS	Photoacoustic spectroscopy
ERS	External reflection spectroscopy
IETS	Inelastic electron tunnelling spectroscopy
SERS	Surface-enhanced Raman spectroscopy
NMR	Nuclear magnetic resonance spectroscopy

ION-SCATTERING SPECTROSCOPY

The most popular techniques based on ion beams can be divided into two groups. The first comprises ion-scattering spectroscopies (low-energy ion scattering, Rutherford back-scattering spectroscopy), and the second secondary-ion mass spectrometries. The distinction lies in the physical property which is measured, ion energies in ISS and quantities of emitted ions in SIMS.

In ISS, an ion beam, usually of noble gas ions (He^+, Ne^+, Ar^+, etc.), is focused on the surface. Collisions of these ions with surface atoms cause variations in the state of motion and energy of the incident ion [1, 2] as represented in Fig. 1A. To a good approximation, the collision of the incident ion with a surface atom can be considered elastic. The energy of the incident ion after the collision (E_1) is given by

$$E_1 = \{\cos e + (M_2^2/M_1^2 - \sin^2 e)^{1/2}/(1 + M_2/M_1)\}^2 E_0 \quad (1)$$

where E_0 is the original energy of the incident ion, M_1 its mass, M_2 the mass of the surface atom and θ the angle of observation. The version of ISS which is most commonly reported uses low energies of the incident ion (E_0), normally in the 500—5000 eV range. This is usually termed low-energy ion scattering (LEIS). In these conditions, only the first layer of the material is observed. Most collisions are single, binary and elastic, so that they obey Eqn. 1 and relate to the first monolayer of the material. Multiple and inelastic collisions cause decreased resolution, but these are less important. In fact, the probability of neutralization increases with the number of collisions and neutral atoms are not detected. Equation 1 indicates that the resolution, $M/\delta M$, is a function of the angle of incidence and of the ratio of the incident ion mass to that of the target. Resolution worsens with increasing M_2/M_1 ratios and decreasing angles of incidence [1].

To obtain quantitative information about surface composition, it is necessary to know how the observed intensity at a given energy of the scattered

ion depends on physical and instrumental factors [1]:

$$I_i = I_0 N_i A(\mathrm{d}\sigma_i/\mathrm{d}\Omega)\delta\Omega T P_i = k_i N_i \qquad (2)$$

where N_i is the surface concentration of the given element i, σ_i is the cross-section, $\delta\Omega$ is the solid angle, T an instrumental factor, A the bombarded area, and P_i the probability that the incident ion will not be neutralized. Both the cross-section and the neutralization probability are functions of the angle of incidence and the ion-to-atom interaction potential.

Absolute quantification by means of Eqn. 2 is difficult or impossible and it is necessary to use a calibration obtained from appropriate standards [1, 2]. Semiquantitative information about surface composition is readily attained but the chemical state of the observed element cannot usually be established by ISS. The experimental arrangement is outlined in Fig. 1B. The sample is placed in an ultra-high vacuum chamber (ca. 10^{-8} Pa). The ion gun is similar to those used for ion bombardment for depth profiling in other techniques, such as XPS. Apart from noble gases, the use of alkali metal ions has been suggested because of their lower tendency to neutralization; their main defect is the loss of selectivity, because ions which have undergone multiple collisions are detected. But charging phenomena in insulating materials are less likely. The energy of the scattered ions is analyzed by a 127° electrostatic analyzer or by a cylindrical mirror analyzer. The latter usually offers better sensitivity.

The application of ISS to polymeric materials has not been extensive, largely because of competition from secondary-ion mass spectrometry (SIMS). Adhesion problems [2, 3], glass/polymer interfaces [4] and polymer surfaces [5—10] have been studied. A combined ISS/dynamic SIMS study of glass/polymer interfaces [4] showed that ISS provides lower resolution than SIMS, because energies instead of masses are analyzed. A study of some polymer surfaces by the LEIS technique has been reported [5]. The technique is extremely sensitive to the presence of surface impurities. For example, inorganic or organometallic compounds used as stabilizers in polymers tend to segregate at the surface. When poly(vinyl chloride) (PVC) containing tin compounds was examined, a large amount of tin was detected at the surface [5]. Concentrations of polar groups such as —OH, —COOH, —O— in polymers

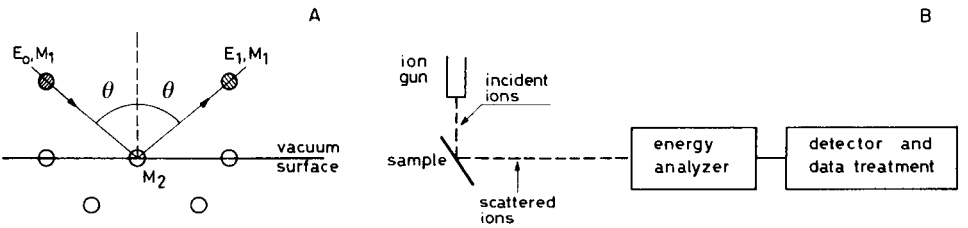

Fig. 1. Ion-scattering spectroscopy. (A) An ion with energy E_0 and mass M_1 is elastically scattered by a surface atom of mass M_2, the ion energy being detected. (B) Experimental arrangement.

have been shown to be higher in the bulk of the polymer than at the surface [5—10]. The conformation of polymer chains near the surface is governed by minimization of surface energy. In polyoxymethylene, the stoichiometric O/C ratio is 1, while the surface ratio detected by ISS is 0.15 [5]. The same trend has been observed in other polymers, copolymers and blends [5—10].

Another ISS technique is Rutherford back-scattering spectroscopy (RBS), which uses a beam of energetic helium ions in the MeV range. Theory and instrumentation are analogous to those for LEIS. Because of surface elastic scattering problems, RBS is inefficient for the detection of elements with masses lower than 28 (silicon). Furthermore, RBS is more penetrating than LEIS; the thickness of the observed layer depends on the energy of the ion beam but is usually several hundred nanometers. One of the rare studies with RBS concerns the diffusion of copper(II) ions in a polypropylene film oxidized between copper foils [11]. The diffusion rates of copper carboxylate complexes in polymeric matrices have been studied [12, 13], as have polymer surfaces which have undergone ion bombardment [14, 15]. The weathering of the surface of bisphenol-A polycarbonate has been determined by RBS after derivatization of the phenol and carboxylic acid groups by thallium(I) ethoxide [16].

SECONDARY-ION MASS SPECTROMETRY

Secondary-ion mass spectrometry (SIMS) has become increasingly important in recent years, particularly in the analysis of semiconductors and polymers. The particles (secondary ions) emitted from the surface on ion or atom bombardment are mass-analyzed. Fast-atom-bombardment mass spectrometry (FABMS) is particularly useful. In the experimental arrangement, an ion gun directs ions or atoms at the surface, with suitable kinetic energy and ion (atom) flux density. Secondary ions are collected through an energy filter and mass-analyzed. The difference between static and dynamic SIMS must be emphasized. In static SIMS, the ion intensity incident on the surface is very small (ca. 10^{-10} A cm^{-2}), so that secondary ions come from the first one or two layers of the material and the surface is not substantially damaged. In dynamic SIMS, the ion current is higher (up to 10^{-7} A cm^{-2}), the surface is rapidly eroded and the analysis is not restricted to the first layers [2, 17, 18]. While static SIMS can be used for surface studies, dynamic SIMS has found applications in depth-profiling studies, e.g., of ion implantation effects on semiconductors.

The processes caused by the impact of an accelerated ion or atom with the surface are indicated in Fig. 2 [2, 17]. The energy of the incident particle is dissipated in a series of collisions and secondary particles are emitted even at a certain distance from the primary impact site. The intensity (I_s) of the signal corresponding to the secondary ion, M^+, as a function of the primary ion flux (i_p) has been described [17] by

$$I_s^M = i_p S R^+ C_M \beta \qquad (3)$$

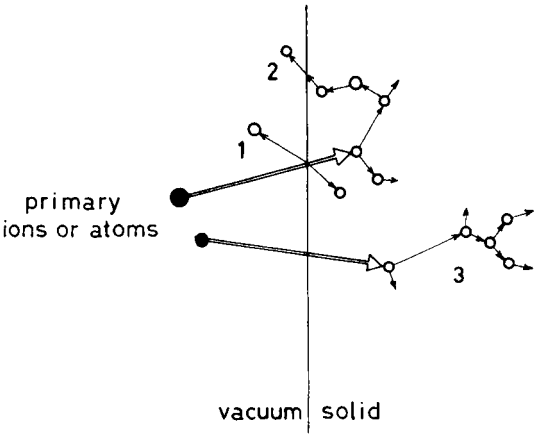

Fig. 2. The physical basis of static SIMS: after the primary particle impact, there is emission of a secondary ion near the impact site (1), emission at some distance (2), and secondary phenomena without emission (3).

where C_M is the surface concentration of M, expressed as coverage, β an instrumental factor, S the sputtering yield (i.e., the number of M particles emitted after each primary ion impact) and R^+ the probability of particle M being emitted as an ion and detected. S and R^+ determine the spectrum; they depend on emission and ionization mechanisms, i.e., on the electronic structure of the material. Various models have been proposed for these mechanisms [17—19]. The complication of SIMS theory causes difficulties in the interpretation of spectra, particularly quantitatively. Sensitivities have to be defined for each fragment and are characteristic of each material.

The sample is analyzed in an ultra-high vacuum chamber, as in ISS. Ion guns based on noble gases (Ne, Ar, Xe) are the most popular. Ions are accelerated by an electric potential which has to be chosen for each ion; e.g., 4-keV energies have been used for Ar^+ and 2-keV energies for Xe^+ [20, 21]. Currents used in static SIMS are now very low (10^{-10} or even 10^{-11} cm^{-2}) to minimize surface damage. Liquid metal guns (Ga, In, Cs) have been used to provide a brilliant and easily-collimated primary ion beam [22].

The use of static SIMS on insulating materials (e.g., polymers) gives rise to charging problems, which cause a decrease in sensitivity and alterations in the relative intensities of peaks. To overcome such problems, an electron gun (flood gun) hitting a broader area than the ion gun can be used. The aim is to neutralize the positive charge induced on the material [20]. Unfortunately, the flood gun can itself have some effect on the observed spectrum [23]. A flood gun has been used to excite secondary ions, to obtain the mass spectrum of poly(butylmethacrylate) [21]. The phenomenon is called electron-stimulated ion emission and has to be minimized in static SIMS experiments; this is achieved by using low electron currents (ca. 0.1 μA cm^{-2}) [20].

Charging problems can be partly avoided by using atoms instead of ions as the primary beam. In FABMS, the ion beam, already accelerated and collimated, is passed through a chamber containing a relatively high pressure of inert gas [24—26]. A fraction of the ions (up to 20%) is neutralized, preserving kinetic energy and direction. An atom beam is obtained, while residual ions are removed electrostatically.

Polystyrene has been studied with both ions and atoms as the primary beam [26]. Quantitative and qualitative differences were observed. The FABMS spectra showed higher intensities and the decrease with time was slower (the rate of decay was a quarter of that observed with ions as the primary beam). The peaks corresponding to high masses were more intense than in SIMS.

Among the analyzers used in static SIMS, the most popular is the quadrupole mass analyzer, which is easy to use and relatively cheap. Magnetic and electrostatic sector analyzers are more effective, particularly for very high masses, but their transmission performance is rather poor. The time-of-flight analyzer [24] has become more often used, because it provides a consistent increase in sensitivity. It shows high transmission; 20—30% of secondary ions are observed, compared to a fraction of 1% with other analyzers. The transmission is constant over the entire mass range and the simultaneous detection of all masses with the same polarity (positive or negative) facilitates and speeds the data averaging [9].

As in conventional mass spectrometry, in static SIMS it is possible to obtain both positive- and negative-ion spectra. Most data now available refer to positive-ion spectra, because negative-ion spectra were considered much less informative [22]. However, negative-ion spectra are particularly useful in detecting groups containing electronegative elements, such as oxygen and halogens.

The negative-ion mass spectrum of polyethylene oxide (PEO) [20] was obtained with 2-keV Xe^+ ions as the primary beam; various high mass peaks were observed, giving qualitative information about the surface conformation. Negative-ion spectra have been used to determine the degree of polymerization of 3-methacryloxypropylsilane on various fillers [27]. Static SIMS is effective in providing a variety of qualitative information about the surface, even if the interpretation is not always straightforward. Its sensitivity is the best among surface techniques (about 10^{-6} coverages can be detected) even though sensitivity can vary widely with the chemical nature of the observed species [22]. The surface damage caused in static SIMS experiments has been widely studied [28]. Variations in chemical composition are important because the energy introduced by primary particles favours differential sputtering of the species present at the surface. Breakage or formation of chemical bonds, enrichment or depletion of particular functional groups, and changes of oxidation state occur as a function of time. Well known is the case of polystyrene, where the XPS shake-up peak associated with aromatic rings disappears after a dose of ca. 10^{14} ions cm^{-2} [20]. Lastly,

morphological changes can occur, in particular amorphization, as well as charging effects. Doses up to ca. 10^{12} ions cm^{-2} do not induce significant surface modifications [20]; at doses over 10^{14} ions cm^{-2}, static SIM spectra cannot be interpreted on the basis of the structure of the parent polymer, because the spectra tend to have a common appearance, owing to $(C_nH_m)^+$ ions [20]. A strong decrease in peak intensities is also observed.

Numerous polymers and copolymers have been studied by static SIMS, e.g., nylon, PTFE (polytetrafluoroethylene) and polypropylene [22, 24] and polystyrene [22]. Nylon has also been studied with a time-of-flight analyzer [9, 24]. The fragmentation pattern observed in static SIMS is typical for each polymer and can be considered a sort of fingerprint. The observed ions can be interpreted in terms of the repetitive unit of the polymer. The SIMS fragmentation patterns are similar to the conventional gas-phase electron-impact mass spectra from the monomers [20].

An example is given by polymethacrylates, which has been studied by several groups [7, 8, 21, 29]. Both the polymer skeleton and pendant groups produce a characteristic fragmentation [21]. The part of the positive-ion spectrum with masses over 100 D is dominated by peaks related to the polymer skeleton.

A sort of fingerprint for polymethacrylates is provided by a particularly intense peak at 69 D, which has been attributed to the formation of a stable dimethylcyclopropyl carbocation [21]. This fragment is prominent in polymethacrylates but not in polyacrylates. It can also be found in other polymers with pendant methyl groups, e.g., polypropylene. The identification of other peaks is more speculative, but the pattern related to the polymer skeleton is reasonably independent of the sidechain. At masses lower than 100, fragmentation of the side-chain produces intense peaks [21]. It is relevant to note that, as in aliphatic esters examined by electron-impact mass spectrometry, the hydrocarbon side-chain R^+ and derived fragments produce intense peaks, while OR^+ and related fragments are less visible. In the case of polymethylmethacrylate, a strong peak occurs at 15 D (CH_3^+), while in polyethylmethacrylate, the peak at 29 ($C_2H_5^+$) is dominant. In polybutylmethacrylates, the intensity ratios of peaks originating from the fragmentation of the side-chain allow the various isomers to be identified unambiguously [21].

Dynamic SIMS has been applied to the study of S-glass silylated with 3-aminopropyltriethoxysilane [4]. Static SIMS has recently been used to characterize quantitatively the bonding of octadecyldimethylchlorosilane (ODS) to silicas used as chromatographic materials [30]; the $SiOH^+/SiO^+$ ratio decreased with increasing ODS coverage, suggesting its reaction with surface silanol groups.

The application of static SIMS to thin (monomolecular) layers of Langmuir-Blodgett fatty acid films on silver has been reported [31]. The degree of unsaturation of the fatty acid is readily determined from such mass spectra.

The relatively easy collimation of ion beams to obtain good spatial resolution has encouraged the use of static SIMS with ions [20, 22] or atoms [32]

for microscopy. With noble gas ions, a resolution of some micrometers is obtainable. Liquid metal ion beams can be collimated to give spatial resolution down to fractions of a micrometer [22]. In atom-beam imaging (FABMS imaging), FAB guns have been modified to improve collimation. Argon atoms provide resolutions comparable to those obtained in static SIMS imaging. Atom beams avoid charging problems. In the usual operating mode, the analyzer is fixed to observe a fragment of given mass. The ion (atom) beam is then rastered on the surface by a computer-guided electrostatic apparatus. The intensity recorded at each observation point is plotted in two dimensions. The use of a time-of-flight analyzer will probably improve the effectiveness of SIMS imaging. By using peaks typical of different compounds, the surface distribution of various components is obtained. The image given by secondary electrons emitted as a consequence of heavy particle bombardment [20, 22] can also be recorded.

Most applications of these techniques concerns the analysis of microcircuits, but images of polymer surfaces have also been obtained [20, 22]. In an interesting application, the fracture surface of a carbon-fiber composite material has been examined [20]. Scanning electron microscopy requires a metal coating so that information about the chemistry of the fracture surface cannot be obtained. In static SIMS imaging, the use of peaks typical of graphite and polymer and graphite alone has shown that some fibers hold residues of the polymeric matrix [20]. Such information is very important in evaluating the fracture mechanism at the surface.

Another space-resolved technique suitable for studying polymer surfaces is the laser microprobe mass spectrometry (LMMS) [9]. Ion emission is induced by an intense laser beam, with a lateral resolution in the 2—100-μm range. It has been applied to the study of dye spots on polystyrene [9] and of various other organic materials [33].

X-RAY PHOTOELECTRON SPECTROSCOPY

X-ray photoelectron spectroscopy (XPS) is one of the most popular spectroscopic techniques available for studying polymer surfaces. Books describe the technique and its applications [34—36], and its applications to polymers have been reviewed [34, 35, 37—39].

The spectrum is obtained by irradiating the sample with a monochromatic x-ray source. Photons can collide with electrons providing their escape energy and emitted electrons acquire a kinetic energy which is equal to the difference between the energy of the incident photon and the binding energy of the electron to the nucleus. For each element and each core level, atomic sensitivity factors, $ASF(i)$, which account for instrumental factors and for the cross-section of the photon/electron collision have been defined. They must be calculated for each instrument; a compilation for the cylindrical mirror analyzer is available [36]. When the experimental XPS intensity, $I(i)$, corresponding to the various elements present at the surface is known, the

relative concentrations, $C(i)$ expressed as atom percent, can be calculated from the equation

$$C(i) = I(i)/ASF(i)/\sum_j I(j)/ASF(j) \quad (4)$$

Emitted electrons are characterized by the inelastic mean free path (IMFP), the value of which depends on the electron kinetic energy. Only the electrons generated near the surface (within a range of a few nanometers) have a finite probability of escaping from the material without changing their state of motion [34—36]. These electrons give rise to the XPS signal, while those which have changed their state of motion contribute to the background. To a first approximation, when the electron kinetic energies exceed ca. 100 eV, the IMFP depends only on the square root of the kinetic energy [34, 35]. The problems of IMFP's in inorganic and organic compounds have been reviewed [40].

The actual constant which characterizes the probability of the electron leaving the material without collisions is the escape death (l), which is a function of the IMFP (Φ) and the angle θ between the axis normal to the surface (z) and the axis of the analyzer: $l = \Phi \cos \theta$. The XPS intensity can be expressed in a simplified form as a function of the number of atoms of the element i in the examined layer, $N(i)$, the atomic sensitivity factor and the electron escape depth $l(i)$ [34]:

$$I(i) = ASF(i) \int_0^\infty N(i) \exp [-z/l(i)] dz \quad (5)$$

A consequence of the exponential dependence expressed in this equation is that more than 95% of the observed electrons come from a layer which has a thickness 3 times the electron escape depth which in turn depends on the IMFP. As the latter has a value, at the commonly used kinetic energies, of 0.5—4 nm [40], the observed layer is 2—12 nm thick.

The instrumentation for XPS has often been reviewed [34—36]. The sample is introduced into an ultra-high vacuum chamber (usually at a background vacuum of 10^{-7}—10^{-8} Pa). The most popular x-ray guns use the K_α lines of magnesium or aluminium, which ensure both good resolution and sensitivity. Emitted electrons are analyzed by a cylindrical or hemispherical analyzer and detected. The XPS resolution is not particularly high (about 0.5 eV) and its sensitivity is low compared to SIMS (10^{-3} coverages can be detected) [34].

Both quantitative (surface concentrations) and qualitative (functional groups) information can be obtained. All elements, except hydrogen and helium, can be observed. Core electrons, with high binding energies, are the origin of the most important spectral features. These electrons are less sensitive to chemical state than valence electrons, but it is still possible to obtain information, even if approximate and often ambiguous, about the chemical state. Because the XPS intensity is a function of the angle of observation, θ

(Eqn. 5), altering this angle provides a non-destructive depth profiling. Of course, the profile is limited by the value of the IMFP in the material.

An alternative is ion bombardment of the surface with an ion gun and collecting the XPS spectra at opportune intervals. Such a technique is not wise for polymeric materials because it alters the surface layer, depleting or enriching it in particular functional groups [34, 35]. Most of the information about polymer surfaces has been drawn from C-1*s* spectra, usually a sum of components relative to different chemical states of the carbon atom at the surface. Line fitting of C-1*s* spectra allows a semiquantitative evaluation of the relative amounts of different functional groups at the surface [34—38]. The C-1*s* spectrum of a floppy disk surface obtained in this laboratory is shown in Fig. 3. Carbon bonded to other carbon atoms or hydrogen provides a component at 284.6 eV, carbon singly bonded to oxygen at 286.2 eV and carboxyl carbon at 288.8 eV; these components are related to the resin used in manufacturing the disk. The components at 291.6 eV (carbon bonded to one fluorine atom) and 293.7 eV (carbon bonded to two or three fluorine atoms) relate to the perfluoroalkyl ethers used as lubricant.

Shake-up peaks, which originate from a two-electron process, provide other information [35, 37, 38]. Beside the emission of a core electron, a simultaneous excitation of a valence electron to an unfilled level can occur.

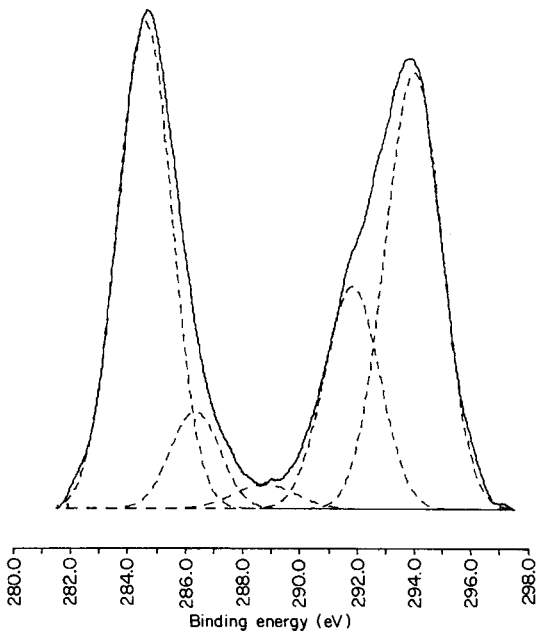

Fig. 3. The C-1*s* spectrum of a floppy disk coated with perfluoroalkyl ether lubricant): (——) original spectrum; (— — —) components.

Shake-up peaks are evident at the lower kinetic energy side of main peaks. Their presence is expected when a polymeric system contains unsaturations. They are particularly prominent in polymers containing pendant aromatic groups [37] and their occurrence indicates the aromaticity of a material [41].

Several studies of x-ray photoelectron spectra of valence electrons, usually accompanied by theoretical calculations of the polymer valence bands, have been reported [42—44]. Obviously, valence electrons are not characteristic of any element, but they reflect the structure of electron bands of a layer which is thicker than that traversed by core electrons and so can be considered representative of the bulk of the polymer. Valence bands are generally studied by solid-state ultraviolet photoelectron spectroscopy, which is otherwise rarely used in polymer studies [45, 46].

Surface of polymers [35—38], copolymers [10, 47, 48] and blends [49, 50] have been studied by XPS. It has been shown that treating polyethylene with a chromic acid/sulphuric acid mixture produces mainly carboxyl groups on the surface [51]. Treating a poly(chlorotrifluoroethylene) surface with methyllithium removes —CF2— near the surface with an increase in the hydrocarbon component (introduction of methyl and unsaturated groups) [52]. The behavior of polyethylene grafted with 1% acrylic acid in contact with water has also been studied [53]; water attracts the acrylic groups to the surface.

Various physical methods have been used to improve the adhesive properties of polymers. By XPS it has been shown that flame treatments induce the formation of hydroxyl, carbonyl and carboxyl groups on polyethylene [54] and polypropylene [55].

Electrical discharge treatment in the presence of oxygen proved effective on the same materials [56, 57]. Electron-beam treatments in the presence of air also favor the formation of oxygen-containing functions [58]. The low-temperature plasma treatment of polymer surfaces is popular [35, 38]; XPS has been applied in studies of water or oxygen plasma treatments of surfaces; these processes provide high densities of carboxylic acid groups [59].

Surface halogenation has also been widely studied [35]. Polypropylene has been treated with a cold plasma of various halomethanes [60]; CF_3Cl and CF_3Br cause respectively the chlorination and bromination of the surfaces, while trifluoromethane produces a film of fluoropolymer on the surface. Surface fluorination with fluorine gas has also been studied [61].

The effect of laser treatment on poly(ethylene terephthalate) (PET) and polymethylmethacrylate (PMMA) has been discussed [62]; with 193-nm radiation, ablative photodecomposition of the surface occurs. For PET, the surface treatment causes oxygen-depletion, indicating removal of carboxyl groups. For PMMA, no preferential removal of oxygen was observed, which suggests decomposition to monomer units. XPS studies on copolymers showed that the surface composition can differ greatly from the bulk composition [10, 47, 48]. In styrene/ethylene oxide copolymers, polystyrene predominates at the surface [47]. In block copolymers of styrene and

dimethylsiloxane, a 1.3—4-nm surface layer of polydimethylsiloxane has been observed. These variations of the surface composition with respect to the bulk have been interpreted as a result of the required minimization of surface energy.

Similarly, the surface-energy minimization can produce surface enrichment in blends, as observed by XPS [49, 50]. In PVC/PMMA blends, a surface excess of PVC is present [49]. Angular dependent studies on polystyrene/poly(vinyl methyl ether) (PVME) blends suggested a composition gradient profile, with surface enrichment in PVME, the component with lower surface tension [50]. The variation in composition in the first few nanometers of the surface layer in blends can be very important; e.g., in biomedical materials, the surface composition governs the biocompatibility of the material. In polyurethanes, enrichment of ether groups at the surface has been observed [63, 64].

The adsorption of molecules on surfaces has also been studied by XPS. Physical absorption of glycine on graphitic surfaces has been observed [65], in a study of the interaction of proteins on biomaterials. A partially orientated double layer, similar in structure to crystalline β-glycine, is stable at the surface.

The surface of fillers for composite materials has been characterized by XPS. Carbon fibers [66—68] and coated glass fibers [69, 70] have been studied. Oxide surfaces treated with alkylamino silanes, normally used as promoters to improve the filler-to-matrix adhesion in composites, have been examined [70]. The bonding of 3-methacryloxypropyltrimethoxysilane to various fillers has been studied by XPS and static SIMS [27]. The fraction of surface covered by the silane and the thickness of the silane layer were estimated by using simplified models based on XPS intensities. Both coverage and thickness influence the mechanical and transport properties of the composite material.

The reactions of epoxides [66] and amines [67] with carbon fibers have been studied, after activation of the fibers by oxidation with sulfuric and nitric acids. The reaction of epoxide or amine groups at the surface was considered a model of the surface reaction of the resins which constitute the matrix in carbon fiber composites. The formation of both epoxide and amine layers on carbon fibers has been demonstrated. The bonding is assumed to be covalent in both cases. Average layer thicknesses can be calculated from XPS data.

Metal/polymer interfaces, and particularly their fracture behavior, have been studied extensively by XPS. These applications have been reviewed [71].

The above paragraphs provide only a very limited sample of the literature concerning XPS applications to the study of polymer surfaces. XPS is the most efficient technique when layers some nanometers thick have to be analyzed.

INTERNAL REFLECTION SPECTROSCOPY

The previously discussed techniques require ultra-high vacuum for operation. All the spectroscopies based on electromagnetic radiation, from radio-frequency to near-ultraviolet, do not need such facilities. In the search for experimental methods for observing a layer of limited thickness with sufficient sensitivity, internal reflection phenomena (internal reflection spectroscopy, IRS) have been examined. Several books and reviews have been written about IRS [72—77]. The technique is also known as attenuated total reflectance (ATR) spectroscopy.

The physical phenomenon on which IRS is based has long been known. An electromagnetic wave incident at the interface between two different media, with refractive indexes n_1 and n_2, respectively ($n_1 > n_2$), is totally reflected. The angle of incidence must be higher than the critical angle, defined by

$$\theta_c = \arcsin (n_2/n_1) = \arcsin (n_{21}) \tag{6}$$

$$E = E_0 \exp [-(2\pi n_1/\lambda)(\sin^2 \theta - n_{21}^2)^{1/2} z] \tag{7}$$

$$\Gamma = [2\pi n_1(\sin^2 \theta - n_{21}^2)^{1/2}/\tau] \tag{8}$$

The theoretical treatment of IRS is not easy; to simplify it, medium 2 is assumed to have a very low absorption [72]. In this approximation, the time-averaged energy flux is zero in medium 2. Instantaneously, the so-called evanescent wave occurs; this is an electromagnetic wave with components in all space orientations; the intensity decreases as a function of the distance from the interface between media 1 and 2 (Fig. 4). The amplitude of the evanescent wave depends on this distance, the amplitude of the electric field at the interface (E_0), the angle of incidence (θ), the wavelength of the radiation (τ) and the refractive index of medium 1 (Eqn. 7).

In the literature, the penetration is often given as d(p), which is the reciprocal of Γ (Eqn. 8). At this thickness, $E = E_0 \times (1/e)$. The meaning of d(s) = $3/\Gamma$ is analogous but then $E = E_0 \times 0.05$.

If the hypothesis of zero absorption of medium 2 is correct, the intensity of the radiation after reflection should be equal to that hitting the sample surface. Internal reflection (ATR) spectroscopy is based on the fact that medium 2 has a net, even if low, absorption [72]. The reflectivity R is less than 1:

$$R = I/I_0 = \exp [-\alpha\, \mathrm{d}(e)] = 1 - \alpha\, \mathrm{d}(e) \tag{9}$$

In this equation, α is the absorption coefficient and d(e) the effective penetration of the evanescent wave. The absorption coefficient is a function of the refractive index of medium 2 and of the wavelength. With the usual absorption coefficients, the reflectivity loss is less than 1%.

In the approximation for low absorption, the absorbance A is given by

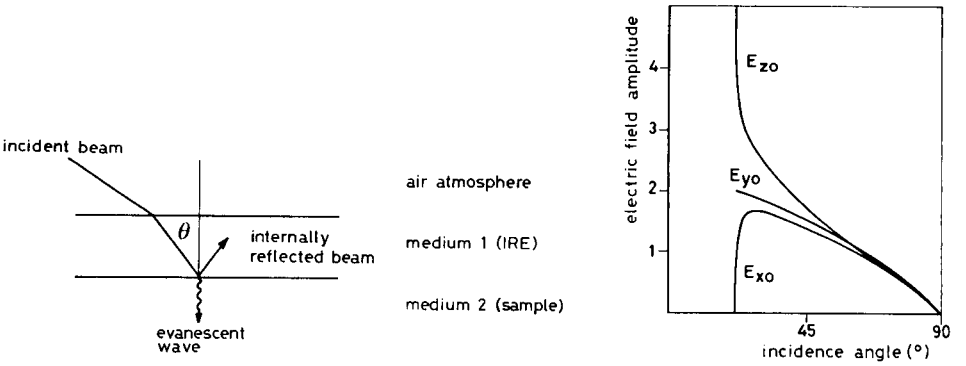

Fig. 4. The physical basis of internal reflection spectroscopy. A wave moving in a medium with refractive index n_1 hits a medium with refractive index n_2 ($n_2 > n_1$). Almost total reflection into medium 1 occurs. The evanescent wave penetrates medium 2.

Fig. 5. Depth dependence of the amplitudes of the evanescent electric field components as a function of angle of incidence, calculated for germanium as the internal reflection element.

$$A = \alpha\, \mathrm{d}(e) = (n_{21}\alpha/\cos\theta) \int_0^t E^2 \mathrm{d}z \tag{10}$$

The final expression is

$$A = \alpha\, \mathrm{d}(e) = (n_{21}\alpha E_0^2)/(2\Gamma \cos\theta) \tag{11}$$

and the effective thickness of the observed layer is given by

$$\mathrm{d}(e) = (n_{21}E_0^2)/(2\Gamma \cos\theta) \tag{12}$$

More sophisticated theoretical treatments [78] do not substantially modify the results. The factors to be considered in calculating the thickness of the observed layer are the angle of incidence, the refractive index of medium 1 and the radiation wavelength. The angle of incidence is particularly important because it influences the amplitude of the electric field at the interface between media 1 and 2 (Fig. 5), altering both penetration and sensitivity, and is present in Eqns. 10—12. Given all the effects, d(e) decreases with increasing angle of incidence.

Medium 1, in contact with medium 2 (the sample) is called the internal reflection element. Its choice determines the critical angle (Eqn. 6), and n_{21} is present in Eqns. 10—12; increase of n_1 induces a decrease of d(e). Within the same technique, the internal reflection spectrum is affected by variation of n_1 as a function of wavelength [72].

The wavelength is present in Eqn. 8 for Γ, which in turn is present in Eqn. 12 for d(e). A decrease in the wavelength means a decrease in the thickness of the observed layer.

Internal reflection spectroscopy has been used in infrared, Raman and fluorescence modifications. Infrared and Raman methods give vibrational

information which allows identification of functional groups in the examined layer. Fluorescence spectroscopy, through the spectrum and the lifetimes of excited states, enables the electronic states of the species in the examined layer to be studied. The wavelengths used in fluorescence and Raman studies are in the 300—700-nm range; a layer with a thickness of hundredths or tenths of a micrometer can be observed [72]. In infrared spectroscopy, a 2.5—16-μm range is scanned and the thickness of the observed layer is several micrometers.

Absorption is measured in the infrared method, but emission is measured in the Raman and fluorescence methods, thus the experimental arrangements are different, as shown in Fig. 6. The sample must be in as intimate contact as possible with the internal reflection element, which is usually a suitably cut single crystal (Fig. 6A). In an infrared reflection study on powders, alterations of the relative intensities of bands were observed with respect to a spectrum of a plaque [79].

The penetration of the infrared radiation can be decreased below the limits allowed by variations in angle of incidence and refractive index of the internal reflection element, by depositing on the examined surface a non-absorbing film of controlled and uniform thickness [75—77]. Of course, this decreases not only the thickness of the observed layer but also the sensitivity, because the intensity of the evanescent field is an exponential function of the dimension normal to the surface (Eqn. 7). Besides penetration, sensitivity and spectral contrast affect the choice of internal reflection element. Increasing n_1 decreases the penetration, sensitivity and spectral contrast. Something similar could be said about the choice of the angle of incidence [72].

In a recent paper [80], the lower limit of the surface layer measurable by Fourier-transform infrared (FTIR)/IRS has been determined. Thin layers of polystyrene were deposited on polyurethane, and a surface layer of 5 nm or even less could be examined by using spectral subtraction. A FTIR/IRS study of Langmuir-Blodgett films of stearic acid which were 1—9 monolayers thick

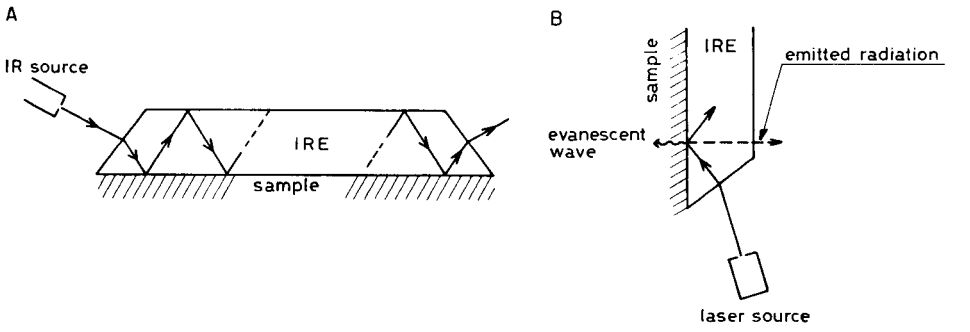

Fig. 6. Experimental arrangements for internal reflection spectroscopy: (A) infrared; (B) Raman. In both cases, the emitted radiation passes to a monochromator (or interferometer) and a detector.

has been published [81], showing good detection even in this less favourable situation.

An ASTM procedure for obtaining internal reflection/infrared spectra is available [82]. The practical aspects of the technique and the related instrumental accessories have been also described [83]. The experimental arrangement outlined in Fig. 6A does not allow a double-beam study. With modern instruments allowing computer-controlled spectral subtraction, it is possible to record a spectrum without the sample and remove possible spurious contributions [72].

From a quantitative point of view, the Lambert-Beer law is not generally valid in this infrared method. There is some absorbance/concentration proportionality, particularly when absorption coefficients are low, but the use of intensity ratios of bonds present in the same sample seems more suitable [84]. Calibration curves based on samples of known concentration have been also suggested [84].

The IRS method with Raman spectroscopy is less popular than the infrared method. The reasons are its lower sensitivity and increased instrumental problems [85]. Emission spectra are collected (Fig. 6B). Excitation is usually done with a laser. The observed layer is shallower than in the infrared method (10—500 nm), depending on wavelength, angle of incidence and internal reflection element [85, 86]. The choice of this element is critical; it must be transparent, with high refractive index and without Raman signals in the zone of interest. Sapphire seems the best [85, 86]. To achieve the best sensitivity, the angle of incidence is usually kept near the critical angle. Again, the contact with the sample must be as intimate as possible. There have been few applications of this technique to polymer surfaces, because of its complexity and lack of sensitivity.

The instrumental problems met in the Raman internal reflection technique are repeated in the fluorescence modification. This technique has found many applications in biology [87], and has also been used to characterize polymer surfaces [88]. The experimental arrangement is similar to that shown in Fig. 6B. Sapphire is again the most used internal reflection element.

The infrared modification has found an extremely wide number of applications in different types of surface analysis of polymers. Part of its popularity can be ascribed to the availability of suitable accessories for commercial infrared spectrometers. Depth profiles in various materials, surface modifications, conformation and orientation have all been studied. Depth profiles between 1 and 10 μm can be obtained; this is not surface in the strictest sense. Internal reflection/infrared spectroscopy is less surface-specific than XPS, but also less sensitive to surface contamination.

Depth profiles of incompatible blends (i.e., mixtures of different phases) for biomedical applications have been obtained by altering the angle of incidence [89, 90]. For Avcothane, an incompatible blend of polyurethane and poly(dimethylsiloxane), it has been observed that increasing the angle of incidence (i.e., decreasing the radiation penetration) increases the intensity

of poly(dimethylsiloxane) signals, which suggests its surface segregation [90]. A depth-profiling study of three-component copolymers (styrene, butadiene and 4-vinylpyridine), again used as biomedical materials, showed surface segregation of 4-vinylpyridine and that macroscopic properties such as hydrophilicity and thrombogenicity depend on the method of preparation [91]. A depth-profiling study of a PVC membrane with crown ethers anchored on it has been presented [92].

In biomaterials, adsorption phenomena are also important. The interaction of polymeric biomaterials with various proteins and blood has been studied [93].

Surface treatments of polymers such as photo-oxidation [94], chemical oxidation [95] and fluorination [96] have been studied. Through peroxide intermediates, —OH, C—O—C, C=O and COOR groups are formed during the photo-oxidation of polypropylene [94]. Chemical oxidation [95] produces the same oxygen-containing functions. Ordinary compression or extrusion processes can introduce a limited quantity of oxidized groups on polymer surfaces [94, 97]. The effect of treating polyethylene with sulfur trioxide fumes, in order to obtain a biomedical material with special anticoagulant properties, has been reported [98]. Plasma treatments have also been studied extensively. Plasma-treated polysiloxane polymers have been examined, particularly in their aging processes [99, 100]. A study of the fracture surface of polyethylene has been reported [101]; the surface terminal group concentration is about an order of magnitude higher than in the bulk. This feature was attributed to breakages of macromolecular chains near the stressed region. The conformational difference between surface and bulk in polyethylene and poly(vinyl alcohol) has been studied [97]. More *trans* isomers were observed at the surface than in the bulk. Polarization techniques have been used to study surface orientation on polypropylene [102]. The application of infrared dichroism in IRS allowed the surface orientation to be quantified [102].

An interesting application of infrared IRS to composite materials has been presented [103]. A polypropylene sheet was printed, using mica plaques, to simulate a polypropylene/mica interface. The polypropylene film was detached and examined by IRS/infrared dichroism. It was observed that at the surface the polypropylene chains assumed a preferential orientation, as if the crystallization had been nucleated by mica.

DIFFUSE REFLECTANCE SPECTROSCOPY

Diffuse reflectance spectroscopy (DRS) has long been used, principally in the u.v./visible region [104]. In recent years, diffuse reflectance in the infrared region has become popular. The introduction of Fourier-transform instruments and improved optics have increased its attraction [105, 106]. Diffuse reflectance is present when the spectrum is a function of both absorption and scattering events, when strongly scattering samples, such as powders,

are examined. The intensity of the radiation arriving on the detector is a function of both the imaginary and real parts of the refractive index, thus exact theory is very onerous. Among the various simplified treatments, the one by Kubelka and Munk [107, 108] has been the most successful. The Kubelka-Munk expression in its simplest form is

$$K/S = (1 - R)^2/2R \tag{13}$$

where R is the diffuse reflectance as measured, and K and S are the empirically estimated absorption and scattering coefficients, respectively.

The Kubelka-Munk model has several limiting conditions: (1) the incoming radiation is monochromatic and completely diffused (actually a low absorption and a low specular reflectivity are sufficient); (2) the extent of the horizontal layer of the sample is infinite and thickness is also infinite (again this condition is not essential); (3) the sample is macroscopically uniform; (4) the sample is not fluorescent; and (5) the optical medium in contact with the top of the specimen has the same refractive index as the medium of the layer. Under suitable conditions, K is proportional to the concentration of the examined species. Other models have been proposed to interpret diffuse reflectance spectra, particularly those of Pitts-Giovannelli and Rozenberg [109], but the Kubelka-Munk equation remains the most used, particularly because it is easy to handle.

Diffuse reflectance spectroscopy is not a surface technique, because it also reflects the bulk composition. It becomes a surface technique if there is a phase deposited on a substrate which does not give a spectrum in the same region. The use of a shallow layer of reflecting powder (usually potassium bromide) to make DRS partly surface-specific has been reported [110]. This is possible because of initial scattering of the incident radiation on the bromide. The radiation then arrives on the sample material from "random" incident angles, thus increasing the scattering at the KBr/sample interface. In coated materials, there is further scattering at the second interface. Because the radiation passes many times through the top layer, the sensitivity is rather better than that of transmission techniques [111].

The diffuse reflectance method can be used in the u.v./visible and infrared regions. In the latter case, it is often called diffuse reflectance infrared Fourier-transform spectroscopy (DRIFT). DRIFT, transmission infrared and FTIR/PAS (photoacoustic spectroscopy, see below) are suitable for similar problems. Transmission FTIR is particularly appropriate for studying adsorption phenomena (such as the silane promoter/filler bond in composite materials). DRIFT has the disadvantage of being instrumentally more complex and less direct in data handling, but it is more sensitive and does not require particular sample treatment. FTIR/PAS and DRIFT have in common the feature that samples can be observed without pretreatment. FTIR/PAS has some suitability for surfaces (the observed layer is several micrometers thick) and is applicable to any type of sample. DRIFT provides more reproducible quantitative data and is by far more sensitive.

The experimental arrangements are outlined in Fig. 7. The radiation sources are similar to those used in the corresponding transmission spectroscopic technique. The difference between the u.v./visible and the infrared arrangements lies in the collection of the scattered radiation. In the former (Fig. 7A), the reflecting sphere used is coated internally with a highly reflecting material (e.g., MgO, NaF). The scattered radiation is then collected by a suitable photomultiplier. In the latter, the reflecting sphere is not efficient enough, and more sophisticated devices are required. The use of hemispherical or ellipsoidal mirrors, with high focusing power, is now common.

For the presentation of results, it is necessary to account for the fact that the Kubelka-Munk assumptions are not completely respected experimentally. Important from a quantitative point of view is that the scattering coefficient S is not constant, but depends on the wavelength, particularly when it becomes comparable to the dimension of the particles studied. Standards are necessary to correct deviations from the ideal Kubelka-Munk behavior. The ratio of the reflectances observed in the sample and in the standard is used at each wavelength: $R' = R(\text{sample})/R(\text{standard})$. In u.v./visible DRS, different standards have been used (MgO, NaF, NaCl, etc.). In infrared DRS, KCl and KBr have been most used; small particles are preferred to optimize scattering. In normal applications, the sample is a powder, which is examined as such. There have also been applications to fibers and polymers (as films or plaques). In the case of powders, spectral characteristics (e.g., bandwidths and relative intensities) have been shown to depend on the particle dimensions. Plots of K/S vs. concentration are not linear when the sample is dispersed in a reflecting material (KCl) [105]; this effect has been verified at high concentrations. The technique can, however, be used for quantitative studies [112].

The commonest application to polymeric materials is the study of silane adhesion promoters on fillers for composite materials. Silanes increase the filler/matrix compatibility. It is important to study the silane-to-filler bonding, so as to understand the action of the silane and its effect on the properties of the material.

Such interactions have also been studied by transmission FTIR [113]. DRIFT is much more sensitive than transmission FTIR; and the sample is

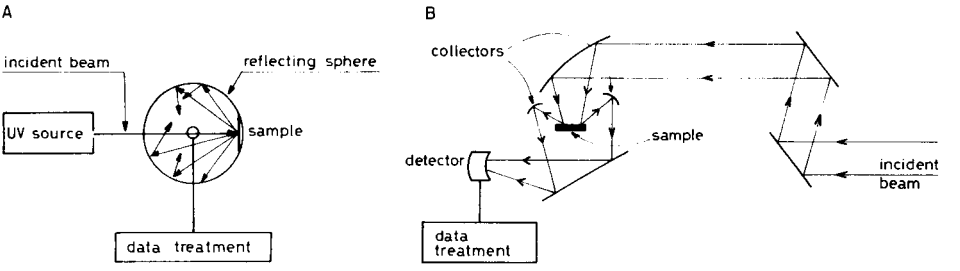

Fig. 7. Experimental arrangements for diffuse reflectance spectroscopy: (A) ultraviolet/visible; (B) Fourier-transform infrared.

not compacted in KBr pellets, so that the physicochemical properties of the adsorbed layer are preserved. In transmission FTIR, it is difficult to study samples with surface specific areas (SSA) of <0.5 m^2 g^{-1}. In DRIFT, the observation of 3.68 mg of silane adsorbed on 1 g of glass with 0.01 m^2 g^{-1} SSA has been reported [106]. The possibility of studying small quantities of silane makes it possible to operate with silane concentrations similar to those normally used in application.

A study of silanes on glass fibers [114] has shown the importance of the orientation of the sample with respect to the incident radiation. Fibers scatter radiation anisotropically, so that the intensity of scattered radiation shows an angular dependence. The latter can be partly eliminated by averaging spectra obtained at different orientations. However, the most efficient way to overcome the problem is to cover the fibers with a shallow layer of reflecting powder [110]. Another problem of glass is its intrinsic strong scattering at <1500 cm^{-1} [110, 112], which prevents study of the silane spectrum in that region.

In a study of the adsorption of 3-aminopropyltriethoxysilane (APS) on oxidized silica, quantitative data about the bonding of the silane have been obtained [115]. Of particular interest are the spectral regions between 3800 and 3000 cm^{-1} (SiO—H and N—H stretch), between 1800 and 1600 cm^{-1} (NH_2 bending) and between 1200 and 800 cm^{-1} (Si—O—Si stretch). An adsorbate coverage of less than a monolayer has been detected. The 3-amino group is important, because it forms hydrogen bonds with surface hydroxyl groups. An important feature of the DRIFT spectra is the observation of Si—O—Si bridges between silane and surface. At higher coverages, silane-silane Si—O—Si bridges are also formed. The two situations have been distinguished by examining the spectrum of APS physisorbed on KBr [115].

A comprehensive series of organic functional groups supported on silica gel has been observed [116]. The matrix background was eliminated by using spectral subtraction techniques, with acceptable semiquantitative results.

DRIFT spectroscopy is not really a surface technique but for polymeric films some variation of sensitivity with depth can be obtained by adding at the surface a reflecting powder, e.g., KBr [110, 111]. In the case of superimposed films, e.g., poly(vinyl fluoride) on poly(ethylene terephthalate), the spectrum of the top layer was found to predominate when this technique was used [111]. For a PMMA film, varying the quantity and particle size of KBr made it possible to observe surface carbonyl groups shifted to lower frequencies because of hydrogen bonding with adsorbed water [111]. DRIFT has some capability for depth profiling, but the observed intensities are not related to depth with any degree of precision. Furthermore, strong alterations of the relative intensities of bands have been observed. The progressive oxidation of a poly(dimethylfulvene) powder showed an increase with time of oxygen-containing functions (OH, C=O, etc.) [105].

Studies of organic compounds in industrial materials by DRIFT, without altering the sample, have been reported [117]. The method is especially

effective for powders and foams. In contrast, the analysis of films of polymeric material can be difficult because specular reflection is stronger than diffuse reflectance, so that the Kubelka-Munk model cannot be used for interpretation. Diffuse reflectance has been used for orientation studies of drawn poly(ethylene terephthalate); even when the specular component predominates, information can be obtained on the molecular orientation of film or fiber surfaces [118].

PHOTOACOUSTIC SPECTROSCOPY

Photoacoustic spectroscopy (PAS) is based on evaluation of the acoustic signals produced by conversion to thermal energy of the energy adsorbed by a solid irradiated with a modulated electromagnetic wave [119—122]. The technique is used mostly for solid, thick and opaque samples. The sample is introduced into a gas-filled cell, one wall of which is transparent to incident radiation; the signal is detected by a microphone. The modulated electromagnetic wave hits the sample and is partly absorbed. The attenuation can be expressed according to the Lambert-Beer law. The optical penetration is usually expressed by the reciprocal of the absorption coefficient at the particular wavelength. The absorbed energy is totally converted into heat in the solid. The theory of PAS deals with the quantity of thermal energy arriving at the surface of the solid [119—121]; this energy flux heats the gas layer in contact with the surface. Because the incident radiation is modulated with a frequency Ω, an acoustic wave with the same frequency is generated.

The thickness of the solid layer contributing to the photoacoustic signal is characterized by the thermal diffusion length, μ:

$$\mu = (2\tau)/(\sigma C\Omega) \tag{14}$$

where τ is the thermal conductivity, σ the density, C the specific heat and Ω the modulation frequency. The original theory provided a unidimensional model of the periodic heat flux from the solid to the gas [123]. The measured signal is given by

$$P = Q \exp\left[-i(\delta + \theta)\right] \tag{15}$$

where $Q = q \exp(-i\Phi)$, $q = K\alpha\mu[2/(\alpha\mu + 1)^2 + 1]^{1/2}$ and $\Phi = \arctan(1 + 2/\alpha\mu)$.

Actually only Q determines the spectrum; δ and θ are phase factors related to the production of the signal and to the instrument, and their values can be obtained examining a standard; q is the modulus and Φ the phase. K is a complex constant accounting for various factors. Both modulus and phase are functions of the absorption coefficient, α, and of the thermal diffusion length, μ.

It is possible to obtain information from a photoacoustic spectrum if spectral parameters, intensity, q, and phase, Φ, are a function of α, i.e., of the incident wavelength. There is saturation when q is not a function of the

wavelength. If $\alpha\mu \gg 1$, then $q = 2^{1/2}K$ and $\Phi = \arctan(1) = \pi/4$. When a saturating material is used, the signal intensity can be normalized, thus eliminating possible variations of incident radiation intensity as a function of wavelength. The instrumental phase factor $(\delta + \theta)$ can also be obtained. Because the absorption coefficient is greater in the presence of strong chromophores and for electronic transitions, the photoacoustic effect is more frequently used in the infrared range. Furthermore, FTIR instruments offer advantages both in calibration and speed of data collection. The measured quantity is usually q. If $\alpha\mu \ll 1$, the valid equation is

$$q = K\alpha\mu[1/(1 + \alpha\mu)]^{1/2} = K\alpha\mu \tag{16}$$

Plots of q vs. α show a linear trend; over limited ranges, q is linearly related to the concentration of the examined species.

In materials presenting strong scattering, the assumption that the absorption of radiative energy of the material depends only on the complex absorption coefficient is not valid. Instead of q, a complex function taking into account scattering events which alter the radiative intensity inside the sample has been proposed [124]:

$$K\alpha\mu = 2^{1/2}q/[(1 + R)\sin(\Phi - \pi/4)] \tag{17}$$

where R is the diffuse reflectance expressed according to Kubelka and Munk [107, 108].

The thermal diffusion length depends only on the physicochemical characteristics of the sample and the modulation frequency (Eqn. 14). In a polymeric material, at normal modulation frequencies, thermal diffusion lengths are micrometers or tens of micrometers. The surface selectivity is equal to or less than that in infrared IRS. As the thermal diffusion length is inversely proportional to the modulation frequency, increasing the latter decreases the depth of the observed layer. But it should be noted that, to observe a layer of only 100 nm, the modulation frequency would have to be in the kHz range.

What has been said refers to solid, thick and opaque samples. Thin samples and thick transparent samples have also been considered. In the first case, if the thermal diffusion length is greater than the film thickness, the spectrum depends on film thickness, absorption coefficient and modulation frequency. In the second case, the observed intensities depend on thermal diffusion length, absorption coefficient and $\Omega^{-3/2}$ [123]. Obviously, different information is obtained, depending on the wavelength used. The commonest case is of infrared radiation, where vibrational information is obtained.

The radiation source for photoacoustic spectroscopy is not particularly different from that used for transmission or reflection infrared spectroscopy. In fact, the photoacoustic cell is usually sold as an accessory of infrared spectrometers. FTIR instruments are now commonly equipped with photoacoustic cells. Such instruments can collect and average spectra very quickly, overcoming sensitivity problems. The heart of the equipment is the photoacoustic cell itself, the construction of which is a very delicate task. A typical apparatus is outlined in Fig. 8. The cell is built with the minimum volume

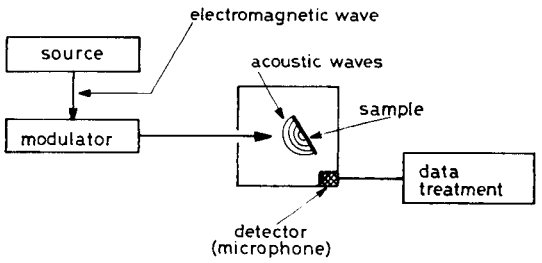

Fig. 8. Experimental arrangement for FTIR/PAS.

that allows introduction of the sample. The amplitude of the photoacoustic signal is inversely proportional to the dimension of the cell. The cell should be as free as possible from mechanical vibrations, which cause spikes in the spectrum. The electrical signal from the sensitive microphone is amplified and processed to yield the spectrum.

The purity of the transport gas is important. Problems are posed by water and carbon dioxide, which have strong infrared absorptions, give large photoacoustic responses and are not easy to remove completely. Several gases have been used to transport the signal; helium is appropriate as it provides good thermal contact with the sample [125].

Various applications of PAS to polymer surfaces have already been reported [74, 119, 121, 125, 126]. An important feature is that sample surfaces can be examined in any form. The dependence of the spectrum on the form of the sample [127] and, in the case of powders, on the particle size [128] has been studied. The spectra of a commercial polymer sample observed in the form of a smooth surface, pellets and powder were found to be similar [127]; but in the powdered samples there was some increase of intensity. A clear dependence of the photoacoustic spectrum on the particle size was demonstrated, particularly when the latter was comparable to the thermal diffusion length [128]. In general, spectral contrast is better with smaller particle sizes, but the reproducibility worsens. The cause lies both in scattering phenomena and in the dependence of the signal intensity on the radiation pathways. The radiation induces photoacoustic signals while both entering and exiting.

From a quantitative point of view, problems arise from the limited range of linearity of the q vs. concentration plots. The use of carbon black as a standard to normalize spectra can itself induce errors, because carbon black tends to adsorb water [129].

When compared with infrared IRS and DRIFT, FTIR/PAS is less direct from an instrumental point of view. However, any sample, even thick ones, with weak scattering or with a rough surface can be examined. A comparative study of infrared IRS and PAS infrared dichroism techniques has been reported for determining surface orientation in films of drawn PET. FTIR/PAS allows the measurement of dichroic ratios, although values were smaller than in infrared IRS, perhaps because the PAS technique gives more

penetration [130]. In a combined study of combined infrared IRS and infrared PAS for incompatible blends, it was shown that the photoacoustic spectra do not depend on sample morphology, but pose problems for quantitative purposes [90].

As in infrared IRS, it is possible to obtain a depth profile by altering the modulation frequency. A study of two-layer samples of epoxy resin on PET has been reported [131]. Spectral subtraction enabled the spectra of both the top layer and the substrate to be obtained.

The effects of thermal oxidation on phenolic resins have been studied [132]. Bands assigned to carbonyl groups appear, because of the oxidation of methylene groups. Transmission spectra suggest a constant increase of oxidation with time, while infrared photoacoustic spectra indicate saturation of the surface after a specific time of treatment. Analogous effects have been observed in the plasma oxidation of a styrene/divinylbenzene copolymer [133]; carbonyl and/or carboxyl (1750—1700 cm^{-1}) and ether-ester (1350—1000 cm^{-1}) signals were observed.

Ultraviolet PAS studies of silicas on which functional groups had been anchored have been reported [124, 134]. In silica functionalized with trimethylsilyl groups, the ratios of the methyl rocking bond to the Si—O stretch band were shown to be proportional to the coverage [135]. Ultraviolet PAS has also been used in studying the chemical effect of mechanical degradation of PVC; it was shown that conjugated double bonds are formed as a consequence of elimination of hydrogen chloride by a radical mechanism induced by mechanical stresses [136].

Photothermal spectroscopy is strictly related to photoacoustic spectroscopy [120]. In this case, the energy of the incident electromagnetic radiation is converted to thermal energy. The latter induces radiative emission at the surface, which is detected.

OTHER VIBRATIONAL TECHNIQUES

Several other vibrational techniques have been devised to solve problems in surface analysis, particularly for the study of films. Polymer films have been studied by using external reflection infrared techniques and emission infrared techniques. Inelastic electron tunnelling spectroscopy (IETS) and surface-enhanced Raman spectroscopy (SERS) are also relevant.

External reflection spectroscopy

Like IRS, external reflection spectroscopy (ERS) can be applied in different regions of the spectrum. In the case of polymer films on metals, mainly infrared ERS has been applied. Reviews have been published [137, 138].

The sample arrangement and the optical phenomena involved in obtaining a spectrum are outlined in Fig. 9. The electromagnetic wave passes from the first medium (atmosphere) to the second medium (polymer) by refraction; this is followed by reflection at the metal/polymer interface and then a second refraction at the polymer/atmosphere interface.

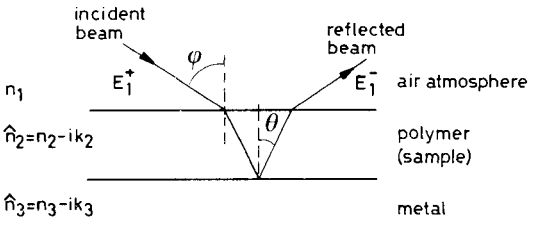

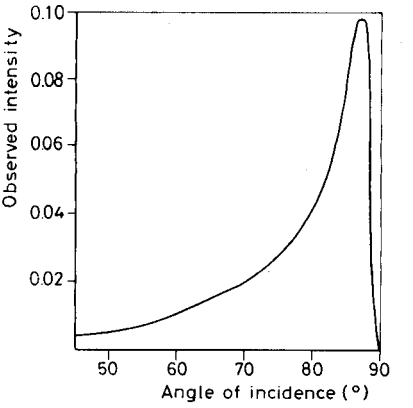

Fig. 9. The physical basis of ERS.

Fig. 10. Infrared ERS: observed intensity as a function of angle of incidence.

The theory of ERS involves the expression of reflectance (E_1^-/E_1^+, Fig. 9) as a function of several parameters, including the refractive index of the polymer, the frequency of the incident radiation and the thickness of the polymer film [139—141]. Given the correct values for such entities, a theoretical calculation of reflectance is possible. Conversely, when the experimental spectrum is known, the thickness and optical constants of the observed layer can be evaluated within certain precision limits. Ellipsometry has also been used to follow the thickness and refractive index of growing thin films [39, 142, 143]. In ERS, the whole layer is observed, not just the surface. An important phenomenon, particularly when very thin films (<10 nm) are examined, is the phase variation of the normal component of the radiation caused by the reflection on a metal. Such a variation (180°) induces suppression of the radiation component normal to the metal surface. The dependence of reflectance on angle of incidence is shown in Fig. 10. No particular problems of sensitivity are encountered in analyses of transparent films. Non-polarized radiation is directed at an angle of about 45° [137, 138]. For very thin films, it is necessary to work at maximum reflectance, with an angle of incidence near 90°. At such angles, illumination of the sample tends to decrease, so that the best compromise between illumination and maximal reflectance must be sought [137]. In an infrared ERS study of polyacrylonitrile on silver, the optical constants were determined and the importance of using polarized radiation for studying <0.5-μm films was emphasized [144]. ERS (or reflection/absorption spectroscopy) requires only conventional infrared instrumentation, apart from the optics necessary to have the radiation following the appropriate path (Fig. 9). Suitable devices have been built to study in-situ reactions [145—147]. The use of a double-beam arrangement has been suggested [148], the clean substrate contribution (aluminum in this case) being subtracted from the sample spectrum. The problem of

sensitivity has been overcome by using more sensitive detectors and by obtaining multiple reflections. Operation at the correct angle is essential. Experimental problems encountered at angles near 90° in grazing-angle infrared reflection spectroscopy have been discussed [149, 150].

Among the applications of infrared ERS, a study of an epoxide adhesive on aluminum produced no evidence for strong aluminum/resin interaction [148].

In a methacrylate adhesive on aluminum, the form and position of the C=O band were shown to depend on the film thickness; this trend was attributed to interactions of the carbonyl group with the aluminum oxide/hydroxide layer present at the interface [151].

Raman spectra have been obtained with similar optics. When the films are orientated anisotropically, this technique can be used to obtain information about the degree of conformational order/disorder in polymer films on metals [152].

Emission spectroscopy

The emission of radiation by polymer films deposited on metals has been studied mainly in the infrared region, although it also occurs in the u.v./visible range [153]. The experimental set-up is outlined in Fig. 11. A polymer film is heated through the metal on which it is deposited. The thermal energy favours transitions from the fundamental energy level to excited levels. The consequent decay can cause the emission of a photon. The spectrum is very similar to that obtained by transmission infrared spectroscopy [154, 155].

Emitted photons are collected and analyzed conventionally. The theory of this type of emission spectroscopy has been discussed [156, 157]. Waves emitted and reflected by the metal surface can interfere destructively, so that the emission intensity depends on the angle of observation. This is analogous to the effect observed in ERS (Fig. 10), but the curve is smoother. Reasonable emission intensities are obtained even at angles near 50° [157–159]. It has been calculated [157] that the maximum emission occurs at an angle of 85°, while at 55° emission is decreased by one third.

Another analogy with ERS is the dependence of the observed intensity and polarization of the emitted wave on the conformation of functional groups with respect to the surface. As in ERS, functional groups parallel to

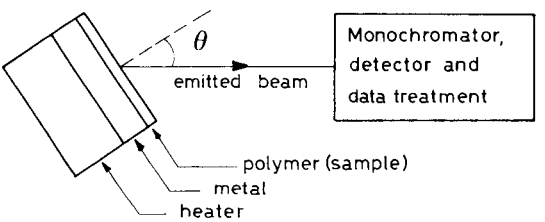

Fig. 11. Experimental arrangement for infrared emission spectroscopy.

the surface do not provide detectable emission [157]; thus information about the orientation of macromolecules on the surface can be obtained [158].

Emission experiments can be done with both conventional infrared [160] and FTIR instruments. In the latter case, sensitivity problems are lessened by quick collection and averaging of a large number of spectra. Greater sensitivity can be achieved by using more efficient detectors, such as mercury cadmium telluride at liquid nitrogen temperature [161]. For thicker layers, there are no problems of sensitivity but auto-absorption of emitted radiation has been reported [161]; this alters the relative intensities of the peaks.

Stray radiation can be eliminated by subtracting the spectrum of the beam splitter (if a FTIR instrument is used) and by using the spectrum of the clean metal surface as the standard. The emission as a function of the intensities pertaining to the sample (I_S), the beam splitter (I_b), and the standard (I_s) is given [159] by

$$E = (I_S - I_b)/(I_s - I_b) \tag{18}$$

Emission spectroscopy is competitive with infrared ERS, with respect to obtainable information and the objects studied. Its disadvantages are its lower sensitivity and increased instrumental complication. But the infrared emission technique can provide information even in the presence of a rough metal surface.

A semiquantitative estimate of the thickness of a styrene/acrylonitrile copolymer film on aluminum has been reported [159]. The spectrum of PET on aluminum has also been described [155].

Inelastic electron tunnelling spectroscopy (IETS)

This is an electroanalytical technique which can provide vibrational, rotational and electronic information, even though it has been used mainly in the vibrational mode.

Figure 12A shows how a sample for IETS is set up. A layer of polymeric material (e.g., adsorbate, adhesive or coating) is deposited on an insulator, and metal electrodes are attached at both sides. An increasing potential is applied to the electrodes, usually 0—500 meV. The system is kept at low temperature (<4.2 K) to maintain all functional groups in the vibrational ground state and to allow superconductivity of the electrodes [162]. When the potential is applied, electrons flow between the electrodes. Elastic tunneling is achieved when the electrons pass through the insulating layer without interacting, i.e., without energy loss. Inelastic tunneling involves the electron losing energy by interaction with a vibrational mode of energy, $h\Omega$, in the insulating layer (Fig. 12B), when the following equation is satisfied:

$$E_1 + eV = E_2 + h\Omega \tag{19}$$

Inelastic tunnelling induces limited (0.01—1%) variations of the cell conductance. It has been shown [163] that for electron/electric dipole interactions, the second derivative of the current (I) with respect to the potential (V) is

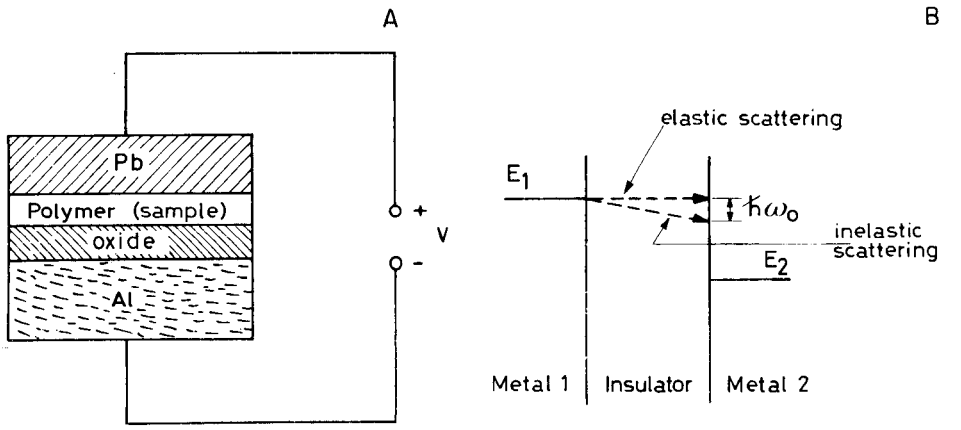

Fig. 12. Inelastic electron tunnelling spectroscopy. (A) Schematic representation of the sample. (B) Physical basis of the technique; the electron passes from a metal where the electron energy is E_1 to a metal where the electron energy is E_2.

equivalent to the vibrational infrared spectrum:

$$d^2I/dV^2 \propto |\langle i|\mu_z|0\rangle|^2 \delta(eV - h\Omega)$$

In the case of electron-induced dipoles, there is an analogy with the Raman spectrum. It is possible to measure d^2V/dI^2, which is proportional to d^2I/dV^2, by adding a low oscillating potential (some 0.3—1.5 meV) to the ramp potential. The measured quantity is the second harmonic of the potential. Plotting d^2I/dV^2 vs. V gives a spectrum containing infrared and Raman bands [162, 163]. The bandwidth is proportional to the temperature and liquid helium is used.

Sample preparation is critical. The thickness of the insulator-coating layer is vital because it governs the junction resistance [162, 164]. The first electrode, usually aluminum, is vapor-deposited on a support. One of the surfaces is oxidized to produce an oxide layer of controlled thickness (a few nanometers). The sample coating is then applied, either from the vapour phase or from solution (the thickness is even less than that of the oxide). Lastly, a lead electrode is deposited from the vapor phase, electric contacts are attached and the sample cell is dipped in liquid helium.

The sensitivity of the technique is quite good for studies of very thin films. The effects of the mode of deposition of lead electrodes are not well known. Equation 19 provides the relationship between the eV and cm^{-1} scales. Both infrared and Raman information can be obtained and both resolution and sensitivity are good, particularly compared with ERS or the emission techniques.

The silane/aluminum oxide interaction has been studied with regard to promoter/filler bonding [165—167]. Studies of the adsorption of methylphosphonic acid on alumina by IETS have been reported [168]. In the case

of 3-aminopropyltriethoxysilane, the NH stretching band was found to be broadened and shifted to lower frequencies, suggesting hydrogen bonding of the amino group with an oxygen either of the substrate or of a Si—O—Si bridge [165]; the Si—C stretching bands were particularly intense, suggesting that Si—C bonds are normal to the surface. In IETS, the exciting electric field is longitudinal [162], not transverse as in infrared. For 3-glycidyloxypropyltrimethoxysilane [166], bands apparently related to C=C and C=O double bonds were observed; they were attributed to the reaction of the epoxide function, giving double bonds with water elimination. It has been shown that monoalkoxysilanes are not adsorbed on alumina whereas trialkoxysilanes are readily adsorbed [167]. The reaction in anhydrous conditions utilizes the surface hydroxide groups present on alumina. The formation of Al—O—Si bonds is probably stabilized by the subsequent condensation of chemisorbed silane molecules to form siloxane oligomers [167].

Studies on adhesion phenomena by analyzing thin adhesive films on aluminum have become quite popular. The use of epoxide films [169], methacrylates [170, 171] and poly(vinyl alcohol) [171] has been reported. In the reaction between a multifunctional amine and a bifunctional epoxide mixture, it has been shown that the amine nitrogen tends to pick up hydrogen atoms from the oxide surface. Al—O—C bonds are formed, with the elimination of Al—OH groups [169]. Several polymer films, poly(vinyl acetate), poly(vinyl alcohol) and PMMA, have been studied on aluminum oxide. Poly(vinyl acetate) undergoes hydrolysis of the ester, and the polymer chemisorbs as poly(vinyl alcohol). Presumably carboxyl absorptions are due to acetates obtained by hydrolysis [170]. For the interaction with aluminum oxide, the formation of Al—O—C bridges has been suggested, even though bonding by hydrogen bonds between hydroxyl groups of the polymer and at the oxide surface has not been completely ruled out [171].

Some rarely applied vibrational techniques

Several other techniques have been developed for the study of films. Infrared surface electromagnetic wave spectroscopy (SEWS) has been applied to the study of organic adsorbates on metal surfaces [172]. Surface picosecond Raman gain spectroscopy and waveguide Raman spectroscopy had similar applications [173].

Surface-enhanced Raman scattering spectroscopy (SERSS) uses the strong increment in intensity of Raman bands associated with functional groups of molecules near (5—20 nm) a rough metal surface, usually silver [174—176]. Its applicability to polymer surfaces (poly-*p*-nitrostyrene) has been reported [174]. The desired surface restriction is obtained, but the sample preparation is complex. Films of phthalocyanine complexes on silver have been studied [176].

Another technique, rather difficult from an instrumental point of view, is waveguide Raman spectroscopy [177, 178]. In order to achieve satisfactory sensitivity, it uses the Raman resonance effect and the conduction of

radiation obtained with a special sample preparation [177]. A study of a cyanine dye on poly(vinyl alcohol) showed a strong interaction of the hydroxyl groups of poly(vinyl alcohol) with the nitrogen in the quinoline ring of the cyanines. Such an interaction has been considered responsible for the polymer/dye adhesion [178].

TRANSMISSION SPECTROSCOPIES

The theory and instrumentation relating to transmission vibrational spectroscopies need not be discussed here. Both the infrared (FTIR) and Raman techniques are well known and widely used, particularly infrared [179, 180]. Transmission techniques observe the whole material. Their application to surface problems is limited to the cases where surfaces and/or interfaces are very broad. They have been applied in studies of the bonding of silanes on fillers with high surface specific area or in compatible blends. Silanes have been studied by infrared [113, 181—186], Raman [187] and ultraviolet [188]. In most cases, the substrate material had a surface specific area greater than 100 $m^2 g^{-1}$. Samples investigated were mostly in the form of KBr pellets or thin layers of silica compacted under high pressure; in the latter case, scattering problems could arise.

The structure of 3-aminopropyltriethoxysilane (APS) on silica has been studied. The silane, depending on the preparation conditions, can be present as a chelate ring or as an extended chain; in the first case, amino groups interact with silica [181]. The structure of APS on silica is particularly sensitive to the pH of the treating solution: at low pH, a form with protonated amine predominates, while at high pH the previously described structures are present [113].

The use of FTIR instead of DRIFT means less experimental complication and a more easily interpretable spectrum. Disadvantages are lower sensitivity and the necessity to use compact samples; such treatment could alter the original sample. Characterization of the reaction at the silane/polymeric matrix interface by FTIR has been reported [189]. The reaction was studied with and without the filler. The reaction of APS was strongly affected by the degree of condensation of the silane in the interphase. Interface studies are important also for compatible blends. FTIR was used to examine why a blend is compatible and which intermolecular interactions are involved in compatibility. The study of conformational and morphological effects is also important.

FTIR is much more precise than dispersive infrared. The signals obtained are particularly suitable for digital treatment, and many modes of data treatment are now used. Spectral addition and subtraction, curve fitting, factorial analysis and derivative spectroscopy [190] may be cited. Least-squares fitting of spectra has been used to calculate the sum of single component spectra which best reproduces the blend spectrum [191]. Factorial analyses, in a substantially equivalent approach, has been applied to estimate the different

components producing a spectrum [192]. Derivative spectroscopy [193] has been used to facilitate spectral interpretation, particularly when partial overlapping of bands occurs.

Finding intermolecular interactions in compatible blends is easier and unequivocal when the observed functional groups have uncoupled vibrational modes. Much work has been done on blends in which one component has a carbonyl or carboxyl group [190]. In polycaprolactone/poly(vinyl chloride) (PCL/PVC) blends, the carbonyl group of PCL has been found to interact with the methine hydrogen of PVC, to form a hydrogen bond. Much more evident is the interaction in systems with hydroxyl groups, as in polyvinylphenol (PVPh) [190]. Actually, polypropiolactone forms blends with PVPh, but not with PVC.

It is always necessary to be cautious in the interpretation, because intermolecular interactions can cause band shifts of some cm^{-1} and/or broadenings. Furthermore, miscibility also depends on other factors, such as the molar concentration of interacting species, distribution of molecular weights, steric considerations, etc. In blends of polystyrene with poly(ethylene oxide) or poly(vinyl methyl ether), which do not contain functional groups with vibrational modes uncoupled from the skeleton, interpretation is difficult. It is not possible to neglect morphological effects or to draw unambiguous conclusions about the presence of intermolecular interactions. Various studies of blend morphology have been reported [190]. A broad range of materials with different fractions of amorphous and crystalline phases has been examined where it was possible to associate particular bands with crystallinity.

NUCLEAR MAGNETIC RESONANCE SPECTROSCOPY

Nuclear magnetic resonance (NMR) spectroscopy is not a surface technique but applications to surface problems have been made under conditions similar to those for transmission infrared spectroscopy. NMR can be used when there is a clearcut distinction between surface and bulk signals. As NMR has poor sensitivity, samples with large specific surface area are necessary.

Application of NMR to surface problems has been reviewed [194, 195]. The silane/filler interaction has been treated in detail [195]. As with infrared, NMR can be applied if a diffuse interface is present, as in compatible blends. NMR spectroscopy can provide very rich information with regard to vibrational and electronic structure and stereochemistry, as well as the state of motion in the system. And, of course, different nuclei can be observed and different experimental techniques are available [196—199]. Solid-state NMR is more complicated than solution NMR, and relaxation times are less favorable in the solid state than in solution. Generally, a solid-state NMR spectrum appears as a broad and not easily interpretable band. The use of high power decoupling, magic angle sample spinning (MASS), and cross polarization make

it possible to obtain solid-state spectra which approximate the spin hamiltonian valid for solution experiments [199].

High power decoupling, in the presence of protons coupled to the observed nucleus, helps to eliminate the effect of direct and indirect coupling constants. High power is necessary for solid samples to cover the bandwidth found in proton spectra [195]. MASS devices [199] spin the sample at high rotation frequencies (3—8 kHz) around an axis forming an angle of 54.7° (magic angle) with the magnetic field direction. Several interactions (shielding tensor anisotropy, quadrupolar coupling, direct coupling) are thus averaged to zero and do not influence the spectrum. High power decoupling and MASS techniques give a "liquid-like" spectrum, but some information is lost. Cross polarization provides increased sensitivity by means of the Hartmann-Hahn effect [199]. Conventional NMR instruments can be adapted to the study of solids by using MASS/cross polarization without important modifications. The study of solids without MASS/cross polarization requires special instruments (wide-line NMR) [197].

Several NMR studies have been devoted to the bonding of silanes to silica gel, which is used as a model for the behavior of glass fibers. Its specific surface area is high (>100 m^2 g^{-1}), suitable for NMR studies [195]. MASS/cross polarization techniques with ^{29}Si have been used to study untreated silica gel surfaces [200, 201]. Hydration/dehydration phenomena were used to probe surface reactivity. Bulk/surface discrimination is provided by cross polarization, which affects only surface silicon atoms vicinal to hydroxide groups. Such silicon atoms can be observed with reasonable sensitivity owing to their preferential relaxation. Silicon atoms bonded to zero, one or two hydroxide groups can be distinguished by the different ^{29}Si chemical shifts. The relative population of silicon atoms bonded to one or two hydroxide groups is sensitive to the treatment. The behavior of silica has been explained by using crystobalite (111 and 100 faces) as the model [200, 201]. Relative ^{29}Si peak intensities have shown that it is more probable for a silane to bond to a silicon atom with two hydroxide groups than to a silane with one hydroxide [201, 202]. If the silane has more than one possibility to form a Si—O—Si bridge, multiple bridges can be observed [203], but an alternative explanation is condensation between silanes. It has been shown that the presence of adsorbed water increases the rate of condensation.

Carbon-13 has also been extensively used to study chemisorbed silanes from the organic side of the molecule [195, 204, 205]. Measuring the chemical shifts in the organic side-chain of the silane made it possible to predict their values on the basis of simple addition rules, when the functional groups present in the chain are known, as in solution NMR [195]. Because NMR is particularly sensitive to molecular motions, the side-chain motion has been studied. Various methods have been used, such as taking into account the entity of cross polarization, chemical shift anisotropy or different (T_1 and T_2) relaxation times [195, 204, 206, 207]. The amount of cross polarization decreases for very long side-chains. The motion of end groups is fast, making

cross polarization less efficient [204]. The motion of phenyl groups anchored to silanes bound to silica has been studied rigorously by using chemical shift anisotropy [206]. Proton T_1 and T_1 (spin locking) relaxation times for silanes with different side-chains (8 and 18 carbon atoms) have been measured [207]. Shorter T_1's and longer T_1 (spin locking) were found in the case of the shorter side-chain, suggesting a freer motion in short chains. Longer chains probably interact either with the silica surface or with other alkyl chains.

Combined studies have been reported in which FTIR, ^{13}C-NMR and ultraviolet PAS [134] or ^{29}Si-NMR, XPS and FTIR/PAS [135] were applied to silylated silica surfaces. NMR offers much qualitative information, but its parameters do not have any immediate quantitative meaning. Vibrational techniques are more sensitive and more easily interpreted.

An interesting application of imaging NMR to the absorption of water in composite materials has been reported [208]. Two epoxide matrices, reinforced with glass fibers, were kept under water for long periods and then examined by H-imaging NMR; the absorption processes observed depended on the properties of the composite material, particularly on the presence of defects providing penetration pathways for water. It seems likely that imaging NMR will offer many other possibilities for non-destructive studies of interfaces.

Another application of NMR to surfaces and interfaces in polymer materials is to compatible blends (diffuse interface); this area has been reviewed [209, 210]. Miscibility in polymer blends is not studied by using traditional parameters (chemical shift, quadrupolar coupling), probably because the interactions between polymer chains are feeble, inducing only small variations. Relaxation phenomena are used [209]; the spin diffusion mechanism allows dispersion to be studied in limited ranges of the magnetization introduced in the system.

The use of proton T_1 (spin locking), obtained by ^{13}C measurements, has proved quite successful [211]. For polystyrene/poly(phenylene oxide) blends, it was observed that, when the blend is compatible, spin diffusion is quick and homogeneous in both polymers, thus a single T_1 (spin locking) is found. The use of T_1 (spin locking) is a one-dimensional NMR technique. Recently, spectra correlating two dimensions have been achieved on the basis of cross-relaxation caused by spin diffusion [212]. In polystyrene/poly(vinyl methyl ether) (PVME) blends, when the blend was compatible, cross peaks between aromatic protons of polystyrene and methyl and methine protons of PVME were found, suggesting a reciprocal interaction [212].

Carbon-13 spin diffusion has been used to study PET/bisphenol-A polycarbonate blends [213]. Compared to ^{1}H spin diffusion, which has a range of a few nanometers, ^{13}C spin diffusion is more selective (tenths of nm) depending on the lower ^{13}C gyromagnetic ratio. Both ^{13}C T_1's and two-dimensional spectra have been used to characterize the blend, allowing hypotheses about intermolecular reactions of these polymers to be formed [213].

CONCLUSIONS

In conclusion, a comparison of the various techniques seems necessary. The choice of criteria is always arbitrary, and here the criteria are divided into two groups, "physical" and "practical".

Four fields of application are considered: polymer surfaces as such, filler surfaces, thin films on supports, and blends (diffuse interface). For each of these fields, the most widely used techniques are indicated. Each technique is characterized by the information that it provides (qualitative, quantitative, depth profiling) and by its physical constraints (thickness of the observed layer, sensitivity).

It is not easy to find a uniform indicator of sensitivity. Here, the mode chosen is to regard the total content (in atomic terms) of the layer of material observed by a particular technique as unity (1) and to express the sensitivity as the fraction, always atomic, that can be estimated. In XPS, for example, a sensitivity of 10^{-2}—10^{-3} means that a 1—0.1% atomic concentration of an element in the few nanometers observed can be detected. The indication of an analogous sensitivity in NMR would refer to the concentration in the whole sample, thus the absolute quantities would be quite different.

TABLE 2

Polymer surfaces

Method	Qualitative information	Quantitative information	Depth profiling	Thickness of observed layer	Sensitivity
ISS	Surface elements	Semiquant.	No	First layer	10^{-4}—10^{-6}
SIMS[a]	Surface functional groups	Difficult	No	<1 nm	10^{-7}
XPS	Surface elements & functional groups	Semiquant.	Yes, angle resolved	4—10 nm	10^{-2}—10^{-3}
IRS infrared	Vibrational spectrum	Semiquant.[b]	Yes, change incid. angle or IRE[c]	1—10 μm	$\approx 10^{-2}$
IRS Raman	Vibrational spectrum	Semiquant.	Yes, change incid. angle or IRE	0.01—0.5 μm	10^{-1}—10^{-2}
DRS infrared	Vibrational spectrum	Semiquant.	Not controlled	Total	10^{-3}—10^{-4}
PAS infrared	Vibrational spectrum	Not very dependable	Yes, change modulation frequency	1—50 μm	10^{-1}—10^{-2}

[a]Static SIMS. [b]Based on band ratios. [c]Internal reflection element.

TABLE 3

Filler surfaces

Method	Qualitative information	Quantitative information	Depth profiling	Thickness of observed layer	Sensitivity
ISS	Surface elements	Semiquant.	No	First layer	10^{-4}—10^{-6}
SIMS[a]	Surface functional groups	Difficult	No	<1 nm	10^{-7}
XPS	Surface elements & functional groups	Semiquant.	Yes, angle resolved	4—10 nm	10^{-2}—10^{-3}
IRS infrared	Vibrational spectrum	Semiquant.[b]	Yes, change incid. angle or IRE[c]	1—10 μm	$\approx 10^{-2}$
DRS infrared	Vibrational spectrum	Semiquant.	Not controlled	Total	10^{-3}—10^{-4}
PAS infrared	Vibrational spectrum	Not very dependable	Yes, change modulation frequency	1—50 μm	10^{-1}—10^{-2}
Transmission infrared	Vibrational spectrum	Quantit.	No	Total	$\approx 10^{-2}$
NMR	Chem. shift, coupling constants, relaxation times	Difficult	No	Total	Low, diff. for diff. nuclei

[a—c] See footnotes to Table 2.

TABLE 4

Thin films

Method	Qualitative information	Quantitative information	Depth profiling	Thickness of observed layer	Sensitivity
SIMS[a]	Surface functional groups	Difficult	No	<1 nm	10^{-7}
XPS	Surface elements & functional groups	Semiquant.	Yes, angle resolved	4—10 nm	10^{-2}—10^{-3}
DRS infrared	Vibrational spectrum	Semiquant.	Not controlled	Total	10^{-3}—10^{-4}

TABLE 4 (continued)

Method	Qualitative information	Quantitative information	Depth profiling	Thickness of observed layer	Sensitivity
PAS infrared	Vibrational spectrum	Not very dependable	Yes, change modulation frequency	1—50 μm	10^{-1}—10^{-2}
ERS infrared	Vibrational spectrum	Semiquant.	No	Total	$\approx 10^{-2}$
Emission infrared	Vibrational spectrum	Semiquant.	No	Total	10^{-1}—10^{-2}
IETS	Vibrational spectrum (IR + Raman)	Semiquant.	No	Total	$\approx 10^{-2}$
SERS	Raman spectrum	Semiquant.	No	5—20 nm	$\approx 10^{-2}$

[a]Static SIMS.

TABLE 5

Blends

Method	Qualitative information	Quantitative information	Depth profiling	Thickness of observed layer	Sensitivity
FTIR	Vibrational spectrum	Quantitative	No	Total	$\approx 10^{-2}$
NMR	Chem. shift, coupling constants, relaxation times	Difficult	No	Total	Low, diff. diff. for diff. nuclei

TABLE 6

Practical comparisons

Method	Instrumentation	Sample preparation	Surface damage
ISS	Reliable (UHV chamber)	None	Yes, limited
SIMS (static)	Reliable, also in data handling (UHV chamber)	None	Yes, limited
XPS	Reliable (UHV chamber)	None	No
IRS infrared	Medium	Good contact with IRE essential	No

TABLE 6 (continued)

Method	Instrumentation	Sample preparation	Surface damage
DRS infrared	Medium	Well distributed sample essential	No
PAS infrared	Reliable, cell efficiency is critical	None	No
ERS infrared	Incidence angle is important	None	No
Emission infrared	Consistent, difficult elimination of stray radiation	Sample as received and heated	No
IETS	Consistent	Critical	No
SERS	Consistent	Critical	No
Transmission infrared	Limited	Powders must be compacted	No
NMR	Consistent	Sample rotation, frequency tuning, cross polarization are critical	No

The comparisons are outlined in Tables 2—5. For all the techniques considered, practical criteria of instrumentation, problems in working conditions and sample preparation, and degree of surface damage are summarized in Table 6.

REFERENCES

1 T. M. Buck, in A. W. Czanderna (Ed.), Methods of Surface Analysis, Elsevier, Amsterdam, 1975.
2 W. L. Baun, Pure Appl. Chem., 54 (1982) 323.
3 W. L. Baun, J. Adhes., 7 (1976) 261.
4 A. T. Di Benedetto and D. A. Scola, J. Colloid Interface Sci., 64 (1978) 480.
5 G. E. Thomas, G. C. J. van der Ligt, G. J. M. Lippits and G. M. M. van der Hei, Appl. Surf. Sci., 6 (1980) 39.
6 W. L. Baun, Appl. Surf. Sci., 6 (1980) 39.
7 J. A. Gradella Jr. and D. M. Hercules, Anal. Chem., 53 (1981) 1879.
8 J. A. Gradella Jr. and D. M. Hercules, Anal. Chem., 52 (1980) 226.
9 D. M. Hercules, Mikrochim. Acta, Suppl. 11 (1985) 1.
10 R. L. Schmitt, J. A. Gardella Jr., J. H. Magill, L. Salvati Jr. and R. L. Chin, Macromolecules, 18 (1985) 2675.
11 H. H. G. Jellinek, in K. L. Mittal (Ed.), Physicochemical Aspects of Polymer Surfaces, Vol. 1, Plenum, New York, 1983.
12 D. L. Allara, C. W. White, R. L. Meek and T. H. Briggs, J. Polym. Sci. Chem. Ed., 14 (1976) 93.
13 D. L. Allara and C. W. White, Adv. Chem. Ser., 169 (1978) 273.
14 T. Venkatesan, S. R. Forrest, M. L. Kaplan, C. A. Murray, P. H. Schmidt and B. J. Wilkens, J. Appl. Phys., 54 (1983) 3150.

15 T. Venkatesan, T. Wolf, D. Allara, B. J. Wilkens and G. N. Taylor, Appl. Phys. Lett., 43 (1983) 934.
16 S. J. Valenty, J. J. Chera, G. A. Smith, W. Katz, R. Argani and H. Backhru, J. Polym. Sci. Chem. Ed., 22 (1985) 3367.
17 J. A. McHugh, in A. W. Czanderna (Ed.), Methods of Surface Analysis, Elsevier, Amsterdam, 1975.
18 N. Treitz, J. Phys. E, 10 (1977) 573.
19 P. Williams, Surf. Sci., 90 (1980) 588; Appl. Surf. Sci., 13 (1982) 241.
20 D. Briggs and M. J. Hearn, Spectrochim. Acta, Part B, 40 (1985) 707.
21 D. Briggs, M. J. Hearn and B. D. Ratner, Surf. Interface Anal., 6 (1984) 184.
22 A. Brown, J. C. Vickerman, Surf. Interface Anal., 6 (1984) 1.
23 D. Briggs and A. B. Wootton, Surf. Interface Anal., 4 (1982) 109.
24 See, e.g., A. F. Dillon, R. S. Lehrle, J. C. Robb and D. W. Thomas, Adv. Mass Spectrom., 4 (1968) 477.
25 F. M. Devienne and J.-C. Roustan, Compt. Rendues, 276C (1973) 923; 283B (1976) 397.
26 A. Brown, J. A. van der Berg and J. C. Vickerman, Spectrochim. Acta, Part B, 40 (1985) 871.
27 F. Garbassi, E. Occhiello, C. Bastioli and G. Romano, J. Coll. Interf. Sci., 117 (1987) 258.
28 S. Storp, Spectrochim. Acta, Part B, 40 (1985) 745.
29 J. E. Campana, J. J. De Corpo, R. J. Colton, Appl. Surf. Sci., 8 (1981) 337.
30 S. J. Simko, M. L. Miller and R. W. Linton, Anal. Chem., 57 (1985) 2448.
31 J. H. Wandass and J. A. Gardella Jr., J. Am. Chem. Soc., 107 (1985) 6192.
32 F. Degreve, J. M. De Long, Surf. Interface Anal., 7 (1985) 177.
33 D. M. Hercules, F. P. Novak and Z. A. Wilk, Anal. Chim. Acta, 195 (1987) 61.
34 D. Briggs and M. P. Seah (Eds.), Practical Surface Analysis, Wiley, New York, 1983.
35 D. Briggs (Ed.), Handbook of X-Ray and Ultraviolet Photoelectron Spectroscopy, Heyden, London, 1977.
36 G. E. Muilenburg (Ed.), Handbook of X-Ray Photoelectron Spectroscopy, Physical Electronics Division, Perkin-Elmer, Norwalk, 1979.
37 A. Dilks, in C. R. Brundle and A. D. Baker (Eds.), Electron Spectroscopy — Theory, Techniques and Applications, Vol. 4, Academic, London, 1981.
38 D. T. Clark, in L. H. Lee (Ed.), Characterization of Metal and Polymer Surfaces, Academic, London, 1977.
39 J. D. Andrade (Ed.), Surface and Interfacial Aspects of Biomedical Polymers, Plenum, New York, 1985.
40 M. P. Seah and W. A. Dench, Surf. Interface Anal., 1 (1979) 2.
41 D. T. Clark and A. Dilks, J. Polym. Sci. Chem. Ed., 14 (1976) 533.
42 J. Riga, J. P. Boutique, J. J. Pireaux and J. J. Verbist, in K. L. Mittal (Ed.), Physicochemical Aspects of Polymer Surfaces, Vol. 1, Plenum, New York, 1983.
43 J.-M. André, J. Delhalle and J. J. Pireaux, in W. Dwight, T. J. Fabish and H. R. Thomas (Eds.), Photon, Electron and Ion Probes of Polymer Structure and Properties, ACS Symposium Series, 162 (1982) 151.
44 J. J. Pireaux, J. Riga, R. Caudano and J. Verbist, Ref. 43, p. 169.
45 W. R. Salaneck, Ref. 43, p. 121.
46 C. Shang Xian, K. Sekim, H. Inokuchi, S. Hashimoto, N. Ueno and K. Sugita, Bull. Chem. Soc. Jpn., 58 (1985) 890.
47 H. R. Thomas and J. J. O'Malley, Macromolecules, 12 (1979) 323.
48 D. T. Clark, J. Peeling and J. M. J. O'Malley, J. Polym. Sci. Chem. Ed., 14 (1976) 543.
49 D. H.-K. Pan and W. M. Prest Jr., J. Appl. Phys., 58 (1985) 2861.
50 H. J. Busscher, W. Hoogsten, L. Dijkema, G. A. Sawatsky, A. W. J. van Pelt, H. P. de Jong, G. Challa and J. Arends, Polym. Commun., 26 (1985) 252.
51 S. Randall Holmes-Farley, R. H. Reamey, T. J. McCarthy, J. Deutch and G. M. Whitesides, Langmuir, 1 (1985) 725.

52 A. J. Dias and T. J. McCarthy, Macromolecules, 18 (1985) 1826.
53 J. Lavielle and J. Schultz, J. Coll. Interface Sci., 106 (1985) 438.
54 D. Briggs, D. M. Brewis and M. B. Konieczko, J. Mater. Sci., 14 (1979) 1344.
55 F. Garbassi, E. Occhiello and F. Polato, J. Mater. Sci., 22 (1987) 207.
56 D. Briggs, C. R. Kendall, A. R. Blithe and A. B. Wootton, Polymer, 24 (1983) 27.
57 D. Briggs and C. R. Kendall, Polymer, 20 (1979) 1053.
58 D. Klee, D. Gribbin and D. Kirch, Angew. Makromol. Chem., 131 (1985) 145.
59 R. G. Nuzzo and G. Smolinsky, Macromolecules, 17 (1984) 1013.
60 M. Strobel, S. Corn, C. S. Lyons, G. A. Korba, J. Polym. Sci. Chem. Ed., 23 (1985) 1125.
61 G. A. Corbin, R. E. Cohen and R. F. Baddour, Macromolecules, 18 (1985) 98.
62 R. Srinivasan and S. Lazare, Polymer, 26 (1985) 1297.
63 V. Sa Da Costa, D. Brier-Russel, E. W. Salzmann and E. W. Merrill, J. Coll. Interface Sci., 80 (1981) 445.
64 M. D. Lelah, L. K. Lombrecht, B. R. Young and S. L. Cooper, J. Biomed. Mater. Res., 17 (1983) 1.
65 W. R. Salaneck, I. Lundström and B. Liedberg, Progr. Coll. & Polym. Sci., 70 (1985) 83.
66 K. Waltersson, Composites Sci. Techn., 22 (1985) 223.
67 K. Waltersson, Composites Sci. Technol., 23 (1985) 303.
68 C. Kozlowski and P. M. A. Sherwood, J. Chem. Soc. Faraday Trans. I, 81 (1985) 2745.
69 G. D. Nichols, D. M. Hercules, R. C. Peek and D. J. Vaughan, Appl. Spectrosc., 28 (1974) 219.
70 P. R. Moses, L. M. Wier, J. C. Lennox, H. O. Finklea, J. R. Lenhard and R. W. Murray, Anal. Chem., 50 (1978) 576.
71 W. J. van Ooij, in K. L. Mittal (Ed.), Physicochemical Aspects of Polymer Surfaces, Vol. 2, Plenum, New York, 1983, p. 1035.
72 F. M. Mirabella Jr., Appl. Spectrosc. Rev., 21 (1985) 45.
73 N. S. Harrick, Internal Reflection Spectroscopy, Wiley, New York, 1967.
74 T. Nguyen, Progr. Org. Coat., 13 (1985) 1.
75 F. M. Mirabella Jr., J. Polym. Sci. Phys. Ed., 21 (1983) 2403.
76 C. B. Hu and C. S. P. Sung, Polym. Prepr., 21 (1980) 156.
77 K. Ohta and R. Iwamoto, Appl. Spectrosc., 39 (1985) 418.
78 G. Mueller, K. Abraham and M. Schaldach, Appl. Opt., 20 (1981) 1182.
79 A. J. Barbetta, Appl. Spectrosc., 38 (1984) 29.
80 K. Ohta and R. Iwamoto, Anal. Chem., 57 (1985) 2491.
81 F. Kimura, J. Umemura and T. Tanenaka, Langmuir, 2 (1986) 96.
82 Standard Practices for Internal Reflection Spectroscopy, ASTM Annual Book 42, E573, 1984.
83 J. K. Barr and P. A. Fluornay, in B. Carroll (Ed.), Physical Methods in Macromolecular Chemistry, Vol. I, M. Dekker, New York, 1969.
84 F. M. Mirabella Jr., J. Polym. Sci. Phys. Ed., 23 (1985) 861.
85 R. Iwamoto, M. Miya, K. Ohta and S. Mima, J. Chem. Phys., 74 (1981) 4780.
86 R. Iwamoto, M. Miya, K. Ohta and S. Mima, J. Am. Chem. Soc., 102 (1980) 1212; R. Iwamoto, M. Miya, K. Ohta and S. Mima, Appl. Spectrosc., 35 (1981) 584.
87 B. K. Lok, Y. Cheng and C. R. Robertson, J. Coll. Interface Sci., 91 (1983) 87.
88 H. Masuhara, N. Mataga, S. Tazuke, T. Murao and I. Yamazaki, Chem. Phys. Lett., 100 (1983) 415.
89 R. Iwamoto and K. Ohta, Appl. Spectrosc., 38 (1984) 359.
90 J. A. Gardella Jr., G. L. Grobe III, W. L. Hopson and E. M. Eyring, Anal. Chem., 56 (1984) 1169.
91 M. D. Lelah, S. L. Cooper, H. Ohnuma and T. Kotaka, Polym. J., 17 (1985) 841.
92 R. Kellner, G. Fischboeck, G. Goetzinger, E. Pungor, K. Toth, L. Polos and E. Lindner, Fresenius' Z. Anal. Chem., 322 (1985) 151.

93 S. Winters, R. M. Gendreau, R. L. Leininger and R. J. Jacobsen, Appl. Spectrosc., 36 (1982) 404.
94 D. J. Carlsson and D. M. Wiles, Macromolecules, 2 (1970) 587, 597; 4 (1972) 174.
95 A. Narebska and Z. Bukowski, Makromol. Chem., 186 (1985) 1411.
96 C. S. Blackwell, P. J. Degen and F. D. Osterholtz, Appl. Spectrosc., 32 (1978) 480.
97 A. E. Tshmel, V. I. Vettegren and V. M. Zolotarev, J. Macromol. Sci. Phys., Part B, 21 (1982) 243.
98 G. Fonseca, J. M. Perena, J. G. Fatou and A. Bello, J. Mater. Sci., 20 (1985) 3283.
99 A. M. Wrobel, J. Kryszewski and M. Gazicki, J. Macromol. Sci. Chem., Part A, 20 (1983) 583.
100 A. M. Wrobel, J. Macromol. Sci. Chem., Part A, 22 (1985) 1089.
101 A. E. Tshmel and V. I. Vettegren, Eur. Polym. J., 12 (1976) 853.
102 F. M. Mirabella Jr., J. Polym. Sci. Phys. Ed., 22 (1984) 1283; F. M. Mirabella Jr., J. Polym. Sci. Phys. Ed., 22 (1984) 1293.
103 A. Garton, S. W. Kim and D. M. Wiles, J. Polym. Sci. Lett. Ed., 20 (1982) 273.
104 G. Kortüm, Reflectance Spectroscopy, Springer, Heidelberg, 1969.
105 M. P. Fuller and P. R. Griffiths, Anal. Chem., 50 (1978) 1906.
106 H. Moulharkt and D. Kunath, Appl. Spectrosc., 34 (1980) 383.
107 P. Kubelka and F. Munk, Z. Tech. Physik, 12 (1931) 593.
108 P. Kubelka, J. Opt. Soc. Am., 38 (1948) 448.
109 See, e.g., H. G. Hecht, Appl. Spectrosc., 37 (1983) 348.
110 S. R. Culler, H. Ishida and J. L. Koenig, Appl. Spectrosc., 38 (1984) 1.
111 S. R. Culler, M. T. McKenzie, L. J. Fina, H. Ishida and J. L. Koenig, Appl. Spectrosc., 38 (1984) 791.
112 M. T. McKenzie and J. L. Koenig, Appl. Spectrosc., 39 (1985) 408.
113 S. Naviroj, S. R. Culler, H. Ishida and J. L. Koenig, J. Coll. Interface Sci., 97 (1984) 308.
114 M. T. McKenzie, S. R. Culler and J. L. Koenig, Appl. Spectrosc., 38 (1984) 786.
115 S. R. Culler, H. Ishida and J. L. Koenig, J. Coll. Interface Sci., 106 (1985) 334.
116 J. A. Davies and A. Sood, Makromol. Chem., 186 (1985) 1631.
117 J. M. Chalmers and M. W. MacKenzie, Appl. Spectrosc., 39 (1985) 634.
118 G. Xue, Macromol. Chem., Rapid Commun., 6 (1985) 811.
119 A. Rosencwaig, Photoacoustics and Photoacoustic Spectroscopy, Wiley-Interscience, New York, 1980.
120 S. O. Karstad and P. E. Nordal, Appl. Surf. Sci., 6 (1980) 372.
121 A. Rosencwaig, Anal. Chem., 47 (1975) 592A.
122 E. P. C. Lai, B. L. Chan and M. Hadjmohammadi, Appl. Spectrosc. Rev., 21 (1985) 179.
123 A. Rosencwaig and A. Gersho, J. Appl. Phys., 47 (1976) 64.
124 L. W. Burggraf and D. E. Leyden, Anal. Chem., 53 (1981) 759.
125 J. F. McClelland, Anal. Chem., 55 (1983) 89A.
126 K. Krishnan, Appl. Spectrosc., 35 (1981) 549.
127 D. W. Vidrine, Appl. Spectrosc., 34 (1980) 314.
128 N. L. Rockley, M. K. Woodward and M. G. Rockley, Appl. Spectrosc., 38 (1984) 329.
129 S. M. Riseman and E. M. Eyring, Spectrosc. Lett., 14 (1981) 163.
130 K. Krishnan, S. Hill, J. P. Hobbs and C. S. P. Sung, Appl. Spectrosc., 36 (1982) 257.
131 N. Teramae, and S. Tanaka, Appl. Spectrosc., 39 (1985) 797.
132 N. Teramae, M. Hiroguchi and S. Tanaka, Bull. Chem. Soc. Jpn., 55 (1982) 2097.
133 D. J. Gerson, Appl. Spectrosc., 38 (1984) 436.
134 D. E. Leyden, D. S. Kendall, L. W. Burggraf, F. J. Pern and M. De Bello, Anal. Chem., 54 (1982) 101.
135 R. W. Linton, M. L. Miller, G. E. Maciel and B. L. Hawkins, Surf. Interface Anal., 7 (1986) 196.
136 M. E. Abu-Zeid, E. E. Nofal, L. A. Tahseen and F. A. Abdul-Rasoul, J. Appl. Polym. Sci., 30 (1985) 3791.

137 D. L. Allara, in L. H. Lee (Ed.), Characterization of Metal and Polymer Surfaces, Academic, London, 1977.
138 H. G. Tompkins in A. W. Czanderna (Ed.), Methods of Surface Analysis, Elsevier, Amsterdam, 1975.
139 R. G. Greenler, J. Chem. Phys., 44 (1966) 310.
140 W. G. Golden, D. S. Dunn and J. Overend, J. Catal., 71 (1981) 395.
141 D. L. Allara, A. Baca and C. A. Pryde, Macromolecules, 11 (1978) 1215.
142 R. P. Netterfield, P. J. Martin, W. G. Sainty, R. M. Duffy and C. G. Pacey, Rev. Sci. Instrum., 56 (1985) 1995.
143 R. T. Graf, J. L. Koenig and H. Ishida, Anal. Chem., 58 (1986) 64.
144 C. A. Sergides, A. R. Chughtai and D. M. Smith, J. Polym. Sci. Phys. Ed., 23 (1985) 1573.
145 H. H. G. Jellinek, H. Kachi and I. Chodak, J. Polym. Sci. Chem., 23 (1985) 2291.
146 S. C. Lin, J. Bulkin and E. M. Pearce, J. Polym. Sci. Chem. Ed., 17 (1979) 3121.
147 C. A. Sergides, A. R. Chughtai and D. M. Smith, Appl. Spectrosc., 39 (1985) 735.
148 G. J. Kemeny and P. R. Griffiths, Appl. Spectrosc., 35 (1981) 128.
149 J. F. Rabolt, M. Juricha nd H. D. Swalen, Appl. Spectrosc., 39 (1985) 269.
150 W. Knoll, M. R. Philpott and W. G. Golden, J. Chem. Phys., 77 (1982) 219.
151 I. Kusaka and W. Suetaka, Spectrochim. Acta, Part A, 36 (1980) 647.
152 J. F. Rabolt, F. C. Burne, N. E. Schlotter and J. D. Swalen, J. Chem. Phys., 77 (1982) 219.
153 P. V. Huong, Adv. Infrared Raman Spectrosc., 4 (1978) 85.
154 D. Kember, D. H. Chenery, N. Sheppard and J. Fell, Spectrochim. Acta, Part A, 35 (1979) 455.
155 J. L. Lauer and L. E. Keller, Appl. Surf. Sci., 9 (1981) 175.
156 R. G. Greenler, Surf. Sci., 69 (1977) 647.
157 D. L. Allara, D. Teicher and J. F. Durana, Chem. Phys. Lett., 84 (1981) 20.
158 K. Wagatsuma, K. Honma and W. Suetaka, Appl. Surf. Sci., 7 (1981) 281.
159 Y. Nagasawa and A. Ishitani, Appl. Spectrosc., 38 (1984) 168.
160 J. Derkosch and W. Mikenda, Mikrochim. Acta, Part II, (1985) 101.
161 P. R. Griffiths, Appl. Spectrosc., 26 (1973) 73.
162 B. F. Lewis, M. Mosesman and W. H. Weinberg, Surf. Sci., 41 (1974) 142.
163 J. Lambe and R. C. Jaklevic, Phys. Rev., 165 (1968) 821.
164 M. G. Simonsen, R. V. Coleman and P. K. Hansma, J. Chem. Phys., 61 (1974) 3789.
165 A. F. Diaz, U. Hetzler and E. Kay, J. Am. Chem. Soc., 99 (1977) 780.
166 D. M. Brewis, J. Comyn, D. P. Oxley and R. G. Pritchard, Surf. Interf. Anal., 6 (1984) 40.
167 J. D. Alexander, A. N. Gent and P. N. Henriksen, J. Chem. Phys., 83 (1985) 5981.
168 M. Higo, Y. Owaki and S. Kamata, Chem. Lett., (1985) 1309.
169 N. M. D. Brown, R. J. Turner, S. Affrossman, I. R. Dunkin, R. A. Pethrick and C. J. Shields, Spectrochim. Acta, Part B, 40 (1985) 847.
170 S. Reynolds, D. P. Oxley and R. G. Pritchard, Spectrochim. Acta, Part A, 38 (1981) 103.
171 R. R. Mallik, R. G. Pritchard, C. C. Harley and J. Comyn, Polymer, 26 (1985) 551.
172 Y. J. Chabal and A. J. Sievers, Phys. Rev. Lett., 44 (1980) 944.
173 J. P. Heritage and D. L. Allara, Chem. Phys. Lett., 74 (1980) 507.
174 D. L. Allara, C. A. Murray and S. Bodoff, in K. L. Mittal (Ed.), Physicochemical Aspects of Polymer Surfaces, Vol. I, Plenum, New York, 1983.
175 H. Ishida and A. Ishitani, Appl. Spectrosc., 37 (1983) 450.
176 C. Jennings, R. Aroca, A.-M. Hor and R. O. Loutfy, Spectrochim. Acta, Part B, 41 (1985) 1095.
177 J. F. Rabolt, R. Santo and J. D. Swalen, Appl. Spectrosc., 34 (1980) 517.
178 J. F. Rabolt, N. E. Schlotter, J. D. Swalen and R. Santo, J. Polym. Sci. Phys. Ed., 21 (1983) 1.

179 J. R. Ferraro and L. J. Basile, Fourier Transform Infrared Spectroscopy, Academic, New York, 1982.
180 D. A. Lang, Raman Spectroscopy, McGraw-Hill, New York, 1977.
181 C. Chiang, H. Ishida and J. L. Koenig, J. Coll. Interface Sci., 74 (1980) 396.
182 H. Ishida and J. L. Koenig, J. Coll. Interface Sci., 64 (1978) 555.
183 H. Ishida and J. L. Koenig, J. Coll. Interface Sci., 64 (1978) 565.
184 H. Ishida, S. Naviroj, K. Tripathy, J. J. Fitzgerald and J. L. Koenig, J. Polym. Sci. Phys. Ed., 20 (1982) 701.
185 S. R. Culler, H. Ishida and J. L. Koenig, J. Coll. Interface Sci., 106 (1985) 334.
186 K. Tsutsumi and H. Takahashi, Coll. Polym. Sci., 1 (1985) 506.
187 J. L. Koenig and P. T. K. Shih, Mater. Sci. Eng., 20 (1975) 127.
188 M. Kawaguchi, M. Komiya and A. Takahashi, Polym. J., 14 (1982) 563.
189 S. R. Culler, H. Ishida and J. L. Koenig, J. Coll. Interface Sci., 109 (1986) 1.
190 M. M. Coleman and P. C. Paynter, Appl. Spectrosc. Rev., 20 (1984) 255.
191 G. Ramana Rao, C. Castiglioni, M. Gussoni, G. Zerbi and E. Martuscelli, Polymer, 26 (1985) 811.
192 M. K. Antoon, K. H. Koenig and J. L. Koenig, Appl. Spectrosc., 31 (1977) 518.
193 G. Leonard, J. L. Halary and L. Monnerie, Polymer, 26 (1985) 1507.
194 T. M. Duncan and C. Dybowski, Surf. Sci. Rep., 1 (1981) 157.
195 A. M. Zaper and J. L. Koenig, Adv. Coll. Interface Sci., 22 (1985) 113.
196 A. Abragam, The Principles of Nuclear Magnetism, Oxford University Press, Oxford, 1961.
197 M. Mehring, High Resolution NMR Spectroscopy in Solids — NMR Basic Principles and Progress, Vol. 11, Springer, Berlin, 1976.
198 R. K. Harris and B. E. Mann (Eds.), NMR and the Periodic Table, Academic, New York, 1978.
199 A. Pines, M. G. Gibby and J. S. Waugh, J. Chem. Phys., 59 (1973) 569; E. R. Andrew, Progr. NMR Spectrosc., 8 (1971) 1.
200 D. W. Sindorf and G. E. Maciel, J. Am. Chem. Soc., 105 (1983) 1487.
201 D. W. Sindorf and G. E. Maciel, J. Phys. Chem., 87 (1983) 1487.
202 D. W. Sindorf and G. E. Maciel, J. Phys. Chem., 87 (1982) 1487.
203 D. W. Sindorf and G. E. Maciel, J. Am. Chem. Soc., 105 (1983) 3767.
204 G. R. Hays, A. D. H. Clague, R. Huis and G. Van der Velden, Appl. Surf. Sci., 10 (1982) 247.
205 C. Chiang, N. Liu and J. L. Koenig, J. Coll. Interface Sci., 86 (1982) 26.
206 D. W. Sindorf and G. E. Maciel, J. Am. Chem. Soc., 105 (1983) 1848.
207 D. Slotfeldt-Ellingsen and H. A. Resing, J. Phys. Chem., 84 (1980) 2204.
208 W. P. Rothwell, D. R. Holecek and J.-A. Vershaw, J. Polym. Sci. Lett. Ed., 22 (1984) 241.
209 J. R. Havens and J. L. Koenig, Appl. Spectrosc., 37 (1982) 226.
210 V. J. McBrierty and D. C. Douglass, J. Polym. Sci. Macromol. Rev., 16 (1981) 295.
211 E. O. Steidkal, J. Schaefer, M. D. Sefcik and R. A. McKay, Macromolecules, 14 (1981) 275.
212 P. Caravatti, P. Neuenschwander and R. R. Ernst, Macromolecules, 18 (1985) 119.
213 M. Linder, P. M. Henrichs, J. M. Hewitt and D. J. Massa, J. Chem. Phys., 82 (1985) 1585.

Analytica Chimica Acta, 197 (1987) 43—50
Elsevier Science Publishers B.V., Amsterdam — Printed in The Netherlands

SPECTROPHOTOMETRIC FIELD MONITOR FOR WATER QUALITY PARAMETERS
The Determination of Phosphate

PAUL J. WORSFOLD* and J. RICHARD CLINCH

Department of Chemistry, University of Hull, Hull HU6 7RX (Great Britain)

HARRY CASEY

Freshwater Biological Association, River Laboratory, East Stoke, Wareham, Dorset BH20 6BB (Great Britain)

(Received 14th October 1986)

SUMMARY

A flow-injection manifold based on reagent injection into the sample stream is described for the determination of phosphate in natural waters. A double-beam photometric detector incorporating light-emitting diodes and photodiodes in enclosed in a 20-cm^3 box. The response is linear over the range 0—2000 $\mu g\ l^{-1}$ phosphate-phosphorus (r = 0.9992) and the limit of detection (2σ) is 12 $\mu g\ l^{-1}$ phosphorus. The reagents are stable for at least 30 days and there is no interference from 10 mg l^{-1} silicate-silicon.

The conventional approach to water quality monitoring is to combine periodic manual sampling with batch analysis in the laboratory [1]. Such a procedure is both labour-intensive and time-consuming, there are likely to be sample stability and contamination problems [2], and the information provided is unlikely to be continuous or immediate. Furthermore, the current trend towards legislation relating to water quality, e.g., the environmental quality objectives (EQOs) stipulated by the EEC [3], is likely to increase the burden on resources available for water monitoring.

There is therefore a growing need for automated on-site monitoring devices [4], but such devices must meet several criteria in addition to those of accuracy, precision, sensitivity and selectivity which are required of laboratory-based methods. These criteria include low power consumption, a facility for periodic recalibration, long-term stability, compact and robust design, a data-logging or direct data-transmission (e.g., telemetry) facility, and most importantly long-term (i.e., at least one week) unattended operation.

Most of the commercial instruments currently available for use in the field are based on electrochemical detection [5] and measure parameters such as pH, temperature, dissolved oxygen and conductivity. Electrochemical monitors, however, are subject to physical and chemical interferences and are available only for a limited number of chemical parameters. Conversely, well-documented spectrophotometric methods are available for a wide range of

0008-2670/87/$03.50

chemical parameters. Also, recent advances in solid-state electronics have assisted in the design of light-emitting diode (LED) photometric detectors, incorporating photodiodes [6] or phototransistors [7—11], which meet the criteria stated above for on-site monitors. One such detector [7] has been used within an injectionless manifold for the determination of silicate and sulphide in situ in the ocean.

The application of flow injection analysis to water pollution studies has already been suggested [12]. This paper considers the design of a flow-injection-based LED photometric detector, with particular reference to its use in automated on-site monitors for the water industry. Results are presented for the determination of phosphate via the molybdenum blue reaction.

EXPERIMENTAL

Reagents

All solutions were prepared in distilled deionized water and all chemicals were of analytical grade (BDH). A stock phosphate solution containing 100 mg l^{-1} phosphorus as phosphate was prepared by dissolving 0.4390 g of potassium dihydrogenphosphate (dried for 2 h at 105°C) in 1 l of water; 5 drops of toluene and 0.4 g of sodium azide were added as preservatives. Working phosphate standards covering the range 0—2000 μg l^{-1} phosphorus were prepared by serial dilution of the stock solution. A 1 μg ml^{-1} phosphorus standard was used for all of the manifold optimization experiments.

The acid/molybdate reagent was prepared by dissolving ammonium heptamolybdate (10 g) in 0.4 M nitric acid (1 l). The ascorbic acid reagent was prepared by dissolving ascorbic acid (80 g) and glycerol (100 g) in water (1 l). Both reagents were stored in brown glass bottles.

Instrumentation and procedures

The reagent-injection manifold design used for this work is based on the so-called "reverse" flow-injection concept [13], which is better called the "reagent-injection" method. A fixed volume of reagent is periodically injected into a continuously flowing sample stream, as shown in Fig. 1. A peristaltic pump (Ismatec Mini S820) was used to propel the sample (phosphate standards) through PTFE tubing (0.5 mm i.d.) at 1.1 ml min^{-1}. The acid/molybdate and ascorbic acid reagents were mixed on-line and continuously pumped through a PTFE rotary valve (Rheodyne 5020) with a 30-μl sample loop. The mixed reagent was manually injected into the sample stream and a 200-cm coil was placed between the injection valve and the detector. The output from the detector was sent to a chart recorder (Tekman Labwriter) set at 1 V f.s.d.

Photometric detector. The circuit diagrams for the LED source and photodiode detector are shown in Fig. 2. A double-beam configuration is used, whereby the untreated sample passes through the reference cell before the addition of reagents and passage through the sample cell. The LEDs for

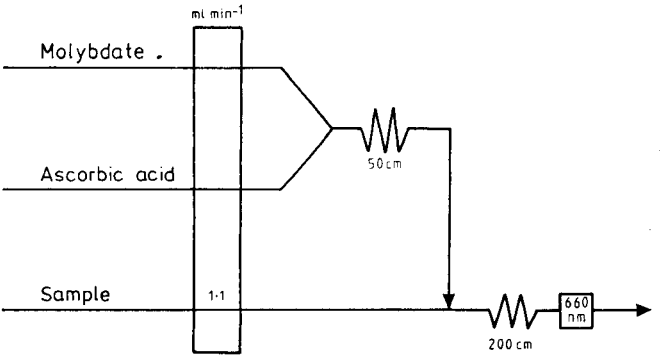

Fig. 1. The reagent-injection manifold for the determination of phosphate. The detector was a dual photometric detector incorporating two red LEDs.

the sample (D4) and reference (D3) cells were ultra-bright red LEDs (Radio Spares 588-263) powered by −5 V, 100 mA regulators (IC4 and IC3, Radio Spares 306-235), with a variable resistor in the reference circuit (R8) providing a coarse zero adjustment for the detector output. The photodiode detector consisted of two silicon photodiodes (D1, sample; D2, reference) with integral current/voltage converters and amplifiers (Radio Spares 308-067), a voltage comparator (IC1) and a voltage follower (IC2). Two variable resistors (R5 and R7) can be used for fine zero adjustment.

The flow cell housing (Fig. 3) consisted of a block of aluminium (20 mm × 20 mm × 20 mm) with two parallel 1.8-mm diameter holes drilled through one side of the cube. Teflon tubing (1.7 mm o.d.; 0.5 mm i.d.) was passed through each hole, one tube being the sample cell and the other the reference cell. Holes were drilled perpendicularly to the teflon tubing to house the two LEDs and the two photodiodes. The path length of the sample and reference beams was therefore 0.5 mm. All components were mounted in an aluminium box.

RESULTS AND DISCUSSION

Detector design

The flow cell was simple to construct, consisting of the same teflon tubing as was used in the remainder of the manifold, and was therefore non-disruptive to the sample stream. Light-emitting diodes were chosen as the light sources for the photometric detector because of their small size, low power consumption (20 mA at 5 V) and cold light output. A constraint in the use of LEDs as sources for photometric detectors is the limited spectral range covered by such devices in the u.v./visible region; only red (λ_{max} = 635 nm), yellow (λ_{max} = 583 nm) and green (λ_{max} = 565 nm) LEDs, each with a bandwidth of 30—40 nm, are readily available. For the determination of phosphate by the molybdenum blue reaction, however, 660 nm is often the wavelength used for detection and the red LED is therefore a suitable light source.

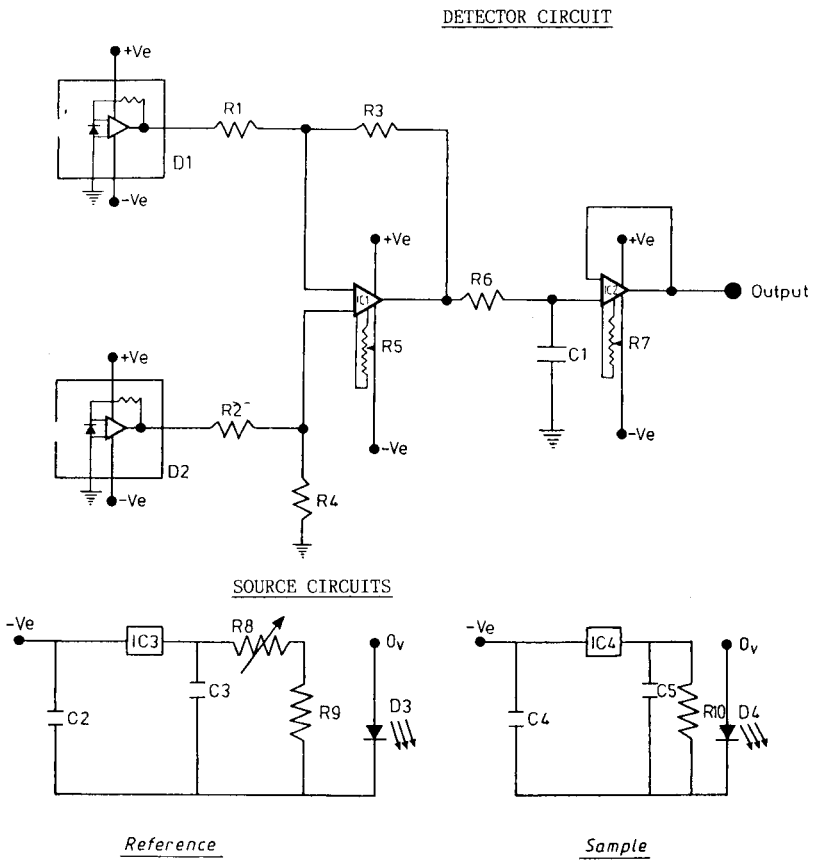

Fig. 2. Circuit diagram of the LED photometric detector. Resistors: R1 4K7, R2 4K7, R3 100K, R4 100K, R5 10K, R6 470 K, R7 25K, R8 1K, R9 1K2, R10 1K5. Capacitors: C1 1.0 μF, C2 220 nF, C3 470 nF, C4 220 nF, C5 470 nF. Diodes: D1 and D2, RS Cat. no. 308-067; D3 and D4, RS Cat. no. 588-263. Integrated circuits: IC1 and IC2 741N, IC3 and IC4 79LO5.

For light detection, a double-beam configuration of photodiodes with integral voltage converters and amplifiers was used in order to minimize drift from temperature changes and detector noise. The sample was pumped through the reference channel prior to the injection of reagent in order to compensate for physical changes in the sample stream (e.g., colour or turbidity). As indicated below, the reproducibility of the results and the stability and sensitivity of the detector were adequate for the routine monitoring of phosphate in river water, but the use of matched photodiodes and/or low noise components would be necessary for certain applications.

Manifold optimization

A reagent-injection manifold was used in order to minimize reagent consumption and therefore maximize the unattended operating lifetime of the

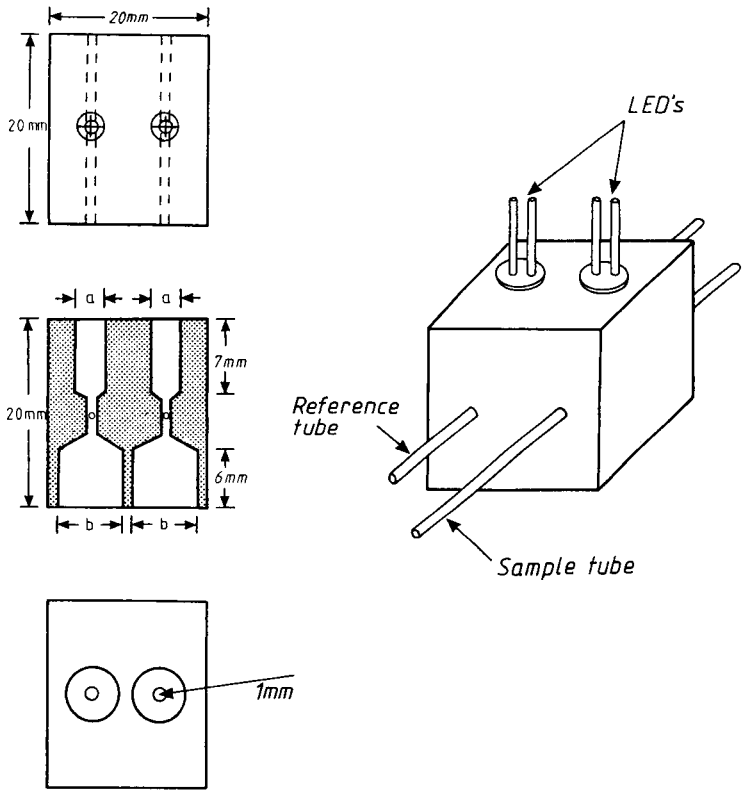

Fig. 3. Flow cell housing made of aluminium. Bores: (a) 5 mm nominal, to fit the LEDs; (b) 8.5 mm nominal to fit the photodiodes.

monitor. In addition, the sensitivity of a reagent-injection manifold can be increased relative to the corresponding conventional manifold providing that excess of reagent is maintained within the reaction zone [13]. The detector response increased with increasing ascorbic acid concentration (0.5—100 g l^{-1}), but a working concentration of 80 g l^{-1} was used as it was difficult to maintain higher concentrations without precipitation. An important parameter governing the unattended operating lifetime of the monitor is reagent stability; it was found that a high concentration of glycerol (100 g l^{-1}). increased the lifetime of the ascorbic acid reagent considerably, from what otherwise would be only a few days. The effect of ammonium molybdate concentration (0.5—20 g l^{-1}) in 0.4 M nitric acid was similarly investigated, and 10 g l^{-1} was shown to be the limiting concentration.

The effect of system variables, e.g., coil length, flow rate and reagent volume, on the sensitivity of reagent-injection procedures in flow injection analysis is known to be different from their effect on conventional sample-injection procedures [13]. In the intended application for this equipment as a field monitor, ambient temperatures must be used for the reaction. The

effect of varying the reaction coil length (35—400 cm) on the response for a sample blank and a 1 μg ml^{-1} phosphate standard is shown in Fig. 4A. The response for the blank is due to refractive index differences between the sample stream and the injected reagent zone, which are minimized at longer coil lengths because of increased dispersion. The response for the 1 μg ml^{-1} standard shows an increase in the extent of reaction at longer coil lengths, because of increased reaction time, in addition to the change in signal caused by the effects of refractive index and dispersion. The sensitivity of the procedure, represented here as the difference between the blank and the 1 μg ml^{-1} standard, therefore, increases with increasing coil length, and a 200-cm reaction coil was used for all subsequent experiments as a suitable compromise between sensitivity and processing time.

The effect of sample flow rate (0.3—2.9 ml min^{-1}) on the sensitivity is shown in Fig. 4B. The sensitivity is somewhat improved at slower flow rates because the increase in the extent of reaction more than compensates for the greater effect of refractive index changes. A compromise flow rate of 1.1 ml

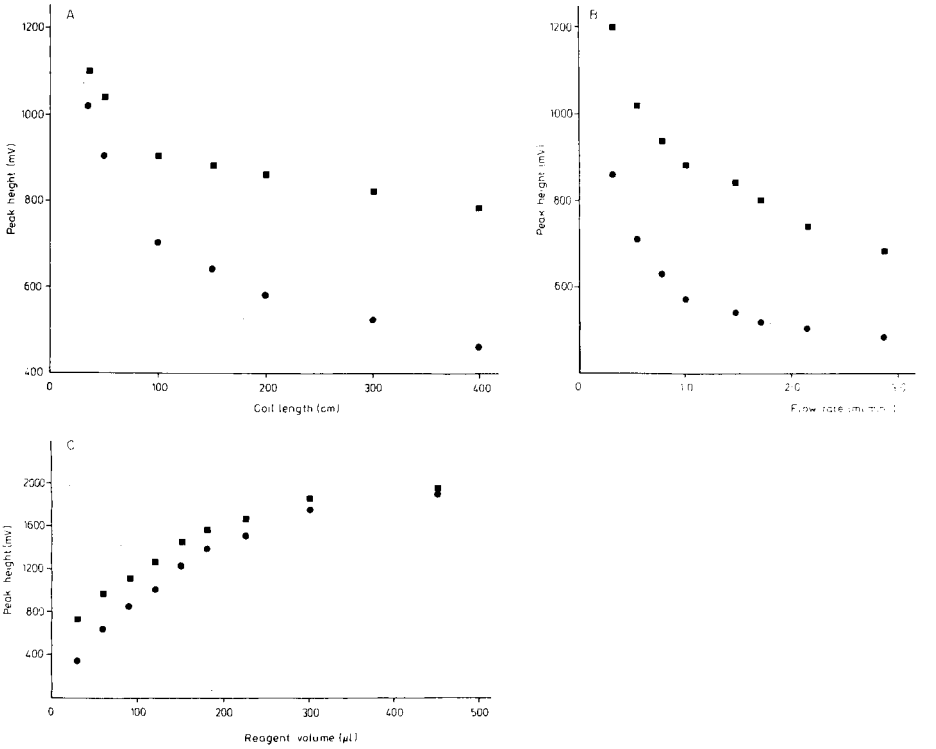

Fig. 4. Effect of manifold variables: (A) reaction coil length; (B) sample flow rate; (C) reagent volume injected. Flow stream: (•) sample blank; (▪) 1 μg ml^{-1} phosphorus (as phosphate) solution. General conditions: 60-μl reagent injection, 1.1 ml min^{-1} sample flow rate, 200-cm reaction coil, except when that condition was varied.

min^{-1} was used for subsequent experiments. The effect of reagent volume (30—450 μl) was also investigated; smaller reagent volumes were shown to give improved sensitivity (Fig. 4C). A reagent volume of 30 μl was used for subsequent experiments.

Calibration and silicate interference

Six phosphate standards covering the range 0—1000 $\mu g\ l^{-1}$ phosphorus as phosphate were processed and a linear calibration graph (r = 0.9995) was obtained; the mean output signal (n = 6) ranged from 230 mV for the blank to 502.5 mV for the top standard. The relative standard deviations (n = 6) for these standards were in the range 0.0—0.9% and the limit of detection (2σ) was 12 $\mu g\ l^{-1}$ phosphorus, which compares favourably with the limits reported for two sample-injection manifolds [13]. Results for an extended range of standards (0—2000 $\mu g\ l^{-1}$ phosphorus) also gave a linear calibration graph (r = 0.9992, n = 7).

Reagent stability is an important prerequisite for a field monitor. The results obtained showed that there was only a small decrease in the response after the reagents had been left in the system for 30 days. The linear calibration equation on day 1 was $y = 0.272x + 228$ (r = 0.9995) and on day 31 was $y = 0.213x + 234$ (r = 0.9967), where x is the concentration ($\mu g\ l^{-1}$ phosphorus) and y is the signal (mV).

For the determination of phosphate in natural waters, the species most likely to interfere with the spectrophotometric procedure is silicate, which competes with phosphate to form a heteropoly acid with the ammonium molybdate. The effect of silicate was evaluated by spiking a 1000 $\mu g\ l^{-1}$ phosphorus standard with various concentrations of silicate (0—1000 $mg\ l^{-1}$ silicon) added as sodium silicate (water glass). Although large silicate concentrations gave rise to serious interferences, 50 $mg\ l^{-1}$ silicon (as silicate) resulted in only a 1% decrease in signal and 10 $mg\ l^{-1}$ silicon, the normal level in river waters, had no effect.

Conclusions

The results presented for the determination of phosphate demonstrate the effectiveness of the LED photometric detector and the feasibility of using a flow-injection approach with spectrophotometric detection as the basis of a field monitor. The reagent-injection procedure shows good sensitivity with low reagent consumption. The reagents are stable for at least 30 days, and sensitivity and linear calibration are maintained over that period. These features are important if long-term unattended operation is to be achieved. Determination of other water-quality parameters such as nitrate and ammonia concentrations have also been shown to be feasible with this approach.

One of us (J. R. C.) thanks the Science and Engineering Research Council for financial support. We thank Mr. D. Mather and Mr. J. Clannachan for their help in constructing the photometric detector.

REFERENCES

1 M. H. I. Coomber and P. J. D. Nicholson, Anal. Proc., 21 (1984) 474.
2 H. Casey and S. M. Walker, International Environment and Safety, October (1981) 16.
3 J. Gardiner and G. Mance, UK Water Quality Standards arising from European Community Directives, WRC Technical Report TR204, 1984.
4 W. W. Pitt, J. Water Pollut. Control Fed., 56 (1984) 548.
5 T. E. Edmonds, Trends Anal. Chem., 4 (1985) 220.
6 T. Imasaka, T. Kamikubo, Y. Kawabata and N. Ishibashi, Anal. Chim. Acta, 153 (1983) 261.
7 K. S. Johnson, C. L. Beehler and C. M. Sakamoto-Arnold, Anal. Chim. Acta, 179 (1986) 245.
8 H. Flaschka, C. McKeithan and R. Barnes, Anal. Lett., 6 (1973) 585.
9 D. Betteridge, E. L. Dagless, B. Fields and N. F. Graves, Analyst, 103 (1978) 897.
10 T. J. Sly, D. Betteridge, D. Wibberly and D. G. Porter, J. Aut. Chem., 4 (1982) 186.
11 M. Trojanowicz, W. Augustynicik and A. Hulanicki, Mikrochim. Acta, 2 (1984) 17.
12 H. Casey and S. Smith, Trends Anal. Chem., 4 (1985) 256.
13 K. S. Johnson and R. L. Petty, Anal. Chem., 54 (1982) 1185.

Analytica Chimica Acta, 197 (1987) 51—56
Elsevier Science Publishers B.V., Amsterdam — Printed in The Netherlands

ASSAY FOR GUANASE IN BLOOD SERUM BY FLOW INJECTION ANALYSIS WITH FLUORESCENCE DETECTION

YOHJI HAYASHI, KIYOSHI ZAITSU and YOSUKE OHKURA*

Faculty of Pharmaceutical Sciences, Kyushu University 62, Maidashi, Higashi-ku, Fukuoka 812 (Japan)

(Received 19th November 1986)

SUMMARY

A sensitive assay for guanase activity in human serum (10 μl) is described. Xanthine, formed enzymatically from the substrate guanine, is determined in a flow system in which columns of immobilized xanthine oxidase, uricase and horseradish peroxidase are connected in that sequence in the flow line. Hydrogen peroxide formed in the enzymatic conversion of xanthine is measured fluorimetrically by reaction with 3-(*p*-hydroxyphenyl)-propionic acid in the system. Linear calibration graphs are obtained for 0.5—500 pmol of xanthine in the 20-μl sample injected. This method permits the assay of guanase activity in the sera of healthy persons and patients with hepatitis.

Guanase (guanine aminohydrolase, EC 3.5.4.3) catalyzes the deamination of guanine to xanthine. The enzyme activity in human serum is increased in patients with liver diseases [1—5]. In the diagnosis, serum guanase activity can be a more sensitive and more quantitative indicator of liver cell damage than glutamate-oxaloacetate transaminase or glutamate-pyruvate transaminase activity [1, 2]. It has been suggested that a screening test of guanase activity in banked blood should be useful for preventing hepatic injury in cases of blood transfusion [2—4].

Many spectrophotometric methods [1—3, 5—12] have been reported for the assay of guanase activity; they are usually insensitive. Highly sensitive radiochemical methods [4, 13, 14] require a radioactive substrate, ^{14}C-labelled guanine. Recently, a sensitive fluorimetric flow-injection determination of hydrogen peroxide was reported [15] which was successfully applied to the determination of adenosine and inosine in human plasma [16]. A highly sensitive flow-injection method for the assay of guanase in human serum has been developed from these procedures, and is reported here. Xanthine formed enzymatically is degraded to hydrogen peroxide by immobilized xanthine oxidase (XOD) and urate oxidase (UOD, uricase) columns. The hydrogen peroxide is quantified by an immobilized horseradish peroxidase (HRP)-mediated reaction with 3-(*p*-hydroxyphenyl)propionic acid (HPPA), an efficient fluorogenic substrate for HRP [17]. Normal and pathological human sera were used to establish the assay procedure.

0003-2670/87/$03.50

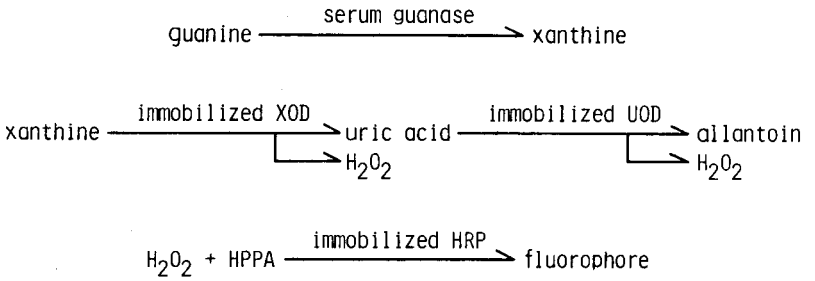

EXPERIMENTAL

Chemicals and reagents

Deionized, triply-distilled water was used. HPPA was obtained from Dojindo Laboratories (Kumamoto, Japan). Tris(hydroxymethyl)aminomethane (Tris; Ultrol grade), horseradish peroxidase (285 purpurogallin units mg^{-1}) and urate oxidase (grade II, 4.0 U mg^{-1}, from *candida* sp.) were from Calbiochem (San Diego, CA), Sigma Chemical Co. (St. Louis, MO.) and Toyobo Biochemicals (Osaka), respectively. Guanine and xanthine were from Nakarai Chemicals (Kyoto). Xanthine oxidase (0.4 U mg^{-1}, from cow's milk, in 3.2 M ammonium sulfate suspension, 10 mM in EDTA) and catalase (Type II, 260 000 U ml^{-1}, from bovine liver, in 30% (v/v) glycerol solution containing 10% (v/v) ethanol), were obtained from Boehringer Mannheim Yamanouchi (Tokyo). Unless otherwise noted, all other chemicals were of reagent grade.

The substrate solution for the guanase reaction was a mixture of 0.1 M Tris/hydrochloric acid buffer (pH 8.0), 2 mM guanine in 0.01 M sodium hydroxide (usable for two weeks), 0.5 U ml^{-1} urate oxidase solution and 40 U ml^{-1} catalase solution (both in 0.1 M Tris/hydrochloric acid buffer, pH 8.0; usable for one week and one day, respectively) in the ratio 35:1:2:2, v/v.

Serum, enzyme reaction and sample solutions

Normal sera were obtained from healthy volunteers in this laboratory. Sera of patients with hepatitis were supplied by Chidoribashi Hospital (Fukuoka).

The substrate solution (400 μl) was pre-incubated at 37°C for ca. 2 min and again incubated for exactly 30 min after addition of 10 μl of serum. The reaction was stopped by addition of 50 μl of 4 M perchloric acid. The resulting mixture was mixed with 90 μl of 2 M potassium carbonate to remove the perchlorate and centrifuged for 10 min at 1000 g. An aliquot (20 μl) of the supernatant solution was used for the flow-injection procedure. For a blank measurement, in order to establish the concentration of endogeneous xanthine and hypoxanthine, the serum was carried through the test procedure except that 2 mM guanine in the substrate solution was replaced with water.

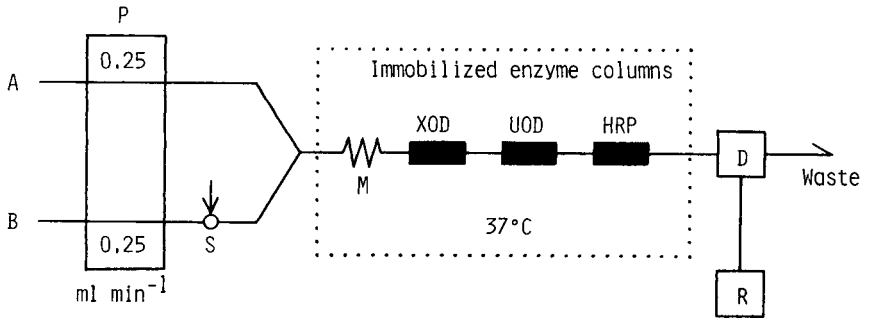

Fig. 1. Schematic diagram of the flow-injection system. A, reagent solution; B, carrier solution; P, pump; S, sample injector; M, mixing coil; D, fluorescence detector; R, recorder.

Flow-injection apparatus and assay procedure for xanthine

A schematic flow diagram of the flow-injection system is shown in Fig. 1. Immobilized xanthine oxidase, urate oxidase and HRP columns prepared as described previously [16] and teflon tubing (0.25 mm i.d.; Gasukuro Kogyo, Tokyo) were used. The reagent solution, which was 5 mM HPPA in 0.1 M Tris/hydrochloric acid buffer (pH 8.0), 0.15 M in sodium chloride and 10 mM in disodium-EDTA, and the carrier solution, which was the same as the reagent solution but without HPPA, were pumped separately with a Sanuki DM2M-1024 pump; both flow rates were 0.25 ml min^{-1}. The sample solution for the test, or the blank solution, was injected through a Rheodyne 7125 syringe-loading sample injector valve (20-μl loop) into the carrier stream. A mixing coil (1 m) and the three enzyme columns built in the flow line were immersed in a water bath at 37°C. The mixing coil served not only to mix the carrier solution (or sample solution) thoroughly with the reagent solution, but also to warm the mixture sufficiently before it reached the enzyme columns. The fluorescence intensity was measured at an excitation wavelength of 305 nm and an emission wavelength of 405 nm with a Shimadzu RF 530 fluorescence spectromonitor equipped with a 12-μl flow cell and a Hitachi 056 chart recorder. For xanthine calibration, 20-μl portions of xanthine standard solutions (0.25—25 μM) were directly analyzed in the flow-injection system. The amount of xanthine formed enzymatically was read from the calibration curve on the basis of net peak height. Guanase activity was expressed as μmoles of xanthine formed per minute per liter of serum at 37°C.

RESULTS AND DISCUSSION

The HPPA concentration in the stream influenced the fluorescence development (peak height). The highest peak was achieved for $\geqslant$4.0 mM HPPA in the reagent solution, thus 5.0 mM HPPA is recommended. Disodium-EDTA was added to the buffer solution to protect xanthine oxidase from certain inhibiting metal ions.

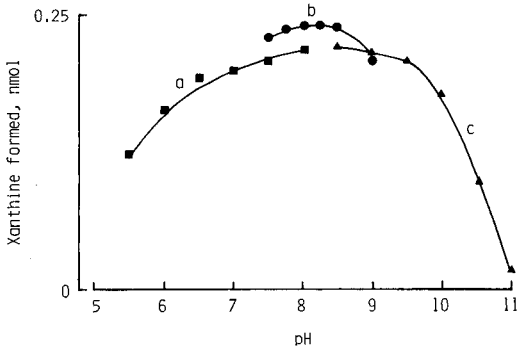

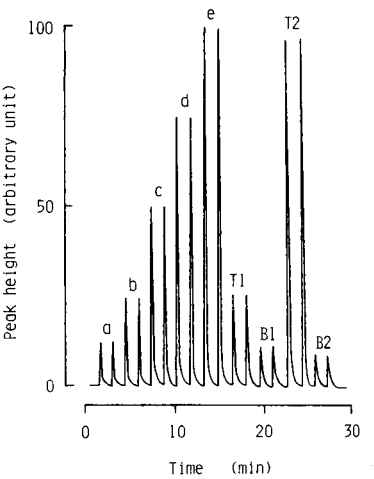

Fig. 2. Effect of pH of buffers for the enzyme reaction on the amount of xanthine formed: (a) 0.1 M phosphate buffer; (b) 0.1 M Tris/hydrochloric acid buffer; (c) 0.1 M 3-cyclohexylaminopropanesulfonic acid/sodium hydroxide buffer. Guanase activity: 0.8 μmol min^{-1} l^{-1}.

Fig. 3. Flow-injection peaks for standards and serum samples. Amounts of xanthine (pmol per 20 μl): (a) 5; (b) 10; (c) 20; (d) 30; (e) 40. Tl and Bl, normal sera; T2 and B2, serum of patient with hepatitis; T and B, test and blank, respectively. Guanase activities (μmol min^{-1} l^{-1}): 0.5 (normal serum) and 3.2 (serum of patient with hepatitis).

The fluorescence from HPPA increased with increasing pH in the range 7.0—8.5. As the immobilized enzymes might be deactivated at higher pH values, pH 8.0 is recommended for the flow system. The peak height increased with decreasing flow rates of the reagent and carrier solutions and the inner pressure in the system increased with increasing flow rate; 0.25 ml min^{-1} was selected for both the reagent and carrier solutions.

Guanase in human serum was most active at pH 7.75—8.50 in 0.1 M Tris/hydrochloric acid buffer (Fig. 2). Tris gave a maximum and constant activity at concentrations of 0.01—0.2 M. Therefore, 0.1 M Tris/hydrochloric acid buffer of pH 8.0 was selected for the enzyme reaction. A maximum and constant activity was obtained in the presence of 40—100 μM guanine in the substrate solution, with an observed Michaelis constant of 7.0 μM; 50 μM (in the substrate solution) was used as a saturated concentration for the enzyme reaction.

Because the concentration of endogenous uric acid in serum is high enough to inhibit the HRP-catalyzed fluorescence reaction of HPPA, the acid should be decomposed by adding urate oxidase to the enzyme reaction mixture; the hydrogen peroxide thus formed was destroyed by using catalase during the enzyme reaction. Urate oxidase and catalase remaining in the enzyme reaction mixture were removed by deproteinization with perchloric acid. A small amount of uric acid was also produced from xanthine in the sample solution.

The resulting uric acid only slightly inhibited the fluorescence reaction, but an immobilized urate oxidase column was placed in the flow line to prevent the inhibition.

The enzyme reaction rate was constant for at least 120 min at 37°C. The amount of xanthine formed after an incubation time of 30 min was proportional to the size of the human serum sample up to at least 20 μl.

For xanthine calibration, xanthine standard solutions were injected into the flow system. The recoveries of xanthine added to serum in the range 0.005—1.5 mM were close to 100%. The calibration graph was linear up to 500 pmol per 20-μl injection volume and passed through the origin. The lower determinable limit (signal/noise ratio = 5) for xanthine was 0.5 pmol per 20-μl injection. Typical peaks obtained for 5—40 pmol of xanthine and for sample and blank runs are shown in Fig. 3. A rapid injection rate (40 h^{-1}) could be attained.

A comparison with a spectrophotometric method based on 8-azaguanine as substrate [7], which produces ammonia (Berthelot reaction) was made for normal and pathological sera. The correlation coefficient was 0.971 (n = 40), and a linear regression equation for the present method (X) against the spectrophotometric method (Y) was $Y = 1.6\,X + 0.059$. The reason for the slope of 1.6 is not known. The within-day precision of the present method was examined by using sera with mean guanase activities of 0.4, 0.8 and 7.2 μmol min^{-1} l^{-1}. The coefficients of variation were 1.2, 0.9 and 1.0% (n = 10), respectively.

Guanase activity in normal sera assayed by the present method was 0.48 ± 0.12 μmol min^{-1} l^{-1} (mean ±s.d., n = 15). The activity in sera of patients with liver diseases was 4.9 ± 3.3 μmol min^{-1} l^{-1} (mean ±s.d., n = 25). These values are in agreement with reported data [1—13].

Bilirubin in serum at concentrations less than 350 μM did not affect the determined activity of guanase but higher concentrations caused an apparent decrease in guanase activity. Ascorbic acid and glucose added to serum at concentrations of 280 μM and 22 mM, respectively, had no effect on the concentrations of xanthine formed.

To check the stability of the immobilized enzyme columns, xanthine solutions (2.5 and 5 μM) were injected 50 times a week into the flow system. The columns were stored at 4°C after being filled with their conservation solution [16], when they were not required for use. The immobilized urate oxidase and HRP columns were stable for at least a year; the xanthine oxidase column was stable for 3 months but a 10% loss of activity was noted after 4 months.

This study provides the first fluorimetric method for the assay of guanase. The method is highly sensitive and precise, and should be convenient for biological investigations and clinical use.

REFERENCES

1 E. E. Mandel and L. R. Macalincag, Am. J. Gastroenterol., 54 (1970) 253.
2 S. Yamasaki, S. Egashira, M. Koga, H. Akagawa and S. Fujii, Kurume Med. J., 29 (1982) 127.
3 K. Kanai, J. Kyoto Prefectural Univ. Med., 79 (1970) 337.
4 S. Fujii, K. Ikenaka, H. Yamada and S. Yamasaki, Rinsho Kagaku, 12 (1983) 208.
5 G. Giusti, B. Galanti and A. Mancini, Enzymologia, 38 (1970) 373.
6 W. T. Caraway, Clin. Chem., 12 (1966) 187.
7 G. Ellis and D. M. Goldberg, Clin. Chim. Acta, 37 (1972) 47.
8 G. Ellis, R. J. Spooner and D. M. Goldberg, Clin. Chim. Acta, 47 (1973) 75.
9 F. Heinz, S. Reckel and J. R. Kalden, Enzyme, 24 (1979) 247.
10 M. Sugiura, K. Kato, T. Adachi, Y. Ito, K. Hirano and S. Sawaki, Chem. Pharm. Bull., 29 (1981) 426.
11 T. Ando, T. Muraoka and H. Okuda, Anal. Biochem., 130 (1983) 295.
12 Y. Nishikawa, K. Fukumoto and F. Watanabe, Clin. Chem., 31 (1985) 103.
13 U. A. S. Al-Khalidi, S. Aftimos, S. Musharrafieh and N. N. Khuri, Clin. Chim. Acta, 29 (1970) 381.
14 C. A. Bennekom, J. P. Laarhoven, C. H. M. M. Bruyn and T. L. Oei, J. Clin. Chem. Clin. Biochem., 16 (1978) 245.
15 Y. Hayashi, K. Zaitsu and Y. Ohkura, Anal. Sci., 1 (1985) 65.
16 Y. Hayashi, K. Zaitsu and Y. Ohkura, Anal. Chim. Acta, 186 (1986) 131.
17 K. Zaitsu and Y. Ohkura, Anal. Biochem., 109 (1980) 109.

Analytica Chimica Acta, 197 (1987) 57—64
Elsevier Science Publishers B.V., Amsterdam — Printed in The Netherlands

DETERMINATION OF THE BENZODIAZEPIN-2-ONES BY CIRCULAR DICHROISM

SOON M. HAN[a], NEIL PURDIE* and KATHY A. SWALLOWS
Chemistry Department, Oklahoma State University, Stillwater, OK 74078-0447 (U.S.A.)
(Received 28th January 1987)

SUMMARY

Formation constants for the 1:1 complexation equilibrium reactions between β-cyclodextrin and the drugs, clonazepam, delorazepam, diazepam (Valium), flurazepam (Dalmane), lorazepam, medazepam, nitrazepam, nordiazepam, oxazepam, and temazepam, were measured by using circular dichroism spectropolarimetry. The range in values is almost one order of magnitude, suggesting a strong structural dependence in the interlocking between the host and different guests. Enthalpy and entropy data for the lorazepam interaction are consistent with data from several earlier studies. Direct determinations of diazepam and flurazepam in pharmaceutical products are within ±2% of the prescribed amounts.

The application of circular dichroism to the identification and determination of drugs, chiral or achiral, has been demonstrated for numerous examples in recent years. The inclusion of achiral examples in the applications of a procedure which seemingly would require that the analyte be optically active, does require that chirality be induced. A very useful mechanism to accomplish this requirement is to complex the achiral, but absorbing, analyte with a chiral, but non-absorbing, host molecule. The two molecular requirements complement each other in the complex to produce a species which is active in circular dichroism. Illustrations of this can be found for phencyclidine (PCP) [1], and its analogs [2], the barbiturates [3], and numerous other drugs [2, 4]. The present work examines another collection of structurally similar substances, the benzodiazepin-2-ones, which by themselves are not optically active, but which do absorb in the ultraviolet (u.v.) by virtue of the presence of the aromatic chromophore. Once again the chiral host molecule is β-cyclodextrin (β-CD). The aqueous buffered β-CD solution becomes the extracting solvent for the determinations.

EXPERIMENTAL

The benzodiazepin-2-ones, clonazepam, delorazepam, diazepam, flurazepam, lorazepam, nitrazepam, nordiazepam, oxazepam, and temazepam, and

[a]Present address: Chemistry Department, Texas Tech University, Lubbock, TX 79409, U.S.A.

0003-2670/87/$03.50

the dehydroderivative, medazepam (all from Hoffmann-LaRoche or Sigma Chemical Co.) were used without further purification. β-Cyclodextrin was obtained from Eastman Kodak.

For the equilibrium studies, solutions were prepared by dissolving the drugs in 0.02 M sodium hydroxide and weighed increments of β-CD were added in such a way that the host was always in excess. Drug concentrations were typically less than 10^{-4} M because of the strong absorption by the aromatic chromophores. Saturation for β-CD at room temperature is approximately 3×10^{-2} M. The sugar is stable in strong alkali for several hours which is very long compared to the few minutes needed for quantifying the drugs. Temperature-dependence data were taken at 15, 25 and 35°C for only lorazepam. Temperatures were controlled to ±0.1°C by using water circulated around the cuvette from an external thermostat (Haake, Model A81). Circular dichroism measurements were made with a JASCO-500A automatic recording spectropolarimeter, equipped with a DP-500N data processor, in the manner previously described over the wavelength range 500—235 nm [3]. Instrument calibration was done with a solution of androsterone in 1,4-dioxan on a daily basis, as recommended by the manufacturer.

The same solution conditions of 10^{-2} M β-CD in 0.02 M sodium hydroxide were selected for the extraction from the pharmaceutical products which were obtained from a local dispensary. The alkali was added to the sugar stock solution just prior to obtaining the spectrum. The products used were tablets containing 5 mg of Valium (Rugby) and capsules containing 30 mg of Dalmane (Mylan). Tablets were crushed and thoroughly mixed by shaking on a Wig-L-Bug for 2 min; then 20-mg portions were withdrawn for extraction into 10-ml or 25-ml aliquots of the alkaline β-CD stock solution. Undissolved solids were removed by centrifugation and the supernatant solution was used to fill the sample cell. Instrument parameters, such as scan rate, sensitivity, and repeat functions, were selected which produced the most favorable signal/noise (S/N) ratio. Several extracts from several tablets were used in the assays.

RESULTS AND DISCUSSION

The general structural formula for the series of benzodiazepin-2-ones is shown in Table 1 where the substituents are identified for each analog. Included also for easy reference are the values obtained for the equilibrium formation constants K_{DS}, and the resultant molar ellipticities, θ_{DS}, at the major maxima in the 250—300-nm wavelength range. Eight of the analogs form an interesting complete subset wherein consecutive substitutions for the four R groups and the accompanying changes in K_{DS} and θ_{DS} might be compared and used to indicate which portion of the benzodiazepin-2-one structure is encompassed in the sugar structure on the formation of the complex. In order better to develop the subsequent discussion, the

TABLE 1

General structure for the benzodiazepin-2-ones and formation constants for β-CD/benzodiazepin-2-one complexes

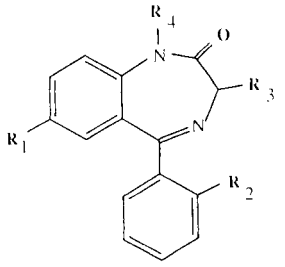

Compound	R_1	R_2	R_3	R_4	K_{DS}	θ_{DS}
Clonazepam	NO_2	Cl	H	H	812	100
Delorazepam	Cl	Cl	H	H	615	587
Diazepam	Cl	H	H	CH_3	208	218
Flurazepam	Cl	F	H	$CH_2CH_2NEt_2$	106	310
Lorazepam	Cl	Cl	OH	H	928	639
Nitrazepam	NO_2	H	H	H	479	72
Nordiazepam	Cl	H	H	H	133	1005
Oxazepam	Cl	H	OH	H	569	751
Temazepam	Cl	H	OH	CH_3	147	206
Lorazepam[a]	Cl	Cl	OH	H	96	246

[a]Result is for the reaction with γ-cyclodextrin.

subset has been arranged in a manner such that nordiazepam is chosen as the basis for substitution and is placed over two consecutive levels which include the molecules in which there is first (a) and second (b) substitution (Fig. 1).

The induced circular dichroism spectra for each of the analytes are shown in Fig 2. The circular dichroism method of detection easily distinguishes this group of drugs from any other, such as the barbiturates [3], the tetracyclines [4], the penicillins [5], or the cephalosporins [5]. It is also capable

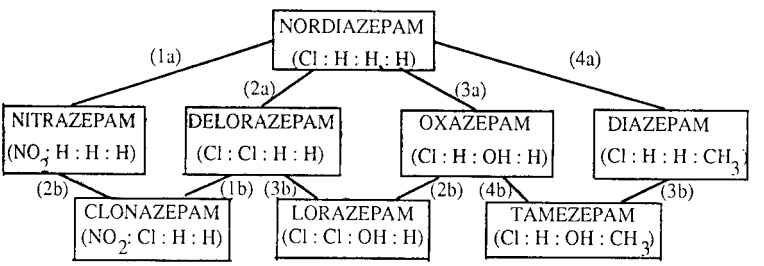

Fig. 1. Subset of successively substituted analogs of nordiazepam. The numerals refer to the R-group subscripts (Table 1).

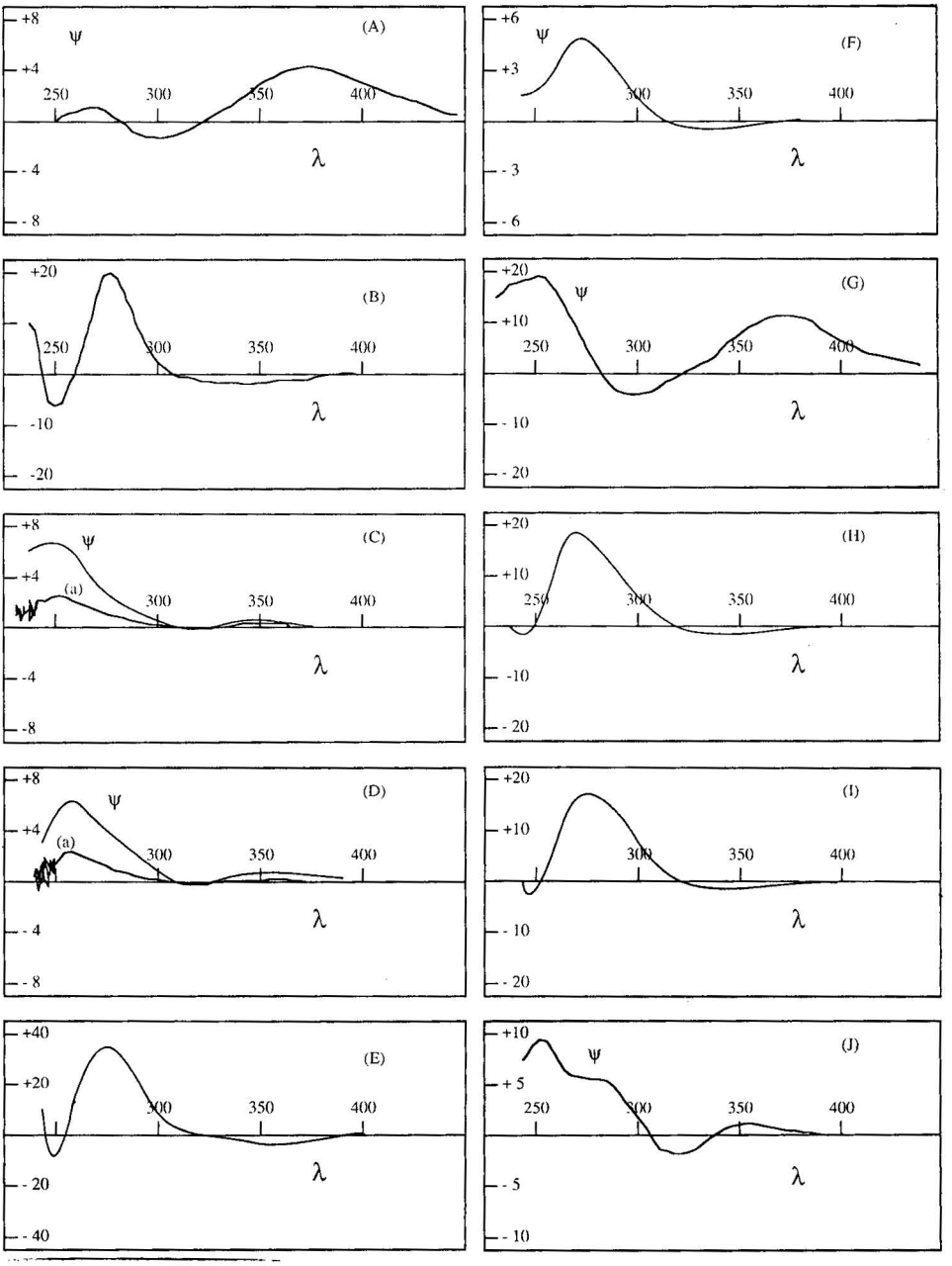

Fig. 2. Induced circular dichroism, spectrum [induced ellipticity (millidegrees) vs. wavelength (nm)] for the 1:1 complex formed between β-CD and drug: (a) clonazepam (C_D = 5.17 × 10^{-5} M; C_S = 6.02 × 10^{-3} M); (B) delorazepam (C_D = 7.711 × 10^{-5} M; C_S = 2.925 × 10^{-3} M); (C) diazepam (C_D = 5.51 × 10^{-5} M; C_S = 7.41 × 10^{-3} M), plus (a) spectrum for the extract; (D) flurazepam (C_D = 5.4 × 10^{-5} M; C_S = 6.82 × 10^{-3} M), plus (a) spectrum for the extract; (E) lorazepam (C_D = 5.73 × 10^{-5} M; C_S = 5.22 × 10^{-3} M); (F) medazepam (C_D = 7.564 × 10^{-5} M; C_S = 3.377 × 10^{-3} M); (G) nitrazepam (C_D = 7.15 × 10^{-5} M; C_S = 7.318 × 10^{-3} M); (H) nordiazepam (C_D = 8.304 × 10^{-5} M; C_S = 2.433 × 10^{-3} M); (I) oxazepam (C_D = 3.67 × 10^{-5} M; C_S = 3.61 × 10^{-4} M); (J) tamazepam (C_D = 7.26 × 10^{-5} M; C_S = 9.727 × 10^{-3} M).

of a degree of distinction among the members of the group. Strong spectral similarities exist for lorazepam and oxazepam, each of which has a hydroxyl group at position R_3, and between diazepam and flurazepam each of which has alkyl substituents at position R_4. The nitro substituents at R_1 in clonazepam and nitrazepam contribute towards a totally new Cotton band of positive sign at longer wavelengths. The spectrum for the β-CD/diazepam complex in strong acid [2] bears a strong resemblance to the spectrum in strong alkali, with the latter being more intense.

The circular dichroism spectra are entirely due to the complex because, when separate, both the free drug and the sugar molecules are optically inactive in the wavelength range of study. The data were processed according to the method described in an earlier publication [3], which amounts to an iterative calculation based on the equations

$$(b[D][S]/\psi) = \{([D] + [S] - [DS])/\theta_{DS}\} - (1/K_{DS}\theta_{DS}) \quad (1)$$

$$K_{DS} = [DS]/[D][S] \quad (2)$$

$$C_D = [D] + [DS]; C_S = [S] + [DS] \quad (3)$$

The calculation is terminated when successive values of K_{DS} and θ_{DS} are invariant. In the equations [D] and [S] refer to the equilibrium drug and sugar concentrations, C_D and C_S are their respective analytical concentrations, b is the cell path length which was 1 cm throughout the study, and ψ is the experimentally measured induced ellipticity. For lorazepam, the values of K_{DS} at other temperatures are 1139 (15°C) and 815 (35°C) from which the calculated values of ΔH and $\Delta S°$ are −2.96 kcal mol^{-1} and 3.6 cal mol^{-1} deg^{-1}, respectively. These thermodynamic values are typical of many others from previous work and further confirm the hydrophobic nature of the center of the sugar structure. None of the other analogs was examined.

The θ_{DS} values found in this interaction are considerably larger than the values already reported for the barbiturate/β-CD associations [4]. The lowest value of 72 observed for nitrazepam is a factor of three greater than the highest barbiturate value, namely 27 for hexobarbital. However, the wider range in θ_{DS} for the benzodiazepin-2-ones suggests a stronger structural dependence. The range of values for K_{DS} is not as broad but the stabilities are on the whole greater than those observed for the barbiturates. This is also true for the comparison of the results for diazepam in 0.1 M hydrochloric acid (K_{DS} = 83; θ_{DS} = 151) [2] versus the present data. One other stability comparison which can be made and which might have a bearing on the later discussion is that for lorazepam in the analogous complexation reaction with γ-cyclodextrin. When offered the larger central cavity of the gamma analog, the stability was observed to decrease by a factor of ten, K_{DS} = 96.

All of the structural variations needed completely to interpret the stability dependence are not satisfied by choosing only eight representatives from the series. Some consistent arguments can, however, be made within the chosen subset, which involves ten single substitution steps converging on three

disubstituted derivatives. First of all, a general trend of increasing stability and decrease in induced ellipticity is observed relative to the values for the designated parent, nordiazepam. When the substituent changes are considered individually, the effects are greatest for R_1 and R_4. This observation is inconsistent with previous results in that it has been generally believed that aromatic rings are the most often preferred guests in the hydrophobic cavity [6], and that a tri-substituted aromatic ring is less likely to be enclosed than a di-substituted one [2, 4]. However, both changes affect the N at position 1, R_4 directly and R_1 by an increase in the electron-withdrawing power on the N lone pair when the substituent is changed from Cl to NO_2, which centers attention on the role of the seven-membered diazo ring.

A better feeling for the structural implications for the complexation reaction comes from comparisons of the changes in K_{DS} and θ_{DS} for reactions involving identical substitution steps. The values are grouped according to the changes in Table 2. When R_1 is changed from Cl to NO_2 (1a and 1b), or R_2 is changed from H to Cl (2a and 2b), the changes in K_{DS} are similar in magnitude and sign implying that the steps are additive and that these centers of activity are remote from the binding site. In contrast, substitutions at R_3 (3a to 3b) and R_4 (4a to 4b) produce irregular changes in K_{DS} suggesting that the diazo ring is directly involved with the sugar on complexing. The data for the interaction of lorazepam with γ-CD adds little which is new, in that one has begun to expect a decrease in the stability of the complex with increasing cavity size.

Data for the two remaining analogs appear to support this interpretation in that for flurazepam the increase in chain length for R_4 leads to a decrease in K_{DS}. This assumes that the effects of Cl or F at position R_3 have similar effects on the rest of the molecule as does phenyl alone. This is not seriously in error because *o*-halophenyl substituents are known to have electron-directing properties similar to phenyl itself. Medazepam has no ketone group and once again the change in θ_{DS} is more representative of the effect observed for changing either R_1 or R_4.

The structural subtleties of molecular association are never fully understood no matter how impartial is the attempt to choose model compounds. Apparent inconsistencies arise when comparisons are made between different guests, such as has occurred in this case between the barbiturates and the benzodiazepin-2-ones, which only serves to point up the limitations of our understanding of such interactions. An aliphatic side chain was preferred in one case but not in the other. Frank [7] has used β-CD as a model system for interpreting the structural selectivities of enzymatic interactions with molecular substrates. Extrapolation from one system to another should be made with caution.

Equilibrium constants for the Valium and Dalmane complexations with β-CD must be known in order to assay the total drug concentration in the commercial products from the measured ellipticities, because the observed values are proportional to the concentrations of the complexed form, [DS],

TABLE 2

Changes in formation constants and induced molar ellipticities with substituents

Substitution step	Substituent change	ΔK_{DS}	$\Delta\theta_{DS}$
1a	Cl to NO_2	+346	−933
1b	Cl to NO_2	+197	−487
2a	H to Cl	+482	−418
2b	H to Cl	+333	+28
2b	H to Cl	+359	−88
3a	H to OH	+436	−254
3b	H to OH	+313	+52
3b	H to OH	−61	−12
4a	H to CH_3	+75	−787
4b	H to CH_3	−422	−545

only. A calibration curve could be prepared to obtain the concentration of the complex by interpolation of the experimentally measured ellipticity, but it is just as convenient to substitute [DS] with ψ/θ_{DS} for the 1-cm cell and solve Eqns. 2 and 3 by microcomputer. Centrifugation is the only separation step in the procedure and it was conveniently done on an instrument with a maximum rpm of 1500. There was no evidence for spectral interferences from other components co-extracted from the products which were either inherently active in circular dichroism or had had activity induced by complexation with β-CD. This is apparent from the similarities between the circular dichroism spectra for the standards and the extracts shown in Fig. 2. None of the other soluble or insoluble ingredients was identified. Because heats of reaction are relatively small, close temperature control is not necessary in the performance of an assay, and the K_{DS} values at 25°C can be used for the ambient conditions. For aliquots taken from any individual tablet or capsule after grinding, the reproducibility in the assay results was better than ±0.2%. The results of the assays for different units taken from the same lot number were found to be 4.94 ± 0.08 mg for Valium and 29.3 ± 0.6 mg for Dalmane, both of which are within ±2% of the prescription amounts. One obvious advantage of the present method over others is that a sophisticated separation procedure is not necessary. While a single assay may take 20 min to complete, simultaneous multiple assays can subsequently be done at a rate of ten per hour if a whole spectral scan is performed, and more frequently if data are taken at a single wavelength.

It is expected that the equilibrium data presented here will also be useful for chromatographic studies of the separation of isomers with cyclodextrins as the chiral stationary phases.

We acknowledge the gift of the various benzodiazepin-2-one standards by Hoffmann-LaRoche.

REFERENCES

1 J. M. Bowen and N. Purdie, Anal. Chem., 53 (1981) 2239.
2 S. M. Han and N. Purdie, Anal. Chem., 56 (1984) 2822.
3 S. M. Han and N. Purdie, Anal. Chem., 56 (1984) 2825.
4 W. M. Atkinson, S. M. Han and N. Purdie, Anal. Chem., 56 (1984) 2827.
5 N. Purdie and K. A. Swallows, Anal. Chem., 59 (1987) 1349.
6 V. W. Saenger, Angew. Chem., 92 (1980) 343.
7 S. G. Frank, J. Pharm. Sci., 64 (1975) 1585.

Analytica Chimica Acta, 197 (1987) 65—70
Elsevier Science Publishers B.V., Amsterdam — Printed in The Netherlands

CRYOGENIC-TEMPERATURE FLUORESCENCE SPECTROSCOPY OF POLYNUCLEAR AROMATIC HYDROCARBONS OF MOLECULAR WEIGHT 328

ANDERS L. COLMSJÖ

Department of Analytical Chemistry, Arrhenius Laboratory, University of Stockholm, S-106 91 Stockholm (Sweden)

(Received 8th October 1986)

SUMMARY

Quasi-linear fluorescence spectra of polynuclear aromatic hydrocarbons with a molecular weight of 328 were recorded at cryogenic temperatures. Thirteen of the sixteen compounds studied showed fluorescence spectra with quasilines at 63 K. Of these, six compounds exhibited highly resolved and intense spectra when dissolved in n-hexane.

Polynuclear aromatic hydrocarbons (PAHs) comprise a group of compounds exhibiting various important biological and chemical properties [1] including mutagenic and carcinogenic effects, rigid and stable chemical structures and a number of unusual spectroscopic properties. The commoner sensitive methods of detection such as mass spectrometry, flame ionization detection, electron-capture detection, room-temperature fluorescence and ultraviolet absorption techniques only give a hint of the structure of such compounds. Therefore, more convincing methods must be used in order to establish the structure of unknown compounds. For example, high-resolution fluorescence techniques can be used based on the Shpol'skii effect [2—4], as has been demonstrated in recent work [5] where PAHs with a molecular weight of 302 were studied and detected in complex samples. In this paper, cata-condensed PAHs with a molecular weight of 328 are described in a similar way with respect to their quasi-linear fluorescence spectra.

EXPERIMENTAL

The sample compartment and the optical set-up were as described previously [6]. The recording unit consisted of an amplifier, a 12-bit A/D converter and an ABC-800 microcomputer, making possible signal treatment, spectral calculations and the storage of spectra on diskettes. Noise reduction as well as wavelength calibration and plotting were done by the computer. The compounds used in this work were either commercially available or obtained from other laboratories.

0003-2670/87/$03.50

RESULTS AND DISCUSSION

There are 39 possible isomers of PAHs with a molecular weight of 328 consisting of systems with six fused benzene rings (Fig. 1). Of these, 16 compounds were available for this study. The solvent used in this and former studies, has, as far as possible, been n-hexane, in order to keep the number of parameters in the spectral library as small as possible. Most compounds that emit quasi-linear fluorescence have proven to do so in n-hexane and the number of multiplets is usually kept to a minimum, in contrast with, for example the results obtained when n-heptane is used as solvent.

The high resolution of the cryogenic-temperature fluorescence spectra is a major advantage for conducting identification studies in unknown samples. Furthermore, if the method is to be used in routine analysis, sensitivity plays an important role. In general, sensitivities at the picogram level can be achieved when the system and method used [6] are applied to compounds exhibiting quasi-linear fluorescence. Important factors that might limit the sensitivity are the molar absorptivity, quantum efficiency, Debye-Waller factor and solubility. The last property is of crucial interest when large molecules are being studied. The solubilities of the PAHs with a molecular weight of 328 are known to be low in most solvents [7]. Very approximately,

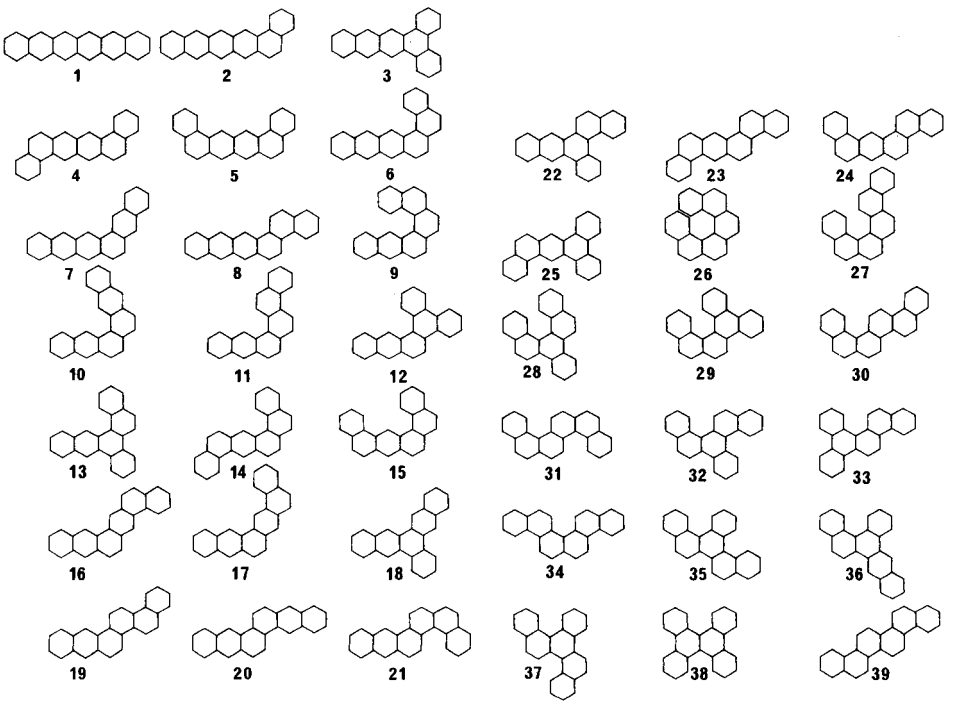

Fig. 1. Isomers of molecular weight 328 consisting of six fused benzene rings.

the minimum solubility required for recording spectra with the system used was estimated to be in the range 0.1—10 pg μl^{-1}. Obviously this limit was well exceeded by most of the compounds studied, yielding high signal-to-noise ratios for saturated solutions. However, the solubility was sufficiently low to prevent the possibility of recording spectra beyond the linear region. Thus with the system used, even saturated solutions of most PAHs with molecular weight 328 cannot cause distortion of a fluorescence spectrum as a result of too high a concentration in n-hexane. One exception is phenanthro(9,10-1)phenanthrene (compound 38, Fig. 1). This solubility limiting factor will shortly be tested on PAHs with even larger molecular weights.

The low-temperature fluorescence properties of the compounds studied are summarized in Table 1. The resolution of the spectra is denoted by a scale +, ++ and +++ rather than by the Debye-Waller factor [8] which is difficult to calculate for incompletely resolved spectra. As in the case of most subgroups of PAHs, large variations can be found among the separate compounds with respect to intensity, resolution and spectral region of their fluorescence spectra. Several compounds are also reported as being weakly or non-fluorescent with respect to the instrumental set-up used. Thus, a compound exhibiting weak, broad-band fluorescence even at cryogenic temperatures will appear to be an even weaker (or zero) emitter in a high-resolution monochromator system. Consequently, compounds such as hexacene and

TABLE 1

Some fluorescence parameters for PAHs of molecular weight 328

Compound number in Fig. 1	Short name[a]	Resolution[b]	Emission maximum (nm)	Excitation wavelength (nm)
1	Hexacene	—	—	—
2	B(a)Pentacene	—	—	—
3	Phe(9,10-b)A	+++	440.1	317
6	Phe(4,3-b)A	++	480.7	331
7	A(1,2-b)A	+	465.1	359
8	Phe(1,2-b)A	++	468.5	313
13	B(c)N(1,2-a)A	+	362.4	322
16	Phe(2,3-a)A	+++	421.9	323
18	B(c)N(2,3-a)A	+++	410.1	317
19	Phe(2,1-a)A	+	400.9	320
20	A(2,1-a)A	+	421.2	308
23	B(h)N(2,1-a)A	+++	398.8	352
25	TB(a,c,h)A	+++	386.6	303
26	Phe(3,4-c)Phe	—	—	—
38	Phe(9,10-1)Phe	+++	381.4	350
39	Phe(2,1-a)Phe	++	370.8	332

[a] A = anthracene/anthraceno, B = benzo, Phe = phenathrene/phenanthro, N = naphtho. [b] +, ++, +++ indicate increasing resolution.

benzo(a)pentacene are reported as being non-fluorescent (Table 1). In contrast, more compact compounds within the group (compounds with a low length-to-breadth ratio) generally exhibit well resolved, low-temperature fluorescence spectra.

Simple and very well resolved spectra were recorded from compounds such as tribenzo(a,c,h)anthracene (Fig. 2A), benzo(a)naphtho(2,1-h)an-

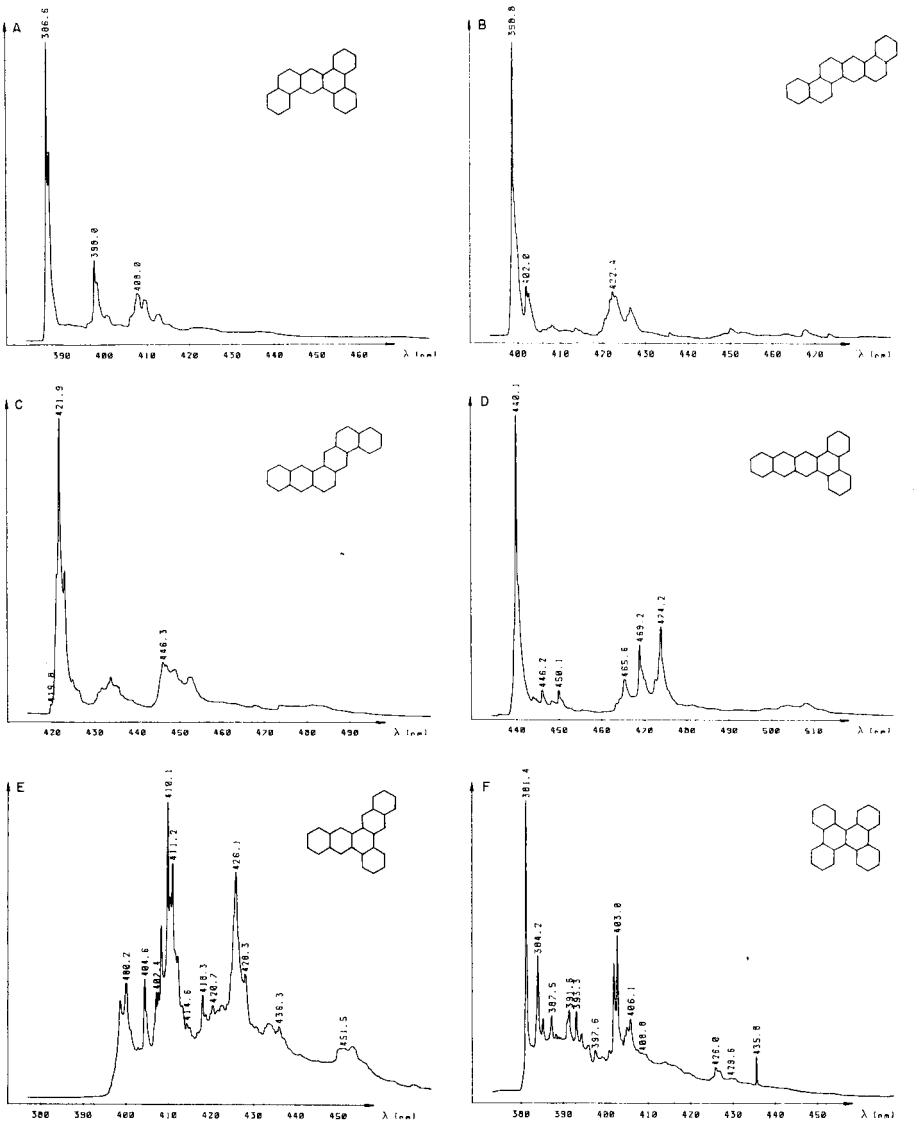

Fig. 2. Fluorescence spectra of polynuclear aromatic hydrocarbons in n-hexane at 63 K: A, tribenzo(a,c,h)anthracene; B, benzo(a)naphtho(2,1-h)anthracene; C, phenanthro(2,3-a)anthracene; D, phenanthro(9,10-b)anthracene; E, benzo(c)naphtho(2,3-a)anthracene; F, phenanthro(9,10-1)phenanthrene.

thracene (Fig. 2B), phenanthro(2,3-a)anthracene (Fig. 2C) and phenanthro(9,10-b)anthracene (Fig. 2D). It may be noted that these all have dibenzo(a,c)anthracene or dibenzo(a,h)anthracene as substructures. The latter compounds are known to exhibit well resolved quasi-linear spectra with simple structures under the same conditions. Another compound in this subgroup is benzo(c)naphtho(2,3-a)anthracene (Fig. 2E), the fluorescence spectrum of which exhibits a more complex, but still quasi-linear, structure. The 0-0′ transition is relatively small, possibly indicating a higher degree of symmetry for the compound. Among the compounds with highly resolved spectra, phenanthro(9,10-1)phenanthrene exhibits a spectrum with complex structure (Fig. 2F).

Figure 3 shows the quasi-linear spectra of anthraceno(1,2-b)anthracene and phenanthro(4,3-b)anthracene, the latter having a slightly better resolved spectrum. The similarity between the two spectra is striking, both having similar vibronic patterns and intensity distributions of the vibronic-coupled emission bands. The influence of the additional benzene ring, which comprises the difference in structure between the compounds, seems to be similar in the two cases, yielding spectra with differences more reminiscent of those caused by substitution.

Another compound reported as being weakly or non-fluorescent is phenanthro(3,4-c)phenanthrene (compound 26, Fig. 1). This might be due to the non-planar structure of the compound, which commonly suppresses the quantum efficiency of a PAH. Benzo(c)phenanthrene is also known to be a non-planar compound with low quantum efficiency.

One of the interesting observations in this study is that most of the compounds exhibit quasi-linear fluorescence spectra in n-hexane. According to the basic and most accepted theory for explaining the Shpol'skii fluorescence, the solutes must fit into the crystal matrix if the phonon bands are not to dominate the spectrum. This is in most cases interpreted as being due to the solute molecules having approximately the same dimensions as the solvent

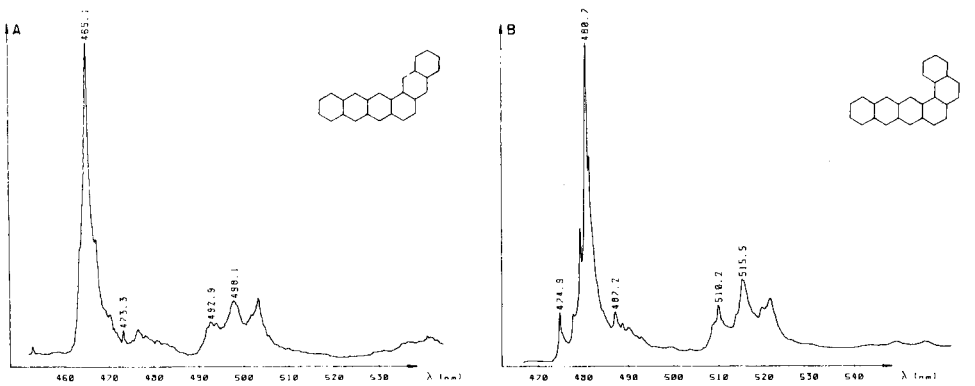

Fig. 3. Fluorescence spectra in n-hexane at 63 K: A, anthraceno(1,2-b)anthracene; B, phenanthro(4,3-b)anthracene.

molecules, the latter being replaced in the crystal by trapped solutes. This way of explaining the effect is probably a simplification of the true state, considering that compounds with from two to six fused benzene rings can emit quasi-linear fluorescence in the same solvent.

This investigation shows the applicability of cryogenic-temperature fluorescence even within groups of compounds for which it is difficult to achieve sensitive quantitation identification by other means. The limiting factor for the moment is the lack of standard compounds, which are difficult to obtain.

The author thanks Stephen Wise for supplying standard compounds and Beryl Holm for reviewing the manuscript.

REFERENCES

1 M. L. Lee, M. V. Novotny and K. D. Bartle, in Analytical Chemistry of Polycyclic Aromatic Compounds, Academic Press, New York, 1981.
2 E. V. Shpol'skii, A. A. Illina and L. A. Klimova, Dokl. Akad. Nauk. SSSR, 87 (1952) 955.
3 E. J. Bowen and B. J. Brocklehurst, J. Chem. Soc., (1954) 3875.
4 A. L. Colmsjö and C. E. Östman, in Atlas of Shpol'skii Spectra and Other Low Temperature Spectra of POM, University of Stockholm, 1981.
5 A. L. Colmsjö and S. A. Wise, Ana. Chim. Acta, 187 (1986) 129.
6 A. L. Colmsjö and U. Stenberg, Anal. Chem., 51 (1979) 145.
7 E. Clar, in Polycyclic Hydrocarbons, Academic Press, New York, 1964.
8 W. C. McColgin, A. P. Marcletti and J. H. Eberly, J. Am. Chem. Soc., 100 (1979) 5622.

Analytica Chimica Acta, 197 (1987) 71—75
Elsevier Science Publishers B.V., Amsterdam — Printed in The Netherlands

CRYOGENIC-TEMPERATURE FLUORESCENCE SPECTROSCOPY OF POLYNUCLEAR AROMATIC HYDROCARBONS OF MOLECULAR WEIGHT 378

ANDERS L. COLMSJÖ

Department of Analytical Chemistry, Arrhenius Laboratory, University of Stockholm, S-10691 Stockholm (Sweden)

(Received 14th November 1986)

SUMMARY

Quasi-linear fluorescence spectra were recorded at 63 K from polynuclear aromatic hydrocarbons with molecular weights of 378, consisting of seven cata-condensed benzene rings. The sensitivity of the method used is clearly sufficient for nine well resolved spectra to be recorded, even though the solubility of the compounds is low in most solvents.

Methods of identifying and quantifying polynuclear aromatic hydrocarbons (PAHs) have attracted much interest during the last decade, and a number of sophisticated analytical methods have been developed [1]. Among these, the chromatographic and spectroscopic properties of the PAHs have been utilized for selective extraction, separation, identification and quantification of individual isomers. For several reasons, the PAHs investigated have mainly been those with a molecular weight up to 300, even though it has been shown that various samples contain PAHs of higher molecular weight [2, 3].

A method for identifying high-molecular-weight PAHs has previously been described for compounds with six fused benzene rings of molecular weight 302 and 328 [4, 5]. In this paper, the selective identification of PAHs with a molecular weight of 378 is discussed, i.e., compounds consisting of seven fused cata-condensed benzene rings. This can again be done with the aid of Shpol'skii fluorimetry, which is a cryogenic-temperature fluorescence technique [6, 7] capable of transforming an ordinary broad-banded fluorescence spectrum at room temperature to a well resolved, quasi-linear spectrum at cryogenic temperatures [8].

EXPERIMENTAL

Both the sample compartment and the optical set-up were as described previously [9]. The recording unit consisted of an amplifier, a 12-bit A/D converter and an ABC-800 microcomputer, and provided signal treatment,

0003-2670/87/$03.50

spectral calculations and the storage of spectra on diskettes. Noise reduction, wavelength calibration and plotting were done by the computer.

RESULTS

The cryogenic fluorescence data for 20 compounds of molecular weight 378 studied are summarized in Table 1. These compounds, the structures of which are given in Fig. 1, are mostly substituted anthracenes or phenanthrenes. Resolution of the spectra is graded on a scale from + to +++, as before [4, 5]. A number of low-intensity spectra of uncertain origin are denoted by w for weak resolution or simply omitted (—).

One of the most interesting points was to establish if the sensitivity of the system was sufficiently high to obtain quasi-linear spectra from PAHs of molecular weight 378. Primarily, solubility was expected to be a strongly limiting factor in addition to the classical parameters such as quantum efficiency, molar absorptivity and Debye-Waller factor. Very approximately, the minimum solubility required for spectra to be recorded with the system used was calculated to be in the range 0.1—10 pg μl^{-1}. Obviously this limit was well exceeded by most of the compounds studied, yielding high

TABLE 1

Fluorescence properties of compounds in Fig. 1

Compound No.	Short name[a]	Resolution[b]	Emission maximum (nm)	Excitation wavelength (nm)
1	TetraB(a,c,h,j)A	++	381.5	335
2	DiN(2,1-a:1,2-j)A	+++	401.4	324
3	DiN(2,3-a:2,3-c)A	+++	404.7	319
4	DiN(2,1-a:2,1-h)A	—	—	—
5	A(2,3-a)Naphthacene	—	—	—
6	DiN(2,1-a:1,2-h)A	+++	412.0	331
7	DiB(a,c)N(2,1-h)A	+++	394.4	317
8	DiB(a,c)pentacene	—	—	—
9	A(2,1-a)B(h)A	++	413.6[c]	325
10	DiB(a,1)pentacene	—	—	—
11	DiN(1,2-b:1,2-h)A	+	460.4	339
12	DiN(2,3-a:2,3-h)A	+++	432.3	336
13	DiB(a,c)N(1,2-i)A	++	425.5	327
14	DiN(2,3-a:2,3-i)Phe	++	413.3[c]	330
15	A(2,1-a)B(j)A	—	—	—
16	DiB(a,c)N(1,2-h)A	+++	406.2	323
17	B(h)Phe(2,3-a)A	+++	422.2	323
18	DiN(1,2-b:1,2-j)A	++	450.6	329
19	B(h)diN(2,1-a:2,1-c)N	w	—	—
20	DiN(1,2-b:2,1-h)A	++	451.2	331

[a] A = anthracene/anthraceno, B = benzo, Phe = phananthrene/phenanthro, N = naphtho. [b] w = weak intensity; +, ++, +++ indicate increasing resolution. [c] Spectra derived from the same compound with a diffuse maximum.

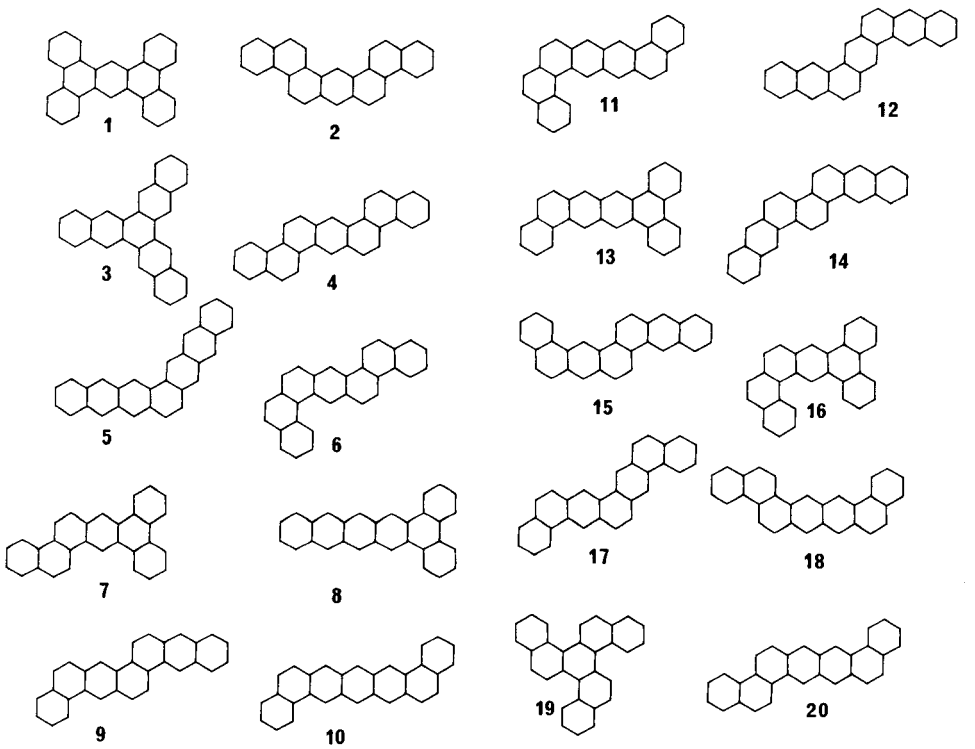

Fig. 1. Isomers of molecular weight 378 investigated.

signal-to-noise ratios for saturated solutions. Moreover, no distortion of spectra arising from any excessive concentration was observed, even though saturated solutions were used.

The solvent used throughout the investigation was n-hexane, for the reasons given previously [4, 5]. Furthermore, because of the number of spectra recorded earlier with n-hexane as solvent, it is possible to identify spectra derived from impurities. This would constitute an obvious risk in studying spectra from high-molecular-weight compounds. So far, the purity of the compounds has appeared to be very high. It would be expected, from the general theory of phonon-less emission lines, that n-hexane is too small a molecule for perfect inclusion of the host molecules in the crystal lattice, thus leading to broad-band emission. However, this is not the case. Many excellently resolved spectra were recorded even though the dimensions of the solvent molecule were much smaller than those of the solute. Compounds with moderately resolved spectra (++), when dissolved in an n-alkane with a longer carbon chain (n-undecane), mostly gave the same or less resolution of the spectrum. A saturated solution of a PAH with a molecular weight of 378 in n-undecane, however, usually showed a more intense spectrum than in n-hexane, because of slightly increased solubility.

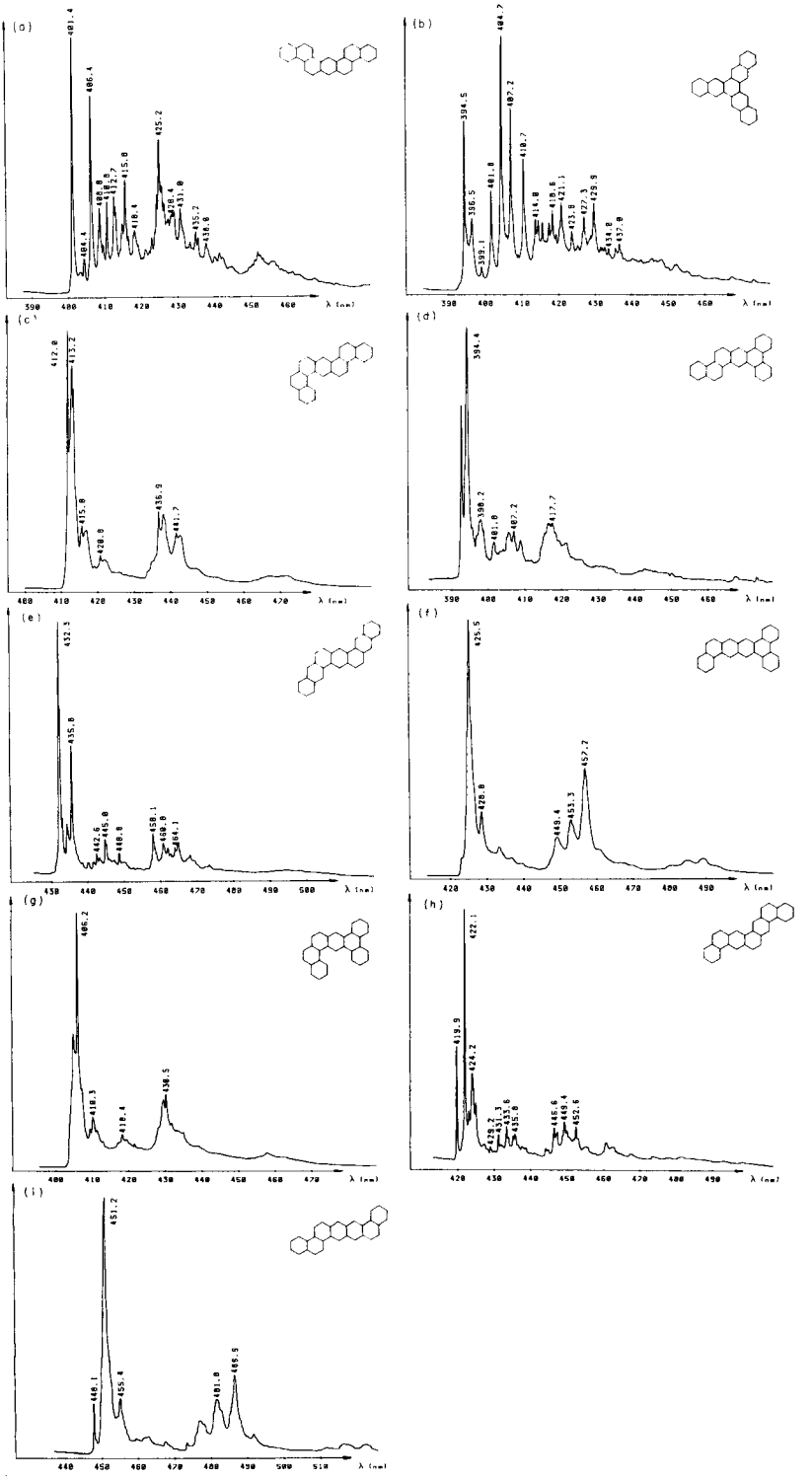

Fig. 2. Fluorescence spectrum of polynuclear aromatic hydrocarbons in n-hexane at 63 K: a, dinaphtho(2,1-a:1,2-j)anthracene; b, dinaphtho(2,3-a:2,3-c)anthracene; c, dinaphtho-(2,1-a:1,2-h)anthracene; d, dibenzo(a,c)naphtho(2,1-h)anthracene; e, dinaphtho(2,3-a:2,3-h)anthracene; f, dibenzo(a,c)naphtho(1,2-i)anthracene; g, dibenzo(a,c)naphtho(1,2-h)-anthracene; h, benzo(h)phenanthro(2,3-a)anthracene; i, dinaphtho(1,2-b:2,1-h)anthracene.

Nine well-resolved spectra are shown in Fig. 2. Very well resolved spectra with numerous quasi-lines of high intensity were obtained from dinaphtho-(2,1-a:1,2-j)anthracene (compound 2; Fig. 2a), dinaphtho(2,3-a:2,3-c)anthracene (compound 3; Fig. 2b), dinaphtho(2,3-a:2,3-h)anthracene (compound 12; Fig. 2e) and benzo(h)phenanthro(2,3-a)anthracene (compound 17; Fig. 2h). As in the case of the six-ring cata-condensed PAHs, well resolved spectra were recorded for compounds having dibenzo(a,c)anthracene or dibenzo(a,j)anthracene as sub-structures, provided that the length-to-breadth ratio was not too large. Thus, if the solubility of a compound with a sub-structure of dibenzo(a,c)anthracene or dibenzo(a,j)anthracene is high enough, the low-temperature fluorescence spectrum of the compound is usually highly resolved. Dibenzo(a,c)naphtho(1,2-i)anthracene (compound 13) was the only compound studied which fulfilled the described sub-structure, and yet had only a resolution denoted by ++.

Unfortunately, the spectra derived from anthraceno(2,1-a)benzo(h)anthracene (compound 9) and dinaphtho(2,3-a:2,3-i)phenanthrene (compound 14) were almost identical, strongly suggesting that one of the compounds had not been properly synthesized. This kind of ambiguity has occurred in most of the investigations of quasi-linear fluorescence of different groups of PAHs made during the last decade at this laboratory, and this emphasizes the versatility of the method for distinguishing between isomeric forms.

Finally, a number of well resolved spectra are shown in Fig. 2c, d, f, g and i. All these spectra are unusual with respect to the spectra recorded earlier (representing more than 200 compounds) but a few striking similarities can be observed. The structure and wavelength interval of the cryogenic fluorescence spectrum of dibenzo(a,c)naphtho(2,1-h)anthracene (compound 7) is similar to, but fully distinguishable from, that of dibenzo(a,e)pyrene [4]. Furthermore, the spectrum of dibenzo(a,c)naphtho(1,2-h)anthracene (compound 16) resembles that of a substituted naphtho(2,3-e)pyrene (but slightly red-shifted) [4].

The author thanks Stephen Wise for supplying standard compounds and Beryl Holm for reviewing the manuscript.

REFERENCES

1 M. L. Lee, M. V. Novotny and K. D. Bartle in Analytical Chemistry of Polycyclic Aromatic Compounds, Academic Press, New York, 1981.
2 M. L. Lee, P. A. Peaden, Y. Hirata and M. Novotny, Anal. Chem., 52 (1980) 2268.
3 T. Romanowski, W. Funcke, J. König and E. Balfanz, J. High Resolut. Chromatogr. Chromatogr. Commun., 4 (1981) 209.
4 A. L. Colmsjö and S. A. Wise, Anal. Chim. Acta., 187 (1986) 129.
5 A. L. Colmsjö, Anal. Chim. Acta, 197 (1987) 65.
6 E. V. Shpol'skii, A. A. Illina and L. A. Klimova, Dokl. Akad. Nauk. SSSR, 87 (1952) 955.
7 E. J. Bowen and B. J. Brocklehurst, J. Chem. Soc., (1954) 3875.
8 A. P. D'Silva and V. A. Fassel, Anal. Chem., 56 (1984) 985A.
9 A. L. Colmsjö and U. Stenberg, Anal. Chem., 51 (1979) 145.

Analytica Chimica Acta, 197 (1987) 77—85
Elsevier Science Publishers B.V., Amsterdam — Printed in The Netherlands

KINETIC SPECTROPHOTOMETRIC DETERMINATION OF INDIUM/GALLIUM MIXTURES

ANTONIA MARÍN, MANUEL SILVA and DOLORES PÉREZ-BENDITO*

Department of Analytical Chemistry, Faculty of Sciences, University of Córdoba, 14004 Córdoba (Spain)

(Received 26th July 1986)

SUMMARY

A kinetic method is presented for the determination of 0.5—5 $\mu g\ ml^{-1}$ gallium based on its activating effect on the copper(II)-catalyzed oxidation of 4,4′-dihydroxybenzophenone thiosemicarbazone by hydrogen peroxide. The reaction is monitored spectrophotometrically at 415 nm. Two sets of reaction conditions are established; one for the direct determination of gallium, and another, in which indium affects the gallium response, for determination of indium. Mixtures of these cations can be determined at $\mu g\ ml^{-1}$ levels and in gallium/indium ratios from 7.5:1 to 1:1.6, with an accuracy and precision of ca. 4.5%.

Various analytical methods for the individual determination of gallium and indium have been developed [1, 2], but kinetic methods have rarely been applied to such determinations. Catalytic [3] and catalytic titration methods [4—6] as well as measurements of fluorescence lifetime [7] have been reported for the kinetic determination of both metal ions. There are a few kinetic methods for the determination of inorganic ions based on their activating effects on several catalyzed non-enzymatic reactions, such as selenium and tellurium [8], mercury [9] and zinc [10]. This paper reports the kinetic determination of gallium/indium mixtures based on their activating effect on the copper(II)-catalyzed oxidation of 4,4′-dihydroxybenzophenone thiosemicarbazone (DBPT) by hydrogen peroxide.

EXPERIMENTAL

Reagents

All experiments were done with analytical-reagent grade chemicals and pure solvents. 4,4′-Dihydroxybenzophenone thiosemicarbazone solutions, 0.1 and 0.3% (w/v), were prepared by dissolving the compound in ethanol. The compound was synthesized by condensation of 4,4′-dihydroxybenzophenone with thiosemicarbazide [11]. Standard gallium solution ($0.9610\ g\ l^{-1}$) was prepared by dissolving gallium chloride (Merck) in 1% (v/v) hydrochloric acid and standardizing by titration with EDTA (8-quinolinol as fluorimetric

0003-2670/87/$03.50

indicator) [12]. Standard indium solution (5.2280 g l^{-1}) was prepared by dissolving the appropriate amount of indium chloride (Merck) in 1% (v/v) hydrochloric acid and standardizing gravimetrically with ammonia [13]. Stock copper(II) solution (1.0260 g l^{-1}) was prepared by dissolving copper sulphate pentahydrate (Merck) in distilled water. It was standardized iodimetrically. These solutions were diluted as required, immediately prior to use.

Apparatus

All spectrophotometric measurements were made on a Perkin-Elmer Lambda 5 spectrophotometer fitted with a device for kinetic measurements and 1-cm quartz cells. The cell compartment was thermostatted by a Peltier system. A PHM 62 pH meter was used with a combined glass/calomel electrode. A Hewlett-Packard HP-85 computer was also used.

Procedures

Determination of gallium. Copper(II) (1.00 μg), the sample volume needed to give a final gallium concentration between 0.5 and 1.5 μg ml^{-1}, 1 ml of 0.45 M ammonium chloride/1.75 M ammonia buffer (pH 9.80), 1.5 ml of 0.3% (w/v) DBPT solution, 3 ml of ethanol and 0.5 ml of 2.4% (v/v) hydrogen peroxide were mixed in that order in a 10-ml volumetric flask and made up to volume with distilled water. A portion of the reaction mixture was immediately transferred to a 1-cm thermostatted cell at 45 ± 0.1°C and the absorbance was recorded at 415 nm as a function of time. The measurements were started exactly 2 min after addition of the oxidant. The rate measured in the absence of gallium was used as a reference. The reaction rate was calculated from the absorbance/time curves and the calibration graph was obtained by linear regression analysis.

Determination of gallium/indium mixtures. Synthetic samples containing various trace concentrations of gallium and indium were determined by two kinetic runs. For a sample containing 5—15 μg of gallium and 2—8 μg of indium, the above procedure enabled gallium to be determined, because indium does not interfere under these conditions. In a second experiment, 1.00 μg of copper(II), 2 ml of 0.1% (w/v) DBPT solution, 2 ml of 0.3% (v/v) hydrogen peroxide, 2 ml of 0.45 M ammonium chloride/1.75 M ammonia buffer (pH 9.80), and the sample volume needed to give a final indium concentration between 0.2 and 0.8 μg ml^{-1} and amounts of gallium between 10 and 50 μg were added in that order and made up to volume in a 10-ml volumetric flask with distilled water. Measurements were made as above, and the indium concentration was established as described below.

RESULTS AND DISCUSSION

Activating effect of gallium

The oxidation of 4,4'-dihydroxybenzophenone thiosemicarbazone (DBPT) by hydrogen peroxide in an ammoniacal medium is catalyzed by copper(II),

and the reaction rate may be measured by the change in the absorbance of the oxidation product at 415 nm [14]. A recent paper described the activating effect of indium on this redox-catalyzed reaction [15]. In this paper, the activating effect of gallium on the same reaction is studied in order to develop a kinetic determination as a prior step for the resolution of indium/gallium mixtures.

The activating effect of gallium on the absorption spectrum obtained for the copper-catalyzed reaction after a reaction time of 5 min is shown in Fig. 1. As can be observed, the oxidation of DBPT is enhanced by the presence of gallium. This activating effect is corroborated by the fact that the reaction does not occur in the absence of the catalyst, copper(II).

Effect of reaction variables

The kinetic determination of gallium(III) is linked to several variables which should be studied and fixed in order to obtain more accurate and reproducible results. The influence of these variables was studied by using initial rate/concentration plots. Likewise, the partial orders for each variable were calculated from the resulting log-log plot. These orders are shown in brackets in Fig. 2.

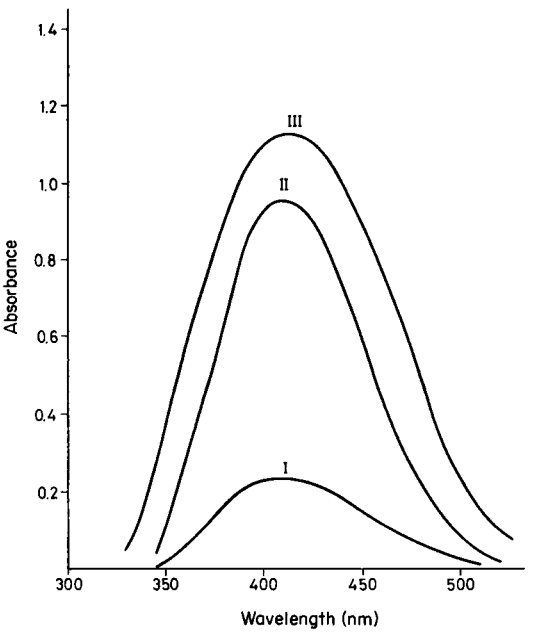

Fig. 1. Activating effect of gallium on the copper(II)-catalyzed oxidation of DBPT by hydrogen peroxide: (I) uncatalyzed reaction; (II) reaction catalyzed by 100 ng ml^{-1} copper(II); (III) as (II) but also activated by 1.5 μg ml^{-1} gallium. Reaction conditions as in Procedure; spectra recorded after 5-min reaction.

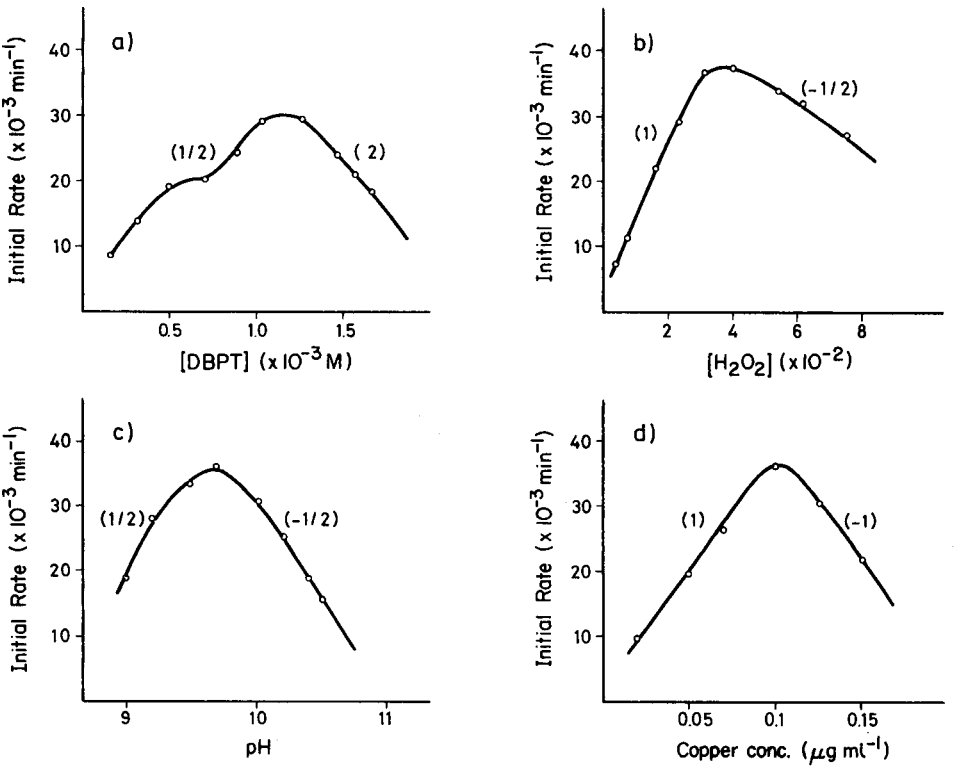

Fig. 2. Effect of chemical variables on the activating effect of gallium (1.0 μg ml^{-1}): (a) DBPT; (b) H_2O_2; (c) pH; (d) Cu^{2+}. (Partial orders are given in parentheses.)

The temperature was varied over the range 20—60°C. The gallium-activated reaction proceeded more quickly as temperatures increased, but became almost constant at 35—45°C. Therefore, 45°C was chosen for the final procedure. The activation energy calculated from the rates was ca. 23.8 kJ mol^{-1}.

The gallium-activated reaction rate was studied as a function of DBPT concentration in the range 0.2—1.6 × 10^{-3} M. The initial rate increased with increasing DBPT concentration up to 1.1 × 10^{-3} M (Fig. 2a) above which it decreased. A concentration of 1.1 × 10^{-3} M DBPT (1.5 ml of 0.3% (w/v) solution) was selected for the determination of gallium. An increase in the hydrogen peroxide concentration up to 4 × 10^{-2} M caused an increase in the initial rate with a first-order dependence (Fig. 2b). Greater concentrations result in a decreased reaction rate. A hydrogen peroxide concentration of 4 × 10^{-2} M (0.5 ml of 2.4% (v/v) solution) was chosen for all subsequent studies.

In order to optimize the concentration of ammonia, its initial concentration was varied in the range 0.017—0.350 M while keeping the concentrations of all the other ingredients constant, and the initial rate measured for each

concentration. From this study, 0.175 M ammonia was chosen as optimum, because smaller and higher values resulted in sharply decreased rates (reaction orders of 2 and −2). This concentration of ammonia was achieved by addition of 1 ml of 0.45 M ammonium chloride/1.75 M ammonia buffer (pH 9.80).

Although the ammonia and pH dependences are not separable, owing to the high concentration of "ammonia" in the reaction medium, its concentration can be considered constant. The variations observed in the initial rate can be attributed to the kinetic dependence on the proton. Thus, the optimum pH found was 9.80 (Fig. 2c) and the reaction order was ½ and −½ for hydrogen ion at pH values below and above 9.80, respectively. This pH value was achieved with 1.0 ml of the above-mentioned buffer solution. Absorbance/time plots for solutions containing different amounts of copper(II) were recorded. A first-order reaction was found for copper concentrations up to 0.1 μg ml^{-1} (1.6×10^{-6} M) above which the order found was −1 (Fig. 2d). Ethanol, ionic strength and order of addition of the reagents did not affect the development of the copper-catalyzed reaction [14]. For the gallium-activated reaction, however, variations in the ethanol concentration between 15 and 55% (v/v) increased the initial rate 2.4 times. Thus, the activating effect of gallium is greatly enhanced by increased ethanol content. Variations in the ionic strength from 0.02 to 0.25 M decreased the rate by ca. 25%. The order of addition of the reagents must be controlled in order to obtain the maximum initial rate and precision. This order, as indicated above, should be copper(II)/gallium/ammonia/DBPT/oxidant.

The effect of the dielectric constant of the solvent on the reaction rate has been described in the literature and is given by the Kirkwood equation [16], which predicts that as the dielectric constant increases, the rate of reaction between two ions with opposite charges decreases. Similar conclusions can be drawn for increases in the ionic strength [17]. From these studies and from the dependence of the initial rate on the ethanol concentration and ionic strength, it can be assumed that an interaction of two ions with opposite charges is the rate-determining step [16, 17].

The initial rate shows a first-order dependence on gallium concentration. There are two linear ranges, one between 0.5 and 1.5 μg Ga ml^{-1}, and another between 1.5 and 5.0 μg ml^{-1} with less sensitivity. The first range was used for the kinetic determination of gallium.

Rate equation

According to the kinetic study, the following rate equation is suggested for the activating effect of gallium on the copper(II)-catalyzed oxidation of DBPT by hydrogen peroxide in an ammoniacal medium:

$$d[DBPT]_{ox}/dt = k[DBPT]^{1/2}[H_2O_2][NH_3]^2[H^+]^{1/2}[Cu^{2+}][Ga^{3+}]$$

where $[DBPT]_{ox}$ is the concentration of the oxidized reagent and k is the rate constant for the activated reaction. The concentration ranges for each variable in which the kinetic equation is applicable are indicated in Table 1.

TABLE 1

Summary of kinetic dependencies for the gallium-activated reaction (V_0 is the initial rate)

Concentration range (M)	Dependence of V_0	Concentration range (M)	Dependence of V_0
2.0×10^{-4}—1.1×10^{-3}	$[DBPT]^{1/2}$	1.6×10^{-10}—1.0×10^{-9}	$[H^+]^{1/2}$
5.0×10^{-3}—4.0×10^{-2}	$[H_2O_2]$	3.9×10^{-7}—1.6×10^{-6}	$[Cu^{2+}]$
1.7×10^{-2}—1.7×10^{-1}	$[NH_3]^2$	7.2×10^{-6}—2.1×10^{-5}	$[Ga^{3+}]$

A comparison with the rate equation for the non-activated catalyzed reaction [14]:

$$d[DBPT]_{ox}/dt = k_1[DBPT]^{-1}[H_2O_2][NH_3][H^+][Cu^{2+}]$$

reveals a change in the sign of the order with respect to DBPT.

Kinetic determination of gallium

The features of the calibration graphs and precision obtained by the initial rate, fixed-time (4 min) and fixed-concentration (0.100 absorbance) methods are shown in Table 2. On account of the greatest precision and widest determination range of the initial-rate method, this was chosen for the kinetic determination of gallium. The detection limit thus achieved, calculated as the value corresponding to three standard deviations of the blank (catalyzed reaction), was 52 ng Ga ml^{-1}.

The effect of many common species was examined to find possible interferences. The tolerance to the species investigated is given in Table 3. Foreign species were added at a maximum level of 100 $\mu g\ ml^{-1}$ (tolerance ratio to gallium, 100). The tolerance ratio for each species was taken as the largest amount yielding an error less than ±5% by the initial-rate method for 1.0 $\mu g\ ml^{-1}$ gallium. Although various ions interfere at the same level as gallium, these generally are not associated with it in real samples, except for aluminium, which must be removed. The high tolerance to indium (up to twice the weight of gallium) is utilized for the resolution of indium/gallium mixtures, as decribed in the next section.

TABLE 2

Figures of merit for the determination of gallium with various types of kinetic measurement

Measurement method	Range ($\mu g\ ml^{-1}$)	Slope (sensitivity)	Corr. coeff. ($n = 6$)	R.s.d. (%)[a]
Initial rate	0.50—1.50	3.33×10^{-2} ml min^{-1} μg^{-1}	0.998	3.1
Fixed time	0.50—1.25	3.09×10^{-2} ml μg^{-1}	0.997	6.9
Fixed concentration	0.75—1.25	6.89×10^{-2} ml min^{-1} μg^{-1}	0.997	6.1

[a]For 11 measurements of 1.0 $\mu g\ Ga^{3+}\ ml^{-1}$.

TABLE 3

Tolerance limits (w/w) for foreign ions in the determination of 1.0 μg ml^{-1} gallium

Tolerance ratio to gallium	Ion
100	NO_3^-, NO_2^-, Cl^-, ClO_2^-, SO_4^{2-}, Br^-, K^+, Na^+
50	AsO_4^{3-}, Ca^{2+}, Ba^{2+}, Sr^{2+}
10	I^-, SCN^-, Co^{2+}, Bi^{3+}
5	EDTA, Fe^{3+}, Zn^{2+}, Cr^{3+}
2	Mg^{2+}, SeO_3^{2-}, Ce^{4+}, In^{3+}, F^-, WO_4^{2-}
1	MoO_4^{2-}, Al^{3+}, Ni^{2+}, Pb^{2+}
<1	CrO_4^{2-}, PO_4^{3-}, tartrate, Mn^{2+}, Cd^{2+}, Ag^+

Kinetic determination of indium/gallium mixtures

In order to determine indium/gallium mixtures, use is made of the following properties. In the kinetic determination of gallium alone, twice its amount of indium is tolerated. When gallium is determined under the experimental conditions for indium alone [15] the sensitivity is decreased, but is greatly enhanced if indium is also present. This effect was studied in order to be of use for the resolution of these mixtures. Several calibration plots of reaction rate vs. gallium concentration for different fixed amounts of indium were recorded. The results (Fig. 3) show that the slope decreases with increase in the indium concentration. There is a direct relationship between the slope

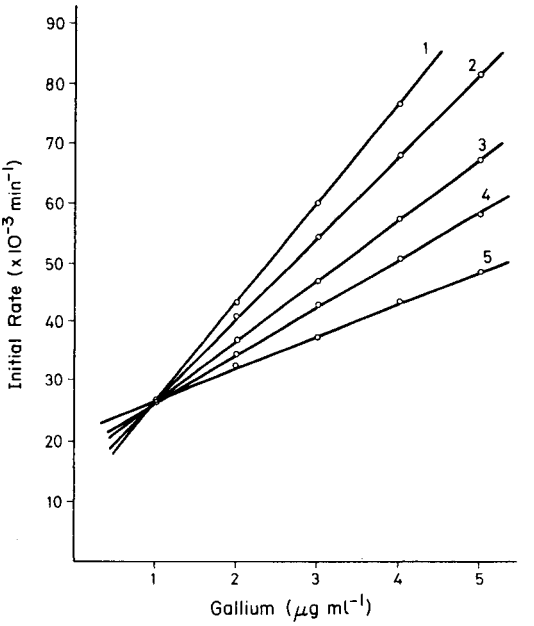

Fig. 3. Calibration plots of initial rate vs. gallium concentration in the presence of the following amounts of indium: (1) 0.0; (2) 0.2; (3) 0.4; (4) 0.6; (5) 0.8 μg ml^{-1}.

of the calibration plot for gallium (Fig. 3) and the indium concentration, i.e., $S = 0.0167 - 0.016\,[In^{3+}]$ where S is the slope of the plot in ml μg^{-1} min^{-1} and the indium concentration is expressed in $\mu g\ ml^{-1}$.

The determination of indium/gallium mixtures is done in two steps. First, the gallium is determined by the first procedure given, which tolerates twice as much indium as gallium. Once the gallium concentration has been evaluated, several known amounts of gallium are added to portions of the sample and the corresponding calibration plot is obtained under the recommended conditions for the second procedure (see Experimental). The slope, S of this graph is measured and the indium concentration is calculated from the equation for S.

The results obtained for several synthetic mixtures of indium and gallium are summarized in Table 4. The determination of gallium/indium mixtures is feasible in the weight ratio range 7.5:1 to 1:1.6. When the recommended procedure was applied to a series of eleven samples with 0.5 $\mu g\ ml^{-1}$ each of indium and gallium, the relative standard deviation (r.s.d.) of the method was 5.5% for indium and 4.2% for gallium. The effects of foreign ions are shown in Table 5. Silver, cadmium and manganese interfere most strongly, but they can easily be separated from indium and gallium.

TABLE 4

Analysis of synthetic mixtures of indium and gallium

Metal taken ($\mu g\ ml^{-1}$)		Indium found ($\mu g\ ml^{-1}$)	Error (%)	Gallium found ($\mu g\ ml^{-1}$)	Error (%)
Indium	Gallium				
0.80	0.50	0.74	−7.5	0.51	2.0
0.50	0.50	0.48	−4.0	0.49	−2.0
0.20	0.50	0.20	0.0	0.51	2.0
0.20	1.00	0.21	5.0	1.06	6.0
0.20	1.50	0.19	−5.0	1.50	0.0

TABLE 5

Tolerance limits (w/w) for foreign ions in the determination of 0.5 $\mu g\ ml^{-1}$ indium and 0.5 $\mu g\ ml^{-1}$ gallium

Tolerance ratio	Ion added
50	Na^+, K^+, Sr^{2+}, Ca^{2+}, Ba^{2+}, AsO_4^{3-}
10	Co^{2+}, Bi^{3+}
5	Fe^{3+}, Cr^{3+}, Zn^{2+}
2	SeO_3^{2-}, Ce^{4+}
1	MoO_4^{2-}, WO_4^{2-}, Mg^{2+}, Pb^{2+}, Al^{3+}, Ni^{2+}
<1	Ag^+, Cd^{2+}, Mn^{2+}

The authors gratefully acknowledge the financial support of the CAICyT.

REFERENCES

1 Z. Marczenko, Separation and Spectrophotometric Determination of Elements, 2nd. edn., Horwood, Chichester, 1986.
2 F. D. Snell, Photometric and Fluorimetric Methods of Analysis. Metals. Part 1, Wiley, New York, 1978.
3 M. C. Mehra and G. Verret, Microchem. J., 25 (1980) 228.
4 H. Weisz and T. Kiss, Z. Anal. Chem., 249 (1970) 302.
5 T. Kiss, Mikrochim. Acta, (1973) 847.
6 T. Kiss, Mikrochim. Acta, Part II, (1975) 471.
7 H. Keizo, M. Kiyotoshi and K. Shirai, Anal. Chim. Acta, 97 (1978) 121.
8 S. P. Klochvskii and G. D. Klochvskaya, Zh. Anal. Khim., 32 (1978) 736.
9 S. P. Klochvskii and G. D. Klochvskaya, Zh. Anal. Khim., 33 (1979) 1749.
10 A. Moreno, M. Silva, D. Perez-Bendito and M. Valcárcel, Analyst, 108 (1983) 85.
11 F. Toribio, J. M. López-Fernandez, D. Pérez-Bendito and M. Valcárcel, Quim. Anal. (Spain), 1 (1982) 21.
12 R. H. A. Crawley, Anal. Chim. Acta, 19 (1958) 540.
13 L. Erdey, Gravimetric Analysis, Part 2, Pergamon, Oxford, 1965, p. 595.
14 J. L. Ferrer-Herranz and D. Pérez-Bendito, Anal. Chim. Acta, 132 (1981) 157.
15 J. L. Ferrer-Herranz and D. Pérez-Bendito, Quim. Anal. (Spain), 3 (1983) 40.
16 K. J. Laidler, Chemical Kinetics, 2nd edn., McGraw-Hill, New York, 1965.
17 M. Kopanika and V. Stara, in G. Svehla (Ed.), Kinetic Methods in Chemical Analysis, Vol. XVIII of Comprehensive Analytical Chemistry, Elsevier, Amsterdam, 1983.

Analytica Chimica Acta, 197 (1987) 87—95
Elsevier Science Publishers B.V., Amsterdam — Printed in The Netherlands

DETERMINATION OF TRACE ELEMENTS IN GALLIUM ARSENIDE BY GRAPHITE-FURNACE ATOMIC ABSORPTION SPECTROMETRY AFTER PRETREATMENT IN GAS STREAMS

I. S. BUSHEINA, J. B. HEADRIDGE* and D. JOHNSON
Department of Chemistry, The University, Sheffield S3 7HF (Great Britain)
K. W. JACKSON[a] and C. W. MCLEOD
Department of Chemistry, Sheffield City Polytechnic, Sheffield S1 1WB (Great Britain)
J. A. ROBERTS
Philips Research Laboratories, Redhill, Surrey, RH1 5HA (Great Britain)
(Received 3rd October 1986)

SUMMARY

Atomic absorption spectrometry (AAS) with a resistively-heated graphite furnace is used for the determination of chromium (0.3—1 atom/10^6 atom) in chromium-doped gallium arsenide after pretreatment in a separate furnace in a stream of argon to remove arsenic, and of manganese and silver (0.03 and 0.04 atom/10^6 atoms, respectively) by a similar procedure after pretreatment with argon and chlorine, the latter to remove both gallium and arsenic as volatile chlorides. Results for chromium were in agreement with those obtained by furnace AAS after dissolution and by spark-source mass spectrometry (SSMS) but AAS after dissolution is more precise. Results for manganese and silver obtained by both gas pretreatments were in good agreement, but were higher than those obtained for presparked material by SSMS, indicating that surface contamination of gallium arsenide was not completely removed by the etching methods used. The procedures established that the concentrations of bismuth, indium and lead in the gallium arsenide sample were below the limits of detection of 3×10^{-3}, 10×10^{-3} and 1×10^{-3} atom/10^6 atoms, respectively. In all cases, calibration graphs were constructed from data obtained with aqueous solutions of appropriate salts.

The electrical properties of semiconductors are closely related to the concentrations of certain trace elements in them. Sometimes a trace impurity within the range 10^{-2}—10^2 atoms/10^6 atoms [ppm (atomic)] is deliberately added as a dopant but there is also interest in determining the concentrations of impurities in the base material itself at concentrations as low as 10^{-4} atoms/10^6 atoms. Determining such low levels of impurities is a formidable task for the analytical scientist and at levels below 0.1 atom/10^6 atoms, few techniques have the required sensitivity. Among these are spark-source mass spectrometry (SSMS), neutron activation analysis and graphite-furnace atomic absorption spectrometry (AAS) with the introduction of solid

[a]Present address: Department of Chemistry, University of Saskatchewan, Saskatoon, Canada.

0003-2670/87/$03.50

samples, which can be used for a range of elements unique to each technique and matrix. Graphite-furnace AAS after dissolution is not quite sensitive enough. Taddia and Lanza [1] quote a limit of detection of 0.06 ppm (atomic) for chromium in gallium arsenide with such a technique.

Graphite-furnace AAS of solid samples has been applied in the Sheffield laboratories for the determination of trace elements in fairly homogeneous materials such as metals [2—6] and glasses [7] with relative standard deviations in the range 5—20% and limits of detection [in approximate ppm (atomic) units] as follows: indium (0.02), thallium (0.001), lead (0.006), antimony (0.02), selenium (0.04), zinc (0.009) and cadmium (0.001) all in nickel-base alloys, bismuth (0.004) and tellurium (0.01) both in copper, and silver (0.0007) in glass. Hence it can be seen that the technique has the sensitivity needed for the determination of more volatile ultra-trace elements in semiconductors at concentrations which can be as low as 10^{-3} ppm (atomic).

In the studies with metals and glasses, the base elements usually had much lower volatilities than the trace elements being determined. However, with some semiconductor materials, including gallium arsenide, a base element is released into the vapour phase at temperatures below 1200°C. This means that very large background absorption can occur when graphite-furnace AAS is used for the determination of trace elements in solid samples of some semiconductors. Normally, a deuterium background corrector cannot correct for such high background absorbances. However, good results have been achieved with either Zeeman or Smith-Hieftje background correction. Hadeishi and Kimura [8] were able to determine a range of elements in solid gallium arsenide by graphite-furnace AAS with Zeeman background correction with the following limits of detection: manganese 0.008, chromium <0.6, copper <0.2 and silver <0.03 atoms/10^6 atoms. Calibration was achieved with solutions of appropriate salts and the furnace was operated under near isothermal conditions. Johnson et al. [9] determined chromium in solid gallium arsenide by graphite-furnace AAS with Smith-Hieftje background correction with a limit of detection of 0.03 atoms/10^6 atoms.

With both methods the interior of the furnace becomes grossly contaminated with arsenic. Investigations were undertaken in this laboratory to see if some or all of the base material could be removed by passing a suitable gas over the gallium arsenide in a separate tube furnace before introducing the solid residue into the cuvette for AAS. In this way, undesirable contamination of the furnace with volatile base elements would be minimized.

Removal of base elements from materials by volatilization in gas streams has been reviewed recently [10]. Suitable gases are argon, chlorine and oxygen. Argon is used when a base element can be volatilized at a relatively low temperature with involatile trace elements remaining in the furnace boat. Chlorine and oxygen are used to convert the elements in the sample to chlorides and oxides, respectively. The volatile chloride or oxide of a base element is removed at a relatively low temperature and less volatile chlorides or oxides of trace elements remain in the furnace boat. In the Sheffield University

laboratory, pretreatment of gallium arsenide with argon or chlorine has been used before the furnace boat is introduced into a graphite cuvette for AAS.

Preliminary investigations showed that gallium arsenide decomposes in a stream of argon at 1150°C with the volatilization of most of the arsenic. The residue is a globule of gallium (b.p. 2403°C). Some elements that are not volatile at 1150°C with their respective boiling points (°C) indicated are indium (2080), lead (1740), antimony (1750), bismuth (1560), silver (2212), chromium (2672), manganese (1962), iron (2750) and copper (2567). It should be possible to determine these elements in the gallium globule by AAS with appropriate heating programs above 1500°C.

It was found that both gallium and arsenic reacted with a chlorine/argon mixture (1 + 5, v/v) at 250°C with the removal of their volatile chlorides in the gas stream. The reaction with undiluted chlorine at this temperature is too vigorous. Arsenic trichloride and gallium trichloride boil at 130°C and 201°C, respectively. Some chlorides not volatile at this temperature, with their respective boiling points (°C) indicated, are silver chloride (1150), lead(II) chloride (950) and manganese(II) chloride (1190). Many anhydrous trichlorides including chromium trichloride are volatile in chlorine at elevated temperatures. In fact, it was found in this study that chromium trichloride was lost from a sample of gallium arsenide along with the base elements on chlorination at 250°C.

Methods are reported here for the determination of chromium in chromium-doped gallium arsenide and ultra-trace concentrations (<0.1 atoms/10^6 atoms) of manganese and silver in gallium arsenide.

EXPERIMENTAL

Gallium arsenide samples

Gallium arsenide slices were provided by Philips Research Laboratories. They were degreased in hot xylene (AristaR grade, BDH Chemicals) and rinsed thoroughly in deionized water. They were placed separately in a small volume of deionized water and a mixture of concentrated nitric and hydrochloric acids (3 + 1; AristaR) was added until the gallium arsenide began to dissolve with the evolution of brown fumes. The etching process was continued for ca. 1 min and the reaction was quenched by adding more deionized water. The gallium arsenide slices were rinsed thoroughly in deionized water and left to dry between filter papers.

A slice was shattered into smaller fragments by placing it on pieces of ashless filter paper, covering with more filter paper and then with tissue paper, and tapping firmly with a small hammer near the centre of the slice. The central pieces were removed by tweezers and again shattered between filter papers until tiny fragments of the semiconductor slice remained, which were suitable for solid-sample AAS. The samples were stored in clean specimen tubes to prevent contamination.

Standard solutions

The stock standard solution (1 mg ml^{-1}) of chromium (as potassium chromate) was prepared in deionized water. Manganese, silver, and lead stock standards (1 mg ml^{-1}) were prepared in 1% (v/v) nitric acid, bismuth in 5% (v/v) nitric acid and indium in 1% (v/v) hydrochloric acid. More dilute standard solutions for calibration graphs were prepared daily from these by appropriate dilution. Their compositions are shown in Table 1.

Apparatus

A Varian-Techtron AA6 atomic absorption spectrometer fitted with a BC6 deuterium lamp background corrector was used in conjunction with an Instrumentation Laboratory IL-555 controlled-temperature furnace Atomizer and a J. J. Instruments CR-552 chart recorder. A sample was placed in the cavity of a pyrolytically-coated graphite microboat, shaped like a small tray, which fitted into the side of the square-sectioned pyrolytically-coated graphite cuvette in the furnace. A damping time constant of 0.26 s was used on the amplifier output of the AA6.

The furnace for pretreatment of gallium arsenide flakes with argon or chlorine was an electrically-heated tube furnace (Amalgams Co., Sheffield, Type T2-12-2) capable of reaching a maximum temperature of 1200°C. It contained a silica tube (75 cm long × 2.5 cm diameter) into which a silica boat (16 cm long × 1.3 cm wide × 0.8 cm deep) could be placed. This boat could accommodate 15 microboats for the IL-555 furnace. High-purity argon or the chlorine/argon mixture (1 + 5, v/v) was passed through concentrated sulphuric acid contained in two Dreschel bottles before entering the furnace.

Procedures

Pretreatment method with argon alone. Select 15 graphite microboats. Introduce one of these into the slot of the cuvette of the IL-555 furnace and heat repeatedly to 2800°C (a step followed by a 5-s hold) with the spectrometer setting shown in Table 2 until there is no blank peak for the element under study. Remove the boat from the furnace and place in the silica boat. Repeat this process with the other 14 boats until all are clean and lined up in the silica boat.

Remove suitably-sized gallium arsenide pieces (see Table 3) from the specimen tube and weigh each accurately to 0.01 mg. Place these in positions

TABLE 1

Composition of calibration solutions for use in the IL-555 furnace

Element	Element conc. ($\mu g\ ml^{-1}$)	Acid conc. (%, v/v)	Element	Element conc. ($\mu g\ ml^{-1}$)	Acid conc. (%, v/v)
Chromium	0.03—0.09	HNO_3 (1)	Bismuth	1	HNO_3 (5)
Manganese	0.1	HNO_3 (1) or HCl (1)	Indium	1	HNO_3 (2)
Silver	0.1	HNO_3 (1) or HCl (5)	Lead	0.1	HNO_3 (1) or HCl (5

TABLE 2

Spectrometer settings for solids, aqueous standards and blanks

Element determined	Lamp current (mA)	Resonance line (nm)	Slit width (nm)
Chromium	5	357.9	1.0
Manganese	5	279.5	0.4
Silver	5	328.1	1.0
Bismuth	8	223.1	0.4
Indium	4	303.9	0.8
Lead	5	283.3	1.0

TABLE 3

Sample size and heating programs for the IL-555 furnace

Element (and form)	Sample size	Heating program[a]
Cr (solid)[b]	2—10 mg	R 750(10), H (10), R 2750(5), H (5)
Cr (aqueous)[c]	10 μl	R 70(15), R 120(15), then as Cr solid[b]
Mn (solid)[b]	5—8 mg	R 75(10), R 175(10), R 500(15), R 1100(15), S 2250, H (5)
Mn (aqueous)[c]	1—5 μl	As Mn solid[b]
Mn (solid)[d]	5—9 mg	R 75(10), R 150(15), R 500(15), R 1000(15), S 2250, H (5)
Mn (aqueous)[e]	1—5 μl	As Mn solid[d]
Ag (solid)[b]	4—6 mg	R 300(15), R 750(5), S 2450, H (15)
Ag (aqueous)[c]	0.5—3 μl	R 75(15), R 120(15), then as Ag solid[b]
Ag (solid)[d]	5—9 mg	R 500(15), R 750(5), R 2750(5), H (20)
Ag (aqueous)[e]	1—4 μl	R 75(15), R 120(15), then as Ag solid[d]
Bi (solid)[b]	3—6 mg	R 500(10), R 600(5), R 2000(5), H (10)
Bi (aqueous)[c]	0.5—4 μl	R 75(15), R 120(15), then as Bi solid[b]
In (solid)[b]	3—6 mg	R 250(10), R 600(10), R 2000(5), H (5)
In (aqueous)[c]	1—7 μl	R 75(15), R 120(15), then as In solid[b]
Pb (solid)[b]	5—10 mg	R 500(15), R 600(5), S 2000, H (15)
Pb (aqueous)[c]	1—10 μl	R 75(15), R 120(15), then as Pb solid[b]
Pb (solid)[d]	10—18 mg	As Pb solid[b]
Pb (aqueous)[e]	1—6 μl	As Pb aqueous[c]

[a]R, ramp to the temperature given over (t) seconds; H(t), hold for (t) seconds; S, step to the temperature given. All temperatures are in °C. [b]After pretreatment in argon. [c]Standard solutions of metal in nitric acid used for calibration graphs to determine trace element in argon-treated gallium arsenide. [d]After pretreatment in chlorine/argon mixture. [e]Standard solutions of metal in hydrochloric acid used for calibration graphs to determine trace element in chlorine/argon-treated gallium arsenide.

2, 3, 5, 6, 8, 9, 11, 12, 14 and 15 of the series of microboats. Leave positions 1, 4, 7, 10 and 13 empty for blanks. Always manipulate samples with plastic-tipped tweezers to prevent possible surface contamination. Slide the silica boat into the silica furnace tube.

Pass argon through the furnace at 750 ml min^{-1} and raise the temperature to 1150°C. Maintain this temperature for 40 min. Switch off the furnace. Each microboat which contained a gallium arsenide flake then contains a gallium globule. Allow the furnace to cool to near room temperature, stop the flow of argon and pull the silica boat backwards out of the furnace. Arsenic from the gallium arsenide flakes will have deposited at the cool end of the silica tube beyond the position occupied by the silica boat.

Pretreatment method with chlorine/argon mixture. Proceed as in the method with argon alone for the first two paragraphs. Then pass a mixture of chlorine (100 ml min^{-1}) and argon (500 ml min^{-1}) through the furnace tube and raise its temperature to 250°C. Maintain this temperature for 40 min and then switch off the furnace. Each microboat, which contained a gallium arsenide flake, will appear to be empty. When the furnace has cooled to near room temperature, stop the flow of chlorine and, after 1 min, stop the flow of argon. Pull the silica boat backwards out of the furnace. Arsenic and gallium trichlorides will have deposited at the other end of the silica tube beyond the hot zone.

Measurement of trace elements in solid residues from pretreated samples. Set up the atomic absorption spectrometer and furnace as outlined in the instruction manual with the instrumental parameters shown in Table 2. Set the heating program for the element as given in Table 3. Obtain recordings of absorbance vs. time for each of the 15 microboats. Measure the areas of all absorbance peaks obtained. If the five "blank" microboats produced absorbance peaks, average their areas to give the blank for the determination. Subtract the blank, if there is one, from the area of each peak obtained from the residues. Obtain the mass of element producing each peak area, corrected for the blank, from the appropriate calibration graph and calculate the concentration of trace element in the sample in $\mu g\ g^{-1}$. Average the ten concentrations and calculate their standard deviation. If necessary, convert the concentrations to ppm (atomic) from the expression: $(\mu g\ g^{-1}) \times M/m$, where M is the average relative atomic mass for the atoms in gallium arsenide [(69.7 + 74.9)/2 = 72.3] and m is the relative atomic mass of the trace element.

Construction of calibration graphs. At appropriate spectrometric settings (see Table 2), heat a graphite microboat in the IL-555 furnace repeatedly to 2800°C until there is no blank for the element under study. Pipette a suitable volume (Table 3) of a standard solution of the element (Table 1) into the microboat and obtain the absorbance peak by use of the heating program shown in Table 3. This program is identical to that for solids except that a drying stage is added if not already incorporated. Repeat the operation six times with various masses of element. Measure each peak area corrected for any acid blank and obtain a calibration graph of peak area vs. mass of element.

Determination of chromium in gallium arsenide after dissolution. Weigh accurately ca. 100 mg of chromium-doped gallium arsenide pieces into a 10-ml PTFE beaker. Add 0.4, 1.1 and 1.5 ml of concentrated hydrochloric

acid, concentrated nitric acid and water, respectively, and warm the beaker on a hot-plate until moderate effervescence occurs. When dissolution is complete, evaporate to 1 ml, transfer the solution and washings to a calibrated plastic tube (1.5 ml), and dilute to the mark.

Prepare a similar solution from an undoped gallium arsenide sample to produce a matrix-matched "blank". Use the spectrometer settings shown in Table 2 and obtain the peak areas for seven 10-μl portions of each solution with the following heating program for the furnace: ramp to 70°C over 15 s, ramp to 120°C over 15 s, ramp to 800°C over 15 s, hold for 5 s, ramp to 2750°C over 10 s, hold for 5 s. Subtract the average blank from the average signal for the solutions prepared from chromium-doped gallium arsenide.

Apply the same heating program to 10-μl portions of standard aqueous chromium solutions within the range 5—50 ng ml^{-1} and 1% (v/v) in nitric acid, prepare a calibration graph of peak area, corrected for any acid blank, vs. mass of chromium, and calculate the chromium content of the sample.

RESULTS AND DISCUSSION

Calibration graphs for chromium, manganese, silver, bismuth, indium and lead were straight lines through the origin. The masses producing 1% absorption were 9 pg of chromium, 2 pg of manganese in nitric acid or 4 pg in hydrochloric acid, 1.5 pg of silver in nitric acid or 3.0 pg in hydrochloric acid, 18 pg of bismuth, 34 pg of indium, and 13 pg of lead in nitric acid or 9 pg in hydrochloric acid.

Results for the determination of chromium and ultra-trace elements in gallium arsenide are shown in Tables 4 and 5. It can be seen from Table 4 that the chromium contents obtained by graphite-furnace AAS after pretreatment of the gallium arsenide with argon at 1150°C are in good agreement with those obtained by the other two methods, verifying that calibration with aqueous standards is permissible. The graphite microboats for the IL-555 furnace act as platforms and allow the release of atomic vapours into a more isothermal argon atmosphere than in normal furnace AAS. However, the new

TABLE 4

Chromium contents of gallium arsenide determined by three different methods

Sample	Chromium content found[a] (atom/10^6 atoms)		
	AAS of solids after pretreatment with argon	AAS after dissolution	SSMS
1	0.37 ± 0.09	0.33 ± 0.02	0.36
2	0.46 ± 0.08	0.55 ± 0.06	0.60
3	0.95 ± 0.22	0.99 ± 0.11	1.20
4	<0.015	—	<0.01

[a]Mean ± SD (n = 10 for solids and n = 7 for solutions).

method is less precise than AAS after dissolution partly because the chromium is not homogeneously distributed within the gallium arsenide samples. Inhomogeneous distribution will be reflected in a higher relative standard deviation (*RSD*) for smaller samples. Samples of 2—10 mg were used in the new method but 100-mg samples were taken for dissolution. Also, chromium appears to be less homogeneously distributed in gallium arsenide (average *RSD* = 21%) than many trace elements in alloys and glasses, typical average *RSD*s for similar methods of analysis being 10% and 8% for lead in nickel-base alloys [6] and glasses [7], respectively. For the determination of chromium in chromium-doped gallium arsenide, the method involving dissolution before AAS is to be preferred.

For the determination of ultra-trace elements in gallium arsenide, however, methods involving dissolution before furnace AAS are usually not sensitive enough and methods involving direct measurements on solids have to be used. It can be seen from Table 5 that the results for manganese and silver after pretreatment of the solid sample with argon or chlorine are in good agreement. However, it is clear that a light etch of sample 5 with nitric and hydrochloric acids did not remove all of the manganese surface contamination because the apparent manganese content is considerably in excess of that determined by spark-source mass spectrometry, where the surface is removed during presparking. For analysis of the other samples in Table 5 a heavier etching was employed. The results for silver are probably high also because of slight surface contamination. Replating of more noble metals on to clean gallium arsenide surfaces can occur when etching solutions are diluted prior to their removal by decantation. When trace elements are determined at concentrations below 0.1 atom/10^6 atoms, great care must also be taken to prevent contamination of clean semiconductor surfaces and graphite microboats from airborne dust particles. If at all possible, work should be done in a clean room with filtered air.

No chromium, bismuth, indium or lead was detected in sample 4; concen-

TABLE 5

Results for the determination of ultra-trace elements in gallium arsenide by three different methods

Element	Sample	Concentration found[a] (atom/10^6 atoms)		
		AAS of solid after pretreatment with Ar	AAS of solid after pretreatment with Cl_2/Ar	SSMS[b]
Manganese	5	0.040 ± 0.007[c]	0.033 ± 0.006[c]	<0.006
Silver	6	0.040 ± 0.004	0.036 ± 0.005	<0.02
Bismuth	4	<0.003	—	<0.03
Indium	4	<0.010	—	<0.03
Lead	4	<0.0012	<0.0014	<0.006

[a]Mean ± SD (n = 10). [b]Surface removed during presparking, before SSMS. [c]Lightly etched.

trations less than the limits of detection are reported. For chromium and lead, these were calculated from twice the standard deviation of peak areas obtained from the five "blank" microboats. These small chromium or lead absorption peaks were equal in area to those of the pretreated gallium arsenide samples. For bismuth and indium, the limits of detection were estimated from the following formula [5]: limit of detection ($\mu g\ g^{-1}$) = (characteristic mass × 0.2 × average *RSD*)/sample mass (g). An average *RSD* of 14%, the average for manganese and silver in Table 5, was used in the formula. The limits of detection of the method are comparable with those for spark-source mass spectrometry, and concentrations of certain ultra-trace elements at 10^{-2} atom/10^{-6} atoms could certainly be determined. Pretreatment of gallium arsenide to remove most of the arsenic and leave a gallium globule containing trace elements led to much less contamination of the furnace and allowed the use of deuterium background correction.

Concentrations of ultra-trace elements at 10^{-4} atom/10^{6} atoms still lie well below the limits of detection of the present method. It might be possible to pretreat 1-g samples of gallium arsenide with chlorine on a larger sample boat for introduction to a specially designed furnace for AAS with expected lower limits of detection for lead and certain other elements but, eventually, a versatile method for multi-element ultra-trace determination at such low levels in semiconductors may be based on inductively-coupled plasma mass spectrometry or other non-spark ablation techniques followed by mass spectrometry.

We thank the Science and Engineering Research Council and Philips Research Laboratories for the award of a studentship to D. Johnson, and the University of El-Fateh, Libya, for a studentship for I. S. Busheina.

REFERENCES

1 M. Taddia and P. Lanza, Anal. Chim. Acta, 159 (1984) 375.
2 A. A. Baker, J. B. Headridge and R. A. Nicholson, Anal. Chim. Acta, 113 (1980) 47.
3 A. A. Baker and J. B. Headridge, Anal. Chim. Acta, 125 (1981) 93.
4 I. S. Busheina and J. B. Headridge, Anal. Chim. Acta, 142 (1982) 197.
5 J. B. Headridge and R. A. Nicholson, Analyst, 107 (1982) 1200.
6 I. S. Busheina and J. B. Headridge, Anal. Chim. Acta, 174 (1985) 339.
7 J. B. Headridge and I. M. Riddington, Analyst, 109 (1984) 113.
8 T. Hadeishi and H. Kimura, J. Electrochem. Soc., 126 (1979) 1988.
9 D. Johnson, J. B. Headridge, C. W. McLeod, K. W. Jackson and J. A. Roberts, Anal. Proc., 23 (1986) 3.
10 K. Bächmann, Talanta, 29 (1982) 1.

Analytica Chimica Acta, 197 (1987) 97—104
Elsevier Science Publishers B.V., Amsterdam — Printed in The Netherlands

DETERMINATION OF SELENIUM IN HUMAN TISSUES BY ATOMIC ABSORPTION SPECTROMETRY

JOANNA FAIRHURST*, BARBARA LLOYD and H. T. DELVES

Department of Chemical Pathology and Human Metabolism, Faculty of Medicine, University of Southampton, Southampton General Hospital, Tremona Road, Southampton SO9 4XY (Great Britain)

(Received 28th July 1986)

SUMMARY

A simple method is described for the determination of selenium in human tissues without the use of perchloric acid. Digestion with nitric and sulphuric acids is followed by hydride generation and atomic absorption spectrometry. Results for NBS bovine liver and IAEA horse kidney reference materials were in good agreement with assigned concentrations, as was also achieved with the perchloric acid digestion. Recovery of added selenium was >90%, and the relative standard deviation was 5.5% for within-batch and 6.9% for between-batch analyses. The values for selenium in heart tissue were 0.9—1.3 $\mu g\ g^{-1}$ dry weight.

Considerable interest has recently been shown in selenium as an essential trace element. Studies have confirmed the detrimental effects of marked selenium deficiency in animals [1] and man [2, 3] and have shown that the associated cardiac lesions can be prevented by selenium supplementation [4]. Moreover, significantly low serum selenium levels have been described in a variety of disease states including cardiomyopathy [5], coronary heart disease [6], coronary atherosclerosis [7] and cancer [8]. It also appears that smoking is associated with lower blood selenium levels [9]. While the measurement of blood levels is a convenient way of assessing selenium status, it is obviously valuable to determine individual tissue levels of this element, as this could provide more detailed knowledge of the role of selenium in organ-specific disease such as cardiomyopathy.

At present, the three main methods for determination of selenium in biological materials are neutron activation analysis, fluorimetry with 2,3-diaminonaphthalene and atomic absorption spectrometry. Of these, the first is time-consuming and requires access to expensive and restricted facilities, but does allow accurate selenium estimation without sample pretreatment. The latter two methods require the digestion and oxidation of tissues, but are more widely available. Atomic absorption spectrometry (a.a.s.) with hydride generation is now accepted as a sensitive and relatively simple method for measuring selenium. Sample preparation for this technique involves either dry ashing (with risk of selenium loss through volatilization

0003-2670/87/$03.50

unless slow, low-temperature methods are used [10], or wet digestion, for which most proposed procedures use perchloric acid [11]. As use of this acid carries the dangers of explosion [12, 13] and contact dermatitis and requires the use of special venting facilities [12], a method avoiding its use has obvious advantages. A simple, rapid method which avoids the use of perchloric acid has been developed for selenium determination in blood [14]. An attempt was therefore made to develop a simple wet-ashing procedure for solid tissue samples which gave data similar to those achieved with perchloric acid.

EXPERIMENTAL

Reagents and apparatus

The antifoam emulsion (DB 110A) was a gift from Dow Corning, and was used as a 1% (w/v) solution in water. All reagents were AnalaR grade (BDH) unless otherwise stated. Deionized water was used throughout. A working stock standard selenium solution (10 μg ml^{-1}) was prepared by transferring exactly 1 ml of selenous acid standard solution (1 mg ml^{-1}) to a 100-ml volumetric flask, adding 1 ml of 16 M nitric acid and diluting to volume with water. Working standard solutions were prepared by transferring 0, 0.5, 1.0, 2.0, 3.0, 4.0 and 5.0 ml of the working stock standard solution of selenous acid to 100-ml volumetric flasks, adding 1 ml of 16 M nitric acid to each and diluting to volume with water. These solutions contained 0, 50, 100, 200, 300, 400 and 500 ng ml^{-1} selenium, respectively.

A Techne Dri-block heater model DB-3H was used for ashing the samples. The heater was fitted with three alloy blocks, each drilled with twelve holes to a depth of 48 mm and a diameter of 16.75 mm. Borosilicate test tubes (16 × 110 mm) were used for sample oxidation. A Tekator Kjeldahl 1007 digester apparatus was used in the comparative study of perchloric acid digestion.

A Perkin-Elmer model 2380 atomic absorption spectrometer and a Perkin-Elmer MHS-20 hydride-generation system were used with the instrumental conditions as in Table 1.

TABLE 1

Instrumental conditions

Atomic absorption measurements			
Radiation source	Perkin—Elmer electrodeless discharge lamp operated at 6W		
Wavelength	196.0 nm		
Spectral band-pass	2.0 nm, restricted slit height		
Measurement mode	Integrated peak area, 19 s, at ×1 scale expansion		
Recorder	Tekman 220/2. Continuous reading at 2 mV f.s.d.		
Hydride generation			
Tube temperature	950°C	Reaction time	10 s
Purge I (argon)	38 s	Reductant delivery	6 ml
Purge II (argon)	25 s	Reaction volume	20 ml

Procedures

Preparation of tissue samples. Tissue samples weighing ca. 20 g were collected at post mortems; samples of heart were taken from the anterior wall of the left ventricle, kidney samples included both cortex and medulla, and liver samples were taken from the anterior surface of the right lobe. All samples were cut into pieces no larger than 20 × 5 × 5 mm with disposable plastic knives, on polystyrene Petri dishes. The samples were washed twice by stirring the cut tissue in 200 ml of 0.15 M sodium chloride for 10 min, drained on filter paper and transferred to polystyrene tubes for storage at −20°C until required. The tissue samples were then defrosted and diced into pieces no larger than 2 mm^3.

Preparation of tissue homogenate. Accurately weigh 5.0 g of diced tissue into a 25-ml measuring cylinder. Add 14 ml of freshly prepared 18 M sulphuric acid/16 M nitric acid (1:1, v/v) to the tissue. Shake and leave to stand for 15 h, before making the homogenate up to a total volume of 20 ml with the sulphuric/nitric acid mixture. Transfer the homogenate to a beaker and stir for 10 min.

Sample oxidation. Transfer duplicate 500-μl portions of tissue homogenate into borosilicate glass tubes. Add 1 ml of 16 M nitric acid and 1 ml of 18 M sulphuric acid and place the tubes into the pre-heated aluminium blocks, at a block temperature which produces a sample temperature of 140—150°C, for 3 h. Remove the tubes, allow to cool to room temperature, and add 2 ml of 6 M hydrochloric acid. Mix by gently shaking the tubes, and replace them in the block pre-heated to 95°C for 30 min. Remove the tubes from the block, allow to cool to room temperature, transfer the samples into the hydride-generation reaction vessels, and dilute with water to a total volume of 20 ml. Add 400 μl of the anti-foam reagent.

Preparation of selenium standards. Transfer duplicate 100-μl volumes of the six working standard solutions into borosilicate glass tubes. Add 1 ml of 16 M nitric acid and 1 ml of 18 M sulphuric acid and thereafter treat the tubes exactly as for the sample oxidation above.

Estimation of tissue dry weight. Label and weigh duplicate 15-ml glass beakers to within 1 mg and weigh 1.0 g of diced wet tissue into each beaker. Dry the tissue samples at 100°C for 48 h and re-weigh. Return the beakers to the oven for a further 24 h at 100°C and weigh again. Repeat until a constant dry weight is achieved, and calculate the final tissue dry weight per gram of wet weight.

Measurement of selenium. Under the instrumental conditions described in Table 1, determine the selenium concentrations in the solution of the ashed samples. Establish a calibration graph by processing the prepared selenium standard solutions. Run the sample solution and blanks in duplicate, and run a working standard solution after every six samples. Calculate the selenium concentrations from the integrated absorbance valves and the calibration graphs. Hence calculate the selenium concentration per gram of tissue (dry weight).

RESULTS AND DISCUSSION

Initial studies showed that determinations based on integrated peak areas were most precise within a range of 10—40 ng of selenium. With a selenium content in heart of around 200 ng per gram of tissue (wet weight), this required determinations to be made on samples containing 0.1—0.2 g of tissue. The most accurate and reproducible results were obtained by preparing a chemical homogenate. Pre-mixing the nitric and sulphuric acid before addition to diced tissue was found to decrease the heat of reaction and hence prevent any selenium loss at this stage.

Optimum conditions for digestion and hydride formation

The total acid volume was kept constant, and the volume ratio of nitric acid to sulphuric acid used for digestion was varied between 1:5 and 5:1. At the two extremes, oxidation of the samples was inadequate and this led to excessive frothing of the reaction mixture during the addition of sodium tetrahydroborate solution, which in turn caused fouling of the connecting tubing and of the quartz absorption cell. The highest peaks were obtained with a 1:1 ratio. The total volume of acid used for digesting 500 μl of chemical homogenate (equivalent to 125 mg of tissue) was varied between 1 and 4 ml. Below 2 ml, the samples were found to char, and had to be discarded. With volumes greater than 2 ml, the selenium absorption signals were less well defined and the sensitivity of the assay was reduced. Thus exactly 2 ml was chosen for use.

The temperature for the digestion was varied between 100 and 160°C. Up to 150°C, the sensitivity was found to increase with increasing temperature. Above 155°C there was loss of sample by spillage during heating. With the block temperature at 155°C, the length of time for which samples were kept in the heating blocks was varied between 1 and 4 h. When heated for <2 h, the selenium peaks were poorly defined and had prolonged lagging edges. Heating for >3 h resulted in decreased sensitivity because of the increased final acid concentration.

The optimum concentration of sodium tetrahydroborate for producing hydrogen selenide from oxidized sample solutions was found to be 5—7% (w/v) in 0.25 M sodium hydroxide. At concentrations less than 4%, the selenium absorption peaks were poorly defined, and had prolonged lagging edges which occasionally extended beyond the 19-s integration period. At concentrations above 7%, the sensitivity decreased.

Calibration, precision and accuracy

Calibration graphs were established by the method of standard additions to a heart homogenate sample by adding 100 μl, 200 μl and 500 μl of homogenate. The calibration graphs were parallel to the line obtained for aqueous standards alone (Fig. 1), indicating no significant matrix effect with these sample sizes. A similar method with 100-μl and 200-μl samples of liver and

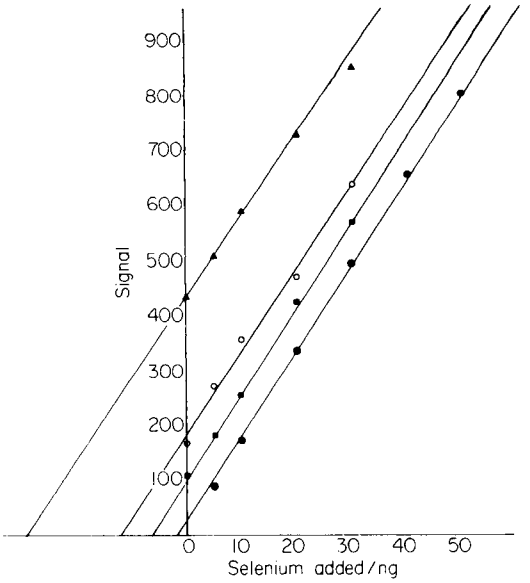

Fig. 1. Effect of tissue matrix on calibration for selenium. Amount of tissue homogenate added to aqueous standards: (●) ○; (■) 100 μl; (○) 200 μl; (▲) 500 μl.

kidney homogenates confirmed that the proposed method is also suitable for these tissues.

Four separate chemical homogenates, each based on 5.0 g (wet weight) of tissue, were prepared from one heart specimen. Replicate analyses of these homogenates were used to estimate within-batch and between-batch precisions. The results are given in Table 2.

The accuracy of the procedure was assessed from the results obtained for three sets of experiments.

Recovery of selenium added to homogenate. Duplicate 100-μl and 500-μl portions of tissue homogenate were transferred to glass tubes; 0, 50, 100, 200 and 300 μl of selenium working standard were added, and the amount of selenium in each sample was determined by the method proposed. The good recoveries of selenium are shown in Table 3.

TABLE 2

Precision of replicate selenium determinations in heart samples

	Within batch	Between batch
No. of determinations	5	20
Mean Se conc. (ng g^{-1})	195.5	197.5
Range (ng g^{-1})	184—208	168—223
Standard deviation (ng g^{-1})	10.7	13.7
Relative standard deviation (%)	5.5	6.9

TABLE 3

Recovery of selenium added to heart homogenate and tissue

Amount of selenium in sample (ng)				Recovery (%)
Initial	Added	Found	Recovered	
Added to homogenate				
5.5	10	14.8	9.3	93
25.0	10	36.0	11.0	110
5.5	20	25.5	20.0	100
25.0	20	45.0	20.0	100
5.5	30	35.0	29.5	98
25.0	30	52.5	27.5	92
5.5	5	10.0	4.5	90
25.0	5	30.7	5.7	114
Added to tissue				
5.6	2.7	8.3	2.7	100
27.8	13.5	40.8	13.0	96

Recovery of selenium added to heart tissue. Dried heart (5.0 g) was accurately weighed into each of two 25-ml measuring cylinders, and 50 μl of stock selenium standard (1 mg ml^{-1} selenium) was added to one of the measuring cylinders. Chemical homogenate of total volume 20 ml was prepared from each of the samples. Duplicate portions of 100 μl and 500 μl of each homogenate were assayed according to the method proposed, and the recovery was estimated from the results obtained for homogenate with and without added selenium (Table 3).

Comparison of digestion efficiency for standard reference materials and samples of heart tissue. In an initial study of the NBS Bovine Liver reference material (1577a), a value of 0.65 ± 0.07 $\mu g\ g^{-1}$ (mean ± SD) was obtained for 5 replicate measurements. Although this was within the assigned range (Table 4), it was 10% low and the precision was somewhat worse than might be expected. Therefore further work was done to ensure that the negative bias was not caused by the omission of perchloric acid from the digestion mixture because it has been claimed that a perchloric/nitric/sulphuric acid mixture is essential to decompose all selenium-containing organic molecules prior to hydride generation and atomic absorption spectrometry [11]. This was investigated by comparing results obtained with the method described here and by a digestion procedure involving perchloric acid. Because no suitable fume cupboard was available, a Kjeldahl digester in which acid vapours were removed using a water vacuum pump was used. Chemical homogenates were prepared from a new bottle of NBS Bovine Liver and from IAEA Horse Kidney and from samples of six hearts. The liver was analyzed 5 times and the remaining homogenates were analyzed in duplicate by using both nitric/sulphuric and nitric/sulphuric/perchloric acid digestions

TABLE 4

Comparison of results obtained after different methods of digestion

Material	Selenium concentration ($\mu g\ g^{-1}$, dry weight)			
	Certified value	Assigned range	HNO_3/H_2SO_4 digestion	$HNO_3/H_2SO_4/HClO_4$ digestion
Bovine Liver (NBS 1577a)	0.71	0.64—0.78	0.721 ± 0.015[a]	0.718 ± 0.025[a]
Horse Kidney (IAEA H-8)	4.67	4.37—4.97	4.86	4.72
Heart A			0.917	0.950
Heart B			0.983	0.992
Heart C			1.308	1.283
Heart D			0.983	0.958
Heart E			1.042	1.092
Heart F			0.892	0.992

[a]Mean ± SD, 5 replicates; all other data are means of duplicates.

in parallel. The results (Table 4) show clearly that the described method gives accurate data by comparison with the results obtained after perchloric acid digestion.

Conclusions

The method described was used in the analysis of samples from several hearts. Results gave a selenium range of 0.9—1.3 $\mu g\ g^{-1}$ (dry weight), which is considerably higher than the one level previously reported for the United Kingdom (0.22 $\mu g\ g^{-1}$ [15]) but is well within the reported international range of 0.21—1.8 $\mu g\ g^{-1}$ [16, 17]. The same method gave selenium values in liver and kidney of 0.91 and 1.7 $\mu g\ g^{-1}$ (dry weight), respectively. These levels again lie within the reported international ranges. In addition, the results show good agreement between the selenium concentrations found by the described method and after digestion with an acid mixture containing perchloric acid. The described method is currently being used to investigate myocardial selenium levels in cardiovascular disease and to establish a reference range of selenium concentrations in heart tissue for the United Kingdom.

The authors thank Dr. P. Gallagher and all the mortuary staff in Southampton hospitals for their co-operation in collecting samples, Miss V. Bunker for providing the comparative data for perchloric acid digestion, and Mrs. Joy Bacon and Mrs. Diane Brown for typing the manuscript.

REFERENCES

1 K. O. Godwin and F. J. Fraser, Q. J. Exp. Physiol., 51 (1966) 94.
2 Keshan Disease Research Group of the Chinese Academy of Medical Sciences, Beijing, China Med. J., 92 (1979) 477.

3 Keshan Disease Research Group of the Chinese Academy of Medical Sciences, Beijing, Carr. Conc. Nutr., 11 (1982) 127.
4 Keshan Disease Research Group of the Chinese Academy of Medical Sciences, Beijing, China Med. J., 92 (1979) 471.
5 O. Oster, W. Prellwitz, W. Kasper and T. Meinertz, Clin. Chim. Acta, 128 (1983) 125.
6 J. Salonen, G. Alfthan, J. Huttunen, J. Pikkarainen and P. Puska, Lancet, 2 (1982) 175.
7 J. Moore, R. Noiva and I. Wells, Clin. Chem., 30 (1984) 1171.
8 J. Salonen, R. Salonen, R. Happetelainen, P. Maenpaa, G. Alfthan and P. Puska, Br. Med. J., 290 (1985) 417.
9 B. Lloyd, R. Lloyd and B. Clayton, J. Epidemiol. Community Health, 37 (1983) 213.
10 T. Gorsuch, The Destruction of Organic Matter, Pergamon, New York, 1970.
11 D. Reamer and C. Veillon, Anal. Chem., 53 (1981) 1192.
12 N. I. Sax, Dangerous Properties of Industrial Materials, Van Nostrand, New York, p. 2144.
13 L. Bretherick, Handbook of Reactive Chemical Hazards, Butterworths, 1979, pp. 777—787.
14 B. Lloyd, P. Holt and H. T. Delves, Analyst, 107 (1982) 927.
15 R. Dickson and R. Tomlinson, Clin. Chim. Acta, 16 (1967) 311.
16 C. Casey, B. Guthrie, G. Friend and M. Robinson, Arch. Environ. Health, 37 (1982) 123.
17 R. Masironi and R. Parr, Selenium and Cardiovascular Diseases, Proceedings of Symposium on Selenium and Tellurium in the Environment, Industrial Health Foundation, Pittsburgh, PA, 1976, pp. 316—322.

Analytica Chimica Acta, 197 (1987) 105—119
Elsevier Science Publishers B.V., Amsterdam — Printed in The Netherlands

A QUANTITATIVE MEASURE OF THE RELIABILITY OF SEARCHES OF SPECTRAL LIBRARIES

P. B. HARRINGTON and T. L. ISENHOUR*

Department of Chemistry and Biochemistry, Utah State University, Logan, UT 84322-0300 (U.S.A.)

(Received 10th November 1986)

SUMMARY

A quantitative measure of library search reliability has been developed. Applications of the quantitative reliability metric (QRM) for evaluating the reliability of library searches for unknown target spectra and the use of this measure to detect the failure of a library search caused by noise, contaminant peaks and missing library spectra are discussed. The effects of noise and composite infrared spectra of mixtures on the QRM are examined for test sets of 561 infrared spectra. The QRM is also used to evaluate the performance of a search of an infrared library compressed by eigenvector projection.

Spectral libraries are important for structure elucidation of complex molecules [1]. Mass spectroscopy (MS) and infrared spectroscopy (IR) are common techniques used for molecular structure determination. The utility of library searching is reflected in the sizes to which these data bases have grown: 79 560 entries for MS and over 95 000 entries for IR libraries [2, 3]. Results of searches of large libraries usually produce lists of nearly identical spectra. A measure of the reliability of the search should facilitate the interpretation of the results.

Intralibrary search results contain information on how a library search performs under ideal circumstances. This information has been used to evaluate library configurations [4, 5]. This same information can also be used for estimating the reliability of a library search which is the likelihood that the closest match is the correct identification. This paper presents a non-probabilistic quantitative measure of the reliability of spectral matches. This metric should perform better than the current methods for evaluating spectral libraries.

Libraries are collections of spectra of known origin which may be created from either raw spectra or spectra in some transformed representation. Several representations exist and vary from minor processing, smoothing or filtering of spectra, to extensive processing such as transforming spectra into the Fourier or eigen domains [6—10].

Measures of similarity have been used varying from simple geometric measures to more elaborate measures which attempt to incorporate spectral

0003-2670/87/$03.50

knowledge such as the probability based matching metric [11, 12]. The similarity metric is an operator which compares two spectra. A reference spectrum of known origin is compared to a target spectrum of unknown identity.

A similarity measure is defined as an operator which gives a value of 1.0 when applied to two spectra which are identical, a value of 0.0 when they are orthogonal and a value of −1.0 when the spectra are inverse. The dot-product metric is an example of a similarity measure with these properties and is given as

$$s = \sum_{i=1}^{n} r1_i \times r2_i \tag{1}$$

where s is the similarity value, $r1$ and $r2$ are spectra that are normalized to unit length and n is the number of components for each spectrum.

Similarity values alone are insufficient for evaluating library search performance. A library search may perform accurately but give low similarity values. Conversely, a similarity value may be large, but the target spectrum may not be correctly identified. Therefore, the closest match to the target spectrum frequently is not the correct identification and lists of closest matches are often used. Similarity values are also not useful for comparing two or more different library searches and other methods have been developed.

An early example of the application of intralibrary searches to evaluate and compare spectral libraries used propagation trees [4]. A spectrum is searched and its list of n closest matching spectra are subsequently searched. Each search of a closest match is represented by a node in a propagation tree which has n more daughter nodes. A tree with n nodes is built to an arbitrary depth. The number of different spectra in a given size of tree indicates the ability of the library search to retrieve similar compounds.

A more recently developed method, the quantitative evaluation of library search performance (QELS), measures differences in performances of library searches [5]. This method compares the n closest matching spectra of a standard library to their index positions in a long list of closest matches acquired from a test library. A weighted sum, S, is calculated from the index positions in the list of closest matches from the test library. The weighting is obtained by dividing each index position from the test library by the corresponding index position from the standard library. A figure of merit is calculated by normalizing with respect to the best and worst possible scores.

Both methods of evaluating performance are useful because they do not use, or depend on, similarity values. The disadvantage of the propagation-tree method is that it is a semi-empirical method.

The QELS method has several disadvantages. The QELS figures of merit depend on the sizes of the libraries because the worst possible score occurs when the order of the n closest matches in the standard library is inverted

and they occur as the last n matches in the test library. If the libraries are large, the figures of merit may become indistinguishable. Another liability of the QELS method is that a standard library is required. High-resolution libraries have been used as standards for ideal performance in the past. Although high-resolution spectra contain more spectroscopic information, they may not be ideal representations if the high-resolution fine structure is not reproduced in the target spectrum.

This method also cannot distinguish between cases for which differences in location between the lists of closest matches from the test and standard libraries are caused by significant or insignificant differences in similarity. The n closest matching spectra may cluster well or poorly around the target spectrum. If the n closest matches in the standard library are all similar to the target compound, then they should all be weighted equally. Conversely, if some of the n closest matches are dissimilar or orthogonal, they should be weighted heavily in evaluating performance.

An improved measure of search performance, the quantitative reliability metric (QRM), is reported in this paper. The QRM was developed to remove the disadvantages of the QELS method and provide a method to measure the reliability of library search results. The standard used by the QRM for ideal performance is the list of closest matches for the intralibrary search of a given spectrum. The selectivity of a library search is defined as the difference in similarity values between adjacent matches in the list of search results. The QRM uses the selectivity of a library search to produce unitless values that are independent of the size of the library and the similarity metric used.

THEORY

The reliability of a library search is evaluated by calculating the differences in the order of closest matches between a search of a target spectrum and the intralibrary search for the target compound. The selectivity of a search is evaluated by calculating the differences in similarity values from the lists of closest matching spectra. The QRM uses both the reliability and selectivity of a search.

The QRM is an extension of the QELS method discussed earlier. Lists of the n intralibrary closest matching spectra are required for each of the spectra in the list of closest matching spectra to a target spectrum. The difference between lists of closest matching spectra obtained from intralibrary and extralibrary comparisons is illustrated below for an acenaphthene spectrum searched against an 8000-compound MS library. The ten intralibrary closest matches for mass spectra of acenaphthene and of 7,8-benzobicyclo(2,2,2)octa-2,5-diene are listed in Table 1. The ten closest matches for an acenaphthene target spectrum are listed in Table 2. This list is more similar to the list of ten closest intralibrary matches for acenaphthene than for 7,8-benzobicyclo(2,2,2)octa-2,5-diene (Table 1).

TABLE 1

Ten closest matches for an intralibrary search for mass spectra of acenaphthene and 7,8-benzobicyclo(2,2,2)octa-2,5-diene

A. ACENAPHTHENE	*B. 7,8-BENZOBICYCLO(2,2,2)OCTA-2,5-DIENE*
(1) Acenaphthene	(1) 7,8-Benzobicyclo(2,2,2)octa-2,5-diene
(2) 7,8-Benzobicyclo(2,2,2)octa-2,5-diene	(2) Acenaphthene
(3) 6-Phenylfulvene	(3) 6-Phenylfulvene
(4) Biphenyl	(4) 1-Naphthyl isocyanide
(5) 1-Naphthyl isocyanide	(5) Biphenyl
(6) Quinoline-2-carbonitrile	(6) *N,N*-Dimethyl-*N'*-D5-Phenylformamidine
(7) *N,N*-Dimethyl-*N'*-D5-Phenylformamidine	(7) Methyl 5-chloroanthranilate
(8) Methyl 5-chloroanthranilate	(8) AR-Chloro-*p*-cymene
(9) 1-Cyanoisoquinoline	(9) Isopropylchlorotoluene
(10) 1,4,6-Trimethyl-2-pyridthione	(10) 5-Chlorobenzofuran-2D

TABLE 2

Library search result list for an acenaphthene mass spectrum

Index	Compound name	Dot product value	QRM(5)
(1)	Acenaphthene	0.982	0.000
(2)	7,8-Benzobicyclo(2,2,2)octa-2,5-diene	0.955	1.211
(3)	6-Phenylfulvene	0.944	0.991
(4)	Biphenyl	0.885	1.832
(5)	1-Naphthyl isocyanide	0.700	3.115
(6)	Quinoline-2-carbonitrile	0.699	3.048
(7)	1-Cyanoisoquinoline	0.680	2.646
(8)	1,1-Dicyano-2-phenylethylene	0.678	2.647
(9)	*N,N*-Dimethyl-*N'*-D5-phenylformamidine	0.668	3.129
(10)	Methyl 5-chloroanthranilate	0.667	3.715

The fundamental difference between the QRM and QELS is that the intralibrary closest matches for each library representation is used (QRM) instead of the intralibrary closest matches of a chosen standard library representation (QELS). The n closest intralibrary matches for a given target compound should be reproducible when the target spectrum and the library spectrum are of equal quality. Differences between the positions of the two lists of closest matching spectra are measured by differences in similarity between the index position where a given closest match appears in the intralibrary search and where that spectrum actually does appear in the target list.

The QRM can be divided into a numerator and a denominator. The numerator calculates the weighted root-mean-squared (RMS) difference in similarity values between the list of closest matching spectra and the intralibrary list of closest matching spectra. The QRM values can be obtained for each entry in the list of search results. All similarity values are obtained from the search results of a target spectrum. Also, QRM values may be obtained for every

reference spectrum in the list of search results. If the list of intralibrary closest matches for a reference spectrum is similar to the list of library search results, a low QRM value will be obtained.

The denominator represents the weighted RMS selectivity measure of the search. The selectivity is obtained by subtracting similarity values of the $(i + 1)$th closest match from the ith closest match. If all the similarity values in the list of closest matches were identical, the selectivity would be zero. The sum of squared weights does not appear in the QRM calculation because both the numerator and denominator contain this term.

The QRM can be calculated for any spectrum, X, in the library. The QRM is given as

$$\mathrm{QRM}(n) = \left[\sum_{i=1}^{n} (s_i \times \Delta s_{i,i*})^2\right]^{1/2} / \left[\sum_{i=1}^{n} (s_i \times \Delta s_{i,i+1})^2\right]^{1/2} \quad (2)$$

where n is the level of comparisons, s_i is the similarity value of the ith closest match in the list of closest matches to a target spectrum, $i*$ is the location in the same list of closest matches of the ith spectrum in the list of intralibrary search results for X, $\Delta s_{i,i*}$ is the difference between the two similarity values, and $\Delta s_{i,i+1}$ is the difference between the ith and the next largest similarity value.

If the two lists match exactly for the n closest matches, n differences will be calculated between identical similarity values and the total will be zero. A weighted sum of squares is obtained from the differences in similarity values, $\Delta s_{i,i*}$. The weight used is the similarity value of the ith closest match in the target list. The root-mean-square is calculated from this sum which indicates the extent of variance between the two lists. The advantage of using a sum of squares as opposed to a sum of absolute values is that a large error will be weighted more than an equal sum of smaller errors. All similarity values are obtained from the list of search results for a target spectrum.

Both the reliability measure (the numerator) and the selectivity measure (the denominator) will become smaller as the library size is increased because the closest matches of a search will be more similar. Therefore, the QRM should be independent of library size. Furthermore, for large libraries, the order of the intralibrary closest matches to a spectrum will be better defined and will form a smaller cluster in the spectra space. The QRM values are unitless and can be used to compare different spectral libraries and similarity metrics.

EXPERIMENTAL

All calculations were done on a Microvax II computer at the Utah State University Department of Chemistry and Biochemistry. The eigenvectors were calculated using IMSL subroutines. All spectra were normalized to unit length and the searches used a dot-product similarity metric.

The IR library consisted of 2300 vapor-phase Fourier-transform infrared (FTIR) spectra collected and distributed by Sadtler Research Laboratories. Low-resolution absorption spectra were digitized at 198 discrete frequencies from 3840 cm^{-1} to 800 cm^{-1} at a 16-cm^{-1} data interval. Construction of a data base containing lists of the 15 intralibrary closest matches for the 2300 spectra in this library required 3 h of computer time.

Twenty-one target spectra were acquired with a Digilab FTS-14 FTIR spectrometer, an IBM IR/85 FTIR spectrometer or a Nicolet 7199 spectrometer adapted to a Varian 3700 gas chromatograph. Separations were done with either 1/4-in. packed SE-30 columns or a 0.2-mm i.d. SE-54 fused silica capillary column.

The MS library consisted of 8000 mass spectra [13] ranging from 21 to 256 a.m.u. Construction of a data base containing lists of the 15 intralibrary closest matches for the 8000 spectra in this library required 50 h of computer time. Target mass spectra were obtained from the CRC Atlas [14].

The test set used to evaluate the QRM was obtained by randomly selecting (without replacement) 561 spectra from the FTIR library described earlier. Twelve noise spectra were obtained by referencing a background spectrum to an adjacent background spectrum. The background spectra were acquired from the gas chromatography/FTIR runs described above. Each spectrum in the test set had one of the twelve noise spectra added to it. Each set of noise and library spectrum was normalized to unit-vector length and summed. The resultant spectrum was normalized to unit vector length. These spectra are composed of real FTIR spectra and hence will be referred to as composite spectra.

The signal-to-noise ratio is obtained from the RMS signal divided by the RMS noise and is given as

$$\mathrm{SNR} = \left[\sum_{i=1}^{v} (n_i + s_i)^2\right]^{1/2} / \left[\sum_{i=1}^{v} n_i^2\right]^{1/2} \tag{3}$$

where n_i is the ith resolution of a noise spectrum, s_i is the ith resolution element of a library reference spectrum and v is the total number of resolution elements. The signal-to-noise ratios for this test set ranged from 1.01 to 1.65 with an average of 1.38 (standard deviation 0.11). The ratio of signal power to noise power can be obtained by squaring the signal-to-noise ratio because the noise was normalized to unit vector length and the denominator is unity.

An FTIR composite spectrum of a mixture was obtained by random sampling of one FTIR library spectrum without replacement and adding to it a second randomly sampled (with replacement) library spectrum. The first spectrum was normalized to a vector length of 0.8 and the second spectrum was normalized to a vector length of 0.2. Both spectra were summed to produce a composite spectrum which was then normalized to a vector length of 1.0. A test set of 561 such spectra was used to evaluate the QRM.

The compressed FTIR library was constructed by projection onto 38 eigenvectors [9, 15]. The eigenvectors were calculated from a covariance about the origin pretreatment matrix using double-precision arithmetic. The projection and normalization of the library were obtained with single-precision arithmetic. Construction of a data base containing lists of the 15 intralibrary closest matches for the 2300 spectra in this library required 40 min of computer time.

RESULTS AND DISCUSSION

Reliability measure

The QRM indicates the reliability of the library search performance. An important application of the QRM is to evaluate the performance for unknown target spectra. Unknown spectra are often obtained at very low levels of concentration and may contain large levels of noise. These spectra will have low similarity values when compared to their correctly matching library entries because library spectra characteristically have low noise levels. Therefore, a similarity measure alone will not indicate how well a search performs.

The QRM is useful for detecting false positives, cases for which the closest match is not the correct identification. Cases do occur for which the closest match in the search list will be correct and also give a large QRM value. This type of error is tolerable because further runs will be done. The confidence level of the QRM is related to the level of comparison, n. The likelihood of not detecting a false positive decreases and the likelihood of incorrectly classifying a positive result as a false positive increases as the level of comparison increases.

A test set of 561 FTIR composite noise spectra was obtained by adding noise spectra to library spectra. Each spectrum in the test set was searched and the QRM value for the closest match and the index position of the correct spectrum in the list of closest matches were stored. Tables 3—5 contain nine categories of QRM values. The low and high designations are the limits of QRM values for each category and Number is the number of searches and QRM values in each category. For the index position of the correct match in each category, the lowest, highest, average and standard deviation are given.

Table 3 gives the index positions of correct matches categorized by the QRM values calculated at a level of 5 for the closest match of each spectrum in the test set. For QRM values less than 0.1, the index position of the correct match ranged between 1 and 3. Table 4 is the same as Table 3 except the level of comparison of the QRM is 10 instead of 5. The number of searches for which the closest match produced a QRM value less than 0.1 decreased from 81 to 15 as the level of the QRM increased from 5 to 10.

Tables 3 and 4 show that when the QRM value increases, so do the cases for which the library search did not function reliably; the correct match is not the closest match. Although cases exist for which the correct match

TABLE 3

Index positions of the correct matches in library search result lists for 561 FTIR noise composite spectra categorized by QRM values at levels of 5 for the closest match

QRM value			Number	Index position of correct match		
Category	Low	High		Low	High	Average[a]
1	0.00	<0.10	81	1	3	1.111 ± 0.354
2	0.10	<0.20	67	1	6	1.090 ± 0.621
3	0.20	<0.30	47	1	2	1.022 ± 0.146
4	0.30	<0.40	48	1	3	1.104 ± 0.425
5	0.40	<0.50	34	1	3	1.059 ± 0.343
6	0.50	<1.00	115	1	20	1.513 ± 2.322
7	1.00	<2.00	95	1	67	3.158 ± 7.966
8	2.00	<4.00	52	1	21	3.520 ± 4.655
9	4.00	<100.00	22	1	86	12.227 ± 23.067

[a]With standard deviation.

TABLE 4

Index positions of the correct matches in library search result lists for 561 FTIR noise composite spectra categorized by QRM values at a level of 10 for the closest match

QRM value			Number	Index position of correct match		
Category	Low	High		Low	High	Average[a]
1	0.00	<0.10	15	1	2	1.200 ± 0.414
2	0.10	<0.20	18	1	2	1.056 ± 0.236
3	0.20	<0.30	41	1	2	1.024 ± 0.156
4	0.30	<0.40	40	1	3	1.075 ± 0.350
5	0.40	<0.50	47	1	2	1.021 ± 0.146
6	0.50	<1.00	149	1	13	1.181 ± 1.103
7	1.00	<2.00	118	1	67	1.975 ± 6.168
8	2.00	<4.00	88	1	28	2.955 ± 4.957
9	4.00	<100.00	45	1	86	8.600 ± 16.958

[a]With standard deviation.

was the closest match and the QRM gave large values, the signal-to-noise ratio of all the composite FTIR spectra with noise was less than 2.0.

The QRM will fail for two situations. The first is when the mapping from spectra space to structure space is not one to one or when several molecular structures give indistinguishable spectra; for example, the xylene isomers are indistinguishable by their mass spectra. The second situation is when the library does not contain enough spectra to form lists of intralibrary closest matches that, excluding the first match, have a unique order.

Table 5 contains the results of the evaluation of the QRM for the 561 composite FTIR spectra of mixtures. The correct match was one of the top three closest matches for all QRM values less than 0.5.

The QRM indicates the reliability of a search result. The QRM at a level of comparison of 5 will typically give values less than 0.1 if the search performs reliably. The QRM at a level of 10 will give values less than 0.5 if the library search performs reliably.

The QRM values are not required for all the spectra in the lists of search results, but only need to be calculated for the closest match. Table 2 gives the search results of a target mass spectrum for acenaphthene, an example of a reliable search. The QRM is plotted as a function of level of comparison in Fig. 1 for the two closest matching spectra to an acenaphthene target spectrum. The QRM values of acenaphthene are 0.0 for acenaphthene to a level of 6. If a library search performs reliably, the QRM will typically give values of 0.0 to a level of 5 or more.

Table 6 gives the ten intralibrary closest matching FTIR spectra for *m*-anisaldehyde and *p*-anisaldehyde. Table 7 gives the search results of a target FTIR spectrum for *p*-anisaldehyde where *m*-anisaldehyde was the closest matching compound. The QRM is plotted as a function of level for both *p*-anisaldehyde and *m*-anisaldehyde in Fig. 2. The QRM values for levels 2 through 14 are lower for *p*-anisaldehyde. The QRM values do not indicate that the *p*-anisaldehyde reference is more similar to the target spectrum than *m*-anisaldehyde, but indicate that the search performed worse for *m*-anisaldehyde than *p*-anisaldehyde and that *m*-anisaldehyde is not likely to be the correct identification.

The QRM is useful in determining whether a target spectrum is contained in a library. If a library does not contain the target spectrum but contains other similar spectra, the similarity values will be high. Table 8 contains the

TABLE 5

Index positions of the correct matches in library search result lists for 561 FTIR mixture composite spectra categorized by QRM values at a level of 10 for the closest match

QRM value			Number	Index position of correct match		
Category	Low	High		Low	High	Average[a]
1	0.00	<0.10	2	1	1	1.000 ± 0.000
2	0.10	<0.20	10	1	2	1.100 ± 0.316
3	0.20	<0.30	29	1	3	1.103 ± 0.409
4	0.30	<0.40	38	1	3	1.105 ± 0.448
5	0.40	<0.50	32	1	3	1.156 ± 2.717
6	0.50	<1.00	131	1	30	1.412 ± 4.211
7	1.00	<2.00	149	1	48	1.846 ± 4.212
8	2.00	<4.00	119	1	41	3.118 ± 5.284
9	4.00	<100.00	51	1	23	4.843 ± 5.612

[a]With standard deviation.

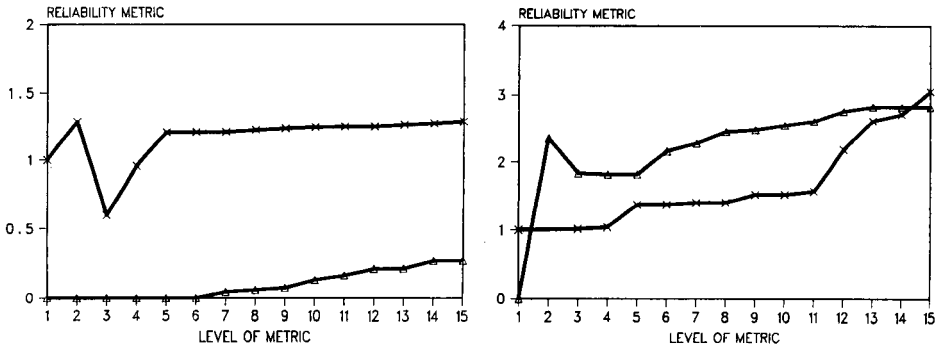

Fig. 1. Plot of QRM values as a function of level (n) for the two closest matching spectra for an acenaphthene MS search. (△) Acenaphthene, the closest matching reference spectrum; (×) 7,8-benzobicyclo(2,2,2)octa-2,5-diene, the second closest match.

Fig. 2. Plot of QRM values as a function of level (n) for the two closest matching spectra for a *p*-anisaldehyde FTIR search. (△) *m*-Anisaldehyde, the closest matching reference spectrum; (×) *p*-anisaldehyde, the second closest match.

TABLE 6

Ten closest matches for an intralibrary search of FTIR spectra for *m*-anisaldehyde and *p*-anisaldehyde

A. m-ANISALDEHYDE	*B. p-ANISALDEHYDE*
(1) *m*-Anisaldehyde	(1) *p*-Anisaldehyde
(2) Carbanilic acid, *N*-ethyl-, ethyl ester	(2) Benzaldehyde, *p*-hydroxy-,
(3) *p*-Anisaldehyde	(3) *m*-Anisaldehyde
(4) Benzaldehyde, 3,4-dimethoxy-,	(4) Benzaldehyde, 3,4-dimethoxy-,
(5) Benzaldehyde, 4-hydroxy-3-methoxy-,	(5) Anthranilic acid, methyl ester
(6) Benzaldehyde, 2,3-dimethoxy-,	(6) Acetophenone, 2′,4′-dimethoxy-,
(7) Ketone, methyl 4-pyridyl,	(7) Benzaldehyde, 2,4-dimethoxy-,
(8) Benzaldehyde, *p*-hydroxy-,	(8) Benzaldehyde, 4-hydroxy-3-methoxy-,
(9) Benzoic acid, 2,4-dimethoxy-,	(9) Anthranilic acid, *N*-methyl-, methyl ester
(10) Cinnamaldehyde, α-bromo-,	(10) Acetophenone, 4*-hydroxy-,

10 closest matches and similarity values for a heptanoic acid, ethyl ester, FTIR target spectrum searched against a library in which that reference spectrum was missing. The QRM is plotted in Fig. 3 as a function of level for the three closest matching spectra. The QRM values for the closest matching spectrum, hexanoic acid, methyl ester, increase rapidly for levels 4 and 5. The dot product values indicate that the search performed satisfactorily, while QRM values greater than 0.1 indicate that the search performed unreliably.

TABLE 7

A library search result list for the search of a *p*-anisaldehyde FTIR spectrum

Index	Compound name	Dot product value	QRM(5)	QRM(10)
(1)	*m*-Anisaldehyde	0.864	1.829	2.544
(2)	*p*-Anisaldehyde	0.862	1.368	1.519
(3)	Benzaldehyde, *p*-hydroxy-,	0.808	2.874	3.386
(4)	Benzoic acid, 2,4-dimethoxy-,	0.754	4.148	4.929
(5)	Carbanilic acid, *N*-ethyl-, ethyl ester	0.735	4.350	5.428
(6)	Benzaldehyde, 3,4-dimethoxy-,	0.726	3.717	4.867
(7)	Benzoic acid, *p*-hydroxy-, pentyl ester	0.725	5.550	6.931
(8)	Acetophenone, 4′-amino-,	0.719	3.472	4.413
(9)	Acetophenone, 2′,4′-dimethoxyl-,	0.719	3.415	4.046
(10)	Benzaldehyde, 4-hydroxy-3-methoxy-,	0.718	4.577	5.884

TABLE 8

Library search result list for the search of the FTIR spectrum of heptanoic acid, ethyl ester when the reference spectrum is not contained in the library

Index	Compound name	Dot product value	QRM(5)	QRM(10)
(1)	Hexanoic acid, methyl ester	0.963	4.186	3.604
(2)	Heptanoic acid, methyl ester	0.960	3.690	4.619
(3)	Hexanoic acid, ethyl ester	0.959	3.098	4.168
(4)	Acetic acid, isopentyl ester	0.957	4.465	4.783
(5)	Hexanoic acid, propyl ester	0.951	3.834	4.872
(6)	Octanoic acid, ethyl ester	0.947	7.748	6.442
(7)	Butyric acid, butyl ester	0.945	5.438	7.400
(8)	Octanoic acid, methyl ester	0.945	6.682	9.521
(9)	Hexanoic acid, isobutyl ester	0.940	4.253	6.236
(10)	Hexanoic acid, pentyl ester	0.939	7.418	6.743

Evaluation of eigenvector-compressed infrared libraries

The QRM is useful for comparing two libraries. A principal advantage of the QRM is that no assumptions are made for ideal library behavior. The lists of closest matches from intralibrary searches for a target spectrum of two different library configurations may be different. The better library configuration may be defined as the library configuration for which the reliability of the search decreases the least when the target spectra contain noise.

An eigenvector-compressed library was created in which the library was reduced to 19% of its original size. The library was transformed by projecting spectra onto 38 eigenvectors. The transformation is given by

$$t_i = \sum_{j=1}^{v} e_{ij} \times d_j \qquad (4)$$

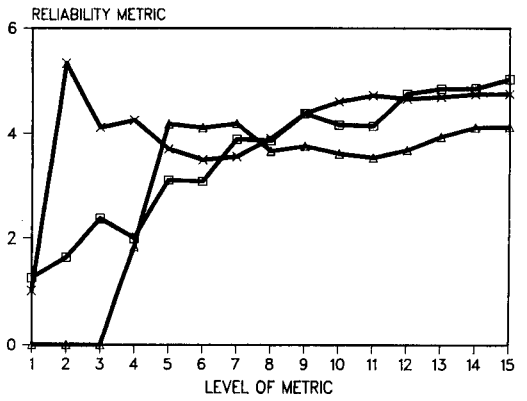

Fig. 3. Plot of QRM values as a function of level (n) for the three closest matching spectra for a heptanoic acid, ethyl ester, FTIR search for which the library does not contain the reference spectrum. (△) Hexanoic acid, methyl ester, the closest matching reference spectrum; (×) heptanoic acid, methyl ester, the second closest match; (□) hexanoic acid, ethyl ester, the third closest match.

where t_i is a component of the transformed spectrum, v is the number of variables, e_{ij} is the jth component of eigenvector i, and d_j is the jth resolution element of the spectrum to be transformed. The compression is achieved when the number of eigenvectors used is less than the number of variables [9, 15].

A Grotch plot is a method for evaluating library-search performance in which the number of correctly identified compounds is plotted as a function of cumulative closest matches [16]. The performance with eigenvector-compressed data is compared to the original library with 21 vapor-phase FTIR spectra in a Grotch plot in Fig. 4. The eigenvector-compressed search performed slightly better than the uncompressed search according to this measure of performance.

The problem of using the location of the correctly matching compound for comparing libraries is that if both libraries correctly identify the compound as the closest match, then no discrimination is achieved between search performance. Both searches correctly identified 15 compounds as closest matches. The QRM method is a more sensitive measure of search performance. For the same test set of 21 samples, the QRM gave only one value of 0.0 at a level of 5 for the uncompressed search of *m*-methylanisole.

A chi-squared goodness-of-fit test indicates that the QRM values obtained from the compressed and uncompressed library searches were not normally distributed [17]. The same set of test spectra was used to evaluate both libraries. Each QRM value obtained from the compressed search was subtracted from the QRM value obtained from the uncompressed search for a given test spectrum. This procedure is used in matched-sample statistical tests. Figure 5 is a histogram of this sample distribution in which the QRM values for the correct compound from the compressed search were subtracted

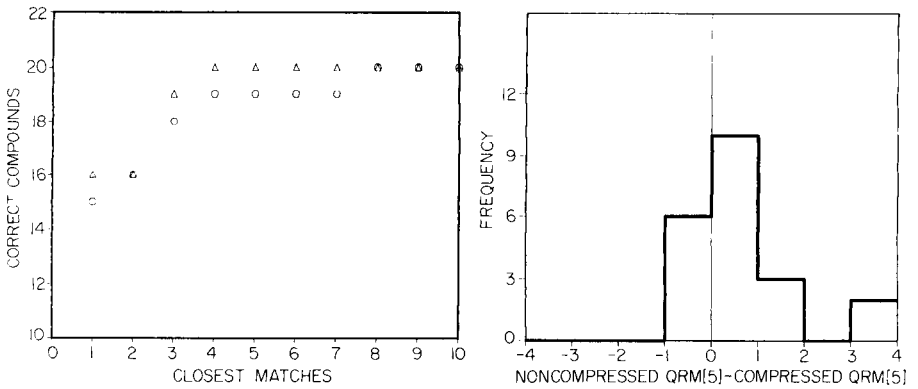

Fig. 4. Grotch plot of an uncompressed FTIR library (○) and an eigenvector-compressed FTIR library (△). The correct identifications are plotted as the cumulative number of closest matching spectra.

Fig. 5. Histogram of the paired differences in QRM values between the uncompressed and eigenvector-compressed libraries. QRM values were obtained with a level of comparison of 5. Values less than 0.0 indicate cases for which the uncompressed search performed better and values greater than 0.0 indicate cases for which the compressed search performed better.

from the matching QRM values obtained from the uncompressed search. The larger the QRM values, the less reliably the search performs. If the differences between the matched sample QRM values are negative, then the non-compressed search performs better; likewise a positive difference will indicate that the compressed search performs better.

Two parameters of a distribution which should indicate differences in search performance are the first and third moments [18]. The first moment is the mean value. The third moment of a distribution measures the symmetry of the distribution X about its mean and is the skewness. Skewness is defined as

$$\mu^{(3)} = [\sum_{i=1}^{n} (x_i - \mu)^3]/n \tag{5}$$

where $\mu^{(3)}$ is the third moment, μ is the mean value, n is the number of samples, and x_i is a paired difference of the QRM values. Skewness indicates the frequency with which one search performs substantially better than the other. Skewness is often normalized to a unitless parameter, γ, which is defined as $\gamma = \mu^{(3)}/\sigma^3$, where γ is the normalized skewness, $\mu^{(3)}$ is the skewness and σ^3 is the cubed standard deviation.

The estimates of the parameters for this sample distribution are the mean ($\hat{\mu}$ = 0.11), the variance ($\hat{\sigma}^2$ = 0.65), the normalized skewness ($\hat{\gamma}$ = 2.51), a

chi-squared statistic ($\tilde{\chi}^2$ = 2.57) obtained from a goodness-of-fit test for normality with 2 degrees of freedom and alpha (α = 0.723), where α is obtained from the X^2 distribution table which is the probability that the chi-squared statistic is not exceeded by a chi-square random variable. The mean difference in search performance is 0.11 which indicates that the average QRM values are lower for the compressed search. The normalized skewness of 2.5 indicates that the compressed search contains more cases for which its search performance is substantially larger than that of the uncompressed search. A positive skewness also indicates that the most probable value, the mode of the distribution, is less than the mean of the distribution. The most probable value, the maximum in the histogram in Fig. 5, is greater than 0.0 which indicates that the compressed search is more likely to perform better than the uncompressed search.

CONCLUSION

The QRM indicates the reliability of library search results for a given compound and provides a method for detecting false positive results. The QRM allows library search performance to be compared without requiring any assumptions of ideal library representations.

If the QRM is used to compare libraries, then intralibrary searches must be run for all the target spectra used to evaluate the libraries. The QRM is a sensitive method for detecting differences in search performance between different library configurations. The normalized skewness is a useful parameter of the matched sample distribution for comparing the performance between library configurations.

If the QRM is used for routine evaluation of performance, a data base containing lists of the intralibrary closest matches for all spectra in the library is required. The creation of this data base will require an amount of computation time which is proportional to the square of the number of library entries. The lists of intralibrary closest matches contain important information which may warrant the computation time required to utilize this information.

Automated structure elucidation from spectra is a formidable task and quality control must be maintained throughout this process. The QRM utilizes rich but difficult-to-obtain information of the clustering of spectroscopic signals to measure the reliability of library search results. A future goal of this research is to develop a probabilistic measure of the reliability of library searches.

This paper was presented at the First Hidden Peak Conference, Snowbird, Utah in June, 1986. The authors thank the previous workers at the University of North Carolina, Chapel Hill, NC, for supplying and assisting in the collection of the GC/FTIR data. The National Science Foundation is acknowledged for its support of this research under grant CHE-8415670.

REFERENCES

1 L. S. Ramos, K. R. Beebe, W. P. Carey, E. M. Sanchez, B. C. Erickson, B. E. Wilson, L. E. Wangen and B. R. Kowalski, Anal. Chem., 58 (1986) 294R.
2 F. W. McLafferty and D. B. Stauffer, Int. J. Mass Spectrom. Ion Phys., 58 (1984) 139.
3 Sadtler Research Libraries, Spectroscopy, 1 (1986) 4.
4 G. T. Rasmussen and T. L. Isenhour, J. Chem. Inf. Comput. Sci., 43 (1979) 1382.
5 M. F. Delaney, F. V. Warren Jr. and J. R. Hallowell Jr., Anal. Chem., 55 (1983) 1925.
6 J. T. Clerc and H. Koenitzer, Stud. Phys. Theor. Chem., 16 (1981) 151.
7 R. B. Lam, S. J. Foulk and T. L. Isenhour, Anal. Chem., 53 (1981) 1679.
8 P. M. Owens and T. L. Isenhour, Anal. Chem., 54 (1983) 1548.
9 G. Hangac, R. C. Wielboldt, R. B. Lam and T. L. Isenhour, Appl. Spectrosc., 36 (1982) 40.
10 S. S. Williams, R. B. Lam and T. L. Isenhour, Anal. Chem., 55 (1983) 1117.
11 K. Varmuza, Pattern Recognition in Chemistry, Springer, Berlin, 1980.
12 G. M. Peysna, R. Venkataraghaven, H. E. Dayringer and F. W. McLafferty, Anal. Chem., 48 (1976) 1362.
13 E. Stenhagen, S. Abrahamson and F. W. McLafferty, Registry of Mass Spectral Data, Wiley-Interscience, New York, 1980.
14 J. G. Grasselli, CRC Atlas of Spectral Data and Physical Constants for Organic Compounds, CRC Press, Cleveland, OH, 1973.
15 P. B. Harrington and T. L. Isenhour, Appl. Spectrosc., 41 (1987) 449.
16 S. L. Grotch, Anal. Chem., 43 (1971) 1362.
17 M. G. Kendall and A. Stuart, The Advanced Theory of Statistics, Vol. 2, Hafner, New York, 1961, Chap. 30.
18 I. Olkin, L. J. Gleser and C. Derman, Probability Models and Applications, Macmillan, New York, 1980.

Analytica Chimica Acta, 197 (1987) 121—128
Elsevier Science Publishers B.V., Amsterdam — Printed in The Netherlands

MICROCOMPUTERIZED ULTRAHIGH-SPEED TRANSIENT DIGITIZER AND LUMINESCENCE LIFETIME INSTRUMENT

T. J. TURLEY, J. N. DEMAS* and D. J. DEMAS
Chemistry Department, University of Virginia, Charlottesville, VA 22901 (U.S.A.)
(Received 2nd February 1987)

SUMMARY

A high-speed transient digitizer and a versatile luminescence lifetime instrument are described. A Z-80-based microcomputer permits rapid acquisition of transients, signal averaging, baseline subtraction, single or double exponential decay fitting, deconvolution, and graphics display of the transient and its semilogarithmic plot of decays on an oscilloscope or an *X-Y* plotter. Data can also be transferred to more powerful computers for further data reduction or higher quality plots. Applications that exploit the speed and convenience of the system are described.

Excited-state lifetimes are ubiquitous and powerful probes of excited-state properties, nature, and kinetics. They are widely used for state assignments, studies of excited-state dynamics, conformational analysis, and both ground and excited-state equilibria [1—4]. Many of these measurements are extremely labor-intensive and computationally demanding. Improvements in the speed of data acquisition and on-line computation of results can permit improved measurements and allow experiments that would have been too expensive or too time-consuming to do otherwise.

Numerous computer-interfaced lifetime instruments or transient recorders have been described [2—7]. These include time-correlated single-photon counting, boxcar integrators, and transient recorders. The first is a widely used luminescence lifetime measurement method that is easily computerized, but is relatively expensive, and not well suited for determination of long lifetimes (>5 μs). It also acquires data slowly unless expensive, mode-locked lasers are used. Boxcar integrators can be very fast (20 ps rise time), but work best with stable signals having high repetition rates. Transient recorders, especially modern interfaceable ones, permit efficient data acquisition and reduction, but tend to be slower (typically >0.1 μs/point).

The Tektronix R7912 ultrahigh-speed transient digitizer is a notable exception to the speed limitation and can record 512 points in a 5 ns single shot (1 GHz bandwidth). In contrast to most designs, this transient digitizer stores by writing on a charged diode array with an electron beam. As the beam sweeps across the array, the diode states are changed. Later, the diodes are interrogated and the results digitized. The digitizer memory tube consists

0003-2670/87/$03.50

of an ultrahigh-speed cathode ray tube (CRT) at one end, the diode target in the middle, and the interrogation scan gun at the other end. The fast CRT tube writes onto the charged diode array rather than onto the normal phosphor screen. Where the beam strikes the array, the diodes are discharged. The scan gun behind the target probes the array with an electron beam; when the scan beam strikes a discharged region, the diodes are recharged. The locations of these charging currents indicate where the CRT wrote on the array which allows digitization of the pattern. This pattern can be stored and transferred to an external computer. While writing can be extremely fast, digitization can take 50—70 ms.

This commercial transient digitizer has several problems. The computer interface is a Tektronix CP bus for their custom computer and software package. Digitized data, stored in an economical form taken directly from the array, must be converted to a single-valued array of intensity vs. time before it is usable. Because Tektronix computers and software are quite expensive, an inexpensive microcomputerized interface and powerful data-reduction software were developed here for the transient digitizer [8]. The system is optimized for luminescence lifetime measurements. This paper outlines the problems of interfacing the digitizer, and the solutions to the problems. The utility of the system is demonstrated by applications to important photophysical and photochemical systems.

EXPERIMENTAL

Hardware considerations

The Tektronix CP bus has 16 bidirectional command and data lines and ten control and handshake lines for control and data transfer. The bus is negative true with open-collector logic drivers. It was necessary for our computer interface to issue commands, monitor digitizer status, and control data transfer. It was also desirable to have provisions for prompt visual display of acquired transients on an oscilloscope and hard-copy graphs on an *X-Y* plotter.

Microcomputer parallel ports were used to control and read data on the CP bus. Control was then predominantly via software. Although transfer rates were slower than a more complex hardware interface, they were more than adequate.

Software considerations

Desired software features included digitizer set-up and control, data transfer to the computer, conversion of the obscure compacted data format of the digitizer to a single-valued waveform (i.e., "normalizing" in Tektronix's nomenclature), data display and plotting, baseline correction, data storage on disks, and uploading data to a more powerful computer. Further, it was desirable to have provisions for signal averaging and data reduction either by fitting the decays by linear least squares to the semilogarithmic plots of

intensity vs. time (single exponential decays) or by deconvolution when the excitation pulse contribution was significant. Finally, to make the system as simple to use as possible, menu-driven software was used.

Interface implementation

The hardware and software have been revised several times. The original computer was an 8080-based Altair 8800B with 8-in. disk drives and an ACTA IV terminal. This computer is now upgraded with North Star 5¼-in. floppy disk drives and a CompuPro 4 MHz S-100 Z-80 CPU board. Although Altair disk BASIC and North Star BASIC were used in some stages, only the latest and most powerful CP/M based Turbo PASCAL versions are discussed here.

Parallel and serial ports were provided by a Processor Technology 3P + S board. This board provided 3-byte-wide latched output ports (A, B, and C),

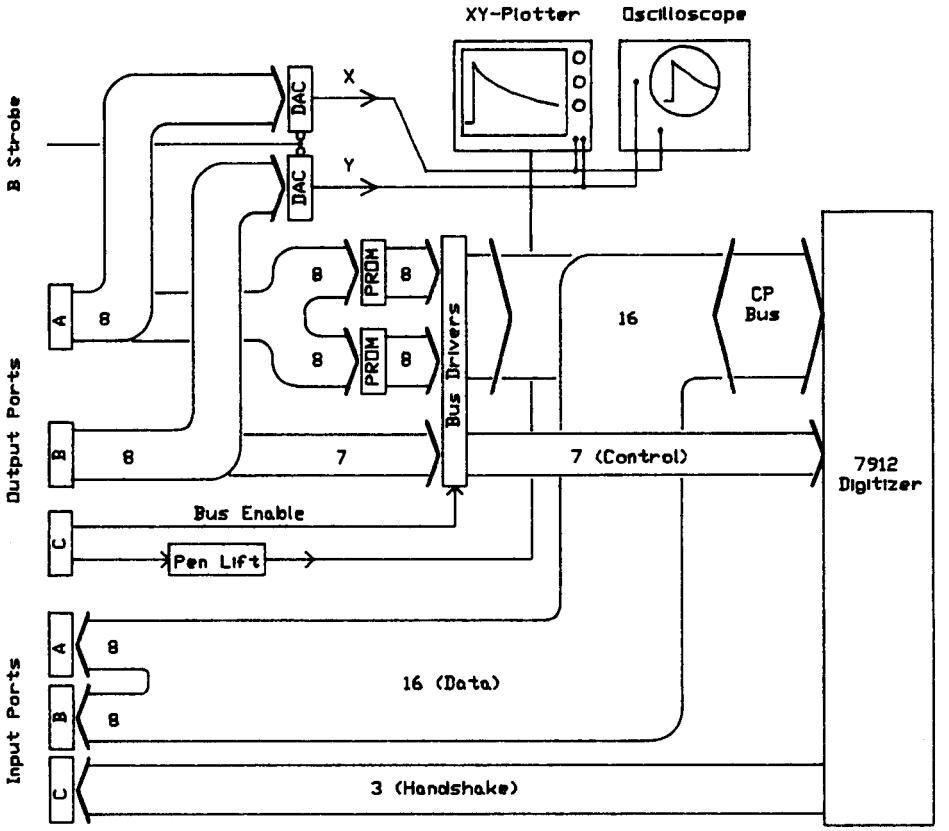

Fig. 1. Schematic representation of the computer interface for the R7912 digitizer. DAC NE5018 8-bit latched DAC (double buffered and triggered by the loading of the B output port); PROM 1702A (256 byte) PROM. The number of lines for each set of connections is indicated.

two-byte-wide (A and B) and one 6-bit (C) input ports, and one serial terminal port.

Complete digitizer control requires 23 computer output lines (16 command/data and 7 control/handshake) and 19 input lines (16 data and 3 handshake). To drive the oscilloscope and *X-Y* plotter, two output bytes were needed for two 8-bit DAC's and a pen lift control bit. This suggested a shortage of output lines.

Figure 1 shows the solution. The number of output lines was reduced by programming the nineteen 16-bit command words into the first 19 words of two-byte-wide 1702A program-only memories (PROM's) with one PROM containing the high byte of the command and the other PROM the low byte. The PROM address lines were driven in parallel by port A. To issue a command, one merely outputs the address of the correct PROM word. Output port B supplied the seven handshake and control lines.

The CP bus was driven through 7438 open-collector NAND gates. To isolate the control/command lines from the bus during set-up, each bit was gated by using the other NAND input line. All of these gate bits were tied together and driven from a bit on port C (bus enabled). During changes in command and status, the bus drivers were gated off. After complete formation of the command and status bits, the drivers were then gated on. A second bit of port C provided pen-lift control.

This arrangement also made it possible to use ports A and B to drive latched *X* and *Y* DAC's. The bus drivers were shut off during DAC output to prevent the digitizer from receiving spurious signals. Although the DAC's were addressed during communications with the digitizer, this presented no problem because they were not in use. Input port C handled the three handshake lines. Details of the circuit and the handshakes are described elsewhere [8].

The R7912 digitizer circuit treats the diode array as a 512 by 512 point matrix (512 vertical columns with 512 quantization levels). The scan gun probes the array by scanning each column sequentially with the address of the column to be scanned stored in the memory of the digitizer followed by digitization information about the column. Column-state information is distinguished from the column address by adding 512 to the latter.

Each column usually has several quantization levels discharged (written) because of the finite width of the write beam. Rather than store the address for every written area, only the addresses of the beginning and the end of the written areas are stored. Thus, the ideal form for the stored data is: the column address, vertical address of the beginning of the written area in the column, vertical address of the end of the written area in the column, next column address, etc.

Artifacts and instrumental features cloud this pristine picture. To save memory, the read circuit stores only the vertical address of the beginning of the written area for traces less than 6 channels wide. Also, for very wide written areas, there may be multiple written segments on a vertical address. Finally, permanent and transient target defects yield spurious points.

Another artifact arises because data writing is analogous to an oscilloscope. The writing beam intensity depends on the rate of change of the waveform; the beam tends to skip and leave unwritten areas on rapidly rising or falling portions. This leaves gaps in the digitized waveform. Further, digitization is continuous and asynchronous with storage, so the first memory location may be for any vertical address. As the digitizer predates microcomputerized instruments, no stored-data massaging is performed. The data transferred to the computer have all the above imperfections.

Several software modules are used. The main Pascal program handles all disk and high-level data-reduction operations. The Pascal program calls a ≈2K machine-language program that sets up the digitizer, transfers the data to the microcomputer, and does a partial normalization. This machine-language routine handles oscilloscopic and plotter data display.

The partial normalization is a simplified version of that recommended by Tektronix in the instruction manual for the R7912 digitizer. All ambiguous columns that have more than two leading or trailing edges are discarded. Vertical addresses that have only one leading and trailing edge are replaced by the average of the leading and trailing edge. Vertical addresses showing only a leading edge are corrected by the required offset of two.

The partially normalized data can be displayed on the oscilloscope to verify data quality. Excessive numbers of bad data points can result from either too high or too low a writing beam intensity. If unacceptable, the digitizer is readjusted and the transient re-recorded. Once a satisfactory transient is recorded, control is returned to the Pascal program where normalization is completed by extrapolating or interpolating the missing points. An option is provided for automatic baseline subtraction by using a previously acquired baseline. Alternatively, a baseline stored in memory or disk can be subtracted.

The user can then examine the normalized data and the semilogarithmic plot of intensity vs. time. This is useful for estimating the degree of non-exponentiality and for selecting the fitting region for the single-exponential fit routine. The Pascal program handles scaling, logarithmic conversions, and data storage. It then transfers control to a machine-language display routine. After inspecting the display, the user returns control to the Pascal program.

The user can display data in tabular form and fit a selected region by least squares to the semilogarithmic plot of intensity vs. time. The results are the lifetime, the pre-exponential factor, and a reduced chi-square.

Simple signal averaging is provided. Any number of transients can be collected (baseline-corrected if desired), normalized, and added together. However, the digitizer occasionally generates bad data that are meaningless or lack much of the transient; these errors are easily caught by visual inspection. To avoid averaging such data, it has been found most reliable for the operator to collect manually, partially normalize, and examine each curve before adding the transient to the accumulating average. Only 2—3 s are required for each decay. Because signal averaging is used only occasionally, this was preferable to designing software to trap all possible errors.

Other features provide for saving or loading data to floppy disk, deleting files, a disk directory, and transferring data to an HP-85 computer. Error trapping permits recovery from common, fatal errors. Program loading is performed automatically, so that even inexperienced users are insulated from the operating system.

Saved data can be reduced either by simplex or double-exponential Marquardt non-linear minimization routines. Alternatively, data can be reduced on the HP-85 computer with its superior graphics. For decay times similar to the 10-ns laser pulse used here, deconvolution software is provided.

Earlier BASIC programs provided plotting of data on a mechanical *X-Y* plotter. Currently, all plotting is done on the HP-85 computer.

Lifetime system

The remainder of the lifetime instrument is conventional [9]. Excitation is via pulsed nitrogen or dye lasers. The digitizer is triggered externally by a photomultiplier tube (PMT) that views the excitation beam via a beam splitter. Solution filters minimize stray radiation, and emissions are viewed through a JY H-10V monochromator. A RCA C7164R signal PMT provides excellent visible and near-infrared sensitivity (>800 nm).

RESULTS AND DISCUSSION

The system is extremely efficient and convenient to use. In the machine-language routine, data collection, data transfer from the digitizer to the computer, and partial normalization takes less than 1 s. Full normalization takes 1—5 s. Set-up for display of the normalized and semilogarithmic plots takes 5 s. Single exponential data fitting takes 30 s if all 512 points are fitted. Typically, a decay may be acquired, displayed, and reduced in <1 min. For replicate runs, collection and reduction of five decays takes less than 3 min. Imprecision for strong signals is about 2%.

System stability was judged by measuring several decay curves (10 ns FWHM) of the same sample. These decays were then deconvoluted one against the other. In the absence of time jitter and noise, the expected lifetime is zero. In practice, the "deconvoluted" decay times ranged from 10 to 100 ps. Thus, overall system noise and stability was less than 100 ps. After over six years of heavy use with no major repairs or maintenance, noise and jitter are now about 300 ps [10]. Presumably, upgrading the laser optics or electronics would improve performance.

The capabilities and ease of use of the system make it a powerful tool. Several studies of reactions of luminescent probes with surfactants [11], cyclodextrins [12], and complex equilibria involving quenchers [13] have been reported. Typical titration curves contained lifetimes (average of ⩾3 decays) taken for 10—60 different quencher or additive concentrations. The system has been used for quenching studies and measurements of solvent exposures for bound probes [14]. In the absence of such an automated system, many of these experiments would have been prohibitively time-consuming.

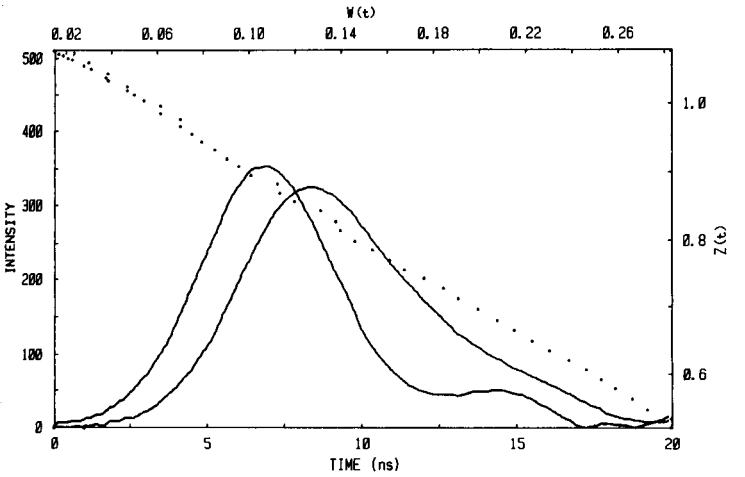

Fig. 2. Decay data for 1 μM rhodamine-B in water. The solid curves, which use the lower and the left axes are $E(t)$ and $D(t)$, with the earlier decay being $E(t)$. The dots, which use the right and upper axes, are the corresponding phase-plane plots. The data for the phase-plane plot are over the 7—13-ns range. Relatively few points are plotted on the phase-plane plot to prevent clutter. The plot was made on a mechanical X-Y plotter except for the axis system and labels.

Deconvolution routines are provided for short lifetimes. Figure 2 shows excitation and luminescence decay curves for rhodamine-B in water. The measured excitation pulse (7 ns FWHM) is wider than the 2-ns lifetime of the dye. Because there is no region free of continued pumping, reduction from the semilogarithmic plots is inaccurate. Deconvolution was by the phase-plane method [4, 10]:

$$Z(t) = K\tau - \tau\, W(t) \tag{1a}$$

$$Z(t) = \int_0^t D(t)\,\mathrm{d}t \Big/ \int_0^t E(t)\,\mathrm{d}t \tag{1b}$$

$$W(t) = D(t) \Big/ \int_0^t E(t)\,\mathrm{d}t \tag{1c}$$

where $E(t)$ and $D(t)$ are the observed excitation and emission decays, respectively, K is the proportionality constant linking $E(t)$ and $D(t)$ in the integral equation, and τ is the luminescence decay time. Plots of $Z(t)$ vs. $W(t)$ should be linear with slopes of $-\tau$. The phase-plane plot is shown in Fig. 2.

The calculated rhodamine-B lifetime was 2.2 ns. A 3.8-ns lifetime for rhodamine-6G under the same conditions agrees well with a phase-angle measurement of 3.6 ns [15]. The dyes were excited at 540 nm and monitored at 560—570 nm to avoid wavelength-dependent transit time variations for $E(t)$ and $D(t)$. However, where wavelength-dependent transit times are a

problem, the phase-plane method can be modified to permit successful deconvolution of lifetimes of about 1 ns for a 10-ns (FWHM) excitation pulse [10].

The hardware and software are much too extensive to describe in detail here. The relevant portions of earlier work [8] and past and existing transient digitizer control-software listings are available for $10 to cover reproduction and mailing.

We thank S. L. Buell, B. L. Hauenstein, Jr., and E. C. Carraway for early software revisions, and M. Grubb and D. Moxness (Tektronix) for electronics assistance. Other group members and numerous physical chemistry students were very helpful in ferreting out problems and making suggestions. We gratefully acknowledge support by the NSF (Grants 82-06279 and 86-00012) and the donors of the Petroleum Research Fund administered by the American Chemical Society.

REFERENCES

1 R. B. Cundall and R. E. Dale (Eds.), Time-Reduced Fluorescence Spectroscopy in Biochemistry and Biology, Plenum, New York, 1983.
2 D. V. O'Connor and D. Phillips, Time-Correlated Single Photon Counting, Academic, New York, 1984.
3 J. R. Lackowicz, Principles of Fluorescence Spectroscopy, Plenum, New York, 1983.
4 J. N. Demas, Excited State Measurements, Academic, New York, 1983.
5 D. G. Taylor, T. J. Turley, M. Rodgers, S. H. Peterson and J. N. Demas, Rev. Sci. Instrum., 51 (1980) 855.
6 T. D. L. Pearson, J. N. Demas and S. Davis, Anal. Chem., 54 (1980) 1899.
7 R. J. Woods, S. Scypinski, L. J. Cline Love and H. A. Ashworth, Anal. Chem., 56 (1984) 1395.
8 T. J. Turley, M. S. Thesis, University of Virginia, 1980.
9 K. Mandal, B. L. Hauenstein, Jr., J. N. Demas and B. A. DeGraff, Inorg. Chem., 87 (1983) 328.
10 E. R. Carraway, B. L. Hauenstein, Jr., J. N. Demas and B. A. DeGraff, Anal. Chem., 57 (1985) 2304.
11 B. L. Hauenstein, Jr., K. Mandal, J. N. Demas and B. A. DeGraff, Inorg. Chem., 23 (1984) 1101.
12 J. I. Cline, III, W. J. Dressick, J. N. Demas and B. A. DeGraff, J. Phys. Chem., 89 (1985) 94.
13 S. W. Snyder, D. E. Raines, P. T. Rieger, J. N. Demas and B. A. DeGraff, Langmuir, 1 (1985) 548.
14 B. L. Hauenstein, Jr., W. J. Dressick, J. N. Demas and B. A. DeGraff, J. Am. Chem. Soc., 105 (1985) 4251.
15 J. N. Demas and R. A. Keller, Anal. Chem., 57 (1985) 538.

Analytica Chimica Acta, 197 (1987) 129—135
Elsevier Science Publishers B.V., Amsterdam — Printed in The Netherlands

OPERATIONAL METHOD FOR SLOPE ESTIMATIONS

G. L. SILVER
Monsanto Research Corporation/Mound, Miamisburg, OH 45342 (U.S.A.)
(Received 31st December 1986)

SUMMARY

The operational method yields an abundance of new slope estimating formulae that apply to equidistant, curvilinear data. The performances of two of these new formulae are compared to the standard formula for center-point slope estimations on three data points. It is demonstrated that the standard formula is only a special case developed from the more general operational approach. New slope formulae at the terminal values of three curvilinear data are derived. Formulae applicable to more than three data points can also be obtained.

In 1985, the operational method of data treatment was introduced [1]; the technique was considered to be a means of exploration because it is easy to learn and can be used to search for unrecognized relationships in data. The method depends on conventions that are easy to master. With the aid of these conventions, new formulae for pointwise interpolation of curvilinear data can be obtained. Continuous interpolation is possible with the aid of a computer [2]. The technique can be expanded into more dimensions, and several two-dimensional formulae have been collected [3].

BACKGROUND

The basis of the operational method can be comprehended through an uncommon interpretation of the incremental form of the Taylor series

$$\phi(x + h) = \phi(x) + h\mathrm{d}\phi(x)/\mathrm{d}x + (h^2/2!)\mathrm{d}^2\phi(x)/\mathrm{d}x^2 + \ldots \quad (1)$$

In this expression, $\phi(x)$ represents some unspecified function of the variable, x, and h represents a small increment to be added to the variable. Equation 1 can be compared to the expansion

$$\exp(hx) = 1 + hx + (hx)^2/2! + \ldots. \quad (2)$$

If the variable, x, in the second expansion is replaced by the differentiation operator $\mathrm{d}/\mathrm{d}x$ (abbreviated D), Equation 2 becomes

$$\exp(h\mathrm{D}) = 1 + h\mathrm{D} + (h^2/2!)\mathrm{D}^2 + \ldots \quad (3)$$

If operators and functions operated upon are considered to be separable,

0003-2670/87/$03.50

Eqn. 3 can be multiplied by $\phi(x)$ (primes represent derivatives)

$$\exp(h\mathrm{D})\phi(x) = \phi(x) + h\phi'(x) + (h^2/2!)\phi''(x) + \ldots$$

with the consequent interpretation

$$\exp(h\mathrm{D})\phi(x) = \phi(x + h) \tag{4}$$

This interpretation is useful as a mnemonic device, but it is not new [4].

Consider the definition of $\cosh(x)$: $\cosh(x) = [\exp(x) + \exp(-x)]/2$. If x is replaced by $h\mathrm{D}$ and this equation is multiplied by $\phi(x)$, then the same interpretation that allows Eqn. 4 suggests

$$\cosh(x)\phi(x) = [\phi(x + h) + \phi(x - h)]/2 \tag{5}$$

Thus if an equation containing $\cosh(x)$ occurs, it can be multiplied by $\phi(x)$ and the $\cosh(x)\phi(x)$ term replaced by the right-hand side of Eqn. 5. An example is

$$\cosh(2x) = 2\cosh^2(x) - 1 \tag{6}$$

Equation 6 is multiplied by $[\phi(x)]^2$ so that every $\cosh(x)$ term can be associated with one $\phi(x)$. This interpretation is taken as axiomatic: it is very useful, if unconventional. Equation 6 thus becomes

$$\phi(x)[\phi(x + 2h) + \phi(x - 2h)]/2 = 2\{[\phi(x + h) + \phi(x - h)]/2\}^2 - \phi^2(x)$$

In this equation, the parameter h represents the spacing on the x-axis between successive, equidistant points on a curve, $\phi(x)$ represents the center point of the curve, and $\phi(x + h)$ represents the function with x incremented by h; it is also represented by the first point to the right of the center point on the curve. The second point to the right of the center point represents $\phi(x + 2h)$, while the two points to the left of the center point are $\phi(x - h)$ and $\phi(x - 2h)$, respectively. Thus if five equidistant values A, B, C, D, E lie on a curve, it is possible for them to be related by the equation

$$C[(A + E)/2] = [(B + D)^2/2] - C^2 \tag{7}$$

There are many such equations. They are useful because some of them have the virtue of representing more than one function that could be passed through the points [1]. Briefly, they may have greater flexibility than other expressions that could be used for the interpolation [3]. Equation 7 and similar equations might remain undetected were it not for the operational method.

Although the hyperbolic identities can be used to derive equations connecting data points, these identities are not as common as the ordinary trigonometric identities. Because the hyperbolic and trigonometric identities can be connected by the symbol i, representing the square root of minus one, most operational formulae have been developed by using trigonometric identities that are homogeneous in sine terms [1, 3]. To use the trigonometric identities in this manner, the following conventions are useful

(a) $ix = h\mathrm{D}$, or $\exp(ix)\phi(x) = \phi(x + h)$,

(b) $\cos(nx)\phi(x) = [\phi(x + nh) + \phi(x - nh)]/2$,

(c) $\sin(nx)\phi(x) = [\phi(x + nh) - \phi(x - nh)]/2i$,

(d) commutative multiplication of functions and operators, and (e) free distribution of functions among operators. The conventions to be observed when dealing with more than one variable have been discussed elsewhere [1].

APPLICATION TO SLOPE ESTIMATIONS

If radian measure is adopted, the approximation

$$x \approx \sin(x) \tag{8}$$

becomes more accurate as x diminishes. Using the Euler identities, this approximation can be rewritten as

$$x = [\exp(ix) - \exp(-ix)]/2i$$

$$\text{or } ix = [\exp(ix) - \exp(-ix)]/2 \tag{9}$$

Multiplying this equation by $\phi(x)$ yields

$$h\phi'(x) = [\phi(x + h) - \phi(x - h)]/2 \tag{10}$$

The standard method for determining the first derivative at the midpoint of three equidistant points A, B, C on a curve is $B' = (C - A)/2h$, where h is the spacing between successive points. This is the interpretation of Eqn. 10, so the operational method has developed the standard equation from $x \approx \sin(x)$. But it is possible to select better approximations to x than its sine, e.g.

$$x = [\tan(x) + 2\sin(x)]/3 \tag{11}$$

$$\text{or } x = [56\sin(x) + 4\sin(x)\cos(x)]/[36 + 24\cos(x)] \tag{12}$$

Equations 8, 11 and 12 are successively better approximations. If x is one radian, for example, the three approximations yield 0.8415, 1.0801, and 0.9995, respectively.

If $\tan(x)$ is rewritten as $\sin(x)/\cos(x)$, and these functions are given their Euler interpretations [1], and if Eqn. 11 is multiplied through by unity (i.e., $\phi(x)/\phi(x)$ on the left and $\phi^2(x)/\phi^2(x)$ on the right), then a new formula for the slope at midpoint B is obtained

$$B' = (1/3h)(C - A)(A + B + C)/(C + A) \tag{13}$$

Similarly, Eqn. 12 yields

$$B' = (1/h)[C^2 + 28B(C - A) - A^2]/[36B + 12(C + A)] \tag{14}$$

where the prime on the letter B indicates first derivative, and A, B, C are considered equidistant. The standard formula, Eqn. 10, is therefore only a

special case of a more general method. Derivative formulae obtained from approximations other than $x \approx \sin(x)$ often have the advantage of incorporating the information available in the numerical value of B, something that the standard formula fails to do. They allow estimation of the derivative dB'/dB, which is not possible with the standard formulae.

Table 1 illustrates the behavior of Eqns. 10, 13 and 14 on three equidistant points A, B, and C given values of 3, 4, and 5, respectively. Some typical operations have also been applied to these values. If the operation is squaring (x^2), for example, then $A = 9, B = 16, C = 25$. It can be seen from Table 1 that the new formulae work about as well as the standard formula: sometimes better, sometimes worse. It is evident that the property of being a better trigonometric approximation does not necessarily result in a better derivative formula in every case. The results in Table 1 must not be interpreted as typical. There are too many new formulae, and too many functions, to allow generalization from these examples [2]. [The interested reader may wish to try another formula: $x = \tan(x)$ yields $B' = B(C - A)/h(C + A)$.]

Operational formulae are not restricted to curves defined by three points. In Eqn. 11, if $\tan(x)$ is replaced by $\sin(x)/\cos(x)$ so that the approximation has two $\sin(x)$ terms and one $\cos(x)$ term, then from the identity $\sin(2x) = 2\sin(x)\cos(x)$, the term $\sin(x)$ can be replaced by $\sin(2x)/2\cos(x)$. This ratio can be substituted for one of the $\sin(x)$ terms in Eqn. 11, or for the other one, or for both $\sin(x)$ terms. Because $\sin(2x)$ becomes $[\phi(x + 2h) - \phi(x - 2h)]/2i$, while $\cos(x)$ becomes $[\phi(x + h) + \phi(x - h)]/2$, three new equations for the slope at the midpoint of five equidistant curvilinear points can be obtained [2]. Still more possibilities arise by substitution of $\cos(x)$ from the identity $\cos(2x) = 2\cos^2(x) - 1$. This is only the beginning, for many other approximations to x in terms of its trigonometric functions could have been used as the starting point for the derivations. While deriva-

TABLE 1

Slope estimations at point B on three equidistant points A, B, and C with values of 3, 4, and 5, respectively

Operation	Slope estimates			True slope
	Eqn. 10	Eqn. 13	Eqn. 14	
None	1.00	1.00	1.00	1.00
x^2	8.00	7.84	7.84	8.00
x^4	272	247	242	256
x^6	7448	6209	5679	6144
$\exp(x)$	64.2	56.6	54.6	54.6
$x^{1/2}$	0.252	0.253	0.253	0.250
$\tan(10x)$	1.76	1.73	1.73	1.70
$\sin(10x)$	0.762	0.766	0.766	0.766
$1/x$	−0.0667	−0.0653	−0.0653	−0.0625
$\ln(x)$	0.255	0.257	0.257	0.250

tive formulae for more and more points can be obtained in this manner, they do not necessarily use the increasing information advantageously. The operational method appears to be strongest when applied to limited data [1].

Example

In the earlier paper [1], the extreme and mirror points were estimated on a spectral curve. The distance of the extreme point from the center point was found by application of the Taylor series. The first derivative at midpoint, $P2$, of the curve can be estimated by Eqn. 14. If Eqn. 14 were perfect, it would always yield the correct value of the derivative at $P2$ using any pair of symmetric points. Thus, the slope at $P2$ can be estimated using either side points $P1$ and $P3$ or E and A (see Fig. 2 in [1]). Because the derivative should be the same whatever points are chosen, it follows that

$$\frac{1}{h}\left[\frac{(P3)^2 + 28(P2)(P3 - P1) - (P1)^2}{36(P2) + 12(P3 + P1)}\right] = \frac{1}{hq}\left[\frac{A^2 + 28(P2)(A - E) - E^2}{36(P2) + 12(A + E)}\right]$$

where h represents the spacing separating $P1$, $P2$, and $P3$, and q represents the fraction of distance h that separates E, $P2$ and A. The value of q is found to be 0.200, an improvement over 0.206 obtained earlier [1].

MORE APPLICATIONS OF THE OPERATIONAL METHOD

Slope estimations by the operational method are not restricted to center points. Consider the expansion

$$1/[\exp(x) + 1] = 1/2 - x/4 + \ldots. \tag{15a}$$

and let $x = h\mathrm{D}$. Multiplying Eqn. 15a by unity, i.e., $\phi(x)/\phi(x)$, yields

$$C' = [2(C - B) - hB']/h \tag{15b}$$

where C' represents the first derivative at terminal value C on the equidistant sequence A, B, C and h is their uniform spacing. Alternatively, the expansions

$$2/[\exp(x) + \exp(-x)] = 1 - x^2/2 + \ldots \tag{16}$$

$$2x/[\exp(x) - \exp(-x)] = 1 - x^2/6 + \ldots \tag{17}$$

can be treated similarly. Solving the resulting simultaneous equations yields

$$C'' = [4C - 2(B + A) - 6hB']/h^2$$

so that a formula for the second derivative at C has been obtained. Reversing the order of points changes the sign of h and gives the derivative at A. Other expansions can be treated similarly [2].

The subject of higher derivatives can be used to illustrate that boundaries on the operational method are not clear. Consider the cosine series

$$\cos(x) = 1 - x^2/2 + \ldots \tag{18}$$

When the symbol i occurs in an exponent, it is given operator status. When it occurs as a coefficient in an infinite series, it is also allowed to have its conventional meaning, $i^2 = -1$. This practice has so far found application only with infinite series [3]. (Equation 8 is only the first term of an infinite series for x in terms of its sine [2]; similar approximations can presumably be expanded into series.) Equation 18 thus becomes

$$\cos(x) = 1 + (ix)^2/2 + \ldots$$

Multiplication by $\phi(x)$ yields

$$[\phi(x + h) + \phi(x - h)]/2 = \phi(x) + (h^2/2)/\phi''(x)$$

an equation that is identical to the standard formula for the second derivative at midvalue B

$$B'' = (C - 2B + A)/h^2 \tag{19}$$

This example suggests that generalization of the technique may prove advantageous. If Eqn. 11 is squared, $-(ix)^2$ substituted for x^2, and $1 - \cos^2(x)$ substituted for every $\sin^2(x)$, the result is

$$-9(ix)^2 = [1 - \cos^2(x)]\,[1 + 2\cos(x)]^2/\cos^2(x)$$

If the left-hand side is multiplied by $\phi^2(x)$, and the right-hand side by $\phi^4(x)/\phi^2(x)$, the operational interpretation of the resulting formula is

$$B'' = (1/h^2)[(C + A)^2 - 4B^2]\,(A + B + C)^2/[9B(C + A)^2] \tag{20}$$

This approximation, not obvious without the operational method, has properties of a second-derivative formula. The series representation of the square root of the cosine function yields a curious equation with the properties of a second-derivative estimator:

$$B'' = (4/h^2)\ \{[B(C + A)/2]^{1/2} - B\} \tag{21}$$

Table 2 compares the predictive properties of Eqns. 19, 20, and 21 on three equidistant points $A = 3$, $B = 4$, and $C = 5$ for some selected functions applied to the points.

TABLE 2

Second-derivative estimations at point B on three equidistant points with values 3, 4, and 5, respectively

Operation	Second-derivative estimates			True value
	Eqn. 19	Eqn. 20	Eqn. 21	
None	0.00	0.00	0.00	0.00
x^2	2.00	1.98	1.97	2.00
x^4	194.0	190.4	178.5	192.0
$\sin(10x)$	−0.641	−0.643	−0.644	−0.643
$1/x$	0.033	0.033	0.033	0.031
$\exp(x)$	59.3	58.8	52.9	54.6
$(x)^{1/2}$	−0.032	−0.032	−0.032	−0.031

Conclusions

The operational method provides a means of searching for unanticipated relationships in numerical analysis. Its axioms are simple and easy to apply. The technique has been used on positive integer powers of angle approximation formulae to demonstrate new slope equations. The standard three-point formulae for first and second derivatives are special cases of the operational method. The new formulae usually apply if the data are restricted to positive numbers, but no method is known for culling the best formulae for particular data configurations. Although empirical, the new technique has not been shown to produce inconsistencies, the critical test of any axiomatic system [5]. The boundaries of the method are not established, but if rigor can be temporarily subordinated to imagination, they seem certain to expand beyond what is presently known.

Mound is operated by Monsanto Research Corporation for the U.S Department of Energy under Contract No. DE-AC04-76-DP00053.

REFERENCES

1 G. L. Silver, J. Comp. Chem., 6 (1985) 229.
2 G. L. Silver, Extensions of the Operational Method, USDOE Report MLM-3382 (25 August, 1986).
3 G. L. Silver, Operational Methods for Data Interpolation, USDOE Report MLM-3277 (1 August, 1985).
4 Z. Kopal, Numerical Analysis, Wiley, New York, 1961, Appendix III.
5 C. R. Wylie, Jr., Foundations of Geometry, McGraw-Hill, New York, 1961, Sect. 1.3.

Analytica Chimica Acta, 197 (1987) 137—148
Elsevier Science Publishers B.V., Amsterdam — Printed in The Netherlands

A NOVEL ADSORBENT FOR THE DETERMINATION OF THE TOXIC FRACTION OF COPPER IN NATURAL WATERS

MANPING ZHANG[a] and T. M. FLORENCE*

CSIRO, Division of Energy Chemistry, Private Mail Bag 7, Menai, N.S.W., 2234 (Australia)

(Received 5th January 1987)

SUMMARY

A novel adsorbent for the determination of the toxic fraction of copper in natural waters is described. Aluminium hydroxide adsorbed on a sulfonic acid cation-exchange resin quantitatively retains copper(II) ions in the absence of organic ligands such as fulvic, humic and tannic acids. In the presence of these ligands, a smaller fraction of copper is adsorbed and can be related to the toxic fraction. The toxic fraction determined by this method agreed well with results of algal assay with the marine diatom *Nitzschia closterium* in seawater and the green alga *Chlorella pyrenoidosa* in a synthetic soft water. The aluminium hydroxide-coated column also quantitatively adsorbs lipid-soluble copper complexes, which can be leached selectively from the column with methanol. The Al:OH ratio on the resin was 1:2 and the conditional stability constants (log K) of the Cu^{2+}-adsorbent complexes in seawater and synthetic soft water were found to be 9.87 and 11.10, respectively; these values are similar to the equilibrium constants for the reaction between Cu^{2+} and algae. The application of this adsorbent in an in-situ instrument for the continuous, unattended determination of the toxic fraction of copper and some other toxic metals in natural waters is outlined.

It is now well established that determination of the total concentration of a metal in a water sample provides little information about its potential toxicity to aquatic organisms [1, 2]. Toxicity varies greatly with the physico-chemical form of the metal present in water; for example, two samples with an identical total concentration of copper may show completely different toxicities if one water has a high concentration of fulvic acid.

Free metal ion is usually the most toxic form of a metal [3, 4] and complexing agents such as fulvic, humic and tannic acids reduce toxicity. Notable exceptions to this rule are lipid-soluble metal complexes (e.g., 8-quinolinol complexes) which may be even more potent than free metal ion [5, 6]. The "toxic fraction" of a metal in a water sample is defined as the percentage of the total metal concentration which is recognised as toxic by a test organism, using a completely ionized inorganic salt of the metal (e.g., chloride or sulfate) as a 100% toxicity reference.

---

[a]On leave from Department of Chemistry, Shandong College of Oceanography, Qingdao, People's Republic of China.

0003-2670/87/$03.50

The toxic fraction is usually determined by a bio-assay or by an electrochemical technique such as anodic stripping voltammetry (ASV) or polarography. Recently, Zorkin et al. [7] reported on a cation-exchange procedure for determining the biologically-active fraction of copper. This method is based on the assumption that Cu^{2+} is the most toxic copper species [3] and that its concentration in a seawater sample of constant composition can be related to the amount of metal sorbed by a sulfonic acid cation-exchange resin.

The development of an in-situ instrument for measuring the average concentrations, over several weeks, of total copper, lipid-soluble copper, and the toxic fraction of copper in seawater or freshwater would be valuable. The corresponding concentrations of zinc, cadmium and lead are also of interest. The instrument would consist of a power source, pump, timer, gauge, filter and adsorbent columns in series for lipid-soluble, toxic and total metal. The development of an adsorbent column for the toxic fraction proved to be the most difficult problem. The cation-exchange method [7] cannot be used for this application because it is an equilibrium system, and cannot integrate the toxic fraction in water containing a varying copper concentration. The cation-exchange resin-bonded copper will simply reflect the toxic copper concentrations in the last column equivalent of seawater to pass through.

The sorbent finally selected for measuring the integrated toxic copper concentration was a sulfonic cation-exchange resin with aluminium hydroxide adsorbed in the resin pores [8, 9]. This adsorbent yields a reasonable estimate of toxic copper in both seawater and a synthetic soft water when compared with toxicity results obtained by algal assays [10].

EXPERIMENTAL

Apparatus and reagents

An EG and G PAR 384 Polarographic Analyzer with a hanging mercury drop electrode was used in the differential-pulse mode for all measurements of total metal by anodic stripping voltammetry (ASV) [11]. Some metals were also determined by atomic absorption spectrometry (AAS) and inductively-coupled plasma emission spectrometry (ICPES).

Merck Suprapur sodium acetate and sodium chloride were used; other reagents were of analytical-reagent grade.

The working area was a Class-100 clean room controlled at a temperature of 25 ± 0.5°C.

Fulvic acid was extracted from garden soil by pyrophosphate extraction, which yields an acid with a very low degree of oxidation [12].

The aluminium hydroxide/cation-exchange columns were prepared as follows: Baker aromatic sulfonic acid disposable extraction columns, H^+ form, containing ca. 1 ml of cation-exchange resin (J. T. Baker Chemical Co., cat. no. 7090-3) were converted to the Na^+ form by passing 10 ml of 1 M sodium chloride through the column, until the pH of the effluent was close

to neutral. The resin was then converted to the Al^{3+} form by passing 10 ml of 0.1 M aluminium chloride. The ion-exchange capacity of a column was 1.1 mmol Na^+.

Determination of aluminium in the effluent showed that 0.16 mmol of Al^{3+} was retained in the column. The column was washed with water to remove excess of Al^{3+}, then 5 ml of 0.5 M ammonia solution was passed through the column to convert the Al^{3+} to aluminium hydroxide, and excess of ammonia was removed by washing with water. When not in use, the column was filled with water to prevent the aluminium hydroxide coating from drying out and losing its adsorptive properties.

Algal assays

The marine diatom *Nitzschia closterium* and the green alga *Chlorella pyrenoidosa* were used in seawater and synthetic soft water, respectively. The assay techniques were as described previously [10, 11].

For *Nitzschia closterium*, the assay medium was filtered seawater collected 2 km off Port Hacking, N.S.W., with 0.5 ml of 0.026 M sodium nitrate and 0.5 ml of 1.28×10^{-3} M dipotassium hydrogenphosphate per 50 ml of seawater. For *Chlorella pyrenoidosa*, the assay medium was 50 ml of standard soft water ($NaHCO_3$, 48 mg l^{-1}; $CaSO_4 \cdot 2H_2O$, 30 mg l^{-1}; $MgSO_4$, 30 mg l^{-1}; KCl, 2 mg l^{-1}) with the addition of 1.0 ml of 0.5 M HEPES buffer (pH 7.0) plus 0.5 ml of the 0.026 M nitrate and 0.5 ml of the 1.28×10^{-3} M dihydrogenphosphate solutions. Cell density was measured after preparation and on three subsequent days using a haemocytometer.

A calibration curve of relative growth rate versus copper concentration was plotted. The toxic concentration of a given metal solution was determined from the measured growth rate and the calibration curve [10].

RESULTS AND DISCUSSION

Algal assay of trace metal toxicity in seawater and freshwater

To compare the fraction of metal retained by the aluminium hydroxide column with the toxic fraction, algal assays were conducted for seawater and freshwater. Figure 1 shows the relative growth rate vs. trace metal concentration curve for Cu, Pb, Cd and Zn in seawater and Fig. 2 shows the relative growth rate vs. copper concentration in soft water.

Table 1 shows the copper concentrations for 50% depression of growth rate in seawater and synthetic soft water, and the toxic fraction for the fulvic, humic, tannic and nitrilotriacetic acid complexes of these metals.

Choice of metal hydroxide for coating

Various metal hydroxides were tested for coating on the cation-exchange resin column. Some could not be immobilized very strongly, and some overestimated the toxic metal fraction. Preliminary experiments showed that aluminium hydroxide coated on Bio-Rad 50W-X8 cation-exchange resin

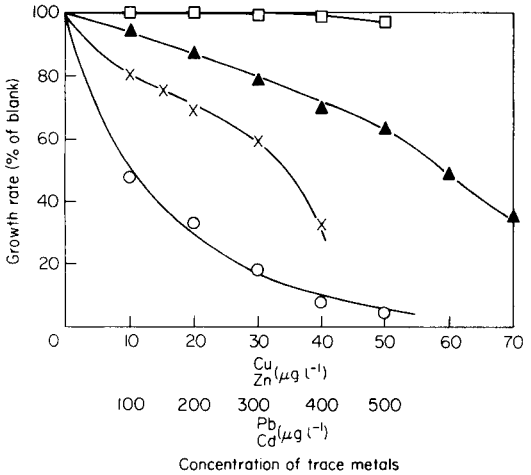

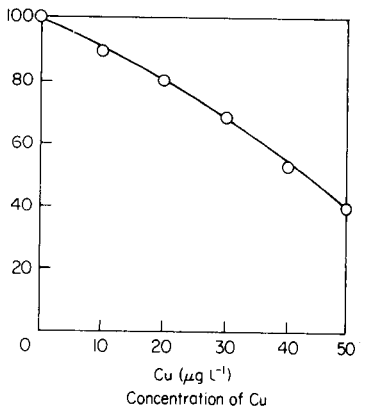

Fig. 1. Trace metal toxicity for algal growth (*Nitzschia closterium*) in enriched seawater: (▲) Zn; (×) Cd; (○) Cu; (□) Pb.

Fig. 2. Toxicity of copper for algal growth (*Chlorella pyrenoidosa*) in enriched synthetic soft water.

TABLE 1

Toxic fraction of copper in seawater and synthetic soft water in the presence of some organic ligands

Organic ligand	Toxic fraction (%)	
	N. closterium[a]	*C. pyrenoidosa*[b]
Fulvic acid, 10 mg l^{-1}	20	42
Humic acid, 10 mg l^{-1}	30	33
Tannic acid, 10 mg l^{-1}	30	30
Nitrilotriacetic acid, 2×10^{-5} M	10	0

[a]50% depression of growth occurred with 9.5 μg l^{-1} copper. [b]50% depression of growth occurred with 43 μg l^{-1} copper.

held promise as a means of estimating the toxic copper concentration. In the absence of organic ligands, this resin adsorbs ionic copper completely and in the presence of some common organic ligands, the metal adsorption decreases.

Efficient immobilization of the aluminium hydroxide on the resin phase required a resin with small particle size (300—400 mesh); larger particles led to leakage of Al^{3+} into the effluent. Commercially-available cation-exchange resin columns (Baker disposable extraction columns) packed with

1 ml of strong cation-exchange resin ($C_6H_5SO_3H$), were used for all subsequent experiments. Coatings of iron(III), cobalt(III) and aluminium(III) hydroxides, and manganese(IV) oxide were prepared on the cation-exchange cartridges and the adsorption properties of these coatings were compared (Table 2). The method of coating the iron(III) and cobalt(III) hydroxides was similar to that described for aluminium hydroxide except that 0.2 M sodium hydroxide was used for conversion to the hydroxides, and hydrogen peroxide was added to oxidize Co(II) to Co(III). The manganese(IV) oxide coating was prepared by adsorbing Mn^{2+} on the column and then passing 0.1 M potassium permanganate.

From Table 2, it is clear that the columns coated with iron(III) or cobalt(III) hydroxide, or manganese(IV) oxide over-estimated the toxic fraction of heavy metals in seawater, whereas the aluminium hydroxide-coated column gave a reasonable correlation with toxic fraction for copper with the ligands studied. However, no sensible correlations were obtained for lead, cadmium, and zinc.

The aluminium hydroxide/cation-exchange resin column is very stable in seawater. After the passage of 1 l of seawater through the column, no increase in aluminium concentration (<1 $\mu g\ l^{-1}$ Al) could be detected in the effluent.

The adsorptive properties of the aluminium hydroxide-coated resin are quite different from those of crystalline aluminium trioxide (Table 3). The Sep-Pak alumina column is a less efficient adsorbent for Zn^{2+}, and does not measure the toxic fraction of copper in the presence of fulvic acid, because the copper-fulvic acid complex is adsorbed on aluminium trioxide. Neither fulvic acid nor its copper complex is adsorbed on the aluminium hydroxide-coated resin.

The capacity of aluminium hydroxide-coated cation-exchange resin column and the effects of pH and flow rate

The capacity of the aluminium hydroxide-coated cation-exchange column was determined by passing 100 ml of seawater containing 10^{-5} M Cu, Pb, Zn and Cd, and the effluent was monitored every 10 ml by using ASV. Complete ($>95\%$) adsorption of copper, lead and zinc was found even after 100 ml of feed solution, but the adsorption of cadmium remained at 20% throughout the experiment. The column can therefore adsorb more than 1 μmol of Cu, Pb and Zn from seawater, which is an adequate capacity for the extraction of 20—30 l of natural or slightly polluted seawater.

To examine the effect of pH on the adsorption, seawater and synthetic soft water containing 10^{-6} M Cu, Pb, Cd and Zn, and adjusted to different pH values in the range 4—8, were passed through aluminium hydroxide columns and the adsorption was measured by ASV. Below pH 4, no metals were adsorbed, and the coated aluminium hydroxide may have been dissolved. Complete adsorption of copper, lead and zinc was obtained above pH 7 in freshwater and above pH 8 in seawater (Fig. 3).

TABLE 2

Adsorption of trace metals on an aluminium hydroxide-coated cation-exchange resin column in the absence and presence of fulvic acid[a]

Hydroxide coating	Fulvic acid concn.	Adsorbed fraction (%)			
		Zn	Cd	Pb	Cu
Fe(III)	None	95	99	100	99
	10 mg l^{-1}	98	99	100	90
Al(III)	None	95	20	100	95
	10 mg l^{-1}	50	20	100	40
Co(III)	None	100	100	90	90
	10 mg l^{-1}	100	100	90	60
MnO_2	None	98	68	99	97
	10 mg l^{-1}	82	35	95	83

[a] 10^{-6} M metals (Cu, Pb, Cd, Zn) added to seawater.

TABLE 3

Comparison of alumina Sep-Pak and aluminium hydroxide-coated cation-exchange resin columns for adsorption of trace metals[a]

Column	Fulvic acid concn.	Adsorbed fraction (%)		
		Zn	Cd	Cu
Alumina	None	43	90	88
	10 mg l^{-1}	40	85	87
Aluminium hydroxide	None	99	20	95
	10 mg l^{-1}	50	20	40

[a] 10^{-6} M Cu, Cd and Zn added to seawater.

Flow rate in the range 3—50 ml min^{-1} had no effect on the adsorption efficiency of Cu^{2+} on the aluminium hydroxide-coated resin column. The very small particle size in the Baker column and the large exchange surface apparently prevented any mass-transfer effects.

Determination of the equilibrium constant for the adsorption of Cu^{2+} on the aluminium hydroxide-coated cation-exchange resin

The equilibrium constant for the Cu^{2+}/aluminium hydroxide association was determined by the graphical method of Loewenschuss and Schmuckler [13], with histidine as the competing ligand (for Cu-histidine, $\log \beta_1 = 10.20$ [14]). The experiment was done by a batch technique with aluminium hydroxide-coated Bio-Rad AG-MP 50 cation-exchange resin. The capacity of the wet adsorbent for copper was 0.10 mmol g^{-1}. Weighed portions of the adsorbent were shaken overnight at 25°C with seawater or synthetic soft

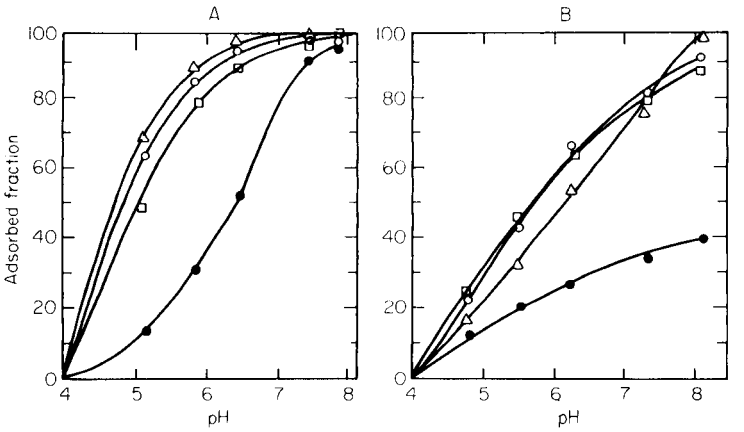

Fig. 3. Adsorption of ionic Cu, Zn, Pb, Cd (10^{-6} M) onto aluminium hydroxide-coated columns at different pH values: (A) soft water; (B) seawater. Metals: (△) Pb; (○) Cu; (□) Zn; (●) Cd.

water containing varying concentrations of Cu^{2+} and histidine, and the concentrations of copper in the supernatant solution were determined; the data for soft water are given in Table 4. The values for the conditional equilibrium constant (log K') for the Cu^{2+}/adsorbent complex were calculated [13] to be log K' = 9.87 in seawater and 11.1 in synthetic soft water. The smaller value in seawater is probably due to some complexing of copper with chloride, and competition for adsorption sites by sodium and magnesium ions.

Previous studies have shown that the equilibrium constants for the reaction between Cu^{2+} and marine algae in seawater have values in the range log K = 9—11 [15]. This explains why the aluminium hydroxide-coated adsorbent with log K' = 9.87 can be used to estimate the toxic fraction of copper in seawater.

Determination of the Al:OH ratio in the aluminium hydroxide-coated cation-exchange resin column

An aluminium hydroxide-coated resin column, as described in the Experimental section, was treated by passing 10.00 ml of standard 0.1 M hydrochloric acid through the column, washing with water, and diluting the effluents to 25 ml. Aluminium and excess of acid were determined in this solution. Aluminium was measured by ICPES, and free acid by potentiometric titration in the presence of oxalate [16].

The Al:OH mole ratio in the column was found to be 1:1.98, so that the species adsorbed on the resin (R) is R—SO_3—$Al(OH)_2$, and not simply $Al(OH)_3$ precipitated in the pores of the resin. The $Al(OH)_2^+$ species, being positively charged, can bond strongly to the negatively-charged sulfonic acid resin.

TABLE 4

Determination of equilibrium constant in soft water for the Cu^{2+} complex with the aluminium hydroxide-coated resin

No.	Cu^{2+} taken[a]	Histidine taken[a]	Resin (wet) (g)	Cu^{2+} in resin (μmol)	Histidine unused (μmol)	CuY in solution[b] (μmol)	Capacity left (μmol)
1	4	8	0.10	1.82	5.82	2.18	8.18
2	8	8	0.15	6.25	6.25	1.75	8.75
3	8	16	0.25	5.22	13.22	2.78	19.58
4	8	16	0.10	4.03	12.03	3.97	6.00
5	8	16	0.20	4.51	10.51	3.49	15.49
6	8	16	0.25	5.13	13.13	2.87	19.87
7	12	24	0.15	7.48	13.48	4.52	8.52
8	12	24	0.20	8.27	20.27	3.73	11.73
9	12	24	0.25	8.31	20.31	3.69	16.70
10	4	8	0.05	1.30	5.30	2.70	3.70

[a] μmoles in 10 ml. [b] Y, histidine.

Adsorption of Cu, Zn, Pb and Cd on the aluminium hydroxide-coated resin for different metal/ligand ratios

Two metal concentrations (0.3×10^{-6} M and 1×10^{-6} M) were used for the adsorption studies with the model ligands, fulvic acid, humic acid and tannic acid at concentrations of 1, 2, 5 and 10 mg l^{-1}. Both seawater and synthetic soft water media were tested. Table 5 shows the results for soft water and seawater, when 10 ml of various metal-ligand mixtures were passed through the columns.

In soft water, cadmium is strongly adsorbed on the aluminium hydroxide-coated column, even in the presence of the organic ligands, but the adsorption from seawater is much weaker. This is probably due to the formation of cadmium-chloride complexes in seawater. With a fixed ligand concentration, metal adsorption increases with increasing metal concentration and with fixed metal concentration, adsorption decreases with increasing ligand concentration. These results show that free metal ion is the adsorbed species.

The adsorbed metal fractions and toxic metal fractions are compared in Table 6. A reasonable correlation was obtained for copper in seawater and soft water with the fulvic acid studied, but the correlation for zinc and cadmium was poor.

Adsorption of some other metals on the aluminium hydroxide-coated resin

The adsorption of Cr(III), Ni(II), Mn(II) and Co(II) was examined by ICPES in seawater and soft water in the absence and presence of fulvic acid. The results are shown in Table 7. In seawater, the aluminium hydroxide-coated resin clearly adsorbs fewer trace metals than in soft water; and in soft water, fulvic acid has less (or no) effect on adsorption, probably because of the lower pH.

TABLE 5

Adsorption of trace metals on aluminium hydroxide-coated cation-exchange resin column from synthetic soft water and from seawater

Ligand	Ligand concn. (mg l^{-1})	Synthetic soft water					Seawater				
		Metal concn. (10^{-6} M)	Adsorbed fraction (%)				Metal concn. (10^{-6} M)	Adsorbed fraction (%)			
			Zn	Cd	Pb	Cu		Zn	Cd	Pb	Cu
Humic acid	1	0.3	100	100	95	50	0.3	95	15	100	74
	2	0.3	100	100	89	48	0.3	73	12	96	65
	5	0.3	96	96	85	30	0.3	71	12	80	62
	10	0.3	96	96	80	25	0.3	64	10	70	52
	1	1.0	100	100	98	96	1.0	98	10	100	85
	2	1.0	98	100	96	96	1.0	80	9	100	75
	5	1.0	98	99	93	93	1.0	75	9	100	62
	10	1.0	99	98	91	92	1.0	70	8	100	55
Fulvic acid	1	0.3	100	98	93	65	0.3	90	10	95	83
	2	0.3	96	96	90	60	0.3	85	8	95	73
	5	0.3	94	94	85	60	0.3	85	8	90	60
	10	0.3	78	89	61	35	0.3	85	7	85	20
	1	1.0	99	99	90	90	1.0	97	20	100	96
	2	1.0	99	99	89	86	1.0	96	10	100	91
	5	1.0	98	97	74	76	1.0	94	8	100	67
	10	1.0	98	98	70	75	1.0	89	7	100	40
Tannic acid	1	0.3	98	99	95	95	0.3	77	10	96	75
	2	0.3	80	98	90	70	0.3	77	9	95	48
	5	0.3	92	98	90	40	0.3	77	8	94	48
	10	0.3	90	96	65	35	0.3	72	8	93	43
	1	1.0	100	100	99	85	0.5	100	20	100	95
	2	1.0	100	100	99	60	0.5	90	10	100	66
	5	1.0	98	100	99	50	0.5	80	1	100	55
	10	1.0	97	100	99	48	0.5	75	1	100	40

TABLE 6

Comparison of adsorbed metal and toxic metal fractions in seawater and soft water in the presence of fulvic acid (10 mg l^{-1})[a]

Metal ion	Seawater		Soft water	
	A	B	A	B
Cu	20	20	35	40
Zn	85	50	78	—
Pb	85	—	61	—
Cd	7	90	89	—

[a] A, adsorbed fraction (%); B, toxic fraction (%).

TABLE 7

Adsorption of trace metals on the aluminium hydroxide-coated resin

Medium[a]	Fulvic acid	Adsorbed fraction (%)			
		Ni(II)	Mn(II)	Cr(III)	Co(II)
Seawater	None	32	10	48	17
Seawater	10 mg l^{-1}	16	10	19	14
Soft water	None	99	99	98	99
Soft water	10 mg l^{-1}	79	99	98	99

[a]Spiked with 2×10^{-5} M of each metal.

Recovery of adsorbed metals from the aluminium hydroxide-coated resin

Adsorbed metal was readily removed from the aluminium hydroxide-coated columns by passing 10 ml of 1 M HCl/0.1 M HNO_3. However, this method also removed the aluminium coating. Adsorbed copper, lead, cadmium and zinc were also quantitatively leached from the column with 10 ml of 0.02 M diethylenetriaminepentaacetic acid (DTPA). With DTPA, the aluminium hydroxide coating was unaffected (no Al^{3+} could be detected in the effluent by ICPES) and, after washing with water, the column could be re-used several times before the resin needed to be re-coated.

Adsorption of lipid-soluble complexes on the aluminium hydroxide-coated resin

Some lipid-soluble organometallic complexes are extremely toxic to aquatic organisms [5, 6]. In seawater, the toxic complexes copper 8-quinolinolate and copper ethylxanthogenate were quantitatively adsorbed on the top of the aluminium hydroxide-coated column as a thin coloured layer. These complexes could be selectively leached from the column by methanol, and ionic copper then removed with DTPA. With this procedure, the aluminium hydroxide-coated column can be used to determine the two most toxic forms of copper, i.e., ionic and lipid-soluble copper (Table 8).

Preliminary study of an in-situ monitoring instrument

There is a need for a simple, inexpensive, reliable instrument for determining the total and toxic copper and other heavy metals in natural waters.

TABLE 8

Adsorption of the lipid-soluble complex formed with 8-quinolinol (8-Q) in 10 ml of seawater on an aluminium hydroxide-coated resin column

Additions	2×10^{-6} M 8-Q/ 1×10^{-5} M Cu^{2+}	6×10^{-6} M 8-Q/ 1×10^{-5} M Cu^{2+}	1×10^{-5} M 8-Q/ 1×10^{-5} M Cu^{2+}
Lipid-soluble fraction (%)	20	60	100
Recovery with methanol (%)	19	55	100

TABLE 9

Trace metal distribution in an aluminium hydroxide-coated resin column and an 8-quinolinol-coated CPG column (8-Q/CPG)

Metal	Metal concn. found (M)[a]				
	Adsorbed on aluminium hydroxide	Adsorbed on 8-Q/CPG	Total	Adsorbed on aluminium hydroxide (%)	ASV-labile (%)
Zn	1.5×10^{-8}	2.7×10^{-9}	1.8×10^{-8}	85	100
Cd	1.9×10^{-11}	2.2×10^{-10}	2.4×10^{-10}	9.1	46
Pb	8.0×10^{-11}	2.3×10^{-10}	3.1×10^{-10}	26	65
Cu	1.3×10^{-9}	5.3×10^{-9}	6.6×10^{-9}	19	30

[a]12 l of seawater was passed through the two columns in series, and the metals were desorbed from the columns and quantified. The metal concentrations given relate to the original seawater.

TABLE 10

Recovery of trace metals on aluminium hydroxide-coated resin column and 8-Q/CPG column when seawater with varying metal concentrations was passed through the columns in series[a]

Metal	Total metal recovery (%)	Metal recovered on aluminium hydroxide column (%)		Metal recovered on 8-Q/CPG column (%)
		Methanol-eluted	DTPA-eluted	
Cd	96	<1	6	94
Pb	80	1	90	9
Cu	91	10	80	10

[a]Three successive 1-l portions of seawater, containing 1×10^{-6} M Cu, Pb, Cd, 1×10^{-7} M Cu, Pb, Cd, and no added metals were passed through the two columns in series. The copper complexing capacity of the seawater (ASV) was 3.5×10^{-8}.

The aluminium hydroxide-coated cation-exchange resin column can be used to determine the toxic fraction (ionic plus lipid-soluble copper), and a small column of 8-quinolinol resin [or controlled-pore glass (CPG) beads coated with 8-quinolinol] in series can be used to adsorb the remaining copper. The copper adsorbed on the two columns equals the total copper in the water sample. Results for a typical seawater are shown in Table 9. The toxic fraction found with the aluminium hydroxide-coated column and ASV-labile measurements [17] are similar. To show that the aluminium hydroxide-coated column can integrate the copper contents in seawater containing varying concentrations of this metal, three separate 1-l portions of seawater to which had been added, respectively, 1×10^{-6} M Cu, Pb, Cd, 1×10^{-7} M Cu, Pb, Cd, and no

added metals were passed in that order through columns of aluminium hydroxide-coated resin and 8-quinolinol-coated controlled pore glass (Pierce Chemical Co.) in series. The metals were then eluted and quantified, and the results are shown in Table 10. Good recovery of copper was obtained. A detailed description of an in-situ instrument will be given in a later publication.

The authors express their gratitude to G. E. Batley and G. K-C Low for helpful discussions and J. L. Stauber, S. J. Buchanan and J. F. Chapman for assisting in the algal assay and ICPES determinations.

REFERENCES

1 T. M. Florence, B. G. Lumsden and J. J. Fardy, Anal. Chim. Acta, 151 (1983) 281.
2 J. Gavis, J. Mar. Res., 41 (1983) 53.
3 W. Sunda and R. L. Guillard, J. Mar. Res., 34 (1976) 511.
4 J. Gavis, R. L. Guillard and B. L. Woodward, J. Mar. Res., 39 (1981) 315.
5 M. Ahsanullah and T. M. Florence, Marine Biol., 84 (1984) 41.
6 J. L. Stauber and T. M. Florence, Aquatic Toxicol., 8 (1986) 223.
7 N. G. Zorkin, E. V. Grill and A. G. Lewis, Anal. Chim. Acta, 183 (1986) 163.
8 C. Gessa, M. L. De Cherchi, P. Melis, G. Micera and L. Strinna Erre, Colloids and Surfaces, 11 (1984) 109.
9 G. Micera, C. Gessa, P. Melis, A. Premoli, R. Dallocchio and S. Deiana, Colloids and Surfaces, 17 (1986) 389.
10 B. G. Lumsden and T. M. Florence, Environ. Technol. Lett., 4 (1983) 271.
11 T. M. Florence, Anal. Chim. Acta, 141 (1982) 73.
12 J. E. Gregor and H. K. J. Powell, J. Soil Sci., 37 (1986) 577.
13 M. Loewenschuss and G. Schmuckler, Talanta, 11 (1964) 1399.
14 A. E. Martell and R. M. Smith, Critical Stability Constants, Vol. 1, Plenum, New York, 1973.
15 T. M. Florence and J. L. Stauber, Aquatic Toxicol., 8 (1986) 11.
16 Oak Ridge Nat. Lab. Report No. TID7015, 1963.
17 T. M. Florence, Analyst, 111 (1986) 489.

Analytica Chimica Acta, 197 (1987) 149—158
Elsevier Science Publishers B.V., Amsterdam — Printed in The Netherlands

DETERMINATION OF URINARY PROSTANOIDS BY CAPILLARY GAS CHROMATOGRAPHY/HIGH-RESOLUTION MASS SPECTROMETRY

DAVID A. HEROLD, JOHN SAVORY*, MICHAEL KINTER, RICHARD ROSS and MICHAEL R. WILLS

Departments of Pathology, Biochemistry and Internal Medicine, University of Virginia Medical Center, Charlottesville, VA 22908 (U.S.A.)

(Received 4th December 1986)

SUMMARY

A stable isotope-dilution gas-chromatography/high-resolution mass spectrometry method for the determination of prostaglandin E_2 (PGE_2) and 6-keto-prostaglandin $F_{1\alpha}$ (6-keto-$PGF_{1\alpha}$) in urine as their methoxime/t-butyldimethylsilyl ether/t-butyldimethylsilyl ester derivatives is described. The derivatives are prepared by a novel derivatization scheme in which the pentafluorobenzyl esters are formed prior to the silylation step in which the t-butyldimethylsilyl esters are formed in an apparent exchange reaction. Recoveries through the entire extraction and derivatization procedure are 70.6% for PGE_2 and 64.4% for 6-keto-$PGF_{1\alpha}$. Quantitation at mass resolutions approaching 10 000 eliminated all interferences in the PGE_2 chromatograms while lower resolutions were sufficient for 6-keto-$PGF_{1\alpha}$. Limits of detection of 50 pg ml^{-1} for each prostanoid were obtained. For PGE_2, a lower limit of detection was obtained at a mass resolution of 10 000 (50 pg ml^{-1}) than was obtained at a mass resolution of 1000 (80 pg ml^{-1}), illustrating the selectivity of detection.

Several thousand reports on the various biological effects of prostanoids have appeared in the literature over the past decade with a large percentage (>40%) including some type of quantification of these compounds. The vast majority of assays used currently to study prostanoids involves some type of immunoassay, usually radioimmunoassay (RIA). The extreme variability of the results obtained by these methods would indicate that many of these procedures are grossly inaccurate. Even the more carefully controlled methods based on gas chromatography/mass spectrometry (GC/MS) probably provide many results that are in considerable error. These errors would be due to interfering compounds, many of prostanoid origin, cross-reacting in an RIA experiment or co-eluting in a GC/MS experiment.

This variability of results for the determination of prostanoids is shown in Table 1, which contains reported concentrations of two prostanoids, 6-keto-prostaglandin $F_{1\alpha}$ (6-keto-$PGF_{1\alpha}$) and thromboxane B_2 (TxB_2), in blood or urine from normal human volunteers. Although the specimens are different in each of the studies cited, the degree of variability seen in normal specimens must indicate a remarkable inter-laboratory variation. Because no stable

0003-2670/87/$03.50

TABLE 1

Comparison of 6-keto-prostaglandin $F_{1\alpha}$ and thromboxane B_2 levels in samples obtained from human volunteers

Concentration or clearance[a]	Biological fluid	Method	Reference
6-Keto-prostaglandin $F_{1\alpha}$			
830 ± 79	Serum	RIA	[1]
273 ± 24	Serum	RIA	[2]
189 ± 39	Plasma	GC/MS	[3]
131 ± 13	Plasma	GC/MS	[4]
125	Plasma	RIA	[5]
115 ± 24	Plasma	RIA	[6]
34 ± 7	Plasma	RIA	[7]
22 ± 3	Plasma	RIA	[6]
0.50—2.49	Plasma	GC/NICI[d]/MS	[8]
<5	Plasma	RIA	[9]
0.6—1.8	Plasma	GC/NICI/MS	[10]
124	Plasma	RIA	[11]
70	Serum	EIA[e]	[12]
<5	Serum	GC/MS	[13]
1.5—1.7[b]	Serum	RIA	[13]
0.4—5.0	Plasma	GC/MS	[14]
9.6[c]	Urine	RIA	[15]
8.9[c]	Urine	GC/MS	[15]
14—19[c]	Urine	RIA	[16]
Thromboxane B_2			
125	Plasma	RIA	[9]
3—45	Plasma	GC/MS	[10]
2.8—10.8	Plasma	GC/MS	[17]

[a]Concentrations in pg ml^{-1} unless otherwise specified. [b]ng ml^{-1}. [c]ng h^{-1}. [d]Negative-ion chemical ionization. [e]Enzyme immunoassay.

materials are available for quality assurance and proficiency testing purposes, normal human specimens, although not ideal, are useful in assessing inter-laboratory variations.

The purpose of the present investigation was to apply stable isotope dilution with quantitation by gas chromatography/high-resolution mass spectrometry in a definitive analytical method to the determination of prostanoids in biological materials. Urine was chosen as the material for study because it represents a complex matrix containing many potential interfering compounds and is of obvious clinical significance. In addition, a novel derivatization procedure has been developed that reduces possible interferences by substantially increasing the molecular weight of the derivatives, provides for the removal of the derivatizing reagents, and yields a derivative of increased stability which shows only one major high mass fragmentation product following electron ionization.

EXPERIMENTAL

Instrumentation

The mass spectrometer used was a double-focusing, reverse-geometry instrument (Model 8230, Finnigan MAT, San Jose, CA 95134) with a SpectroSystem 300 data system. The instrument was operated in the electron ionization (EI) mode using 70-eV electrons with a source temperature of 250°C, the conversion dynode at 5000 V and the electron multiplier at 2000–2200 V. Resolution, as noted in the text, was defined by $M/\Delta M$ with a 10% valley. Data were acquired in the selected ion monitoring mode at a rate of 1 cycle per second with a dwell time of 410 ms per channel per cycle. Tetraiodophthalic anhydride and 5,10,15,20-tetrakis(*p*-methoxyphenyl)-21*H*, 23*H*-porphine were admitted into the ion source via direct probe to provide appropriate lock-masses, *m/z* 651.603 and *m/z* 734.289, respectively.

A Varian 3700 gas chromatograph was equipped with a DB-1 (J.W. Scientific, Rancho Cordova, CA 95670) methyl silicone bonded-phase fused silica capillary column, 30 m × 0.25 mm, with a 0.25-μm film thickness. Samples were injected using an on-column injector (OCI-3, Scientific Glass Engineering, Austin, TX 78759) at an oven temperature of 200°C followed by a 15°C min^{-1} ramp to 290°C.

Reagents

All solvents, including water, used in the extraction and derivatization procedures and for cleaning purposes were glass-distilled HPLC-grade reagents (Bodman Chemicals, Media, PA 19063). Cartridges (C_{18} Sep-Pak) were supplied by Waters Associates.

Reagents used in the preparation of prostaglandin derivatives were as follows: *N,N*-diisopropylethylamine (Aldrich Chemical Co.), pentafluorobenzyl bromide (PCR Research Chemicals, Gainesville, FL 32602), methoxylamine hydrochloride (2% in pyridine; Pierce Chemical, Rockford, IL 61105), and *N*-methyl-*N*-(t-butyldimethylsilyl)trifluoroacetamide (MTBSTFA; Pierce). Prostaglandin E_2 (PGE_2) and 6-keto-prostaglandin $F_{1\alpha}$ (6-keto-$PGF_{1\alpha}$) standards were obtained from Cayman Chemical (Denver, CO 80205) and their deuterated analogs PGE_2-3,3,4,4-d_4 (d_4-PGE_2) and 6-keto-$PGF_{1\alpha}$-3,3,4,4-d_4 (d_4-6-keto-$PGF_{1\alpha}$) from Merck and Co./Isotopes (St. Louis, MO 63116). Tritiated PGE_2 and 6-keto-$PGF_{1\alpha}$ were obtained from New England Nuclear (Boston, MA 02118). All prostaglandin standards were stored at −70°C.

Preparation of glassware

All glassware and Reacti-vials (Pierce) used in the extraction and derivatization steps were cleaned by soaking in a 2% RBS-35 (Pierce) solution, rinsed with deionized water, acetone, and air-dried. Glassware was then silylated with a 5% solution of chlorotrimethylsilane (Pierce) in toluene (1 h at room temperature), rinsed with methanol, and air-dried overnight. This procedure was repeated before each experiment.

Extraction

For each sample, 23.6 and 26.9 ng of d_4-PGE_2 and d_4-6-keto-$PGF_{1\alpha}$, respectively, were added to 10.0 ml of urine which was then acidified to pH 2.5—3.5 with formic acid. The acidified sample was applied by glass syringe to a C_{18} reverse-phase Sep-Pak column preconditioned with dichloromethane (10 ml), acetonitrile (10 ml), and water (20 ml). The Sep-Pak column was then washed first with 10 ml of water, then with 10 ml of 15% acetonitrile/85% water (v/v, pH adjusted to 2.5 with formic acid) and the prostaglandins were eluted with 10 ml of acetonitrile/water (40/60 v/v, pH adjusted to 2.5 with formic acid) into a 50-ml centrifuge tube.

The PGE_2 was then extracted from the eluate by adding 10 ml of a hexane/dichloromethane (50/50 v/v) solution to the tube, vortexing, and transferring the organic layer to a clean 50-ml centrifuge tube. A small amount of sodium chloride helped to separate the layers. The 6-keto-$PGF_{1\alpha}$ was then extracted from the eluate with three 5-ml aliquots of ethyl acetate. The combined organic fractions were evaporated to near dryness and transferred with three 200-μl portions of methanol to a 1.0-ml Reacti-vial and evaporated under argon for derivatization.

Preparation of derivatives

Methoximation. The residue from the extraction was dissolved in 50 μl of 2% methoxylamine hydrochloride in pyridine and heated at 70°C for 1 h. The solvent was then evaporated at room temperature in a stream of dry argon and the residue dried under vacuum for 5 min.

Pentafluorobenzyl esters. The vacuum-dried residue was dissolved in 30 μl of acetonitrile. Portions (10 μl) of 33% pentafluorobenzyl bromide in acetonitrile and of 10% diisopropylethylamine in acetonitrile were added and the samples were incubated at room temperature for 15 min. The solvent was then evaporated at room temperature in a stream of dry argon and the residue dried under vacuum for 5 min.

Silylation. This residue was dissolved in 50 μl of acetonitrile and 40 μl of MTBSTFA and 10 μl of pyridine were added and the samples were incubated at 40°C for 1.5 h. The solvent was then evaporated at room temperature under a stream of dry argon and the residue dried under vacuum.

Hexane extraction. The residue was dissolved in 100 μl of water and extracted with three 200-μl aliquots of hexane. The hexane fractions were combined and evaporated at room temperature in a stream of dry argon.

Quantitation by gas chromatography/mass spectrometry

The final residue was dissolved in 20 μl of tetradecane, and a 1-μl aliquot was injected onto the chromatographic column. The prostaglandins of interest were quantitated by selected-ion monitoring in the positive-ion mode using fragment ions at nominal masses *m/z* 666 (PGE_2), *m/z* 670 (d_4-PGE_2) and *m/z* 798 (6-keto-$PGF_{1\alpha}$), *m/z* 802 (d_4-6-keto-$PGF_{1\alpha}$). For studies at higher resolution (5000 and 10 000), the exact mass calculated from the

element composition of the fragment ion was used in selected-ion monitoring modes using a reference lock-mass.

RESULTS

Extraction recoveries

The recoveries through the initial urine extractions and final derivatization were evaluated by using urine samples spiked with [^{3}H]-PGE_2 and [^{3}H]-6-keto-$PGF_{1\alpha}$. The recoveries of duplicate experiments are shown in Table 2. The recoveries listed are those obtained after each step and are cumulative with the absolute recoveries for each step shown in parentheses. The initial extractions give almost quantitative recoveries. Also, the recoveries shown for the derivatization steps are excellent and indicate that the expected derivatives are being formed in high yield. This extraction procedure is considerably simpler than that used previously in this laboratory for the determination of prostanoids in plasma [18]. This earlier procedure had used C_{18} Sep-Pak, and silica Sep-Pak solid-phase extractions followed by high-performance thin-layer chromatography, after which the appropriate zones were scraped from the plates for derivatization. The complexity of these various steps, necessary to eliminate interferences, led to considerable losses (50% recovery). These steps were found to be unnecessary in the present procedure because of the new derivatization scheme and the high resolution capabilities of the mass spectrometer. This extraction procedure was optimized for maximum recovery and clean-up by adjustment of pH and eluting solvent mixtures. Urine specimens extracted by the procedure described above gave brown residues on evaporation, but were still acceptable for the derivatization steps.

Derivatization and GC/MS studies

Most workers measuring PGE_2 and 6-keto-$PGF_{1\alpha}$ use derivatization schemes which form the methoxime/trimethylsilyl ether/pentafluorobenzyl

TABLE 2

Cumulative[a] percent recoveries of [^{3}H]-PGE_2 and [^{3}H]-6-keto-$PGF_{1\alpha}$ added to urine

Assay step	Recovery (%)	
	[^{3}H]-PGE_2	[^{3}H]-6-keto-$PGF_{1\alpha}$
After C_{18} Sep-Pak	92.5	91.0
After dichloromethane/hexane extraction	71.2 (77.0)	22.8 (25.1)
After ethyl acetate extraction (× 3)	89.2 (96.4)	86.6 (95.2)
After transfer to Reacti-Vial	86.5 (97.0)	82.4 (95.2)
After derivatization and extraction into hexane	75.3 (87.1)	72.5 (88.0)
After reconstitution in tetradecane	70.6 (93.8)	64.4 (88.8)

[a]Percent recoveries for the individual steps are shown in parentheses.

ester or form the methyl ester rather than the pentafluorobenzyl ester. These derivatives are relatively unstable in the presence of small amounts of water and exhibit extensive fragmentation when electron ionization is used. Therefore, studies based on the pentafluorobenzyl ester have generally used negative-ion chemical ionization, for which the pentafluorobenzyl ester is particularly suitable, while positive-ion chemical ionization has generally been used for the methyl ester derivatives. However, electron ionization is to be preferred over chemical ionization mainly because the ion source stays cleaner, yielding maximum sensitivity for a longer time. Also, the sensitivity needed can be obtained at higher mass resolutions by electron ionization. To circumvent these disadvantages, the use of the t-butyldimethylsilyl derivatives was investigated here. Other workers have described the use of these derivatives and have noted their advantages in terms of improved stability (even in the presence of water) and sensitivity, because the degree of fragmentation using electron ionization is decreased [19–21].

Methoxime derivatives were found to be essential in the present study. Attempts were made to derivatize the hydroxyl and carboxyl groups of PGE_2 and 6-keto-$PGF_{1\alpha}$ leaving the keto group intact. However, it proved impossible to chromatograph these compounds successfully. All subsequent work, therefore, included the preparation of methoxime derivatives as a first step in the GC/MS procedure.

An attempt was also made to derivatize both the hydroxyl and carboxyl groups in one step by direct action of MTBSTFA in acetonitrile and pyridine at temperatures up to 60°C for 1 h. However, the expected t-butyldimethylsilyl ether and ester derivatives could not be prepared in good yield. The lack of success in preparing the t-butyldimethylsilyl ester derivative directly by using MTBSTFA led us to resort to the earlier derivatization procedure in which the pentafluorobenzyl ester was prepared before the final preparation of the trimethylsilyl ethers. When this approach was used, but with the substitution of MTBSTFA for *N,O*-bis(trimethylsilyl)trifluoroacetamide (BSTFA), both the t-butyldimethylsilyl ethers and the t-butyldimethylsilyl

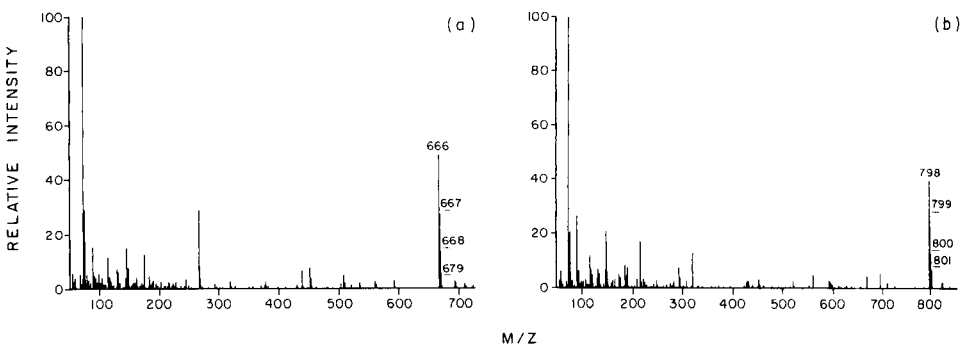

Fig. 1. Electron-ionization mass spectra of (a) prostaglandin E_2 and (b) 6-keto-prostaglandin $F_{1\alpha}$ as their methoxime/t-butyldimethylsilyl ether/t-butyldimethylsilyl ester derivatives.

ester were formed, apparently by an exchange reaction with the pentafluorobenzyl ester. The mass spectra of these derivatives for PGE_2 and 6-keto-$PGF_{1\alpha}$ under electron ionization conditions are shown in Fig. 1. These spectra are notable for an intense fragment ion $[M^{+\cdot}—C_4H_9\cdot]^+$ which makes these derivatives well-suited to selected ion monitoring because these ions carry a large fraction of the ion current for these compounds.

Quantitative measurements

Lock masses. For high-resolution mass spectrometry based on multiple ion monitoring, it is necessary to provide the instrument with a lock mass. This provision is achieved by continuously admitting a compound with a suitable mass spectrum into the ion source. Two compounds were chosen with predicted stability which potentially would produce a molecular ion suitable for the determination of PGE_2 and 6-keto-$PGF_{1\alpha}$. Tetraiodophthalic anhydride (m.w. 651.603) was found to provide a suitable lock mass for PGE_2 and 5,10,15,20-tetrakis(*p*-methoxyphenyl)-21*H*,23*H*-porphine (m.w. 734.289) was found to provide a suitable lock mass for 6-keto-$PGF_{1\alpha}$ with the EI spectra of these compounds showing the molecular ion to be the base peak.

Sensitivity and detection limit. The sensitivities, (*S*, expressed in counts pg^{-1}) and limits of detection (*LOD*, expressed in pg ml^{-1}) for PGE_2 in urine at a series of mass resolutions (*R*) are as follows: $R = 1000$, $S = 49.5$, $LOD = 80$; $R = 5000$, $S = 9.1$, $LOD = 60$; $R = 10\,000$, $S = 3.6$, $LOD = 50$. As can be seen from these data, the lowest limit of detection in this system is obtained at a resolution of 10 000 despite the fact that this resolution provided the lowest absolute sensitivity. Mass resolution of 1000 in fact gave a sensitivity more than 10-fold greater but a higher limit of detection. This is an excellent illustration of the fundamental principle of highly selective mass spectrometric detection techniques: increased selectivity causes a decrease in the sensitivity of the assay, but because of a more rapid decrease in the noise, a resultant increase in the signal-to-noise ratio leads to improved limits of detection.

A standard calibration curve for PGE_2 is shown in Fig. 2. As expected, this curve is linear for lower concentrations of PGE_2 with a deviation from linearity at higher concentrations which is a result of the increasing contribution of endogenous d_4-PGE_2 to the internal standard signal [22]. At the levels generally encountered in urine specimens, however, these contributions were insignificant, allowing prostanoid concentrations to be calculated directly from the observed signal ratios [22].

Urine samples. Selected-ion-monitoring chromatograms for PGE_2 in typical urine samples are shown in Fig. 3 at mass resolutions of 1000, 5000, and 10 000. The "clean" chromatograms obtained are in part due to the high molecular weight of the prostanoid derivatives, allowing operation in a mass range where fewer interferences are encountered and the removal of the derivatizing reagents (and any other polar constituents) via a hexane/water extraction, both unique features of the scheme proposed here. In these

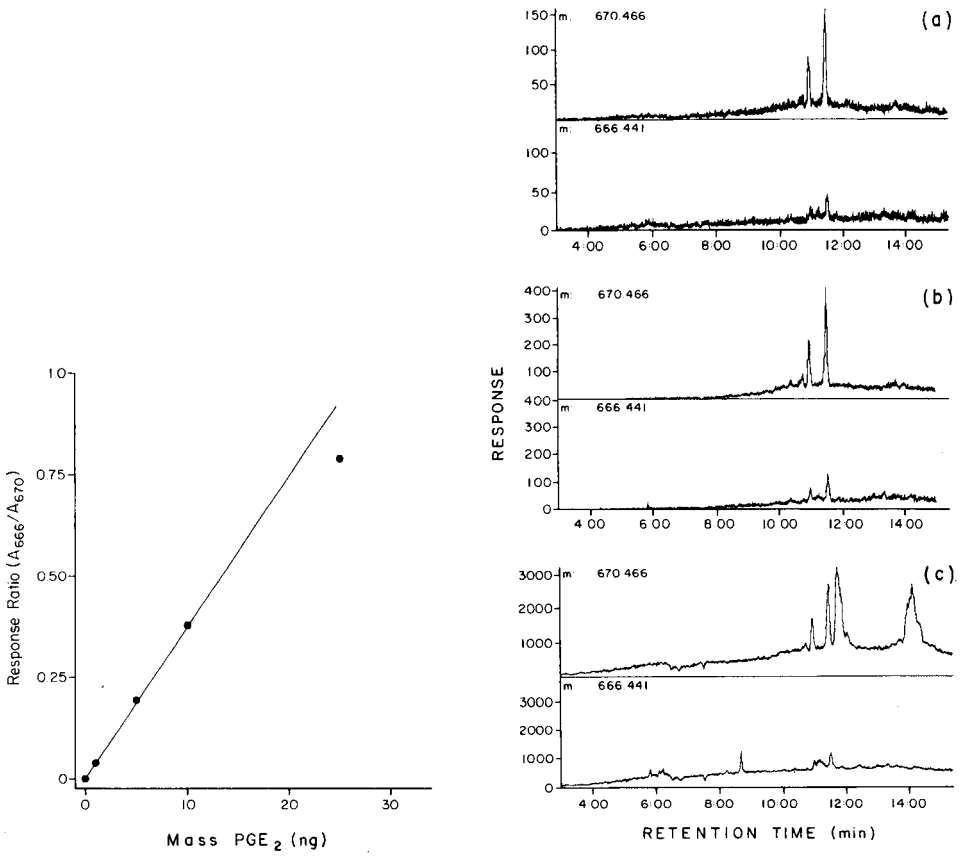

Fig. 2. Calibration curve for the determination of PGE_2 in urine by stable-isotope-dilution selected-ion monitoring.

Fig. 3. Selected-ion monitoring chromatograms for the determination of PGE_2 in a urine specimen obtained at different mass resolutions: (a) 10 000; (b) 5000; (c) 1000.

chromatograms, the doublet observed is a result of the formation of *syn* and *anti* methoxime isomers.

Figure 3, however, also shows that interferences are encountered at a mass resolution of 1000 and that resolutions between 5000 and 10 000 are needed to eliminate these interferences. It has been found that these higher resolutions are needed in routine determinations to ensure interference-free chromatographs. As previously discussed, these resolutions do provide the lowest limits of detection despite lower sensitivities. These reduced sensitivities, however, can lead to less precise measurements as a result of poorer counting statistics although this may be offset by more accurate baseline determinations.

In the GC/MS determination of 6-keto-$PGF_{1\alpha}$, no interferences were observed. These interference-free chromatograms are the result of the clean-up

and derivatization procedure, because many interferences were observed using unit resolution with the previous clean-up and derivatization methods [18]. Chromatograms again showed the separation of the *syn* and *anti* methoxime isomers with limits of detection in the 50—100 pg ml^{-1} range.

In human and dog urine specimens, the ranges for PGE_2 concentrations were 80—570 pg ml^{-1} (human specimens, 12 individuals) and 800—4300 pg ml^{-1} (dog specimens, 6 individuals). For 6-keto-$PGF_{1\alpha}$ in human and dog urine specimens, the concentration ranges were 77—185 pg ml^{-1} (human specimens, 6 individuals) and 500—1600 pg ml^{-1} (dog specimens, 6 individuals). It is important to note that these data are not presented as a clinical study but rather as indicative values for evaluation of this method. From these data one can see that the limits of detection afforded by high resolution mass spectrometry are needed for the determinations.

Conclusion

The present investigation has led to the development of a stable isotope-dilution GC/MS procedure for urine prostanoids. The use of a new derivatization scheme together with the application of high-resolution mass spectrometry has enabled chromatograms to be produced with no interferences in the prostanoid peaks. This reference method developed for the determination of urinary prostanoids should lead to a much better understanding of the role of these compounds in biological processes.

Funding for the purchase of the high-resolution mass spectrometer was obtained from the National Institutes of Health, Division of Research Resources Shared Instrumentation Grant Program, grant number 1-S10-RRO-2418-01. Additional funding supporting this research by the John Lee Pratt Fund of the University of Virginia is also gratefully acknowledged.

REFERENCES

1 H. G. Morris, N. A. Sherman and F. T. Sheperdson, Prostaglandins, 21 (1981) 771.
2 L. Viinikka and O. Ylikorkola, Br. J. Pharmacol., 72 (1981) 299.
3 C. N. Hensby, G. A. FitzGerald, L. A. Friedman, P. J. Lewis and C. T. Dollery, Prostaglandins, 18 (1979) 731.
4 C. N. Hensby, P. J. Barnes, C. T. Dollery and H. Dargie, Lancet, II (1979) 1162.
5 L. M. Demers and D. D. Derck, in B. Samuelsson, P. W. Ramwell and R. Paoletti (Eds.), Advances in Prostaglandin and Thromboxane Research, Vol. 6, Raven Press, New York, 1980, p. 193.
6 M. D. Mitchell, Prostaglandins Med., 1 (1978) 13.
7 A. Edlund, W. Bomfin, L. Kaijser, C. A. Edlund, E. Pinca and A. Wennalm, Prostaglandins, 22 (1981) 323.
8 I. A. Blair, S. E. Barrow, K. A. Waddell, P. J. Lewis and C. T. Dollery, Prostaglandins, 23 (1982) 579.
9 C. Johnston, F. Carey and R. A. Forder, Clin. Sci., 67 (1984) 633.
10 H. Schweer, J. Kammer and H. W. Seyberth, J. Chromatogr., 338 (1985) 273.
11 M. Sekin, Nippon Naibumpi Gakkai Zasshi, 61 (1985) 1.
12 T. Tonai, K. Yokota, T. Yano, Y. Hayashi, S. Yamamoto, K. Yamashita and H. Miyazaki, Biochim. Biophys. Acta, 836 (1985) 335.

13 C. Chiabrando, M. W. Castognoli, A. Noseda, R. Fanelli, G. Rajtar, C. Cerletti and G. de Gaetano, Prostaglandins Leukotrienes Med., 16 (1984) 79.
14 B. J. Smith, R. M. Ross, C. R. Ayers, M. R. Wills and J. Savory, J. Liq. Chromatogr., 6 (1983) 1265.
15 R. Zipser, A. Morrison, G. Laffi and R. Duke, J. Chromatogr., 339 (1985) 1.
16 A. Barden, L. J. Beilin, R. Vandongen and I. Rouse, Clin. Sci., 68 (1985) 601.
17 D. A. Herold, B. J. Smith, R. M. Ross, F. Marquis, J. Savory, M. R. Wills and C. R. Ayers, paper presented at the 32nd Annual Conference on Mass Spectrometry and Allied Topics, San Antonio, TX, May 1984.
18 B. J. Smith, D. A. Herold, R. M. Ross, F. G. Marquis, R. L. Bertholf, C. B. Ayers, M. R. Wills and J. Savory, Res. Commun. Chem. Pathol. Pharmacol., 40 (1983) 73.
19 M. Tada, H. Maksuda, T. Kuzuya, M. Inui and H. Abe, Jpn. Circ. J., 49 (1985) 276.
20 A. C. Bazan and D. B. Knapp, J. Chromatogr., 236 (1982) 201.
21 A. Aly, K. Green and C. Johansson, Acta Physiol. Scand., 122 (1984) 583.
22 B. N. Colby and M. W. McCaman, Biomed. Mass Spectrom., 6 (1979) 225.

Analytica Chimica Acta, 197 (1987) 159—167
Elsevier Science Publishers B.V., Amsterdam — Printed in The Netherlands

IMPROVED QUANTITATION OF 2,4-DICHLOROPHENOL IN PLANT TISSUES BY HIGH-PERFORMANCE LIQUID CHROMATOGRAPHY WITH AMPEROMETRIC DETECTION

DAVID J. CHESNEY and DENNIS E. TALLMAN*
Department of Chemistry, North Dakota State University, Fargo, ND 58105 (U.S.A.)
ALLEN A. PECKRUL, LEONARD W. COOK and JAMES R. FLEEKER
Department of Biochemistry, North Dakota State University, Fargo, ND 58105 (U.S.A.)
(Received 25th September 1986)

SUMMARY

For the determination of 2,4-dichlorophenol (DCP) residues in plant tissues, the use of high-performance liquid chromatography with amperometric detection decreases the quantitation limits by a factor of five compared to those obtained with gas chromatography with Hall conductivity detection. It also avoids the clean-up and derivatization procedures required for electron-capture detection. After extraction of DCP from plant tissue by steam distillation and collection in toluene, an alumina clean-up column is used to remove electroactive interferences from the samples. The DCP is then extracted into aqueous alkaline solution, neutralized, and diluted with acetonitrile to ca. 50% (v/v). An alternative clean-up made use of an in-line, pre-column electrochemical procedure, in which case the alumina column was not used. The components were separated with a reverse-phase column and detected with a polychlorotrifluoroethylene/graphite composite electrode at an applied potential of +1.0 V vs. Ag/AgCl. The quantitation limit for DCP in the plant tissues was 100 pg per injection (0.05 mg kg^{-1}).

The herbicide 2,4-dichlorophenoxyacetic acid (2,4-D) is partially metabolized in plants by conversion to 2,4-dichlorophenol (DCP). Prior to approval for the use of 2,4-D on food crops, the U.S. Environmental Protection Agency (EPA) requires residue data for both the parent herbicide and DCP. The use of high-performance liquid chromatography (HPLC) to determine DCP in complex plant matrices has been very limited [1], probably because of superior selectivity and sensitivity of the gas chromatographic method. Liquid chromatography with ultraviolet (UV) spectrophotometric detection has been used to determine DCP in environmental samples either directly [2] or, more commonly, after liquid-liquid extraction and preconcentration [2, 3] or pre-column enrichment [4]. However, determination of phenols in complex environmental samples with UV detection often is limited by inadequate sensitivity and unseparated interferences [5].

Samples with high organic content require the use of a suitably selective detector to minimize matrix interferences [6]. Liquid chromatography with electrochemical detection (LC/EC) provides superior selectivity for suitable

0003-2670/87/$03.50

analytes. Although the advantages of LC/EC in residue determinations have been discussed [7, 8], few applications in this area have been reported [7, 9—11].

This report describes the utility of LC/EC for determinations of DCP residues. The method involves separation of DCP residues from the sample matrix by steam distillation [12] followed by alkaline extraction to transfer the phenol back into the aqueous phase. Co-distilled interferences can be removed either by a column clean-up procedure or by the use of in-line pre-column electrochemical oxidation. The determination requires only a minimum of sample handling, yet provides good sensitivity and chromatographic resolution, even in complex plant matrices. The proposed method is compared to the more established and routine methods of gas chromatography with Hall conductivity detection (GC/Hall) [13] and liquid chromatography with UV spectrophotometric detection (LC/UV) with respect to sensitivity, limits of quantitation and the degree of sample handling required to provide adequate removal of interferences.

EXPERIMENTAL

Reagents

All chemicals used were research grade unless otherwise specified. The DCP was obtained from the U.S. EPA Standards Repository (Research Triangle Park, NC). Toluene, acetonitrile, methanol and acetone were HPLC grade. A stock solution containing 500 μg ml^{-1} DCP in acetone was prepared. Working standards for the GC/Hall method were prepared by serial dilution with toluene to cover the range 0.1—0.8 μg ml^{-1} DCP. Intermediate stock solutions for LC/EC were prepared by dilution of the 500 μg ml^{-1} stock to 10 μg ml^{-1} in acetonitrile. Working standards were prepared by further dilutions in water to cover the range 0.005—0.5 μg ml^{-1} DCP. A solution of 1 μg ml^{-1} DCP in methanol was used to spike the plant tissues for recovery studies.

The water used for the HPLC mobile phase and dilution of standard solutions was prepared by passing distilled water through a Waters 4-cartridge Milli-Q water purification system. This water was further purified by triple distillation in glass, the final step of which was a sub-boiling distillation, and was stored over chloroform to remove particulates and prevent bacterial growth [14]. Chromatographic mobile phases were filtered through Whatman GF/F glass microfibre filters.

Apparatus

The LC system has been described [15]. A coiled stainless-steel pulse dampener (Li-Chroma-Damp II, Alltech Associates, Deerfield, IL) was added between the pump and injector to smooth flow fluctuations. The main column (4.6 mm × 15 cm) contained C-8 stationary phase on 5-μm packing (Altex Ultrasphere). The electronic potentiostats and power supplies,

constructed in house, were of standard configuration. The applied potential was monitored with a Keithley Model 178 digital multimeter. Current output from the potentiostat was directed to a Fisher Recordall Series 5000 strip-chart recorder. An ESA Model 5021 conditioning cell (Bedford, MA) was placed in-line between the injector and column for selective oxidation of co-eluting electroactive impurities. The amperometric detector was of the thin-layer configuration; the working electrode was composed of Kelgraf, a conducting composite of graphite (15% w/w) and polychlorotrifluoroethylene (PCTFE). This electrode was prepared as described previously [16], except that the entire disk was prepared from the conductive composite, eliminating the insulating sheath of PCTFE surrounding the central Kelgraf plug. The interface between the Kelgraf and the insulating sheath was a significant source of noise, and a full-disk Kelgraf electrode (composite material occupying the entire flow channel of the amperometric detector) provided improved signal-to-noise ratios. Electrodes were polished with 1-μm alumina on Kitten-Ear felt (Mark V Laboratories, East Granby, CT) mounted on a lapping wheel. An LDC/Milton Roy spectromonitor D variable-wavelength detector was used with the LC system described above for the spectrophotometric determinations.

A Tracor Model 550 gas chromatograph equipped with a Tracor Model 700 Hall conductivity detector was used with a glass column (1.8-m × 2-mm i.d.) packed with 10% OV-1 on 80/100 Gas-Chrom Q (Alltech Associates, Deerfield, IL). Nitrogen was the carrier gas at a flow rate of 20 ml min^{-1}. Column temperature was 135°C, and the column inlet, column outlet and transfer line were at 210°C, 240°C, and 250°C, respectively. Methanol (HPLC grade) was the electrolyte solvent with a flow rate of 0.2 ml min^{-1} and the hydrogen flow was 30 ml min^{-1}. The detector furnace temperature was 900°C.

Procedures

All samples were stored in glass jars with aluminum foil seals at −20°C. Hay samples were chopped into 2—3-cm lengths and thoroughly mixed. Portions of this mixture were ground for 30 s in a coffee mill prior to steam distillation as were seed samples. Plant material (10—20 g) was placed in a 2-l round-bottom flask and spiked at the 0.05 or 0.1 $\mu g\ g^{-1}$ level. Distilled water (300 ml) was added, followed by 25 ml of phosphoric acid (85%) and 10 ml toluene. The flask was fitted with an extraction adapter [17] and condenser. Water was added to the extractor. The flask contents were heated and steam-distilled for 2 h with stirring, the distillate being passed through a layer of toluene trapped in the extractor. After cooling, the toluene layer was collected. The condenser and extraction apparatus were rinsed with an additional 10 ml of toluene which was added to the first portion. The combined toluene extract was dried over anhydrous sodium sulfate prior to gas chromatography.

For HPLC, the toluene extract was passed through a 2-g column of partly deactivated aluminum oxide (prepared by adding 4% distilled water to W-200

acid alumina, mixing well, and allowing to equilibrate for 12 h before use) and the DCP was eluted with 50 ml of water-saturated ether. The DCP was partitioned into aqueous solution by shaking the ether eluate with 5 ml of 1 M NaOH. The bulk of the ether layer was removed with a disposable pipet. The aqueous layer was purged with nitrogen to remove residual ether and transferred to a 50-ml volumetric flask. The solution was diluted with 20 ml of acetonitrile and 10 ml of glacial acetic acid and brought to the mark with water. This solution was separated by HPLC.

For some samples, the alumina-column clean-up was eliminated in favor of in-line electrochemical clean-up. For these samples, the combined toluene extract was extracted with 5 ml of 1 M NaOH. The toluene layer was discarded and the aqueous layer extracted with three 5-ml portions of ether. Residual ether was removed and the aqueous sample taken through the procedures described above. The in-line electrochemical clean-up was used in those samples for which the alumina column was found to be unsuitable.

Standard solutions for the LC/EC procedure were prepared weekly in water. These solutions were stable for a week at room temperature. The mobile phase consisted of acetonitrile/water (40:60 v/v), 0.1 M in sodium perchlorate and 0.1% (v/v) in acetic acid. This solution was filtered each day to ensure removal of particulates. Recovery studies were done by spiking plant material prior to sample workup as noted above.

The Kelgraf working electrode was roughened initially with 600-grit sandpaper, followed by polishing with 1-μm alumina on a rotating lapping wheel. The electrodes were held in place by a plexiglas jig which caused a mass of ca. 80 g to press down on the electrode surface. This jig was rotated 90° every 2 min. Other studies indicate that nearly equivalent S/N ratios can be obtained with Kelgraf electrodes resurfaced with 600-grit sandpaper, without any subsequent polishing. Following the polishing step, the electrode was sonicated 5 min each in HPLC-quality water, methanol and chloroform. The electrode was then dried and placed in the flow cell. A 127-μm gasket spacer (Bioanalytical Systems, West Lafayette, IN) was used to form the flow channel. While Kelgraf electrodes appear to provide superior signal-to-noise response [15], any commercially available electrochemical detector could be used, with some sacrifice in limit of detection.

Initial equilibration of an electrode was done overnight under flow in a low-pressure recycling system containing the desired mobile phase, with the electrode potential maintained at the potential to be used the next day (typically 1.10 V vs. Ag/AgCl). Before use, the applied potential was switched to −1.10 V for 1 min and then back to +1.10 V and the electrode background current allowed to settle (typically within 20—30 min). The detector cell was then placed on-line with the HPLC system and samples were processed. Overnight conditioning was done only once unless the detector cell was removed from the HPLC and allowed to dry. Under these circumstances, the entire electrode pretreatment procedure was repeated. The potential of the in-line conditioning (clean-up) cell, when used, was typically set at +0.30 or +0.35 V vs. its internal reference electrode.

RESULTS AND DISCUSSION

The response of the LC/EC system to standard solutions of DCP was found to be linear in the range of 0.005—0.5 $\mu g\ ml^{-1}$ (0.1 g—10 ng injected), covering the expected range for the plant samples. A series of 21 injections of 0.1 $\mu g\ ml^{-1}$ DCP gave an average response of 15.0 nA with a relative standard deviation of 0.9%; background currents were typically in the range 20—40 nA. With the in-line conditioning cell activated, the background current tended to vary slightly from day to day for unknown reasons. Peak-to-peak baseline noise was ca. 100—200 pA, independent of the on/off state of the conditioning cell, resulting in a limit of detection (signal-to-noise ratio of 2) of ca. 40 pg injected.

Chlorinated phenols such as DCP are difficult to oxidize [18, 19]. This limits the degree of electrochemical selectivity one can obtain because of the high applied potentials required to effect an oxidative response. The hydrodynamic voltammogram in Fig. 1 indicates that DCP does not begin to oxidize until a voltage of +0.85 V vs. Ag/AgCl is applied, and the current response never reaches a maximum. An applied potential of +1.10 V was chosen to maximize the current response while keeping the background current at an acceptable level.

In initial determinations, the alumina-column clean-up procedure was used. Excellent results were found in most cases, particularly for wheat and barley samples, with well-resolved DCP peaks and quantitation limits (S/N = 5) in the 100-pg range, corresponding to 50 $\mu g\ kg^{-1}$ in the original plant material. However, some samples, particularly straw and hay, presented a highly complex and variable sample matrix and chromatograms.

A study of the current/potential behavior of components in interfering peaks in selected samples indicated that their current responses reached

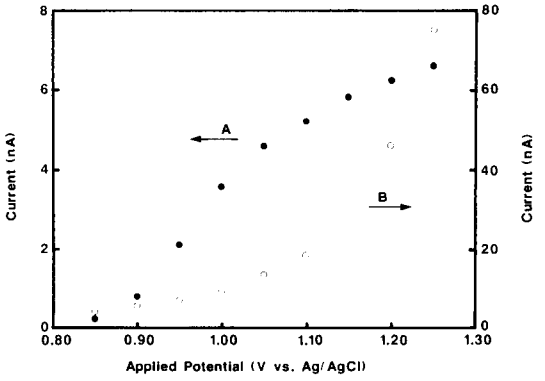

Fig. 1. Hydrodynamic voltammogram of 2,4-dichlorophenol (0.05 $\mu g\ ml^{-1}$) with a Kelgraf working electrode; injection volume, 20 μl; mobile phase, 40% acetonitrile, 0.1 M sodium perchlorate, 0.1% acetic acid; flow rate, 0.88 ml min^{-1}. A(•), DCP peak height; B(○), background current.

maxima well before the oxidation threshold for DCP. This difference in electrochemical behavior was exploited by placing the ESA coulometric conditioning cell in-line between the injector and the column as described above. It was found that an applied potential of +0.35 V (vs. the internal reference electrode) was the maximum applied potential which would not cause DCP to be oxidized to an appreciable extent. The use of this in-line electrochemical conditioning technique provided substantially increased resolution in most cases (Fig. 2). No deleterious effects on chromatographic resolution or peak shape nor any pressure variations or other negative effects were observed as a result of the pre-column placement of the conditioning cell [20]. It is not known whether the interfering compounds were removed from the chromatograms by conversion to chromatographically similar but non-oxidizible products, or if follow-up chemical reactions were taking place which produced new, chromatographically dissimilar products which may or may not have been electroactive. Extraneous chromatographic peaks with retention times greater than that of DCP did appear in some samples when the conditioning cell was used; when the conditioning cell was turned off, these peaks disappeared.

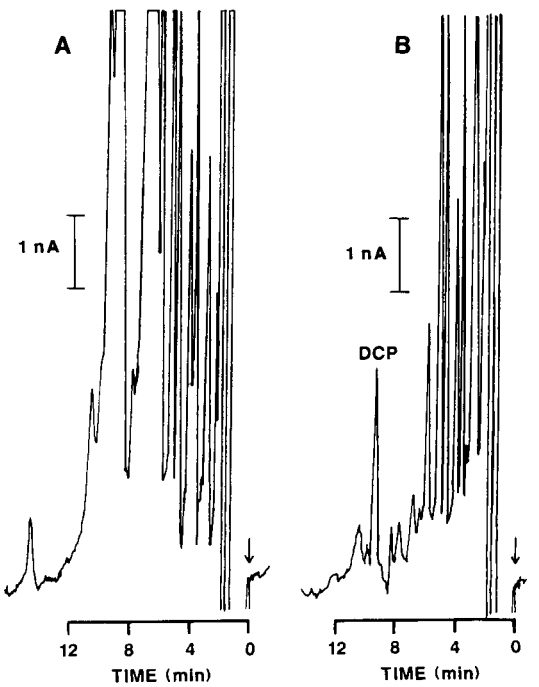

Fig. 2. Liquid chromatographic separation of a soybean hay sample with electrochemical detection. Chromatographic conditions as in Fig. 1. Applied potentials: (A) detector at +1.10 V with conditioning cell disconnected; (B) detector at + 1.10 V with conditioning cell at +0.30 V.

TABLE 1

Recoveries and maximum DCP residue found for various plant tissues

Plant tissue		Recovery (%) ±s.d. (n)	DCP added ($\mu g\ kg^{-1}$)	Maximum DCP residue found ($\mu g\ kg^{-1}$)
Barley[a]	grain	77 ± 1.7 (3)	50	<50
	straw	87 ± 1.2 (3)	50	<50
	forage	78 ± 2.3 (3)	50	115
Wheat[a]	grain	77 ± 2.5 (3)	50	<50
	straw	85 ± 4.7 (3)	50	<50
	forage	68 ± 4.5 (3)	50	162
Soybean[b]	seed	90 ± 1.5 (3)	50	<50
	seed	72 ± 3.6 (3)	100	—
	straw	94 ± 1.8 (4)	50	774
	straw	84 ± 3.4 (3)	200	—

[a]Alumina-column clean-up; 3 ml of 85% phosphoric acid used during steam distillation.
[b]Electrochemical clean-up; 25 ml of 85% phosphoric acid used during steam distillation.

As can be seen from Table 1, recoveries of sample spikes varied with the type of clean-up used. For wheat and barley samples, the alumina-column clean-up was used exclusively and recoveries averaged 78% at the 50 $\mu g\ kg^{-1}$ level. Soybean samples were treated primarily by the in-line electro-oxidative clean-up, and recoveries were substantially better (ca. 92% at the 50 $\mu g\ kg^{-1}$ level). Subsequent investigation of wheat and barley samples subjected to both clean-up procedures verified that ca. 10% lower recovery was obtained with the alumina column. However, even though a portion of the DCP was lost in the alumina column, the precision for replicate samples of each plant tissue type was very good (Table 1), and this procedure appears to be very promising. It is also noted that recovery is somewhat dependent on DCP concentration, with higher DCP concentrations yielding somewhat lower recoveries (Table 1). The origin of this behavior is being studied. Amounts of DCP found in these samples ranged from below the limit of quantitation (50 $\mu g\ kg^{-1}$) to 774 $\mu g\ kg^{-1}$ for soybean straw (Table 1).

For direct comparisons to other detection modes, several soybean hay and seed samples were prepared as detailed above and processed on each of three systems: GC/Hall, LC/UV and LC/EC. Samples were injected into the gas chromatograph from the toluene solution following steam distillation; they were also extracted with alkaline solution for the LC procedures. The LC/UV measurements were made at a wavelength of 287 nm and produced a relatively simple chromatogram, with a well-resolved DCP peak, but did not provide adequate sensitivity for the determination of residues at the levels needed for plant samples (Fig. 3A). The GC/Hall system had adequate sensitivity for determination of DCP residues, but the DCP peak eluted on the trailing edge of the solvent peak making accurate quantitation difficult

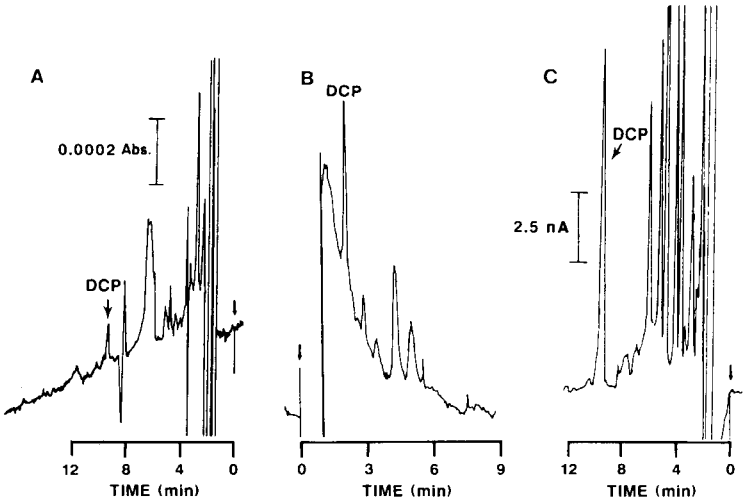

Fig. 3. Chromatograms for DCP in a spiked soybean hay sample. Chromatographic conditions as in Fig. 1, except for B (see text). (A) LC/UV, 287 nm, 1.7 ng DCP injected. (B) GC/Hall, 2.2 ng DCP injected. (C) LC/EC, 1.7 ng DCP injected, detector at +1.10 V, conditioning cell at +0.30 V.

(Fig. 3B). Based on the slope of the baseline and injections of DCP standards, the limit of quantitation on the GC/Hall system was estimated to be ca. 0.5 ng injected. In contrast, the LC/EC system provided well-resolved, easily quantifiable peaks for most samples. A typical chromatogram is shown in Fig. 3C.

The chromatogram obtained for one soybean-hay sample without the use of the in-line conditioning cell showed interferences preceding and following the DCP peak. Use of the conditioning cell at an applied voltage of +0.35 V removed part of the interferences while use of the amperometric cell with the working electrode at +0.95 V removed the remaining interferences but reduced the DCP peak response slightly. Although the nature of the various electroactive interferences is not known, given the ubiquitous presence of naturally-occurring phenolic acids [21], it seems reasonable that such compounds may be responsible for the observed interferences. It was noted that the extent of interferences increased as the volume of phosphoric acid added to decrease foaming in the still pot was increased; this tends to support the suggestion that phenolic acids are involved because the increased acidity would enhance the hydrolysis of phenolic acid esters. It is possible that the use of some surfactant could reduce sample foaming to a manageable level, and permit the use of lower concentrations of phosphoric acid. This possibility is being studied.

This work was supported in part by the Interregional Project No. 4 of the U.S.D.A. and the North Dakota Water Resources Research Institute (Project

No. 6582); it is published as journal article No. 1531 of the North Dakota Agricultural Experiment Station.

REFERENCES

1 U. Banasiak, R. Binner, M. Stock, H. Beitz and H. J. Goedicke, Arch. Phytopathol. Pflanzenschutz, 18 (1982) 359.
2 M. W. Dong and J. L. DiCesare, J. Chromatogr. Sci., 20 (1982) 517.
3 K. Ugland, E. Lundanes, T. Greibrokk and A. Bjorseth, J. Chromatogr., 213 (1981) 83.
4 R. L. Smith and D. J. Pietrzyk, J. Chromatogr. Sci., 21 (1983) 282.
5 G. Blo, F. Dondi, A. Betti and C. Bighi, J. Chromatogr., 257 (1983) 69.
6 R. S. K. Buisson, P. W. W. Kirk and J. N. Lester, J. Chromatogr. Sci., 22 (1984) 339.
7 P. T. Kissinger, K. Bratin, W. P. King and J. R. Rice, ACS Symp. Ser., 136 (1980) 57.
8 H. A. Moye, in H. A. Moye (Ed.), Anal. Pestic. Residues, Chem. Anal. Vol. 58, Wiley, New York, 1981, p. 157.
9 D. E. Ott, J. Assoc. Off. Anal. Chem., 61 (1978) 1465.
10 W. Buchberger, H. Malissa and K. Winsauer, Mikrochim. Acta, Part I (1984) 53.
11 G. J. Clark, R. R. Goodin and J. W. Smiley, Anal. Chem., 57 (1985) 2223.
12 G. Y. P. Kan, F. T. S. Mah, N. L. Wade and M. L. Bothwell, J. Assoc. Off. Anal. Chem., 64 (1981) 1305.
13 L. W. Cook, F. W. Zach, H. J. Klosterman and D. W. Bristol, J. Agric. Food Chem., 31 (1983) 268.
14 C. J. Decedue and W. P. Unruh, BioTechniques, March/April (1984) 78.
15 D. E. Weisshaar, D. E. Tallman and J. L. Anderson, Anal. Chem., 53 (1981) 1809.
16 D. E. Weisshaar and D. E. Tallman, Anal. Chem., 55 (1983) 1146.
17 S. C. Fang and P. Theisen, J. Agric. Food Chem., 7 (1959) 770.
18 M. Akerblom and B. Lindgren, J. Chromatogr., 258 (1983) 302.
19 D. N. Armentrout, J. D. McLean and M. W. Long, Anal. Chem., 51 (1979) 1039.
20 G. W. Schieffer, Anal. Chem., 52 (1980) 1994; 53 (1981) 126.
21 D. A. Roston and P. T. Kissinger, J. Liq. Chromatogr., 5 (1982) 75.

Analytica Chimica Acta, 197 (1987) 169—176
Elsevier Science Publishers B.V., Amsterdam — Printed in The Netherlands

ROOM-TEMPERATURE PHOSPHORIMETRIC DETERMINATION OF BIOGENIC INDOLE COMPOUNDS ADSORBED ON A THIN-LAYER CHROMATOGRAPHIC PLATE

NAOTAKA KURODA, HITOSHI NOHTA and YOSUKE OHKURA*

Faculty of Pharmaceutical Sciences, Kyushu University 62, Maidashi, Higashi-ku, Fukuoka 812 (Japan)

(Received 6th October 1986)

SUMMARY

A simple and sensitive method is described for the determination of biogenic indole compounds adsorbed on cellulose or alumina plates for thin-layer chromatography by room-temperature phosphorimetry. The optimum conditions were investigated for 5-hydroxyindole-3-acetic acid and indole-3-acetic acid. The compounds are spotted on the plates, which are then sprayed successively with sodium citrate or sodium acetate, and sodium iodide solutions. The plates are dried completely under a stream of dry nitrogen, and immediately dipped in molten paraffin. The phosphorescence is stable for at least 3 h even in moist air. The limits of detection for nine biogenic indole compounds tested are between 2 and 300 pmol per sample spot.

In recent years, solid-surface room-temperature phosphorimetry has been developed as a useful analytical technique because of its simplicity and high selectivity. Several methods have been reported for the room-temperature phosphorimetric determination of biochemically and clinically important compounds [1—4].

Low-temperature (77 K) phosphorescence (LTP) of biogenic indole compounds has been studied thoroughly [5—7]. More recently, it was found that room-temperature phosphorescence (RTP) of indole compounds can be observed when they are adsorbed on cellulose filter paper [8], ion-exchange filter paper [9, 10] or sodium acetate powder [4] as support material. Although these techniques do not require cryogenic equipment, it is necessary to keep the support materials dry in a stream of argon [8, 11] or nitrogen [9, 10, 12]; the phosphorescence intensity is susceptible to atmospheric humidity.

It is shown here that reproducible RTP intensities of indole compounds can be obtained even in moist air when the compounds are spotted on cellulose and alumina plates for thin-layer chromatography (TLC) and coated with paraffin after drying, and that the RTP intensities increase in the presence of sodium iodide as a heavy atom perturber, and sodium acetate or sodium citrate. 5-Hydroxyindole-3-acetic acid (5-HIAA) and indole-3-acetic acid (IAA) were used as model compounds to establish suitable conditions

0003-2670/87/$03.50

for a general analytical method for indole compounds. The RTP characteristics of indole compounds were also compared with those for LTP.

EXPERIMENTAL

Reagents and apparatus

All chemicals and solvents were of reagent grade, unless otherwise stated. Deionized, distilled water was used. Indole-3-acetic acid and serotonin-creatinine sulfate were purchased from Wako (Osaka, Japan). Other indole compounds and paraffin (m.p. 68—70°C) were obtained from Nakarai Chemicals (Kyoto, Japan). Indole compounds were dissolved in methanol/water (1:4, v/v) for RTP measurements and in ether/ethanol (4:1, v/v) for LTP measurements. The TLC plates used (20 × 20 cm) were of cellulose, aluminum oxide 60 F_{254} and silica gel 60 on aluminum backing sheets (all from Merck).

Uncorrected RTP spectra and intensities were measured with a Hitachi MPF-3 spectrofluorimeter equipped with a Hitachi phosphoroscope attachment and a sample holder in the sample compartment; the spectral bandwidths of the excitation and emission monochromators were 40 nm and 16 nm, respectively, the exciting beam was 2 mm in width and 30 mm in length on the TLC plate. The sample holder was built as described by Paynter et al. [13] with minor modifications, as shown in Fig. 1. Uncorrected LTP spectra and intensities were measured with the spectrofluorimeter equipped with a Hitachi quartz Dewar flask in place of the sample holder, in quartz sample tubes (4.0 mm i.d., 5.0 mm o.d., 200 mm long; sample volume ca. 150 μl) [14]. The phosphorescence lifetimes were measured on a Hitachi V-550 synchroscope.

Procedure

The sample solution was spotted on to a strip of TLC plate (1 × 3 cm) from a micropipette (Wiretrol, Drummond). The applied volumes of sample solutions were 2 μl for alumina and silica-gel plates and 1 μl for cellulose plates; the diameters of the sample spots were 4.0, 3.8 and 5.0 mm, respectively. The plate was dried by blowing hot air (ca. 60°C) and sprayed with 1 M sodium acetate, sodium citrate or sucrose (ca. 5 μl cm^{-2}). The sodium citrate solution is recommended. After drying in the same manner, the plate was sprayed with 3 M sodium iodide (ca. 5 μl cm^{-2}) and again dried. The plate was placed in a plastic box (12 × 9 × 5 cm high) equipped with a gas inlet and a vent and dried completely by passing dry nitrogen through the box at 2 l min^{-1} for ca. 10 min. The gas was dried by passing it successively through a calcium chloride column (30 cm × 2 cm i.d.) and a phosphorus pentoxide column (15 cm × 2.5 cm i.d.). The plate was immediately dipped in paraffin melted in an oil bath at 100°C. After the paraffin had solidified, the plate was placed in the sample holder and the RTP intensity was measured. For the reagent blank, the procedure was the same except that the sample solution was replaced with methanol/water (1:4, v/v).

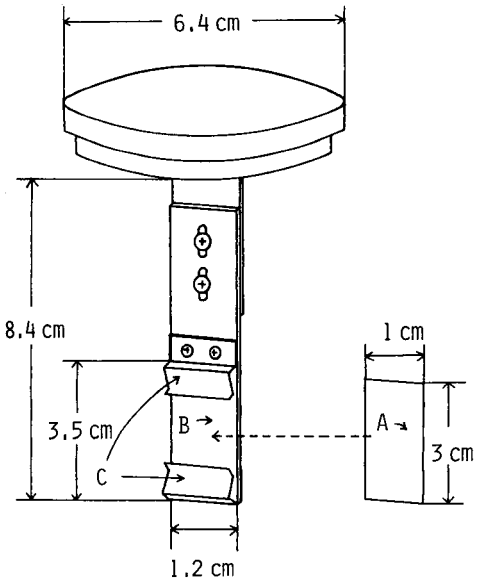

Fig. 1. Schematic diagram of sample holder for RTP measurement. The TLC plate strip (A) is fixed in place (B) by clips (C). The holder is fitted to a Hitachi phosphoroscope attachment instead of a Hitachi quartz Dewar flask assembly, the exciting beam irradiates the plate at 45°, and RTP is measured at right angles to the exciting beam.

RESULTS AND DISCUSSION

The RTP spectra of 5-HIAA adsorbed on a cellulose plate had excitation and emission maxima at 310 and 450 nm, respectively (Fig. 2). On irradiation at 310 nm, a very weak blank phosphorescence was observed; its intensity was 0.6% of that given by 1 nmol μl^{-1} 5-HIAA. The excitation and emission maxima of 5-HIAA on alumina and of IAA on both plates are summarized in Table 1.

When the cellulose and alumina plates were not treated with paraffin, the RTP intensities of 5-HIAA (1 nmol per spot) decayed immediately when the plates were left standing in the sample compartment after drying (Fig. 3). In contrast, with paraffin-treated plates, the RTP intensities of 5-HIAA were stable for at least 3 h and then decreased slightly with time (Fig. 3). Drying of the plate by blowing hot air was not sufficient to give reproducible RTP intensities but the intensities were reproducible after complete drying of the plates in a stream of dry nitrogen for more than 7 min; 10 min was selected for the recommended procedure. Indole-3-acetic acid also gave similar results. No significant RTP was observed from 5-HIAA or IAA on a silica-gel plate under any of the conditions examined.

Reproducible RTP intensities could be obtained for sample spots of diameter 3.5—7.0 mm. Therefore, sample sizes of 1 μl (cellulose plate) and 2 μl (alumina plate) were used.

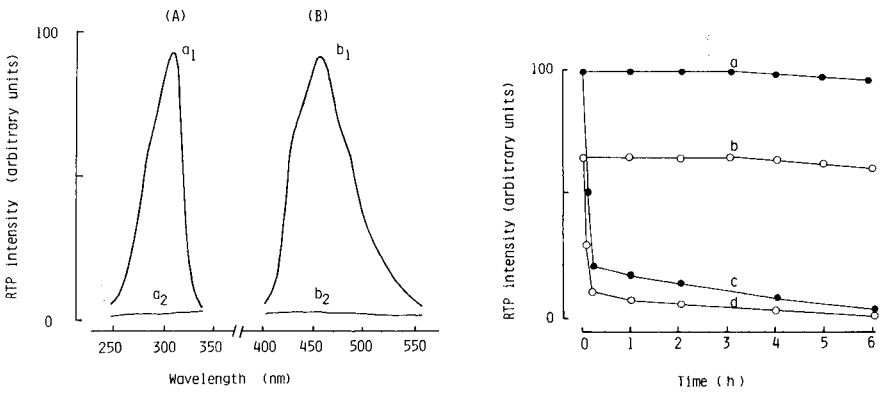

Fig. 2. The RTP spectra of 5-HIAA on a cellulose plate: (A) excitation (450-nm emission); (B) emission (310-nm excitation). (a_1 and b_1) 1 nmol μl^{-1} 5-HIAA was treated as in the recommended procedure; (a_2 and b_2) blank corresponding to a_1 and b_1.

Fig. 3. Stability of RTP intensities of 5-HIAA (1 nmol per spot): (a, c) on cellulose; (b, d) on alumina. 5-HIAA was treated as in the recommended procedure with (a, b) and without (c, d) the paraffin treatment. The atmospheric humidity was 72% at 25°C.

An increase in RTP intensities of some compounds has been observed in the presence of an alkali metal iodide as a heavy atom perturber [3, 8—10, 12]. The RTP intensities of 5-HIAA and IAA were enhanced most when the plates were sprayed with 3—4 M sodium iodide; 3 M is recommended.

Compounds without a heavy atom (sodium acetate [11, 15], sodium citrate [16], boric acid, alanine and sucrose [17]) have also been reported to influence RTP intensity. These compounds, and sodium tartrate, sodium gluconate and inositol, were investigated as spray reagents. Sodium acetate, sodium citrate and sucrose effectively enhanced the RTP intensities of 5-HIAA and IAA. The effects of these compounds were examined under various acidic and alkaline conditions on the plates; the plates were spotted with hydrochloric acid or sodium hydroxide before the sample spotting. When the plates were sprayed with sodium acetate or sodium citrate, large enhancements of RTP intensities of 5-HIAA and IAA on both plates were observed in the neutral range (Figs. 4 and 5). Sucrose also enhanced the RTP of 5-HIAA and IAA in the neutral range on alumina plates but not on cellulose plates.

In the absence of sodium acetate, sodium citrate or sucrose, maximum RTP intensities were obtained under alkaline conditions, as reported previously [1, 3]. These observations suggest that treatment of the plate with hydrochloric acid or sodium hydroxide is not required. The relative RTP intensities and detection limits for 5-HIAA and IAA thus obtained are summarized in Table 1. The lowest detection limits for 5-HIAA and IAA on both plates were attained after spraying with sodium citrate; 1 M sodium citrate gave almost the maximum RTP intensities and is recommended.

TABLE 1

Excitation and emission maxima for RTP, relative intensities (*RPI*) and detection limits (*DL*) for 5-HIAA and IAA

Compound[a]	Plate	Spray reagent[b]	$\lambda_{ex}/\lambda_{em}$ (nm)	*RPI* Sample/blank	*DL*[c] (pmol per spot)
5-HIAA	Cellulose	Sodium citrate	310/450	100[d]/0.60	6
		Sodium acetate	310/450	109/1.10	10
		Sucrose	310/450	25/0.50	20
		None	310/460	16/0.30	19
	Alumina	Sodium citrate	310/450	41/0.08	2
		Sodium acetate	310/450	42/0.12	3
		Sucrose	310/450	30/0.38	13
		None	310/450	3/0.07	23
IAA	Cellulose	Sodium citrate	290/450	69/0.75	11
		Sodium acetate	290/450	87/1.00	11
		Sucrose	290/450	15/0.50	33
		None	290/450	15/0.30	20
	Alumina	Sodium citrate	290/445	15/0.04	3
		Sodium acetate	290/445	16/0.06	4
		Sucrose	290/445	23/0.17	7
		None	290/445	5/0.04	8

[a]1 nmol applied per spot. [b]Spray reagents were all 1 M solutions. [c]Defined as the amount giving an intensity twice the background. [d]The intensity of 5-HIAA on cellulose was taken as 100.

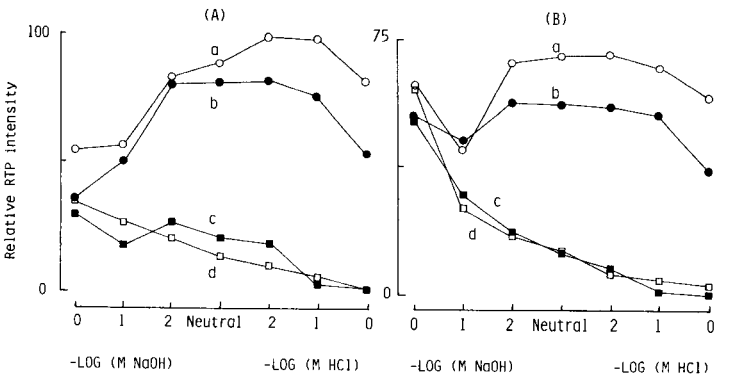

Fig. 4. Effect of the treatment of the cellulose plate with hydrochloric acid or sodium hydroxide on RTP intensities: (A) 5-HIAA; (B) IAA (both 1 nmol per spot). The plate was spotted with various concentrations of hydrochloric acid or sodium hydroxide and then spotted with the sample solution. Spray solution: (a) 1 M sodium acetate; (b) 1 M sodium citrate; (c) 1 M sucrose; (d) none. Otherwise the procedure was as recommended. The intensity from 5-HIAA on a cellulose plate treated with 0.01 M hydrochloric acid was taken as 100.

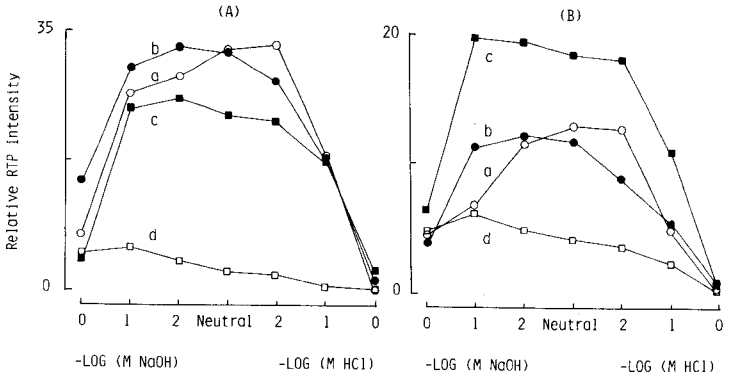

Fig. 5 Effect of the treatment of the alumina plate with hydrochloric acid or sodium hydroxide, on RTP intensities. Samples and treatments as in Fig. 4.

The RTP and LTP characteristics, relative intensities and detection limits of nine indole compounds of biological importance obtained by this method are listed in Table 2. Although the RTP intensities of the compounds on alumina plates were lower than those obtained on cellulose plates, the detection limits obtained for alumina plates were better because of its lower blank value.

The RTP and LTP excitation maxima of indole compounds having a hydroxyl or methoxyl group at the 5-position were at longer wavelengths than those of the other indole compounds tested. The lifetimes of RTP of indole compounds were very much shorter than those of LTP (Table 2). This is probably caused by the heavy atom effect [17]. The tendency was similar to that observed with 2-naphthalene sulfonate [18].

The calibration graphs for 5-HIAA and IAA were linear from 10 pmol to 250 nmol on cellulose and alumina plates. The precision was established by repeated assays (n = 10) for 1 nmol of 5-HIAA or IAA per spot on both plates. The relative standard deviations were 4.6 and 4.8%, respectively, for cellulose and 5.1 and 4.9%, respectively, for alumina.

The proposed method is sensitive, precise and rapid enough to measure 60 samples within 1 h. Therefore, this method should be useful for the determination of indole compounds in biological samples after separation by thin-layer chromatography on a cellulose or alumina plate; this is now in use in this laboratory with a laboratory-constructed TLC scanner/RTP detection system.

TABLE 2

Characteristics for RTP and LTP, relative intensities and detection limits of biogenic indole compounds

Compound[a]	Room temperature								Low temperature			
	Cellulose plate				Alumina plate				$\lambda_{ex}/\lambda_{em}$ (nm)	*RPI*[b,d]	*DL*[b,e]	Lifetime (s)
	$\lambda_{ex}/\lambda_{em}$ (nm)	*RPI*[b]	*DL*[b,c]	Lifetime (ms)	$\lambda_{ex}/\lambda_{em}$ (nm)	*RPI*[b]	*DL*[b,c]	Lifetime (ms)				
5-HIAA	310/450	100	6	34	310/450	41	2	26	310/450	100	190	4.8
Serotonin	310/450	64	9	32	310/450	18	5	20	310/450	78	240	1.3
5-Hydroxy-L-tryptophan	310/450	71	8	23	310/450	33	2	19	310/450	82	230	4.1
Melatonin	310/450	59	10	39	310/450	5	16	21	310/440	94	200	5.3
IAA	290/450	69	11	45	290/445	15	3	23	290/435	91	420	6.3
Indole	290/450	2.5	300	20	290/445	0.3	150	—[f]	290/435	59	650	7.4
Tryptophol	290/450	48	16	37	290/445	3	15	23	290/435	57	670	6.3
Tryptamine	290/450	53	14	27	290/445	18	3	28	290/435	58	660	7.0
L-Tryptophan	290/450	59	13	30	290/445	19	2	21	290/435	82	470	7.3

[a]RTP, 1 nmol per spot; LTP, 10 nmol ml^{-1}. [b]*RPI* and *DL* defined as in Table 1. [c]Given in pmol per spot. [d]The intensity of 5-HIAA was taken as 100. [e]Given in pmol ml^{-1}. [f]Not detectable at 1 nmol per spot.

REFERENCES

1 S. L. Wellons, R. A. Paynter and J. D. Winefordner, Spectrochim. Acta, Part A, 30 (1974) 2133.
2 R. J. Hurtubise, Solid Surface Luminescence Analysis, M. Dekker, New York, 1981.
3 T. Vo-Dinh, E. L. Yen and J. D. Winefordner, Anal. Chem., 48 (1976) 1186.
4 R. M. A. von Wandruszka and R. J. Hurtubise, Anal. Chem., 49 (1977) 2164.
5 P. A. St. John, J. L. Brook and R. H. Biggs, Anal. Biochem., 18 (1967) 459.
6 L. V. S. Hood and J. D. Winefordner, Anal. Biochem., 27 (1969) 523.
7 O. Hutzinger and M. Zander, Anal. Biochem., 28 (1969) 70.
8 M. L. Meyers and P. G. Seybold, Anal. Chem., 51 (1979) 1609.
9 J. J. Aaron, M. Andino and J. D. Winefordner, Anal. Chim. Acta, 160 (1984) 171.
10 M. Andino, J. J. Aaron and J. D. Winefordner, Talanta, 33 (1986) 27.
11 R. T. Parker, R. S. Freedlander, E. M. Schulman and R. B. Dunlap, Anal. Chem., 51 (1979) 1921.
12 H. T. Karnes and S. G. Schulman, Anal. Chim. Acta, 164 (1984) 257.
13 R. A. Paynter, S. L. Wellons and J. D. Winefordner, Anal. Chem., 46 (1974) 736.
14 N. Kuroda, H. Nohta and Y. Ohkura, Anal. Chim. Acta, 175 (1985) 163.
15 I. M. Jakovljevic, Anal. Chem., 49 (1977) 2048.
16 E. L. Y. Bower and J. D. Winefordner, Anal. Chim. Acta, 102 (1978) 1.
17 R. T. Parker, R. S. Freedlander and R. B. Dunlap, Anal. Chim. Acta, 120 (1980) 1.
18 G. J. Niday and P. G. Seybold, Anal. Chem., 50 (1978) 1577.

Analytica Chimica Acta, 197 (1987) 177—186
Elsevier Science Publishers B.V., Amsterdam — Printed in The Netherlands

URINARY ARSENIC SPECIATION BY HIGH-PERFORMANCE LIQUID CHROMATOGRAPHY/ATOMIC ABSORPTION SPECTROMETRY FOR MONITORING OCCUPATIONAL EXPOSURE TO INORGANIC ARSENIC

B. S. CHANA* and N. J. SMITH

Health & Safety Executive, Occupational Medicine & Hygiene Laboratory, 403 Edgware Road, London NW2 6LN (Great Britain)

(Received 3rd November 1986)

SUMMARY

Total urinary arsenic determinations are often used to assess occupational exposure to inorganic arsenic. Ingestion of sea food can increase the normal background levels of total arsenic in urine by up to an order of magnitude, but this arsenic has relatively little toxicity; it is tightly bound as arsenobetaine. The excretion of inorganic arsenic and its metabolites dimethylarsenic acid (DMA) and monomethylarsonic acid (MMA) is not influenced by the consumption of arsenic from sea food. Specific measurements of DMA, MMA and inorganic arsenic provide a more reliable indicator or exposure than total urinary arsenic levels. An automated atomic absorption method involving high-performance liquid chromatographic separation of the arsenic species and continuous hydride generation is described for the determination of arsenite, arsenate, DMA and MMA at μg As l^{-1} levels. The method is used to study normal urinary arsenic levels in laboratory staff and arsenic excretion by exposed workers.

Arsenic can occur in both inorganic and organic forms and these show large differences in their metabolism and toxicity [1]. Exposure to arsenic occurs in occupations such as smelting, glass making and pesticide manufacture and use. Soluble compounds of arsenic can readily be absorbed both orally and by inhalation, the extent of absorption being dependent on the solubility of the compound [1]. The excretion pathways are such that urine forms the main route of elimination. Inorganic arsenic undergoes considerable biotransformation in the body, both monomethyl and dimethyl derivatives being formed [2—4]. The proportions of inorganic and methylated species in the urine can vary although dimethylarsenic acid is generally the major metabolite [3]. Elimination kinetics are such that arsenic is cleared very rapidly from the blood to the urine with a half life in the body of ca. 30 h [5]. Complex organo-arsenicals occur in sea foods, and arsenic ingested in this form is not metabolised but excreted unchanged with a very short half-life [2, 6].

The problems of interpreting urinary arsenic measurements have been discussed [3, 7]. Methods for estimating urinary arsenic based on the determination of total arsenic will not differentiate between the components

arising from occupational exposure and those arising from dietary intake. Roy [8] suggested that the most suitable method of monitoring workers exposed to arsenic is to measure the concentration of arsenic in the urine at the end of a working week. However, he agreed that the ingestion of sea food in the previous 48—72 h would invalidate urinary arsenic as a measure of occupational exposure, if the analytical method is not specific for individual arsenic species. In a study of arsenic concentrations in the urine of unexposed and occupationally exposed subjects, Mappes [9] stated that in the occupational setting, a total arsenic determination can be made 24 h after most meals containing fish without error. Buchet et al. [3], however, recommend the determination of inorganic arsenic, monomethylarsonic (MMA) and dimethylarsenic acid (DMA) in urine for biological monitoring of workers exposed to inorganic arsenic. Stoeppler and Apel [10] suggested that the methodology for arsenic speciation that is now available allows occupational exposure and dietary intake to be distinguished and should be used in routine biological monitoring of exposed workers.

Numerous approaches have been applied to the determination of arsenic species in various matrices. Pacey and Ford [11] reported a method based on ion-exchange chromatography for the separation of arsenate, MMA and DMA, with arsenite being obtained by difference from total arsenic, although no real applications were given. Ricci et al. [12] developed an automated method using ion chromatography and atomic absorption spectrometry (a.a.s.) for the speciation of arsenic compounds in air samples. This method required the use of two buffers for elution and allowed 10—15 samples to be analysed before the column had to be regenerated. Morita et al. [13] used various anion- and cation-exchange columns followed by inductively-coupled plasma atomic emission spectrometry for the detection of arsenic species, and successfully applied the method to the analysis of a seaweed sample. More recently, Tye et al. [14] used high-performance liquid chromatography (h.p.l.c.) for the separation of arsenite, arsenate, MMA and DMA, and applied this technique in the analysis of water samples. Buchet et al. [15] used sodium tetrahydroborate for the generation of arsines with their subsequent collection in liquid nitrogen before selective volatilisation, whilst Foa et al. [7] followed a procedure based on ion chromatography, separating the arsenic species with various eluants. This paper reports a method that will allow the separation of arsenite, arsenate, MMA and DMA in urine by h.p.l.c. with detection of the separated arsenic species by continuous hydride generation/a.a.s.

EXPERIMENTAL

Apparatus

The h.p.l.c. system included automated sample injection and solvent and column switching valves. Waters 510 and Waters 590 programmable solvent delivery pumps and Waters solvent-selecting and column-switching valves

were used. Samples were introduced onto the column with a Waters Wisp auto-injector. The arsenic species were separated on a strong anion-exchange column (25 cm × 4.5 mm i.d.) of 10-μm Ionospher (Chrompak). A 1.5-cm guard column (MPLC) with a RP-18 guard cartridge placed before the anion-exchange column was used to remove most of the organic components from urine that would otherwise bind irreversibly to the packing material in the anion-exchange column. A conditioning column (Scientific Glass Engineering) packed with silica was used to pre-saturate the mobile phase with silica.

The continuous hydride generation was based on the addition of sodium tetrahydroborate to the acidified column effluent. Sulphuric acid and reductant were introduced into the column effluent stream by a model 202U peristaltic pump (Watson Marlow) operated at 20% of its maximum pumping speed. Acidflex tubing (yellow/yellow), and standard tubing (green/green), both from Elkay Laboratory Products, were used for sulphuric acid and reductant, respectively. Three 10-turn mixing coils (Gradko International, part no. 15-37) and a gas-liquid separator (Fig. 1.) were connected to the stream after the addition of acid and reductant. Argon added via a flow meter carried the hydrides to an electrically-heated quartz furnace for a.a.s.

A Perkin-Elmer 3030 atomic absorption spectrometer equipped with a hydride system (MHS-20) and an electrodeless discharge lamp operated at 8 W were used for arsenic determination at 193.7 nm, at a bandwidth of 0.7 nm and a 5× scale expansion. The quartz furnace of the MHS-20 was maintained at 900° C. Signals were recorded on a Waters 740 data module and measured as peak heights. A Hamilton Microlab M programmable diluter was used to prepare matrix-matched standards.

Standards and reagents

Deionized, double-distilled water was used throughout. The arsenic trichloride (1000 mg l^{-1}) solution was a Spectrosol reagent (BDH). Stock solutions (1000 mg As l^{-1}) of arsenate, DMA and MMA, without any stabilisers, were prepared from sodium arsenate (Sigma), dimethylarsenic acid (Sigma) and methylarsonic acid (Pfaltz and Bauer) and stored at −20°C until required. Working standards of 0.1, 0.2, 0.4, 0.6, 0.8 mg As l^{-1} for each species were freshly prepared daily in water. Concentrated sulphuric acid was diluted to 3 M. Sodium tetrahydroborate (2% w/v) was prepared in sodium hydroxide solution (0.5% w/v) and filtered through a Whatman grade 4 filter before use. Phosphate buffer was prepared from 0.03 M sodium dihydrogenorthophosphate, and its pH was adjusted to 6.2—6.3 with 0.03 M disodium hydrogenorthophosphate, before filtration through a 0.45-μm filter.

Procedures

Urine samples were collected in polycarbonate bottles, without preservatives, and were filtered through a 0.45-μm filter. If further treatment was delayed by more than 12 h, they were stored at −20°C. The diluter was used to add 50 μl of each working standard to 950 μl of urine (obtained from a

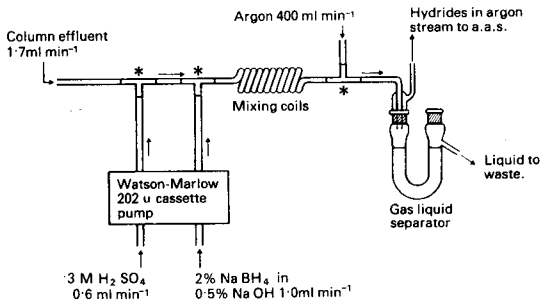

Fig. 1. Continuous hydride generation system. The gas/liquid separator consists of a U tube (MF21/2) and a bottle head (MF28/2) (Fisons Scientific Equipment), modified as shown. The T-pieces (*) were from Technicon (part number 116-0200-00).

person known to have had a fish-free diet) to give matrix-matched standards of 5, 10, 20, 30 and 40 μg l^{-1} with respect to arsenic for each arsenic species. These standards were also filtered through a 0.45-μm filter before use.

The normal analytical sequence consisted of five standards, one quality-control sample, then six samples followed by another quality-control sample. While the samples and matrix-matched standards were being prepared and loaded into the autosampler carousel, the effluent from the h.p.l.c. system was connected to the continuous hydride generation/a.a.s. system. After ca. 40 min, when the arsenic electrodeless discharge lamp emission and the hydride generation system were stable, the carousel was loaded and analyses were initiated.

The combination of an auto-injector, a programmable 590 pump, a 510 pump and solvent- and column-switching valves allowed sample loading, automated on-line sample clean-up and precolumn regeneration to be done sequentially and automatically. The chromatographic separation was achieved in phosphate buffer (0.03 M, pH 6.2—6.3) at 1.7 ml min^{-1}; 30 s after injection of sample the precolumn regeneration sequence (by the 590 pump) was initiated automatically. The precolumn was backflushed between each sample with 3 ml of water, 7 ml of methanol and 4 ml of water before further equilibration with phosphate buffer.

Total arsenic was also measured. This was achieved by arsine generation/a.a.s. after the urine samples and matrix-matched standards had been digested with a mixture of concentrated nitric and perchloric acids. Appropriate safety precautions were taken in handling perchloric acid. Arsenic trichloride was used to prepare the matrix-matched standards. A urine sample (from a person on a fish-free diet) spiked with equal amounts (10 μg As l^{-1}) of arsenite, arsenate, DMA and MMA was used as a control, which was analysed at the beginning and end of each run.

RESULTS

The development of this h.p.l.c./hydride generation/a.a.s. system depended on establishing both a robust h.p.l.c. system capable of automated

processing of a large number of samples without column deterioration, and an efficient and reproducible system for hydride generation and delivery to the spectrometer.

The h.p.l.c. separation

A range of anion-exchange silica-based column packings was tested and discarded before a 10-μm Ionospher column with a conditioning column was found to be a satisfactory combination. The main problem was the limited life of the earlier column systems; separation power deteriorated after only a limited number of sample injections. The use of the Ionospher column with a RP-18 guard cartridge, and a conditioning column to pre-saturate the mobile phase, however, had an adequate lifetime (400 injections) and maintained good chromatographic separation of the four arsenic species (Fig. 2). The retention times of the four arsenic species remained constant within an analytical run of 7 h. Gradual decrease in the retention times of arsenate and DMA was observed, however, and after ca. 400 injections there was some loss in resolution between DMA and arsenate. It was then possible to resolve DMA and arsenate by decreasing the buffer concentration to 0.025 M, thereby extending the life of the column without any significant loss in sensitivity.

Hydride generation

The addition of sodium tetrahydroborate to the acidified column effluent resulted in considerable formation of hydrogen and disruption of the contin-

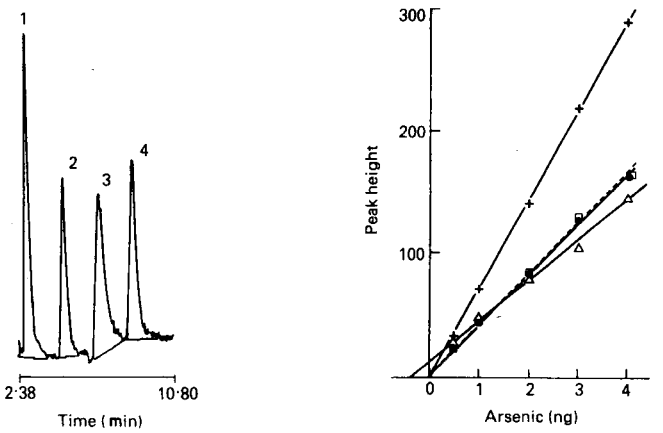

Fig. 2. Chromatogram of urine from a subject on a fish-free diet spiked with equal amounts (40 μg As l^{-1}) of: (1) arsenite; (2) monomethylarsonic acid; (3) dimethylarsenic acid; (4) arsenate.

Fig. 3. Calibration graphs constructed from 100-μl injections of spiked urine standards: (+) arsenite; (△) DMA; (•) MMA; (□) arsenate.

uously flowing liquid stream. Various geometries of mixing coils and gas/liquid separator, various concentrations of sulphuric acid and reductant, and different argon flows were investigated to establish optimum yields of hydrides without blurring of the chromatographic separation. The optimum conditions are shown in Fig. 1. Variations of ±10% in these specified conditions could be tolerated with only minor effects on sensitivity and reproducibility.

Seven injections (100 μl) of urine spiked with equal concentrations (40 μg As l^{-1}) of arsenite, MMA, DMA and arsenate were made to assess the reproducibility of peak-height and peak-area measurements. The relative standard deviations and the relative signal responses are shown in Table 1. Peak-height measurements were more reproducible.

Typical calibration graphs for each of the arsenic species are shown in Fig. 3. These were obtained by injecting the same volume (100 μl) of different concentrations of urine-spiked standards and plotting peak height for each arsenic species against amount added to the column. The intercept for DMA reflects the endogenous concentration in the urine for making the matrix-matched standards. The differences in the slopes of the calibration graphs are partly due to the different rates of conversion of each arsenic species to its hydride and partly because peak heights decrease with increasing chromatographic retention times.

The detection limits, based on twice the standard deviation of replicates of known low concentration (endogenous concentration + 5 μg As l^{-1}) were 2 μg As l^{-1} for all four species. Between-run relative standard deviations (n = 21) were assessed by spiking a urine sample from an occupationally unexposed subject with ca. 10 μg As l^{-1} with respect to each species. Portions of the sample were stored at −20°C to try to prevent the oxidation of arsenite which has been shown to occur on storage at room temperature [15]. The values obtained were 5.1% (arsenite), 3.8% (MMA), 5.3% (DMA) and 7.2% (arsenate).

Analysis of urine samples

Urine samples, together with recent dietary history, were obtained from occupationally unexposed laboratory staff. The samples were analysed for total arsenic and then speciated to establish normal levels of metabolites of

TABLE 1

Relative standard deviations (r.s.d.) and mean relative signal responses for arsenite, MMA, DMA and arsenate (arsenite = 100; n = 7)

Species	Arsenite	MMA	DMA	Arsenate
Peak height signal	100	98	55	65
R.s.d. (%)	4.5	4.6	5.4	2.3
Peak area signal	100	97	100	76
R.s.d. (%)	4.9	5.7	9.4	2.0

inorganic arsenic. The samples were grouped according to dietary histories of sea-food intake (Table 2). In subjects with recent sea-food intake (<1 day) the mean total urinary arsenic was over 15-fold higher than from subjects with no history of sea-food ingestion. The total concentration of the four individual species varied very much less, although it appeared that DMA (major arsenic species) is raised to some extent immediately after sea-food ingestion.

Urine samples collected from twelve workers occupationally exposed to inorganic arsenic were grouped according to their recent sea food consumption (Table 3). All subjects who had recently consumed sea food showed a considerable increase in total arsenic levels compared to the speciation total. The percentage increase ranged from 65% to 255%. Clearly, in the absence of speciation studies, the measurement of total arsenic levels would lead to serious over-estimation of the arsenic excretion resulting from occupational exposure. However, for those who had not recently consumed sea-food, the sum of individual arsenic species approaches the total arsenic level.

DISCUSSION

Total urinary arsenic estimations have been used for assessing occupational exposure to inorganic arsenic. Our experience and that of others [16] show that the ingestion of sea food can increase the normal background levels of total arsenic in urine by an order of magnitude. The arsenic from sea food has relatively low toxicity, is tightly bound to an organic molecule which has been identified as arsenobetaine [17, 18]. The excretion of inorganic

TABLE 2

Concentrations of arsenic species in urine samples from occupationally unexposed laboratory staff

Days after eating sea food	No. of subjects	Urinary arsenic[a] ($\mu g\ l^{-1}$)				
		Arsenite	MMA	DMA	Sum of arsenic species[a]	Total
<1	7	1.1 (1—2)	2.6 (1—4)	19.6 (7—54)	23.3 (7—58)	259 (53—1303)
<3	10	1	2.1 (1—3)	9.3 (3—25)	12.4 (3—28)	120 (19—510)
>3	8	1	1.4 (1—2)	5.0 (1—10)	7.4 (1—10)	29 (8—69)
0[b]	14	1	1.7 (1—3)	5.5 (1—29)	8.2 (1—31)	14.6 (3—53)

[a]No arsenate was detected. Mean values are given with ranges in parentheses. [b]No sea food consumed.

TABLE 3

Concentration of arsenic species in urine samples. Subjects A1—7 had recently eaten sea food, subjects B1—5 had not

Sample	Urinary arsenic ($\mu g\ l^{-1}$)					
	Arsenite	MMA	DMA	Arsenate	Sum of arsenic species	Total arsenic
A1	5	7	38	n.d.[a]	50	98
2	3	2	18	n.d.	23	135
3	4	6	55	n.d.	65	231
4	1	7	25	4	37	147
5	18	9	38	13	78	137
6	3	4	30	n.d.	37	61
7	6	8	42	n.d.	56	102
B1	15	11	72	n.d.	98	105
2	26	31	127	2	186	195
3	25	28	124	3	180	195
4	5	11	33	n.d.	49	51
5	4	3	41	n.d.	48	46

[a]Not detected.

arsenic and its metabolites (DMA and MMA) has been said not to be influenced by the excretion of arsenic from sea food [7, 15]. Specific measurement of DMA, MMA and inorganic arsenic should thus provide a more reliable indicator of exposure than total urinary arsenic levels.

Methods which were previously available for the measurement of arsenic species in urine involve lengthy procedures, which cannot easily be automated and therefore are not suited for routine monitoring of workers exposed to inorganic arsenic. The method described here is an automated one which allows the measurement of arsenite, arsenate, DMA and MMA in urine in one process. The method is free of interference from the organoarsenic compounds from sea food as these are not reduced by sodium tetrahydroborate to their corresponding arsines and are therefore not detected [15]. The method is easy to set up and once in operation requires minimum operator attention. Filtration of the urine samples is the only sample preparation required and up to five samples per hour can be analysed.

A useful life for the separating column was achieved by adding a precolumn and a conditioning column packed with silica to the h.p.l.c. system. The major improvement resulted from the use of a conditioning column. The precolumn, placed before the separating column, removed the majority of the organic components from urine that would otherwise bind irreversibly to the packing material in the separating column. The conditioning column, between the pump and the injector, ensured that the mobile phase dissolves any silica from the conditioning column rather than from the separating column.

With this method the reduction of each arsenic species to its corresponding hydride in a continuous stream is not necessarily complete. Increase in concentrations of acid and reductant increased the signal from arsenate but decreased the response from DMA. Conditions for continuous hydride generation were optimised to give the best signal for the four arsenic species, although preference was given to the DMA response as DMA is the predominant arsenic species present in urine. It has long been accepted, however, that reproducibility can be achieved in a continuous flow system even if the chemical reaction is not complete [19].

Urine samples obtained from occupationally unexposed laboratory staff were analysed for individual arsenic species by the method described here and for total arsenic. The data show that sea food consumed up to 3 days before sampling causes the total urinary arsenic concentration to be considerably increased, thus demonstrating the interference of this dietary arsenic in the monitoring of occupational exposure to inorganic arsenic. This is in agreement with the findings of Foa et al. [7] and lends support to the view that 3 days or more should elapse before the influence of diet on total urinary arsenic levels can be disregarded.

The influence of diet on the total arsenic in the species monitored is very much less than on total arsenic. As is shown, sea food consumed up to a day before sampling raises the mean arsenic speciation total to a very much smaller extent than the mean total arsenic. The data clearly indicate that speciation techniques should be used for the biological monitoring of exposure to inorganic arsenic, as has been suggested elsewhere [3, 7, 10]. Compared to total arsenic methods, the arsenic speciation method described here is simple, automated, not prone to losses and contamination, does not require digestion with nitric and perchloric acids and is not influenced by arsenic from dietary sources.

We thank D. Gompertz for valuable advice and discussion.

REFERENCES

1 R. J. Fielder, E. A. Dale and S. D. Williams, HMSO London, Toxicity Review 16: Inorganic Arsenic Compounds, Health and Safety Executive, London, 1986.
2 E. A. Crecelius, Environ. Health Perspect., 19 (1977) 147.
3 J. P. Buchet, R. Lauwerys and H. Roels, Int. Arch. Occup. Environ. Health, 48 (1981) 71.
4 G. K. H. Tam, S. M. Charbonneau, F. Bryce, C. Pomroy and E. Sandi, Toxicol. Appl. Pharmacol., 50 (1979) 319.
5 J. Mealy, G. L. Brownell and W. H. Sweet, Arch. Neurol. Psychiatry, 81 (1959) 310.
6 A. Chapman, Analyst, 51 (1926) 548.
7 V. Foa, A. Colombi, M. Maroni, M. Buratti and G. Calzaferri, The Sci. Total Environ., 34 (1984) 241.
8 M. Roy, Occup. Health in Ontairo, 4 (1983) 17.
9 R. Mappes, Staub-Reinhalt. Luft, 42 (1982) 133.
10 M. Stoeppler and M. Apel, Fresenius' Z. Anal. Chem., 317 (1984) 226.
11 G. E. Pacey and J. A. Ford, Talanta, 28 (1981) 935.

12 G. R. Ricci, L. S. Shepard, G. Colovos and N. E. Hester, Anal. Chem., 53 (1981) 610.
13 M. Morita, T. Uehiro and K. Fuwa, Anal. Chem., 53 (1981) 1806.
14 C. T. Tye, S. J. Haswell, P. O'Neill and K. C. C. Bancroft, Anal. Chim. Acta, 169 (1985) 195.
15 J. P. Buchet, R. Lauwerys and H. Roels, Int. Arch. Occup. Environ. Health, 46 (1980) 11.
16 S. S. Pinto, M. O. Varner, K. W. Nelson, A. R. Labbe and L. D. White, J. Occup. Med., 18 (1976) 677.
17 J. S. Edmonds and K. A. Francesconi, Tetrahedron Lett., 18 (1977) 1543.
18 J. B. O. Luten, O. Riekwel-Booy and A. Rauchbaar, Environ. Health. Perspect., 45 (1982) 165.
19 R. J. Henry and D. C. Cannon, in J. W. Winkelman (Ed.), Clinical Chemistry, Principles and Technics, 2nd edn., Harper and Row, New York, 1974, p. 225.

Analytica Chimica Acta, 197 (1987) 187—194
Elsevier Science Publishers B.V., Amsterdam — Printed in The Netherlands

LACTATE BIOSENSOR BASED ON HUMAN ERYTHROCYTES

JAROSLAV RACEK
Department of Clinical Biochemistry, Faculty Hospital, 305 99 Plzeň (Czechoslovakia)

(Received 29th July 1986)

SUMMARY

An amperometric lactate biosensor based on human erythrocytes is described. The erythrocyte suspension is retained near the platinum electrode by means of a semipermeable membrane. The response is based on lactate dehydrogenase activity in the erythrocytes and uses the oxidation of NADH by hexacyanoferrate(III) and amperometric detection of the resulting hexacyanoferrate(II). The limit of detection is 2.8×10^{-5} mol l^{-1}, and the response is linear up to 1 mmol l^{-1} lactate in the analyzed solution (11 mmol l^{-1} in a blood sample). The response time is 7 min, and the useful lifetime is 2 weeks. The response is influenced only by reducing substances (uric acid) and malic acid. The effect of uric acid is readily compensated, and there is insufficient malic acid in blood to affect the results.

Determination of lactate is of a great significance in medicine (detection of lactic acidosis in shock patients and sportsmen), in detection of food spoilage, etc. Recently, various types of enzyme electrodes have been used for this purpose in place of spectrophotometric methods. Four kinds of lactate-converting enzymes can be immobilized on the surface of a measuring electrode: yeast lactate dehydrogenase, E.C. 1.1.2.3 [1—5], animal lactate dehydrogenase, E.C. 1.1.1.27 [6—13], lactate oxidase, E.C. 1.1.3.2 [14—18] and decarboxylating lactate oxidase, E.C. 1.13.12.4 [19]. Many microbial sensors which use whole cells instead of an isolated enzyme have been described recently, but only one type of cellular biosensor has been proposed for lactate determination. It is based on immobilization of cells of the aerobic yeast *Hansenula anomala* on a platinum anode. These cells contain lactate dehydrogenase (L-lactate: ferricytochrome c oxidoreductase, E.C. 1.1.2.3) in high activity [20—22]. This paper describes another system with immobilized whole cells for lactate determination: this lactate biosensor is based on the lactate dehydrogenase (L-lactate: NAD^+ oxidoreductase, E.C. 1.1.1.27) activity of human erythrocytes.

EXPERIMENTAL

Preparation of cell suspension

Blood of healthy human volunteers (blood donors) was collected in vessels with sodium fluoride (2 mg per 1 ml of blood). The erythrocytes were

0003-2670/87/$03.50

separated by centrifugation and washed twice with isotonic sodium phosphate buffer, pH 7.4; the same buffer was added to give a volume equal to that of the original blood. Later, whole blood was used without any pretreatment with the same results.

Apparatus and procedures

The principle of lactate determination is as follows: lactate dehydrogenase in the erythrocytes catalyses conversion of lactate to pyruvate in the presence of NAD^+; the reduced form of this coenzyme is re-oxidized by hexacyanoferrate(III) and the resulting hexacyanoferrate(II) is detected amperometrically by its oxidation at a platinum anode.

The lactate biosensor contained a platinum electrode with a platinum disk 2 mm in diameter at one end, polarized at 0.35 V. The reference Ag/AgCl electrode was immersed in sodium phosphate buffer (0.2 mol l^{-1}), pH 7.4 containing potassium chloride (0.1 mol l^{-1}). A small chamber above the platinum electrode was filled with the cell suspension and covered with a semipermeable Visking membrane by means of an O-ring (Fig. 1).

During the measurement the tip of the biosensor was put into a glass vessel, the temperature of which was maintained at 25°C. The vessel was filled with 3.0 ml of working solution, i.e., isotonic Tris/HCl buffer, pH 9.0, containing potassium hexacyanoferrate(III) (5.0 mmol l^{-1}), NAD^+ (1.0 mmol l^{-1}) and phenazine methosulfate (0.5 mmol l^{-1}). This solution was prepared just before measurements were made. Before the series of measurements, the electrode was immersed in this solution for several minutes, so that the internal pH (in the chamber) was equilibrated to the value of 9.0. The current between the platinum anode and the reference electrode was measured using a picoammeter BM 545 (Tesla Brno, ČSSR); 0.3 ml of sample was added and a second reading was taken after the current had stabilized. The solution was mixed with a magnetic stirrer. The current started to increase after 10 s, and became constant within 7 min. After the measurement had been completed, the electrode was immersed into sodium phosphate buffer (0.2 mol l^{-1}, pH 7.4) again and stored at 4°C.

The results obtained with the cellular biosensor were compared with those obtained by an ultraviolet procedure for blood plasma lactate. The lactate kit used was fully enzymatic (Monotest 19 × 5, Best. No. 149.993; Boehringer Mannheim); the measurements were made on an OLLI-3000 analyzer (Ollituote, Espoo 32, Finland).

Reagents

Standard sodium L-lactate solutions (1.0 mol l^{-1}) were prepared from a stock solution of sodium lactate (SPOFA, ČSSR) by dilution with distilled water. When venous blood plasma or blood was used, 1 drop of fluoride/EDTA solution (Best. No. 243.710, Boehringer Mannheim) was added to 1.0 ml of the blood immediately after its collection.

Sodium phosphate (pH 7.0, 7.4 and 8.0) and Tris/HCl (pH 8.0, 8.5, 9.0

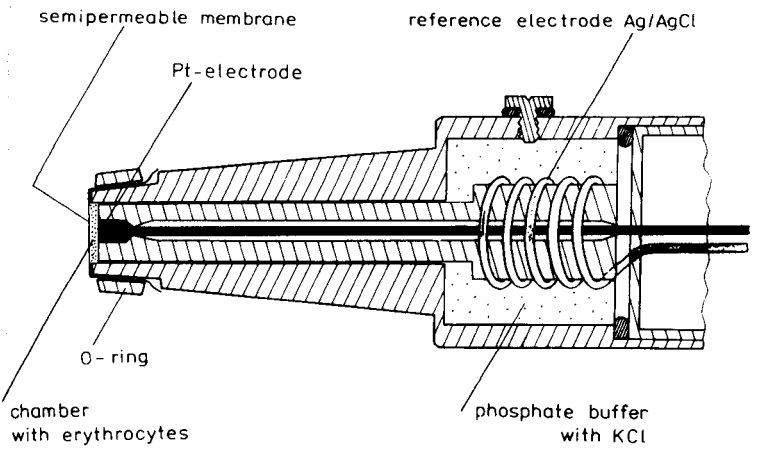

Fig. 1. Cross-section of erythrocyte lactate biosensor.

and 9.5) buffers were prepared in concentrations of 0.2 mol l^{-1} and their osmolality was corrected with distilled water (for phosphate buffer) or sodium chloride (for Tris/HCl buffer) to give a value of 285 mmol kg^{-1}. All other reagents were purchased from Lachema Brno (ČSSR) and were of analytical grade.

RESULTS

Figure 2 shows calibration graphs obtained with the erythrocyte biosensor under the finally recommended conditions. A lactate concentration of 1.0 mmol l^{-1} in the measuring vessel (corresponding to 11 mmol l^{-1} in the biological material) elevated the current by ca 0.18 μA. This lactate concentration was also found to be the upper limit for the linear response of the biosensor. The lower limit of detection was 2.8×10^{-5} mol l^{-1} in the measuring vessel, i.e., 0.3 mmol l^{-1} in the sample.

The effect of reagent concentrations was investigated. The concentration of one of the compounds was changed while the others remained constant, and the maximal response to lactate (20 mmol l^{-1} in the measuring vessel) was recorded. The optimal concentrations in the working solution were as follows: >1.0 mmol l^{-1} NAD^+, 0.5 mmol l^{-1} phenazine methosulfate (a further increase of its concentration caused a depression of the response) and >5.0 mmol l^{-1} hexacyanoferrate(III). The isotonic Tris/HCl buffer, pH 9.0, was replaced by other isotonic buffers (Tris/HCl or sodium phosphate as described above) of various pH values between 7.0 and 9.5. However, pH 9.0 was found to provide the greatest response to lactate (Fig. 3).

Interferences

Reducing substances (ascorbic acid, uric acid, and compounds with sulfhydryl groups) can interfere directly with the electrochemical process because they are oxidized at the platinum anode. A second possible inter-

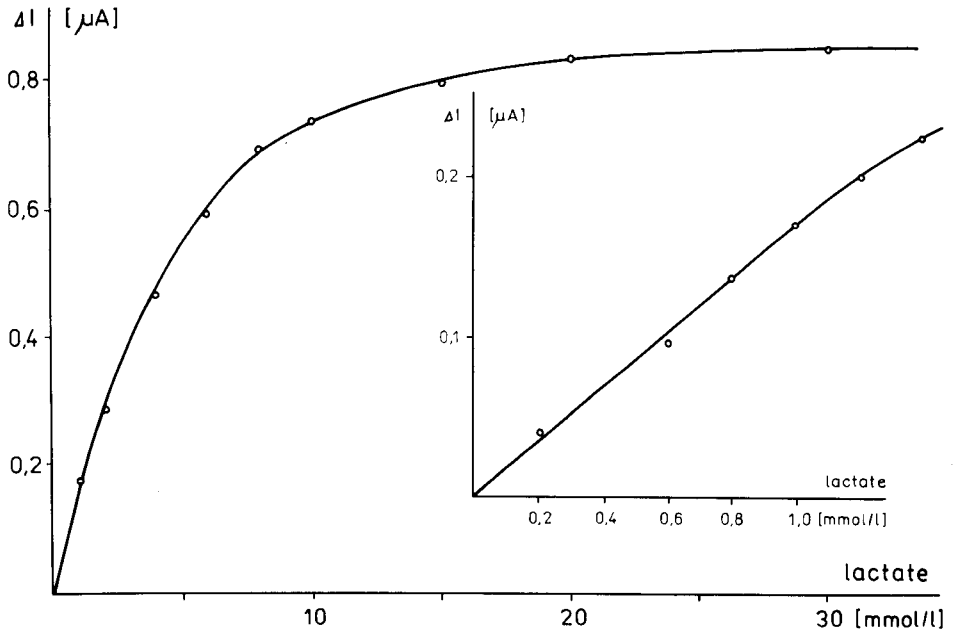

Fig. 2. Calibration graphs for an erythrocyte lactate biosensor (lactate concentration is that in the measuring vessel; concentration in original sample is 11 times higher).

ference mechanism is their reduction of hexacyanoferrate(III). These compounds were tested at a concentration of 11 mmol l^{-1}; 0.3 ml of the stock solution was diluted with 3.0 ml of working solution so that the final concentration of reducing substance in the measuring vessel was 1.0 mmol l^{-1}. Their influence has already been described in detail [21] and is summarized in Table 1. The degree of interference of reducing substances, especially of uric acid, can be significant when biological material (blood plasma) is analyzed for lactate. When uric acid is present it is necessary to subtract the sample blank value from the measured current in the following way. Blood plasma is added to the modified working solution in which NAD^+ is absent. The current rises owing to the reducing substances which are present in the plasma and reaches a constant value 2—3 min after blood plasma addition. NAD^+ (0.1 ml, 33 mmol l^{-1}, in isotonic Tris/HCl buffer, pH 9.0) is added and the current increase over the next 7 min corresponds to the lactate concentration.

The effect of non-reducing compounds present in blood plasma in higher concentrations either normally (various compounds, such as amino acids, sugars, ketones, etc.) or abnormally (drugs, toxins, etc.) was tested. These compounds in aqueous solutions, were added to the working solution so that their final concentrations in the measuring vessel were 1.0 mmol l^{-1}. The biosensor response to these solutions was compared with the response to the lactate solution alone at the same concentration. The only interfering substance found was L-malate which gave 21.8% of the response

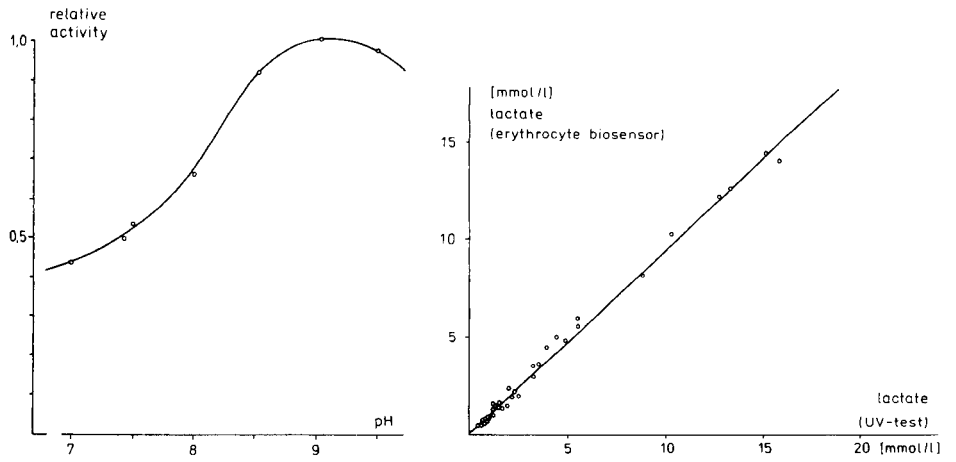

Fig. 3. Dependence of the response on the pH of the working solution.

Fig. 4. Comparison of results for lactate obtained by the erythrocyte biosensor and an ultraviolet spectrophotometric method.

TABLE 1

Effect of some reductants (1.0 mmol l^{-1}) on the erythrocyte biosensor response

Reductant	Electrode response (μA)	Upper limit of values in blood (mmol l^{-1})	Positive error in lactate conc. (mmol l^{-1})
Cysteine	0.082	0.033	0.02
Ascorbic acid	0.154	0.079	0.07
Uric acid	0.121	0.416	0.36

of lactate at equimolar concentration. The compounds tested were alanine, arginine, aspartate, citrulline, glutamate, glutamine, glycine, histidine, isoleucine, leucine, lysine, phenylalanine, serine, valine; fructose, galactose, glucose; acetoacetate, acetone, citrate, glycerol, 3-hydroxybutyrate, malate, oxalate, 2-oxoglutarate; ethanol, ethylene glycol, mannitol, methanol, phenobarbital, salicylate and sorbitol.

Analytical performance

The precision of the method was calculated from 20 repeated estimations of lactate concentration in pooled blood plasma and serum. It was calculated as a relative standard deviation and was found to be 4.01% for pooled blood plasma (mean concentration = 1.16 mmol l^{-1}) and 3.66% for pooled blood serum (mean concentration = 3.10 mmol l^{-1}). Table 2 demonstrates the recovery of the procedure. Lactate standards were added to pooled blood plasma, and each sample was analyzed three times.

TABLE 2

Recovery of standard additions of lactate

Lactate (mmol l^{-1})		Recovery (%)	Lactate (mmol l^{-1})		Recovery (%)
Added	Found		Added	Found	
0.0	1.16	—	6.0	7.05	98.2
2.0	3.05	94.5	8.0	8.87	96.4
4.0	5.36	105.1			

The lactate concentration was determined in 35 blood plasma samples collected from patients admitted to the Faculty hospital in Plzeň and from sportsmen after maximal physical exercise. The results obtained with the biosensor compared favourably with those of the spectrophotometric test (Fig. 4). The equation for this plot is $y = 0.183 + 0.946\,x$ with a correlation coefficient (r) of 0.995 ($n = 35$).

The biosensor response to lactate decreased by ca. 10% of its original value over two weeks if the biosensor was kept in isotonic sodium phosphate buffer, pH 7.4 at +4°C when not in use. This pH was found to be better for retaining enzyme activity in erythrocytes than the working pH of the biosensor. The measurements were performed daily, always in one series of 10—20 determinations.

DISCUSSION

Lactate electrochemical biosensors are usually based on lactate-converting enzymes which are placed on the surface of an electrode [1—19]. The common disadvantage of these biosensors is their limited stability if immobilizing techniques are not used for enzyme stabilization. The necessity of enzyme isolation, purification and then immobilization complicates the preparation of such lactate electrodes. The yeast lactate electrode with immobilized cells of *Hansenula anomala* [20—22] does not need these steps in the biosensor preparation. However, it is necessary to induce specific enzyme activity in the cells by their repeated culture in a lactate medium, and the resulting biosensor is not quite specific [21, 22].

In the present investigation, it was decided to use human erythrocytes for lactate biosensor construction to overcome all the problems mentioned above. The high activity of lactate dehydrogenase in erythrocytes (36 μg^{-1} at 25°C) [23], easy accessibility and the very few active metabolic pathways found in erythrocytes in comparison with other cells and tissues [24] were the reasons for the choice. It was decided to use indirect determination of NADH with hexacyanoferrate(III) as it is more sensitive than direct NADH re-oxidation at the electrode [6, 8] and does not need any electrode pretreatment. Amperometric detection of the resulting hexacyanoferrate(II) was chosen because of the quicker establishment of equilibrium than in

potentiometric detection [22, 25]. The enzyme diaphorase is often used as an electron mediator between NADH and hexacyanoferrate(III) [26]. However, because the erythrocyte membrane is impermeable to this enzyme, phenazine methosulfate had to be used instead.

The optimal concentrations of NAD^+ and phenazine methosulfate found in this work agree with the values given by most other authors [8, 11, 13, 27]. While Chen and Liu [13] used a 20 mmol l^{-1} hexacyanoferrate(III), 5 mmol l^{-1} is assumed to be sufficient for achieving the greatest enzyme reaction rate. The alkaline pH of the working solution represents the best pH for conversion of lactate to pyruvate [12, 13].

The linearity and sensitivity (Fig. 1) as well as the reproducibility of the test are comparable with those obtained with yeast lactate biosensors [20, 22]. However, there is some difference in other properties, such as the response time of the biosensor and its selectivity. The erythrocyte biosensor needs 7 min to reach a constant current response, which is longer than in a yeast biosensor [20], Nevertheless, slow establishment of equilibrium (up to 10 min) has been found in all biosensors based on immobilized NAD^+-dependent lactate dehydrogenase [7, 13].

Erythrocytes are highly specialized cells which lose many of their organelles (nucleus, mitochondria, ribosomes) during their development. Anaerobic glycolysis represents one of the few active metabolic pathways which can be found in matured cells [24]. That is why practically no interferences by metabolites were observed in lactate determination with this erythrocyte biosensor. The only such compound which interferes is malate, but its influence can be neglected because of the minimal malate concentration in blood plasma. The biosensor response to malate is dependent on the presence of NAD^+, and it may be a sign of malate dehydrogenase activity in erythrocytes, because lactate dehydrogenase itself does not catalyse the conversion of this substrate [28]. Pyruvate inhibition of lactate dehydrogenase [29] was not observed because of the rapid removal of the second product of the enzymatic reaction, NADH. The selectivity of the erythrocyte biosensor is thus much better than that of a yeast biosensor where interference of glucose, pyruvate, many amino acids, ketones, ethanol and some other compounds can occur, especially as the biosensor ages [21].

The influence of reducing substances causing a positive error in lactate determination was expected because of their electrochemical oxidation at the anode. Previously, the possibility of eliminating the effect of uric and ascorbic acids was studied [21]. For a yeast lactate biosensor, this cannot be done without previous irreversible enzyme inhibition. Two identical yeast electrodes are necessary for this purpose; enzyme activity in the cells on one of these electrodes is inhibited by oxalate [22]. The procedure is thus complicated and the response time duplicated. In contrast, the erythrocyte biosensor offers the elimination of all interferences by means of a sample blank value which can be easily obtained without inhibition of enzyme activity in the cells.

The advantages of the erythrocyte biosensor in comparison with enzyme lactate biosensors and a yeast lactate biosensor can be summarized as follows. Erythrocytes are readily obtained, and the induction of enzyme synthesis in the cells by their repeated cultures in a medium containing the substrate is not necessary. Enzyme isolation, purification and immobilization with possible loss of activity during these steps is avoided. Interference of non-reducing metabolites is negligible and the influence of reducing compounds can be eliminated by subtraction of the sample blank value. These properties together with sufficient sensitivity and reproducibility make the erythrocyte biosensor very suitable for lactate determination in biological fluids such as blood plasma and whole blood.

REFERENCES

1 D. L. Williams, A. R. Doig, Jr. and A. Korosi, Anal. Chem., 42 (1970) 118.
2 P. Racine and W. Mindt, Experientia, Suppl., 18 (1971) 525.
3 H. Durliat, M. Comtat and A. Baudras, Clin. Chem., 22 (1976) 1802.
4 H. Durliat and M. Comtat, Anal. Chem., 13 (1980) 2106.
5 W. P. Soutter, F. Sharp and D. M. Clark, Brit. J. Anaesth., 50 (1978) 445.
6 W. J. Blaedel and R. A. Jenkins, Anal. Chem., 48 (1976) 1240.
7 W. J. Blaedel and R. C. Engstrom, Anal. Chem., 52 (1980) 1691.
8 A. Schelter-Graf, H.-L. Schmidt and H. Huck, Anal. Chim. Acta, 163 (1984) 299.
9 J.-M. Laval, C. Bourdillon and J. Moiroux, J. Am. Chem. Soc., 106 (1984) 4701.
10 M. Cenas, J. Rozgaité and J. Kulys, Biotechnol. Bioeng., 26 (1984) 551.
11 A. Malinauskas and J. Kulys, Anal. Chim. Acta, 98 (1978) 31.
12 F. Scheng and G. D. Christian, Clin. Chim. Acta, 91 (1979) 295.
13 A. K. Chen and C. C. Liu, Biotechnol, Bioeng., 19 (1977) 1785.
14 F. Mizutani, K. Sasaki and S. Yukio, Anal. Chem., 55 (1983) 35.
15 L. C. Clark, Jr., L. K. Noyes, T. A. Grooms and C. A. Gleason, Clin. Biochem., 17 (1984) 288.
16 L. C. Clark, Jr., L. K. Noyes, T. A. Grooms and M. S. Grooms, Critical Care Med., 12 (1984) 461.
17 G. Nagy, L. H. von Storp and G. G. Guilbault, Anal. Chim. Acta, 66 (1973) 443.
18 F. Mizutani, T. Yamanaka, Y. Tanabe and K. Tsuda, Anal. Chim. Acta, 177 (1985) 153.
19 M. Mascini, D. Moscona and G. Palleschi, Anal. Chim. Acta, 157 (1984) 45.
20 J. Racek, J. Musil, Clin. Chim. Acta, 162 (1987) 129.
21 J. Racek, J. Musil, Clin. Chim. Acta, (1987) in press.
22 B. J. Vincké, M. J. Devleeschouwer and G. J. Patriarche, Anal. Lett., 18 (1985) 593.
23 E. Schmidt and F. W. Schmidt, Diagnostik, 8 (1975) 427.
24 S. M. Rapoport, Medizinische Biochemie, 7th edn., VEB Verlag Volk und Gesundheit, Berlin, 1977, p. 619.
25 R. M. Ianiello, T. J. Lindsay, A. M. Yacynych, Anal. Chem., 54 (1982) 1980.
26 A. K. Chen, C. C. Liu and J. G. Schiller, Biotechnol. Bioeng., 21 (1979) 1905.
27 A. A. Malinauskas and J. J. Kulys, Biotechnol. Bioeng., 21 (1979) 513.
28 H.-J. Hohorst, in H. U. Bergmeyer (Ed.), Methoden der enzymatischen Analyse, 2nd edn., Berlin, Akademie-Verlag, 1970, Vol. 1, p. 1425.
29 A. L. Latner and A. W. Skillen, Isoenzymes in Biology and Medicine, Academic Press, London, 1968, p. 33.

Analytica Chimica Acta, 197 (1987) 195—202
Elsevier Science Publishers B.V., Amsterdam — Printed in The Netherlands

A PIEZOELECTRIC CRYSTAL DETECTOR FOR DETERMINATION OF ACETOIN IN AIR

ERIC C. HAHN[a], AHMAD A. SULEIMAN[b] and GEORGE G. GUILBAULT*

Universal Sensors, Inc., P.O. Box 736, New Orleans, LA 70148 (U.S.A.)

JAMES R. CAVANAUGH

U.S. Department of Agriculture, Eastern Regional Research Center, Philadelphia, PA 19118 (U.S.A.)

(Received 7th August 1986)

SUMMARY

A method is presented for the determination of acetoin (3-hydroxy-2-butanone) in air with a piezoelectric crystal detector coated with semicarbazide. The response time is about 5 min, is fully reversible, and is selective for acetoin in the presence of the interferences normally found in air. The detector has a sensitivity of 12.4 Hz l μl^{-1} for acetoin and the response varies linearly with concentration in the 50—80 $\mu l\, l^{-1}$ range.

Since the first observance of the piezoelectric phenomenon by Pierre and Jacques Curie [1], subsequent research by Sauerbrey [2, 3] led to the discovery of a linear relationship between the change in the oscillating frequency of a piezoelectric crystal and the change in mass of its electrical surface. This discovery provided the incentive for extensive research into the application of piezoelectric crystal detectors in many areas of analytical chemistry. Hlavay and Guilbault [4], as well as Alder and McCallum [5], have presented thorough reviews of the theory of piezoelectric crystal detectors and many of the applications.

Acetoin, 3-hydroxy-2-butanone, is present in many drinks and foods and reliable methods for its determination are needed. In a previous study [6], the use of tetrabutylphosphonium chloride was reported as a coating substrate for acetoin. Although this substrate possessed reasonable sensitivity and good response time (less than 1 min), many interferences were observed. This paper describes the development of a detector for acetoin by using a piezoelectric crystal detector coated with neutralized semicarbazide. This compound is used in classical organic analysis to produce derivatives of ketones for identification [7].

[a]Present address: U.S. Customs Laboratory, Room 326 Customhouse Building, 423 Canal Street, New Orleans, LA 70130, U.S.A.
[b]Present address: Department of Chemistry, University of New Orleans, Lakefront, New Orleans, LA 70148, U.S.A.

0003-2670/87/$03.50

EXPERIMENTAL

Apparatus and chemicals

The apparatus and use of the piezoelectric crystal detector were the same as described previously [6]. The piezoelectric crystals used were AT-cut, 9-MHz quartz crystals with gold-plated electrodes on both sides, premounted in holders used commonly in electronics (International Crystal Manufacturing Co.). The frequency counter (Model No. SM-2420) and the power supply (Model No. IP-2728) were from Heathkit Electronics or Veritechnology Electronics Corp. A low-frequency Model OX transistor oscillator (International Crystal Manufacturing Co.) was modified to effect the oscillation of the 9-MHz crystal at its third overtone of 27 MHz.

Acetoin and semicarbazide hydrochloride were obtained from Eastman Organic Chemicals.

Preparation and properties of coating material

The semicarbazide coating material was prepared by dissolving 100 mg of semicarbazide hydrochloride in 10 ml of 1:1 acetone/ethanol, followed by the addition of 5 ml of 6 M ammonia solution. The clear solution was allowed to stand for a few minutes to ensure the complete neutralization of the hydrochloric acid, and was then applied to both electrode surfaces of the piezoelectric crystal by means of a glass rod. A small drop of the solution was placed in the center of the electrode surface and allowed to evaporate. Another small drop was deposited onto the center of the surface and allowed to evaporate. In this way, circles of the coating material were deposited onto both sides of the electrode surface. The crystal was placed in the detector cell, and, under a dry nitrogen flow of approximately 50 ml min^{-1}, was heated to 65°C for 15 min to remove volatile compounds. The resultant coating was assumed to be neutralized semicarbazide.

This application technique was repeated until a net frequency decrease of ca. 4000 Hz was observed for the crystal. This amount was selected after it had been shown that the sensitivity of the coated crystal toward acetoin remained essentially constant for coatings corresponding to frequency changes in the range of 3000—5000 Hz.

The detector showed a drift of less than 2 Hz in 15 min and the baseline noise level was ±3 Hz when operating at 27 MHz. The temperature of the detector cell and acetoin bubbler was controlled at 25 ± 1°C, the detector cell was insulated with asbestos, and the acetoin bubbler was immersed in a water bath; all tubing was wrapped in asbestos to minimize temperature fluctuations. In the absence of these precautions, the noise level was ±6 Hz.

Generation of acetoin vapor

Initial attempts to generate reliable acetoin concentrations in the 1—100 $\mu g\ l^{-1}$ range proved unsuccessful because the inner walls of the tubing became coated with the acetoin. To obtain reliable exposure of the detector

to acetoin in this range, a series of flow meters and valves was set up in conjunction with a thermostated bubbler containing the acetoin. Acetoin levels so generated proved reliable and reproducible for more than an hour. The apparatus is represented in Fig. 1.

The bubbler consisted of an impinger with a drawn-out tip. Because the nitrogen bubbles formed were of the order of 3 mm in diameter, and because the flow rate was 100—200 ml min^{-1}, the residence time of the nitrogen in the acetoin was too brief to permit saturation of the nitrogen with the analyte. Consequently, the concentration of acetoin in the eluting gas stream could not be calculated from the vapor pressure data. This necessitated an external calibration of the acetoin in the gas stream.

The calibration was done with a gas chromatograph equipped with a flame ionization detector and a 2 ft. × 1/8 in. stainless-steel column packed with 5% OV-1 on Chromosorb P. Injector and detector temperatures were both 180°C and the column temperature was held at 70°C. Nitrogen carrier gas flow rate was 35 ml min^{-1}. Two calibration methods were used. This served both as an internal check of the calibration as well as confirmation of its reproducibility.

In one method, a known volume of acetoin was placed in an evacuated 250-ml gas-sampling bulb. The bulb was heated to ensure complete volatilization of the acetoin. Nitrogen, dried with a molecular sieve, was added to achieve atmospheric pressure, then 2.5 ml of this gas was injected into a second evacuated 250-ml gas-sampling bulb, nitrogen was added, and a 2.5-ml aliquot was injected into the gas chromatograph from a gas-tight syringe. Concentrations were calculated using the ideal gas law. In another method, a known volume of acetoin was mixed with acetophenone and the

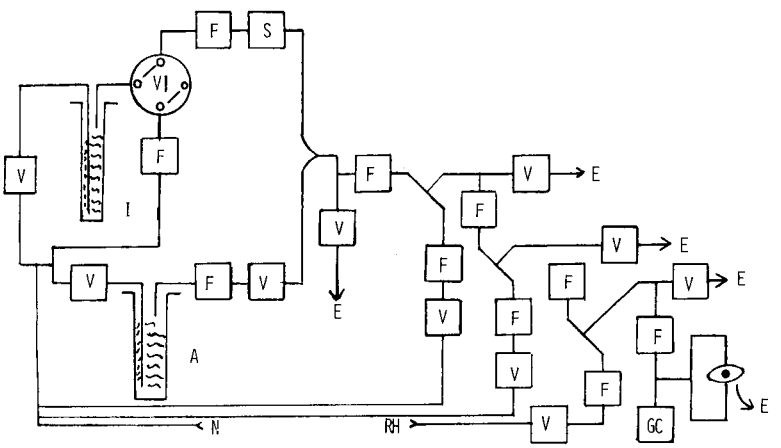

Fig. 1. Schematic representation of apparatus for generation of acetoin vapor: V, regulating valves; VI, 4-way valve; F, flow meters; S, stopcock valves; GC, gas sampling port of gas chromatograph; (•) semicarbazide piezoelectric crystal; N, dry nitrogen; RH, air at 58% relative humidity; A, acetoin; I, interferent; E, effluent vent.

liquid was injected into the gas chromatograph. Acetophenone was chosen because it eluted after the acetoin. A calibration curve was generated by using different concentrations of acetoin. A linear plot of amount injected vs. area was observed for 1—6 ng of acetoin. Good agreement was obtained between the two methods, indicating that absorption of acetoin on the glass walls of the sampling bulb was not a problem.

RESULTS AND DISCUSSION

Investigation of coating materials

A study was conducted with over 25 possible coating materials to be used in the injection-mode type of detection. No coating material was found which responded both quickly and strongly to acetoin. Therefore, attention was focused on the continuous mode of detection. This allows use of coatings which might respond more slowly to acetoin than to possible interferents. Several possibilities are summarized in Table 1. In all cases, the particular coating material was dissolved in a suitable solvent, such as chloroform or ethanol, and deposited on both electrode surfaces by means of a glass rod, and the solvent was evaporated by passing dry nitrogen over the electrode surfaces. A report by Day and Anderson [8], as well as further information supplied by the U.S. Dept. of Agriculture, indicated that alcohols, such as 1- and 2-octanol, may also be present in the food products under investigation. Hence, a secondary study was undertaken to find a coating material which showed little response to 1-octanol. Because the results of this study indicated that semicarbazide gave little response to this alcohol (14 Hz in 7-min exposure to 100 mg l^{-1} 1-octanol in 90 ml min^{-1} dry nitrogen), it was decided to focus on this coating material.

Effect of flow rate on response and response time

Two investigations were undertaken in this area. The first study was done with dry nitrogen as carrier gas. The response was completely reversible and a maximum response of 873 Hz for 22 μl l^{-1} acetoin vapor was found after 5 min with a carrier gas flow rate of 90 ml min^{-1}. In a similar experiment involving wet air (58% relative humidity) as the carrier gas, the response was found to be fully reversible and the maximum response was 283 Hz with a carrier gas flow rate of 200 ml min^{-1} (Fig. 2). The sensitivity in wet air (12.4 Hz μg^{-1}) was considered adequate for field use and the use of humidified air as carrier gas would tend to reduce effects of ambient moisture. Unless stated otherwise, all subsequent experiments were done with air of approximately 58% humidity.

The effects of flow rate of wet air on detector response were studied. Results indicated that the shortest response times (<5 min) were obtained with flow rates between 170 and 230 ml min^{-1} (see Fig. 3).

The ratio of the response (Hz) to the response time (min) was used as an indication of detector performance. As shown in Fig. 4, this ratio approaches

TABLE 1

Study of coatings for the detection of acetoin

Coating[a]	Injection mode response (Hz)[b]	Continuous mode[c]	
		Response (Hz)	Response time (min)
Silicone Oil DC-200	0	5	10
OV-1	0	4	10
Apiezon L	0	5	10
Squalane	0	4	10
Carbowax 400	3	2450	9
Carbowax 550	4	2620	9
Carbowax 1000	4	2670	9
Carbowax 1540	4	2710	9
Carbowax 6000	4	2700	9
Carbowax 20M	4	2920	9
Carbowax 20M-TPA	3	2930	9
Dibutyl phthalate	0	3100	10
Dioctyl phthalate	0	3300	10
DEG succinate	1	3060	10
DEG sebacate	1	3070	10
DEG adipate	1	3070	10
Quadrol	0	100	10
Tergitol NPX	1	2250	10
Triton X-100	1	1900	10
Ucon LB-550-X	1	2140	10
2,4-Dinitrophenylhydrazine	2	220	10
Semicarbazide HCl	2	240	9
Semicarbazide	16	1970	8
Triethanolamine	0	80	10
EG succinate	1	1960	10
Amine 220	1	110	10

[a]To give frequency change of 3700—4100 Hz. [b]To 2.5 ml of 7.7 mg l^{-1} acetoin in nitrogen carrier stream. [c]50 μg l^{-1} acetoin in dry nitrogen at 90 ml min^{-1}.

a maximum at a flow rate of about 200 ml min^{-1}. Unless stated otherwise, this flow rate was used in all subsequent studies.

Sensitivity of acetoin detector

The effluent gas from the system depicted in Fig. 1 was passed through a 250-ml sample bulb, and a 2.5-ml aliquot was injected into a gas chromatograph for absolute calibration. Constant detector frequency after 5 min indicated that equilibrium had been attained in this time. Consequently, samples for gas chromatography were taken after purging the analyte stream for 5 min. The crystal was given sufficient time between runs to return to its baseline frequency and remain stable for 2 min before another run was made. From the peak area obtained from gas chromatography, the concentration of acetoin in the carrier gas stream was evaluated and plotted against

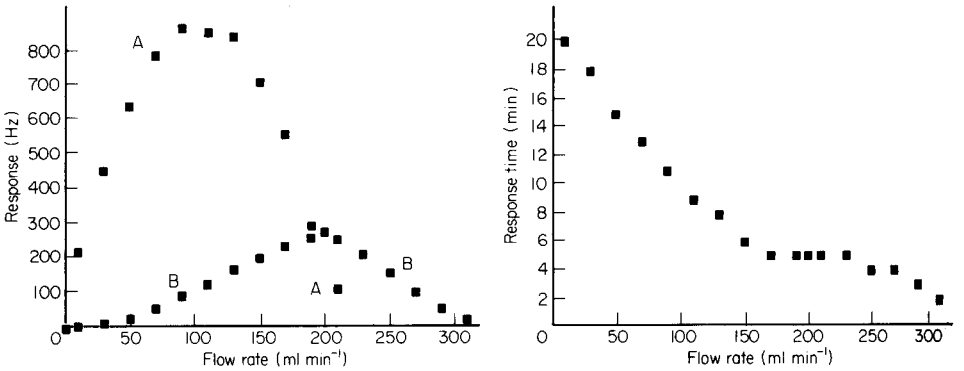

Fig. 2. Effect of flow rate on detector response. (A) Response in dry nitrogen; (B) response in 58% relative humidity air Conditions: 22 μl l^{-1} acetoin; crystal coated with neutralized semicarbazide to give 4000-Hz frequency change.

Fig. 3. Effect of flow rate on detector response time. Conditions: 51.4 μl l^{-1} acetoin; crystal as in Fig. 2; 58% relative humidity air.

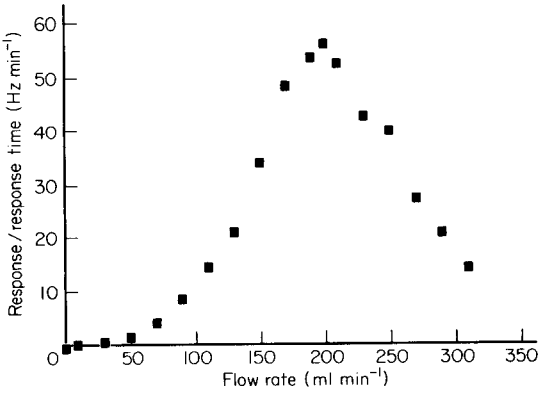

Fig 4. Effect of flow rate on ratio of detector response to response time.

the detector response. The relationship was linear for acetoin concentrations of 5—50 μg l^{-1} with a slope (sensitivity) of 12.4 Hz μg^{-1}.

Repetitive determinations of the response to acetoin (51 μg l^{-1}) for different crystals showed precision of ±1.1% (633 ± 7 Hz). Six repetitive determinations at 5.2 and 51.4 μg l^{-1} showed reproducibility of ±2.4 and ±0.24%, respectively.

Interferences

Interference studies were done by passing potential interferents alone and with acetoin through the system (see Fig. 1). Results for selected interferents alone, summarized in Table 2, show that the detector is much more sensitive to acetoin than to the other compounds selected for study. When

TABLE 2

Responses for potential interferences

Substance	Concentration ($\mu g\ l^{-1}$)	Response[a] (Hz)	Absolute sensitivity (Hz l μg^{-1})	Relative sensitivity
Acetone	3119	13	0.0042	0.000001
Ethanol	2418	22	0.0091	0.000001
Chloroform	2000	1	0.0005	0.000000
Acetaldehyde	2000	0	0.0000	0.000000
n-Hexyl acetate	50	18	0.3600	0.000029
Ethyl butyrate	150	27	0.1500	0.000015
n-Octanol	100	14	0.1400	0.000011

[a]After 5 min. The response to 0.1 $\mu g\ l^{-1}$ acetoin was 1240 Hz, giving an absolute sensitivity of 12,400 Hz l mg^{-1} and a relative sensitivity of 1.

these same compounds were mixed with 51.4 $\mu g\ l^{-1}$ acetoin and passed through the system, frequency changes ranged from 628 to 631 Hz, relative to a value of 632 Hz for acetoin alone. It is concluded that these compounds cause no significant problems at these concentration levels.

To evaluate effects of moisture, the effluent from the detector cell was passed into a jar in which a relative humidity gauge was mounted. For a 51.4 $\mu g\ l^{-1}$ acetoin sample, the signal decreased from about 710 Hz at 0% humidity to about 630 Hz at 40% humidity, and remained relatively constant up to about 90% humidity. The response then decreased by about 22% between 90 and 95% relative humidity. At 97% relative humidity, the detector overloaded and was useless.

Use as a field detector

To test the detector system in a manner analogous to a field situation, a flow system was developed in which the sample stream could be passed alternately through a chloroform scrubber and activated charcoal filter or directly to the detector. The chloroform scrubber would remove acetoin but not moisture and permit an analyte-free baseline to be established. The response of this system for a 51.4 $\mu g\ l^{-1}$ acetoin sample passed through the chloroform scrubber for 1 h was essentially as reported for the system in Fig. 1. This indicates that the chloroform does not become saturated with acetoin for this length of time and further that water is not removed from the sample. After approximately two hours of operation, the detector sensitivity increased somewhat, indicating that moisture was being absorbed by the chloroform. It is recommended that a few drops of water be added to the chloroform bubbler on an hourly basis to avoid this problem. This system has been used for over 30 days without noticeable change in detector sensitivity.

We thank the U.S. Department of Agriculture for their financial support of this research.

REFERENCES

1 See, e.g., F. W. Maarsen, M. C. Smit and J. Matze, Recl. Trav. Chim. Pays-Bas, 76 (1957) 713.
2 G. Z. Sauerbrey, Z. Phys., 155 (1959) 206.
3 G. Z. Sauerbrey, Z. Phys., 178 (1964) 457.
4 J. Hlavay and G. G. Guilbault, Anal. Chem., 49 (1977) 1980.
5 J. F. Alder and J. J. McCallum, Analyst, 108 (1983) 1169.
6 A. A. Suleiman, E. C. Hahn and G. G. Guilbault, Anal. Lett., 17 (1984) 2205.
7 R. L. Shriner, R. C. Fuson and D. Y. Curtin, The Systematic Identification of Organic Compounds, 5th edn., Wiley, New York, 1964, p. 134.
8 E. A. Day and D. F. Anderson, J. Agr. Food Chem., 13 (1965) 2.

Analytica Chimica Acta, 197 (1987) 203—215
Elsevier Science Publishers B.V., Amsterdam — Printed in The Netherlands

PLANAR ARTIFICIAL BIOMEMBRANES OPTIMIZED FOR BIOCHEMICAL ASSAY

ULRICH J. KRULL

Chemical Sensors Group, Department of Chemistry, Erindale College, University of Toronto, Mississauga, Ontario L5L 1C6 (Canada)

(Received 25th September 1986)

SUMMARY

Langmuir-Blodgett monolayer and planar bilayer lipid membrane (BLM) experiments are used to study the relative significance of dipolar potential and packing/fluidity in the control of the permeability of phospholipid/steroid BLMs to potassium ion. Practical chemical construction of BLMs designed to achieve particular dipolar potentials and packing/fluidity characteristics are described. The ability to modify selectively the salient physical properties of BLMs allows optimization of the ion permeability and receptor activity of the membrane. The use of BLMs to quantify drug response and receptor activity is illustrated by examples involving valinomycin, phloretin, concanavalin A and auxin receptor.

The introduction of the bilayer lipid membrane (BLM) as an analogue of the cell membrane has stimulated research activity directed towards elucidation of the role of biomembranes in cellular processes. Early work with antibody/antigen and enzyme/substrate pairs showed electrochemical activity as a function of selective binding when these structures were located in BLMs formed from crude lipid extracts [1]. These observations formed the basis of proposals to use BLMs as chemical transducers for various organics and biochemicals by means of selective interactions with membrane-embedded receptors [2]. Subsequent study has tentatively evaluated the quantitative characteristics and structural features of artificial chemoreceptive membranes [2—4] and has paved the way for another potential application of these membranes. This other application is based on the ability of these systems to provide information about both selective and non-selective molecular interactions in the membranes, and penetration of various chemicals of biological or environmental interest.

Many studies of the properties of membranes (receptor action, selective agents used for tissue labelling and imaging, and transport of environmental toxins) are presently done with animals. Such procedures are difficult, owing to the large number of experiments required and the general need for dissection, tissue preparation, separation and subsequent measurements. Ideally, artificial membranes could be used as models for natural tissues to overcome these deficiencies. The quantitative application of BLMs for drug assay was

0003-2670/87/$03.50

suggested in the work of Thompson et al. [5] in their investigation of lipid-membrane assay of antibiotics. The poor reproducibility of such experiments demonstrated that membrane properties were highly dependent on lipid chemistry and on the presence of any structure-modifying agents, even if present at trace concentrations. Most reliable work correlating the electrochemical response of membranes to biochemical activity has therefore concentrated on the use of well-defined lipid compositions which are formulated from purified starting materials and are monitored chromatographically [6]. The use of such protocols has dramatically improved experimental reproducibility and has definitively established the BLM as an important tool in selected areas of investigation, such as formation of transmembrane ion conductive channels by multi-subunit proteins [7] and by polypeptides [8].

This work has tentatively established the relative significance of dipolar potential and packing/fluidity properties of BLMs in the control of transmembrane permeability to potassium ion. This was done by correlating monolayer compression measurements of dipolar potential and average molecular area with the temperature dependence of ion permeability through BLMs. In association with previous experimental work [4], this provides sufficient information for engineering membranes of physically desired character by chemical manipulation of molecular content. This may have important ramifications with respect to the study of new drugs and chemicals which are designed to bind with proteinaceous receptors in specific tissues, as well as those which are membrane-permeable toxins or are used for tissue labelling or imaging by selectively passing into specific types of cell membranes in the absence of associated functional receptors. Model systems demonstrating permeability control of antibiotics, interaction of toxins and the measurement of the physiological activity of receptors are described.

EXPERIMENTAL

Materials and equipment

The phospholipid used was lyophilized egg phosphatidyl choline (PC; Avanti Biochemicals, Birmingham, AL). The steroids used were 5-cholesten-3β-ol, 5,7-cholestadien-3β-ol, 5-cholesten-3β,7α-diol, 5α-cholestan-3β,5α,6β-triol, 5α-cholestan-5α,6α-epoxy-3β-ol, 5-cholesten-3β-ol-7-one and 5α-cholestan-3-one (Research Plus, Bayonne, NJ).

Phloretin and valinomycin (Sigma Chemical Co.) were prepared in methanolic solution. The concanavalin A and glycogen (Sigma) system was an artificial receptor-based reaction pair, and the auxin receptor system [9] was an example of a natural hormone receptor.

Standard thin-layer chromatography and high-resolution gas chromatography were used to elucidate the phosphatidyl choline/steroid chemistry [6]. Methylation of phosphatidyl choline was necessary for capillary gas chromatography. All chemicals were of reagent-grade quality.

The BLM support housing consisted of two identical perspex half-cells

separated by a teflon sheet (0.1-mm thickness) containing a circular aperture (1-mm diameter) in which the BLM was formed. An external direct current (d.c.) potential (+25 mV) was applied across the membrane between two Ag/AgCl reference electrodes (Orion Research, Cambridge, MA) extended with agar salt bridges. The external circuitry consisted of a d.c. power supply, and a digital electrometer (Keithley System 1, Keithley Instruments, Cleveland, OH) for data acquisition. The solution cell and sensitive electronic equipment were isolated in a grounded Faraday cage. An infrared heat source was used to heat the cell for operation at elevated temperatures. The Langmuir-Blodgett thin-film trough was a Lauda film Balance Type 1974 (Sybron-Brinkmann, Toronto, Canada).

Procedures

The phosphatidyl choline/steroid mixture used to form BLMs consisted of 20 mg each of phosphatidyl choline and steroid in 1 ml of dry n-decane. The mixture was introduced into the teflon aperture between the two solution compartments containing 0.1 M KCl by using a fine sable hair brush. The membrane formed spontaneously and was monitored by optical reflectivity and electrical properties. For Arrhenius barrier measurements, the transmembrane cationic current was measured as a function of temperature from 21° to 30°C, varied at approximately 0.5°C min^{-1}. All other experiments were done at 21 ± 1°C. A variable-volume micropipette was used to add electroactive agents to the bathing electrolyte. Concentrations of valinomycin and phloretin in the electrolyte were 10^{-7} M and 4×10^{-6} M, respectively. The methanol concentrations in the aqueous electrolyte never exceeded 1% by volume. Experiments with concanavalin A have been reported [10] and involved 10^{-6} M lectin, 10^{-4} M Ca^{2+} and Mn^{2+} and a 2% (by volume) saturated aqueous solution of glycogen. The reagents were added in the order listed.

Auxin receptor is a naturally-derived receptor system which has been demonstrated to have biochemical activity that depends on environmental conditions and chemical stimulation. The activated receptor can transport H^+ across a BLM and therefore can control transmembrane ion currents. Membranes containing auxin receptor were prepared from coleoptiles and primary leaves of maize (*Zea mays*, cv. Blizzard). The procedure for the collection, isolation and purification of the receptor has been described [9]. The solution containing the purified receptor was lyophilized in 100-μl aliquots and stored dry at 4°C until needed. Each aliquot was reconstituted in 100 μl of distilled water and 10-μl volumes were introduced directly into electrolyte in the electrochemical cell along with the stimulant, naphthalene acetic acid (methanolic solution), and adenosine triphosphate (final concentrations ca. 10^{-8}, 10^{-5}, 10^{-6} M, respectively).

In all electrochemical experiments, chemical properties of the lipid membranes were altered by oxidizing the steroid component of a phosphatidyl choline/5-cholesten-3β-ol mixture or by using pure phosphatidyl choline/steroid mixtures.

For the trough experiments, approximately 2 mg each of phosphatidyl choline and steroid were dissolved in 5 ml of hexane. After sonication in an ultrasound bath to ensure homogeneous dispersion, approximately 100 μl of solution was slowly transferred to a 0.1 M KCl electrolyte subphase in the trough by means of a syringe. A period of at least 10 min was allowed to ensure complete removal of the volatile solvent before compression experiments were initiated. Dipolar potential was measured by placing a capacitative probe within 1 mm of the monolayer surface on the trough. The air gap was controlled by means of a small-volume positive-pressure pump which provided constant filtered air flow.

RESULTS

The Arrhenius energy barrier to potassium ion permeability of BLMs was experimentally estimated from the dependence of the electrochemical current on temperature. Additional information about molecular association was established by use of Langmuir-Blodgett thin-film trough compression techniques, and consisted of data for average molecular area and dipolar potential. This work correlates the results of these experimental methods and demonstrates that a relationship exists between average molecular area, dipolar potential and the Arrhenius energy barrier. Identification of the significance of these properties to the control of ion permeability has provided sufficient information for the design of specialized artificial biomembranes. A summary of results, presented in Table 1, shows the values of the physical parameters of interest for monolayers at a surface pressure of 30 mN m^{-1} (estimated surface pressure for BLMs [11]). Tables 2 and 3 include the transmembrane ion currents obtained from standard concentrations of the electroactive stimulants which altered the electrostatic fields and packing/

TABLE 1

Summary of bilayer and monolayer results for phosphatidyl choline/steroid membranes[a]

Steroid	BLM Arrhenius energy barrier[b] (eV)	Monolayer properties[c]	
		Average molecular area (nm^2)	Dipolar potential (mV)
5-Cholesten-3β-ol	1.18 ± 0.03	0.458 ± 0.014	490 ± 15
5,7-Cholestadien-3β-ol	0.80 ± 0.25	0.440 ± 0.050	475 ± 25
5-Cholesten-3β-ol-7-one	0.63 ± 0.04	0.450 ± 0.010	205 ± 20
5α-Cholestan-3β,5α,6β-triol	0.49 ± 0.16	0.462 ± 0.009	200 ± 20
5α-Cholestan-5α,6α-epoxy-3β-ol	0.35 ± 0.04	0.481 ± 0.011	550 ± 25
5α-Cholestan-3-one	0.19 ± 0.02	0.528 ± 0.028[d]	660 ± 15[d]

[a]Equal weight ratios of phosphatidyl choline and steroid. [b]From [4]. [c]Calculated at a surface pressure of 30 ± 1 mN m^{-1}. [d]Calculated just before collapse pressure of 26.2 ± 1.5 mN m^{-1}.

TABLE 2

Electrochemical response of BLM to 10^{-7} M valinomycin for various lipid chemical compositions

Chemical composition[a]	Average molecular area (nm^2)	Dipolar potential (mV)	Relative change in BLM ion current[b]
PC + 5-cholesten-3β-ol	0.458 ± 0.014	490 ± 15	10
PC + 5-cholesten-3β-ol-7-one	0.450 ± 0.010	205 ± 20	50
PC + 5α-cholestan-3β,5α,6β-triol	0.462 ± 0.009	200 ± 20	100
PC + 20% air-oxidized 5-cholesten-3β-ol	—	—	2.0
PC + 30% air-oxidized 5-cholesten-3β-ol	—	—	1.7
PC + 40% air-oxidized 5-cholesten-3β-ol	—	—	1.5

[a]Products from air-oxidation of cholesterol have been described [6]. [b]Ion current increase measured as ratio of largest ion current response to the initial current before valinomycin addition.

TABLE 3

Electrochemical response of BLM to 4×10^{-6} M phloretin for various lipid chemical compositions

Chemical composition	Average molecular area (nm^2)	Dipolar potential (mV)	Relative change in BLM ion current[a]
PC + 5α-cholestan-3β,5α,6β-triol	0.462 ± 0.009	200 ± 20	2
PC + 5-cholesten-3β-ol	0.458 ± 0.014	490 ± 15	5
PC + 5α-cholestan-3-one	0.528 ± 0.028	660 ± 15	7

[a]Ion current increase measured as ratio of largest ion current response to the initial current before phloretin addition.

fluidity parameters of the BLMs. Tables 4 and 5 demonstrate the control of transmembrane ion current by selective receptors, and the optimization of the signal by adjustment of transmembrane ion conductivity and receptor conformation.

Adjustment of hydrogen ion concentration was used to examine the proton transport of auxin-receptor, which had been reconstituted in BLMs. Conformation of the receptor binding site, and therefore auxin binding activity, was dependent on pH; the activity was maximal at pH 5.3. At higher pH values, decreased availability of H^+ and decreased hormone-binding activity resulted in a concerted reduction of ion current. At lower pH, receptor activity again decreased, but was partially offset by the greater concentration of H^+ available for transport. Measurements of electrochemical responses were made by integration of transmembrane ion currents for a standard period of time at various pH values. The results for receptor activity and electrochemical response obtained at pH 5.3 were arbitrarily chosen to

TABLE 4

Electrochemical response of BLM for concanavalin A/glycogen interaction for various lipid chemical compositions

Chemical composition	Average molecular area (nm^2)	Dipolar potential (mV)	Relative change in BLM ion current[a]
PC + 5-cholesten-3β-ol	0.458 ± 0.014	490 ± 15	4
PC + 95% 5-cholesten-3β-ol + 2% 5,7-cholestadien-3β-ol + 2% 5α-cholestan-5α,6α-epoxy-3β-ol + 1% 5-cholesten-3β-ol-7-one	0.46 ± 0.02	440 ± 15	7
PC + 80% 5-cholesten-3β-ol + 7% 5-cholesten-3β-ol-7-one + 7% 5α-cholestan-3β,5α,6β-triol + 6% 5α-cholestan-5α,6α-epoxy-3β-ol	0.50 ± 0.01	500 ± 15	8
PC + 30% air-oxidized 5-cholesten-3β-ol	—	—	12

[a]Ion current increase measured as ratio of largest ion current response to the initial current before concanavalin A addition.

TABLE 5

Electrochemical response of BLM for auxin receptor stimulation with standard concentration of naphthalene-1-acetic acid

pH	Normalized accepted activity[a] (%)	Normalized electrochemical response[a] (%)		
		Lipid prep. A	Lipid prep. B	Lipid prep. C
4.0	0	5 ± 5	0	0
4.5	25	58	14	0
5.0	90	95	25	2
5.5	95	95	23	1
6.0	75	82	20	0
6.5	40	32	6	0
7.0	20	10	1	0

[a]Data from [9]. Lipid compositions were derived from differentially air-oxidized cholesterol.
Lipid preparation A: PC + 85% of 5-cholesten-3β-ol + 4% of 5-cholesten-3β,7α-diol + 4% of 5-cholesten-3β-ol-7-one + 4% of 5,7-cholestadien-3β-ol, and 3% other steroids. Lipid preparation B: PC + 90% of 5-cholesten-3β-ol + 2% of 5-cholesten-3β,7α-diol + 2% of 5-cholesten-3β-ol-7-one + 2% of 5,7-cholestadien-3β-ol, and 4% other steroids. Lipid preparation C: PC + 5-cholesten 3β-ol.

represent 100% activity and response. This calibration of activity and response allowed normalization of results obtained at other pH values to prepare the comparison shown in Table 5.

DISCUSSION

Permeability of the BLM

Ion permeability through a membrane can be described as a three-step process involving ion partitioning into a membrane, transport through the membrane, and desorption of the ion into the opposing solution. Physical properties of lipid membranes can be adjusted to alter ion current by modification of the four following features [12]. Firstly, the phospholipid acyl chain length and/or the residual hydrocarbon solvent content within a BLM can control the thickness of the membrane, and therefore the extent of the hydrophobic zone of low dielectric constant located in the interior of the membrane. An ideal Born interaction energy can be calculated for ions in the non-polar interior of the membrane as follows

$$W_B = Z_i^2/8\pi\epsilon\epsilon_0 r_i$$

where Z_i represents the ionic valency, r_i the ionic radius, ϵ the environmental dielectric constant and ϵ_0 the permittivity of free space. The integration of the Born energy barrier across the hydrophobic width of the membrane provides an indication of the magnitude of the opposition to ionic permeability through the zone of low dielectric constant. The ideal image potential would also be altered as a function of the thickness of the membrane as indicated by the following relationship:

$$W_{im} \propto Z_i^2/(4\pi\epsilon\epsilon_0)\, Y_i$$

where Y_i represents the distance between the ion and the surface of the membrane.

Secondly, the extent of unsaturation of the phospholipid acyl chains has been related to the control of the fluidity and thickness of BLMs [12]. The choice of the term fluidity is ambiguous because the molecular motion of lipids can be axial or lateral, and the term does not account for the proximity of neighbouring lipid molecules. It will be assumed that greater lipid mobility will also provide for a decreased lipid packing (density), and the effects of the unsaturated acyl chains will therefore relate to packing/fluidity alterations. An increase in the extent of acyl chain unsaturation causes an increase in the rate constant of ionic translocation, and results in the observation of higher ionic currents due to increased molecular fluidity and decreased packing density.

Thirdly, the chemical alteration of the headgroup (polar) area can result in substantial differences in the extent of hydrogen bonding and the magnitude of the dipolar potential. The dipolar potential originates from the anisotropic structure of the membrane. Dipolar moieties in the polar headgroup zone have a time-averaged alignment which results in the establishment of a net electrostatic polarization. The dipolar potential or Volta potential at liquid/gas or liquid/liquid interfaces, ΔV, can be regarded as the average dipole-based electrostatic voltage perpendicular to the BLM surface.

The average molecular dipole moment perpendicular to the plane of the membrane, $\mu_\perp$, can be represented [3] as $\mu_\perp = \Delta V/4\pi n$, where n is the number of molecules in a defined area. If the molecular area, A, is considered, then the expression can be rewritten as $\mu_\perp = A\Delta V/12\pi$.

The polar zone of the membrane contains phosphorus-nitrogen, carbonyl, hydroxyl and hydration water moieties, which combine to establish the dipolar potential. This positive potential attains a magnitude of hundreds of millivolts within the membrane. The potential will influence the passage of formally charged ions or dipolar species through the membrane, and will affect the surface partitioning of polarized species. The interfacial zone between the phospholipid headgroups and the aqueous electrolyte solution may provide a surface which contains selective binding sites. These sites may be directly controlled by the dipolar potential, and may act to provide a local concentration of solute or ion at the surface, which is available for transmembrane transport. Such a localized concentration of the permeating species is much more important than bulk solution concentration in the determination of transmembrane permeability [13]. Further electrostatic effects based on charged lipid headgroups can be observed, and in some instances can be correlated to Gouy-Chapman double-layer potentials [14]. The dipolar potential can still provide a significant effect on the permeability of charged membranes and should not be ignored.

Fourthly, the preparation of BLMs from mixed lipid systems such as phospholipid and steroid can lead to concurrent alterations of dipolar potential, fluidity and packing. The partition coefficients evaluated for a number of different ions have been found to be relatively independent of the presence of certain common steroids; however, large permeability changes due to dipolar potential and packing/fluidity alterations have been observed [12].

Previous experimental work has indicated that the properties of charge, size and hydrophobicity of the permeating ion, the ion adsorption plane, the density and the mobility of the lipid, the dielectric distribution and the dipolar potentials of BLMs are the most significant features which combine to establish the magnitude of the transmembrane ion current. It is possible to maintain most of these variables at fixed values, and still dramatically alter the physical properties of a membrane to adjust the transmembrane permeability of simple inorganic or hydrophobic ions [4]. A standardized lipid mixture based on equivalent molar ratios of phospholipid and various steroids produces a series of membranes of similar properties (including dielectric characteristics) for permeability studies using any one particular permion. Dipolar potential and packing/fluidity parameters may be subsequently altered to investigate effects on partitioning and translocation rate constants of ions, as well as interactions of membranes with organics.

The chemical nature of the permeating species and the mechanism of permeation must be considered in the determination of the significance of the various properties of membranes to the control of transmembrane permeability. The process of penetration of ions or solutes through standard lipid

matrices is dominated by steric features, electronic distribution, formal charge and physical size of the permeating species. This must be the case because the membrane can be physically described in terms of electrostatic and lipid mobility/structural features. The use of K^+ ion as the only significant permion, and the use of membranes of similar Born energy and image potential characteristics, has provided standardization of the properties of the system so that control of transmembrane permeability was achieved by adjustment of dipolar potentials and packing/fluidity characteristics.

The incorporation of approximately equal mole-fraction concentrations of each of the various steroids into the phospholipid provided a method for the controlled chemical modification of the membrane. These modifications lead to observation of the influence of the extra polar species of the steroids on ion permeability of the membrane by alteration of dipolar and steric properties of the headgroup zone. The experiments examined packing/fluidity and dipolar-potential properties of the membrane to establish the relative significance of these parameters to transmembrane ion conduction (applicable to transmembrane permeability of uncharged solutes as well).

Steric factors are related to packing/fluidity properties and are partially based on the physical volume occupied by lipid molecules. Such factors can be correlated with the structure and mobility of the acyl chains, which are densely packed in the anisotropic structure of the BLM at surface pressures near 30 mN m^{-1} [11]. Migration of permeating species such as ions down an electrical potential or concentration gradient through the acyl chain zone must be influenced by axial chain rotation, which would sweep out a transient volume suitable for temporary containment of the permeant species [15]. The results of the temperature dependence of ion permeability of BLMs indicated that the structures of the different steroids clearly had a large influence on the Arrhenius energy barrier. This barrier represented the highest energy which ions had to overcome to pass through the membrane, and was a collective result of steric barriers, low dielectric constants and electrostatic potentials.

A comparison of the Arrhenius barrier values and dipolar potential results of Table 1 does not indicate that a simple relationship exists between the two parameters, and suggests that the dipolar potential may not be the parameter which controls the maximum value of the ion energy barrier [4]. Previous electrochemical [4, 14] and spectroscopic/calorimetric results [16, 17] have indicated that it is difficult, and perhaps impossible, to differentiate molecular interactions completely from dipolar potentials because these parameters operate synergically. The dipolar potential is directly influenced by conformational changes caused by molecular interactions within the headgroup zone of the membrane, and molecular interactions (and the structure of the membrane) are directly influenced by dipolar potentials [18]. The control of ion permeability of BLMs by dipolar potentials can therefore occur by interaction of the permeating species with the electrostatic field and/or by steric hindrance associated with a structural modification

induced by the dipolar potential. However, to a first approximation the experimental results indicate that the permeability of BLMs to uncharged species of low dipole moment can be engineered simply by using the average molecular areas expressed in Table 1 for calibration of packing/fluidity. The correlation of the Arrhenius barrier data to measurements of average molecular area indicates that steroid concentration and structure can be used to control reproducibly the permeability of BLMs and that simple Langmuir-Blodgett compression experiments can be used to quantify relative packing/fluidity characteristics of lipid membranes.

A high correlation between Arrhenius energy barrier values and transmembrane ion currents has never been established in these experiments, but was expected because of the large differences in the magnitudes of the measured energy barriers. Ion current is dependent on the mechanism of permeation as well as the Arrhenius energy barrier, and therefore should be dependent on the Arrhenius prefactor. Transport of ionic species is controlled by at least three fundamental processes: molecular interactions of lipids provide steric hindrance to transmembrane migration and correlate with the Arrhenius barriers for ions; dipolar potentials influence ion entrance into the area of steric hindrance; dipolar potentials may provide localized concentrations of permeable species at the membrane/solution interface. The Arrhenius model can provide a mathematical approximation of the permeability of ionic species through a BLM. The model must include consideration of the Arrhenius energy barrier (largely derived from packing/fluidity properties) and also an Arrhenius prefactor which is directly related to the magnitude of the dipolar potential. Such a prefactor is expected to reflect an exponential dependence of ion concentration at the membrane surface (and therefore ion permeability) on the experimentally measured corresponding monolayer dipolar potentials.

BLM chemical response

Langmuir-Blodgett technology provides a method suitable for design and characterization of the structures of BLMs, and can be used to prepare optimized models suitable for investigation of partitioning and permeability by ionic and neutral species. Such uses of lipid membranes permit significant improvements in the correlation of in vivo biochemical permeability events when contrasted with the results derived from simplistic hydrocarbon partitioning experiments which are still often used.

The cyclic polypeptide valinomycin (m.w. 1111) is an example of a large organic molecule that can partition into lipid membranes. The antibiotic properties of this compound are immediately obvious in electrochemical experiments using BLMs because valinomycin has the ability to complex K^+ ion in its interior, and can shuttle large quantities of ions across the membrane. The large size of the valinomycin/K^+ complex, and the external hydrophobic amino acid sheath provide reduction of the electrostatic energy barriers to ion translocation. The size and charge of this permeating species

indicate that it should be sensitive to packing/fluidity and dipolar potential properties of lipid membranes. The results of Table 2 confirm that both these properties can be independently adjusted by chemical modifications of the membranes, and that the ion-carrier complex is sensitive to such modifications. The results listed in Table 1 provided the basic physical characterization of the different membranes, and were used in the results presented in Table 2.

A second common electroactive probe used in studies of BLMs is the dipolar agent, phloretin (m.w. $\approx$ 275). This species has a relatively large partition coefficient favouring lipid membrane incorporation, and has a dipole moment of 5.6 which apparently aligns in the headgroup zone in opposition to the standing dipolar potential. The resulting reduction in the magnitude of the dipolar potential necessarily alters transmembrane ion current. Previous work has shown that the low concentrations of phloretin used in the experiments summarized in Table 3 only alter the dipolar potential (not the packing/fluidity) of BLMs. The results of Table 3 indicate how the sensitivity of membranes to dipolar perturbants may be enhanced by appropriate manipulation of lipid content.

BLM receptor activity

Concanavalin A was present as a large tetrameric protein at the pH used in this work, and was activated with Ca^{2+} and Mn^{2+} ions to provide a selective binding site for saccharide residues on each monomeric protein sub-unit [10]. The tetravalent binding capacity of the concanavalin A was used to bind multiple saccharide residues from a polysaccharide to prepare an aggregate by polymerization. This process led to various forms of electrochemical response when the concanavalin A was located on the surface of the membrane. One such distinct response can be described as a continuous increase in ion current which was observed as polymerization proceeded, and was most commonly observed if oxidized lipid was present. This form of electrochemical signal is used in Table 4 to summarize the response of concanavalin A to polysaccharide for various chemical compositions of BLMs, and indicates that the response is sensitive to both dipolar potential and packing/fluidity properties. These results support the hypothesis that the ion-current signal is due to perturbation of the structure and/or electrostatic fields of the lipid membrane rather than the formation of formal conductive channels or pores (which are relatively insensitive to dipolar fields and packing/fluidity effects). This work provides an example of how BLMs may be used to assist the elucidation of mechanistic information.

Well-defined protocols for reconstitution of proteinaceous receptors into membranes [19], and the present ability to tailor physical properties of membranes to meet specific requirements, can be combined to improve opportunities for development of a reproducible technique for quantitation of receptor activity. Alterations in membrane-associated conductance or permeability caused by receptor stimulation could provide methods for the

evaluation of action of natural or artificial drugs, hormones or substrates. Previous electrochemical work has confirmed that reconstituted receptors can provide useful dose/response correlations which are suitable for biosensor development [2]. The results described in Table 5 for the auxin receptor further demonstrate that the chemical content of BLMs can be controlled to optimize the activity of reconstituted receptor systems, providing increased sensitivity. This was accomplished by adjusting the environment of the receptor to presumably meet its conformational requirements for hormone binding, and to optimize its partitioning and mobility in the lipid matrix. Control of the ion current originated with the hydrogen-ion translocation mechanism of the protein, thereby eliminating the usual influence of the physical properties of the lipid matrix on the ion permeability.

Conclusions

Widespread use of planar BLMs has been reported for investigation of anesthetic action, immunochemical activity, enzymatic function, antibiotic action and specialized receptor events. Control of the structure of BLMs could be used to optimize many of these previous applications, and provides a well-characterized basis for further toxicological and pharmacological determinations. Research must address the correlation of the molecular structure of lipids with properties of membranes to supersede the trial-and-error approach which is presently necessary for the preparation of desired BLMs. A chemometrics approach could be implemented to resolve this multidimensional chemical parameter problem.

The author is indebted to the Natural Sciences and Engineering Research Council of Canada for support of this work, to M. A. Venis of Shell Research Ltd., Sittingbourne, U.K. for provision of the auxin receptor, and to M. Thompson of the University of Toronto for many helpful discussions.

REFERENCES

1 H. Ti Tien, Bilayer Lipid Membranes, M. Dekker, New York, 1974.
2 U. J. Krull and M. Thompson, IEEE-Electron Devices, 32 (1985) 1180.
3 M. Thompson and U. J. Krull, Anal. Chim. Acta, 147 (1983) 1.
4 U. J. Krull, M. Thompson, E. Vandenberg and H. E. Wong, Anal. Chim. Acta, 174 (1985) 83.
5 M. Thompson, P. J. Worsfold, J. M. Holuk and E. A. Stubley, Anal. Chim. Acta, 104 (1979) 195.
6 U. J. Krull, M. Thompson and A. Arya, Talanta, 31 (1984) 489.
7 M. Criado, H. Eibl and F. J. Barrantes, J. Biol. Chem., 259 (1984) 9188.
8 P. Lauger, J. Membr. Biol., 57 (1980) 163.
9 M. Thompson, U. J. Krull and M. A. Venis, Biochem. Biophys. Res. Commun., 110 (1983) 300.
10 M. Thompson, U. J. Krull and L. I. Bendell-Young, Bioelectrochem. Bioenerg., 13 (1984) 255.
11 A. Georgallas, D. L. Hunter, T. Lookman, M. J. Zuckerman and D. A. Pink, Eur. Biophys. J., 11 (1984) 79.

12 P. Lauger, R. Benz, G. Stark, E. Bamberg, P. C. Jordan, A. Fahr and W. Brock, Q. Rev. Biophys., 14 (1981) 513.
13 S. McLaughlin, in F. Bonner and A. Kleinzeller (Eds.), Current Topics in Membranes and Transport, Vol. 9, Academic, New York, 1977, p. 71.
14 D. A. Haydon and V. B. Myers, Biochim. Biophys. Acta, 307 (1973) 429.
15 N. P. Franks, J. Mol. Biol., 100 (1976) 345.
16 S. H. White and G. I. King, Proc. Natl. Acad. Sci. USA, 82 (1985) 6532.
17 B. A. Lewis and D. M. Engelman, J. Mol. Biol., 166 (1983) 211.
18 E. Neumann, in G. Milazzo (Ed.), Principles of Electric Field Effects in Biological Systems: Topics in Bioelectrochemistry and Bioenergetics, Vol. 4, Wiley, New York, 1981, p. 113.
19 A. Darszon, J. Bioenerg. Biomembr., 15 (1983) 321.

Analytica Chimica Acta, 197 (1987) 217—227
Elsevier Science Publishers B.V., Amsterdam — Printed in The Netherlands

FLOW-INJECTION ANALYSIS WITH A COATED TUBULAR SOLID-STATE COPPER(II)-SELECTIVE ELECTRODE

J. F. VAN STADEN* and C. C. P. WAGENER
Department of Chemistry, University of Pretoria, Pretoria 0002 (South Africa)
(Received 29th October 1986)

SUMMARY

The incorporation, behaviour and suitability of a home-made coated tubular solid-state copper(II)-selective electrode into the conduits of a flow-injection system is described. The compact tubular sensor (volume 7.8 μl) is constructed from a copper tube and Tygon tubing, treated with ammonium sulphide to give the copper/copper sulphide electrode and conditioned in an ascorbic acid medium. Interferences of foreign ions are similar to those found in batch analysis, but are less severe in the flow-injection system. Changes in carrier stream pH between 1 and 3 affected the electrode response, but sample pH has no or little influence in the range 1—7 depending on the copper(II) ion concentration in the samples. With 30-μl samples the flow-through electrode system covers a working range up to 5000 mg dm^{-3} with a detection limit of 0.5 mg dm^{-3}. The system is suitable for the determination of copper(II) in effluent and tap water (relative standard deviation $< 1.75\%$ for 0.5—912 mg dm^{-3} copper) and acidic copper sulphate plating solutions (relative standard deviation $< 1.21\%$ for 87—4135 mg dm^{-3} copper) at a sample frequency of about 80 h^{-1}. The results obtained agree well with results by a standard atomic absorption spectrometric method.

Extensive studies on copper ion-selective electrodes have been reported by various research groups during the last decade and much attention has been given to the use of this electrode system in chemical analysis [1—17]. Solid-state copper ion-selective electrodes have been prepared in different ways. They are usually prepared from the sulphide or selenide precipitates of copper(I) or copper(II) as the active material and generally in the presence of the appropriate silver salts. Homogeneous and heterogeneous electrodes have been constructed, the homogeneous electrodes being based on copper salts alone or on copper and silver salts, and the heterogeneous ones on precipitate-based membranes with a polymeric matrix. In most of the methods reported, manual methods were used in chemical analysis using copper-selective electrodes.

The use of electrochemical detection in flowing streams has become more common [18—21]. Several types of solid-state membranes have been applied in the design of flow-through ion-selective electrodes. Some novel flow-through tubular arrangements for ion-selective electrodes have been described [22—26] for flow-injection systems, but so far the polymeric

0003-2670/87/$03.50

membrane type of sensors based on mobile carriers [23—26] or moulded supporting materials [22] have been used. A tubular solid-membrane copper-(II)-selective electrode in which a pellet is embedded in the polymer Polypol PS-230 was constructed by Van der Linden and Oostervink [22]; the flow-through channel in the body and the pellet was made by careful drilling. The tubular mode of construction was recently extended to the concept of coated tubular solid-state ion-selective electrodes [27—30] incorporated into the conduits of flow-injection systems.

In the present paper, a simple and cheap coated tubular solid-state homogeneous copper(II) sulphide electrode membrane was constructed and incorporated into a flow-injection system. This flow-injection system was applied to the determination of copper in effluent and tap water as well as copper sulphate plating bath solutions.

EXPERIMENTAL

Preparation of the copper sulphide electrodes

The same concept as the one used for the construction of a chloride-selective electrode [27] was followed for the basic design of the coated tubular flow-through solid-state copper-selective membrane electrode, but with a few modifications. The unit consisted of a 10 mm × 1 mm i.d. copper pipe connected to two pieces (20 mm × 0.5 mm i.d.) of Tygon tubing at both ends. An inner wire of a shielded cable was wound around the outside body of the copper pipe to ensure electrical contact between the electrode and the Ionalyzer instrument. The whole unit was isolated with Araldite epoxy resin. The internal wall of the copper pipe was cleaned by pumping about 5 cm^3 concentrated nitric acid through the tube followed by distilled water. The copper/copper sulphide electrode was activated by deposition of copper sulphide as a fine membrane on the inner wall of the copper tube. The coating was done by circulation of 0.001 mol dm^{-3} ammonium sulphide at a rate of 2.00 cm^3 min^{-1} through the tube for 120 min. The electrode was pretreated with 0.02 mol dm^{-3} ascorbic acid for 120 min at the same flow rate. The volume of the flow-through cell was about 7.8 μl. The electrode was stored in 0.02 mol dm^{-3} ascorbic acid.

Flow system

The electrodes were incorporated into the conduits of a flow-injection system with basic design similar to those previously used [27, 29]. A Carle microvolume two-position sampling valve (Carle Catalogue No. 2014) containing two identical sample loops was used; each loop had a volume of 30 μl. The sampling unit (Cenco) was used together with a Cenco peristaltic pump that supplied a constant stream of samples to the sampling valve system. The timing of the sampler unit was 45 s for sampling with zero wash time and valve actuation at 43 s. The sampling valve system was synchronized with the Cenco sampler unit.

The carrier and reagent streams were pumped with a Cenco peristaltic pump operating at 10 rpm. Tygon tubing (0.51 mm i.d.) was used to construct the manifold. Mixing coils were made by winding appropriate lengths of Tygon tubing on Perspex rods (15 mm o.d.). The carrier stream, a solution of the ionic-strength-adjustment buffer (see below), was pumped at a constant flow-rate of 3.90 cm^3 min^{-1}. A pulse suppressor coil (200 cm × 0.51 mm i.d.) was incorporated between the peristaltic pump and the sampling valve. Samples taken from the turntable of an automatic sampler were injected automatically from a 30-μl sampling loop into the carrier stream by means of the two-position valve. While one loop served the carrier stream, a sample was drawn through the other loop at a constant flow rate of 2.00 cm^3 min^{-1}. Injected samples were mixed with the carrier stream in a 105 cm × 0.51 mm i.d. mixing coil; an extra flow (1.40 cm^3 min^{-1}) of ionic-strength-adjustment buffer was added further downstream, to improve the hydrodynamic flow, and mixed in a second mixing coil (160 cm × 0.51 mm i.d.) before the potential was measured at room temperature in the coated tubular electrode. Potentials were recorded with an Orion Research (model 901) microprocessor Ionalyzer connected to a Cenco recorder (model 34195-041). The tubular indicator electrodes were used with an Orion 90-02 double-junction reference electrode with 10% (w/v) potassium nitrate as the outer chamber filling solution, placed in a vessel downstream from the indicator electrode just before the solution went to waste [27].

Reagents and solutions

All chemicals used were of analytical reagent-grade unless otherwise specified. Solutions were prepared with double-distilled/deionized water. The stock solutions were prepared by weighing and standardized by appropriate classical analytical methods. Working standard copper(II) solutions were prepared by appropriate dilutions to cover the range 0—5000 mg dm^{-3} copper(II). All solutions were degassed before measurements by use of a water vacuum pump.

RESULTS AND DISCUSSION

The construction and preparation of home-made tubular electrodes are simple and easy to conduct. However, the electrode properties and response depend entirely on the method of preparing the precipitates as well as conditioning of the electrode. Results obtained in studies of the copper/copper(II) sulphide electrodes indicated that it was possible to coat the inner wall of the tubular metal cylinder by using three different methods: (i) anodic deposition with circulation of sodium sulphide solution; (ii) circulation of the hydrogen sulphide gas through the tube; or (iii) circulation of an ammonium sulphide solution through the tube.

Results showed that circulation of the ammonium sulphide solution was not only the cheapest and easiest way, but it was also clear that electrodes

prepared with this solution gave an activated copper(II) sulphide membrane with satisfactory electrochemical behaviour for the purpose intended. To decrease the oxidative dissolution of copper ions from the membrane material, careful conditioning of the electrode was a prerequisite. Stable and reproducible potentials were achieved when the electrodes were treated in 0.02 mol dm^{-3} ascorbic acid for 120 min; this confirmed results obtained by earlier workers [5, 11, 12]. A 0.002 mol dm^{-3} formaldehyde solution as antioxidant buffer was also incorporated into the ionic-strength adjustment buffer to retard oxidation of the membrane and prolong the lifetime of the electrode [6, 9]. Typical calibration curves illustrating the linear response of the electrode are presented in Fig. 1. When standard working copper(II) solutions in 1.0 mol dm^{-3} potassium nitrate were aspirated at 3.90 cm^3 min^{-1} into a single-line manifold to the detector until a steady-state signal was obtained, the electrode showed a linear response between about 10 and 5000 mg dm^{-3}. The calculated Nernstian response of the

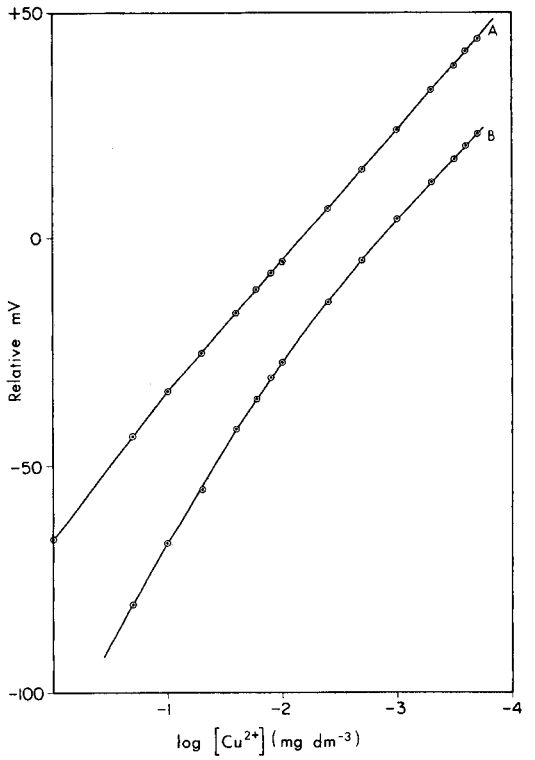

Fig. 1. Experimental calibration curves showing the response range: (A) aspiration of standard working copper(II) solutions in 1.0 mol dm^{-3} potassium nitrate at 3.90 cm^3 min^{-1} in a single-line manifold system to the detector until a steady-state was just obtained; (B) single-line manifold with 3.90 cm^3 min^{-1} carrier stream of 1.0 mol dm^{-3} potassium nitrate and a sample volume of 30 μl.

tested electrode was 29 ± 1 mV per decade (Curve A). Pick et al. [5] used 0.02 mol dm^{-3} ascorbic acid as reducing medium to prolong the half-life of the electrode membrane, a method which was also implemented to store the tubular copper-selective electrode. However, pretreatment of the electrode in this way resulted in an increased slope which was probably due to the formation of copper(I) ions, as postulated by Harsányi et al. [12]. There was a tendency for the slope to increase for concentrations below 10 mg dm^{-3} which is just the opposite of the results obtained by Harsányi et al. [12]. This is probably due to a predominant role by copper(I) ions formed during storage. The dynamic linear response range was less (Curve B) than that shown in Curve B when a sample volume of 30 μl was injected into a single-line flow-injection system with a carrier stream of 3.90 cm^3 min^{-1}. The deviation of the curve also started at higher concentrations than similar curves for chloride- [27] and iodide-selective [29] electrodes. The coated tubular copper-selective electrode also took a relatively long time to stabilize every morning and it was necessary to do a test run of about 30 min every morning under the same conditions as were to be used for the rest of the day.

Preliminary experiments were conducted to optimize the flow-injection system parameters as well as the performance of the electrode itself. Good results were obtained by using the same flow-injection system parameters like line length, transmission tube inside diameter, carrier stream flow rate and sample volume as previously described for the chloride-selective electrode [27]. It was, however, necessary to increase the addition of the reagent solution further downstream to 1.40 cm^3 min^{-1} in order to maintain a reasonable sample throughput. Although the basic design of the electrode was still a tubular cylinder [27], a plain copper tube was used as the main body of the electrode and the volume of the tubular assembly was decreased to about 7.8 μl, which provided good performance.

The influence of pH and foreign ions on the performance of the electrode was examined. The influence of pH was tested in two series of experiments, by changing the pH of the ionic-strength-adjustment buffer and by changing the pH of the samples. Figure 2A shows the influence of pH on the peak heights of a series of standard copper(II) solutions prepared in distilled water, injected into an ionic-strength-adjustment buffer of 1.0 mol dm^{-3} potassium nitrate at different pH values as carrier solution. There was a large decrease in peak heights when the pH was changed from 3 to 1, which would have a powerful effect on the precision and accuracy of results for copper samples from acidic plating baths which contain a high concentration of sulphuric acid. The peak heights reached a maximum between a pH of 3 and about 5. Although the effect was slight, the peak heights for copper(II) concentrations above 1000 mg dm^{-3} tended to decrease at pH values above 5. It was therefore necessary to use a buffered solution as the carrier stream for reliable results. Figure 2B shows the influence of pH on the peak heights of standard copper(II) solutions at different pH values injected into unbuffered 1.0 mol dm^{-3} potassium nitrate as carrier. The peak heights did not

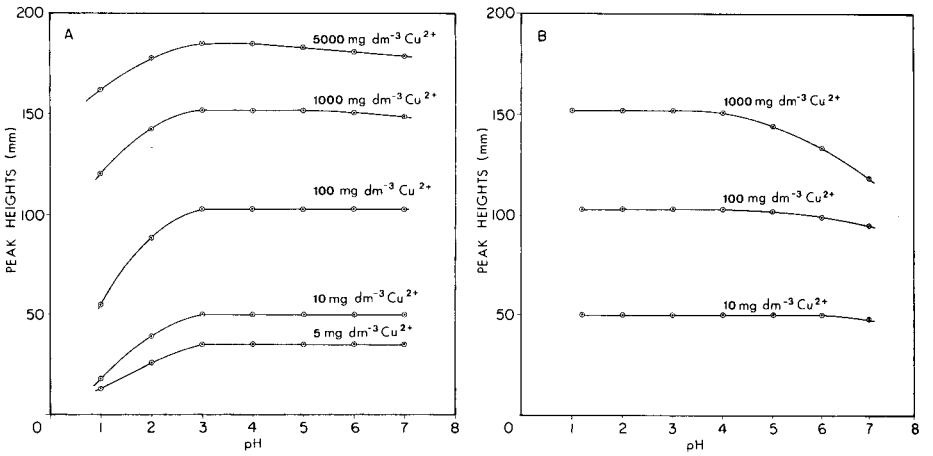

Fig. 2. Influence of pH on peak heights of a series of standard copper(II) solutions injected into an ionic-strength-adjustment buffer of 1.0 mol dm^{-3} potassium nitrate: (A) standard solutions in distilled water with carrier solutions at different pH values (B) standard solutions at different pH values with carrier solution pH unadjusted. Sample volume injected, 30 μl.

change over the pH range 1—7 for the 10 mg dm^{-3} copper(II) solution, but tended to decrease at higher pH values for more concentrated copper-(II) solutions, mainly because precipitates were formed in the standard solutions.

The influence of foreign ions on the determination of copper was investigated by preparing a series of standard solutions containing only the interfering ion and by adding various salts to 5, 10, 20 and 40 mg dm^{-3} solutions of copper(II). The presence of ammonia destroyed the electrode response rapidly, because of the formation of the soluble stable tetrammine copper-(II) complex. Silver and mercury(II) ions interfered because of the formation of insoluble sulphide precipitates on the copper(II) sulphide membrane. This resulted in sharp potential change of the electrode because of a change in resistance on the electrode membrane [2]. Although the effect was slower with 30-μl sample injections than with a continuously aspirated sample, the copper(II) sulphide membrane was eventually replaced by a film of silver sulphide or mercury(II) sulphide. The determination of 5, 10, 15 and 20 mg dm^{-3} solutions of copper(II) was, however, not affected by the presence of up to 5000 mg dm^{-3} Na^+, K^+, Ca^{2+}, Mg^{2+}, Pb^{2+}, Zn^{2+}, Co^{2+} or Ni^{2+}. The interference of Fe^{3+} ions is illustrated in Fig. 3, with different ionic-strength-adjustment buffers as carrier streams. With 1.0 mol dm^{-3} potassium nitrate at pH 3 as carrier stream, there was a notable interference of iron(III) in concentrations above 60 mg dm^{-3} (Fig. 3A). Adjustment of the pH of the carrier to 4.8 with acetate buffer decreased the interference of iron(III) (Fig. 3B). This trend was enhanced to a level where the interference of 100 mg dm^{-3} Fe^{3+} was less than 10% on 5 mg dm^{-3} copper(II) by using

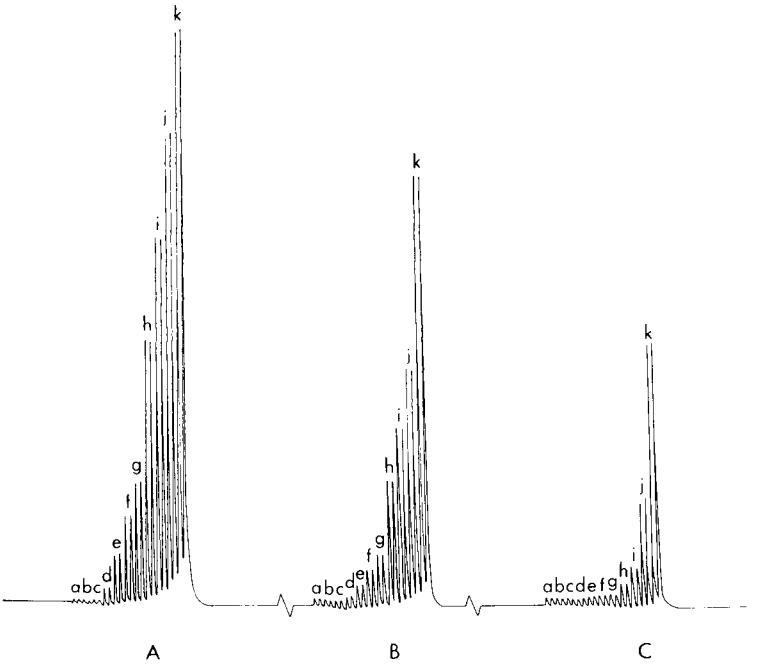

Fig. 3. Typical strip-chart recording illustrating the interference of iron(III) on the proposed flow-injection system. A series of standard iron(III) solutions was injected (30 μl), each in duplicate. Recorder paper speed, 2 mm min^{-1}; recorder range 20 mV. Iron(III) concentrations (mg dm^{-3}): (a) 5; (b) 10; (c) 20; (d) 40; (e) 60; (f) 80; (g) 100; (h) 250; (i) 500; (j) 1000; (k) 2000. Carrier solution: (A) 1.0 mol dm^{-3} potassium nitrate at pH 3; (B) as in (A) but adjusted to pH 4.8 with 0.05 mol dm^{-3} acetate buffer; (C) a combination of 0.05 mol dm^{-3} sodium fluoride, 0.05 mol dm^{-3} acetate buffer and 1.0 mol dm^{-3} potassium nitrate at pH 4.8.

a combination of 0.05 mol dm^{-3} sodium fluoride, 0.05 mol dm^{-3} acetate buffer and 1.0 mol dm^{-3} potassium nitrate as the carrier/reagent stream.

The interferences of chloride and bromide were also evaluated. Figure 4 shows the interference of chloride and bromide. Chloride interfered remarkably in the determination of copper(II) when the concentration of the interferent rose above 250 mg dm^{-3} (Fig. 4A, I); this was confirmed with mixed sample solutions (Fig. 4A, II). With bromide, the tolerable level was even lower (Fig. 4B, I) at 100 mg dm^{-3}, which again was confirmed (Fig. 4B, II) with mixed sample solutions. The interference of chloride is a disadvantage to the electrode as the determination of copper(II) in swimming pools was ruled out.

The proposed flow-injection system with the coated tubular solid-state copper(II)-selective electrode was, however, suitable for analyzing effluent and tap water samples with a chloride interference of less than 250 mg dm^{-3}, as well as copper sulphate plating bath solutions. For the effluent and water samples, a mixture 0.05 mol dm^{-3} in acetate (pH 4.8), 0.05 mol dm^{-3} in

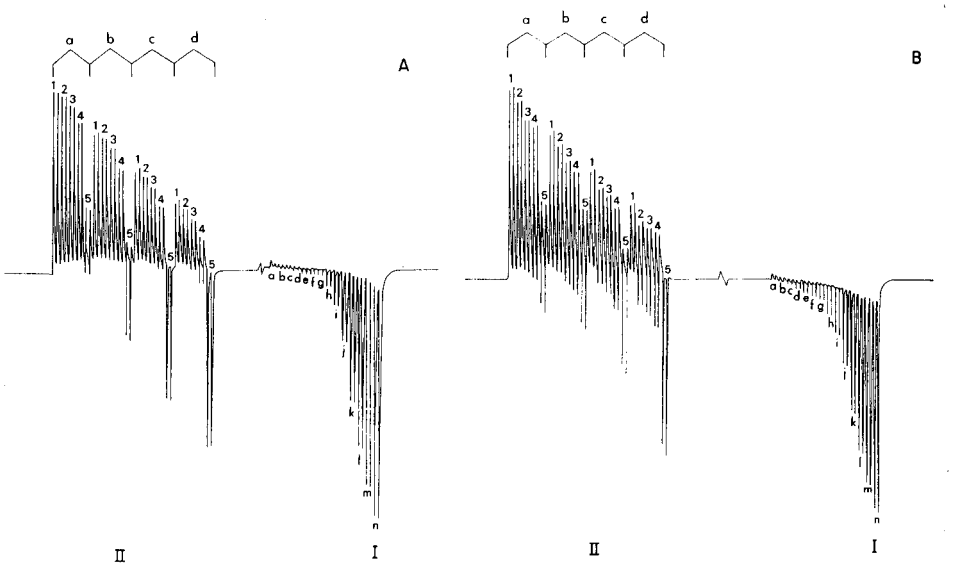

Fig. 4. Typical strip-chart recordings illustrating the interference of chloride (A) and bromide (B) on the proposed flow-injection system with 1.0 mol dm^{-3} potassium nitrate at pH 3 as carrier stream. Conditions: 30-μl injections in duplicate; recorder paper speed, 2 mm min^{-1}; recorder range, 20 mV. (I) Recorder trace for a series of standard chloride (or bromide) solutions with different concentrations (mg dm^{-3}): (a) 5; (b) 10; (c) 20; (d) 40; (e) 60; (f) 80; (g) 100; (h) 250; (i) 500; (j) 1000; (k) 2000; (l) 3000; (m) 4000; (n) 5000. (II) Recorder trace for a series of mixed standard chloride (or bromide) and copper(II) solutions. Copper(II) concentrations (mg dm^{-3}): (a) 40; (b) 20; (c) 10; (d) 5. Chloride (or bromide) concentration (mg dm^{-3}): (1) 0; (2) 250; (3) 500; (4) 1000; (5) 5000.

sodium fluoride, 0.002 mol dm^{-3} in formaldehyde (as antioxidant) and 1.0 mol dm^{-3} in potassium nitrate was used as the carrier stream. Real sample throughput of copper(II) samples, as well as carry-over and reproducibility of results, is dependent on the flow system, with the main contribution arising from the practical response time of the tubular copper(II)-selective electrode. Results indicated that the practical response time of the copper(II)-selective electrode was slower than that of the chloride-selective electrode [27]. The practical response time was, however, fast enough to give a sample throughput of about 80 samples per hour as presented by the recorder output in Fig. 5. The samples were injected in random order to test carry-over effects, which were found to be negligible. The performance and reproducibility of the proposed method for effluent and tap water are summarized in Table 1. Good agreement of results was obtained between the proposed flow-injection system and a standard atomic absorption spectrometric method. The lower limit of detection was 0.5 mg dm^{-3}. Although the sample throughput (80 h^{-1}) is relatively high, the procedure is still characterized by good reproducibility (<1.75%).

The proposed flow-injection system was also applied to the determination

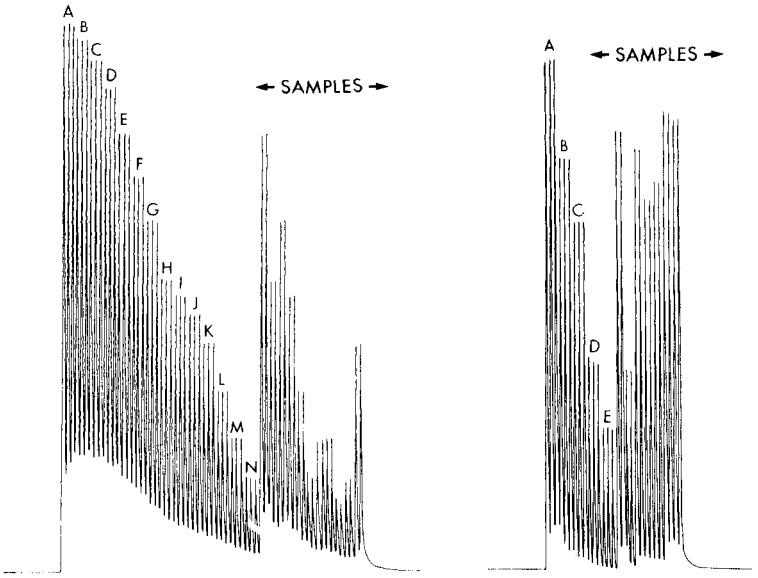

Fig. 5. Recorder trace for the flow-injection determination of copper(II) in effluent and tap water. From left to right, 5—5000 mg dm^{-3} standard copper(II) solutions followed by routine samples; standard solutions were injected in triplicate and samples in duplicate. Recorder paper speed, 2 mm min^{-1}; recorder range, 20 mV. Copper(II) concentrations (mg dm^{-3}): (A) 5000; (B) 4000; (C) 3000; (D) 2000; (E) 1000; (F) 500; (G) 250; (H) 100; (I) 80; (J) 60; (K) 40; (L) 20; (M) 10; (N) 5.

Fig. 6. Recorder trace for the flow-injection determination of copper(II) in acidic copper sulphate plating bath solutions. From left to right, 40—5000 mg dm^{-3} standard copper(II) solutions followed by routine samples. Conditions as for Fig. 5. Copper(II) concentrations (mg dm^{-3}): (A) 5000; (B) 1000; (C) 500; (D) 100; (E) 40.

of copper(II) in acidic copper sulphate plating bath solutions where there is a need for simple, rapid measurements [31]. Acid matrix interference was eliminated by preparing the standard copper(II) solutions in the same acid concentration (67.5 g dm^{-3} sulphuric acid) as the samples. The concentration of acetate buffer was increased to 1.0 mol dm^{-3} in the carrier solution; the other components remained 0.05 mol dm^{-3} sodium fluoride, 0.002 mol dm^{-3} formaldehyde and 1 mol dm^{-3} potassium nitrate. A typical recorder output for the determination of copper(II) in plating bath solutions at a sampling rate of 80 determinations per hour is given in Fig. 6. Samples were injected in random order and carry-over from one sample to another was negligible. The final results (Table 2) again compare favourably with the results obtained from a standard atomic absorption spectrometric procedure. This procedure was also characterized by good reproducibility (<1.21%).

TABLE 1

Performance and reproducibility of the proposed flow-injection method for the determination of copper(II) in effluent and tap water samples[a]

Sample	Copper(II) concentration (mg dm^{-3})		R.s.d. (%)
	Atomic absorption	Flow injection	
1	918	912	0.66
2	93	95	1.14
3	154	151	0.95
4	74	76	1.25
5	19	17	1.56
6	7.9	8.2	1.66
7	0.5	0.5	1.75
8	4.5	4.8	1.68
9	0.9	1.3	1.72
10	3.3	3.0	1.69
11	4.4	4.1	1.69
12	30	32	1.36

[a]Mean results of 15 tests in each case, with relative standard deviation for the flow-injection method.

TABLE 2

Performance and reproducibility of the proposed flow-injection method (FIA) for the determination of copper(II) in acidic copper sulphate plating bath solutions[a]

Sample	Copper(II) concentration (mg dm^{-3})		R.s.d. (%)
	Atomic absorption	Flow injection	
1	1914	1905	0.46
2	85	87	1.21
3	993	1000	0.51
4	531	525	0.64
5	689	692	0.59
6	2101	2107	0.41
7	4139	4135	0.27
8	2621	2630	0.36
9	2893	2884	0.34
10	566	571	0.61

[a]Mean result of 15 tests in each case, with relative standard deviation for the flow-injection method.

The authors thank the Council for Scientific and Industrial Research, Pretoria and the University of Pretoria for financial support. They also thank Miss M. L. Aveling for assistance with some of the experiments.

REFERENCES

1 H. Hirata, K. Higashiyama and K. Date, Anal. Chim. Acta, 51 (1970) 209.
2 M. Mascini and A. Liberti, Anal. Chim. Acta, 53 (1971) 202.
3 G. Johansson and K. Edström, Talanta, 19 (1972) 1623.
4 J. Pick, K. Tóth and E. Pungor, Anal. Chim. Acta, 61 (1972) 169.
5 J. Pick, K. Tóth and E. Pungor, Anal. Chim. Acta, 65 (1973) 240.
6 M. J. Smith and S. E. Manahan, Anal. Chem., 45 (1973) 836.
7 W. J. Blaedel and D. E. Dinwiddie, Anal. Chem., 46 (1974) 873.
8 J. M. van der Meer, G. den Boef and W. E. van der Linden, Anal. Chim. Acta, 85 (1976) 317.
9 A. Hulanicki, M. Trojanowicz and T. K. vel Krawczyk, Water Res., 11 (1977) 627.
10 G. J. M. Heijne and W. E. van der Linden, Anal. Chim. Acta, 93 (1977) 99.
11 E. Pungor, K. Tóth, M. K. Pápay, L. Pólos, H. Malissa, M. Grasserbauer, E. Hoke, M. F. Ebel and K. Persy, Anal. Chim. Acta, 109 (1979) 279.
12 E. G. Harsányi, K. Tóth and E. Pungor, Anal. Chim. Acta, 152 (1983) 163.
13 J. Gulens, Ion-selective Electrode Rev., 2 (1980) 117.
14 D. Midgley, Ion-selective Electrode Rev., 3 (1981) 43.
15 J. Veselý, D. Weiss and K. Štulik, Analysis with ion-selective electrodes, Horwood, Chichester, 1978.
16 H. Freiser, Ion-selective electrodes in analytical chemistry, Vol. 2, Plenum, New York, 1980.
17 J. Koryta and K. Štulik, Ion-selective electrodes, 2nd edn., Cambridge University Press, Cambridge, 1983.
18 J. Růžička, E. H. Hansen and E. A. Zagatto, Anal. Chim. Acta, 88 (1977) 1.
19 E. Pungor, Zs. Fehér, G. Nagy, K. Tóth, G. Horvai and M. Gratzl, Anal. Chim. Acta, 109 (1979) 1.
20 K. Tóth, G. Nagy, Zs. Fehér, G. Horvai and E. Pungor, Anal. Chim. Acta, 114 (1980) 45.
21 J. Růžička and E. H. Hansen, Flow Injection Analysis, Wiley, New York, 1981.
22 W. E. van der Linden and R. Oostervink, Anal. Chim. Acta, 101 (1978) 419.
23 M. E. Meyerhoff and P. M. Kovach, J. Chem. Educ., 60 (1983) 766.
24 A. J. Frend, G. J. Moody, J. D. R. Thomas and B. J. Birch, Analyst, 108 (1983) 1357.
25 M. Mascini and G. Palleschi, Anal. Chim. Acta, 100 (1978) 215.
26 S. Alegret, J. Alonso, J. Bartroli, J. M. Paulis, J. L. F. C. Lima and A. A. S. C. Machado, Anal. Chim. Acta, 164 (1984) 147.
27 J. F. van Staden, Anal. Chim. Acta, 179 (1986) 407.
28 J. F. van Staden, Anal. Lett., 19 (1986) 1407.
29 J. F. van Staden, Fresenius' Z. Anal. Chem., 325 (1986) 247.
30 J. F. van Staden, Analyst, 111 (1986) 1231.
31 M. S. Frant, Plating (East Orange, NJ), July (1971) 686.

Analytica Chimica Acta, 197 (1987) 229—237
Elsevier Science Publishers B.V., Amsterdam — Printed in The Netherlands

REVERSIBLE IMMOBILIZATION OF AN ANTIBODY WITH A THIOL-SUBSTITUTED SORBENT
Application to Enzyme Immunoassays

J. L. BOITIEUX*, R. GROSHEMY and D. THOMAS

Laboratoire de Technologie Enzymatique, Université de Technologie de Compiègne, BP 233,60206 Compiègne (France)

F. ERGAN

Institut de Recherche en Biotechnologie, Conseil National de Recherche du Canada, Hôpital Royal Victoria 687 avenue des Pins ouest, Montreal H3A 1A1 (Canada)

(Received 10th March 1986)

SUMMARY

A new sensor is described for a specific protein; enzyme-linked immunosorbent assays are combined with electrochemical measurements. Specific sensors are proposed based on immobilization of an antibody by ligands onto artificial protein-based membranes, combined with a computerized system, for the determination of various antigens or haptens. Specific antibodies labelled by ribonuclease are reversibly bound to the membrane by using cysteine as the ligand. Two enzymes are used: ribonuclease is used for reversibly linking the immuno-complex to the insoluble matrix via disulfide bridges; β-D-glucose oxidase is used for labelling the antigen. The measurement consists of an immunological process and an enzymatic reaction. The protein-based membrane activated with thiol groups is fixed over an oxygen electrode. After incubation of the free antigen and the antigen labelled with glucose oxidase with specific antibodies linked by ribonuclease, the reaction medium is introduced in a continuous flow cell. The oxygen consumption by the enzyme reaction is measured on-line with the electrode in contact with a standard glucose solution. This response is correlated to the antigen concentration of the sample. The signal is directly proportional to the oxygen consumption. The reproducibility with use of the same membrane is $< 5\%$. Cleavage between the immuno-complex and the thiol-containing membrane by dithiothreitol is 98% complete.

Enzyme immunoassay has developed considerably in recent years especially with respect to the design of new sensors [1, 2]. Other solid-state electrochemical sensors such as the ion-sensitive field effect transistor (ISFET) and chemical field-effect transistor (CHEMFET) have also been described [3, 4]. The rates of formation and dissociation of the antigen/antibody complex are relatively small, so an analytical system has been considered which will allow the assay of almost any biologically active material without having to use another support, the specific antibodies being linked reversibly to electrochemical sensors. Some approaches to this technology have already been studied in the area of affinity chromatography [5, 6].

The present paper concerns a new sensor for a specific protein that has

0003-2670/87/$03.50

been developed by incorporating enzyme immunoassay with electrochemical measurements. The originality of this work consists in fixing a specific antibody on a protein-based membrane via a bridging group to study the reversibility of this immuno-complex. This application derives from biospecific affinity chromatography applied to the determination of antigens or haptens. The reversible immobilization of antigen/antibody complexes labelled with glucose oxidase for development of an automatic computerized system is described. Sulfhydryl groups (from cysteine) are immobilized on the surface of a protein-based membrane by means of a gelatin solution. Cysteine was fixed on a polypropylene film coated with pig-skin gelatin polymerized with glutaraldehyde. It gave excellent reversible fixation of reduced ribonuclease (RNase)-labelled rabbit antibodies. The active membrane is fixed over an oxygen electrode in the measuring cell.

To illustrate the application of this device, rabbit IgG is studied as a model antigen. The reaction medium is injected into the cell, after incubation of the antigen-coupled glucose oxidase and of the antigen to be determined with the corresponding antibodies coupled to a pre-established concentration of reduced RNase. The activity of the glucose oxidase is measured with a standard glucose solution. The amount of linked enzyme is inversely proportional to the concentration of antigen in the medium. After the measure-

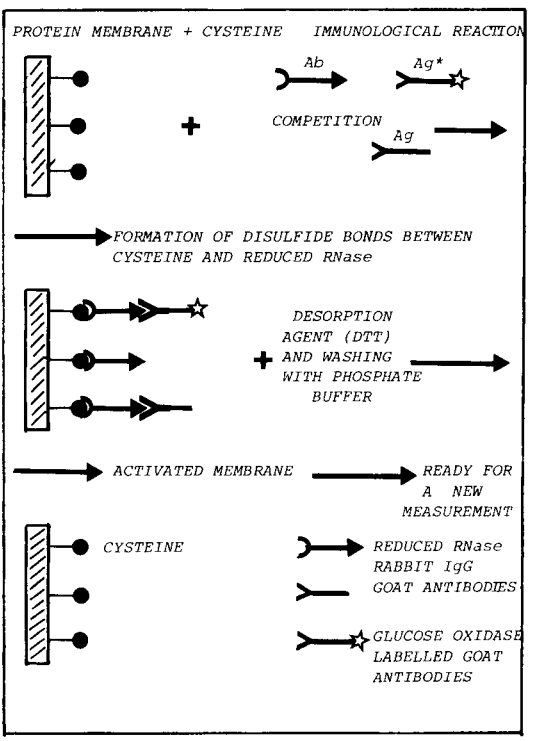

Fig. 1. Sequence of events for the competitive assay of goat IgG. Ab: Antibody, Ag: Antigen.

ment, the disulfide bonds that have been formed between the immunocomplex coupled to the reduced RNase and the cysteine are broken by injection of a dithiothreitol (DTT) solution. The principle of the system is shown in Fig. 1.

EXPERIMENTAL

Apparatus and reagents

The measuring apparatus consisted of an oxygen electrode (Clark electrode, Radiometer G-5404610) and oxygen analyzer (Radiometer pHM-71). Control of this circuit were achieved by an Apple-II microcomputer and a graphics recorder connected to the analyzer. This apparatus has recently been described [7]. A schematic representation of the measuring system is shown in Fig. 2. The gas-selective membrane was a modification of the commercially available model.

Glucose oxidase (E.C. 1.1.3.4, type II, specific activity 18400 U g^{-1}), RNase and mercaptoethanol were from Sigma Chemical Co. Pig-skin gelatin came from the Rousselot Laboratory (Ribécourt 60400, France). Glutaraldehyde and other reagents were of analytical grade (Merck). Rabbit IgG (lyophilized) and anti-rabbit IgG (goat) were obtained from Miles Laboratories.

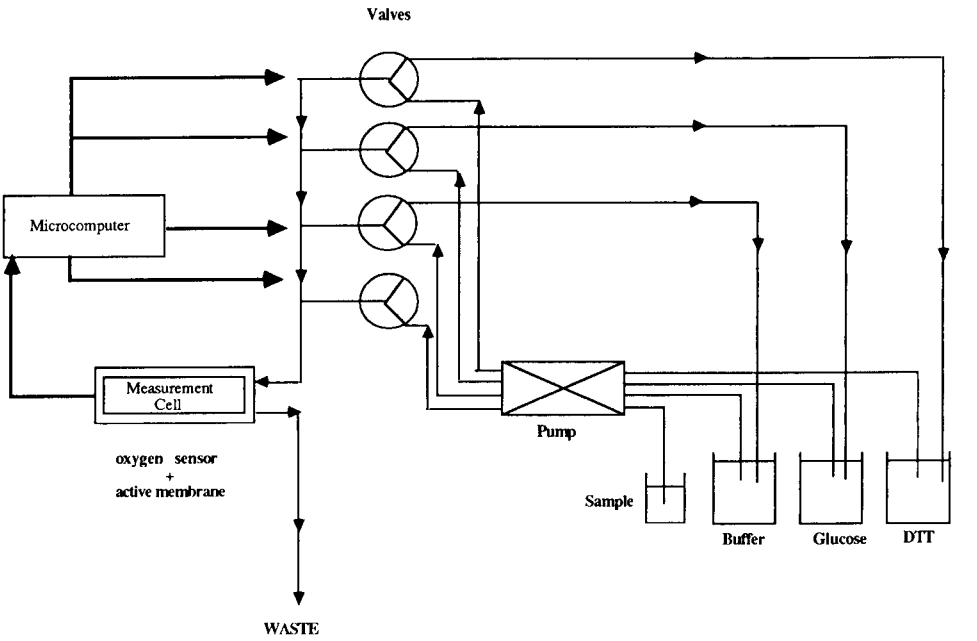

Fig. 2. Schematic diagram of the immunosensor and measuring cell, with a flow system for antigen or antibody determination.

Methods

Preparation of the modified protein carrier. Preliminary studies of immobilization of specific antibodies on different types of protein carriers showed that the greatest amount of antibodies was retained on a membrane of pig-skin gelatin [8]. This gelatin, when acid-treated, has on its surface a significant number of free amine groups. Pig-skin gelatin was dissolved in 100 ml of 0.1 M phosphate buffer, pH 6.8, by heating for 1 h in a water bath at 50°C. A portion (1 ml) of this solution was spread on a polypropylene film (7 cm × 5 cm, ca. 0.05 mm thick to obtain good mechanical stability). The polypropylene was treated beforehand with lauryl sulfate (0.5% w/v in phosphate buffer) to increase the adhesion of the gelatin. The film was left at room temperature until it was dry. This membrane was immersed in glutaraldehyde (1% in 0.01 M phosphate buffer, pH 5.2) for 5 min. The excess of glutaraldehyde was washed out thoroughly with distilled water. The activated membrane was immersed in an aqueous 0.2 M cysteine solution for 1 h. The majority of the amine groups of cysteine reacted with reactive groups of the membrane. The sulfhydryl groups on each membrane were determined spectrophotometrically as described by Ellman [9] after different incubation times. The concentrations of sulfhydryl groups fixed on the membrane are shown in Table 1.

Preparation of the IgG/RNase. Three coupling methods were studied, the one-step glutaraldehyde technique described by Avrameas and Guilbert [10], the carbodiimide technique [11] and the *p*-benzoquinone technique [12]. In the glutaraldehyde technique, 4 ml of reduced RNase (2.4 mg ml^{-1}) was incubated for 2 h at room temperature with 5 mg of IgG, 0.05 ml of a 1% glutaraldehyde solution and 0.5 ml of 0.1 M phosphate buffer, pH 6.8. After dialysis overnight at 4°C against the phosphate buffer, the conjugate was precipitated by adding ammonium sulphate. Further fractionation on Sephadex G-25 of the dialysed conjugate, equilibrated with 0.01 M phosphate buffer, pH 6.8, was used to eliminate the free enzyme.

The carbodiimide technique is derived from the method used by Nakane et al. [11] for coupling acid phosphatase to IgG. A 4-ml portion of reduced RNase solution (2.4 mg ml^{-1}) was incubated with 5 mg of goat IgG and 20 mg of 1-ethyl-2-(3-dimethylaminopropylcarbodiimide) in 0.5 ml of distilled water. This was followed by dialysis against 0.5% sodium chloride solution at room temperature. The conjugates obtained were isolated by chromatography on Sephadex G-25. The *p*-benzoquinone technique consisted first

TABLE 1

Dependence of sulfhydryl group concentration (μmol ml^{-1} cm^{-2}) on incubation time and cysteine concentration

Incubation time	30 min			60 min			90 min		
Cysteine (M)	0.1	0.2	0.01	0.1	0.2	0.01	0.1	0.2	0.01
SH conc.	0.237	0.478	0.049	0.274	0.572	0.09	0.463	0.567	0.08

of treatment of an antibody with an excess of *p*-benzoquinone, removal of excess of reagent, and coupling of the "activated" IgG to a marker substance. To 3 mg of rabbit IgG in 0.7 ml of 0.15 M sodium chloride were added 10 μl of 1 M phosphate buffer, pH 6.0, and 0.2 ml of ethanol containing 6 mg of *p*-benzoquinone. The preparation was kept at room temperature in the dark for 1 h and passed through a Sephadex G-25 column (0.9 × 4 cm), equilibrated with 0.15 M sodium chloride. The first coloured fraction containing the activated antibody was collected in a volume of ca. 1 ml. To this first fraction (1 ml), 0.2 ml of a 1% RNase solution in 0.1 M phosphate buffer, pH 6.8, was added, followed by one-tenth of the volume of 1 M carbonate/hydrogencarbonate buffer, pH 9. This mixture was left at 4°C for 15 h and the reaction was then stopped by addition of one tenth of the volume of 1 M lysine, pH 7.5. After 4 h, the mixture was dialysed overnight at 4°C against 0.1 M phosphate buffer, pH 6.8, and centrifuged for 20 min at 40 000g. The solution was filtered through a sterile Millipore membrane (0.22 μm) and an equal volume of glycerol was added.

Preparation of glucose oxidase-labelled goat antibody. A 10-mg portion of glucose oxidase (16.1 U mg^{-1}) was dissolved in 1 ml of a 1% glutaraldehyde solution in 0.1 M phosphate buffer, pH 6.8. The mixture was left for 18 h at room temperature. Glucose oxidase was purified by gel filtration on a Sephadex G-25 fine column (0.9 × 60 cm) equilibrated with 0.15 M sodium chloride. The fractions of the first peak containing the glucose oxidase were pooled and concentrated with polyethyleneglycol 2000. To the glucose oxidase solution were added 2 mg of goat IgG and 0.5 ml of 0.1 M carbonate/hydrogencarbonate buffer, pH 9.5. After a 24-h incubation at 4°C, the functional groups still free were inactivated by 0.5 ml of 0.2 M lysine solution, pH 6.8. The glucose oxidase/antibody conjugates were purified by fractionation on Sephadex G-200 equilibrated with 0.01 M phosphate buffer, pH 6.8, to eliminate the free enzyme. The fractions of the first peak were pooled and distributed in sterile 0.2-ml portions. This solution could be stored at 4°C for several months without significant loss in activity.

Assay. Discs (10-mm diameter, ca. 0.05 mm thick) were cut from the thiolated protein membrane and fixed round the tip of the oxygen electrode in the measuring cell. After incubation of RNase-labelled rabbit IgG (50 μl of conjugate diluted 10 times) for 1 h, the mixture was pumped into the measuring flow cell for 5 min. The immuno-complex thus bound to the thiolated membrane was washed with 0.01 M phosphate buffer, pH 6.8, for 30 s. The marker glucose oxidase activity was measured in the presence of a standard glucose solution (5 g l^{-1}). The consumption of oxygen estimated by the sensor is proportional to the enzyme activity retained on the active membrane and consequently to the antigen concentration. The presence of dithiothreitol (25 nM) enables the disulfide bonds between the RNase-labelled rabbit IgG and the cysteine fixed onto the protein membrane to be broken. The cell was first filled with phosphate buffer (0.01 M, pH 6.8) for 15 s to obtain a steady-state signal which represented the zero reference potential.

Spectrophotometric determination of reduced RNase/rabbit IgG complexed to glucose oxidase antibody conjugates. Portions (10 μl) of RNase/rabbit IgG solution diluted with 90 μl of phosphate buffer (0.01 M, pH 6.8) were incubated with 50 μl of glucose oxidase conjugate (diluted 1 + 9) for 2 h at room temperature on the thiolated membrane. After washing, the disks were immersed in 2.9 ml of 5×10^{-4} M 3,3'-diaminobenzidine solution containing 0.1 mg of peroxidase, and 100 μl of 5 g l^{-1} glucose solution. Enzymatic activity was monitored at 450 nm.

Reduction of RNase. The RNase (10 mg) and 0.48 g of urea were mixed with 0.02 ml of mercaptoethanol in 0.5 ml of distilled water. After dissolution, the pH was adjusted to 8.5 with aqueous 5% (w/v) trimethylamine solution. The mixture was incubated for 4 h at room temperature and the pH was adjusted to 4 with 1 M acetic acid. The reduced RNase obtained was purified by chromatography on Sephadex G-25 equilibrated with 0.1 M acetic acid. The fractions of the first peak were pooled and distributed in sterile 0.2-ml fractions. They could be stored at 4°C for several days without significant loss of activity.

RESULTS

Two types of disulfide bridges formed via cysteine bound to the gelatin membrane over the oxygen electrode were studied. The bridges were either with rabbit IgG conjugates or with reduced RNase/IgG conjugates. These reactions are illustrated in Fig. 3. In order to improve this reversible binding, attempts were made to couple rabbit IgG (unreduced) to an enzyme which contains potentially more sulfhydryl groups than the membrane. RNase was chosen; it has 4 disulfide bridges (between amino acids 26 and 84, 40 and

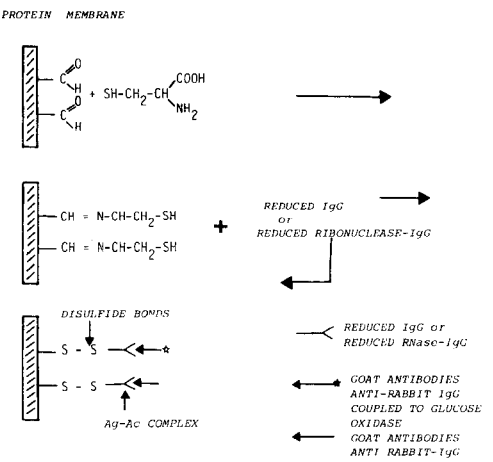

Fig. 3. Schematic representation and biochemical structure of the reversible bienzymatic system for goat anti-rabbit IgG.

95, 65 and 72 and 58 and 110) and therefore, after reduction, 8 sulfhydryl groups.

Three techniques were evaluated for coupling RNase to IgG. The conjugate obtained by glutaraldehyde coupling is named conjugate A. Conjugate B was obtained by coupling previously reduced RNase to IgG by the carbodiimide technique. Conjugate C was prepared with unreduced RNase binding via the carbodiimide technique. The concentrations of free sulfhydryl groups found for 1-ml solutions of each of these conjugates are shown in Table 2. The conjugate prepared from unreduced RNase showed a higher concentration of sulfhydryl groups than those prepared with previously reduced RNase. This is certainly due to the fact that there is a concomitant reduction and partial denaturation of IgG during the coupling with RNase. A dramatic decrease of sulfhydryl group concentration was observed after a 15-day storage, which decreased further after 30 days for each type of conjugate.

Reduced RNase that had not been coupled to IgG had an average sulfhydryl concentration of 7×10^{-8} mol ml^{-1}, which is more than in reduced IgG (2.6×10^{-8} mol ml^{-1}). Immunological tests through immunodiffusion of these immuno-complexes showed that there was no alteration of the immunological sites. To evaluate these properties, double diffusion tests were made on agar-coated slides by the method of Campbell et al. [13]. They showed an important precipitation reaction between glucose oxidase-labelled goat antibodies, anti-rabbit IgG and conjugate A. For conjugates B and C the precipitation reactions were less important. Calibration graphs were obtained for different dilutions of each glucose oxidase. Labelled goat antibody conjugates were measured amperometrically with the oxygen electrode. This electrode was coated with the thiolated membrane which had been saturated with RNase-labelled rabbit IgG. Figure 4 shows that the variation of the electrode signal after 1 min for the different conjugates was proportional to the enzyme activity, and consequently to the antigen concentration, i.e., the goat antibodies.

Measurements of the glucose activity of the conjugate were reproducible for the same membrane, with a relative standard deviation of 0.3% ($n = 7$) at a rate of oxygen consumption of 1.46 mm Hg s^{-1}. Studies done through the spectrophotometric measurement of the glucose oxidase activity of these immuno-

TABLE 2

Free sulfhydryl bonds of RNase as achieved by various conjugation techniques[a]

Time	SH concentration (μmol ml^{-1})		
	A	B	C
On preparation	102.4	6.34	29.4
After 15 days	29.4	1.98	17.2
After 30 days	14.7	1.91	7.35

[a]See text for identification of conjugates A—C.

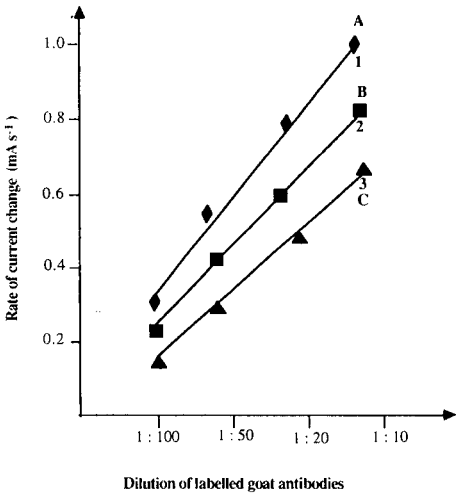

Fig. 4. Effect of dilution of goat anti-rabbit IgG labelled with glucose oxidase, on the electrode signal for the conjugates produced by the three methods: (1) conjugate A; (2) conjugate B; (3) conjugate C.

complexes with reduced IgG showed that the amount of reduced IgG immobilized on a membrane was 35%. Amperometric measurements of the glucose oxidase activity of the immuno-complexes showed that 35% of conjugate A was fixed on the membrane; 17% of conjugate B and 42% of conjugate C. The results are summarized in Table 3. Conjugates A and C gave the best overall results, better than those obtained when RNase reduction increased the binding of the IgG/RNase complex to the thiolated membrane. The choice between conjugates A and C is difficult; conjugate C seems better because it generally showed higher glucose oxidase activity.

The breaking of the disulfide bridges formed between cysteine bound to the protein membrane on the electrochemical sensor and RNase-labelled rabbit IgG was achieved by 25 mM dithiothreitol. The rate of disulfide-bridge breaking was such that 72% of the immuno-complex was uncoupled

TABLE 3

Immunological properties of different conjugates (for identification, see text)[a]

RNase/IgG conjugate	A	B	C
Presence of free thiols	+++	+	+
Immunodiffusion test	++	+	+
Glucose oxidase activity (mm Hg s^{-1})	0.57	0.42	0.70
RNase/IgG conjugate bound to membrane (%)			
Spectrophotometry	35	17	42
Amperometry	35	17	44

[a] +++ very positive, ++ positive, + slightly positive.

after 2 min, 98% after 7 min and 100% after 15 min. These results are very encouraging.

The electrode can be used continuously over many months without apparent loss in response. Repeated assays (n = 7) done with the same sample of goat antibody and the same membrane for each type of RNase/IgG complex (coupling and uncoupling) in the same run gave standard deviations of ca. 5%. However, the variation between different membranes was much higher (20%), but this is not a handicap, except that it necessitates recalibration after each membrane change. This computerized enzyme immunosensor allowed 20 sample measurements per hour. The measurement time included the washing step between samples, the sampling step and the oxygen measurement.

Conclusions

The use of reversible systems based on disulfide-bridge formation and rupture in order to establish competitive enzyme immunological assays of antigenic substances by means of amperometric measurements has given encouraging preliminary results. The measurement technique is not yet fully tested but a fully computerized system has been achieved, based on the indirect reversibility of immuno-complexes which will allow for decreased measuring time and provide a large number of measurements with the same protein carrier, without having to change the membrane after each assay.

This work was made possible with the help of INSERM (Contract no. 858006).

REFERENCES

1 T. T. Ngo and H. M. Lenhoff, Biochem. Biophys. Res. Commun., 99 (1981) 496.
2 C. R. Lowe, FEBS Lett., 106 (1979) 405.
3 S. D. Caras, D. Danmuta and J. Janata, Anal. Chem., 57 (1985) 1920.
4 J. Janata and G. F. Blackburn, Ann. N.Y. Acad. Sci., 428 (1984) 286.
5 J. Carlson, H. Drevin and R. Axen, Biochem. J., 173 (1978) 723.
6 G. F. Srelig and A. Meister, J. Biol. Chem., 257 (1982) 5092.
7 J. L. Boitieux, G. Desmet and D. Thomas, Anal. Chim. Acta, 163 (1984) 309.
8 J. L. Boitieux, G. Desmet and D. Thomas, FEBS Lett., 93 (1978) 133.
9 G. L. Ellman, Arch. Biochem. Biophys., 82 (1959) 70.
10 S. Avrameas and B. Guilbert, C.R. Acad. Sci., 273 (1971) 2705.
11 P. K. Nakane, R. Sri and G. B. Pierce, J. Histochem. Cytochem., 14 (1966) 55.
12 T. Ternynck and S. Avrameas, Ann. Immunol., 1270 (1976) 197.
13 D. H. Campbell, J. S. Garvey, N. E. Cremer and D. H. Sussdorf, Methods in Immunology, 2nd edn., W. A. Benjamin, New York, 1970, p. 198.

Analytica Chimica Acta, 197 (1987) 239—248
Elsevier Science Publishers B.V., Amsterdam — Printed in The Netherlands

STAIRCASE VOLTAMMETRY AS A RAPID DETECTION METHOD FOR ANODIC STRIPPING DETERMINATION OF LEAD

BO SVENSMARK

Department of General and Organic Chemistry, University of Copenhagen, The H. C. Ørsted Institute, DK-2100 Copenhagen Ø (Denmark)

(Received 22nd September 1986)

SUMMARY

Rapid-scan staircase voltammetry is used to strip lead plated on a rotating mercury film electrode. With potential steps of 10 mV every 64 μs, the entire stripping of the metals is made in only 4 ms. Noise is reduced by averaging several current measurements on each step. The method allows quantification of 0.1 μg l^{-1} lead within a total time of less than 4 min. Because of the rapid scan, the rotation of the electrode can continue during the stripping step. Oxygen does not affect the measurements although a small decrease in current is observed. The method is tested on a sample of sea water. Some results are also given for cadmium.

Anodic stripping voltammetry is well established for determinations of heavy metals at trace and ultratrace concentrations [1—3]. Its high sensitivity derives from the initial plating step and the effectiveness of this step has been improved by application of rotating electrodes and mercury film electrodes [4—8].

The stripping step has not been improved to the same degree. Several techniques have been used for stripping: linear-scan voltammetry, differential-pulse voltammetry [9—11], a.c. voltammetry [12], square-wave and staircase voltammetry [13—16] and chronopotentiometry [17, 18]. Differential-pulse, a.c. and pulse voltammetry have good noise rejection but perform best at low scan rates. The linear-scan method is simple but not as sensitive and noise-free as the more advanced wave-forms. Staircase voltammetry can be considered as a digital version of linear-scan voltammetry. Both methods are characterized by low noise rejection, but with the possibility for improved sensitivity at high scan rates. Staircase voltammetry has been used in anodic stripping [15]. The capabilities of the method have not been developed fully, however, because the scan rates were below the optimum for the method. Square-wave voltammetry at moderate high scan rates, up to 0.5 V s^{-1}, has been used for anodic stripping of heavy metals in the presence of dissolved oxygen [16].

In the present work, staircase voltammetry at high scan rates (156 V s^{-1}) is used to give high sensitivity for lead at very short detection times (5 ms).

0003-2670/87/$03.50

This allows fast determinations of lead without the need for deoxygenation, rest periods or interruption or electrode rotation or stirring. The possibility of quantifying heavy metals in oxygen-containing solutions has several advantages. The total time requirement is reduced and determinations in flowing, natural waters are possible. Maybe the most important point is that the chemical conditions, and so the speciation of heavy metals in solution, do not change. Lecomte et al. [19] reported that in some cases deoxygenation by simple nitrogen purging gave completely unreliable results.

EXPERIMENTAL

Reagents, cells and electrodes

Mercury(II) nitrate and nitric acid were of analytical grade. The standard lead solution was Fluka Titrisol (1.000 g l^{-1}). Diluted lead solutions were 0.29 M in nitric acid. Water was deionized twice on ion-exchange resin columns.

The cells were polyethylene cups made by cutting 25-ml polyethylene flasks in two. The cups were supported in a Metrohm electrode stand. The working electrode was a rotating Beckman glassy carbon electrode (6-mm diameter) carefully polished by hand with 1-μm alumina polishing paste. A mercury film was formed by electrochemical reduction of 100 mg l^{-1} mercury in 0.29 M nitric acid at a potential of −1.0 V vs. SCE. This reduction was done in two steps, first for 5.0 s and then for 30.0 s. The film was kept at a rest potential of 0.0 V vs. SCE after the reductions; it was stable for 2—8 h, but was quite sensitive to air. The film was therefore covered by a hanging water drop during transfer and cleaning operations to prevent evaporation of mercury. The reference electrode was a Gould mercury sulphate electrode and the counter electrode was a platinum wire.

Instrumentation

The potentiostat was home-made and designed for fast response (Fig. 1). The control loop contains only one operational amplifier (I; Harris HA5160). The cell was connected to the potentiostat by a shielded cable, through which the reference electrode was connected via the central wire and the counter electrode via the shield wire. This diminished the capacity to ground and speeded up the response of the reference electrode. The working electrode was connected to a current follower (II; Harris HA5160) with a feed-back resistor of 200 ohm. An active low-pass filter (V; Harris HA6160, 12 dB/octave) provided positive feed-back for compensation of ohmic resistance in solution. The filter function allows a higher feed-back ratio without oscillations [20]. The input and output to the control instrument were buffered and amplified (III, IV; Harris HA5160).

The applied potential waveforms were generated by a dedicated microcomputer which simultaneously sampled the current signals. The computer was a Motorola M6800 CPU with 16K RAM. The interface contains a

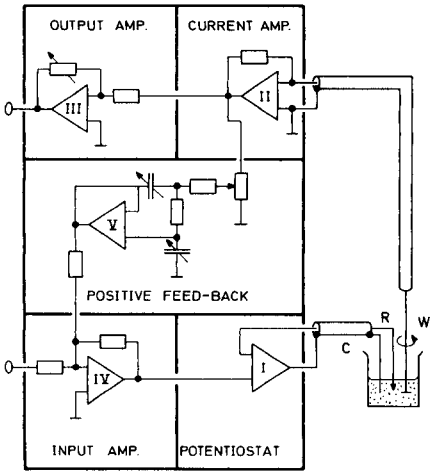

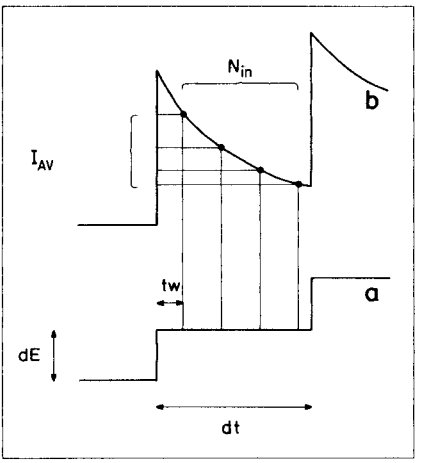

Fig. 1. Potentiostat design. Operational amplifiers: (I—IV) Harris HA5160; (V) Harris HA6160. W, Working electrode; R, reference electrode; C, counter electrode.

Fig. 2. Potential (a) and current (b) as a function of time. dE, Step height (mV); dt, step length (μs); N_{in}, number of input samples; t_w, waiting time (μs); $I_{AV.}$, current averaged over N_{in} points (nA).

16-channel, 12-bit 250-kHz AD converter (Datel DAS-250) and two 12-bit 400-kHz DA converters (Datel DAC-HK12). Each converter was interfaced to the microcomputer by a 32-point (16-bit) FIFO buffer. Data transfer to the RAM was controlled by a direct-memory-access controller (Motorola DMA, MC6844). The timing was controlled by two 3 × 16-bit programmable timers (Motorola PTM, MC6840). Programs were written with a cross-assembler on a RC4000 or RC8000 mainframe computer. The assembled code was stored on the RC8000 computer and loaded into the microcomputer through a local network. After start-up, the microcomputer ran independently of the mainframe computer. The overall performance of the system allowed up to 4000 12-bit current measurements at 100 kHz. In bursts, a few hundred points could be sampled at 250 kHz. The experimental curves were displayed point by point on a CRT monitor. Curves and experimental settings as well as comments could be printed on an Epson FX-50 printer with dot graphics written in assembler.

Standard experimental conditions

The following conditions were used unless otherwise stated. The solution was 10.0 ml of 10 ng ml^{-1} lead in 0.29 M nitric acid. The plating time was 10.0 s at −1.0 V in solutions in contact with air; no deoxygenation was used. The electrode rotation speed was 40 rps during plating and stripping. No rest period was used.

For detection, the positive staircase ramp was from —1.0 V to 0.0 V vs. SCE. The ramp consisted of 100 steps 10 mV high and 64 μs long. The entire scan takes 6.4 ms and the overall scan rate is 156 V s^{-1}. The current was sampled at 16, 32, 48 and 64 μs after the beginning of a step. The average of these 4 points is the observed current I (see Fig. 2). The background under the current peak was approximated by a straight line connecting two points on each side of the peak. Both background points and the peak itself were indicated by cursors controlled manually from the keyboard. The peak current was calculated by the microcomputer as the vertical distance from the peak to the straight line. For most series of experiments, the cursor coordinates could be left unchanged after the initial setting for the actual case. For IR compensation, the positive feed-back was adjusted to 90% of the setting where oscillations began. The time constant for the filter was normally 1.0 μs, but 0.5 μs was used in some cases. The experiments were repeated 3—7 times; results are given as the mean value and the relative standard deviation (%, *RSD*) of the mean.

The observed currents are presented in normalized form

$$I_n = I_{obs}(10\ dt)/(64\ dE\ c_0\ t_d)$$

where I_n is the normalized current, I_{obs} the observed current (both in nA), dt the step length (μs), dE the step height (mV), c_0 the bulk concentration of analyte (ng ml^{-1}) and t_d is the (deposition) time (s).

THEORY

The theory for staircase voltammetry stripping at film electrodes was developed by Christie and Osteryoung [21] who gave the following expression for the current

$$I = q_M g n\, dE/dt \qquad (1)$$

where q_M is the charge corresponding to the amount of metal deposited in the plating step, g is a current function dependent on dE and a thickness parameter ($l^2/D\ dt$), where l is the film thickness and D is the diffusion coefficient, n is the number of electrons exchanged, dE is the step height, and dt is the step length. In the case of a thin film, as used in the present study, the current function g is independent of the thickness parameter, but decreases with increasing values of dE [21].

For a rotating disc electrode, the charge q_M accumulated during the plating step is given by $q_M = k\, c_0\, \omega^{1/2}\, t_d$ where c_0 is the bulk concentration which can be assumed to be constant for all reasonable deposition times, ω is the rotation speed, t_d is the deposition time, and k is a constant. The variable quantity in a real determination is q_M because the other parameters (dE, dt, etc.) are normally kept constant during a run. The important relationships in practice are the variations of current I with t_d, c_0 and $\omega^{1/2}$. For confirmation of theory, the dependence of I on $1/dt$ and dE is also important.

It necessary to study how the charging current affects the results at the high scan rates used. The charging current is proportional to scan rate $I_c = C_{dl}\, dE/dt$ where C_{dl} is the double-layer capacitance and dE/dt is the first derivative of the potential function with respect to time. For staircase voltammetry, dE/dt is theoretically a delta function at the beginning of each step and zero on each step. The effective electrode potential E_e is less than the input potential function E_i because of R_u (the uncompensated resistance). Thus $E_e = E_i - IR_u$. In effect the electrode circuit is equivalent to a simple capacitor (C_{dl}) in series with a resistor (R_u), which behaves as a low-pass filter. The current at the beginning of a step is therefore not a high delta function but a peak; the effective potential, E_e, approaches the final value more slowly than the steep step function

$$E_e = E_i\,[1 - \exp(-t/R_u C_{dl})]$$

where t is the time from the start of the step. The uncompensated resistance should be as small as possible to charge the double layer quickly (and to prevent distortions of the faradaic current); it can be reduced by applying a positive feedback in the potentiostat. Here, this is assumed and R_u is the residual uncompensated resistance: R_u is the resistance (in solution) minus R_+, the setting of the feed-back resistor. When R_u approaches zero, the setup will start to oscillate. Initially, the oscillations are damped but at $R_u = 0$, they are undamped and may ruin the electrode surface. Thus, R_+ is a compromise between distortions and oscillations [20].

RESULTS

In the experiments done here, the background current consisted mainly of the double-layer charging current (Fig. 3); the electrode double-layer could be completely charged in 20 μs. A recording of the total current as a function of time (Fig. 4, trace a) shows clearly the initial charging current spikes at each step. To achieve a smooth curve, 16 points were measured at each step. Subtraction of the charging current gave the apparent faradaic current (Fig. 4, trace b). The charging current was obtained by parallel shift of a part of the curve from a region without faradaic current. Because of the induced charging current [22], the two components of the current cannot be separated completely in this simple way; but the faradaic current does not increase immediately. After averaging of the current measurements on each step, the analytical signal is presented as a current/potential function (Fig. 5).

The effect of the simple averaging techniques on the noise level is summarized in Table 1. The relative standard deviation for 7 repeated measurements decreased from 4.6 to 1.0% when the number of points in the average increased from 1 to 8. The step height, dE, and so the overall scan rate (dE/dt), affected the sensitivity and noise level (Table 2). The signal increased with scan rate but a small decrease was observed in the normalized current when the scan rate increased. The step length, dt, affected the normalized current in a similar way (Table 2).

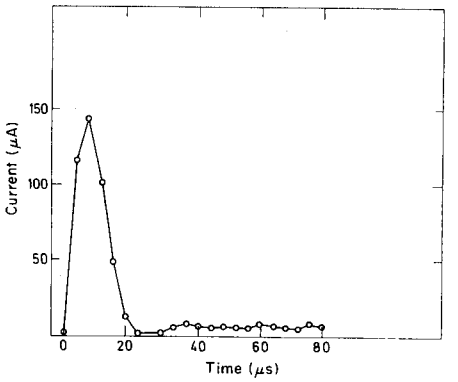

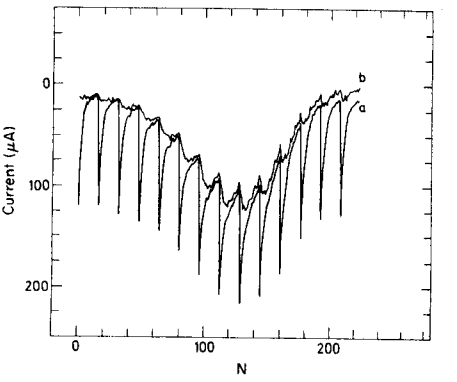

Fig. 3. The charging current as a function of time on a single step. The current was sampled at intervals of 4 μs.

Fig. 4. (a) Total current as a function of time; (b) apparent faradaic current obtained by subtraction of the charging current from the total current. N is the number of current samples; 16 points were sampled at each step (dt = 256 μs).

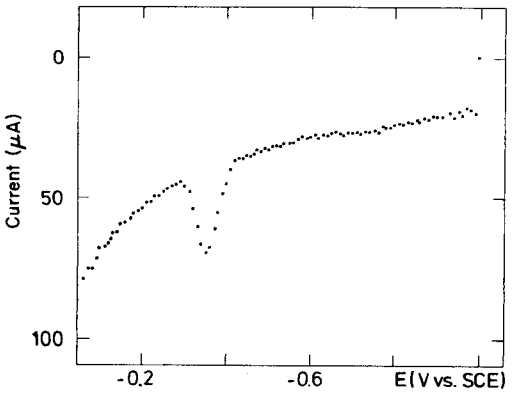

Fig. 5. Staircase stripping voltammogram for 10 ng ml^{-1} lead, showing the averaged current as a function of potential. The step from the first to the second point corresponds to the charging current. t_d = 10 s.

For thin mercury films, the signal should be independent of the thickness [21]. The normalized currents observed with increasing film thickness were 834, 764, 745 and 735 nA for mercury deposition times of 10, 20, 35 and 65 s, respectively; relative standard deviations were around 2%. Thus the signals were almost independent of thickness except for the very thin film (10-s deposition time; 10 ng ml^{-1} lead).

All the above experiments were run in solutions which had not been degassed and were in contact with air. An increase in current (8%) was observed

TABLE 1

Effect of variation of number of input samples, N_{in} (dt = 128 μs)

N_{in}	1	2	4	8
I_n (nA)	450	803	814	825
RSD(exp) (%)	4.64	2.15	1.37	1.01
RSD(calc) (%)[a]	(4.64)	(3.28)	(2.32)	(1.64)

[a] *RSD* calculated on the assumption of a constant (current-independent) error, *RSD*(calc.) = $RSD/(N_{in})^{1/2}$ are given in parentheses.

TABLE 2

Effects of variation of step height, dE, and step length, dt

dE[a] (mV)	I_n[b] (nA)	Scan rate (V s^{-1})	dt[c] (μs)	I_n[b] (nA)	Scan rate (V s^{-1})
2	1288 (6.2)	31	256	1195 (8.2)	39
4	1188 (3.8)	63	128	1000 (0.6)	78
8	1095 (0.4)	125	64	1013 (1.2)	156
12	1061 (0.3)	188	32	984 (0.4)	313
16	987 (2.0)	250	24	988 (0.5)	417
20	938 (0.6)	313	16	986 (0.4)	625

[a] At constant dt = 64 μs. [b] With *RSD* (%) in parentheses. [c] At constant dE = 10 mV.

when the solution and cell were purged with nitrogen for 3—7 min. The effect of oxygen seems to affect the reproducibility in other cases (e.g., cadmium in natural waters and biological growth media) somewhat more than reported here. However, the measurements were in all cases reliable and usable. For example, with no purging, I_n for 10 ng ml^{-1} lead was 813 nA (*RSD* 1.7%); with purging for 3—7 min, the average I_n was 884 nA (*RSD* 2.2%).

The electrode rotation speed (ω) was varied over the range 10—80 rps with $\omega^{1/2}$ t_d kept constant at 179 (t_d = 28.3 s at 40 rps). The normalized currents observed has a mean vlaue of 593 with *RSD* of 1.5%, showing that the theoretical relationship was achieved.

The normalized current for lead as a function of deposition time is shown in Table 3. For a deposition time of 10 s, the mean normalized current was 660 (*RSD* 0.9%) for six lead concentrations over the range 3.6—55 ng ml^{-1} Pb. All these data indicate that linear response is obtained; the normalized current does not change with rotation speed, plating time or concentration. The relative error in a single determination is ca. 1%.

The effect of the positive feed-back on the current can be seen in Table 3. Without feed-back, the current is diminished and this effect is proportional to the absolute current; the response is linear only at moderate currents (2—10 s deposition time). Another effect of the feed-back is seen indirectly

TABLE 3

Effect of deposition time, t_d, on normalized current, I_n, with and without IR compensation

t_d (s)	I_n^a (nA)	I_n^b (nA)	t_d (s)	I_n^a (nA)	I_n^b (nA)
1[c]	(913) (8.6)[d]	(794) (11.8)	20	973 (0.3)	793 (1.4)
2	975 (2.6)	828 (2.1)	50	954 (0.2)	695 (0.3)
5	951 (1.9)	865 (2.4)	100	976 (0.5)	593 (0.6)
10	973 (1.0)	836 (0.4)			
Average	967 (1.2)[a]	768 (13.6)[b]			

[a]IR compensation on. [b]IR compensation off. [c]Not included in average. [d]*RSD* (%) for 7 measurements.

in Table 3; for these results, the relative standard deviation is a little higher than in most other experiments because the feed-back had to be near the limit of oscillation to keep the response linear at the highest concentrations. The linearity is good but the repeatability is slightly below normal.

The method was tested on a sample of sea water taken 100 m from the coast off Nivå in Sjælland (Denmark). The water was filtered through a 0.45-μm filter and tested without further pretreatment (degassing or addition of electrolyte or buffer). The pH of the water was 8.0. Analysis with a plating time of 60 s gave a value of 0.58 $\mu g\ l^{-1}$ lead (*RSD* 7.3%). The concentration was evaluated by standard addition. Cadmium could be determined with exactly the same procedure, except a plating time of 120 s; the value found was 0.13 $\mu g\ l^{-1}$ (*RSD* 5.6%). These results are higher than the literature values (0.02—0.2 $\mu g\ l^{-1}$ for Pb and 0.02—0.07 $\mu g\ l^{-1}$ for Cd [23]). The present high values are probably due to contamination because the laboratory is not fitted for ultra-trace determinations, but the high levels could be due to polluted water from the sewage treatment plant 500 m south of the sampling place.

DISCUSSION

Most of the investigated parameters gave the expected effects, i.e., the normalized current was constant. This holds for analyte concentration, plating time and rotation speed. Some parameters showed slight deviations but they are without significance in using the method for analytical purposes. This was the case for the variation of noise with N_{in}, the effect of mercury film thickness and the effect of oxygen. The only variables that gave significant deviations were dE and dt. The theory predicts an effect for dE (actually a higher effect than observed) but no effect for dt. The observed decrease with increasing scan rate (dE/dt) is probably due to the effect of residual

uncompensated resistance because the effect of this error is expected to be more severe at short times, i.e., for variations within a single step. For analytical purposes these deviations are unimportant because dE and dt are fixed during all determinations.

The normalized current could change a lot from one day to another. This is caused by the electrodes (e.g., differences between mercury films, degradation of the films by current transients) and not by the detection method. Normally this type of error does not occur within one day.

The optimum conditions depend on analyte concentration and on the instrumentation and electrode geometry. The fastest scan for convenient stability was 10-mV steps of length 64 μs. For metals with slow electron transfers, in low conducting media or for higher stability, a dt of 256 to 1024 μs is recommended. A reasonable resolution of the current peak is obtained for dE between 4 and 12 mV. The low limit for dt is set by the instrumentation because a minimum of four current samples should be taken at each step. Another problem when the sweep rate is too high is the setting of the positive feed-back; it becomes too critical. The positive feed-back is necessary to keep the current linear at high plating times or high concentrations. However, the response is linear, if the product of plating time and concentration is kept lower than 200 s $\times$ μg l^{-1} even without positive feed-back.

The method can be used for quite high analyte concentrations, up to 10 mg l^{-1}, with plating times down to 0.1 s. At such small plating times, the current observed is too high because the concentration profiles at the rotating electrode surface are not stationary at the very beginning of plating. In such experiments, the plating time should be held constant.

The instrumental detection limit is not a fixed value but is inversely proportional to the plating time. The results show that 0.6 μg l^{-1} could be determined with a precision better than 10% with a plating time of 60 s in natural waters at natural pH in the presence of oxygen. The results show that the relative standard deviation settles at a value about 1% for a plating time $\times$ concentration product of 100 s $\times$ μg l^{-1}. Further increase of the plating time only increases the possible errors owing to the uncompensated resistance.

Compared to the classical differential pulse technique, the advantage of the present technique is not primarily a higher sensitivity but rather the short time required for a complete analysis. The differential pulse method requires typically a rest period of 25 s and a scan at 10 mV s^{-1} over 1 V takes 125 s; a 156 V s^{-1} scan over the same range takes 6.4 ms. The time difference between the methods could then be used to extend the plating time for staircase voltammetry by 2 min within the same total time. The importance of being able to analyse in the presence of oxygen was stressed in the Introduction. Instrumentally, this technique is also very simple because the rotation of the electrode (or flow in a flow cell) need not be interrupted for rest period or detection. The computer need only control the potential; no further controls for degassing or stirring are needed.

I thank Svend Aage Laursen for skilful construction of the potentiostat. This work was supported by the Danish Natural Science Research Council, grant no. 511-15013 for the instrumentation.

REFERENCES

1 J. Wang, Stripping Analysis, VCH Publishers, Deerfield Beach, FL, 1985.
2 F. Vydra, K. Stulik and E. Julakova, Electrochemical Stripping Analysis, Horwood, Chichester, 1976.
3 H. W. Nürnberg, Pure Appl. Chem., 54 (1982) 853.
4 E. Barendrecht, Nature, 181 (1958) 764.
5 K. W. Gardiner and L. B. Rogers, Anal. Chem., 25 (1953) 1393.
6 M. M. Nicholson, J. Am. Chem. Soc., 79 (1957) 7.
7 K. Z. Brainina, Talanta, 18 (1971) 513.
8 T. M. Florence, J. Electroanal. Chem., 27 (1970) 273.
9 G. C. Barker and A. W. Gardner, Fresenius' Z. Anal. Chem., 173 (1960) 79.
10 E. P. Parry and R. A. Osteryoung, Anal. Chem., 37 (1965) 1634.
11 J. B. Flato, Anal. Chem., 44 (1972) 75A.
12 W. L. Underkofler and I. Shain, Anal. Chem., 37 (1965) 218.
13 J. A. Turner, J. H. Christie, M. Vukovic and R. A. Osteryoung, Anal. Chem., 49 (1977) 1904.
14 J. Osteryoung and R. A. Osteryoung, Anal. Chem., 57 (1985) 101A.
15 U. Eisner, J. A. Turner and R. A. Osteryoung, Anal. Chem., 48 (1976) 1608.
16 M. Wojciechowski, W. Go and J. Osteryoung, Anal. Chem., 57 (1985) 155.
17 D. Jagner, Anal. Chem., 50 (1978) 1924.
18 L. Kryger and D. Jagner, Anal. Chim. Acta, 78 (1975) 251.
19 J. Lecomte, P. Mericam, A. Astruc and M. Astruc, Anal. Chem., 53 (1981) 2372.
20 D. Britz, Electrochim. Acta, 25 (1980) 1449.
21 J. H. Christie and R. A. Osteryoung, Anal. Chem., 48 (1976) 869.
22 L.-H. L. Miaw and S. P. Perone, Anal. Chem., 51 (1979) 1645.
23 B. Magnusson and L. Rasmussen, Mar. Pollut. Bull., 3 (1982) 81.

Analytica Chimica Acta, 197 (1987) 249—256
Elsevier Science Publishers B.V., Amsterdam — Printed in The Netherlands

SWEPT-POTENTIAL OXIDATIVE DETECTION IN FLOW STREAMS

DALE S. OWENS, CHERYL M. JOHNSON and PETER E. STURROCK*
School of Chemistry, Georgia Institute of Technology, Atlanta, GA 30332-0400 (U.S.A.)
ALONZO JARAMILLO
Chemistry Department, Universidad del Valla, A. A. 25360, Cali (Colombia)
(Received 15th January 1987)

SUMMARY

A swept-potential electrochemical detector, operated in the oxidative staircase voltammetric mode, is demonstrated for the high-performance liquid chromatography of a mixture of catecholamines. Voltammetric limits of detection are approximately 30 pg or 1 nM and chromatographic limits of detection are approximately 250 pg. The use of a platinum working electrode in a wall-jet cell configuration, with potential pulses for cleaning and activation between each sweep, results in a cell that has maintained a constant response for over a year without mechanical refinishing of the electrode surface.

The basic concepts, instrumentation, and applications of swept-potential electrochemical detection in flow streams have been discussed in previous papers [1—4]. These applications were all based on reduction reactions at a static mercury-drop electrode with square-wave voltammetry. The oxidative detection of carbamates, using a wall-jet cell with a platinum electrode, was described in a previous paper [5]. However, this work did not use a potential sweep; measurements were made at a constant potential, interrupted by periodic potential pulses to clean and reactivate the electrode surface.

This paper reports experiments on oxidative swept-potential detection with catecholamines as the test compounds. The factors controlling the signal-to-noise ratio, and hence limits of detection, are discussed. Results are compared to earlier work by Caudill et al. [6].

EXPERIMENTAL

The instrumentation has been fully described [2]. The only changes for the present work were the use of the wall-jet cell used before [5] and designed by Berger [7], instead of the PARC 310 cell used for reductions, and the use of a high-speed switching accessory to actuate the injector valve [8].

Several new versions of the control software were generated to investigate various waveforms. An additional feature of the control software allows the potential of the working electrode to be maintained between experiments to avoid an open circuit across the cell at the end of each experiment.

0003-2670/87/$03.50

All chromatography was done in an isocratic mode with a Zorbax-ODS column (150 X 4.6 mm i.d.) and a Haskel pneumatic-amplifier pump (model 26740). Injections of 10 μl were used in all cases. The mobile phase was 5% acetonitrile/95% aqueous 0.05 M citrate buffer at pH 5.2, 0.001 M in EDTA. The flow rate was usually adjusted to 0.8 ml min^{-1}. Early runs were done with mobile phase that had been purged with nitrogen. However, this was found to be unnecessary and was discontinued for later runs.

Standard solutions of the catecholamines (Sigma Chemical Co.) were prepared daily in oxygen-free 0.1 M perchloric acid and stored in an ice bath during the day.

RESULTS AND DISCUSSION

The first attempts at swept-potential detection of the catecholamines by using square-wave voltammetry on a platinum electrode were very disappointing. Sometimes a small peak would result from a large injection and at another time no detectable response would be found. It is now known that the poor response was the result of two factors, rapid fouling of the electrode surface and a poor choice of excitation waveform.

Successful detection of the catecholamine was obtained by using direct current (d.c.) with cleaning pulses, as previously reported [5, 7, 9] for other analyte systems. After the control program had been modified to include cleaning and activation pulses between each potential sweep, detector performance improved but remaines unsatisfactory in the square-wave voltammetric mode.

The primary problem of square-wave voltammetry at the platinum electrode is the background current obtained in the absence of any analyte. Not only is the background current large, but the rate of current decay is very slow. Thus the usual time delay, so effective for avoiding the capacitance current on mercury, is not effective for avoiding the background current on the platinum electrode. As reported by Schuette and McCreery [10], the major component of this background is faradaic rather than capacitive current.

In hydrodynamic flow, the situation can be even less favorable than indicated by Schuette and McCreery [10] for unstirred solutions, because most of the soluble product of the forward step is swept away before it can be reacted in the reverse step. Thus, one of the prime advantages of square-wave voltammetry is lost while the background current from surface reactions is not decreased in hydrodynamic flow and is almost doubled by the reverse step.

In contrast, staircase voltammetry is favored in hydrodynamic flow in comparison to unstirred solution. The faradaic current is enhanced over that in unstirred solution because there is no appreciable depletion of analyte from the region near the electrode surface, an advantage shared by d.c. amperometry and to a lesser extent by square-wave voltammetry. In addition,

the background faradaic current is much less than that for square-wave voltammetry because of the smaller potential pulses applied. For example, steps of 10 mV for staircase voltammetry might correspond to 50 mV forward and −40 mV reverse for square-wave voltammetry. In brief, the advantages of the larger potential pulses in square-wave voltammetry are decreased by hydrodynamic flow while the surface nature of the background faradaic reactions on the solid electrode acts as a disadvantage. In addition, for the same sampling time and step size, the sweep rate with staircase voltammetry is twice that for square-wave voltammetry. This is an important factor in obtaining adequate resolution on the time axis.

Other pulsed waveforms, such as differential pulse, normal pulse, and differential double pulse, have been used for voltammetric oxidation of catecholamines [11—13]. Unfortunately, these waveforms result in such slow potential sweeps that the techniques are not suitable for application to high-performance liquid chromatography (h.p.l.c.) or flow injection analysis.

Rapid-sweep experiments, especially with pulsed waveforms, require cells with rapid-response characteristics. Thin-layer cells and coulometric cells have long time constants because of their large electrode areas and high resistances and are poor choices for rapid-sweep applications. Berger [7] has discussed the design criteria for the wall-jet cell used in this study, which has a platinum-disk working electrode at 0.81-mm diameter and an inlet jet of 57-μm i.d. fused-silica tubing. The collection efficiency of this cell is such that the current response is similar to that of a thin-layer cell with a working electrode of 3-mm diameter (i.e., the current density is approximately 14-fold greater for the wall-jet cell), yet the response time of the wall-jet cell is much shorter, making it suitable for rapid-sweep and pulsed operation.

Instrumentation also plays an important role in the comparison of d.c. amperometry, staircase voltammetry, and square-wave voltammetry at solid electrodes in hydrodynamic flow. It is quite simple to introduce a d.c. offset signal into the current amplifiers for d.c. amperometry and to operate the amplifiers at very high gain. This simple approach is not feasible with the voltammetric experiments because the magnitude of the background is highly dependent on the electrode potential. Even introduction of a linear-ramp offset current is not effective because the change of background current with electrode potential is highly nonlinear. Thus, for the voltammetric techniques, the amplifiers are operated at a lower gain in order to keep the current response within the output range of the amplifiers and analog-to-digital converter throughout the potential sweep. The amplifier gain for square-wave voltammetry was usually a factor of eight lower than for staircase voltammetry, which in turn was a factor of 64 lower than for d.c. amperometry. Operation of the amplifiers at lower gain results in fewer analog-to-digital converter (ADC) levels for a given current response, resulting in poorer signal-to-noise ratios for the voltammetric techniques as compared to d.c. amperometry.

Figure 1 illustrates a typical chromatogram of catecholamines obtained with d.c. amperometry, with periodic cleaning pulses. Typical limits of detection for this type of experiment are 9 pg injected. These limits of detection are calculated on the basis of twice the standard deviation of the baseline after application of Fourier transform (FT) filter [14] with the cutoff factor chosen to minimize any distortion of the analyte peak. Such filtering is entirely appropriate because the instrument has no filter circuits except for the gated integrator used to accumulate the signal during one sampling window. The time constant for the integrator is 1 ms and the usual sampling window is 16.7 ms to minimize 60-Hz noise. Over the range from 0.75 to 164 ng injected, the detector response for norepinephrine was linear with a sensitivity (slope) of 1.500 ± 0.007 nA ng^{-1} and a standard error of 1.04 nA. The negative region between peaks B and C is related to perchloric acid in the sample. Possibly, perchloric acid eluting at that time might cause a chemical oxidation of the electrode surface, leading to a decrease in the electrochemical oxidation of the surface and a lower background current.

Figure 2 illustrates a three-dimensional representation of a typical chromatogram of catecholamine standards with a staircase voltammetric detector.

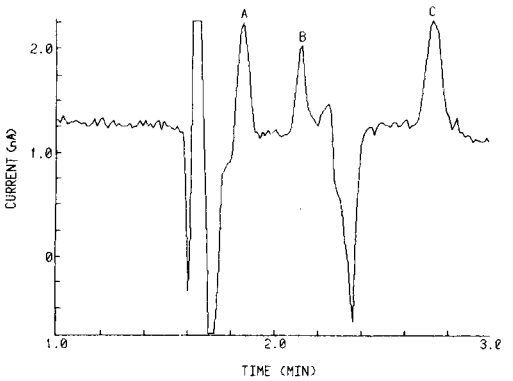

Fig. 1. Direct-current detection of catecholamines. Peaks: A, 0.75 ng norepinephrine, B, 0.80 ng epinephrine; C, 0.82 ng dopamine. Electrode potential, 0.90 V vs. Ag/AgCl with cleaning pulses to 3.0 V and 0.50 V every 0.74 s; flow rate, 1.0 ml min^{-1}. Raw data with no filtering or smoothing.

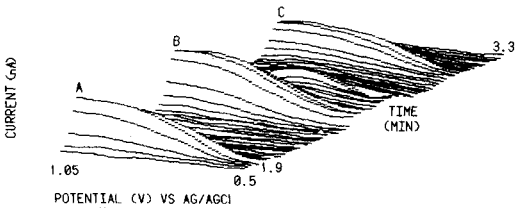

Fig. 2. Swept-potential chromatogram of catecholamine standards. Peaks: A, 6.1 ng norepinephrine; B, 8.4 ng epinephrine; C, 4.9 ng dopamine. Estimated peak molar concentrations: A, 2.0×10^{-7}; B, 2.3×10^{-7}; C, 1.2×10^{-7}. Staircase waveform; 10-mV steps 16.7 ms wide; sweep repetition, 1.21 s; flow rate, 0.8 ml min^{-1}.

One sweep was chosen as a voltammetric baseline and subtracted from all sweeps. Then each subtracted sweep was FT-filtered with the cutoff factor chosen to minimize distortion of the voltammogram from one of the peaks. The sigmoidal shapes of the voltammograms, as predicted for hydrodynamic flow, are evident.

Voltammetric limits of detection were estimated on a molar basis after comparison of the chromatographic response to the response from an injection of the same volume and concentration into the flow-injection system, to correct for chromatographic band broadening. These limits are estimated to be approximately nanomolar for dopamine and norepinephrine, corresponding to about 30 pg injected.

Because the response of electrochemical detectors is proportional to concentration rather than mass, mass limits of detection can be improved greatly by scaling down the chromatography. Thus, a change to microbore columns would be expected to show a marked lowering of the mass limits of detection, provided that the detector response does not deteriorate with the reduced volume flow rate used with microbore columns. The theoretical equations for the wall-jet cell [15] indicate that a decrease in volume flow rate can be compensated by a decrease in the radius of the working electrode and the diameter of the inlet jet.

Figure 3 illustrates a chromatogram obtained from the data file of Fig. 2 by educing those points with a common potential. In comparison to Fig. 1, Fig. 2 contains fewer points. Furthermore, as explained above, the amplifier gain was lower for the experiment illustrated in Figs. 2 and 3, and therefore the signal-to-noise ratio is poorer. Limits of detection are estimated to be about 250 pg injected. Sweep-to-sweep variation resulting from flow noise

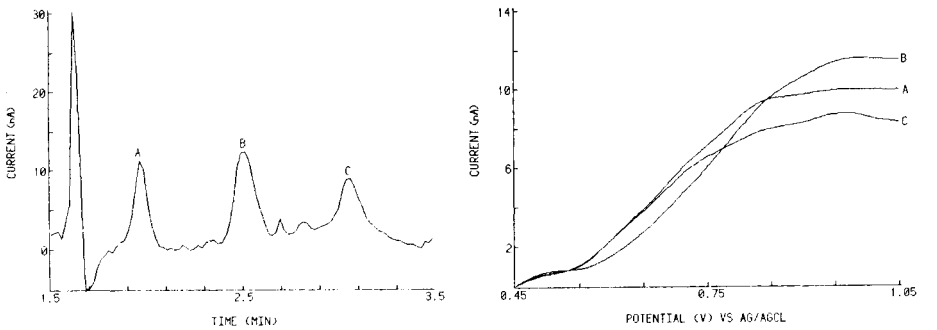

Fig. 3. Constant-potential chromatogram of catecholamine standards. The figure is constructed from the data file of Fig. 2 by plotting those points taken at an electrode potential of +0.90 V vs. Ag/AgCl.

Fig. 4. Hydrodynamic voltammograms of catecholamines. The three voltammograms are the three sweeps taken from the respective peaks of Fig. 2.

is the probable reason that the chromatographic limits of detection are poorer than the voltammetric limits of detection cited above.

Over the range 6.1—168 ng injected, the detector response for norepinephrine was linear with a sensitivity of 1.794 ± 0.043 nA ng^{-1} and a standard error of 5.3 nA. It is evident that the current sensitivity is slightly greater for the voltammetric technique even though the limits of detection are inferior because of the inability to offset the background currents and the subsequent operation of the amplifiers at lower gain. The swept-potential chromatographic limits of detection are about a factor of 30 poorer than those of d.c. amperometry, consistent with a factor of 64 lower gain, a concurrent decrease in electronic noise, and a 20% increase in sensitivity.

Figure 4 illustrates the hydrodynamic voltammograms of the three catecholamines obtained from the chromatographic peaks of Fig. 2. Differences in half-wave potential and slope are evident. Although the differences in oxidation potentials are not dramatic in the case of the catecholamines, they can be expected to be more so in other chemical systems. The important point to realize is that all three complete voltammograms were obtained from a mixture in one experiment with small amounts of analyte.

Application of the swept-potential detection to real samples is illustrated in Fig. 5. The sample is typical of a number of samples supplied by another research group [16] and is an extract of whole rat hearts from male CD rats which had been dosed with a test compound in 0.9% saline. The absence of dopamine (peak C in Figs. 2 and 3) is expected for these samples.

The periodic cleaning pulses are very important. The cell used in this work had been in use for almost three years and, during that time, the platinum surface of the working electrode had never been polished or cleaned mechanically. During early swept-potential experiments, the control program did not include the application of cleaning pulses; instead, runs with d.c. amperometry with cleaning pulses were interspersed between swept-potential runs in order to restore the electrode response, which was observed to decay by a factor of almost 100 after a few days of use without cleaning pulses. Since the inclusion of cleaning pulses in the control program, the response of the cell has remained virtually constant for over a year.

Another important experimental feature is the maintenance of electrode potential between chromatographic runs. After a period of time with the cell

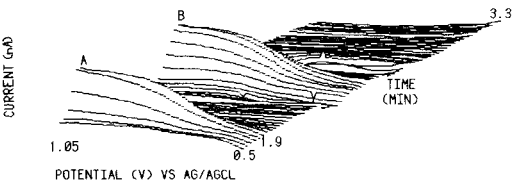

Fig. 5. Swept-potential chromatogram of rat heart extract. Peaks A and B correspond to 8.6 ng of norepinephrine and to 11.9 ng of epinephrine injected, respectively. All conditions as in Fig. 2.

in open circuit, the baseline voltammograms are observed to change for perhaps 10—15 min. before reaching a steady state. This is in contrast to the reduction-mode experiments with a static mercury-drop electrode and is attributed to surface changes on the platinum electrode. It was found that if the potential of the platinum electrode is maintained between chromatographic runs, a steady baseline is reached after only a few sweeps and never shows the magnitude of changes observed when the cell has been open-circuited. These observations should be relevant to other workers who practice almost ritualistic procedures in preparing platinum electrodes and rely on the first sweep for special significance. The reproducible baseline voltammograms obtainable in flow streams serve as a powerful incentive to performing voltammetry by flow injection analysis rather than in bulk solution.

As earlier reported by Caudill et al. [6], this work indicates that staircase voltammetry is an acceptable waveform for rapid-sweep oxidations on solid electrodes. However, there are many differences in experimental detail and some differences in the conclusions reached. In other cases, there is insufficient information with which to make a valid comparison. Although the waveform is nominally the same, our step width is typically 16.7 ms compared to Caudill's 100 ms. This narrower (shorter) step width is possible because of the faster time constant of the potentiostat used ($\approx$10 μs vs. 10 ms) and possibly a faster time constant for the cell. This allowed the resolution on both the potential and time axes to be increased in the work described here. Typically, a 10-mV step and a sweep repetition of 1.5—2 s were used, compared to the 50-mV step and 3-s sweep repetition used by Caudill et al.

Mass limits of detection are quite dependent on the chromatographic parameters which are different between this work and the work of Caudill et al. However, the swept-mode chromatographic limits of detection in this work are approximately a factor of 15 better. A fundamental difference is that the present voltammetric limits of detection are better than the chromatographic limits of detection while Caudill et al. reported the reverse. This implies that the factors controlling the limits of detection are different in the two experiments.

Another important difference is that the wall-jet cell with platinum working electrode, coupled to the use of cleaning pulses, resulted in a stable response with virtually no cell maintenance as compared to the repolishing required to restore response of carbon electrodes. Because the effective area of the multifiber electrode used by Caudill et al. [6] was not specified, it is not possible to compare current density and capture efficiency of the cells.

Although significant improvements have resulted from this work, the limits of detection do not compare favorably with those of d.c. amperometry. Future work in this laboratory will explore several paths. Some improvement can be expected by increasing the dynamic range of the current-measuring circuit by increasing the number of bits of the ADC from the present 12. Another approach would be to average several background

voltammograms and to use this data base to generate a nonlinear current offset. This would require an increase from the present 8 bits of the current offset control DAC but would allow operation of the current amplifiers at higher gain with concurrent improvement in signal-to-noise ratio and improved limits of detection.

Another promising avenue would be to follow the lead of other workers who are exploring the advantages of microarray electrodes [17—20]. Because of the radial flow lines across the surface of the electrode in the wall-jet cell, the optimum electrode here should be a regular array of platinum or gold dots (or concentric circles) rather than the random active sites or the straight lines presently used.

This work was supported in part by NIH Grant R03 RR02542-01 and by NIH Grant BRSG No. 2S07 RR7024-21. The programming assistance of Huggins Msimanga is gratefully acknowledged.

REFERENCES

1 J. Scanlon, P. Flaquer, G. Robinson, G. O'Brien and P. Sturrock, Anal. Chim. Acta, 158 (1984) 169.
2 P. Reardon, G. O'Brien and P. Sturrock, Anal. Chim. Acta, 162 (1984) 175.
3 M. Thomas, H. Msimanga and P. Sturrock, Anal. Chim. Acta, 174 (1985) 287.
4 D. Owens and P. Sturrock, Anal. Chim. Acta, 188 (1986) 269.
5 M. Thomas and P. Sturrock, J. Chromatogr., 357 (1986) 318.
6 L. Caudill, A. Ewing, S. Jones and M. Wightman, Anal. Chem., 55 (1983) 1877.
7 T. Berger, U.S. Patent 4,496,454, Jan 29, 1985.
8 M. Harvey and S. Stearns, Anal. Chem., 56 (1984) 837.
9 S. Hughes and D. Johnson, Anal. Chim. Acta, 132 (1981) 11.
10 S. Schuette and R. McCreery, J. Electroanal. Chem., 191 (1985) 329.
11 R. Lane and A. Hubbard, Anal. Chem., 48 (1976) 1287.
12 J.-L. Ponchon, R. Cespuglio, F. Gonon, M. Jouvet and J. F. Pujol, Anal. Chem., 51 (1979) 1483.
13 W. Beck, W. Brooks and M. Fillenz, J. Electroanal. Chem., 125 (1981) 205.
14 E. Aubanel and K. Oldahm, Byte, 10 (1985) 207.
15 H. Gunasingham and B. Fleet, Anal. Chem., 55 (1983) 1409.
16 S. May, Ga. Inst. Tech., private communication.
17 K. Wehmeyer, M. Deakin and M. Wightman, Anal. Chem., 57 (1985) 1913.
18 C. Chidsey, B. Feldman, C. Lundgren and R. Murray, Anal. Chem., 58 (1986) 601.
19 A. Bard, J. Crayston, G. Kittlesen, T. Shea and M. Wrighton, Anal. Chem., 58 (1986) 2321.
20 L. Fosdick and J. Anderson, Anal. Chem., 58 (1986) 2481.

Analytica Chimica Acta, 197 (1987) 257—264
Elsevier Science Publishers B.V., Amsterdam — Printed in The Netherlands

DETERMINATION OF SELENIUM BY MEANS OF COMPUTERIZED FLOW CONSTANT-CURRENT STRIPPING AT CARBON FIBRE ELECTRODES.
Application to Human Whole Blood and Milk Powder.

CHI HUA, DANIEL JAGNER* and LARS RENMAN

Department of Technical Analytical Chemistry, Chemical Centre, University of Lund, P.O. Box 124, S-221 00 Lund (Sweden)

(Received 9th December 1986)

SUMMARY

The main features of the flow constant-current stripping analysis for selenium(IV) are formation of a mercury film on a carbon fibre sensor in a chloride medium containing mercury(II), electrolysis in the sample at −0.20 V vs. SCE for 15—60 s, and subsequent stripping (reduction) of the mercury(II) selenide formed on the electrode surface, by means of a constant current of 0.40 μA in an acidic magnesium chloride solution containing Triton X-100. During stripping, the potential vs. time gradient is monitored at a real-time measuring rate of 25.6 kHz. All experimental parameters are under computer control. A standard addition method is used and the results are calculated and reported, both digitally and graphically. Equations relating the magnitude of the constant current to the concentration of reducible species, and, in particular, of dissolved dioxygen, are derived. Milk powder and whole blood reference samples were analyzed by high-pressure digestion in nitric acid and dilution with hydrochloric acid, in order to reduce selenium(VI) to selenium(IV), and then constant-current stripping. The results obtained by this method were lower than those obtained by the reference technique, but the values agreed within one standard deviation of the two techniques. Ions, such as iron(III) and lead(II), known to interfere with electrochemical stripping for selenium(IV) in batch analysis did not interfere in the flow approach.

Selenium is most frequently determined electrochemically or spectrometrically, after hydride generation. In the former approach, both anodic [1, 2] and cathodic [3, 4] stripping voltammetry procedures have been used. An alternative method would appear to be constant-current reductive stripping with potentiometric measurement, i.e., real-time monitoring of the potential vs. time transient during reduction of the oxidized species on the electrode surface with a constant current. When used in conjunction with computerized flow instrumentation, this approach might offer advantages with respect to ease of automation and of cleansing the electrodes between stripping cycles. Moreover, deoxygenation of the sample would not be necessary and interference from reducible species in the sample would be eliminated.

The purpose of the present work was to investigate whether constant-current stripping could be used to advantage for the determination of selenium

0003-2670/87/$03.50

in biological samples. Carbon fibres were investigated as possible sensors, because their use simplifies handling of the flow system considerably [5].

EXPERIMENTAL

Flow electrodes and instrumentation

The working electrode was a carbon fibre, 10 μm in diameter, mounted through a PVC tube with an inner diameter of 0.5 mm, as described previously [5]. A platinum tube mounted downstream from the working electrode was used as counter electrode followed by a saturated calomel reference electrode (SCE) [6]. All potentials reported below are vs. SCE.

A computerized flow potentiometric and constant-current stripping analyzer, described in detail elsewhere [6], was used in all investigations. In this instrument, six different solutions can be sucked, in random order, into the flow cell; the flow rate, the electrolysis potential, and opening and closing of inlet valves are under computer control. During stripping, a constant current of programmable magnitude and direction is allowed to pass through the cell. After recording of the stripping curve, E (V) vs. t (s), at a real-time sampling rate of 25.6 kHz, and, normally, after differentiation, subtraction of the background and digital filtration, the stripping peak is located and integrated within a specified potential width. Subsequently, the differential of the stripping curve, dt/dE vs. E is displayed on the printer/plotter. In the present investigation, the main experimental parameters were: flow rate 1.5 ml min^{-1}, reductive current 0.4 μA, peak-searching potential range —0.38 to —0.53 V, peak integration width ±0.07 V around peak potential, averaging filter width 0.03 V, and Savitzky-Golay filter width of 0.015 V [6], the potential resolution being 0.001 V.

Reagents

All chemicals were of analytical grade except the mineral acids, which were of Suprapur grade. All dilutions were made with Millipore-Q water. Stock solutions, 100 mg l^{-1}, of mercury(II) and selenium(IV) were prepared by diluting Titrisol (Merck) ampoules with 1 M hydrochloric acid.

Milk powder reference samples CRM 150, 151 and 063 were obtained from the Commission of the European Communities, Community Bureau of Reference (BCR), Brussels.

Human blood samples were obtained from the Department of Occupational Health, University of Lund. Three of these, referred to as samples A, B and C below, were chosen as reference samples and analyzed for selenium by means of neutron activation analysis.

The mercury plating solution was 100 mg l^{-1} mercury(II) in 2 M magnesium chloride/0.5 M hydrochloric acid.

The stripping solution was 2 M magnesium chloride/0.20 M hydrochloric acid containing 0.3% (v/v) Triton X-100.

The test solution was 5 M hydrochloric acid containing 2 mg l^{-1} mercury(II) and 2 μg l^{-1} selenium(IV).

Procedures

Sample decomposition. For whole blood, transfer 300 μl of the sample to a quartz high-pressure digestion tube. Add 3 ml of concentrated nitric acid, close the tube and heat it at 80°C for 40 min and then at 180°C for approximately 7 h. Allow to cool and then add 7 ml of concentrated hydrochloric acid. Boil gently for 30 min in order to convert selenium(VI) to selenium(IV). Finally, add 20 μg of mercury(II) and dilute to 10 ml.

For blood sample B, a 600 μl sample was used, owing to the lower selenium content of this sample.

For milk powders, digest 50 mg of the samples in the same way as for the whole blood samples above.

Constant-current stripping. For digested whole blood, the procedure is as follows. The mercury plating solution is allowed into the cell and a potential of 0.02 V is applied for 4 s in order to remove the mercury film on the electrode used in previous cycles. The same procedure is also applied when a fresh carbon fibre electrode is used. Subsequently, a new mercury film is plated onto the carbon fibre by applying the potential sequence: −0.30 V for 5 s, potential off for 2 s, −0.50 V for 5 s, potential off for 2 s, and, finally, −0.85 V for 20 s. The sample solution is then allowed into the cell and an electrolysis potential is applied for 15 s, after which the stripping solution is sucked into the cell. One minute later the reductive constant current is applied in the potential range −0.20 to −0.80 V. After 5 s at −0.80 V, a potential of −0.20 V is applied again for 5 s, after which the background is recorded. An identical electrolysis/stripping cycle is then repeated on a blood sample spiked with 150 μg l^{-1} selenium(IV).

During the electrolysis/stripping cycle for the spiked sample the differential of the background-corrected stripping curve from the previous run is displayed on the printer/plotter, together with values for peak potential and area. Analogous results are displayed for the spiked sample, after which the computer calculates the selenium(IV) concentration in the sample by means of the usual equations for standard addition.

Electrolysis/stripping cycles in sample and spiked sample can be repeated any pre-chosen number of times in order to estimate the reproducibility. The computer then reports the mean value and the standard deviation.

For digested milk powder, the procedure is the same as that for whole blood with the exceptions that the sample is electrolyzed for 60 s and that the magnitude of the selenium(IV) standard addition is 150 μg kg^{-1}.

RESULTS AND DISCUSSION

Electrode reactions

The electrode reactions taking place during the determination of selenium(IV) with mercury electrodes have been investigated by means of cathodic stripping voltammetry [3, 4]. According to these studies, the potentiostatic deposition reaction is

$$Hg + H_2SeO_3 + 4H^+ + 4e^- \rightarrow HgSe(Hg) + 3H_2O \quad (1)$$

where HgSe(Hg) denotes mercury(II) selenide on the mercury surface, and the stripping reaction in acid medium is

$$HgSe(Hg) + 2H^+ + 2e^- \rightarrow H_2Se + Hg \quad (2)$$

In media with high copper(II) concentrations, the electrode reactions that have been suggested are

$$Cu^{2+} + 2e^- \rightarrow Cu(Hg) \quad (3)$$

$$2Cu(Hg) + H_2SeO_3 + 4H^+ + 4e^- \rightarrow Cu_2Se(Hg) + 3H_2O \quad (4)$$

$$Cu_2Se(Hg) + 2H^+ + 2e^- \rightarrow 2Cu(Hg) + H_2Se \quad (5)$$

In order to elucidate the electrode reactions ocurring in the constant-current stripping analysis for selenium in the acid digest of biological material, the test solution was analyzed according to the procedure described above for acid digests of whole blood. The procedure was repeated after the addition of 0.2 mg l^{-1} copper(II) to the sample. Both experiments yielded identical stripping peak potentials, i.e. at —0.45 V, showing that reactions (3—5) are not applicable to the present study, because the copper(II) concentration in the acid digest was far below 0.2 mg l^{-1}.

That reaction 2 was the relevant reduction reaction for constant-current stripping was confirmed by processing a whole blood digest as in the procedure described above and varying the hydrochloric acid concentration in the stripping medium in the range 0.01—1 M. The shift in peak potential agreed well with a two-proton reaction. A hydrochloric acid concentration of 0.20 M was chosen finally, because this yielded a selenium stripping peak at approximately —0.45 V where the signal-to-background ratio was optimal.

Dependence of stripping time on stripping current

Assuming that reduction of selenium(IV) is not rate-determining and that the only electrode reaction occurring during stripping is reduction of mercury(II) selenide, the stripping time, t_{strip}, would, in accordance with potentiometric stripping theory [7], be inversely proportional to the stripping current, i_{strip}, as

$$t_{strip} \propto D_{Se(IV)}\,[Se(IV)]\; t_{el}\; A\; \delta_{el}^{-1}/i_{strip} \quad (6)$$

where [Se(IV)] is the selenium(IV) concentration in the sample, $D_{Se(IV)}$ the diffusion coefficient, t_{el} the time of electrolysis in the sample, A the electrode surface area, and δ_{el} the thickness of the diffusion layer during electrolysis in the sample, all quantities being expressed in their normal units.

During stripping in the magnesium chloride medium, however, other reactions also take place at the electrode surface, the most important side-reaction being the reduction of dissolved dioxygen to water. Because the transport of dioxygen to the electrode surface is diffusion-controlled, the current

required for the reduction of dioxygen, i_O, will be proportional to

$$i_O \propto D_O [O_2] A \delta_{strip}^{-1} \quad (7)$$

where $[O_2]$ is the concentration of, and D_O the diffusion coefficient for, dissolved dioxygen in the stripping medium and δ_{strip} is the diffusion-layer thickness during stripping. Equation 6 thus has to be modified

$$t_{strip} \propto D_{Se(IV)} [Se(IV)] t_{el} A \delta_{el}^{-1} / (i_{strip} - i_O) \quad (8)$$

or, if all experimental parameters except stripping current are kept constant,

$$t_{strip} \propto 1/(i_{strip} - i_O) \quad (9)$$

The validity of Eqn. 9 was examined by processing the test solution according to the procedure for digested whole blood as described above. Stripping was done in the stripping medium, the stripping current being varied between 0.4 and 5 μA. By plotting t_{strip} vs. i_{strip}, a linear relationship was obtained for $i_{strip} > 3$ μA, which on extrapolation yielded a value of 0.22 μA for i_O, the same value being obtained by least-squares regression using Eqn. 9.

The practical implication of Eqn. 9 is that the stripping current must be considerably higher than the current needed for the reduction of reducible species in the stripping medium in order to diminish the influences from fluctuations in the latter. Thus in stripping media with a high content of dissolved dioxygen, it is necessary to exploit very rapid reduction reactions. Because the reduction of mercury(II) selenide is highly reversible, this is not a problem in the present study. For less reversible reactions, the concentration of reducible species in the stripping medium must be lowered, e.g., by using concentrated salt solutions such as 5 M calcium chloride [8]. In such solutions, the dissolved dioxygen content is very low, as is the diffusion coefficient, owing to the high viscosity (cf. Eqn. 7).

Linear range

The linear range was investigated by processing solutions containing 5 M hydrochloric acid, 2 mg l^{-1} mercury(II) and 0.1—5 μg l^{-1} selenium(IV) according to the procedure described above for digested milk powder. A linear relationship between stripping time and concentration was obtained up to 1.5 μg l^{-1} selenium(IV). By decreasing the sample electrolysis time, the linear range could be expanded accordingly.

The same experiments were repeated without the addition of 2 mg l^{-1} mercury(II) to the sample solution. No increase in linear range was observed. This indicates that formation of mercury(II) selenide is solely a surface reaction. Mercury(II) is added in the procedures described above only in order to improve the reproducibility.

Improved linear range can, however, be achieved by accumulating a number of stripping curves in the computer, each curve being obtained after a short period of electrolysis in the sample. Because the selenium(IV) concentration in the acid digests of this study was always within the linear range, this possibility was not exploited.

Effect of deposition potential and concentration of hydrochloric acid on sensitivity

The effect of deposition potential on sensitivity was investigated by processing the test solution according to the procedure described above for whole blood, using deposition potentials between —0.10 and —0.50 V. Maximum response was obtained at potentials above —0.20 V and no response was obtained below —0.40 V. The experiment was repeated at a constant deposition potential of —0.20 V and with hydrochloric acid concentrations in the range 2—6 M. The sensitivity increased with increasing concentration of hydrochloric acid as is shown in Fig. 1 (cf. Eqn. 1). Hydrochloric acid concentrations above 6 M could not be investigated owing to rapid deterioration of the carbon fibre sensor, probably caused by reactions between the PVC tube and the strong hydrochloric acid.

It is beyond the scope of this paper to elucidate in detail which equilibria in the $Se/Hg/Cl^-/e^-/H^+$ system are involved in the electrochemical determination of selenium. This will, however, be the subject of a separate study using the HALTAFALL program [9], with which both redox and precipitation equilibria can be taken into consideration.

Long-term stability of the carbon fibre sensor and the use of Triton X-100

The long-term stability of the carbon fibre sensor was investigated by means of consecutive electrolysis/stripping cycles in an acid digest of milk powder reference sample CRM 150. Although there were slight individual

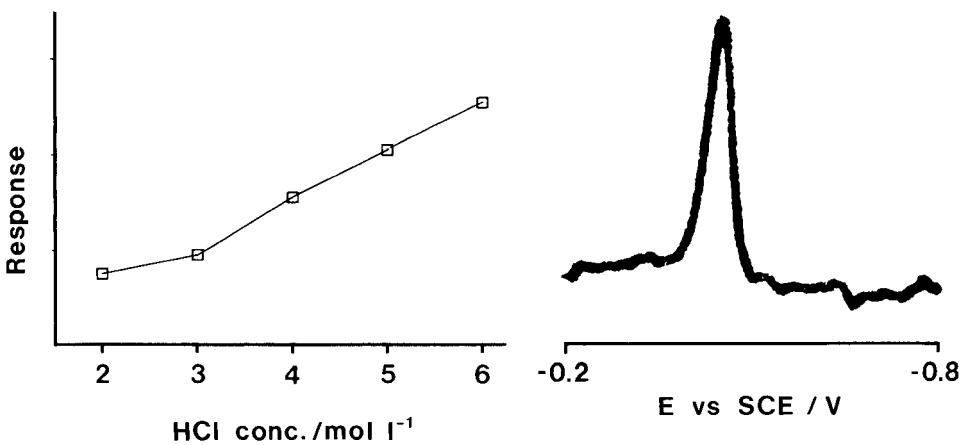

Fig. 1. Effect of hydrochloric acid concentration on the stripping time. Electrolysis for 60 s at —0.20 V vs. SCE in a solution containing 2 mg l^{-1} mercury(II) and 2 μg l^{-1} selenium(IV). Constant-current stripping in 2 M magnesium chloride containing 0.20 M hydrochloric acid and 0.3% (v/v) Triton X-100. Response is in arbitrary units.

Fig. 2. Constant-current stripping curve, dt/dE vs. E, obtained after 15 s of electrolysis at —0.20 V vs. SCE in digested whole blood sample A. The stripping medium is the same as in Fig. 1.

variations between electrodes, most of the electrodes tested could be used for more than 500 electrolysis/stripping cycles. Removal of the mercury film between stripping cycles at the mildly oxidizing potential of 0.02 V increased the long-term stability. This is probably due to simultaneous removal of organic matter adsorbed on the electrode surface.

Without the addition of Triton X-100 to the stripping solution, a split selenium stripping peak was sometimes obtained. Although the total area under the split peak yielded correct values for the stripping time, the formation of a split peak interfered with the peak-searching routines in the controlling computer program. Thus, in order to obtain accurate results in a fully automated procedure, it is necessary to add Triton X-100 to the stripping solution.

Interferences and reproducibility

Interference from elements previously reported to interfere in the batch electrochemical stripping determination of selenium(IV) was examined by processing the test solution according to the procedure for digested whole blood, before and after the addition of the interfering element. The results are summarized in Table 1, together with the reproducibility of consecutive electrolysis/stripping cycles.

As is apparent from Table 1, none of the elements investigated interfered significantly with the determination of selenium(IV). This is, of course, a consequence of the flow approach used in this study: the interfering elements are not present in the stripping medium. The reduction of these elements does thus not interfere with the reduction of mercury(II) selenide, which would have been the case in a batch system (cf. Eqns. 7 and 8.)

Analysis of milk powder and whole blood

The constant-current stripping curve obtained in the analysis of whole blood sample A is shown in Fig. 2. The results from eight analyses of the milk powder reference substances and the three whole blood samples, previously analyzed by neutron activation, are summarized in Table 2. From this it can be seen that the constant-current stripping technique yields lower

TABLE 1

Interference study on ions known to interfere with the electrochemical stripping of selenium(IV) in batch analysis

Metal ion M	Concentration ratio Se(IV):M	Recovery ± s.d. (n = 5) (%)
As(III)	1:10	103.4 ± 6.3
Cu(II)	1:100	95.6 ± 8.8
Fe(III)	1:100	99.5 ± 3.1
Zn(II)	1:100	99.0 ± 8.4
Pb(II)	1:100	105.6 ± 9.2

TABLE 2

Results obtained for reference samples

Reference sample	Type of sample	Selenium content			
		Certified value ($\mu g\ kg^{-1}$)	Neutron activation value ($\mu g\ l^{-1}$)	Value found ± s.d. (n = 8)	
				($\mu g\ kg^{-1}$)	($\mu g\ l^{-1}$)
CRM 150	Milk powder	127	—	123 ± 9	
CRM 151	Milk powder	125	—	119 ± 15	
CRM 063	Milk powder	88	—	73 ± 11	
A	Whole blood	—	82		76 ± 8
B	Whole blood	—	53		44 ± 6
C	Whole blood	—	96		88 ± 16

values than those obtained by other techniques. For four of the six samples, however, the difference is less than one standard deviation of the value obtained by the stripping method. If the relative uncertainty of the reference values is assumed to be 5%, all six values are in agreement within one standard deviation of the techniques.

REFERENCES

1 R. W. Andrews and D. C. Johnson, Anal. Chem., 47 (1975) 294.
2 R. W. Andrews and D. C. Johnson, Anal. Chem., 48 (1976) 1056.
3 S. B. Adeloju, A. M. Bond and M. H. Briggs, Anal. Chem., 56 (1984) 2397.
4 S. Forbes, G. P. Bound and T. S. West, Talanta, 26 (1979) 473.
5 Huang Huiliang, Chi Hua, D. Jagner and L. Renman, Anal. Chim. Acta, 193 (1987) 61.
6 L. Renman, D. Jagner and R. Berglund, Anal. Chim. Acta, 188 (1986) 137.
7 D. Jagner, Analyst, 107 (1982) 593.
8 H. Eskilsson, D. Jagner and C. Haraldsson, Anal. Chim. Acta, 175 (1985) 79.
9 N. Ingri, W. Kakotowicz, L. G. Sillen and B. Warnqvist, Talanta, 14 (1967) 1261.

Analytica Chimica Acta, 197 (1987) 265—273
Elsevier Science Publishers B.V., Amsterdam — Printed in The Netherlands

DETERMINATION OF URANIUM(VI) IN SEAWATER BY MEANS OF AUTOMATED FLOW CONSTANT-CURRENT CATHODIC STRIPPING AT CARBON FIBRE ELECTRODES

CHI HUA, DANIEL JAGNER* and LARS RENMAN

Department of Technical Analytical Chemistry, Chemical Centre, University of Lund, P.O. Box 124, S-221 00 Lund (Sweden)

(Received 9th December 1986)

SUMMARY

Uranium(VI) is determined in an automated flow system by means of constant-current reductive stripping with a mercury film-coated carbon fibre electrode and catechol as adsorptive reagent at pH 8.6. Interference from iron(III) is eliminated by addition of sulphite. Increased linear range between stripping signal and sample uranium(VI) concentration can be obtained by adding, in the computer, several stripping curves, each obtained after a short period of adsorptive accumulation. It is shown that the hanging mercury drop electrode can be used for the determination of uranium(VI) by means of computerized constant current stripping without the need for inert gas bubbling. The results obtained for uranium(VI) in two reference seawater samples, NASS-1 and CASS-1, were 2.90 and 2.68 $\mu g\ l^{-1}$ with standard deviations ($n = 8$) of 0.57 and 0.75 $\mu g\ l^{-1}$, respectively.

Because of the importance of uranium in the nuclear industry, the electrochemical properties of this element have been thoroughly investigated. For the electrometric determination of uranium(VI), at the $\mu g\ l^{-1}$ level, however, very few methods are sufficiently sensitive. One of these exploits the catalytic current in nitrate medium [1] and the others are based on cathodic stripping subsequent to adsorptive accumulation on the working electrode surface. For adsorptive preconcentration of uranium(VI) complexes on the hanging mercury drop electrode (HMDE), tributyl phosphate, tripropyl phosphate [2] and diisopropylmethyl phosphate [3] have been used. Uranium(VI) has also been determined after adsorption onto glassy carbon electrodes coated with trioctylphosphine oxide [4, 5]. The most sensitive methods are, however, based on the adsorption of the uranium(VI)/pyrocatechol complex as first discussed by Matysik [6]. This method was later refined and applied in the analysis of natural waters by Lam et al. [7] and by van den Berg and Huang [8], using differential-pulse cathodic stripping voltammetry on the HMDE. Because this technique demands sample deoxygenation, and because the HMDE is difficult to incorporate into a flow cell with a small dead volume, the procedure is, however, rather difficult to automate. It was thus decided to investigate if the differential-pulse technique could be converted to a

0003-2670/87/$03.50

constant-current stripping technique by using a mercury film electrode as has been previously shown to be possible for the determination of nickel(II) and cobalt(II) [9] and of molybdenum(VI) [10]. When used in connection with computerized flow instrumentation [11] and with carbon fibre as substrate for the mercury film [12], the method can be made highly automated. Furthermore, the computerized approach would make it possible to overcome a major general problem in adsorptive stripping voltammetry, namely, the non-linear relationship between stripping signal and sample concentration of analyte at high analyte concentrations or long adsorptive accumulation times. By adding, in the computer, several constant-current stripping scans, each obtained after a short period of adsorptive accumulation, the linear range with respect to sample concentration of analyte and total period of adsorptive accumulation can be increased considerably.

EXPERIMENTAL

Flow electrodes and instrumentation

A 10-μm carbon fibre inserted perpendicularly to the flow direction in a 30-mm PVC tube with an inner diameter of 0.5 mm was used as working electrode [12]. The platinum tube counter electrode [12] and the thin-layer saturated calomel reference (SCE) electrode [11] were mounted downstream from the working electrode. All potentials given below are versus the SCE.

A Princeton Applied Research static mercury drop electrode (Model 303 SMDE) with a drop diameter of 0.62 mm was used in the comparison between mercury film and mercury drop electrodes.

The computerized flow potentiometric stripping analyzer described in detail elsewhere [11] was used in all experiments. In this analyzer, six different solutions can be sucked, in random choice order, through the flow electrodes. The flow rate, electrode potential, stripping current magnitude, opening and closing of magnetic valves and potential measurement rate are under computer control. During stripping, the computer registers the potential (E) vs. time (t) transient and, after background subtraction and digital filtration, locates and integrates the stripping peak on the dt/dE vs. E transform of the stripping curve and then displays the results on a printer/plotter and a strip-chart recorder [11]. After the processing of a sample and of a sample containing a standard addition of uranium(VI), the computer program evaluates and reports the sample concentration of uranium(VI), using the normal equations for standard addition.

The experimental parameters used in this investigation were, unless otherwise stated: reductive current 0.9 μA, flow rate 1 ml min^{-1}, potential measurement rate 25.6 kHz, averaging filter 0.030 V, Savitzky-Golay filter 0.015 V, peak-searching potential range —0.62 to —0.82 V, and peak integration width 0.20 V around the located peak potential. For all measurements and calculations, a potential resolution of 0.001 V was used.

Reagents

All reagents were of analytical grade. Stock solutions of metal ions (1 mg l^{-1}) were prepared by diluting atomic absorption spectrometry standards (Janssen Chimica) with Millipore-Q water. A stock buffer solution (1 M) was prepared by dissolving piperazine-*N*,*N*′-bis-2-ethanesulphonic acid (PIPES) and sodium hydroxide in a molar ratio of 1:1 in 0.50 M ammonia. Catechol stock solution (0.1 M) was obtained by dissolving catechol in Millipore-Q water.

Seawater reference samples from off Southeast Bermuda (NASS-1) and off Halifax Harbour (CASS-1) were purchased from the National Research Council of Canada.

Procedure used for the determination of uranium in seawater

Nitric acid was added to 30 ml of seawater to reach a pH of 2 and the mixture was treated ultrasonically in order to expel carbon dioxide. The PIPES buffer was added to a total concentration of 0.01 M and the pH was adjusted to 7.5 with sodium hydroxide after which 30 mg of sodium sulphite was added followed by catechol to a total concentration of 0.002 M. Finally the pH was adjusted to 8.6. The same sample preparation was used for a seawater sample spiked with 5 μg l^{-1} uranium(VI). The two solutions were then placed at two inlets of the flow analyzer, three of the other four inlets being used for a mercury plating solution consisting of 200 mg l^{-1} mercury(II) nitrate in 0.1 M nitric acid, a cleaning solution consisting of 1 M sodium hydroxide in 50% (v/v) ethanol, and Millipore-Q water.

In the initial step of the computerized procedure, the mercury plating solution was allowed into the cell and a potential of 0.60 V was applied for 15 s in order to remove the mercury film from the previous run. Then a fresh mercury film was plated onto the carbon fibre, the potential vs. time sequence being −0.10 V for 2 s, −0.40 V for 10 s, −0.90 V for 10 s, −0.10 V for 2 s, −0.40 V for 10 s, −0.90 V for 10 s and finally −1.30 V for 30 s.

The unspiked sample was then allowed into the cell and a potential of −0.10 V was applied for 100 s prior to stripping in the sample. Stripping was terminated at a potential of −1.20 V and after 5 s at this potential the adsorption potential of −0.10 V was again applied for 1 s after which the background was recorded. Finally, the electrodes were rinsed with the cleaning solution at a potential of −0.10 V for 90 s and with Millipore-Q water until the next run. The spiked sample was processed in the same way except that the time for adsorptive accumulation was decreased from 100 s to 40 s.

RESULTS AND DISCUSSION

Composition of stripping solution

In previous applications based on constant-current stripping after adsorptive accumulation, stripping media containing high concentrations (5 M) of calcium chloride were exploited [9, 10]. The reason for this was that such media contain only low concentrations of dissolved dioxygen and that the

high viscosity of these solutions enabled the diffusional transport of dioxygen to the electrode surface during stripping to be kept very small. Consequently, most of the reductive current applied during stripping was involved in the reduction of the adsorbed species and only a minor part in the reduction of reducible species diffusing to the electrode during stripping. In connection with the constant-current reductive stripping of mercury(II) selenide, however, it was found that constant-current stripping was also possible in solutions with a high content of dissolved dioxygen, provided that the reduction process at the electrode surface was not rate-limiting [13]. For this reason, initial experiments were directed at reducing the uranium(VI)/catechol complex in the sample solution, thus avoiding the extra time needed for medium exchange. These experiments were successful, and so no attempts were made to investigate other possible stripping media. In this connection, it might be noted that stripping medium exchange is not as advantageous in adsorptive stripping as it is in potentiometric or constant-current stripping of amalgamated elements. The reason for this is that in adsorptive stripping the stripping potential is not affected by complexation reactions in the same straightforward way as in stripping of amalgamated metals [14]. Consequently, overlapping adsorptive stripping peaks can normally not be resolved simply by adding a suitable complexing agent to the stripping medium.

Reduction mechanism, effect of pH, catechol concentration, and adsorptive deposition potential

The reduction mechanism and the solution equilibria in the uranium(VI)/catechol system were investigated by van den Berg and Huang [8]. Their results were confirmed in the present study. The effects of variations in pH, total catechol concentration and adsorptive deposition potential are shown in Fig. 1(a—c). In these investigations, a 0.50 M sodium chloride solution containing 10 $\mu g\ l^{-1}$ uranium(VI), 0.01 M PIPES and 0.1% (w/w) sodium sulphite was electrolyzed for 30 s prior to stripping.

Linear range and precision

The linear range was investigated by analyzing the reference seawater NASS-1 according to the procedure described above and varying the time for adsorptive accumulation between 0 and 120 s. The results are shown in Fig. 1(d). The same seawater sample was also analyzed after standard additions of 0—10 $\mu g\ l^{-1}$ uranium(VI) and at a fixed time of adsorptive accumulation of 40 s. From these experiments, it was concluded that the relationship between stripping time and sample concentration of uranium(VI) was linear as long as the product of the time for adsorptive accumulation and sample uranium(VI) concentration was less than 400 s $\mu g\ l^{-1}$. Because the uranium(VI) concentration in seawater is less than 5 $\mu g\ l^{-1}$ it was concluded that, provided that the time for adsorptive accumulation in the uranium(VI) spiked sample was decreased from 100 s to 40 s, all data should lie within the linear range.

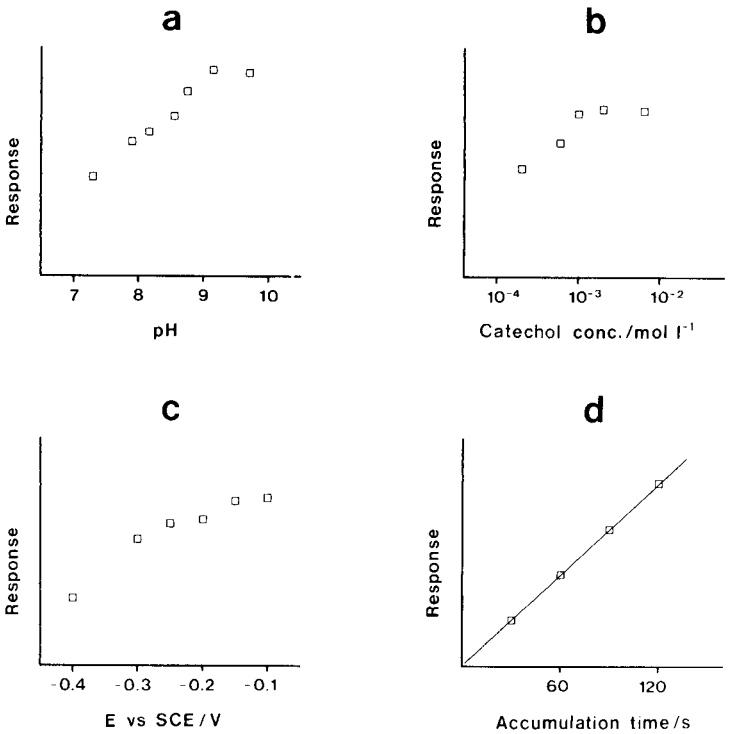

Fig. 1. Effect of pH (a), total catechol concentration (b), adsorptive accumulation potential (c) and time of adsorptive accumulation (d) on the stripping signal in a 0.50 M sodium chloride solution containing 10 μg l^{-1} uranium(VI). When not subject to variations, the pH, total catechol concentration, adsorptive accumulation potential and time were 8.4, 0.002 M, −0.10 V and 30 s, respectively. For (d), the reference seawater sample NASS-1 was used instead of the 0.50 M sodium chloride solution, and the pH was 8.6. Responses are given in arbitrary units.

The non-linear relationship between stripping signal and analyte concentration typical of adsorptive stripping is illustrated in Fig. 2. Here a 0.50 M sodium chloride solution was pretreated in the same way as described for seawater, and then analyzed with (Fig. 2a) and without (Fig. 2b) computer-accumulated stripping scans. In Fig. 2(a), the time for adsorptive accumulation was 10 s prior to stripping and background subtraction, as described for the seawater samples. Seven such background-corrected scans were accumulated in the computer memory after which the peak area was evaluated. In Fig. 2(b), the time for adsorptive accumulation was 70 s and the peak area from a single scan was evaluated. The two procedures were repeated after standard additions of 20, 50, 80 and 120 μg l^{-1} uranium(VI). As can be seen from Fig. 2, the linear range can be expanded considerably by accumulating several scans, each scan being obtained after a short period of adsorptive accumulation.

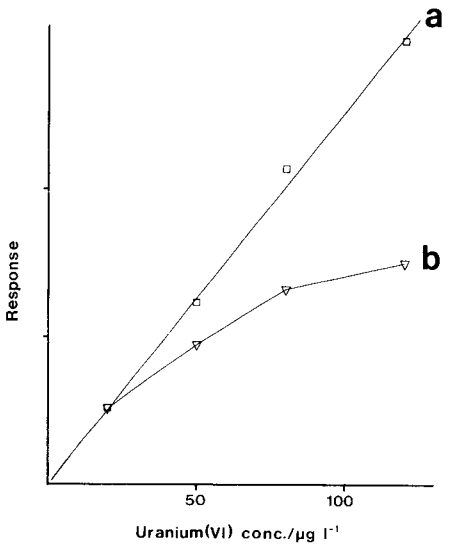

Fig. 2. Extension of linear range by means of computer-accumulated stripping scans in 0.50 M sodium chloride containing 0.002 M catechol and 0.01 M PIPES buffer at pH 8.6. Curves: (a) seven accumulated background-corrected scans obtained after 10-s adsorptive accumulation at —0.10 V for each scan; (b) background-corrected curve obtained from a single scan after 70-s adsorptive accumulation at —0.10 V. Responses are given in arbitrary units.

A 0.50 M sodium chloride solution to which 3.0 $\mu g\ l^{-1}$ uranium(VI) had been added was analyzed by the above procedure for seawater. Ten consecutive analyses yielded a mean value for uranium(VI) of 3.14 $\mu g\ l^{-1}$ with a standard deviation of 0.36 $\mu g\ l^{-1}$. No measurable amounts of uranium(VI) were found in the unspiked sodium chloride sample.

Possible interferences

Possible interferences from Bi(III), Fe(III), Sn(IV), Cd(II), Zn(II), Sb(V), V(V), Pb(II) and Cu(II) were investigated by adding these species to 0.50 M sodium chloride. Only lead(II) gave a stripping peak close to that of uranium(VI). The sensitivity for lead(II) was, however, much less than that for uranium(VI) and measurable stripping peaks for lead(II) were obtained only at concentrations exceeding 1 $\mu g\ l^{-1}$. The interference from iron(III) was eliminated by the addition of sulphite.

Organic surfactants naturally present in seawater can interfere with the determination of uranium(VI) by means of adsorptive competition. Triton X-100 is often used as a model for such surfactants and it has been shown that some coastal waters contain surfactants equivalent to 0.01—0.05 $mg\ l^{-1}$ Triton X-100 [8]. When 0.50 M sodium chloride was substituted for seawater and analyzed according to the procedure for seawater described above, after the addition of 3 $\mu g\ l^{-1}$ uranium(VI), it was found that the addition of 1 $mg\ l^{-1}$

Triton X-100 decreased the stripping signal by 20%. The stripping peaks were, however, reproducible and the uranium(VI) concentration could be determined by means of standard additions.

Uranium(VI) in seawater

The seawater reference samples NASS-1 and CASS-1 were analyzed for uranium(VI) as described above. Figure 3 shows the stripping curves obtained for NASS-1 before (curve a) and after (curve b) the standard addition of 5 $\mu g\ l^{-1}$ uranium(VI), the time for adsorptive accumulation being 100 and 40 s, respectively.

Eight consecutive analyses of the two reference samples yielded an average value of 2.90 $\mu g\ l^{-1}$ for NASS-1 and 2.68 $\mu g\ l^{-1}$ for CASS-1, the standard deviations being 0.57 and 0.75 $\mu g\ l^{-1}$, respectively. No certified values exist for uranium(VI) in NASS-1 and CASS-1. The values obtained do, however, agree with reports indicating that the normal value of uranium(VI) in 3.5% salinity seawater is 3.3 $\mu g\ l^{-1}$ [8, 15].

Comparison between mercury film and HMDE

Because most adsorptive stripping experiments are done with the HMDE and differential-pulse stripping techniques, and because this investigation had shown that constant-current stripping can be applied in non-deoxygenated sample solutions, the performance of the HMDE in reductive constant-current stripping was investigated. In these experiments, 100 ml of 0.50 M sodium chloride was spiked with 3 $\mu g\ l^{-1}$ uranium(VI) and pretreated in the same way as the seawater samples above. The experimental conditions were the same as those for seawater with the exception that the procedure for renewal of the mercury film was replaced by manual extrusion of a new mercury drop and that the stripping current was 10 μA.

For the first experiment, quiescent solution was used with a 100-s period for adsorptive accumulation. The results obtained on the strip-chart recorder and printer/plotter are shown in Fig. 4(a) and (b). In the second experiment, a magnetic stirrer was operated for 60 s and stripping was initiated 40 s after the stirrer had been stopped (Fig. 4c and d).

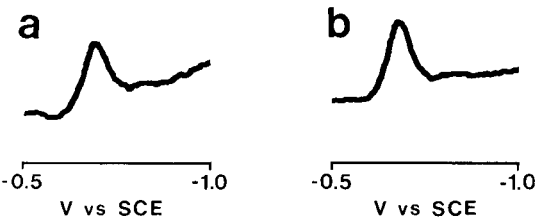

Fig. 3. Constant-current stripping peaks obtained in the analysis of reference seawater NASS-1 before (a) and after (b) the standard addition of 5 $\mu g\ l^{-1}$ uranium(VI). Adsorptive accumulation at —0.10 V for 100 s (a) and 40 s (b).

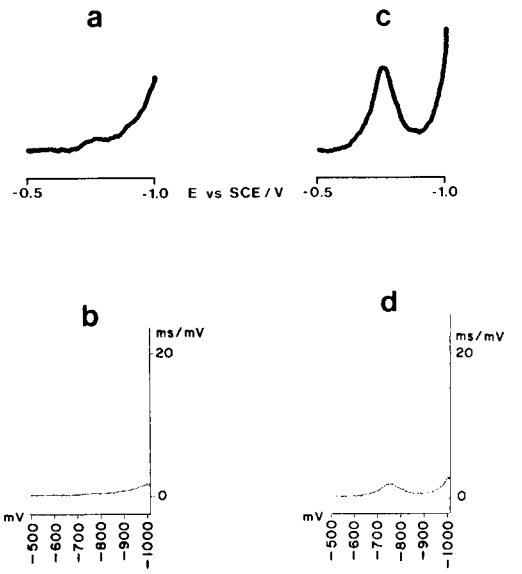

Fig. 4. Constant-current stripping in 0.50 M sodium chloride containing 0.002 M catechol, 0.01 M PIPES buffer and 3 $\mu g\ l^{-1}$ uranium(VI) at the HMDE. Curves: (a, b) adsorptive accumulation in quiescent solution at −0.10 V for 100 s; (c, d) adsorptive accumulation at −0.10 V for 60 s in stirred solution and then for 40 s in quiescent solution. Curves (a) and (c) were obtained on a strip-chart recorder; (b) and (d) are the same data obtained on a printer/plotter.

From Fig. 4 it can be seen that constant-current stripping for uranium(VI) is indeed possible in non-deoxygenated solutions. It can also be seen, by comparison with Fig. 3, that the sensitivity with the HMDE is similar to that of the carbon fibre electrode provided that mass transport to the electrode surface is enhanced by means of stirring. It can also be seen that the peak potentials for the two electrodes are approximately the same.

Although not yet fully proven, these results imply that computerized constant-current stripping might be used to eliminate the need for deoxygenation in adsorptive stripping with the HMDE. Results obtained in the adsorptive stripping determination of iron(III) using solochrome violet RS as the reagent and the HMDE as the working electrode in non-deoxygenated solution clearly indicates this possibility also in solutions not containing sulphite; details of this procedure will be reported later. Obviously, it would also make it possible to increase the linear range by means of accumulating several stripping scans as described for the carbon fibre electrode.

REFERENCES

1 J. V. Collat and J. J. Lingane, J. Am. Chem. Soc., 76 (1954) 4214.
2 H. Berge and H. Ringsrtorff, Anal. Chim. Acta, 55 (1971) 193.

3 H. Sohr and L. Liebetrau, Fresenius' Z. Anal. Chem., 219 (1966) 409.
4 K. H. Lubert, M. Schnurrbusch and A. Thomas, Anal. Chim. Acta, 144 (1982) 123.
5 K. Izutse, T. Nakamura, R. Takizawa and H. Hanawa, Anal. Chim. Acta, 149 (1983) 147.
6 J. Matysik, Ann. Univ. Mariae Curie-Sklodowska, Sect. AA, 21 (1966) 31.
7 N. K. Lam, R. Kalvoda and M. Kopanica, Anal. Chim. Acta, 154 (1983) 79.
8 C. M. G. van den Berg and Z. Q. Huang, Anal. Chim. Acta, 164 (1984) 209.
9 H. Eskilsson, D. Jagner and C. Haraldsson, Anal. Chim. Acta, 175 (1985) 79.
10 Chi Hua, D. Jagner and L. Renman, Anal. Chim. Acta, 192 (1987) 103.
11 L. Renman, D. Jagner and R. Berglund, Anal. Chim. Acta, 188 (1986) 137.
12 Huang Huiliang, Chi Hua, D. Jagner and L. Renman, Anal. Chim. Acta, 193 (1987) 61.
13 Chi Hua, D. Jagner and L. Renman, Anal. Chim. Acta, 197 (1987) 257.
14 D. Jagner, Analyst, 107 (1982) 593.
15 T. H. Ku, K. G. Knauss and G. G. Mathieu, Deep-Sea Res., 24 (1977) 1005.

Analytica Chimica Acta, 197 (1987) 275—280
Elsevier Science Publishers B.V., Amsterdam — Printed in The Netherlands

Short Communication

ISODIFFERENTIAL DERIVATIVE APPROACH TO THE SPECTROPHOTOMETRIC DETERMINATION OF NICKEL AND COBALT MIXTURES

F. GARCIA SANCHEZ*, M. HERNANDEZ LOPEZ and J. C. MARQUEZ GOMEZ

Department of Analytical Chemistry, Faculty of Sciences, The University, Malaga-29071 (Spain)

(Received 12th May 1986)

Summary. A graphical method for measuring derivative amplitudes in binary mixtures with overlapping spectra is described. The method is based on the interference-free character of the isodifferential points in the derivative calibration graphs. Cobalt and nickel mixtures are analyzed in the range 0.01—2.5 $\mu g\ ml^{-1}$ by the formation of coloured chelates with benzyl-2-pyridylketone 2-pyridylhydrazone, with relative standard deviations $\leqslant 1.5\%$.

Several very sensitive reagents have been proposed for the individual spectrophotometric determination of nickel and cobalt. However, determination of both in a mixture is often troublesome because of the considerable overlap between their broad absorption spectra [1]. Generally, the resolution of such binary mixtures requires the measurement of total absorbance at two wavelengths and solving a set of simultaneous equations. Derivative spectra, however, provide additional possibilities in this respect. Derivative spectrophotometry enhances the detectability of minor spectral features; its consequent capability to discriminate between closely related spectral features make it useful in several areas of analytical spectrometry [2, 3]. Recently the use of rapid "scanning" diode-array spectrophotometers [4, 5] giving digital data output, offers new possibilities for the resolution of mixtures [6], particularly when combined with modern liquid chromatography [7, 8]. Several approaches have been used in the above reports for the quantitative evaluation of the derivative amplitudes of analyte solution mixtures with closely related spectral shapes, generally based on trial and error.

The model used in this paper is based on the fact that Beer's Law is obeyed for the nickel and cobalt complexes of a particular ligand in the concentration range studied, and therefore is also obeyed for the total absorbance. The derivative absorbances (first and second) of a compound band are also the sum of its component derivative absorbances.

0003-2670/87/$03.50

Experimental

Apparatus and reagents. Spectral measurements were made with a Shimadzu UV-240 Graphicord recording spectrophotometer in 1-cm quartz cells. The spectra were obtained with a spectral bandwidth of 0.5 nm, a scanning speed of 3 nm s^{-1} and recording chart speed of 10 nm cm^{-1}. First and second derivative ultraviolet spectra were obtained with a Shimadzu derivative spectrum attachment with optional program/interface (model OPI-2) giving first to fourth derivatives, $\Delta\lambda$ 1, 2 and 4 nm.

The synthesis of benzyl-2-pyridylketone 2-pyridylhydrazone (BPKPH) was as reported previously [9]. Solutions (1×10^{-3} M) were prepared weekly by dissolving 0.0288 g of BPKPH in 100 ml of absolute ethanol. A 0.1 M nickel stock solution was prepared from nickel nitrate hexahydrate and standardized gravimetrically with dimethylglyoxime. Cobalt stock solution (0.1 M) was prepared from cobalt nitrate hexahydrate and standardized by EDTA titration (xylenol orange indicator). Working solutions were prepared by appropriate dilutions with water. A pH 9.0 buffer solution was prepared from 0.1 M boric acid and 0.1 M sodium hydroxide. Unless otherwise stated, the reagents used were of analytical-reagent grade. Distilled, demineralized water was used throughout.

Determination of binary mixtures. Place an aliquot of a sample containing 0.25—1.001 μg ml^{-1} cobalt and 0.5—2.00 μg ml^{-1} nickel into a 10-ml volumetric flask. Add 5 ml of 1×10^{-3} M BPKPH ethanolic solution and 2 ml of pH 9.0 borate buffer and dilute to the mark with deionized water. Record the first-derivative spectrum between 400 and 550 nm against a reagent blank, with $\Delta\lambda$ = 4 nm, at a scanning speed of 3 nm cm^{-1}. Measure the first-derivative analytical value as the vertical difference in the absorbance change (dA) scale from the corresponding iso-differential point (λ_1 = 483 nm for nickel, λ_2 = 453 nm for cobalt) to the intersection with the first-derivative curve. The concentration of nickel and cobalt in the sample is found from calibration graphs previously run under the same conditions as those for the mixture.

Results and discussion

BPKPH behaves as a sensitive chromogenic ligand for several metal ions [10]. Under alkaline conditions, the ligand is tridentate and the complexes, formed with the anionic form of the ligand, are only sparingly soluble in water. The chelates are soluble, however, if the medium contains sufficient ethanol. BPKPH reacts with cobalt(II) to form a yellow-orange complex with absorption maximum at 483 nm, over the pH range 2—13.5 [10]. The complexation of BPKPH with nickel occurs in a narrower pH range; maximal and constant absorbance is obtained in the pH range 10—13 at the absorption maximum of 453 nm. In 50% ethanol, chelate formation is complete with both metals after addition of borate buffer of pH 9.0, with a five-fold molar excess of BPKPH. Colour development is instant and the colour is stable for at least 4 h. Slight variations in absorbance can be obtained by modifying the

concentration of ethanol on the medium. No changes in absorbance were observed when the order of addition of the reagents was changed. A mole ratio plot shows that the mole ratio of cobalt or nickel to BPKPH at pH 10.40 is 1:2.

Figure 1A shows the spectra obtained for the nickel and cobalt complexes. The absorption spectrum of the 1:1 metal ion mixture consists of a broad band which is the sum of the individual components, and which does not allow discrimination between the components. The first derivatives of these spectra are shown in Fig. 1B. Again, the severe overlap of the derivative spectra makes it difficult to determine each metal ion. Suitable selection of the wavelength from which the derivative amplitudes are measured, however, allows accurate determination of nickel and cobalt in mixtures from the first-derivative spectra, as will be demonstrated below. Figure 2A shows the absorption spectra of two series of solutions containing increasing concentrations of the BPKPH chelates of nickel and cobalt. Again they emphasize that the closely related spectral behaviour of both chelates provides superimposed spectra at practically all wavelengths and concentration ratios, and individual quantitation is impeded.

The wavelengths of maximum absorption of the chelates are 453 (nickel) and 483 nm (cobalt) at all concentrations. At each wavelength, the change in absorbance dA with changing wavelength is zero for one of the chelates, so that the other component can be determined without interference at that wavelength. This can be seen in Fig. 2B. From Fig. 2A and B it may be inferred that greatest sensitivity would be obtained when the first-derivative

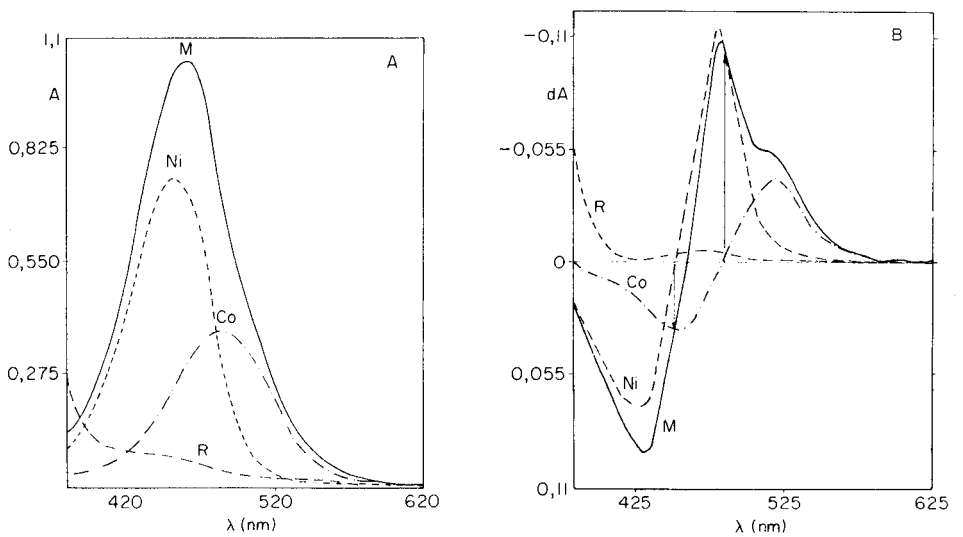

Fig. 1. (A) Absorption spectra of reagent (R), cobalt complex (Co), nickel complex (Ni) and mixtures of cobalt + nickel (1:1) (w:w) complexes (1 μg ml^{-1} Co^{2+} or Ni^{2+}, 5 × 10^{-4} M BPKPH; pH 10.4). (B) First derivatives of the spectra in (A).

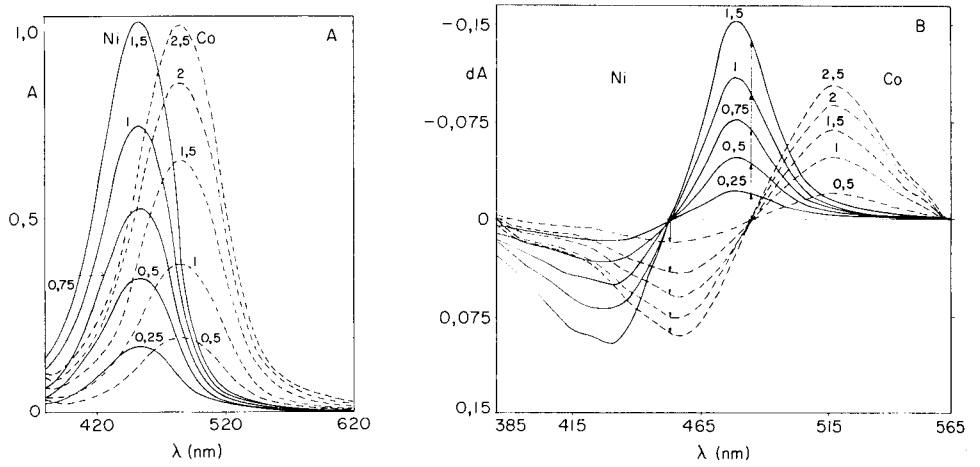

Fig. 2. (A) Absorption spectra of two series of cobalt and nickel complexes at the concentrations ($\mu g\ ml^{-1}$) indicated on the curves (5×10^{-4} BPKPH; pH 10.4). (B) Superimposed first derivatives of the spectra in (A).

amplitude of component 1 is zero at the same wavelength at which the first-derivative amplitude of component 2 is maximal. This condition is satisfied at the wavelength where the first derivative of component 1 is zero and the second derivative of component 2 is zero. In turn, this is satisfied when the wavelength difference between absorption maxima corresponding to both absorbing species is equal to the half band-width of each spectral band.

These considerations are of analytical interest because it becomes possible to predict if two overlapping bands can be measured satisfactorily by using the isodifferential derivative approach. Only a few data about the fundamental spectra of the overlapping compounds are needed, i.e., maximum spectral intensity (A), half band-width at half maximum intensity ($1/2\ B$) and separation between wavelength maxima of both compounds (C).

Although the spectral profiles of two compounds can vary in a broad manner, the considerations can be simplified if the overlapping bands are confined to a decreased spectral zone in which they have a Gaussian profile. On this assumption, the absorbances of bands 1 and 2 are given as a function of λ (wavelength) by

$$I_1(\lambda) = A_1 \exp\left[(-\lambda - C_1)^2/2B_1^2\right] \tag{1}$$

$$I_2(\lambda) = A_2 \exp\left[(-\lambda - C_2)^2/2B_2^2\right] \tag{2}$$

The first derivative of band 1 is expressed as

$$dI_1(\lambda)/d\lambda = \left[-A_1(\lambda - C_1)/B_1^2\right] \exp\left[-(\lambda - C_1)^2/2B_1^2\right] \tag{3}$$

and the second derivative of band 2 as

$$d^2I_2(\lambda)/d\lambda^2 = (A_2/B_2^2)\left\{\left[(\lambda - C_2)^2/B_2^2\right] - 1\right\} \exp\left[-(\lambda - C_2)^2/2B_2^2\right] \tag{4}$$

The maximum sensitivity and precision are obtained in the isodifferential derivative method when the first derivative amplitude of a component is zero. The solutions for $d^2I_2(\lambda)/d\lambda^2 = 0$ and for $dI_1(\lambda)/d\lambda = 0$ are satisfied when $C_1 = \lambda$ and $(\lambda - C_2)/B_2 = 1$, i.e., when $C_1 - C_2 = B_2$. These conclusions are illustrated in Fig. 3, in which two overlapping Gaussian bands are examined for three distinct values of ratios B_1/B_2 and A_1/A_2.

From Fig. 2A it may be seen that the band maxima separation for the nickel and cobalt chelates is 30 nm. The half band-width corresponding to the nickel chelate is 35 nm and that for the cobalt chelate is 40 nm. As $C_1 - C_2 = B_2$ the half band-width must optimally be 30 nm so there is only a small difference from this optimal value in first-derivative amplitude (Fig. 2B).

The dependence of the first- and second-derivative spectra on the instrumental parameters follows the general patterns of derivative spectroscopy [11]. Thus $\Delta\lambda = 4$ nm, a medium scanning speed (3 nm cm^{-1}) and the response time associated with the derivative circuit give satisfactory results.

The calibration graphs prepared by plotting absorbance and dA against nickel and cobalt concentrations (in $\mu g\ ml^{-1}$) were linear for 0—1.25 $\mu g\ ml^{-1}$ and 0—2.25 $\mu g\ ml^{-1}$, respectively. The equations obtained by the least-squares treatment of data for mixtures were $dA = 0.104[Ni] - 0.007$, $r = 0.9994$ ($n = 5$), and $dA = 0.038[Co] - 0.001$, $r = 0.9954$ ($n = 5$). The analytical characteristics are summarized in Table 1.

The results obtained for the determination of each ion in various binary mixtures are shown in Table 2. The method gives satisfactory results.

We thank The Comisión Asesora de Investigación Cientifica y Tecnica for supporting this study (Project No. 3007/83 C02-02).

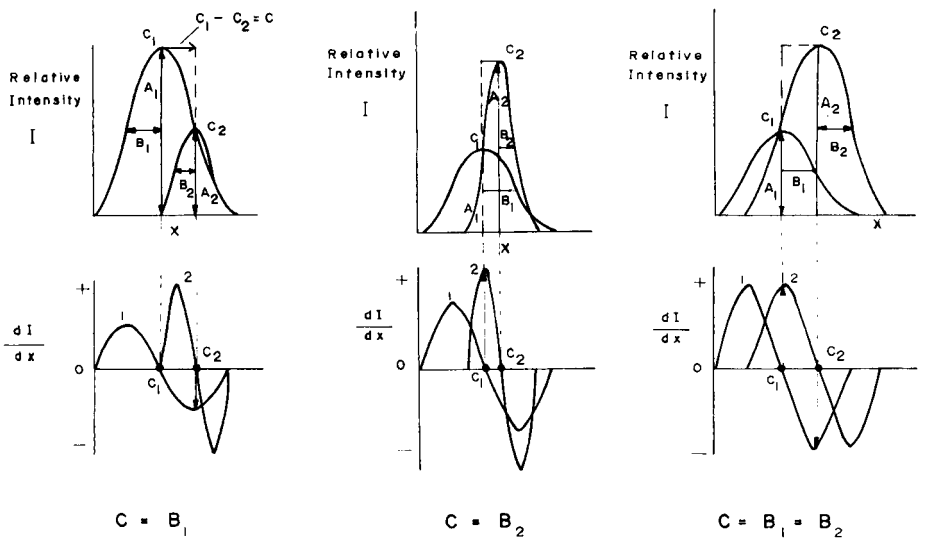

Fig. 3. Effect of band-width and separation between wavelength maxima on the usefulness of the isodifferential derivative approach.

TABLE 1

Characteristics of the first-derivative isodifferential procedure

Metal	Sensitivity[a]	Detection limit[b] ($\mu g\ ml^{-1}$)	Linear range ($\mu g\ ml^{-1}$)	*RSD* (%)
Cobalt	1.05×10^{-3}	0.0138	0.045—2.25	1.34 ($n = 5$)
Nickel	8.00×10^{-4}	0.0065	0.022—1.25	0.75 ($n = 5$)

[a]From slope of calibration graph. [b]3σ value.

TABLE 2

Analysis of binary mixtures of nickel and cobalt

Ratio Ni:Co (w/w)	Nickel ($\mu g\ ml^{-1}$)		Error (%)	Cobalt ($\mu g\ ml^{-1}$)		Error (%)
	Taken	Found[a]		Taken	Found[a]	
1:20	0.100	0.110 ± 0.008	+10.0	2.000	1.995 ± 0.018	−0.2
1:4	0.500	0.494 ± 0.001	−1.2	2.000	2.040 ± 0.034	+2.0
1:2	0.500	0.501 ± 0.021	+0.0	1.000	0.963 ± 0.017	−3.7
1:1	1.000	0.923 ± 0.015	−7.7	1.000	0.963 ± 0.015	−3.7
1:1	0.500	0.520 ± 0.010	+4.0	0.500	0.523 ± 0.013	+4.6
2:1	1.000	1.005 ± 0.002	+0.5	0.500	0.530 ± 0.010	+6.0
7.5:1	1.500	1.485 ± 0.005	−1.5	0.200	0.184 ± 0.015	−8.0
10:1	1.000	0.998 ± 0.012	−0.2			

[a]Mean ± SD of three separate determinations.

REFERENCES

1 Z. Marczenko, Spectrophotometric Determination of Elements, Horwood, Chichester, 1976.
2 G. Talsky, L. Mayring and H. Kreuzer, Angew. Chem., Int. Ed. Engl., 17 (1978) 785.
3 T. C. O'Haver, Anal. Proc., 19 (1982) 22.
4 D. G. Jones, Anal. Chem., 57 (1985) 1057A.
5 D. G. Jones, Anal. Chem., 57 (1985) 1207A.
6 D. T. Rossi and H. L. Pardue, Anal. Chim. Acta, 175 (1985) 153.
7 M. J. Milano and E. Grushka, J. Chromatogr., 133 (1977) 352.
8 B. J. Clark, A. F. Fell, H. P. Scott and D. Westerlund, J. Chromatogr., 286 (1984) 261.
9 J. J. Laserna, A. Navas and F. Garcia Sanchez, Anal. Chim. Acta, 121 (1980) 295.
10 F. Garcia Sanchez, A. Navas, J. J. Laserna and A. Arbaizar, Analyst, 107 (1982) 35.
11 J. Medinilla, F. Ales and F. Garcia Sanchez, Talanta, 33 (1986) 329.

Analytica Chimica Acta, 197 (1987) 281—284
Elsevier Science Publishers B.V., Amsterdam — Printed in The Netherlands

Short Communication

SPECTROPHOTOMETRIC AND SPECTROFLUORIMETRIC DETERMINATION OF IODIDE BY EXTRACTION OF ICl_2^- WITH RHODAMINE B

M. A. AL-HAJJAJI

Department of Chemistry, Faculty of Applied Sciences and Engineering, Umm Al-Qura University, P.O. Box 3711, Makkah Al-Mukarramah (Saudi Arabia)

(Received 12th November 1986)

Summary. Iodide is determined after oxidation with nitrous acid in 5 M hydrochloric acid to ICl_2^-. The ion-pair formed with rhodamine B is extracted into toluene and measured spectrophotometrically ($0.5—5 \times 10^{-5}$ M) or spectrofluorimetrically ($1—10 \times 10^{-6}$ M). The relative standard deviations were 1.8% for the determination of 5×10^{-6} M iodide ($n = 5$) by spectrofluorimetry and 2.3% ($n = 50$) for 1×10^{-5} M iodide by spectrophotometry. Periodate, iodate and iodine responded exactly as iodide.

Iodides are used extensively in the preparation of pharmaceuticals and in photography. Trace amounts of iodide are required by animal and plant life. The determination and separation of macro and micro quantities of iodide were reviewed by Williams [1], while spectrophotometric and spectrofluorimetric procedures have been summarized by Snell [2], Zak [3] and Marczenko [4]. The catalytic activity of iodide is still used in recent literature for the determination of the ion [5, 6]. Iodate can be separated from iodide by extracting tetraphenylarsonium iodide [5].

Basic dyes such as triphenylmethane dyes have been applied for the spectrophotometric determination of different elements after their extraction as ion-pairs from acidic media into organic solvents [7]. The absorbance of the organic layer is measured. The compounds used to extract iodine as triiodide are crystal violet [8], brilliant green [9], neutral red [10], methylene blue [11] and nitron [12, 13]. Iodine in other forms can be extracted with brilliant green (I_2Cl^-, I_2Br^- [14], crystal violet (I_2Cl^- [15]), basic blue K (I_2Br^- [16]) and Nile blue (I^- [17]). Other reagents include the xanthene dyes such as butylrhodamine B [18], rhodamine 6G and rhodamine B [19]. The last two reagents were used to extract iodide at pH 1—5 (rhodamine 6G) and pH 0.5—1.0 (rhodamine B) into benzene/isoamyl acetate. Bromide, sulphide, dichromate and iron(III) interfered. In this report, iodide is oxidized with nitrous acid in 5 M hydrochloric acid to form ICl_2^-, which is extracted into toluene as an ion-pair with rhodamine B. The absorbance or fluorescence of the organic layer is a measure of the iodide concentration.

0003-2670/87/$03.50

Experimental

Apparatus. A Beckman Model 35 u.v./visible double-beam spectrophotometer was used to measure absorbance (at 564 nm). Fluorescence measurements were made with a Perkin-Elmer model MPF-44-B spectrofluorimeter; the excitation and emission wavelengths were 350 nm and 593 nm, respectively, the slit widths were 5 nm (for both excitation and emission) and the signal gain was 1 on the ratio mode. Silica and quartz 10-mm cuvettes were used.

Reagents. Unless otherwise mentioned, all solutions were made with analytical-grade chemicals dissolved in deionized, double-distilled water.

Method. To a 25-ml volumetric flask, add, in the following order, the iodide solution, 2.5 ml of 0.01 M sodium nitrite and 2.5 ml of aqueous 0.02 M rhodamine B. Dilute to the mark with hydrochloric acid so that the final acid concentration is 5 M. Transfer the contents of the flask to a separating funnel and extract with two 5-ml portions of toluene. The extraction must be done in the dark with minimum exposure to light. Measure the absorbance or fluorescence of the extract within 10 min of extraction. Obtain a blank by the same procedure, replacing the iodide solution with distilled water.

Results and discussion

The oxidation of iodide to iodine(I) was discussed by Laitinen [20]. One of the oxidants that can be used is nitrous acid, which was chosen in this investigation as superior to iodate [21] when the interference by reductants is considered. The reaction between iodide and nitrous acid in 5 M hydrochloric acid is [22]:

$$I^- + 2HNO_2 + 2H^+ + Cl^- \rightarrow ICl + 2NO + 2H_2O$$

In this medium, iodine chloride reacts further with chloride to produce ICl_2^-, which has a formation constant of 1.7×10^2 [20]. This anion is extracted into toluene as the ion-pair with rhodamine B.

Effect of solvent. Besides toluene, methyl isobutyl ketone, chloroform, heptane and carbon tetrachloride were tried as possible extractants for the ion-pair. Only toluene was successful. The stability of the complex in the organic layer was followed spectrophotometrically. The absorbance decreased with time. This decrease was faster on exposure to light; the organic layer lost 37% of its absorbance in 1 h compared to a 16% loss for the same period in the dark. The composition of the ion-pair was established spectrophotometrically by Job's method of continuous variation [23] to be 1:1 ($C_{25}H_{33}N_2O_3^+ \cdot ICl_2^-$).

Effect of reagents. The effect of hydrochloric acid concentration was investigated because of its importance in the formation of iodine chloride and its chloride complex and in the lowering of the blank signal as it protonates the organic dye preventing its transfer to the organic layer except as the ion-pair; 5 M hydrochloric acid was optimum in this respect. The optimum

TABLE 1

Effect of various ions (1×10^{-4} M) on the determination of 0.250 μmol of iodide by the spectrophotometric method

Ion	Found[a]	Relative[b] error (%)	Ion	Found[a]	Relative[b] error (%)
Br^-	0.255	2.0	Al^{3+}	0.244	−2.4
BrO_3^-	0.248	−0.8	Ba^{2+}	0.260	4.0
Cl^-	0.253	1.2	Ca^{2+}	0.250	0.0
ClO_3^-	0.260	4.0	Cd^{2+}	0.244	−2.4
ClO_4^-	0.295	18.0	Co^{2+}	0.255	2.0
F^-[c]	0.244	−2.4	Cu^{2+}	0.257	2.8
SCN^-[c]	0.285	14.0	Mg^{2+}	0.260	4.0
	0.333[d]	33.5	Mn^{2+}	0.250	0.0
SO_3^{2-}[c]	0.244	−2.4	NH_4^+	0.255	2.0
SO_4^{2-}[c]	0.260	4.0	Ni^{2+}	0.260	4.0
MoO_4^{2-}[c]	0.250	0.0	Pb^{2+}	0.258	3.2
NO_3^-	0.260	4.0	Sb(V)	0.246	−1.6
CH_3COO^-[c]	0.253	1.2	Sr^{2+}	0.255	2.0
$C_2O_4^{2-}$[c]	0.258	3.2	Zn^{2+}	0.255	2.0

[a]Average of two measurements. [b]Iodide/interferent mole ratio is 1:10. [c]Added as potassium or sodium salts. [d]Iodide/thiocyanate mole ratio is 1:30.

concentration of rhodamine B for extracting 5×10^{-5} M iodide was 2×10^{-3} M. The extraction of iodide by 2×10^{-3} M rhodamine B gave rise to a constant absorbance at nitrite concentrations $> 5 \times 10^{-3}$ M. Control of the nitrite concentration is necessary because of its partial loss in the highly acidic reaction medium. Large amounts of nitrite may also cause nitrosation of the phenyl rings of the dye.

Effect of diverse ions. The effect of several ions on the determination of iodide was investigated as shown in Table 1. Positive interference was observed from 1×10^{-4} M thiocyanate or perchlorate. This can be attributed to iodide contamination of these general-purpose reagents. Periodate, iodate and iodine responded as iodide and the method can therefore be used for the determination of total iodine.

Linear calibration graphs were obtained for both spectrophotometric ($0.5—5 \times 10^{-5}$ M) and spectrofluorimetric ($1—10 \times 10^{-6}$ M) methods. The relative standard deviations were 1.8% ($n = 5$) for the spectrofluorimetric determination of 5×10^{-6} M iodide and 2.3% ($n = 50$) for the spectrophotometric determination of 1×10^{-5} M iodide. The apparent molar absorptivity was 2.02×10^4 l mol^{-1} cm^{-1}.

Mr. Khalid M. Mirza is thanked for his excellent technical assistance.

REFERENCES

1 W. J. Williams, Handbook of Anion Determination, Butterworths, London, 1984, p. 391.

2 F. D. Snell, Photometric and Fluorometric Methods of Analysis (Nonmetals), Wiley-Interscience, New York, 1981, p. 290.
3 B. Zak, in D. F. Boltz and J. A. Howell (Eds.), Colorimetric Determination of Nonmetals, Wiley-Interscience, New York, 1978, p. 139.
4 Z. Marczenko, Spectrophotometric Determination of Elements, Horwood, Chichester, 1976, p. 296.
5 S. D. Jones, C. P. Spencer and V. W. Truesdale, Analyst, 107 (1982) 1417.
6 C. P. Sivaraman and S. Rajeswari, Indian J. Mar. Sci., 12 (1983) 177.
7 D. T. Burns, Anal. Proc., 19 (1982) 355.
8 S. A. Lomonosov, N. I. Shukolyukova and V. I. Chernoukhova, Zh. Anal. Khim., 28 (1973) 2389.
9 G. F. Proskuryakova, R. V. Shiveikina and M. S. Chernavina, Izv. Vyssh. Uchebn. Zaved. Khim. Khim. Tekhnol., 6 (1963) 729.
10 M. Tsubouchi, Bull. Chem. Soc. Jpn., 44 (1971) 554; Anal. Chim. Acta, 54 (1971) 143.
11 A. Gantschewa, Mikrochim. Acta, (1967) 601.
12 N. Gantchev and D. Atanasova, C.R. Acad. Bulg. Sci., 25 (1972) 1669.
13 N. Gantchev and A. Kireva, Mikrochim. Acta (1972) 889.
14 L. N. Lapin, Tr. Kom. Anal. Khim. Akad. Nauk SSSR, 11 (1960) 323.
15 B. Morches and G. Tölg, Z. Anal. Chem., 200 (1964) 20.
16 N. K. Podberezskaya and E. A. Shilenko, Zavod. Lab., 32 (1966) 918.
17 W. Likussar, G. Pokorny and H. Zechmann, Anal. Chim. Acta, 49 (1970) 97.
18 N. K. Podberezskaya and E. A. Shilenko, Zavod. Lab., 39 (1973) 774.
19 E. Ramanauskas, L. Bunikiene, K. Grigoniene and Z. Neverdauskiene, Tr. Khim. khim. Tekhnol. (Gor'kii), 35 (1973) 119; Anal. Abstr., 29 (1975) 4B186.
20 H. A. Laitinen, Chemical Analysis, McGraw-Hill, New York, 1960.
21 T. V. Ramarkrishna and N. Balasubramanian. Indian J. Chem., 214 (1982) 217.
22 H. T. S. Britton and H. G. Britton, J. Chem. Soc., (1952) 3892.
23 P. Job, Ann. Chim., 9 (1928) 113.

Analytica Chimica Acta, 197 (1987) 285—289
Elsevier Science Publishers B.V., Amsterdam — Printed in The Netherlands

Short Communication

SPECTROPHOTOMETRIC DETERMINATION OF BISMUTH AFTER EXTRACTION OF HEXADECYLTRIBUTYLPHOSPHONIUM TETRAIODOBISMUTHATE(III) BY MICROCRYSTALLINE BENZOPHENONE

D. THORBURN BURNS* and N. TUNGKANANURUK

Department of Analytical Chemistry, The Queen's University of Belfast, Belfast BT9 5AG (Northern Ireland)

(Received 14th November 1986)

Summary. Bismuth (0—110 μg) is determined spectrophotometrically at 495 nm after its adsorptive extraction from dilute sulphuric acid as hexadecyltributylphosphonium tetraiodobismuthate(III) on microcrystalline benzophenone and dissolution of the solid phase in carbon tetrachloride. The effects of acidity, diverse ions and masking studies are reported. The system is applied to the determination of bismuth in pharmaceutical samples.

One of the classical spectrophotometric methods for the determination of bismuth is based on the yellow colour of the tetraiodobismuthate(III) anion [1—3]. A variety of onium cations has been reported for the extraction of complex anions of main group and transition metals [4, 5]. The tetraiodobismuthate(III) anion has been extracted as an ion pair with benzyldimethylphenylammonium [6], tetraphenylphosphonium [7] or tetraphenylarsonium [8] cations by conventional liquid extraction but not to date by a solid/liquid system [9], although some chelate systems have been extracted in that way [10—14]. No previous reports have been made of the application of the hexadecyltributylphosphonium cation as an ion-pairing reagent for anionic metal complexes.

The present communication describes the adsorptive ion-pair extraction of hexadecyltributylphosphonium tetraiodobismuthate(III) with microcrystalline benzophenone. The separated solid benzophenone is dissolved in carbon tetrachloride and the determinations completed spectrophotometrically at 495 nm. The system has been successfully applied to the determination of bismuth in pharmaceutical products.

Experimental

Apparatus. Pye-Unicam SP 8-400 and SP 6-550 u.v./visible spectrophotometers were used for recording absorption spectra and for routine measurements, respectively, with matched quartz 1-cm cells.

Reagents and solutions. Hexadecyltributylphosphonium bromide [Fluka,

0003-2670/87/$03.50

purum ~ 97% (Br)] was used as supplied. Elemental analysis gave 65.9% C, 12.1% H ($C_{28}H_{60}PBr$ requires 66.2% C, 11.9% H). A 1.0% (w/v) stock solution was made in aqueous 10% (v/v) methanol. A stock 100 $\mu g\ ml^{-1}$ bismuth(III) solution was prepared by dissolving 0.2321 g of hydrated bismuth nitrate $Bi(NO_3)_3 \cdot 5H_2O$ (AnalaR, >98% pure, BDH) in 5 ml of concentrated nitric acid and diluting to exactly 1 l with water. More dilute standard solutions were prepared as required. The potassium iodide/ascorbic acid reagent solution was prepared by dissolving 10 g of reagent-grade potassium iodide and 1 g of ascorbic acid in water and diluting to 100 ml. The benzophenone solution was 20% (w/v) in acetone. All other reagents were of analytical grade. Twice-distilled water was used throughout.

General procedure. Place an aliquot containing up to 100 μg of bismuth(III) in an Erlenmeyer flask with a ground-glass stopper. Add 3.0 ml of 0.5 M sulphuric acid, 2.0 ml of potassium iodide/ascorbic acid reagent solution and 1.0 ml of the 1% (w/v) reagent solution. Swirl to mix and allow to stand for 3 min. Add 2.0 ml of the 20% benzophenone solution, stopper the flask and shake vigorously for 30 s. Filter the orange separated solid through a sintered glass filter (No. 2 porosity). Wash with water, drain or suck dry, dissolve the solid from the filter with carbon tetrachloride and make up to volume with that solvent in a 10-ml volumetric flask. Dry the solution by addition of 1 g of anhydrous sodium sulphate. Measure the absorbance at 495 nm against a reagent blank prepared in the same way.

Digestion of pharmaceutical samples. Samples (to contain 40—50 μg Bi) were placed in 100-ml Kjeldahl flasks and concentrated nitric acid was added followed by 72% perchloric acid, as indicated below. The mixture was warmed (CARE) [15] gently to complete oxidation, filtered, if necessary, into a 200-ml volumetric flask and made up to volume with distilled water. The following volumes (ml) of nitric acid, 72% perchloric acid and water, respectively, were used: bismuth carbonate tablet (3.0, 1.0, 20); 0.5 g of bismuth subgallate ointment (4.0, 2.0, 20); 2 ml of bismuth carbonate suspension (2.0, 2.0, 10).

Examination of main experimental variables

The low-melting-point solids naphthalene, diphenyl, 1,4-dichlorobenzene and benzophenone were each examined for their adsorptive/extraction properties by using the microcrystalline solid formation procedure from acetone solution. Benzophenone showed the highest recovery (apparent molar absorptivity = 9.7×10^3 l mol^{-1} cm^{-1}) of the solids examined when dissolved, and was adopted for use. The apparent molar absorptivities of the extracted bismuth complex were 5,9, 5.3 and 3.7 (each $\times 10^3$ l mol^{-1} cm^{-1}), for 1,4-dichlorobenzene, diphenyl and naphthalene, respectively, when dissolved in carbon tetrachloride.

Various solvents with different functional groups, including alcohols, ketones, esters, ethers, chlorinated and aromatic hydrocarbons, were examined to dissolve the ion pair along with the benzophenone. The ion pair was

soluble and stable in carbon tetrachloride, benzene, chloroform, chlorobenzene, dichloromethane, acetonitrile, ethyl acetate, amyl acetate, toluene, isopropanol, 2,2-dimethoxypropane, and 1,1,2,2-tetrachloroethane but was unstable in dimethylformamide, dimethylsulphoxide, methyl ethyl ketone, methyl isobutyl ketone, dioxane, acetyl acetone, trichloroethylene, diethyl ketone, xylene, methanol, propylene carbonate, amyl alcohol, pentan-1-ol and pentan-2-ol. It was not soluble in all other solvents examined. Carbon tetrachloride was chosen for further study because the ion pair gave the highest molar absorptivity (at 495 nm) in this solvent.

Various onium salts were examined by the general procedure; hexadecyltributylphosphonium bromide showed the highest apparent molar absorptivity of the dissolved solid and was thus used in the subsequent work. The absorption maximum is 495 nm, and the reagent blank was found to be negligible at this wavelength.

The effects of varying the amounts of potassium iodide/ascorbic acid solution, hexadecyltributylphosphonium bromide, 0.5 M sulphuric acid and benzophenone solution were examined for 50 μg of bismuth(III). For each variable, the absorbance increased up to a constant value with increase in volume added and then decreased slowly except for benzophenone which remained constant. Convenient amounts in the plateau regions are specified in the general procedure. Replacement of sulphuric acid by hydrochloric, nitric, perchloric or phosphoric acid gave slightly lower recoveries. Ascorbic acid could be replaced by other reducing agents such as sodium sulphite, hydrophosphite or thiosulphate without adverse effect. The extent of extraction was found to be unaffected by ionic strength, or by phase-volume ratios up to 5:1 water/benzophenone in acetone, or by order of addition of reagents provided there was a delay of 3 min prior to addition of the benzophenone solution. Dissolved extracts were stable for at least 5 h in diffuse daylight but were unstable in direct sunlight.

The composition of the complex was established spectrophotometrically by Job's method of continuous variation [16] and by the mole-ratio method [17, 18] to be $[C_{28}H_{60}P][BiI_4]$.

Results and discussion

A linear calibration graph was obtained over the range 0—110 μg of bismuth in 10 ml of the final carbon tetrachloride solution. For the determination of 50 μg of bismuth, the relative standard deviation was 0.59% (10 results).

The possible interferences of various anions and cations were checked spectrophotometrically for 50 μg of bismuth. The results of the interference and masking studies are summarized in Table 1. The only ions that interfered significantly were Sb(III), Fe(III) and Sn(II) at 100:1 weight ratios, Cu(II) (25:1), Te(IV) (20:1) and Pb (30:1). The interferences from Sb(III), Sn(II) and Te(IV) can be masked by addition of ammonium fluoride and that of Fe(III) and Cu(II) by sodium hydrogensulphite. Lead(II) can be tolerated up

TABLE 1

Effect of various ions on the determination of 50 μg of bismuth

Ion[a]	Ion/Bi (w/w)	Absorbance change[b] (%)	Ion[a]	Ion/Bi (w/w)	Absorbance change[b] (%)
Ag(I)	50	−30	Cu(II)	25	−25
	1	—		5	—
Hg(I)	50	−44		40	—[g]
	5	—	Pb(II)	30	+30
Hg(II)	100	−66		4	−8
	50	—		1.5	—
Pd(II)	20	+115	F^-	500	+5
Cd(II)	20	−69		200	—
	10	—	ClO_4^-	500	+16
Ce(III)	100	−5		250	+7
	50	—		50	—
Ga(III)	100	−13	VO_3^-	500	+142
	60	−7		50	—
	20	—	CN^-	1000	−5
Ru(III)	5	+23		500	—
	1	—	EDTA	1000	−5
As(III)	100	−8		500	—
	50	—	$S_2O_3^{2-}$	1000	−9
V(IV)	100	−8		250	—
	50	—	WO_4^{2-}	50	−24
Sn(II)	100	−18		10	—
	100	—[c]	Tartrate	1000	−4
Sb(III)	100	−86		500	—
	100	—[c]			
Fe(III)	100	−10			
	50	—			
	100	—[d]			
	100	—[e]			
Te(IV)	20	—[f]			

[a]Cations added as chloride, sulphate or nitrate; anions added as sodium or ammonium salts. [b]Ions causing less than a 2% change in absorbance are regarded as not interfering. [c]0.5—1.0 ml of 10% (w/v) NH_4F solution added. [d]1.0 ml of 1% (w/v) ascorbic acid solution added. [e]0.5 ml of 5% (w/v) $NaHSO_3$ solution added. [f]5 drops of 10% (w/v) NH_4F solution added without adding 0.5 M H_2SO_4. [g]After addition of 2 ml of 10% (w/v) $NaHSO_3$ and KI solutions, centrifuge, add 1% (w/v) $C_{24}H_{60}PBr$ solution to supernatant liquid and proceed as in the general procedure.

to a ratio of 1.5:1, but no suitable masking agent was found for larger amounts. Under the conditions of the general procedure, the following cations in a weight ratio of 100:1 were without appreciable effect: Na^+, NH_4^+, Ca^{2+}, Mg^{2+}, Co^{2+}, Mn^{2+}, Ni^{2+}, Zn^{2+}, UO_2^{2+}, Al^{3+}, Cr^{3+}, La^{3+}, Zr(IV) and Nb(V). Cations which interfered were Hg(II), Ga(III), As(III), Ce(III) and V(IV) at $\geqslant$100:1, Ag(I) and Hg(I) at $\geqslant$50:1 and Cd(II) and Pd(II) at $\geqslant$20:1 ratios. Among anions which did not interfere were bromide, chloride, nitrate, acetate, carbonate, sulphate, phosphate and oxalate at 1000:1 ratios.

TABLE 2

Analysis of selected bismuth-containing pharmaceutical products

Sample	Bismuth taken[a] (mg)	Bismuth found[b] via BiI_4^- (mg)	Bismuth found[c] by AAS (mg)
Bismuth carbonate tablets	53.3	54.54 ± 0.06	54.6
Bismuth subgallate ointment	45.9	45.79 ± 0.08	45.9
Bismuth carbonate suspension	49.2	51.08 ± 0.06	51.1

[a]Specification. [b]Mean ±95% confidence for 5 replicates. [c]Average 5 s integration, standard deviation of 0.15.

Solutions obtained from tablets, a suspension of bismuth carbonate and an ointment containing bismuth subgallate were analysed by the general procedure and also independently by atomic absorption spectrometry (AAS). The results (Table 2) show excellent agreement and are consistent with the specifications of the products examined. The method is rapid and precise. The interferences are less than for the simple aqueous phase measurement of the tetraiodobismuthate(III) ion.

REFERENCES

1 F. B. Stone, J. Soc. Chem. Ind. London, 6 (1887) 416.
2 F. D. Snell and C. T. Snell, Colorimetric Methods of Analysis. Vol. I, Inorganic. Chapman and Hall, London, 1936.
3 H. Onishi, Photometric Determination of Traces of Metals. Part II a: Individual Metals, Aluminium to Lithium. Wiley, New York, 1986.
4 A. J. Bowd, D. T. Burns and A. G. Fogg, Talanta, 16 (1969) 719.
5 D. T. Burns, Anal. Proc., 19 (1982) 355.
6 K. C. Bayon and H. K. Das, Curr. Sci., 53 (1984) 312.
7 N. Matano and A. Kawase, Trans. Nat. Res. Inst. Met., 1 (1959) 69.
8 N. K. Baishya and G. Baruah, Curr. Sci., 45 (1976) 94.
9 D. T. Burns, J. M. Jones and N. Tungkananuruk, Trends. Anal. Chem., 4 (1985) VI.
10 M. Gautam and B. K. Puri, Mikrochim. Acta, Part I, (1979) 515.
11 B. K. Puri, M. Gautam and T. Fujinaga, Bull. Chem. Soc., Jpn., 52 (1979) 3415.
12 B. K. Puri, C. L. Sethi and A. Kumar, Mikrochim Acta, Part I, (1983) 361.
13 B. K. Puri and A. K. Gapta, Croat. Chem. Acta, 58 (1985) 91.
14 K. Ishida, B. K. Puri, M. Satake and M. C. Mehra, Talanta, 32 (1985) 207.
15 Analytical Methods Committee, Analyst, 84 (1959) 214.
16 P. Job, Ann. Chim. Paris, 9 (1928) 113.
17 J. H. Yoe and A. L. Jones, Ind. Eng. Chem. Anal. Ed., 16 (1944) 111.
18 K. Momoki, J. Sekino, H. Sato and N. Yamaguchi, Anal. Chem., 41 (1961) 1286.

Analytica Chimica Acta, 197 (1987) 291—293
Elsevier Science Publishers B.V., Amsterdam — Printed in The Netherlands

Short Communication

SPECTROFLUORIMETRIC DETERMINATION OF 16α-HYDROXYESTRONE BY REACTION WITH HEXACYANOFERRATE(III) AND ARGININE IN ALKALINE SOLUTION

YOSHIHISA YAMAGUCHI*, CHOZO HAYASHI and KIYOSHI MIYAI

Central Laboratory for Clinical Investigation, Osaka University Hospital, 1-1-50 Fukushima, Osaka 553 (Japan)

(Received 3rd November 1986)

Summary. The reaction of 16α-hydroxyestrone with hexacyanoferrate(III) and arginine in alkaline solution at 95°C produces a fluorescent compound that is measured at 490 nm ($\lambda_{(ex)}$ = 395 nm). Most other steroids do not interfere. The calibration is linear for 0.5—50 μg of analyte.

Ultraviolet detection based on the Δ^4-3-keto group has been widely used after separation of steroids by high-performance liquid chromatography [1]. New fluorimetric methods for the determination of some urinary steroids based on reaction with glycinamide [2, 3], benzamidine [4, 5] or glycylglycine [6] were recently developed. These methods have the advantage of being highly selective and sensitive. In this communication, a method is reported for the determination of 16α-hydroxyestrone (3,16α-dihydroxy-1,3,5-[10]-estratrien-17-one) with hexacyanoferrate(III) and arginine in alkaline solution to form a fluorescent product.

Experimental

Reagents and apparatus. Steroid standards (Sigma Chemical Co.) were used as received. Two solutions were used to produce the fluorescent product. Reagent A was a solution of sodium hydroxide (10 g), boric acid (1 g) and potassium hexacyanoferrate(III) (100 mg) in water (100 ml). Reagent B was a 0.8% (w/v) solution of arginine in water. Fluorescence was measured with a Model MPF-4 spectrofluorimeter (Hitachi).

Procedure. Pipet 5—50 μl of a standard methanolic 1 mg ml^{-1} solution of the steroid into a test tube, add 1.5 ml each of reagents A and B, and mix well. Heat in a water bath at 95°C for 10 min. After cooling, measure the fluorescence intensity at 490 nm ($\lambda_{(ex)}$ = 395 nm).

Results and discussion

Fluorescence spectra (Fig. 1) of the reaction product show maxima at 395 nm (excitation) and 490 nm (emission). Some other steroids such as corticosterone and testosterone fluoresce at 420 nm ($\lambda_{(ex)}$ = 345) and other

0003-2670/87/$03.50

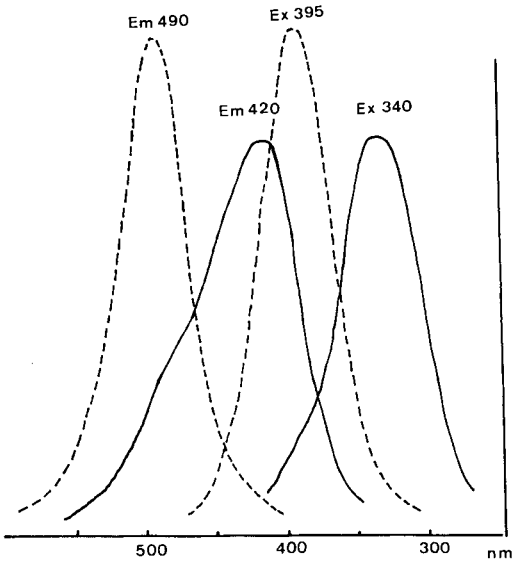

Fig. 1. Excitation and emission spectra: (--) 16α-hydroxyestrone, 5 μg; (—) corticosterone, 100 μg.

TABLE 1

Reactivity of steroids with hexacyanoferate(III) and arginine in alkaline solution

Steroid	Fluorescence intensity[a]	
	395/490 nm	340/420 nm
16α-Hydroxyestrone	100	100
Estrone	15	n.d.[b]
16β-Hydroxyestrone	8	n.d.[b]
Estradiol	5	10
Estriol	2	6
Corticosterone	1	35
Testosterone	0.5	15
Cortisol	n.d.[b]	10
16α-Hydroxydehydroepiandrosterone	n.d.[b]	10
16α-Hydroxyandrostenedione	n.d.[b]	10
16-Ketotestosterone	n.d.[b]	8
Tetrahydro-11-ketocorticosterone	n.d.[b]	4
Tetrahydrocorticosterone	n.d.[b]	3

[a]Relative to 16α-hydroxyestrone as 100. Tetrahydro-11-deoxycortisol, tetrahydrocortisone, tetrahydrocortisole, 11-deoxycortisol, androstenediol, cortol, androsterone and dehydroepiandrosterone were not detected at either set of wavelengths. [b]n.d., not detected.

estrogens fluoresce at 490 nm ($\lambda_{(ex)}$ = 360—395 nm). The fluorescence intensity increased rapidly with reaction time up to 5 min and more slowly up to 15 min; a time of 10 min is recommended. The calibration graph for 16α-hydroxyestrone obtained under the recommended conditions was linear from 0.5 to 50 μg of analyte. The responses given by other steroids, compared to that given by 16α-hydroxyestrone, are shown in Table 1.

The fluorescent product was also formed in the absence of hexacyanoferrate(III) but the fluorescence intensity of the reagent blank was increased significantly and many other steroids also gave rise to fluorescence. To avoid these problems, therefore, hexacyanoferrate(III) was added. The volume of alkaline solution added also affected the procedure, in that at low concentrations of sodium hydroxide, 20-keto-21-ol steroids also reacted and the fluorescence intensity of the reagent blank again increased.

16α-Hydroxyestrone is present in urine from pregnant women and new born babies. This procedure should be applicable to its determination in urine from these subjects in a post-column detection system after high-performance liquid chromatography.

REFERENCES

1 A. M. Caldarella, G. E. Reardon, E. Canalis, C. H. Altshuler, J. Hologgitas and J. A. Clayton-Hopkins, Clin. Chem., 28 (1982) 538.
2 T. Seki and Y. Yamaguchi, Anal. Lett., 15(B13) (1982) 1111.
3 T. Seki and Y. Yamaguchi, J. Liquid Chromatogr., 6 (1983) 1131.
4 Y. Yamaguchi and T. Seki, Anal. Biochem., 142 (1984) 204.
5 T. Seki and Y. Yamaguchi, J. Chromatogr., 305 (1984) 188.
6 Y. Yamaguchi and T. Seki, Anal. Chim. Acta, 160 (1984) 267.

Analytica Chimica Acta, 197 (1987) 295—301
Elsevier Science Publishers B.V., Amsterdam — Printed in The Netherlands

Short Communication

MONITORING OF GLUCOSE IN BIOLOGICAL FLUIDS BY FOURIER-TRANSFORM INFRARED SPECTROMETRY WITH A CYLINDRICAL INTERNAL REFLECTANCE CELL

BILL BAUER and TERI A. FLOYD*[a]

Department of Chemistry, University of Idaho, Moscow, ID 83843 (U.S.A.)

(Received 21st November 1986)

Summary. The feasibility of using internal reflectance infrared spectrometry to monitor changing glucose concentrations in biological fluids is described. A FTIR spectrophotometer and a cylindrical internal reflectance cell are used to obtain spectra of glucose in normal saline solutions, blood serum, and cerebral spinal fluid. The slopes obtained for the standard additions of glucose to each of these solutions compare well and indicate that although the changes in absorbance are small, they are quantifiable. The working range was 0—8 mg ml^{-1}, which brackets normal blood glucose concentrations.

Most of the commonly used methods for the determination of glucose in biological fluids utilize glucose oxidase to catalyze the oxidation of glucose by oxygen to gluconic acid and hydrogen peroxide [1—3]. Glucose is then quantified by monitoring one of the products or reactants of this reaction by a suitable method. In real-time monitoring, devices that utilize these methods often suffer problems arising from the stability, selectivity, and diffusion rates of the reagents [4]. An ideal glucose monitor for biological systems should monitor changing glucose concentrations directly and comprise components that will be stable over very long periods of time.

Glucose has, of course, an infrared (IR) spectrum. The use of direct IR transmission spectrometry with aqueous-based systems is complicated by the typically low molar absorptivities of most analytes and by the very strong background absorbance of water. Thin-film cells with very short pathlengths are available as a means of lessening the latter problem, but are difficult to fill reproducibly and have limited use in flowing systems. To circumvent these problems, attenuated total reflectance (ATR) with digital subtraction of the background water spectrum has been used for the quantitation of low levels of analytes in aqueous and biological environments [5, 6]

Attenuated total reflectance is most typically done with flat-plate multiple internal reflection cells. Recently, cylindrical internal reflectance cells that use cylindrical crystals have become available [7—9]. These cells have a

[a]Present address: Applied Geotechnology Inc., 300 120th Ave. NE, P.O. Box 3885, Bellevue, WA 98009-3885, U.S.A.

0003-2670/87/$03.50

higher signal-to-noise ratio (S/N) ratio because they utilize more of the IR energy, are much easier to make leak-proof, and are available in low-volume flow-cell designs that make them well suited for continuous monitoring applications.

Internal reflectance liquid cells of both types have been successfully used in many industrial applications for process control in aqueous solutions [7—9]. Additionally, Gendreau and Jakobsen [10, 11] have studied biological systems such as blood serum, blood plasma and whole blood using Fourier-transform infrared (FTIR) internal reflectance techniques. Kaiser [12] patented a monitor consisting of a flat ATR cell with a CO_2 laser as a source which was claimed to be able to detect glucose, ethanol and uric acid in dried whole blood or directly from living tissue, such as the human tongue. Results for aqueous solutions were presented.

The primary focus of the work presented here was to investigate the feasibility of measuring changes in glucose concentrations in biological fluids using IR spectroscopy and an internal reflectance cell for liquids. Results presented indicate that even though the measured absorbances for glucose at concentrations normally found in biological fluids are quite small, changes in concentration can be measured reproducibly.

Experimental

A stock 50 mg ml^{-1} glucose solution was prepared by dissolving 5.00 g of anhydrous D-glucose (Sigma Chemical Co.) in 100 ml of normal (0.9%) saline solution (American McGraw). Blood samples were obtained fresh from co-workers as they were needed. Frozen cerebral spinal fluid samples were obtained by courtesy of Dr. Jay Hunter (St. Joseph Hospital, Lewiston, ID).

The internal reflectance cell was the CIRCLE cylindrical internal reflectance accessory (Barnes Analytical Division, Spectra-Tech, Stamford, CT). A 5-ml sample was loaded into the "open boat" CIRCLE cell and spiked with 0.16-ml additions from the stock glucose solution. Spectra were taken before and after the addition of the glucose on a Digilab FTS 15/80 FTIR spectrophotometer (Digilab, Cambridge, MA) equipped with a fast scan, narrow-band MCT detector. Because of an apparent error in the Digilab Version 2.81 subtraction software installed on our instrument, the digitized spectra were downloaded to an IBM PC for data manipulation. Spectra were normalized by a two-point baseline correction program that calculated a linear function which could be subtracted, point by point, from the spectrum to force the two points to zero absorbance. In the Version 4.00 Digilab software package, which was later installed on our instrument, the error has been corrected.

Results and discussion

The strong water bands and their effects are evident in Fig. 1A in which the spectra of normal saline solution and blood serum appear to differ very little. The only exception is the amide II band at about 1550 cm^{-1} [13] in the serum spectrum which appears only as a shoulder on the 1640 cm^{-1}

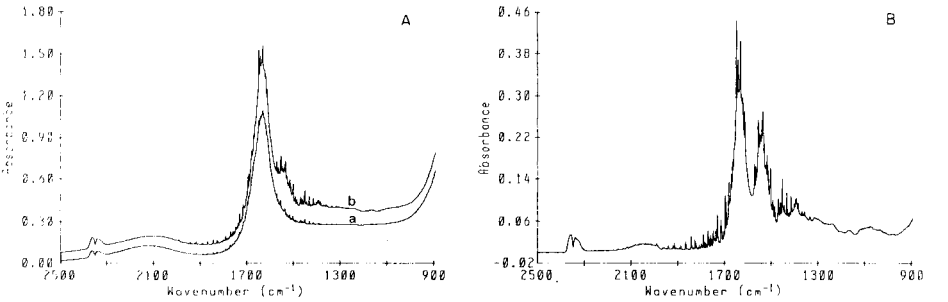

Fig. 1. (A) Spectra (FTIR with cylindrical internal reflectance cells) for (a) normal saline solution and (b) blood serum (offset 0.1 absorbance). (B) Spectrum obtained by subtracting the normal saline spectrum from the serum spectrum in (A).

peak of water. The subtraction of the normal saline spectrum from that of the serum results in the spectrum shown in Fig. 1B. The amide I and II bands (1650 and 1550 cm^{-1}) are now clearly evident as well as further structure down to about 950 cm^{-1} which is usually attributed to proteins [10, 11, 13]. Imposed on this protein background should be the spectra of glucose and other carbohydrate species with peaks that would appear at approximately 1160, 1107, 1080, and 1036 cm^{-1}, with the 1080 and 1036 cm^{-1} peaks being the most prominent and indicative of glucose. Figure 2 gives an expanded view of the spectra of normal saline solution, an 8.0 mg ml^{-1} glucose solution, blood serum and cerebral spinal fluid from 1300 to 980 cm^{-1}. Again, even in this expanded view, major differences between each of the spectra are difficult to see, but now the 1080 and 1036 cm^{-1} peaks of glucose are a little more evident, as is some protein structure in the blood serum and the cerebral spinal fluid. Figure 3 shows the result of subtracting the spectrum of normal saline solution from those of the glucose solution, blood serum and cerebral spinal fluid. The glucose bands in the spectrum of the glucose solution are clearly evident and the carbohydrate bands can be seen in the

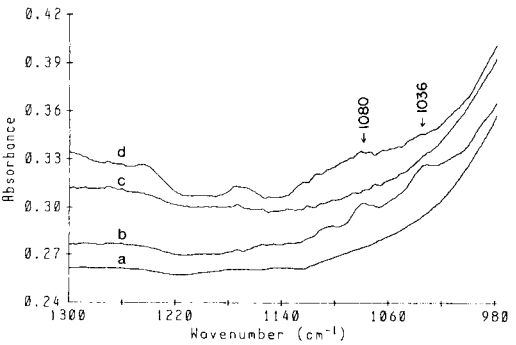

Fig. 2. Unsubtracted spectra: (a) normal saline; (b) glucose solution; (c) spinal fluid (offset 0.04 absorbance); (d) blood serum (offset 0.01 absorbance.)

blood serum spectrum but are not easily identified in the spectrum of cerebral spinal fluid.

The spectra in Fig. 3 tend to indicate that quantitation of an actual glucose concentration in blood serum might be very difficult, if not impossible, because of the large degree of overlap between the glucose spectrum and the unknown, variable background spectrum of glucose-free blood serum. In this work, however, it is "changes" in glucose concentrations that have to be quantified and not the actual quantities. Gendreau and Jakobsen [11] and Gendreau et al. [13] have reported that after exposure for about 4 min, the blood proteins absorbed onto the surface of an internal reflectance crystal in both static and flowing systems form a protein layer of a fairly consistent nature that will remain on the surface of the crystal. They also reported that glycoproteins and carbohydrate species have a tendency to undergo rapid surface adsorption and desorption. The somewhat consistent nature of the background spectrum of blood proteins and the fast adsorption/desorption kinetics of the carbohydrates onto the surface should allow the changes in blood sugar levels to be quantified by using the slope of a calibration curve derived from plotting glucose concentration vs. absorbance at a particular wavenumber.

Because of the limited sample volumes available, a standard-addition method was used to determine if consistent slopes relating absorbance and glucose content could be obtained in normal saline solution, blood serum and cerebral spinal fluid. Figure 4 shows a series of spectra for 0.16-ml additions of the stock 50 mg ml^{-1} glucose solution to serum from which the background spectrum of water has been subtracted. A two-point local baseline at 1185 and 970 cm^{-1} was used to normalize the spectra. The 1080 and 1036 cm^{-1} bands clearly show the greatest change with increasing glucose content; either can be used to construct calibration curves, but the 1036 cm^{-1} band has the greater sensitivity. The calibration plot based on the 1036 cm^{-1} peak yielded a slope of $3.0 \times 10^{-3} \pm 1 \times 10^{-4}$ ml mg^{-1} with $R_2 = 0.984$.

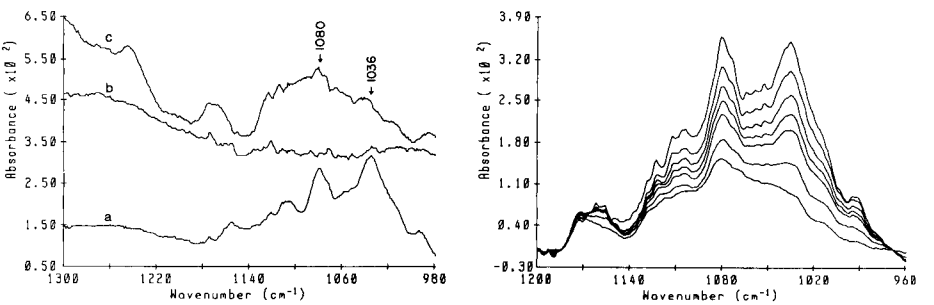

Fig. 3. Spectra with the normal saline background spectrum subtracted: (a) glucose solution; (b) spinal fluid (offset 0.036 absorbance); (c) blood serum (offset −0.002 absorbance).

Fig. 4. Series of background-corrected spectra for 0.16-ml additions of a standard 50 mg ml^{-1} glucose solution to a solution of blood serum.

The presence of the carbohydrate bands imposed on the protein background is evident and the additions of glucose appear to have a limited effect on the background spectrum. Similar results are obtained for standard additions of glucose to normal saline solution and cerebral spinal fluid but the background absorbance is much less complicated and intense in either of these solutions.

Because of the relatively small changes in absorbance with changing glucose content and the much larger background signal, the data exhibit a low signal-to-noise ratio which shows up as relatively large variations in the calculated slopes of the individual calibration curves. This scatter is clearly shown in Table 1 (column 2) by the large standard deviations for the mean slopes of the standard curves obtained from the addition of glucose to normal saline solution, blood serum and cerebral spinal fluid. These variations can be shown to be largely of a random nature if a comparison is made to the standard deviations of the calculated average slopes also shown in Table 1 (column 3). These slopes were obtained by normalizing the data for several individual calibration curves to zero by subtracting the absorbance representing no glucose added to the solution from each of the others in the series of additions. The absorbance values representing one addition of the 50 mg ml^{-1} glucose solution were then averaged. Similar averages were calculated for all the other additions to generate new data sets representing the average absorbance change per addition of glucose. These new data sets were then processed by a variance-weighted linear-regression program to yield the slopes in Table 1 (column 3). The consistency of the standard deviations for the slopes in Table 1 implies that the measurement of increasing glucose concentration is not affected greatly by the protein background in the blood serum. The lower slope of the blood serum data is an artifact caused by dilution of the proteins during the standard-addition procedure combined with the baseline-correction procedure. In general, the slopes and standard deviations agree quite well with each other, indicating that an IR/ATR method may be suitable for monitoring changes in glucose content in biological solutions.

Gendreau et al. [13] have shown that, even though the rate of adsorption and desorption of blood proteins onto the ATR crystal becomes constant

TABLE 1

Mean slopes for standard-addition curves of glucose and slopes from replicate standard-addition curves calculated by variance-weighted linear least squares

Base solution	Standard addition curves Slope (10^{-3} ml mg^{-1})	Calculated by weighted linear least squares Slope (10^{-3} ml mg^{-1})	R^2
Normal saline	2.95 ± 0.15	3.07 ± 0.05	0.9955
Blood serum	2.66 ± 0.20	2.65 ± 0.05	0.9896
Spinal fluid	2.99 ± 0.27	3.02 ± 0.05	0.9963
Overall	2.89 ± 0.23	2.90 ± 0.04	0.9977

within about 4 min, these processes continue for many hours, preferentially adsorbing and desorbing different blood proteins with time. This continuing process will provide a constantly, though probably slowly, changing background spectrum that will also contribute to errors in glucose measurements in blood serum over time. These fluctuations coupled with the normal instrumental noise could be very important when a two-point method such as that applied here is used to normalize the baseline from spectrum to spectrum because an error can occur in any one of three points. This effect would be of less importance if only one selected wavelength were monitored continuously.

Generally, the types of errors that contribute to the variances in the measured slopes will tend to average out because of their random nature. Of greater importance if this technique is to be used as a method for the real-time monitoring of glucose levels, are interferents that will significantly affect the resulting glucose measurements. In living systems, the sample matrix will be complicated by the presence of blood cells. The matrix can also be expected to fluctuate with changes in diet, activity or any other of a wide range of variables (e.g., stress and illness). The effects of these variables on the ability of an IR/ATR monitor to track glucose levels has yet to be investigated.

In conclusion, the IR method presented offers potential for monitoring changes in glucose concentrations in biological fluids. Similar slopes were obtained from the standard curves obtained from the standard addition of glucose to normal saline solution, blood serum and cerebral spinal fluid, indicating that the background absorbances of these solutions did not significantly interfere with the glucose measurements. This method may be well suited for the real-time monitoring of changing glucose concentrations but not for routine determinations unless a better model of the glucose-free blood protein spectrum can be obtained and then subtracted from the normal blood spectrum. Current work centers on developing a mathematical/spectral model of the blood background.

The authors thank Barnes Analytical, a division of Spectra-Tech, for the loan of the CIRCLE accessory.

REFERENCES

1 G. A. Gough, J. Y. Lucisano and P. H. S. Tse, Anal. Chem., 57 (1985) 2351.
2 S. D. Caras, D. Petelenz and J. Janata, Anal. Chem., 57 (1985) 1920.
3 N. L. Malavolti, D. Pilosof and T. A. Nieman, Anal. Chem., 56 (1984) 2191.
4 L. B. Wingard, Jr., Fed. Proc., Fed. Am. Soc. Exp. Biol., 42 (1983) 288.
5 D. Kuehl and R. Crocombe, Appl. Spectrosc., 38 (1984) 907.
6 J. S. Wong, A. J. Rein, D. Wilks and P. Wilks, Jr., Appl. Spectrosc., 38 (1984) 32.
7 A. Rein and P. Wilks, Jr., Am. Lab., 14 (1982) 152.
8 P. Wilks, Jr., Ind. Res. Dev., Sept. (1982) 132.
9 E. G. Bartick and R. G. Messerschmidt, Am. Lab., 16 (1984) 56.
10 R. M. Gendreau and R. J. Jakobsen, Appl. Spectrosc., 32 (1978) 326.

11 R. M. Gendreau and R. J. Jakobsen, J. Biomed. Mater. Res., 13 (1979) 893.
12 N. Kaiser, Methods for Determining the Contents of Metabolic Products in the Blood, U.S. Patent No. 4, 169,676, Oct. 1979; IEEE Trans. Biomed. Eng., 8 (1979) 597.
13 R. M. Gendreau, S. Winters, R. I. Leininger, D. Fink, C. R. Hassler and R. J. Jakobsen, Appl. Spectrosc., 35 (1981) 353.

Analytica Chimica Acta, 197 (1987) 303—308
Elsevier Science Publishers B.V., Amsterdam — Printed in The Netherlands

Short Communication

DETERMINATION OF TOTAL TIN AND TRIBUTYLTIN IN MARINE BIOLOGICAL MATERIALS BY ELECTROTHERMAL ATOMIC ABSORPTION SPECTROMETRY

J. C. MCKIE

Marine Laboratory, P.O. Box 101, Victoria Road, Aberdeen (Great Britain)

(Received 1st September 1986)

Summary. Total tin and tributyltin in marine biological tissue are determined at the sub-$\mu g\ g^{-1}$ level by graphite-furnace atomic absorption spectrometry. Total tin is extracted by digestion with nitric acid, and tributyltin is extracted by n-hexane after treatment with hydrochloric acid. A matrix modifier (ammonium dihydrogenphosphate), and a stabilized-temperature platform furnace are used to overcome matrix effects. Zeeman background correction is used. Results of analyses of oyster (*Crassostrea gigas*), salmon (*Salmo salar*) and a reference material (Bowen's kale) are presented. The detection limit for both methods is ca. 30 ng of tin with a relative standard deviation (n = 6) of 7.8% for a sample containing 200 ng of tin.

The total world production of organotin compounds was 30 000 tonnes in 1984. The main uses of these compounds are as stabilizers for PVC, miticides in crop protection and as biocidal agents in a number of applications [1]. Tributyltin derivatives have become increasingly used as antifouling agents, particularly in the marine environment [2]; their advantages are well known but there is concern over their biological effects on non-target organisms. Bis(tributyltin)oxide (TBTO) is extremely toxic to a range of marine organisms; for example, the 15-day LC_{50} (concentration which causes the death of 50% of the animals tested in 15 days) of TBTO to mussel larvae is ca. 0.1 $\mu g\ l^{-1}$ [3]. Deleterious effects on oysters have been reported from several shellfish growing areas [4—6]. French and UK legislation now restricts the sale of organotin antifouling paints for use on small boats.

The assessment of these hazards requires reliable methods for determining total tin and tributyltin in marine tissue. Current methods for the determination of total and TBTO in marine biota achieve initial separation by gas or high-performance liquid chromatography [7—10] or chelation and liquid/liquid extraction [6, 11] with subsequent detection by techniques such as graphite-furnace atomic absorption spectrometry (AAS), fluorimetry and flame photometry. The method described below incorporates the best features of these procedures in order to produce a simplified method with good sensitivity suitable for routine analysis for total tin in marine biological tissues. Recent improvements in electrothermal AAS, e.g., the use of a

0003-2670/87/$03.50

stabilised-temperature platform furnace, Zeeman background correction and matrix modification with ammonium dihydrogenphosphate, are applied to overcome difficulties arising from the use of nitric acid digests of biological tissues for total tin determination. A similar procedure is described for TBT; the necessary prior separation from inorganic and other organotin species involves n-hexane extraction of the tissue after treatment with hydrochloric acid [11, 12] to remove TBT and other tin compounds, followed by washing with sodium hydroxide [13] to remove inorganic and mono- and dibutylated tin compounds. The combined procedures give a sensitive and reliable method for TBT in marine fish and shellfish.

Experimental

Apparatus. A Perkin-Elmer Z3030 atomic absorption spectrometer, with a HGA-600 graphite furnace, AS60 autosampler attachment and Anadex printer DP9 501B, was used. Digestion flasks were cleaned with hot concentrated nitric acid (1 h) and rinsed with water. All other glassware was cleaned by soaking in (1 + 1) hydrochloric acid for 2 days, and rinsed with water. Digest solutions were stored in 25-cm^3 polystyrene vials with polyethylene caps (Nunc, Roskilde, Denmark).

Reagents. All water used was double-distilled. A commercial 1000 $\mu g\ cm^{-3}$ tin(II) chloride standard solution (BDH) was used to make a 1 $\mu g\ cm^{-3}$ working standard in a reagent blank solution; this was stable for 4 weeks.

Procedure for total tin. Weigh accurately ca. 1.0 g of finely homogenized (but not dried) sample tissue into a short-necked, round-bottomed 150-cm^3 silica flask. Add 20 cm^3 of nitric acid and heat overnight on a hot-plate at 60°C. Then evaporate the solution to 4—6 cm^3 at 275°C; do not evaporate to dryness as tin may be lost. Cool the solution and transfer it quantitatively to a Nunc vial, rinsing with 16 cm^3 of 25% (w/v) ammonium dihydrogenphosphate solution. Dilute to 25 cm^3 with water; the modifier concentration in the final solution is 15% (w/v). This solution is used for AAS under the conditions given in Table 1. Calibration is done with inorganic tin standards made up in reagent blank (i.e., (1 + 4) HNO_3/15% (w/v) $NH_4H_2PO_4$).

Procedure for tributyltin. Weigh accurately ca. 1.0 g of finely homogenized (but not dried) tissue and transfer to a 250-cm^3 pyrex conical separating funnel, washing the weighing vessel with 40 cm^3 of hydrochloric acid. Shake mechanically for 90—120 min. Add accurately 100 cm^3 of n-hexane, shake for 45—50 min and allow to settle for at least 4 h. Pour off the acid layer and discard. Add 130 cm^3 of 3% (w/v) sodium hydroxide solution and shake for 30—40 min. Allow to separate (4—6 h) and pipette a 50-cm^3 aliquot of the n-hexane into a 100-cm^3 pyrex beaker. Add 10 cm^3 of concentrated nitric acid to the beaker and evaporate the n-hexane on a hot-plate at a surface temperature of 120°C. Evaporate the acid solution to 4—6 cm^3. Cool the solution and transfer it to a Nunc vial as described above, diluting to 25 cm^3, to provide the solution for AAS (Table 1). Four blanks should be run with each batch of 20 samples; calibration is identical to that for total tin.

TABLE 1

Recommended instrumental conditions for total tin and tributyltin determinations

Spectrometer			
Wavelength	286.3 nm	Graphite tubes	Pyrolytically coated, with L'vov Platform
Irradiation source	EDL, 6—8 W		
Spectral bandwidth	0.7 nm	Sheathing gas	Argon
Signal processing	Peak height or peak area	Cooling water flow	4 l min^{-1}
Read delay	0.3 s	Sample aliquot	5 to 10 μl

Furnace program

	Dry	Dry	Ash	Atom	Clean
Temp. (°C)	80	140	800	2100	2700
Ramp (s)	3	30	30	0	1
Hold (s)	10	15	60	2[a]	1

[a]Gas stop, read signal.

Results and discussion

Extraction, separation and decomposition of TBT. Visual observation of the dispersion of various marine tissues showed that dissolution rates varied but contact with hydrochloric acid for 6 h was adequate for all samples; overnight treatment was convenient. After extraction with n-hexane [14], the extracts were washed with sodium hydroxide solution [12]. The possibility of inorganic or other butylated tin species passing through the procedure to the final solution was assessed by the addition of 250 μg of inorganic or dibutylated tin to 1-g samples of oyster tissue found to contain 0.19 μg Sn g^{-1} as TBT (*RSD* = 12%, n = 6). The tin measured (0.20 μg g^{-1}, *RSD* = 6.1%, n = 5) indicated that no significant carryover had occurred.

After separation, the TBT extract was mixed with nitric acid. Evaporation of the solvent solution without acid addition led to large (>50%) losses of TBT, possibly by volatilization [14] or precipitation [15]. Evaporation in the presence of nitric acid overcame these difficulties. The subsequent digestion in the TBT procedure was less vigorous than that in the total tin method, and it was considered possible that TBT might not be completely decomposed. The sensitivities of TBTO and inorganic tin were compared by preparing a 1000 μg Sn cm^{-3} TBTO solution by dissolving TBTO in anhydrous acetic acid. A secondary 1 μg cm^{-3} solution in anhydrous acetic acid was prepared from this, and working solutions were prepared by dilution with reagent blank solution. Calibration graphs prepared in this way were not significantly different in gradient or linear working range from those obtained from inorganic tin in reagent blank, or inorganic tin in reagent blank plus 0—2% (v/v) acetic acid (Fig. 1). It was concluded that TBT, after the extraction and mild digestion, could be estimated routinely by calibration with inorganic tin standards in reagent blank.

Matrix modification and background correction. Pruszkowska et al. [16] discussed the use of matrix modifiers and platform furnaces in the

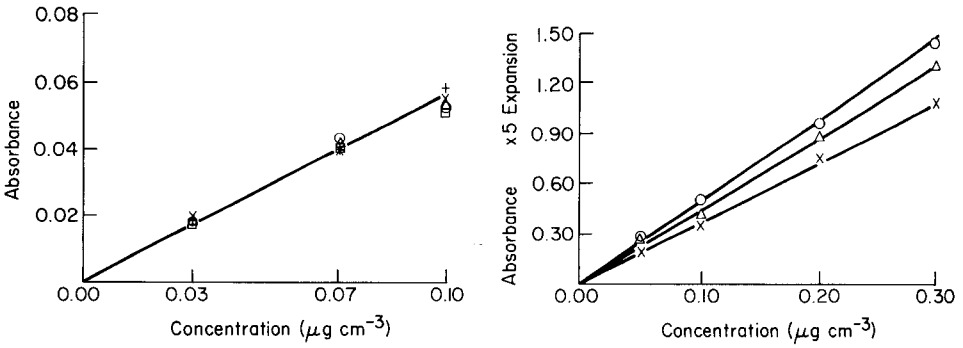

Fig. 1. Comparisons of calibration graphs: (×) inorganic tin in blank matrix; (○) inorganic tin in 1% (v/v) acetic acid; (△) TBT in 1% (v/v) acetic acid; (□) TBT in 2% (v/v) acetic acid; (+) inorganic tin in 2% (v/v) acetic acid.

Fig. 2. Calibration graphs for inorganic standards prepared in 5% (×), 10% (△) and 15% (○) ammonium dihydrogenphosphate solution.

determination of inorganic tin in certain solutions. They concluded that 0.8% (w/v) ammonium dihydrogenphosphate solution overcame many matrix interferences including those of chloride and sulphate [17]. Hinderberger et al. [18] found that the same concentration was adequate for the determination of lead, cadmium, chromium and nickel in a range of biological materials. Both groups used weak (1 + 99) nitric acid solutions. The much more acidic digests (1 + 4 HNO_3) described above required a much higher modifier concentration (15% w/v $NH_4H_2PO_4$) to prevent matrix interference (Fig. 2). With this concentration of modifier it was found that the standard addition curves from inorganic tin spikes added to the final digests were linear, and the gradients were not significantly different from that of a calibration graph obtained for inorganic tin standards. The matrix modifier raised the volatilization temperature of the tin to $>1000^{\circ}$C. This enabled the bulk of the background interference to be removed at the ashing stage, and decreased the background absorbance to a level well within the capability of the Zeeman correction system [19].

In the total tin method, high background absorbances (up to 1 s) can be encountered. A consequence of using the Zeeman effect for correction is the need to use the 286.3-nm tin line. The 224.6-nm line, although 25% more sensitive, suffers from non-linearity at relatively low absorbances. When the 286.3-nm line was used in the peak-height mode, a sensitivity (to produce 0.0044 absorbance) of 11 pg of tin was obtained. In the peak-area mode, the sensitivity was 25 pg, which may be compared with 23 pg reported by Pruszkowska et al. [16] using similar signal processing. These results were obtained using a stabilized-temperature platform furnace, which maintains a population of free atoms in the tube by atomization into a furnace environment where the platform and its surroundings are approaching thermal

equilibrium. Earlier work on a conventional (non-stabilized) platform furnace had found a sensitivity of ca. 100 pg (peak height) [20].

Blanks. The low concentrations of tin expected in fish and shellfish (up to perhaps 5 $\mu g\ g^{-1}$) suggested that contamination of equipment and reagents would have to be avoided. The acid treatment of digestion and extraction flasks was found to decrease blanks to undetectable levels, and no tin contribution from pipette tips, Nunc vials, or the auto-sampler was found. The main source of blank signal was the reagents, primarily the matrix modifier. This source of tin varied between batches of chemical and must be reliably established for each set of samples. Reagent blanks of 1.4 ng Sn cm^{-3} (*RSD* = 16%, $n = 20$) were obtainable, but the reagent blank typically was 5 ng cm^{-3}. Tin can be extracted from matrix modifier solutions, however, by use of an electrolytic reagent cleaner (e.g., ESA model 2014P), with an applied potential of −1.4 V.

Calibration and performance. The recoveries of TBT and inorganic tin spikes (each 2.5 μg Sn) from blank digests were 2.52 μg (*RSD* = 3.0%, $n = 6$) and 2.39 μg (*RSD* = 4.0%, $n = 6$), respectively. Recoveries from oyster tissue of spikes of TBT (0.20 μg Sn g^{-1} wet wt.) and inorganic tin (1.35 $\mu g\ g^{-1}$) were 0.20 $\mu g\ g^{-1}$ (*RSD* = 16%, $n = 3$) and 1.36 $\mu g\ g^{-1}$ (*RSD* = 8%, $n = 3$), respectively. The standard addition graphs and the recoveries of inorganic tin and TBT from blank digests and shellfish digests indicated that the total tin digest matrix does not interfere with the determination, and that sensitivities for the tin species tested are not significantly different from the sensitivity for inorganic tin standards. Both methods were therefore calibrated with standards made up from inorganic tin stock solutions diluted with reagent blank, i.e., (1 + 4) HNO_3/15% (w/v) $NH_4H_2PO_4$). Under the operating conditions given in Table 1, a linear calibration graph was obtained up to 150 ng Sn cm^{-3} (3.8 $\mu g\ g^{-1}$ of sample). The range can be extended upwards by greater dilution with reagent blank. The 2σ detection limit for total tin was 1.2 ng Sn cm^{-3} (0.03 $\mu g\ g^{-1}$ for a 1-g sample). A 10 ng cm^{-3} standard gave a mean absorbance of 0.038 (*SD* = 0.00082, $n = 6$). The precision of the methods was shown by replicate analyses of salmon muscle and whole oysters. For salmon flesh, the mean total tin content was 1.06 $\mu g\ g^{-1}$ wet weight (*RSD* = 9.4%, $n = 6$) and for the whole body of an oyster was 2.37 $\mu g\ g^{-1}$ wet weight (*RSD* = 7.4%, $n = 6$). The values for TBT in further specimens of the above were 0.77 μg Sn g^{-1} (*RSD* = 4.9%, $n = 6$) and 0.18 $\mu g\ g^{-1}$ (*RSD* = 13%, $n = 6$).

Conclusions

The methods presented have proved to be reliable in routine use in this laboratory in studies of the accumulation of tin from antifoulants in scallops and Pacific oysters [21]. Twenty total tin or ten TBT determinations can be done per day. No certified marine reference material for total tin or TBT is available; analysis of Bowen's kale gave 0.13—0.17 $\mu g\ g^{-1}$ total tin, which is in reasonable agreement with a recent value of 0.22 ± 0.067 $\mu g\ g^{-1}$ [22] for this reference material.

The author thanks members of the Chemistry Section of the Marine Laboratory, and J. Pirie in particular, for valuable assistance and discussions.

REFERENCES

1 M. D. Muller, Fresenius' Z. Anal. Chem., 317 (1984) 32.
2 M. J. Waldock and D. Miller, ICES CM/E12 (1983).
3 A. R. Beaumont and M. D. Budd, Mar. Pollut. Bull., 15 (1984) 402.
4 C. Alzieu, M. Heral, Y. Thibaud, M. J. Dardighac and M. Feuillet, Rev. Trav. Inst. Peches Marit., 45 (1982) 100.
5 C. R. Rodriquez and F. C. Lopez, Rev. Trav. Inst. Peches Marit., 47 (1985) 89.
6 M. J. Waldock and J. E. Thain, Mar. Pollut. Bull., 14 (1983) 411.
7 K. L. Jewett and F. E. Brinckman, J. Chromatogr. Sci., 19 (1981) 583.
8 H. A. Meinema, T. W. Burger, G. Versluis de Haan and E. C. Gevers, Env. Sci. Technol., 12 (1978) 288.
9 T.-H. Yu and Y. Arakawa, J. Chromatogr., 258 (1983) 189.
10 B. Zimmerli and H. Zimmermann, Fresenius' Z. Anal. Chem., 304 (1980) 23.
11 G. W. Bryan, P. E. Gibbs, L. G. Hummerstone and G. R. Burt, J. Mar. Biol. Assoc., 66 (1986) 611.
12 H. Iwai, O. Wada and Y. Arakawa, J. Anal. Toxicol., 5 (1981) 300.
13 V. F. Hodge, S. L. Seidel and E. D. Goldberg, Anal. Chem., 51 (1979) 1256.
14 S. Kojima, Analyst, 104 (1979) 660.
15 A. Chapman, personal communication (1984).
16 E. Pruszkowska, D. C. Manning, G. R. Carnrick and W. Slavin, At. Spectrosc., 4 (1983) 87.
17 M. Tominage and Y. Umezaki, Anal. Chim. Acta, 110 (1979) 55.
18 E. J. Hinderberger, M. L. Kaiser and S. R. Koirtyohann, At. Spectrosc., 2 (1981) 1.
19 F. J. Fernandez, W. Bohler, M. M. Beaty and W. B. Burnett, At. Spectrosc., 2 (1981) 73.
20 W. Slavin, G. R. Carnrick, D. C. Manning and E. Pruszkowska, At. Spectrosc., 4 (1983) 69.
21 I. M. Davies, J. C. McKie and J. D. Paul, Aquaculture, 55 (1986) 103.
22 W. R. Wolf, Biological Reference Materials, Wiley, New York, 1985.

Analytica Chimica Acta, 197 (1987) 309—313
Elsevier Science Publishers B.V., Amsterdam — Printed in The Netherlands

Short Communication

ATOMIC ABSORPTION SPECTROMETRIC/HYDRIDE GENERATION DETERMINATION OF TRIBUTYLTIN AND DIBUTYLTIN IN SEA WATER AT THE NANOGRAM PER LITRE LEVEL

P. W. BALLS

Department of Agriculture and Fisheries for Scotland, Marine Laboratory, PO Box 101, Aberdeen AB9 8DB (Great Britain)

(Received 12th December 1986)

Summary. A relatively simple system is described for the determination of tributyltin and dibutyltin in sea water at the ng l^{-1} level. It is based on hydride generation followed by cryogenic trapping on a silanized glass wool column, transport to a quartz cuvette atomizer, and detection by atomic absorption spectrometry. Detection limits (3σ) of 2 ng Sn l^{-1} are obtained for both species.

Recently concern has been expressed over the deleterious environmental effects of tributyltin (TBT) on shellfish [1] and molluscs [2, 3]; TBT in natural waters originates from antifoulant paints used on boats and moored structures. Some species such as the dogwhelk, *Nucella lapillus*, show abnormalities at very low TBT concentrations (ca. 1—2 ng Sn l^{-1}) [3]. The British government has recently set a "safe" target water concentration of 8 ng Sn l^{-1} (as TBT) [4]. Analytical methods should therefore be suitable for use at and below this concentration, but relatively high detection limits have been reported in recent work, e.g., 30 ng Sn l^{-1} [5] and 200 ng Sn [6]. Another consideration is that for widespread use the method should be relatively simple and require only readily available equipment.

Several authors have described the determination of organotin species in sea water, [7—10]; the species were reduced to their volatile hydrides which were stripped from solution with a carrier gas. After trapping and chromatographic separation, they were detected either by atomic absorption spectrometry (AAS) with a graphite furnace or quartz tube atomizer, or by flame atomic emission spectrometry. The method developed here is based on the work of Andreae and Byrd [8]. The technique was optimized for the determination in sea water of TBT and one of its degradation products, dibutyltin (DBT).

Experimental

Apparatus. The apparatus used is illustrated in Fig. 1. The reaction vessel (200, 550 or 1100 ml) was of pyrex glass with a 29/42 ground-glass neck. Helium (70 ml min^{-1}) was introduced through a fine frit, which ensured

0003-2670/87/$03.50

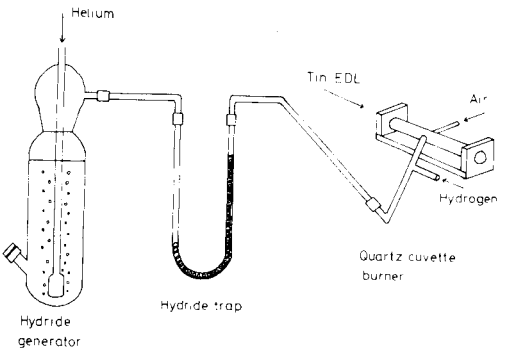

Fig. 1. Hydride-generation apparatus and quartz tube atomizer.

good mixing and efficient stripping of hydrides from solution. Sodium tetrahydroborate was introduced via a teflon-backed silicone rubber septum (13-mm diameter) from a disposable polypropylene syringe with a stainless steel needle. All connecting tubing was of Pyrex glass (6 mm o.d., 3 mm i.d.). The number of joints was kept to a minimum; joints were held with 6 mm i.d. teflon tubing. In order to minimize adsorption, which causes sensitivity losses and peak tailing, it was essential to silanize all surfaces. This was done by filling all parts of the system (except the reaction vessel) with a 2% solution of dimethyldichlorosilane in 1,1,1-trichloroethane (BDH) and leaving them at room temperature for several hours. The component parts were then drained and dried at $\geqslant 110°C$. The hydride trap should be silanized daily. The hydride trap (30 cm × 6 mm o.d.) was half packed with silanized glass wool. Water vapour from the reaction vessel condensed in the empty part of the tube and did not block the tube. In order to prevent the condensation of tributyltin hydride, it was necessary to heat the connecting tubing with 3 m nichrome wire (22 SWG, Baird and Tatlock, 6.5 Ω) attached to a d.c. power supply (24 V, 2 A). The hydride trap was heated independently by ca 1.4 m of nichrome wire and a second power supply (10 V, 1.5 A). Details of the atomizer and spectrometer are given below.

Reagents and solutions. Aqueous 2% (w/v) sodium tetrahydroborate was prepared from high-purity reagent (BDH or Aldrich). This reagent has a large inorganic tin blank which can be decreased by the addition of 1 ml of 2 M sodium hydroxide to 100 ml of the reductant solution [8]. The sodium hydroxide was first cleaned by coprecipitation with lanthanum nitrate [11]. AnalaR nitric acid (BDH) was used to prepare 5 M acid for sample acidification and 1 M for the standards.

Solutions containing 1000 mg Sn l^{-1} as tributyltin fluoride and dibutyltin oxide (Fluka) were prepared in absolute ethanol and anhydrous acetic acid, respectively. Working standards (0.2 mg Sn l^{-1}) were prepared weekly, from the stock solution, in 1 M nitric acid. Calibrations were prepared in sea water with no detectable TBT or DBT.

Methods. Three reaction vessels (200, 550 and 1100 ml) were used, the

largest being suitable for low concentrations. The reaction vessel was filled with sea water and acidified to ca. pH 2 by the addition of 5 M nitric acid (0.2, 0.5 or 1 ml according to sample volume). The sample was degassed for 5 min to remove air and volatile species. The heating of the hydride trap was stopped and the trap cooled in liquid nitrogen. Sodium tetrahydroborate solution was injected (2, 4 or 8 ml according to sample volume) and the reaction was allowed to proceed for 3 min. During the reaction the pH increased to 6—8, a range which has been reported as optimal for hydride generation [8]. No increase in yield was observed for times greater than 3 min. At the end of this time, the liquid nitrogen was removed, the hydride trap was heated, and the detector output was recorded on a chart recorder. Typical traces are shown in Fig. 2A and B.

Results and discussion

Choice of detector. A graphite furnace and a quartz cuvette atomizer were tested. The graphite furnace was investigated first but considerable difficulties were encountered in introducing the sample stream. Initially the sample was introduced via the internal purge inlet of the furnace. A signal was obtained for DBT but not for TBT; this was attributed to condensation of the hydride at the cold spot caused by the cooling water of the furnace. This difficulty could not be overcome by circulating warm water. A TBT signal

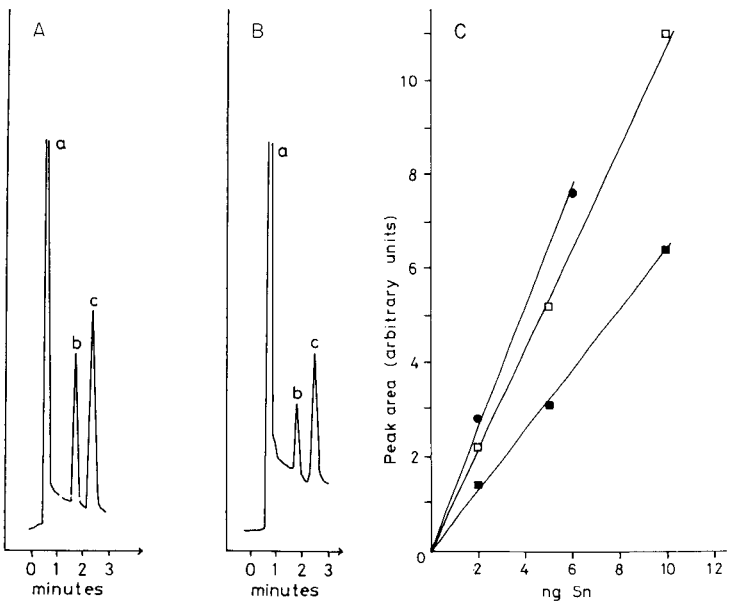

Fig. 2. (A) Peaks obtained for spiked sea water: (a) Sn(IV); (b) Bu_2SnH_2 ; (10 ng Sn); (c) Bu_3SnH (20 ng Sn). (B) Peaks obtained for a sea water sample (200 ml): (a) Sn(IV); (b) Bu_2SnH_2 (5 ng Sn); (c) Bu_3SnH (15 ng Sn). (C) Calibration graphs for TBT for different sample volumes: (●) 200 ml; (□) 550 ml; (■) 1100 ml.

was successfully obtained by introducing the sample stream through an alumina tube (Goodfellow Metals) into the open end of the furnace (window removed). This was considered unsatisfactory, however, because the intensity of the light source was diminished. Additionally, it was not possible to secure the inlet tube sufficiently firmly to eliminate spurious peaks caused by vibration.

Because of these difficulties the graphite furnace was abandoned in favour of the quartz tube burner. The quartz tube (7 cm × 0.9 cm i.d.) was based on a design by Andreae [12], and contained a hydrogen-rich flame. Air (200 ml min^{-1}) and hydrogen (330 ml min^{-1}) were introduced as shown in Fig. 1, which produced a stable flame. The burner was held in an aluminium holder mounted in an atomic absorption spectrometer (Perkin-Elmer model 603). The light source was a tin electrodeless discharge lamp (Perkin-Elmer) operated at 8 W, and absorbance measurements were made at the 224.6 nm tin line, with a spectral slit-width of 0.1 nm. This arrangement functioned satisfactorily.

Removal of water vapour from the gas stream. Water vapour tends to destroy the silanized coating of the glassware, which leads to a decrease in sensitivity and reproducibility. A simple cold trap is unsuitable because this also removes TBT hydride. Drying agents such as sodium sulphate and molecular sieves have also been reported to remove the higher-boiling point hydrides [13]. An attempt was made, therefore, to remove the water vapour from the gas stream with a Dry-Perm drier (International Science Consultants, Model DP-3), which passes the gas stream through a length of Nafion (Dupont) tubing which is permeable to water vapour. A molecular sieve was packed around the tube to absorb the moisture. This system was very effective at removing water vapour. However, although the drier did not remove DBT from the gas stream, TBT was retained, probably by condensation in the untreated tube. It was not possible, therefore, to dry the gas stream and this makes frequent silanization essential.

Analytical performance. Figure 2 shows that the procedure gives a sequence of peaks, in the order inorganic tin, DBT and TBT. Ideally the method should give an identical response for each organotin species for the same tin concentration. This is sometimes the case, but the sensitivity for TBT was often observed to be less than that for DBT. Variations are principally due to differences in trapping efficiency. Three freshly silanized traps were compared and in all cases the sensitivity was lower for TBT than DBT, the peak area ratios being 0.635, 0.395 and 0.730. These results are probably due to variations in the quality of the silanization.

An additional source of variable sensitivity is the sample volume. Figure 2C shows calibration graphs for TBT obtained by using the same trap but varying the sample volume. There is evidently some decrease in stripping efficiency with increasing sample volume. This is similar to the effect reported by Olson et al. [14], for a hydride-generation method. The variable sensitivities outlined above, however, do not present practical problems

because the reproducibility for a particular set of conditions is good (see below).

The method gives a linear response up to at least 80 ng Sn (as TBT), based on peak-height measurements. This is considerably better than the 13 ng reported by Randall et al. [15] and is sufficient for all but the most contaminated samples. Six determinations of 5.0 ng Sn (as TBT fluoride) in 1.1 l of sea water gave a mean result of 5.1 ng Sn with a standard deviation of 0.4. Thus the relative standard deviation is 8% and the 3σ detection limit is 1.2 ng tin.

Although there are no organotin species associated with the reagents used, there is a large inorganic tin blank (ca. 20 ng Sn). This primarily arises from the sodium tetrahydroborate; the nitric acid contributes only 2—3 ng Sn. Interpretation can be a problem when the organotins appear as small peaks on the shoulder of the inorganic tin peak. This problem was decreased by using the minimum quantity of sodium tetrahydroborate. The method described here uses half the quantity recommended elsewhere [8], with no loss in sensitivity.

Water samples should be taken and stored in brown glass bottles (1 or 2.5 l). Samples were stored in the dark at room temperature were observed to be stable for at least two weeks. Between sampling trips, the bottles should be cleaned with detergent and rinsed with tap and distilled water.

Communications with Dr Jim Byrd, Skidaway Institute of Oceanography, were of great value in developing this method.

REFERENCES

1 M. J. Waldock and J. E. Thain, Mar. Pollut. Bull., 14 (1983) 411.
2 A. R. Beaumont and M. D. Budd, Mar. Pollut. Bull., 15 (1984) 402.
3 G. W. Bryan, P. E. Gibbs, L. G. Hummerstone and G. R. Burt, J. Mar. Biol. Assoc. U.K., 66 (1986) 611.
4 Organotin in Antifouling Paints — Environmental Considerations. Pollution Paper No 25. HMSO, London, 1986.
5 J. J. Cleary and A. R. D. Stebbing, Mar. Pollut. Bull., 16 (1985) 350.
6 L. Ebdon, S. J. Hill and P. Jones, Analyst, 10 (1985) 515.
7 V. F. Hodge, S. L. Seidel and E. D. Goldberg, Anal. Chem., 51 (1979) 1256.
8 M. O. Andreae and J. T. Byrd, Anal. Chim. Acta, 156 (1984) 147.
9 O. F. X. Donard, S. Rapsomanikis and J. H. Weber, Anal. Chem., 58 (1986) 772.
10 A. O. Valkirs, P. F. Seligman, P. M. Stang, V. Homer, S. H. Lieberman, G. Vafa and C. A. Dooley, Mar. Pollut. Bull., 17 (1986) 319.
11 D. S. Lee, Anal. Chem., 54 (1982) 1682.
12 M. O. Andreae, Anal. Chem., 49 (1977) 820.
13 A. Woollins and W. R. Cullen, Analyst, 109 (1984) 1527.
14 C. L. Matthias, G. J. Olsen, F. E. Brinckman and J. M. Bellama, NBSIR, 20 (1986) 609.
15 L. Randall, O. F. X. Donard and J. H. Weber, Anal. Chim. Acta, 184 (1986) 197.

Analytica Chimica Acta, 197 (1987) 315—321
Elsevier Science Publishers B.V., Amsterdam — Printed in The Netherlands

Short Communication

A STUDY OF ARSENIC(III) AND ARSENIC(V) REDUCTION AND OF ARSINE DECOMPOSITION IN HYDRIDE-GENERATION ATOMIC ABSORPTION SPECTROMETRY

NARSITO[a] and J. AGTERDENBOS*

Laboratory for Analytical Chemistry, State University of Utrecht, Croesestraat 77A, 3522 AD Utrecht (The Netherlands)

(Received 16th September 1986)

Summary. The difference in behaviour of arsenic(III) and arsenic(V) in their conversion to arsine by reduction with sodium tetrahydroborate, and the role of the addition of oxygen and hydrogen to the carrier gas in the production of arsenic atoms are described.

Hydride-generation atomic absorption spectrometry (AAS) has been applied for the determination of arsenic at the ng ml^{-1} level, and much work has been done on the influence of several parameters such as the pH of the analyte solution [1, 2], the carrier gas flow rate [2, 3], the absence or presence of oxygen in the heated quartz tube [4] and the atomization temperature [3, 4]. The atomization mechanism in the heated quartz tube has also been studied [4, 5].

The difference in behaviour of arsenic(III) and arsenic(V) has been noted several times [1, 2, 6]. Arsenic(III) is converted to the hydride in solutions of pH lower than 5; arsenic(V) requires strongly acidic solutions. Therefore, determination of arsenic(III) and of total arsenic is possible on different portions of a sample solution and so the concentration of arsenic in each of its oxidation states may be determined [2]. Some authors [6] state that even with a high concentration of sodium tetrahydroborate, the signal obtained from arsenic(V) is up to 10% lower than the arsenic(III) signal. In some procedures, arsenic(V) is reduced to arsenic(III) with iodide prior to the hydride generation [7]. The difference in behaviour is often attributed to the lower reaction rate of arsenic(V) with the tetrahydroborate [1, 2]. The high decomposition rate of tetrahydroborate under the usual experimental conditions [8] supports the assumption that kinetic reasons may play a role. No proof seems to have been given that it does cause low absorbance values, so an investigation of this possibility was one of the aims of the present work.

During this work, it was observed that the presence of too much oxygen

[a]On leave from Gadjah Mada University, Department of Chemistry, Sekip Unit III, Yogyakarta, Indonesia.

0003-2670/87/$03.50

in the carrier gas resulted in a considerable signal decrease, a phenomenon earlier found if selenium was the analyte [9]. Therefore the role of oxygen in the case of arsenic was also studied. Finally, the role of the addition of extra hydrogen to the carrier gas was studied, as it has been shown that for selenium this decreases the absorbance [10].

Experimental

Apparatus. The apparatus used was as described before [11, 12]. It was a continuous flow type and gases could be added not only at the reaction cross where analyte and reagent solutions were mixed, but also in an extra gas inlet just before the heated quartz tube. A wavelength of 193.7 nm and a slit width of 300 μm were used.

Reagents. All reagents were of analytical reagent grade. The sodium tetrahydroborate solution contained some sodium hydroxide (0.2 g per 100 ml). A stock solution containing 1000 μg ml^{-1} arsenic(III) was prepared from arsenic trioxide. A similar stock solution of arsenic(V) was prepared from a Merck Titrisol solution. Working arsenic solutions were prepared by appropriate dilution with 3 M hydrochloric acid.

Procedure. The hydride was generated by mixing analyte and tetrahydroborate solutions in the reaction cross at 4.0 ml min^{-1} each. A 500 ml min^{-1} or 300 ml min^{-1} flow of carrier gas (nitrogen) was used to sweep the hydride through a spiral glass coil and a gas/liquid separator into an electrically heated quartz tube. Additional gases (nitrogen, air, oxygen or hydrogen) entered through an extra gas inlet after the gas/liquid separator just before the quartz tube. The absorbance of arsenic was measured as a peak height on a chart recorder. In order to check whether any of the arsenic(III) or arsenic(V) was still present after its reaction with tetrahydroborate, the liquid in the waste after the gas/liquid separator was analyzed. Enough hydrochloric acid was added to make the acidity 3 M and 1% (w/v) tetrahydroborate was used in all cases to ensure complete conversion to the hydride.

Results and discussion

Influence of air, oxidation state of arsenic and reagent concentration. In a first series of experiments, the influence of the addition of air (10 ml min^{-1}), of the reagent concentration, and of the oxidation state of the analyte on the reduction efficiency and on the absorbance were studied. In these experiments 50 ng ml^{-1} arsenic(III) or arsenic(V) was used, and the cuvette temperature was 900°C. All absorbance values in Table 1 have been corrected for dilution by hydrogen evolved [10]. The carrier gas flow was 500 ml min^{-1}.

The results presented in Table 1 indicate that when a low concentration of tetrahydroborate is used, the presence of air in the carrier gas causes a considerable suppression of the absorbance, both for arsenic(III) and arsenic(V). For a possible explanation, it must be considered that stoichiometrically the amount of oxygen present in 10 ml min^{-1} of air is equivalent to the hydrogen evolved by 4 ml min^{-1} of 0.05% sodium tetrahydroborate [10]. So the results

TABLE 1

Arsenic absorbance signals generated from arsenic(III) and arsenic(V) and from the residues

Analyte	$NaBH_4$ (% w/v)	Corrected absorbance				
		Arsenic (50 ng ml^{-1})		Waste	Total	
		A_1[a]	A_2[b]	A_w[b]	$A_1 + 2A_w$[c]	$A_2 + 2A_w$[c]
As(III)	0.05	0.315	0.062	0.138	0.591	0.338
	0.10	0.406	0.371	0.078	0.562	0.527
	0.20	0.471	0.472	0.047	0.565	0.566
	0.50	0.563	0.568	0.010	0.583	0.588
	1.0	0.581	0.588	0.000	0.581	0.588
	2.0	0.454	0.562	0.000	0.454	0.562
As(V)	0.05	0.034	0.000	0.264	0.562	0.528
	0.10	0.111	0.098	0.218	0.547	0.534
	0.20	0.251	0.248	0.137	0.525	0.522
	0.50	0.484	0.491	0.026	0.536	0.543
	1.0	0.562	0.573	0.000	0.562	0.573
	2.0	0.463	0.551	0.000	0.463	0.551

[a]No air added. [b]10 ml min^{-1} air added. [c]The factor 2 is a dilution factor.

suggest that under the prevailing conditions the presence of excess of hydrogen in the carrier gas plays an important role in ensuring complete formation of analyte atoms. Table 1 further shows that at reagent concentrations between 0.2 and 1.0%, the addition of air does not influence the results, but when a 2% reagent solution is applied the absence of air causes lower absorbance values than expected from the other experiments. This suggests

TABLE 2

Reduction efficiency for arsenic(III) and arsenic(V) at various tetrahydroborate concentrations, calculated from the data given in Table 1

$NaBH_4$ (%, w/v)	Reduction efficiency (%)			
	Arsenic(III)		Arsenic(V)	
	1[a]	2[b]	1[a]	2[b]
0.05	53	18	6	0
0.10	72	70	20	18
0.20	83	83	48	47
0.50	97	97	90	90
1.0	100	100	100	100
2.0	100	100	100	100

[a]No air added. [b]10 ml min^{-1} of air added.

that here the addition of oxygen favours the formation of analyte atoms in the cuvette.

Table 2 shows that there is a significant difference in the reduction efficiency between arsenic(III) and arsenic(V) at sodium tetrahydroborate concentrations lower than 1.0%. It suggests that under these conditions arsenic(III) reacts more quickly than arsenic(V). At low concentrations of tetrahydroborate, arsenic(III) is converted to the hydride more efficiently than arsenic(V). Complete conversion of both arsenic(III) and arsenic(V) can be achieved at sodium tetrahydroborate concentrations of 1.0% or higher. This means that the difficulty of the difference in sensitivity for arsenic(III) and arsenic(V) usually met with in a batch system can be overcome.

Influence of additional oxygen and hydrogen. In a further study of the role of additional oxygen, arsine was generated from a 25 ng ml^{-1} arsenic(III) solution by 1.0% (w/v) sodium tetrahydroborate solution and swept into the quartz tube by 300 ml min^{-1} of nitrogen carrier gas. An additional nitrogen flow of 500 ml min^{-1} was added through the extra gas inlet together with the additional oxygen, so that the total gas flow was about 900 ml min^{-1}. It was assumed that the addition of oxygen gave no significant increase in the gas flow rate.

Figure 1 shows that at high oxygen flows the concentration of arsenic

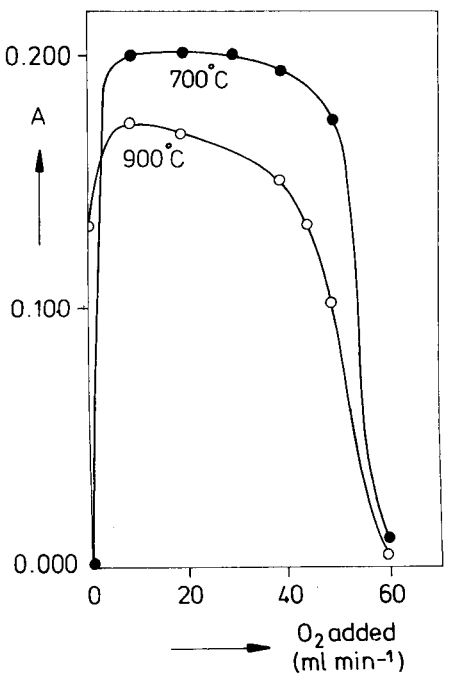

Fig. 1. The influence of oxygen in the flow gas on the peak-height absorbance of arsenic at two different atomization temperatures.

atoms is decreased considerably. A similar phenomenon has been observed for selenium [9]. As the hydrogen flow generated by the reaction of the tetrahydroborate with acid was about 80 ml min^{-1} [10], the amount of oxygen required to decrease the signal is slightly more than the flow (40 ml min^{-1}) necessary to react with hydrogen to form water. Obviously, under these conditions some excess of oxygen is required for decreasing the signal. The reason of the decrease is possibly that the excess of oxygen reacts with the arsenic atoms to form an arsenic oxide. It should be noted that in this work no effort was made to exclude the presence of oxygen in the system. The amount present is very small, probably not more than 0.1%, and so it will not influence the above conclusions, but it is certainly more than enough to convert all arsine to arsenic atoms according to a reaction of the type:

$$4AsH_3 + 3O_2 \rightleftharpoons 4As + 6H_2O \quad (1)$$

Therefore, if this reaction occurs, high absorbances should be found even without the addition of oxygen.

Figure 1 shows that, if no oxygen is added, absorbances are low (or zero) at 700°C and 900°C. This may be explained by the assumption that at the very low oxygen concentration present (below 0.1%), the above reaction is too slow to give full conversion during the short residence time of the gas mixture in the quartz tube (addition of 10 ml of oxygen increases its content more than ten-fold).

To study the influence of additional hydrogen, a 300 ml min^{-1} nitrogen carrier flow was used. Through the extra gas inlet, 20 ml min^{-1} of air and the additional hydrogen were added. The total gas flow was kept constant at 740 ml min^{-1} by the addition of an appropriate nitrogen flow through the extra gas inlet. The hydride was generated from 50 ng ml^{-1} arsenic(III) solution by a 0.25% (w/v) reductant solution in order to minimize the amount of hydrogen produced by the reaction of the tetrahydroborate with acid (ca. 20 ml min^{-1} of hydrogen is produced). Although the conversion of arsenic to arsine was only ca. 90% (see Table 1), the repeatability of the measurement was good.

The following reaction also seems possible for the formation of arsenic atoms:

$$2AsH_3 \rightleftharpoons 2As + 3H_2 \quad (2)$$

Thermodynamically [3], only very small amounts of arsenic atoms can be expected to be present in the quartz tube at the usual temperature, if this reaction governs the decomposition of arsine. This contradicts experiments described here and elsewhere [3, 4]. It means that reaction 2 is not the source of the arsenic atoms present. The conclusion is supported by the results given in Table 3, which shows that the degree of decomposition is fairly independent of temperature and that decomposition is not reversed by an excess of hydrogen. In this respect arsenic behaves differently to selenium [10].

TABLE 3

Influence of hydrogen on the arsenic absorbance at two different temperatures. The total gas flow was constant

Hydrogen (ml min^{-1})		20[a]	120	220	320	420
Absorbance	700°C	0.186	0.196	0.182	0.182	0.179
	900°C	0.156	0.174	0.162	0.157	0.149

[a]From decomposition of tetrahydroborate.

An objection against a radical mechanism of decomposition [4] is that the equilibrium concentration of hydrogen atoms at 700°C is only 0.1—1% of the arsine concentration [8], and no evidence is available that in situations like here, the actual concentration exceeds the equilibrium concentration by the factor required.

As far as reaction 1 is concerned, at first sight it seems contradictory to the observations of Welz and Melcher [4] that hydrogen is required for the formation of analyte atoms. The observations mentioned above, however, suggest that under the usual conditions hydrogen and oxygen molecules react (nearly) quantitatively and so it seems possible that the hydrogen used in the experiments of Welz and Melcher removes the excess of oxygen and so prevents the arsenic atoms disappearing by their reaction with oxygen to form an arsenic oxide. Experiments [5] showing that even the presence of some residual hydrogen in the carrier gas from the tubing causes a signal, indicate that very small amounts of hydrogen are sufficient to allow arsenic atoms to be produced. Therefore it may be concluded that none of the present observations, nor published data contradict the assumption that reaction of arsine with oxygen occurs to produce arsenic atoms. According to these views, the role of oxygen is oxidation of the arsine and the role of hydrogen is prevention of the oxidation of the arsenic atoms by the oxygen in excess of the arsine. Moreover, the role of both gases may be to form radicals, which probably participate in arsine oxidation. A proof that radicals play a role in the mechanism was given recently [8].

One of the authors (N) thanks the Netherlands University Foundation for International Cooperation (NUFFIC) for financial support. Thanks are also due to R. W. Bussink for help in the preparation of the manuscript.

REFERENCES

1 J. Agget and A. C. Aspell, Analyst, 101 (1976) 341.
2 A. G. Howard and M. H. Arbab-Zavar, Analyst, 106 (1981) 213.
3 D. Bax, J. T. van Elteren and J. Agterdenbos, Spectrochim. Acta, Part B, 41 (1986) 1007.
4 B. Welz and M. Melcher, Analyst, 108 (1983) 213.
5 B. Welz and M. Schubert Jacobs, Fresenius' Z. Anal. Chem., 324 (1986) 832.

6 K. C. Thompson and D. R. Thomerson, Analyst, 99 (1974) 595.
7 B. J. A. Haring, W. van Delft and C. M. Bom, Fresenius' Z. Anal. Chem., 310 (1982) 217.
8 J. Agterdenbos and D. Bax, Fresenius' Z. Anal. Chem., 323 (1986) 783.
9 J. Agterdenbos, J. P. M. van Noort, F. F. Peters and D. Bax, Spectrochim. Acta, Part B, 41 (1986) 283.
10 D. Bax, F. F. Peters, J. P. M. van Noort and J. Agterdenbos, Spectrochim. Acta, Part B, 41 (1986) 275.
11 J. Agterdenbos, J. P. M. van Noort, F. F. Peters, D. Bax and J. P. ter Heege, Spectrochim. Acta, Part B, 40 (1985) 501.
12 J. Agterdenbos and D. Bax, Anal. Chim. Acta, 188 (1986) 127.

Analytica Chimica Acta, 197 (1987) 323—325
Elsevier Science Publishers B.V., Amsterdam — Printed in The Netherlands

Short Communication

DETERMINATION OF COPPER IN NATURAL WATERS BY ATOM-TRAPPING ATOMIC ABSORPTION SPECTROMETRY AFTER LIQUID/LIQUID EXTRACTION

S. BRADSHAW, A. J. GASCOIGNE and J. B. HEADRIDGE*[a]

Department of Chemistry, The University, Sheffield S3 7HF (Great Britain)

J. H. MOFFETT

Department of Chemistry, School of Pure and Applied Sciences, University of the South Pacific, P.O. Box 1168, Suva (Fiji)

(Received 24th November 1986)

Summary. Copper (1—100 ng ml^{-1}) is determined in natural waters by atom-trapping atomic absorption spectrometry after extraction of its 1-pyrrolidinecarbodithioate complex into isobutylmethylketone. Results are in good agreement with those obtained by conventional carbon-furnace atomic absorption spectrometry.

Copper in natural waters at levels of 1—100 ng ml^{-1} can readily be determined by carbon-furnace atomic absorption spectrometry. However, many laboratories, particularly in developing countries, possess only a flame atomic absorption spectrometer and this technique is usually not sensitive enough for the direct determination of copper in waters. To assist in the prospecting for copper minerals in Fiji, a relatively simple method based on flame atomic absorption spectrometry (a.a.s.) was needed for the determination of copper in natural waters. It was known that the limit of detection for copper in waters by flame a.a.s. could be lowered significantly by preconcentrating the analyte by liquid/liquid extraction [1] or by atom-trapping [2]. It was decided to combine both methods to produce a convenient method with a very low limit of detection. Such a method involving preconcentration of copper by extraction of its 1-pyrrolidinecarbodithioate complex into methyl isobutyl ketone (MIBK) [3], is described here. Work was started in Fiji and completed in Great Britain. Copper was determined in twelve samples of natural waters collected in Co. Durham, Derbyshire and Sheffield in England.

Experimental

Water samples and solutions. Water samples were collected in polythene bottles. These were pretreated by filling with 8 M nitric acid, pouring out the acid and allowing the inverted bottles to drain. They were not rinsed. All nitric acid used was AristaR grade (BDH). A standard solution of copper

[a]Formerly at the University of the South Pacific.

0003-2670/87/$03.50

sulphate (1% w/v in copper and 0.1 M in nitric acid) was prepared. More dilute standards were obtained by diluting it with 0.1 M nitric acid.

Ammonium 1-pyrrolidinecarbodithioate (APCD) solution (1.6×10^{-2} M) was prepared immediately before use by dissolving 0.13 g of APCD in 50 ml of water containing 0.5 ml of 0.1 M ammonia solution.

Equipment for atom-trapping a.a.s. This was similar to that described by Khalighie et al. [2]. The burner for the air/acetylene flame had a slit length of 10.4 cm and fitted into a Perkin-Elmer 300S atomic absorption spectrometer coupled to a JJ Instruments CR552 chart recorder. The 324.8-nm copper line from a Pye Unicam hollow-cathode lamp was employed. The flow rates of air and acetylene were adjusted so that no carbon particles deposited on the cooled silica tube during the collection period while an MIBK solution of the copper complex was being nebulized. These flow rates were 28 and 6 arbitrary units for air and acetylene, respectively. The lower edge of the silica tube (4 mm outside diameter) was fixed at 15 mm above the burner top. The light path from the hollow-cathode lamp passed just above the silica tube such that the tube was only just low enough to cause no attenuation of light intensity, which would result from partial blockage of the light beam.

Equipment for carbon-furnace a.a.s. Concentrations of copper in natural waters were also determined directly by carbon-furnace a.a.s.; 10 μl of sample or standard was pipetted onto a graphite microboat which was inserted into the cuvette of an Instrumentation Laboratory IL555 furnace, positioned within a Varian Techtron AA6 atomic absorption spectrometer. Measurements were again made at 324.8 nm under conditions that gave good sensitivity and reproducibility.

Method for the determination of copper by atom-trapping a.a.s. after liquid/liquid extraction. To 50 ml of water sample, 1 ml of 5 M nitric acid, 2 ml of APCD solution and 10 ml of MIBK were added. The solution was shaken for 2 min, the layers were allowed to separate, and the organic layer was collected in a small flask. This solution was nebulized and copper was collected on the atom-trap for 3 min. Whilst pure MIBK was nebulized, the cooling water was ejected from the silica tube and the peak of absorbance vs. time was recorded. The maximum absorbance was noted.

A series of standard solutions containing copper(II) at concentrations of 10—100 ng ml^{-1} was treated in a similar way and a calibration graph was drawn for peak absorbance, corrected for a small copper blank from the distilled water used in preparing the solutions, vs. concentration of copper. The concentrations of copper in the natural water samples were read from this graph.

Results and discussion

The calibration graph was a straight line passing through the origin. The results for the determination of copper in twelve samples of natural water are shown in Table 1, compared to results obtained by carbon-furnace a.a.s.

TABLE 1

Copper contents of natural waters determined by two independent a.a.s. methods

Sample	Copper found (ng ml^{-1})				
	Atom trapping[a]	Carbon furnace		Atom trapping[a]	Carbon furnace
Killhope 1	8	8	Ecton Hill 1	10	10
Killhope 2 (park level mine)	24	23	Ecton Hill 2	36	35
Dowgang mine	25	25	Ecton Hill 3	48	47
Rampgill mine	11	11	Ecton Hill 4	29	31
Cambokeels 1	51	51	Sheffield mains water	6	6
Cambokeels 2 (horse level)	17	17	Sheffield University Chemistry Dept.[b]	91	90

[a] After extraction. [b] After storage in a roof tank.

The standard deviation of ten determinations of Sheffield mains water (5.8 ng Cu ml^{-1}) was 0.17 ng ml^{-1} (r.s.d. = 2.9%). The 3σ limit of detection calculated from this value was 0.5 ng ml^{-1}. The concentrations of copper producing 1% absorption were 0.79 and 0.75 ng ml^{-1} by atom-trapping a.a.s. after liquid/liquid extraction and carbon furnace a.a.s., respectively.

The results obtained by atom-trapping a.a.s. after extraction are in excellent agreement with those obtained by carbon-furnace a.a.s. Therefore the former method can be recommended when carbon-furnace a.a.s. is not available. Naturally, it is somewhat slower because of the additional time needed for extraction and atom-trapping (about 6 min more per sample). The method is 165 times more sensitive than conventional flame atomic absorption spectrometry.

We thank the Research Committee of the University of the South Pacific for a grant towards this work and Dr. P. R. Ineson of the Department of Geology, University of Sheffield, for collecting water samples in Co. Durham.

REFERENCES

1 M. Kanke, Y. Hayashi, T. Kumamara and Y. Yamamoto, Nippon Kagaku Zasshi, 92 (1971) 983.
2 J. Khalighie, A. M. Ure and T. S. West, Anal. Chim. Acta, 107 (1979) 191.
3 M. Murakami and T. Takada, Talanta, 32 (1985) 513.

Analytica Chimica Acta, 197 (1987) 327—332
Elsevier Science Publishers B.V., Amsterdam — Printed in The Netherlands

Short Communication

AN INTERFERENCE EFFECT IN THE USE OF INDUCTIVELY-COUPLED ARGON PLASMA SPECTROMETRIC DETECTION FOR HIGH-PERFORMANCE LIQUID CHROMATOGRAPHY

GARY K.-C. LOW, GRAEME E. BATLEY* and STEPHEN J. BUCHANAN

CSIRO, Division of Energy Chemistry, Lucas Heights Research Laboratories, Private Mail Bag 7, Sutherland, N.S.W., 2232 (Australia)

(Received 3rd October 1986)

Summary. When arsenic species are determined by liquid chromatography with an inductively-coupled plasma detector, samples containing high concentrations (> 0.1 M) of easily ionizable elements, such as Na and K, can give rise to a spurious chromatographic peak. This peak is caused by a change in the emission background when the easily ionizable element in the matrix is eluted from the HPLC column as a concentrated slug. The effect cannot be attributed to scattered radiation from salt particles, or changes in aerosol transport efficiency or the physical dimension of the plasma.

In speciation studies, element-specific detection systems such as atomic absorption spectrometry (AAS) and inductively-coupled plasma atomic emission spectrometry (ICP/AES) are being increasingly used to detect species separated by high-performance liquid chromatography (HPLC). The inherent sensitivity and selectivity of these spectrometric techniques coupled with the preconcentration and resolution achievable by HPLC have resulted in sensitive, specific methods for arsenic [1], lead [2], tin [3], chromium [4] and selenium species [5].

The existence of matrix effects in the direct nebulization of samples in ICP/AES is well documented [6—9]. Easily ionizable elements such as sodium and potassium have been shown to affect the emission, while the presence of volatile organic compounds significantly alters the excitation properties of the plasma, resulting in a substantial net reduction of the required signal [10]. Mechanisms based on physical and chemical factors such as aerosol generation, transport efficiencies, shifts in ionization, enhanced collisional excitation and ambipolar diffusion have been postulated to explain changes in signal intensity [6]. Where the analyte is nebulized as a pulse, as occurs in the effluent from HPLC columns, the nature of these interference effects has largely been unexplored. While background interference problems would not be expected to differ from those of continuous nebulization, components of the sample matrix, separated by the column, could produce pulses of easily ionizable elements which could have significant effects on the background emission signals at the required wavelength.

0003-2670/87/$03.50

Because spurious peaks were observed during the determination of arsenic species in biological samples by HPLC with ICP/AES detection, interference effects were more fully investigated to elicit both their nature and their origins.

Experimental

Instrumentation. The HPLC system comprised a Waters model M45 solvent-delivery system, a U6K injector, a 25 cm × 4.1 mm i.d. Hamilton PRP-X100 anion column and a 25 cm × 4.1 mm i.d. Vydac 201Tp 5 μm C_{18} column (Hamilton Company). For the resolution of five arsenic species, these columns were used in conjunction with an automated switching valve as described previously [11].

The flow rate of the mobile phase into the nebulizer of the ICP/AES system was 2 ml min^{-1}. This system comprised a Labtest Plasma 2000 generator and matchbox, and a 0.5-m Ebert monochromator fitted with a 2100 groove mm^{-1} grating blazed at 260 nm. The optimized ICP parameters were 0.9 kW r.f. power, 1 l min^{-1} gas flow and 12–18 mm observation height (above top coil). The monochromator was peaked to the emission line of the analyte and was unaltered during each chromatographic run. The detection signal was recorded simultaneously by a Watanabe Servorecorder SR6312 and a locally built STD bus-based microcomputer which quantified the areas of the recorded peaks. Unless otherwise stated, a TR-30-A3 concentric glass nebulizer (J. E. Meinhard Associates, Santa Anna, CA) was used.

Reagents. Standard solutions for arsenic determination (750 mg As l^{-1}) and eluants were prepared from reagent-grade chemicals as described previously [12]. The eluant was 3×10^{-3} M ammonium dihydrogen-orthophosphate adjusted to pH 6.

Results and discussions

Formation of interference peaks. A typical application of ICP/AES detection in HPLC is to arsenic species in sea-water or urine samples, with separation on an anion-exchange column [1, 11, 12]. A column switching technique enables five arsenic species, As(V), As(III), monomethylarsonic acid (MMA), dimethylarsinic acid (DMA) and arsenobetaine to be resolved [11]. During examination of a series of urine samples enriched in arsenobetaine, an additional peak was obtained at a retention time which did not correspond to those of the other common arsenic species (Fig. 1). By collecting the eluant fraction containing this peak and directly aspirating it, it was shown not to contain arsenic. Systematic injection of major urine components, showed that sodium chloride was solely responsible for the spurious peak (Fig. 2).

The elution of sodium was followed at the sodium emission line at 330.2 nm. A sharp peak was evident initially, followed by a broader, more diffuse peak (Fig. 2D). However, if the sample was acidified to pH 3 prior to injection, a larger sharp peak was observed, presumably resulting from a different retention mechanism on the reverse-phase column. In strong electrolyte

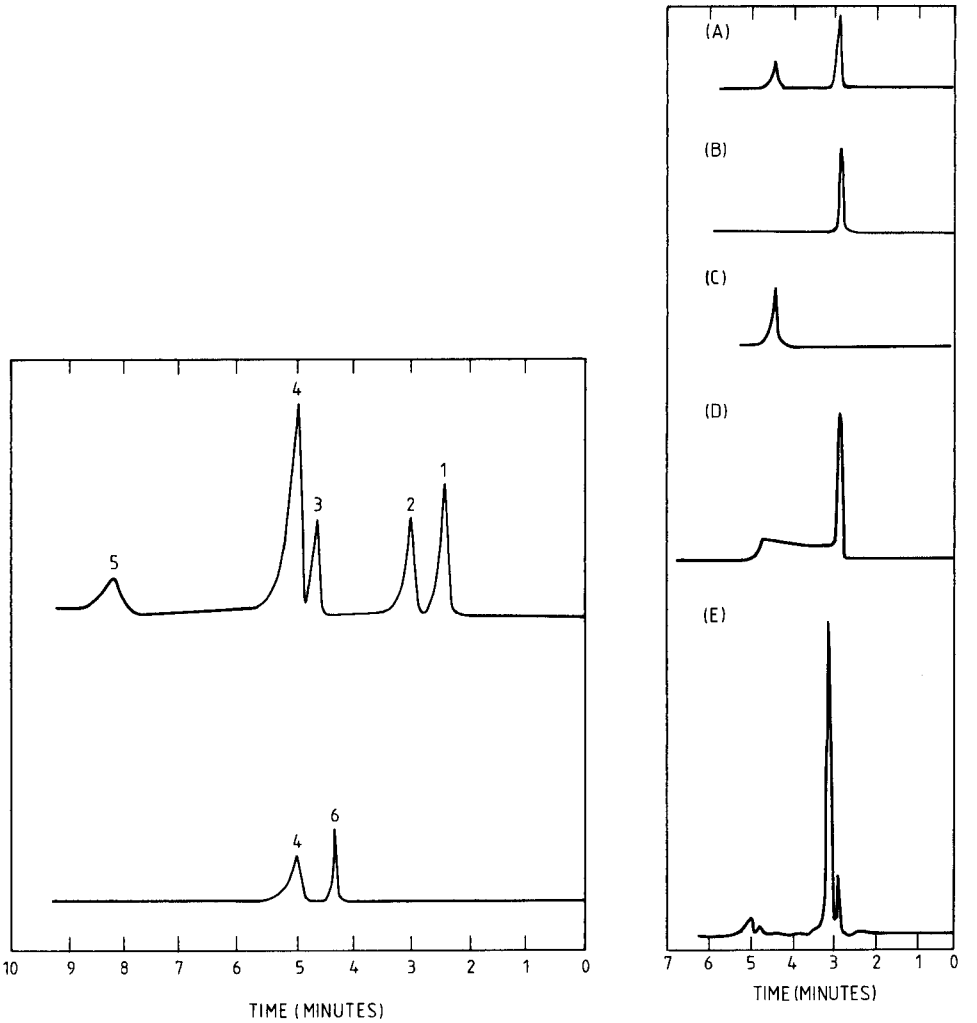

Fig. 1. The top chromatogram shows the separation of a standard mixture of arsenic species in water using a combined system of anion-exchange and C_{18} reverse-phase columns via a column-switching system. Peaks: (1) dimethylarsinic acid; (2) monomethylarsenic acid; (3) arsenic(III); (4) arsenobetaine; (5) arsenic(V). The bottom chromatogram shows the appearance of the spurious peak (6) prior to the elution of arsenobetaine (4) in a urine sample.

Fig. 2. Elution profiles from the C_{18} column only: (A) a urine sample containing arsenobetaine, monitored at the arsenic emission line (228.8 nm); (B) 0.51 M sodium chloride at 228.8 nm; (C) arsenobetaine in distilled water at 228.8 nm; (D) 0.51 M sodium chloride at the sodium line (330.2 nm); (E) as (A), but monitored at carbon emission line (193.09 nm).

solutions, the extent of exchange of the hydronium ions of the silanol groups ($\geqslant$Si-OH + $H_2O \rightleftharpoons \geqslant SiO^- + H_3O^+$) is regulated by the pH of the medium. At pH 3 the surface groups of the silica are completely undissociated, and lose their exchangeability.

When a 400 mg l^{-1} solution of arsenobetaine in 0.51 M sodium chloride was gradually diluted to 0.13 M sodium chloride, and equal volumes of each solution were injected onto the C_{18} column, the spurious peak height was found to decrease with the square root of the salt concentration, whereas the arsenobetaine peak decreased proportionally to concentration. Maessen et al. [7] observed a similar relationship for continuously aspirated, easily ionizable elements.

The spurious peak was also observed on injection of other electrolytes. For ionic strengths equivalent to 0.17 M NaCl, the peak height increased in the order $KCl < Na_2SO_4 < NaH_2PO_4 < NaNO_3 < NaCl$.

The formation of ghost peaks need not be restricted to the example of arsenic determination. Indeed, measurement at emission wavelengths other than those for arsenic in the range 190—250 nm revealed the same peak, originating from an increase in background continuum emission. This is evident in Fig. 2E where the spurious peak appeared even at the carbon emission line.

Effect of scattered radiation of eluting electrolytes on plasma background. A possible explanation for the peak is that it arises from a change in background caused by scattered radiation from the large concentration of eluting salt. The most intense emission lines of sodium have intensities several decades higher than the natural background [13] and these lines may be major contributors to background shifts through spurious reflections or scattering by optical components. This possibility was eliminated by using a dye solution filter at the entrance slit of the spectrometer, to filter out any stray light contributions above 550 nm, near the intense sodium emission lines at 588.99 and 589.59 nm. These lines are 60 and 30 times, respectively, more intense than the 330.24- and 330.33-nm sodium lines. The chromatograms obtained for arsenic speciation in sodium chloride solutions were identical, including the presence of the spurious peak, with or without the optical filter.

Physical disturbance of the plasma by the eluting electrolytes. The elution of an easily ionizable element as a concentrated slug from the HPLC column may temporarily change the physical dimensions of the plasma [14, 15] and therefore affect the emission background during the period of the elution of the spurious peak. To ascertain this, both still photographs and multi-frame film were taken during the entire chromatographic run. Measurements on the photographic enlargements of the plasma during the periods before, during and after the elution of the spurious peak showed no discernible difference in the dimensions of the plasma.

It is unlikely that the change in the background emission would arise from the shift in ionization equilibrium [6, 16] because measured ratios of Ar(I)

(357.25 nm) to Ar(II) (356.43 nm) remained constant throughout the chromatographic run.

Transport efficiency. In conventional ICP/AES, transport efficiency is defined as the ratio of the amount of analyte entering the plasma to the amount of analyte aspirated, and it is possible that a salt may affect this efficiency, especially when it elutes as a slug from the HPLC column. In the case where analyte is being aspirated as a slug, the transport efficiency is based on the integrated mass of analyte in the slug.

Transport efficiencies were measured by a direct method similar to that described by Smith and Browner [17]. A cellulose fibre filter (22 × 8 mm) was connected to the end of the delivery tube and sodium chloride solutions containing europium (400 mg l^{-1}) were aspirated for 30 s, with a 30-s aspiration of dilute hydrochloric acid between successive solutions. The filters were washed with 3 × 2.5 ml of 1 M hydrochloric acid and 2 ml of distilled water and the washings diluted to 10 ml. The europium retained by the filter was determined as a percentage of the total europium by ICP/AES measurements of these solutions at 382.0 nm. The results of triplicate measurements (Table 1) showed that, at least up to 0.51 M sodium chloride, the transport efficiency was not significantly altered.

To show that the spurious peak was not an artefact of the nebulization system used, a crossed-flow GMK nebulizer system was used in place of the concentric glass nebulizer system. The GMK nebulizer, reputed to be less affected by changes in salt concentration [8], gave no difference in the ratios of the spurious peak to arsenobetaine peak heights from those in the chromatograms obtained previously.

Conclusions

When an easily ionizable element is presented as a major component in the sample matrix and is eluted as a concentrated slug from the HPLC column into the plasma, it can manifest itself as a spurious chromatographic peak. This is important in studies of speciation, in that the appearance of an unexpected peak in an HPLC/element-specific detection system cannot be assumed automatically to be a different species of the same element. If the spurious peak cannot fully be resolved from the analyte peak, over-estimation of the analyte may occur. It is important therefore, not only to resolve species of an element from each other, but also to separate these species from the interfering peak.

TABLE 1

Effect of sodium chloride on the transport efficiency of an ICP/AES nebulization system

NaCl concentration[a] (M)	0.00	0.17	0.51	1.71
Transport efficiency[b] (%)	0.64 ± 0.02	0.63 ± 0.02	0.61 ± 0.01	0.57 ± 0.01

[a]In a solution containing 400 $\mu g\ l^{-1}$ europium. [b]Mean ± range.

REFERENCES

1 D. S. Bushee, I. S. Krull, P. R. Demko and S. B. Smith, Jr, J. Liq. Chromatogr., 7 (1984) 861.
2 M. Ibrahim, T. W. Gilbert and J. A. Caruso, J. Chromatogr. Sci., 22 (1984) 111.
3 D. T. Burns, F. Glocking and M. Harriott, Analyst, 106 (1981) 921.
4 I. D. Krull, K. W. Panaro and L. L. Gerhsman, J. Chromatogr. Sci., 21 (1983) 460.
5 J. P. McCarthy, J. A. Caruso and F. L. Fricke, J. Chromatogr. Sci., 21 (1983) 389.
6 M. W. Blades and G. Horlick, Spectrochim. Acta, Part B, 36 (1981) 881.
7 F. J. M. J. Maessen, J. Balke and J. L. M. de Boer, Spectrochim. Acta, Part B 37 (1986) 517.
8 J. Lee, J. R. Sedcole and M. W. Pritchard, Spectrochim. Acta, Part B, 41 (1986) 217.
9 J. R. Botto, Spectrochim. Acta, Part B, 40 (1985) 397.
10 P. W. J. M. Boumans and M. Ch. Lux-Steiner, Spectrochim. Acta, Part B, 37 (1982) 97.
11 G. K.-C. Low, G. E. Batley and S. J. Buchanan, J. Chromatogr., 368 (1986) 423.
12 G. K.-C. Low, G. E. Batley and S. J. Buchanan, Chromatographia, 22 (1986) 292.
13 R. K. Winge, V. J. Paterson and V. A. Fassel, Appl. Spectrosc. 33 (1979) 206.
14 W. Slavin, Anal. Chem., 58 (1986) 589A.
15 S. R. Koirthyohann, J. S. Jones, C. P. Jester and D. A. Yates, Spectrochim. Acta, Part B, 32 (1977) 455.
16 G. R. Kornblum and L. de Galan, Spectrochim. Acta, Part B, 32 (1977) 455.
17 D. D. Smith and R. R. Browner, Anal. Chem., 54 (1982) 533.

Analytica Chimica Acta, 197 (1987) 333—337
Elsevier Science Publishers B.V., Amsterdam — Printed in The Netherlands

Short Communication

EXTRACTION OF LANTHANIDES WITH 8-QUINOLINOL IN THE PRESENCE OF 6-AMINO-4,4′-(5-NONYL)-2,2′-BIPYRIDINE

S. TAGUCHI[a], M. HOJJATIE and H. FREISER*

Strategic Metals Recovery Research Facility, Department of Chemistry, University of Arizona, Tucson, AZ 85721 (U.S.A.)

(Received 19th December 1986)

Summary. 6-Amino-4,4′-(5-nonyl)-2,2′-bipyridine (ADNBP) is studied for adduct formation in combination with 8-quinolinol (HQ) for lanthanide extractions. Ytterbium, praseodymium and lanthanum are extracted as mixed complexes, $LnQ_3 \cdot$ ADNBP. 8-Quinolinol did not form self-adducts in these systems under the given conditions. Extractabilities are enhanced dramatically by ADNBP.

Numerous chelating reactants, either alone or combined with selected compounds suitable for adduct formation, have been studied to separate individual lanthanides by extraction [1—8]. In some cases, adduct-forming reagents improve extractability dramatically. In a previous paper, 4,4′-di(5-nonyl)-2-2′-bipyridine (DNBP) was studied for adduct formation in combination with 8-quinolinol (HQ) [7]. In this system, Yb, Ho, Eu and Pr were extracted as $LnQ_3 \cdot HQ \cdot$ DNBP and La as LaQ_3, and a higher self-adduct complex, such as $LnQ_3 \cdot 2HQ \cdot$ phen, found in the 1,10-phenanthroline (phen) system, was not observed. The reduced ability to form self-adducts may well be due to steric effects of the nonyl groups of DNBP. Extractability and separations were not much improved in this system. In the present study, 6-amino-4,4′-(5-nonyl)-2,2′-bipyridine (ADNBP) is proposed for adduct formation. Because the amino group is a strong electron-donating group, complex stability should be increased and, thus, extractability and perhaps selectivity might be improved.

Experimental

Apparatus. The ^{1}H-NMR spectra were measured at 60 MHz with a Varian EM-360L spectrometer, and at 250 MHz with a Bruker WM-250 spectrometer on samples containing tetramethylsilane as an internal standard. Mass spectra were measured with a Hewlett-Packard Model 5930A dodecapole spectrometer or a Varian MA7311A spectrometer equipped with a Varian SS-200 data

[a]Permanent address: Department of Chemistry, Toyama University, Toyama, Japan.

0003-2670/87/$03.50

system. The infrared spectra were obtained with a Perkin-Elmer 1800 spectrometer.

Reagents. Lanthanide (Yb^{3+}, Pr^{3+}, La^{3+}) solutions were prepared from the corresponding chlorides. 8-Quinolinol (Eastman Kodak) was purified by recrystallization from ethanol and dissolved in chloroform just prior to use. The buffer stock solution was 12-M tris(hydroxyamino)-methane (Tris); this solution contained 0.425 M sodium tartrate to prevent the formation of lanthanide hydroxides. Arsenazo-III was used as an aqueous 0.5% solution. The ADNBP was synthesized by treatment of DNBP with sodium amide according to the Chichibabin method [9—12]: 4 g of DNBP (Reilly Tar and Chemical Co.) purified by recrystallization from ethanol and 0.8 g of sodium amide were dissolved in dry toluene at 70°C under nitrogen, and refluxed for 72 h. After cooling, the mixture was treated with 10 ml of 10% (w/v) sodium hydroxide and 60 ml of water, and finally extracted with ethyl acetate. A deep brown oil was collected (4 g, 95%) by concentration. This oil was loaded on a silica gel column and eluted with chloroform to recover 77% of the unreacted starting material. Then the adsorbed material was eluted with ethyl acetate and 1 g of ADNBP (23% yield) was obtained by concentration. Nuclear magnetic resonance data (250-MHz H^1-NMR; $CDCl_3$): δ 8.63 (singlet, 1H, aromatic); 8.61 (singlet, 1H, aromatic); 8.41 (singlet, 1H, aromatic); 7.33 (doublet, 1H, aromatic); 7.31 (doublet, 1H, aromatic), 2.67 (multiplet, 2H, CH protons), 1.68 and 1.32 (multiplet, 24 H, CH_2 protons) and δ 0.99 ppm (triplet, 12 H, CH_3 protons). IR data (neat): 3351 cm^{-1} ($-NH_2$), 1603 (C=C aromatic). Mass spectral data, *m/z* (relative intensities): 423 (M^+, 29.1), 408 (7.1), 407 (4.7), 381 (31.24), 368 (68.7), 325 (100), 232 (60.2), 71 (32.9), 57 (75.4) and 55 (55).

Determination of distribution ratios. A 10-ml portion of buffered lanthanide solution and an equal volume of the reagent solution were equilibrated in a vial by shaking vigorously for 2 h. After separation of phases, equal-volume aliquots of both phases were pipetted. The lanthanides in the aqueous phase were determined by the arsenazo-III method after adjustment of pH to 2.6 ± 0.1 with formic acid [1]. The lanthanides in the organic phase were back-extracted into equal volumes of pH 5 formate buffer solution by shaking for 2 h [5], and also determined by the arsenazo-III method.

Results and discussion

The extraction equilibria for Yb, Pr and La with 8-quinolinol in the presence of ADNBP were evaluated by the slope method. The slopes of three in the plots of log D vs. pH for each lanthanide under the given conditions indicate release of three protons in the extraction (Fig. 1). Plots of log D — 3 pH vs. log $[ADNBP]_o$ (Fig. 2) gave slopes of unity for each metal, indicating a single ADNBP molecule in the adducts. Finally, plots of log D — 3 pH vs. log $[HQ]_o$ (Fig. 3) had slopes of three, indicating three 8-quinolinol molecules in the extracted complexes.

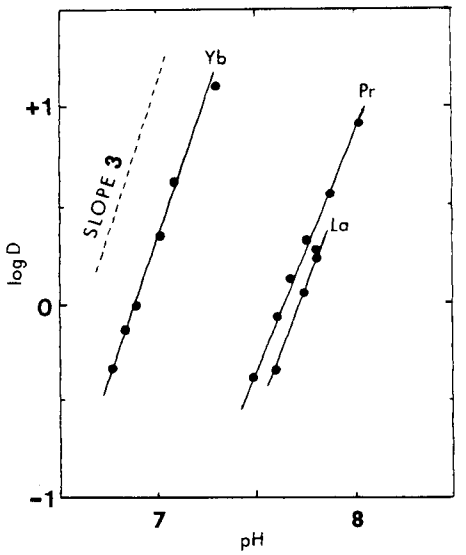

Fig. 1. Relationships between log D and pH. Aqueous phase: $[Ln^{3+}] = 2 \times 10^{-5}$ M, [tartrate] = 0.034 M, [Tris] = 0.0096 M. Organic phase: $[HQ]_o$ = 0.1 M in chloroform, $[ADNBP]_o$ = 0.003 M in chloroform.

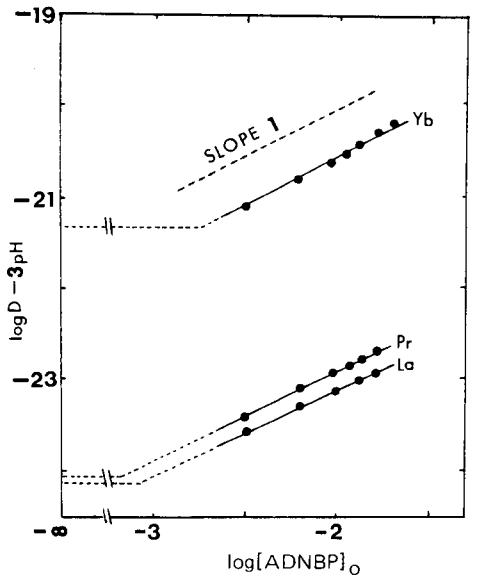

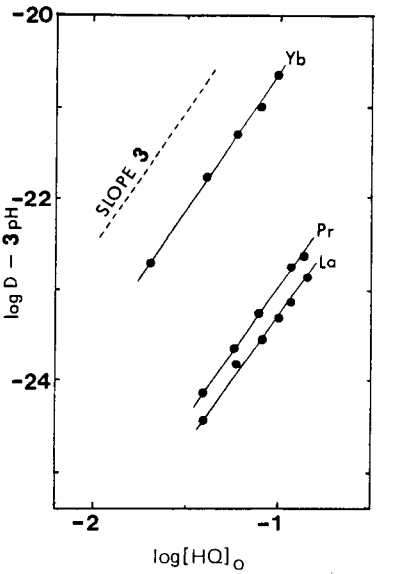

Fig. 2. Relationships between log D − 3 pH and log $[ADNBP]_o$. Conditions as in Fig. 1 except for ADNBP concentration.

Fig. 3. Relationship between log D − 3 pH and log $[HQ]_o$. Conditions as in Fig. 1 except for HQ concentration.

From these results, the overall reaction can be expressed as

$$LnT_2^- + 3HQ(org) + ADNBP(org) \overset{K'_{ex}\beta_{0,1}}{\rightleftharpoons} LnQ_3 \cdot ADNBP(org) + 3H^+ + 2T^- \quad (1)$$

where $\beta_{0,1}$ is the formation constant of the adduct in the organic phase from the chelate LnQ_3 and ADNBP, and K'_{ex} is the conditional constant of the extraction of the simple 8-quinolinolate, LnQ_3, from the tartrate complex, LnT_2^-, and is defined as

$$K'_{ex} = \beta_3 K_{DC} K_a^3 / K_{DR}^3 \beta_2 C_T^2$$

where K_a and K_{DR} are the acid dissociation and distribution constants of 8-quinolinol, β_3 and K_{DC} are the overall aqueous-phase formation constant and distribution constant of LnQ_3, and β_2 and C_T are the formation constant of the lanthanide tartrate complex and total concentration of tartrate. The overall extraction constant of reaction 1 can be expressed as

$$K'_{ex}\beta_{0,1} = D\,[H^+]^3/[HQ]_o^3[ADNBP]_o \quad (2)$$

where D is the distribution ratio of the lanthanide. Values of $K'_{ex}\beta_{0,1}$ can be calculated from the equilibrium extraction data by means of Eqn. 2 (Table 1).

TABLE 1

Values of extraction constants, separation factors (SF) and half-extraction pH

	La^{3+}		Pr^{3+}		Yb^{3+}
Log K'_{ex} [a]	−21.1		—		—
$pH_{1/2}$	8.03				
Log $K'_{ex}\beta_{3,0}$ [b]	—		−18.71		−15.24
SF				3.47	
$pH_{1/2}$	—		8.24		7.08
Log $K'_{ex}\beta_{2,1}$ [c]	—		−17.30		−13.68
SF				3.62	
$pH_{1/2}$	—		7.79		6.56
Log $K'_{ex}\beta_{1,1}$ [d]	—		−18.94		−15.91
SF				3.03	
$pH_{1/2}$	—		7.96		6.98
Log $K'_{ex}\beta_{0,1}$ [e]	−17.58		−17.40		−15.15
SF		0.18		2.75	
$pH_{1/2}$	(7.70)[f]		(7.66)[f]		(6.89)[f]
	7.19[g]		7.13[g]		6.38[g]

[a—e]Stoichiometry of extracted complexes (where HQ is 8-quinolinol): (a) LnQ_3 [1]; (b) $LnQ_3 \cdot 3HQ$ [1]; (c) $LnQ_3 \cdot 2HQ \cdot$ phen [1]; (d) $LnQ_3 \cdot HQ \cdot$ DNBP; (e) $LnQ_3 \cdot$ ADNBP.

Experimental conditions: for aqueous phase $[Ln^{3+}] = 1-2 \times 10^{-5}$ M, [tartrate] = 0.034 M, [Tris] = 0.0096 M; for organic phase, $[HQ]_o = 0.1$ M, [adduct reagent]$_o$ = 0.1 M. [f]Results at $[ADNBP]_o = 0.003$ M. [g]Calculated value from log $K'_{ex}\beta_{0,2}$ at $[ADNBP]_o$ = 0.1 M to compare with other systems.

The $pH_{1/2}$ values of the present system are much lower than in other systems, under comparable conditions, demonstrating that ADNBP is effective for adduct formation. It is more effective for lighter lanthanides than for heavier, however, so that separations are not much improved.

This research was supported by a grant from the Department of Energy.

REFERENCES

1 T. Hori, M. Kawashima and H. Freiser, Sep. Sci. Technol., 15 (1980) 861.
2 M. Kawashima and H. Freiser, Anal. Chem., 53 (1981) 284.
3 O. Tochiyama and H. Freiser, Anal. Chem., 53 (1981) 874.
4 O. Tochiyama and H. Freiser, Anal. Chim. Acta, 131 (1981) 233.
5 E. Yamada and H. Freiser, Anal. Chem., 53 (1981) 2115.
6 Y. Sasaki and H. Freiser, Inorg. Chem., 22 (1983) 2289.
7 S. Taguchi and H. Freiser, Solv. Extr. Ion Exch., in press.
8 S. Motomizu and H. Freiser, Solv. Extr. Ion Exch., 3 (1985) 637.
9 A. E. Chichibabin and O. A. Seide, J. Russ. Phys. Chem. Soc., 46 (1914) 1216.
10 H. D. Tjeenk Willink, Jr. and J. P. Wihaut, Rec. Trav. Chim., 53 (1934) 275.
11 M. T. Leggler, Org. React., 1 (1942) 91.
12 J. E. Parks, B. E. Wagner and R. H. Holm, J. Org. Metal. Chem., 56 (1973) 53.

Analytica Chimica Acta, 197 (1987) 339—342
Elsevier Science Publishers B.V., Amsterdam — Printed in The Netherlands

Short Communication

DETERMINATION OF STABILITY CONSTANTS OF A COPPER/CITRIC ACID COMPLEX BY ION-EXCHANGE CHROMATOGRAPHY AND ATOMIC ABSORPTION SPECTROMETRY

MARK R. PITLUCK[a], BRUCE D. POLLARD[b] and DANIEL T. HAWORTH*
Department of Chemistry, Marquette University, Milwaukee, WI 53233 (U.S.A.)
(Received 7th May 1986)

Summary. The method is based on separation of free copper ion from the complex by ion-exchange chromatography and determination of the free copper ions by atomic absorption spectrometry. Parameters that influence the separation and determination of the free metal are evaluated. Calculation of the conditional stability constant and the number of binding sites per citric acid (L) molecule was based on a Scatchard plot. The conditional stability constants found for the CuL^{2-} complex were pK = 5.04 at pH 7.0 and pK = 4.76 at pH 6.2 and ionic strength 0.10 M. The number of binding sites per molecule was unity.

A combined ion-exchange chromatographic/atomic absorption spectrometric method is developed for the determination of stability constants and combining ratios. Citric acid (2-hydroxyl-1,2,3-propanetricarboxylic acid) is a well-known masking agent [1]. Copper binding by citric acid (H_4L) has been widely studied. The H_3LCu^+, H_2LCu, $HLCu^-$ and LCu^{2-} complexes are known [2] and the LCu^{2-} species predominate at pH > 6 [3]. This complex is used as a model to evaluate the method.

Calculation of the conditional stability constant for the copper/citric acid complex from the experimental data is based on the Scatchard plot [4]. The Scatchard parameter, ν, for the copper/citric acid solution is defined as $\nu = [LCu^{2-}]/C_L$, where $[LCu^{2-}]$ is the concentration of the complex and C_L is the analytical concentration of citric acid. The conditional stability constant, K', can be evaluated from

$$\nu/[Cu^{2+}] = K'n - K'\nu \quad (1)$$

where $[Cu^{2+}]$ is the concentration of free copper ion and n is the number of binding sites per citrate ion. A plot of $\nu/[Cu^{2+}]$ vs. ν should yield a straight line with a negative slope equal to the conditional stability constant and intercept equal to $n\,K'$. Uncomplexed Cu^{2+} concentration is quantified by

[a]Present address: Pfizer Central Research, Groton, CT 06340, U.S.A
[b]Present address: ARCO Chem. Co., Newtown Square, PA 19073, U.S.A.

0003-2670/87/$03.50

atomic absorption spectrometry (AAS) after separation from complexed copper, and the latter is quantified by difference between total and uncomplexed copper.

Experimental

Preparation of solutions. A stock copper solution (ca. 1.5×10^{-2} M) was prepared from copper nitrate (Gold Label; Aldrich Chemical Co.) and its concentration was verified with AAS. Other concentrations were prepared by dilution of this stock. A stock solution (1.00×10^{-2} M) was prepared from citric acid (Gold Label, Aldrich Chemical Co.).

A series of copper/citric acid solutions was prepared with a copper concentration of 2.00×10^{-4} M and citric acid concentrations between 2.00×10^{-4} and 1.00×10^{-3} M. The ionic strength of each solution was adjusted to 0.10 M with 0.20 M sodium nitrate and the pH was adjusted to 6.2 or 7.0 with a sodium hydroxide or nitric acid solution.

Instrumentation. The liquid chromatograph consisted of a Tracor 995 isochromatographic pump, Rheodyne 7125 injector equipped with a 100-μl loop, and a Tracor 960 ultraviolet (UV) detector. Solvent was selected with a series of solenoid valves. An ion-exchange column (40 mm long, 1.6 mm i.d.) was constructed of teflon tubing and 316 stainless steel Swagelok column end-fittings with 2-μm stainless steel frits. The column was slurry-packed with HC-Pellionex SCX (37—53 μm particle size; Reeve Angel, Clinton, NJ), a strong cation-exchange resin consisting of a polystyrene/divinylbenzene copolymer base with sulfonic acid functional groups. The resin has an exchange capacity of 60 μeq g^{-1} (dry weight) and is stable between pH 2 and 10.

The outlet of the UV detector was connected to the premix burner of the atomic absorption spectrometer (Instrumentation Laboratory 251 AA/AE) with 1/16 in. teflon tubing and appropriate Swagelok fittings. The spectrometer was interfaced to a Rockwell International Aim 65 microcomputer.

Chromatographic parameters. Solutions were injected onto the ion-exchange column using a 100-μl loop and a water mobile phase at 4.0 ml min^{-1}. The negatively charged copper/citric acid complex eluted from the column at the bed volume while the free copper ions were retained. After 30 s, the mobile phase was switched to 0.10 M barium nitrate for 15 s to elute the adsorbed copper. Barium nitrate was chosen because the high exchange constant for Ba^{2+} produces minimal band spreading of the copper ions being eluted. The mobile phase was switched to 0.10 M sodium nitrate for 15 s to remove barium ions from the resin and then back to water for 3.5 min to remove excess of sodium ions. Additional injections were made at the end of the water rinse cycle and the mobile phase sequence was repeated. A 20-μl loop was substituted for the 100-μl loop when the free metal concentration of the copper/citric acid solutions exceeded the linear dynamic range of the system; copper calibration standards of higher concentrations were then used.

Spectrometric parameters. The parameters for the spectrometer were: 324.7 nm wavelength, 640 μm slitwidth, 0.2 mA per count, intensity at 4 V, 620 V on the photon multiplier, 2 mA lamp current, and 22 mA deuterium lamp current. The aspiration rate of the premix burner was set at 2.0 ml min^{-1} for a chromatographic flow rate of 4.0 ml min^{-1}. The aspiration rate as a function of chromatographic flow rate was optimized for signal-to-noise.

Calibration. The calibration graph was linear over the copper concentration range 2.50×10^{-5}—1.00×10^{-4} M with a typical slope and intercept of 4.9×10^4 cm l mol^{-1} and 0.20 cm, respectively. Calibration was repeated for each series of copper/citric acid solutions. The relative standard deviation (*RSD*) for the peak height of copper standards ($n = 4$) was usually less than 6%. The major contributor to the *RSD* was flicker noise of the premix burner; to compensate for the flicker noise, sample solutions were bracketed with appropriate standards.

Results and discussion

Typical chromatograms are shown in Fig. 1. Parameters that affected the peak shape of the copper standard peak were pH and ionic strength of solution. Decrease in pH and increase in ionic strength caused peak broadening and tailing. The copper standards were matched in pH and ionic strength to the sample solutions to reduce differences in the peak shapes.

The most probable source of error in this method is dissociation of the complex during the separation step. Dissociation of the complex during the separation was not expected to be significant because the complex was in contact with the ion-exchange column for only 0.7 s. The fact that peak parameters (peak width, tailing and asymmetry) of copper ion peak separated from the complex were equivalent to peaks of the copper standard solutions tends to support this expectation.

Scatchard parameters are shown in Fig. 2 for pH 6.2 and 7.0 and ionic strength 0.10 M. The logarithm of the conditional stability constant obtained from the slope is 5.04 ± 0.03 at pH 7.0 and 4.76 ± 0.04 at pH 6.2. The value of SiO_4 at pH 7 is in reasonable agreement with the value of 5.2 reported by LeFebvre [5] at the same pH. Values reported by others are 4.4 and 5.95 [6] at ionic strengths of 2.0 and 0.5, respectively, and 5.2 at an ionic strength of 1.0 [2], all in the pH range 4.8—7.0. Differences are attributed to different solution conditions. Additional influencing factors are that the concentration of citric acid in this study was 2×10^{-4}—1×10^{-3} M while most other studies involved concentrations of 1.5×10^{-2} M and greater.

The number of binding sites per citric acid molecule was calculated to be 1.03 ± 0.03 for solutions at pH 7.0 and 0.91 ± 0.04 for solutions at pH 6.2. It is emphasized that this method will apply only for complexes with dissociation rates that are slow relative to the chromatographic process.

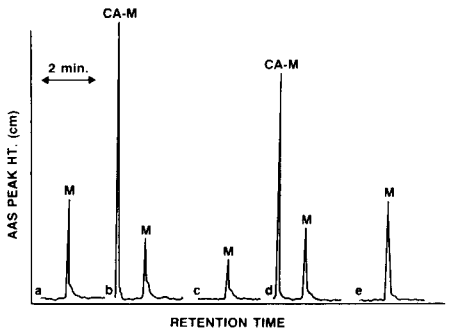

Fig. 1. Typical chromatograms for copper standards (a, c, e) and copper/citrate solutions (b, d). M represents the free copper ion and CA-M represents citric acid/copper complex.

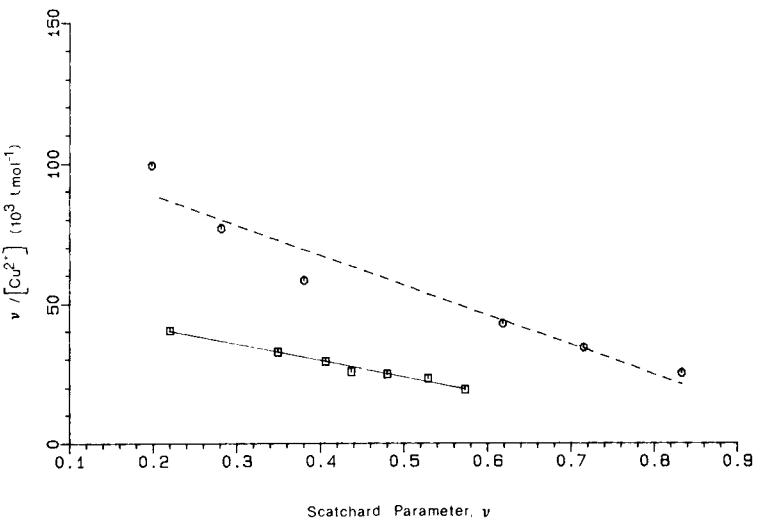

Fig. 2. Scatchard plots for Cu(II) binding by citric acid at ionic strength 0.10 M: (□) at pH 6.2; (○) at pH 7.0. Each point is the average of four separate solution preparations and treatments.

REFERENCES

1 I. M. Kolthoff, E. B. Sandell, E. J. Meehan and S. Bruckenstein, Quantitative Chemical Analysis, Macmillan, NY, 1969.
2 L. G. Sillen and A. E. Martell, Stability Constants of Metal-Ion Complexes, The Chemical Society, London, 1964, p. 479.
3 R. C. Warner and J. Weber, J. Am. Chem. Soc., 75 (1953) 5086.
4 G. Scatchard, Ann. N.Y. Acad. Sci., 51 (1949) 660.
5 J. Lefebvre, J. Chem. Phys., 54 (1957) 581.
6 I. R. Still and P. Wikberg, Inorg. Chim. Acta, 46 (1980) 147.

Analytica Chimica Acta, 197 (1987) 343—346
Elsevier Science Publishers B.V., Amsterdam — Printed in The Netherlands

Short Communication

REVERSED-PHASE ION-PAIR SEPARATION OF SEVERAL WEAK ORGANIC ACIDS FOUND IN URINE

FREDERICK H. WALTERS

Department of Chemistry, University of Southwestern Louisiana, Lafayette, LA 70504 (U.S.A.)

(Received 29th July 1986)

Summary. Retention data are presented for homovanillic acid, 5-hydroxyindoleacetic acid, *p*-hydroxyphenylacetic acid, vanillic acid and hippuric acid on reversed-phase C-18 columns with aqueous and 10% (v/v) methanolic acetic acid buffers. These data are fitted to a model and window diagrams are constructed from calculated model parameters. The optimum pH for separation of these acids is 4.2—4.4.

The weak organic acids studied here all occur in urine, interfere with one another in some methods, and are all physiologically significant. Vanillylmandelic acid and homovanillic acid are urinary metabolites of ephinephrine and norephinephrine. Hippuric acid is a urinary metabolite used to test liver function after administration of benzoic acid. 5-Hydroxyindoleacetic acid is the urinary metabolite of serotonin.

Homovanillic acid (often measured with vanillymandelic acid) is the most important of the above group. Chromatographic methods presently used include high-performance liquid chromatography (HPLC) with ion-exchange columns [1], ion exchange followed by ion-moderated partition [2], two-dimensional HPLC [3], liquid chromatography on alumina, Sephadex G-10 and ion-exchange columns [4] and gas chromatography with electron-capture detection [5].

Deming and coworkers [6—8] have utilized window diagrams to optimize these separations after fitting retention data to a simple model [7] based on weak-acid equilibria. Calculated model parameters (t_{HA}, t_A, and pK_a) were then used to construct window diagrams of relative retention vs. pH. From these window diagrams, optimum conditions could be chosen for the separation of a mixture of the organic acids.

In this communication, reversed-phase ion-pair chromatography with an ultraviolet detector is utilized to study the separation of four weak organic acids found in urine along with homovanillic acid. There are more sensitive electrochemical [9, 10] and fluorescence detectors [11] available for these components but the emphasis here will be on establishing the optimum separation conditions between these five acids by using window diagram methodology.

0003-2670/87/$03.50

Experimental

Homovanillic acid (4-hydroxy-3-methoxyphenylacetic acid), 5-hydroxyindole-3-acetic acid, *p*-hydroxyphenylacetic acid, vanillic acid (4-hydroxy-3-methoxybenzoic acid) and hippuric acid were obtained from Aldrich Chemicals. Samples were dissolved in the eluting solvent before injection. Dilute (1 M) acetic acid and sodium hydroxide were used to make the eluting buffer and HPLC-grade ethanol was used as an organic modifier.

The liquid chromatographic setup consisted of a Tracor Model 960 ultraviolet fixed-wavelength detector (254 nm), an LDC Constametric III pump, a Hewlett-Packard Model 3390 Integrator and an Alltech 10-μm C_{18} reversed-phase column (25 cm × 4.6 cm i.d.).

Results

Retention data for homovanillic acid, 5-hydroxyindole-3-acetic acid, *p*-hydroxyphenylacetic acid, vanillic acid and hippuric acid are tabulated in Table 1. The eluent pH was varied from 3.9 to 6.15 and aqueous acetate and 10% methanolic acetate buffers were used. The 10% methanol decreases the retention times significantly and allows better chromatographic behavior on the column. The pH range chosen brackets that of the pK_a values of the weak acids studied. Several other acids (*p*-hydroxymandelic acid, vanillymandelic acid, 3,4-dihydroxymandelic acid) had retention times less than 3 min in the methanolic buffer solutions indicating that their pK_a values are < 4. The data were then fitted to the function

$$t = (t_{HA} + t_A\ 10^{(pH - pK_a)})/(1 + 10^{(pH - pK_a)})$$

using a simplex, nonlinear least-squares computer program similar to that described by O'Neill [12]. Here, t is the observed retention time and t_{HA} and t_A are the retention times of the molecular form and anion of the acid,

TABLE 1

Retention data for selected organic acids on a reversed-phase C_{18} column in the pH range 3.9—6.15

Compound	Retention time (min) at different pH							
	Aqueous media[a]					Methanolic media[b]		
	3.90	4.40	4.75	5.0	6.15	4.75	5.85	6.15
Homovanillic acid	12.90	10.06	6.79	5.63	1.88	16.87	13.44	9.34
5-Hydroxyindole-3-acetic acid	7.84	6.70	5.17	4.29	1.69	26.20	10.52	8.09
p-Hydroxyphenylacetic acid	7.66	6.31	4.41	3.57	1.38	16.99	7.19	4.95
Vanillic acid	11.12	8.99	5.99	4.82	1.32	25.03	7.83	4.94
Hippuric acid	5.01	4.48	4.14	3.85	2.69	16.35	8.29	5.07

[a] Aqueous acetate buffer (0.06 M) at 3.3 ml min^{-1}. [b] 10% methanolic acetate buffer at 2.5 ml min^{-1}.

respectively. Values of t_{HA}, t_A and pK_a obtained for each acid are reported in Table 2.

The values of pK_a duplicated those obtained in the literature [13]. Price et al. [7] used vanillic acid under similar conditions with citrate buffers (10% methanol); their values for t_{HA}, t_A and pK_a for vanillic acid were 16.59, 2.75 and 4.53, respectively. The pK_a value is in good agreement with that shown in Table 2. The values obtained for the pK_a of 5-hydroxyindole-3-acetic acid are different in the aqueous and 10% methanolic buffers. The reason for this could be inaccuracies in measuring the long retention times for this compound in the aqueous buffer as well as the scarcity (3 points) of retention data.

From the data in Table 2, window diagrams can be drawn for both solvents (Fig. 1). When dilute buffered acetic acid is the solvent, the optimum occurs near pH 4.2 (Fig. 1A). The V-shaped indentation is not observed for the dilute methanolic acetic acid buffer where the optimum pH is near 4.5 (Fig. 1B). The retention times are noticeably less in the methan-

TABLE 2

Values for t_{HA}, t_A, and pK_a for selected weak organic acids on the C_{18} column

Compound	Aqueous media[a]			Methanolic media[b]		
	t_{HA} (min)	t_A (min)	pK_a	t_{HA} (min)	t_A (min)	pK_a
Homovanillic acid	25.36	12.99	4.41	17.53	2.62	4.40
Vanillic acid	58.97	5.51	4.51	14.72	1.63	4.51
p-Hydroxyphenylacetic acid	58.31	6.31	4.17	13.69	1.99	4.17
Hippuric acid	172.82	7.55	3.50	11.37	3.62	3.50
5-Hydroxyindole-3-acetic acid[c]	112.58	5.65	4.09	9.60	2.42	4.57

[a]Aqueous acetate buffer (0.06 M). [b]10% methanolic acetate buffer. [c]Literature value [13] for pK_a = 4.54.

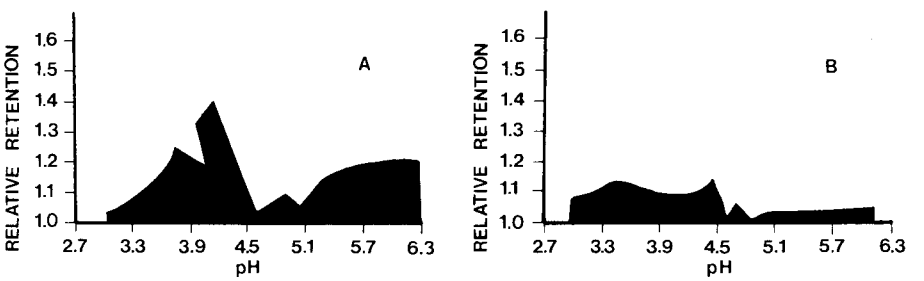

Fig. 1. Window diagrams for weak organic acids: (A) in aqueous acetic acid buffers; (B) in 10% methanolic acetic acid buffers.

olic solvent, but provide an adequate separation (see volumes given for pH 4.4 in Table 1).

The help of Her Tsang Chen of the Chemical Engineering Department in programming the simplex nonlinear least-squares program is acknowledged.

REFERENCES

1 T. Toluda, M. Masanou and Z. Tamura Koyokomori, Bunseki Kagaku, 33 (1984) E331.
2 S. R. Binder and G. Sivorinovsky, J. Chromatogr., 336 (1984) 173.
3 G. M. Anderson, K. R. Schlicht and P. J. Cohen, Anal. Biochem., 144 (1985) 27.
4 B. H. Westerlink, F. J. Bosker and J. F. O'Hanlon, Clin. Chem., 28 (1982) 1745.
5 S. W. Dziedzic, L. B. Dziedzic and S. E. Gittow, J. Lab. Clin. Med., 82 (1973) 829.
6 S. N. Deming and M. L. H. Turoff, Anal. Chem., 50 (1978) 546.
7 W. P. Price, R. Edens, D. L. Hendrix and S. N. Deming, Anal. Biochem., 93 (1979) 233.
8 W. P. Price and S. N. Deming, Anal. Chim. Acta, 108 (1979) 227.
9 R. F. Seegal, K. O. Brosch and B. Bush, J. Chromatogr., 273 (1983) 253.
10 J. Durtrieu and Y. A. Delmotte, Fresenius' Z. Anal. Chem., 317 (1984) 124.
11 T. G. Rosano, H. H. Brown and J. M. Meola, Clin. Chem., 27 (1981) 228.
12 R. O'Neill, Appl. Stat., 20 (1971) 338.
13 E. P. Serjeant and B. Dempsey (Eds.), IUPAC Ionization Constants of Organic Acids in Aqueous Solution, Pergamon, Oxford, 1979.

Analytica Chimica Acta, 197 (1987) 347—352
Elsevier Science Publishers B.V., Amsterdam — Printed in The Netherlands

Short Communication

INTEGRATED-CIRCUIT BIO-CALORIMETRIC SENSOR FOR GLUCOSE

H. MURAMATSU

Seiko Instruments, Research and Development Department, Takatsukashinden, Matsudo-shi, Chiba 271 (Japan)

J. M. DICKS

Biotechnology Centre, Cranfield Institute of Technology, Cranfield, Bedfordshire MK43 0AL (Great Britain)

I. KARUBE*

Research Laboratory of Resources Utilization, Tokyo Institute of Technology, Nagatsuta-cho, Midori-ku, Yokohama 227 (Japan)

(Received 9th September 1986)

Summary. Two integrated-circuit temperature-sensitive devices, each composed of three Darlington-connected npn transistors and a CMOS constant-current circuit, are used for calorimetric determination of glucose concentration. One device is modified with a cellulose triacetate/1,8-diamino-4-aminomethyloctane membrane and used for glutaraldehyde immobilization of glucose oxidase. The difference in steady-state output voltage of the enzyme-modified sensor compared to the unmodified sensor after addition of glucose is related to the temperature change induced by the enzyme-catalyzed reaction. Glucose is determined in the range 5—100 mM after signal analysis by fast-Fourier transform. The enthalpy change approximates to that of a spherical silicon conduction model.

Numerous publications have dealt with the detection of chemical substances by biological means [1—3]. The inherent advantages of using biological systems are high selectivity, ambient reaction conditions and novel biochemical characteristics. The detection device, the transducer, can exploit aspects of the biological reaction such as a change in current, light emission, mass or heat. Most enzymatic reactions are associated with heat evolution, making calorimetry almost universally applicable to biosensor development.

Mosbach and Danielsson [4], Danielsson [5] and Scheller et al. [6] have reported extensively on the enzyme thermistor system, highlighting the attractiveness of the technique for quantifying a large number of substances, simply by changing the enzyme column on-line with the thermistor. There are, however, several disadvantages in using thermistor detection: non-linear resistance/temperature properties and variation of response between thermistors, change of resistance with time because of gradual ageing, and self-heating of the thermistor caused by current flow. Self-heating can be reduced by using a bridge circuit, but for a small detection device, such as would be suitable for in vivo use, the low signal-to-noise ratio caused by the connection to

0003-2670/87/$03.50

the bridge makes thermistors impractical for microsensor application. The enzyme thermistor was designed for flow analysis, hence the size of the enzyme column and associated peripherals is not a problem.

The aim here was to construct a micro bio-calorimetric sensor, suitable for the assay of small sample volumes and possible in vivo use. Integrated-circuit temperature-sensitive devices do not suffer from the problems associated with conventional thermistors. Because a change in temperature changes the potential of the transistor assembly, self-heating and ageing do not occur, voltage/temperature characteristics are linear and variation between integrated circuits can be minimized to high tolerance levels. This paper describes a new method for glucose detection by using glucose oxidase immobilized on the surface of a temperature-sensitive integrated-circuit device, and the techniques applied for construction of the system.

Experimental

Materials. 1,8-Diamino-4-aminomethyloctane and cellulose triacetate were obtained from Asahi Kasei Co. and Eastman Kodak Co., respectively. Glutaraldehyde was from Kanto Kagaku Co. All other chemicals were of commercial analytical grade. All aqueous solutions were made up in distilled water.

Construction of the thermal sensor. The integrated-circuit (IC) thermal sensors used (Seiko Instruments Inc.) were composed of three Darlington-connected npn transistors, wherein the collector of each transistor is connected in common, the base of the first is connected to the common collector, and the emitter of the third transistor is connected to a CMOS constant-current circuit (Fig. 1). The total dimensions of the IC thermal sensor are $1 \times 1 \times 0.3$ mm and the sensor is coated with a silicon nitride layer (0.95 μm thick). The sensors require only a 3-V power supply and exhibit excellent linearity of voltage/temperature dependence (10 mV $^{\circ}C^{-1}$) in the range -40°C to 80°C [7, 8].

Two IC thermal sensors were bound inside a plastic case and electrical connection was made to the IC with a conventional aluminum IC bonder. The case was encapsulated with insulating epoxy resin (two component, setting time 5 min) except for the surface of the thermal sensors. The membrane used for enzyme immobilization was formed by casting a solution

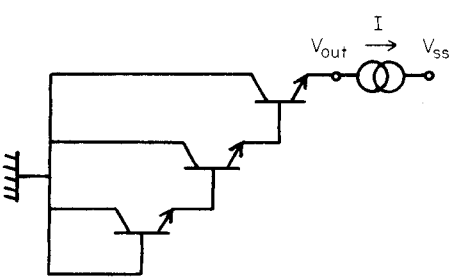

Fig. 1. Circuit diagram of the IC thermal sensor.

containing cellulose triacetate (50 mg ml^{-1}), 1,8-diamino-4-aminomethyl-octane (20%) and glutaraldehyde (2%) in dichloromethane onto the surface of one thermal sensor [9]. After 24 h, the membrane was re-treated with glutaraldehyde (2% in water) for 1 h and immersed in glucose oxidase solution (1 mg ml^{-1}, 0.05 M phosphate buffer pH 7) for 12 h at 20°C. After reaction, the membrane was washed thoroughly with the phosphate buffer (pH 7) and stored at 4°C.

The measurement system consisted of digital voltmeters (Hewlett-Packard, model 3478A), power supply (Metronix, model 521C) and personal computer (Nippon Electronics Company, model PC-9801E). The above-described biocalorimetric sensor was connected to the power supply. Each output voltage was measured by the voltmeters which were connected to the computer with a GP-IB (IEEE-488). Temperature control was maintained with a stirred thermostated bath connected via the computer to a third IC thermal sensor. In this way, the temperature of the bath could be held to within ±0.01°C. Data from the thermal sensors was processed by the computer every 0.5 s and either continuously displayed on a monitor or stored on floppy disk.

Procedure. The thermal sensor system was applied to batch determinations of glucose. The sensors were placed into a 5-ml cell containing 2 ml of the pH 7 phosphate buffer in the thermostated bath at 30°C. After the temperature of the bath and the output voltage of the thermal sensors became constant, an aliquot of glucose solution stored in the water bath (0.2 ml, pH 7) was injected into the sensor compartment. The difference between the output voltage of the sensor modified with the glucose oxidase membrane, and that of the unmodified sensor was related to the enthalpy change resulting from the enzymatic reaction. The difference in stationary output voltage after glucose addition was used as the measure of glucose concentration.

The activity of the immobilized enzyme was also evaluated spectrophotometrically by measuring the absorbance change at 535 nm of a solution containing glucose (10 mM), peroxidase (4 mg dl^{-1}), *o*-dianisidine (0.66 g dl^{-1}) and phosphate buffer (pH 7, 0.05 M) after reaction with the immobilized enzyme on the thermal sensor. The activity in mol s^{-1} was estimated by comparison with the absorbance change effected by the free enzyme after complete reaction with glucose of known concentration.

Results and discussion

Response of the sensor. The normal operational output voltage of the thermal sensors was ca. 1.2 V at 30°C, with a voltage difference in the range ±0.01 mV between the two integrated circuits. Figure 2A shows a typical response of the thermal sensors to the injection of a portion of glucose solution (2 mM final concentration). As can be seen, high-frequency noise made isolation of the response signal from the raw data difficult; fast Fourier transform (FFT) was used to remove it [10, 11]. The FFT signal is shown in Fig. 2B. The FFT signal was then passed through a filter window (Fig. 2C) to remove the high-frequency noise (Fig. 2D). The reduction range for the

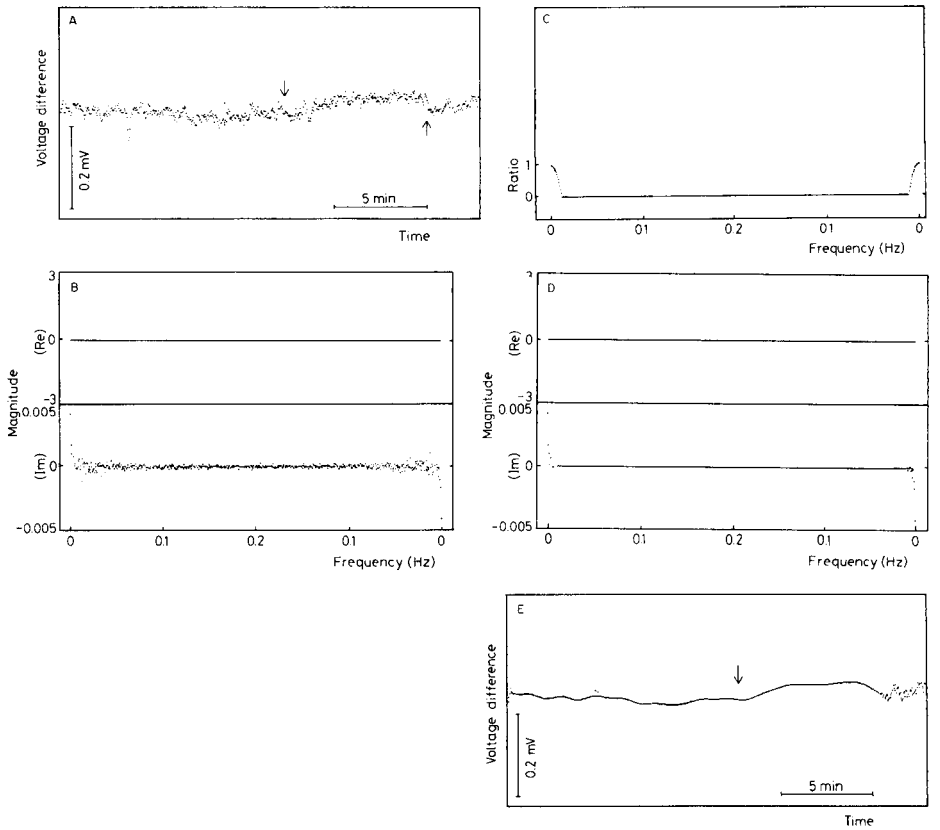

Fig. 2. (A) Voltage difference response of the thermal sensors to 2 mM glucose; each of the 512 points shown corresponds to 5 computer-averaged data points measured every 0.5 s; from left to right, the arrows indicate the injection of glucose sample (2 mM final concentration) and the onset of stirring. (B) Fast-Fourier transform (FFT) of (A) showing the real component (upper part) and the imaginary component (lower part). (C) Filter window to remove high-frequency noise. (D) Convolution of (B) and (C). (E) Response after removal of high-frequency noise from (A) by FFT; the arrow indicates sample injection.

high-frequency noise was 94%. The filtered FFT signal was subjected to reverse FFT to produce the response displayed in Fig. 2E, in which the enthalpy change caused by the enzyme reaction can be seen. The temperature difference between the two thermal sensors is 0.003°C (applying the 10 mV $^{\circ}C^{-1}$ characteristic) for 2 mM glucose. The results before and after FFT for 100 mM glucose are shown in Fig. 3. Although the response in Fig. 3A can be distinguished from the noise prior to FFT, and Fig. 3B still indicates some error at the start and end of the run near the edge of the FFT window, the FFT-treated signal clearly identifies the change in enthalpy as an initial slope. The time required for the enthalpy change to reach a stationary state is dependent on the mass diffusion of glucose through the immobilization

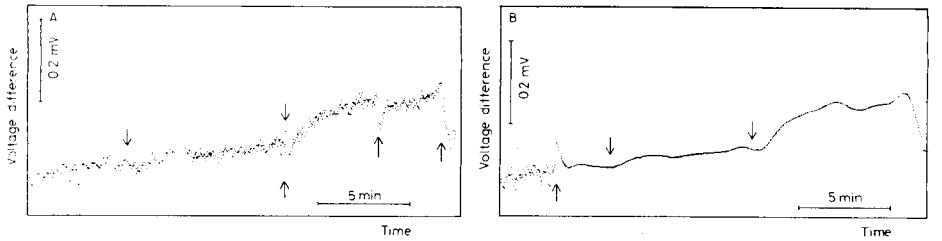

Fig. 3. (A) Voltage difference response of the sensors to glucose injection; the downward arrows indicate injection of glucose samples (1 mM and 100 mM final concentration) and the upward arrows indicate stirring points. (B) Response after removal of high-frequency noise from (A) by FFT; here the upward arrows indicate error caused by FFT.

membrane and the enzyme reaction rate. The stationary response time is 2 min for 2 mM glucose and 4 min for 100 mM glucose. Because glucose concentrations below 100 mM produce a faster response from the sensor, the major limitation to the rate of enthalpy change would appear to be the mass diffusion rate. In Figs. 2A and 3A, the decrease in IC voltage output indicated by the arrows is a result of stirring the solution during sample addition.

The calibration curve for glucose is shown in Fig. 4. Glucose in the range 5—100 mM can be determined; the sensor gave no detectable response to 100 mM fructose.

Thermal diffusion model. Spectrophotometric measurement of the immobilized enzyme activity gave a value of 1.15×10^{-5} mol s^{-1} for 10 mM glucose. The enthalpy change for the enzymatic conversion of glucose to gluconolactone by glucose oxidase is 80 kcal mol^{-1} [3], giving a calculated steady-state heat generation rate for immobilized enzyme catalysis of 1×10^{-3} kcal h^{-1}.

The Fourier rule governing the enthalpy of a sphere at steady state is given [12] by $q = -\lambda A(dT/dx)$, where q is the thermal conduction rate (kcal h^{-1}), λ is the thermal conductivity (kcal m^{-1} h^{-1} K^{-1}), A is the surface area (m^2), T is temperature (Kelvin), and the conduction distance is x (m). For a sphere of 1-mm diameter, this equation gives $dT/dx = q/4\lambda(x + 5 \times 10^{-4})^2$, and $q = 1 \times 10^{-3}$ kcal h^{-1} for 10 mM glucose.

The thermal conductivities of water and silicon are 0.5 and 148 kcal m^{-1} h^{-1} K^{-1} [13], giving a calculated value of T, from the equation for dT/dx of 0.32°C for water and 0.001°C for silicon. This latter value is reasonable compared with the actual measured value of 0.005°C at 10 mM glucose. The measured enthalpy change thus approximates to the calculated case for spherical silicon conduction owing to the high thermal conductivity of silicon.

The minimum detectable concentration of 2 mM and the very poor linearity of the system might greatly be improved by coupling the product of the first reaction to a second enzymatic catalysis, thereby amplifying the total enthalpy change in the system [6]. Further studies are directed at improving the sensitivity of this bio-calorimetric sensor.

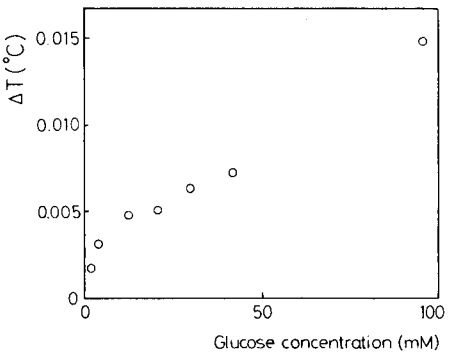

Fig. 4. Calibration plot for glucose (30°C, pH 7, 0.05 M phosphate buffer).

The authors thank Mr. M. Namiki and Mr. M. Gouda (Seiko Instruments) for supplying the IC sensors and for invaluable information, and Drs. K. Kajiwara and E. Tamiya (Tokyo Institute of Technology) for useful discussions.

REFERENCES

1 T. Seiyama, K. Fueki, J. Shiokawa and S. Suzuki (Eds.), Proceedings of the International Meeting on Chemical Sensors, Kodansha Ltd., Tokyo, 1983.
2 S. Suzuki (Ed.), Ion Selective Electrodes and Enzyme Electrodes (in Japanese), Kodansha, Tokyo, 1981.
3 S. Suzuki (Ed.), Biosensors (in Japanese), Kodansha, Tokyo, 1984.
4 K. Mosbach and B. Danielsson, Anal. Chem., 53 (1981) 83A.
5 B. Danielsson, Appl. Biochem. Biotech., 7 (1982) 127.
6 F. Scheller, N. Siegbahn, B. Danielsson and K. Mosbach, Anal. Chem., 57 (1985) 1740.
7 K. Tanaka, M. Kamiya and Y. Namiki, Sensor Technology (in Japanese), 10 (1982) 42.
8 Y. Namiki, M. Kamiya, E. Kojima and K. Tanaka, Japanese Patent S.59-47467, 1984.
9 E. Watanabe, K. Toyama, I. Karube, H. Matsuoka and S. Suzuki, Appl. Microbiol. Biotechnol., 19 (1984) 18.
10 H. Kawada, Y. Chiga and S. Minami, Interface (in Japanese), 9 (1983) 261.
11 D. E. Smith, Anal. Chem., 48 (1976) 221A.
12 S. Fujita, Chemical Engineering (in Japanese), Vol. I, Iwanami, Tokyo, 1976, p. 49.
13 Y. Morino (Ed.), Kagaku-Binran Kisohen (in Japanese), Vol. 2, Japanese Chemical Society, Maruzen, Tokyo, 1975, p. 983.

Analytica Chimica Acta, 197 (1987) 353—359
Elsevier Science Publishers B.V., Amsterdam — Printed in The Netherlands

Short Communication

FLOW-INJECTION DETERMINATION OF PHOSPHATE SPECIES IN DETERGENTS WITH A CALCIUM ION-SELECTIVE ELECTRODE

PETER W. ALEXANDER* and JAVAPA KOOPETNGARM

Department of Analytical Chemistry, University of New South Wales, P.O. Box 1, Kensington, N.S.W. 2033 (Australia)

(Received 4th December 1986)

Summary. A calcium ion-selective electrode is applied for the determination of ligands which complex calcium ions. The response of the electrode is measured when ligand solutions are injected into a buffered carrier stream containing calcium. Injections of EDTA, citrate, tripolyphosphate and pyrophosphate provide peaks with heights dependent on both the ligand and calcium concentrations. Ligand concentrations down to 2×10^{-5} M can be detected. Tripolyphosphate in detergents is easily determined. Use of the electrode has advantages over spectrophotometric methods for phosphates in flow systems.

Calcium ion-selective electrodes have been widely studied [1], mainly for the determination of calcium in a broad range of sample matrices. The use of such electrodes for indirect determinations of chelating ligands seems not to have been explored, and the present communication reports on this type of application.

In non-flow systems, the calcium ion-selective electrode (ISE) has been used for detecting end-points in complexiметric titrations of calcium ions and carboxylic acids [2, 3]. Determinations of stability constants of complexes formed between calcium and some carboxylic acids [4], and of the chelating properties of detergent builders [5] with the calcium ISE have been reported. In flow analysis, the calcium PVC membrane electrode has been used for determinations of calcium (e.g., the determination of calcium ion in natural and potable waters and wash liquors [6, 7]), for potentiometric titration of calcium with EDTA [8, 9] and for determinations of ionised calcium in blood serum [10—12], including other applications of the calcium ISE [13—15]. Indirect flow-injection determinations of organic ligands and metal ions have been successfully achieved with other electrodes including a copper-membrane electrode [16] and a copper metal electrode [17], but the calcium electrode may have advantages over the copper-type electrodes for some applications.

In this study, the calcium electrode is used in a flow-injection system as an indicator electrode for the indirect determination of various phosphate ions. The response of the electrodes used is related to the amount of ligand

0003-2670/87/$03.50

injected into a buffered carrier stream containing calcium ion. The carrier conditions are similar to those required for ion-chromatographic separation of phosphates with sodium trimesate [18] with indirect photometric detection. The electrode method is shown to allow determination of the phosphate species in detergents without the need for colorimetric reagents, as used with liquid chromatographic separation of polyphosphates with u.v. detection after post-column reaction with molybdate [19, 20].

Experimental

Apparatus. The flow system consisted of a Desaga STA multipurpose pump (Model 131900) operated at maximum speed with pump tubes of 1.42 mm inner diameter connected to an injection port and a flow-through cell.

The potentiometric flow cell contained an Orion research double-injection reference electrode (model 90-02) and a calcium ion-selective electrode fitted with a flow-through cap of a design previously described [21]. The reference electrode was placed downstream in the waste reservoir. Sample solutions were injected either from a microlitre syringe through a custom-made stainless-steel injection port with a rubber septum or by use of an Omnifit injection valve with an injection loop (usually 100 μl or 250 μl).

Manifolds were made of polyethylene tubing (1.14 mm inner diameter) and an Omnifit T-connector in a two-channel system. The sample solution was injected into a flow stream of either potassium nitrate solution or borate buffer and then mixed with calcium ion in buffer at the T-junction before reaching the indicator electrode. The flow rates of the sample stream and the buffered calcium stream were each set at 4.75 ml min^{-1}.

The electrodes were coupled to an Activon pH-ion-mV-temperature meter (Model 108) connected to an Omniscribe series D5000 chart recorder. The analog output from the meter was also interfaced to an Apple IIe microcomputer via an analog-to-digital converter (John Bell Engineering Co.), which was of 8-bit successive approximation design. The software for real-time data acquisition, data storage and data processing was developed in this laboratory. Electrode potential readings were displayed on the video monitor in real time and stored on a disk with the Apple IIe system. The data were later plotted on a Watanabe *X-Y* plotter, and could be compared with the analog data recorded on the chart recorder. Digital smoothing of data was achieved by a 9-points averaging method prior to plotting.

Reagents. Borate buffer solution (pH 9.4) was prepared by dissolving disodium tetraborate in distilled water. The carrier stream containing calcium ion was prepared by mixing calcium nitrate solution with the appropriate buffer to obtain the appropriate concentration. Ammonia buffer solution (pH 9.4) was prepared by dissolving ammonium nitrate and ammonia solution in distilled water. All solutions were prepared from analytical-grade reagents and were deaerated before use in the flow system.

Procedures. Solutions of calcium ion were injected into the carrier stream

containing borate buffer to investigate the electrode response to calcium ion activity. For flow-injection studies of complexing ligands, solutions of EDTA, citrate, tripolyphosphate and pyrophosphate were injected into a flow stream containing 10^{-4} M calcium in 0.05 M borate buffer or 10^{-2} M calcium in 0.5 M ammonia buffer.

The samples of detergents analysed were: (A) a green fluorescent liquid, (B) a green liquid, (C) an opaque blue liquid, (D) a white powder, (E) a blue powder, and (F) another blue powder. The phosphate contents in these samples, evaluated by high-performance liquid chromatography with an anion-exchange column and a post-column u.v. detector [19], were: (A) 1.9% pyrophosphate, (B) 7.9% pyrophosphate, (C) 12.0% tripolyphosphate, (D) 12.3% tripolyphosphate, (E) 32.8% tripolyphosphate, and (F) 33.0% tripolyphosphate.

The multiple standard addition method of Gran was used for the evaluation of phosphate in detergent samples. An appropriate amount of each sample was dissolved in 0.05 M borate buffer to give ca. 1×10^{-3} M phosphate. A series of standard phosphate solutions was added to each aliquot of the sample solutions. The peak heights after injections of these solutions were used in the Gran plot method [22] and the amount of phosphate in each sample was then calculated.

Results and discussion

This indirect determination of complexing ligands by flow injection analysis is based on the partial complexation of the injected ligand by calcium ions present in the carrier stream. The response of the calcium ISE to the residual free calcium ion activity in the flow stream is monitored after injection of the phosphate ions. The peak height depends on the concentration of the injected phosphate but also depends on the dispersion in the system and on the response range of the calcium ISE.

In an initial study of the electrode response to uncomplexed calcium ions, calcium solutions were injected into a borate buffer carrier stream at pH 9.4 (Fig. 1). The slope of the plot of peak height against the logarithmic calcium concentration was 30.2 mV, in agreement with the expected slope for a divalent metal ion.

In the studies of various phosphate ions, solutions of each type of phosphate were prepared in 0.05 M borate buffer and then injected into a flow stream containing 10^{-4} M calcium in 0.05 M borate buffer. The output for 250-μl injections of different tripolyphosphate solutions is shown in Fig. 2. Figure 3A shows a calibration plot for tripolyphosphate standards from the peaks in Fig. 2. The plot is compared with calibration plots for other ligands which react with calcium; EDTA gave the most sensitive effect but obviously any ligand forming a strong complex with calcium ions can be determined with greater or lesser sensitivity by this procedure. Table 1 indicates the relationship between the stability constants of the complexes formed and the sensitivity of the responses for different ligands. The calibration plot

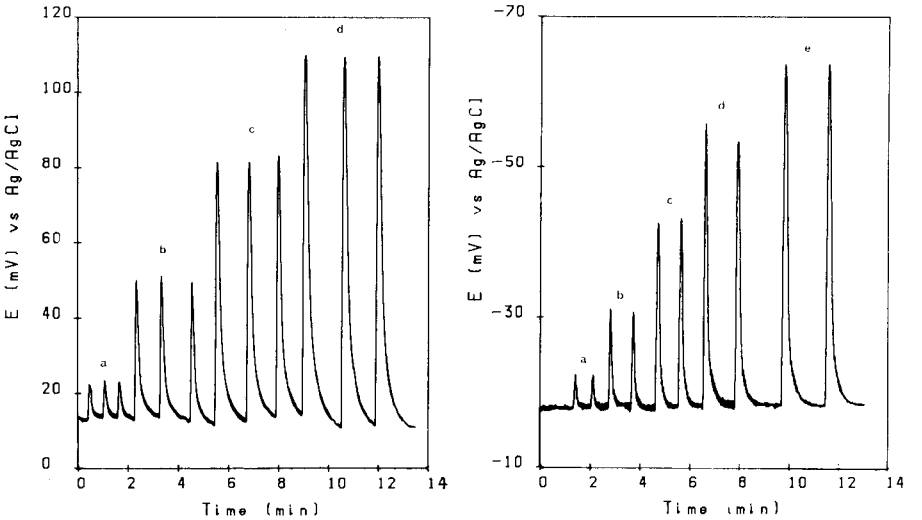

Fig. 1. Peaks obtained for 250-μl injections of Ca^{2+} into 0.05 M borate buffer at pH 9.4 at a total flow rate of 9.5 ml min^{-1}. Concentration of injected solutions: (a) 1×10^{-5} M; (b) 1×10^{-4} M; (c) 1×10^{-3} M; (d) 1×10^{-2} M.

Fig. 2. Peaks obtained for 250-μl injections of tripolyphosphate into 10^{-4} M Ca^{2+} in 0.05 M borate buffer at pH 9.4 at a total flow rate of 9.5 ml min^{-1}. Concentrations of injected samples: (a) 1×10^{-4} M; (b) 3×10^{-4} M; (c) 1×10^{-3} M, (d) 3×10^{-3} M, (e) 1×10^{-2} M.

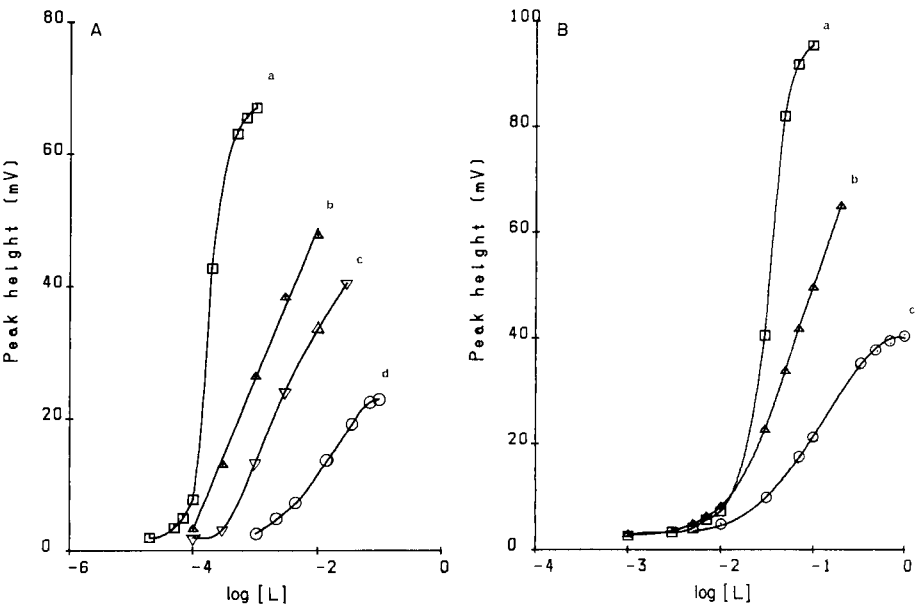

Fig. 3. Calibration plots for 250-μl injections of different ligands (L): (a) EDTA; (b) tripolyphosphate; (c) citrate; (d) pyrophosphate. Reagent stream: (A) 10^{-4} M Ca^{2+}/0.05 M borate buffer at pH 9.4; (B) 10^{-2} M Ca^{2+}/0.5 M ammonia buffer pH 9.5/0.5 M KNO_3. Flow rate 9.5 ml min^{-1} in all cases.

TABLE 1

Relationship between conditional stability constants and peak heights observed for ligand solutions (1×10^{-3} M) injected into borate buffer pH 9.4 containing 1×10^{-4} M calcium

Ligand	Peak height (mV)	log K'[a]	Ligand	Peak height (mV)	log K'[a]
Tripolyphosphate	26.43	8.40	EDTA	67.0	12.59
Pyrophosphate	13.26	5.18	Citrate	2.57	2.37
Orthophosphate	—[b]	2.35			

[a]Calculated as described by Inczedy [23]. [b]Not detectable.

for pyrophosphate (Fig. 3A) is much less sensitive than that for tripolyphosphate, as expected from Table 1. Figure 3B shows the calibration plots for EDTA, citrate and tripolyphosphate solutions injected into a 1×10^{-2} M calcium stream at pH 9.5. The sigmoidal curves obtained are shifted towards higher ligand concentrations, as expected for the reaction with a higher calcium concentration.

The above-described procedure with the borate buffer was examined for the determination of phosphate species in samples of commercially available detergents. The detergents (see Experimental section) were dissolved in water, and diluted to give 1% solutions in the borate buffer. Table 2 shows the results obtained for the determination of total complexing ligands in these samples, compared with the values obtained by liquid chromatographic (l.c.) determination of individual phosphate components. Samples C—F with high tripolyphosphate content showed good agreement with the l.c. values, the differences being no greater than 3%. The data show large errors for samples A and B where the pyrophosphate content was low; the high results for the pyrophosphate are no doubt caused by interferences from

TABLE 2

Determination of phosphate species in detergent samples by the proposed method

Sample	Phosphate (%)		Difference (%)
	Found[a]	L.c.	
A[b]	3.41 (0.25)	1.9	+79.5
B[b]	9.08 (0.41)	7.9	+14.9
C[c]	12.25 (0.42)	12.0	+2.1
D[c]	11.92 (0.51)	12.3	—3.1
E[c]	32.36 (2.61)	32.8	—1.3
F[c]	33.19 (1.77)	33.0	+0.6

[a]With standard deviation (n = 5) in parentheses. [b]As sodium pyrophosphate. [c]As sodium tripolyphosphate.

other complexing species in the detergent, and the proposed method would require a separation step before pyrophosphate could be determined with acceptable accuracy. The separation could be achieved by ion chromatography [19, 20]; the potentiometric method described here would eliminate the need for post-column spectrophotometric reactions.

Conclusions

The sensitivity of this indirect flow-injection determination of complexing ligands with the calcium ion-selective electrode depends on the Ca^{2+} concentration in the carrier stream. A similar concept has been applied in the indirect determination of amino acids and metal ions with copper electrodes [17]. In the buffered electrolytes studied here, better sensitivity was achieved for injections of EDTA solution than for tripolyphosphate or citrate solutions because of the relative formation constants with calcium. Interferences can therefore occur if individual ligands must be determined.

This electrode detection method is obviously applicable in ion-chromatographic separations of phosphates. The electrode method would have considerable advantages over the u.v. detection method [19, 20] with a post-column reaction between eluted phosphate species and molybdate reagent. The feasibility of using the calcium electrode as a detector in general liquid chromatography depends on matching mobile-phase conditions required for the separation of solution components with those established above for the calcium electrode. Separation of inorganic phosphates, for example, has been reported [18] at pH 8 in sodium trimesate and the possibility of using the calcium electrode appears to be attractive.

The authors are grateful to the Australian Government for the award of a Fellowship to J.K. from the Australian Development Assistance Bureau.

REFERENCES

1 G. Nagy, Zs. Feher, K. Toth and E. Pungor, Hung. Sci. Instrum., 41 (1977) 27.
2 A. K. Mukherji, Anal. Chim. Acta, 40 (1968) 354.
3 J. Kalous, K. Vytras and A. Terberova, Collect. Czech. Chem. Commun., 48 (1983) 1137.
4 B. J. Birch, A. Craggs, G. J. Moody and J. D. R. Thomas, J. Chem. Educ., 55 (1978) 740.
5 J. A. Blay and J. H. Ryland, Anal. Lett., 4 (1971) 653.
6 J. D. R. Thomas, in E. Pungor and I. Buzas (Eds.), Anal. Chem. Symp. Ser., 18 (Modern Trends in Analytical Chemistry, Part A) (1984) 141.
7 A. J. Frend, G. J. Moody, J. D. R. Thomas and B. J. Birch, Analyst, 108 (1983) 1357.
8 J. Růžička, E. H. Hansen and H. Mosbaek, Anal. Chim. Acta, 92 (1977) 235.
9 S. Kanamori and H. Ikegami, J. Oceanogr. Soc. Jpn., 36 (1980) 177.
10 R. Virtanen, Anal. Chem. Symp. Ser., 8 (Ion-Selec. Electrodes, 3) (1981) 375.
11 J. Růžička and J. C. Tjell, Anal. Chim. Acta, 47 (1969) 475.
12 E. H. Hansen, J. Růžička and A. K. Ghose, Anal. Chim. Acta, 100 (1978) 151.
13 G. A. Ortolano, R. C. Stuart, K. R. Wunschel, Jr., E. A. Kaiser, R. P. Hummond and A. K. Swong, Microchem. J., 2 (1983) 409.
14 P. Anker, D. Amman, P. C. Meier and W. Simon, Clin. Chem., 30 (1984) 454.

15 J. Thode, J. Wandrup, F. Aas and O. Siggard-Andersen, Scand. J. Clin. Lab. Invest., 42 (1982) 407.
16 C. R. Loscomb, G. B. Cox and J. A. W. Dalziel, J. Chromatogr., 166 (1978) 403.
17 P. W. Alexander, P. R. Haddad and M. Trojanowicz, Anal. Chim. Acta, 171 (1985) 151; Anal. Lett., 17 (1984) 309.
18 H. Small and T. E. Miller, Jr., Anal. Chem., 54 (1982) 462.
19 N. Yoza, K. Ito, Y. Hirai and S. Ohashi, J. Chromatogr., 196 (1980) 471.
20 Y. Hirai, N. Yoza and S. Ohashi, J. Chromatogr., 206 (1981) 501.
21 P. W. Alexander and P. Seegopaul, Anal. Chem., 52 (1980) 2403.
22 E. P. Serjeant, Potentiometry and Potentiometric Titrations, Wiley, New York, 1984, pp. 225—229.
23 J. Inczedy, Analytical Applications of Complex Equilibria, Horwood, Chichester, 1976, pp. 317—368.

Analytica Chimica Acta, 197 (1987) 361—365
Elsevier Science Publishers B.V., Amsterdam — Printed in The Netherlands

Short Communication

TEMPERATURE EFFECTS ON AMPEROMETRIC DETECTION AT NICKEL OXIDE ELECTRODES IN FLOW-INJECTION SYSTEMS

BEN S. HUI and CALVIN O. HUBER*

Department of Chemistry, University of Wisconsin-Milwaukee, Milwaukee, WI 53201 (U.S.A.)

(Received 21st October 1986)

Summary. A flow-through nickel oxide electrode is used for the detection of selected organic molecules in a flow-injection system. Sensitivity is enhanced more than ten-fold for some compounds at 105°C relative to 25°C. Diffusion-controlled currents are obtained for some species at the higher temperature. Linear response extends to 10^{-7} M with detection limits in the nanogram range in some cases. The higher temperature increases the rate of saponification of ethyl acetate and also allows the determination of acetone. Typical relative standard deviations are 1—3%.

Fleischmann et al. [1] reported that alcohols and amines are oxidized at a nickel anode in aqueous alkaline solution. They showed that the rate-determining step is oxidation of the substrate by Ni(III) formed anodically on the nickel surface. This electrode reaction has been applied to measurements of a number of organic species including amino acids and proteins [2, 3]. The reactions are kinetically controlled and thus have relatively high temperature dependence. Cyclic voltammetry reported by Gomez et al. [4] has shown that Ni(III) oxide forms at less positive applied potential as temperature increases. In the present report, the nickel oxide electrode with the flow-injection technique at elevated temperature is applied to the determination of selected organic molecules. Both enhancement of the electron-transfer rates and enhancement of pre-detector reaction rates yield analytical advantages.

Experimental

Reagents. All chemicals were of reagent grade and water was double-distilled. The background electrolyte was 0.1 M sodium hydroxide containing 1×10^{-5} M nickel sulfate as suspended nickel hydroxide to enhance long-term stability of electrode activity.

Apparatus. The flow-injection system included a gravity-feed carrier-electrolyte reservoir and a Rheodyne Model 50 sample-injection valve with a 25-μl sample loop. The PTFE tubing (0.8 mm i.d.) length from the injector to detector was 20 cm. The detector cell was a three-electrode system. The body of the cell was machined from a teflon block to provide 0.8-mm

0003-2670/87/$03.50

channels and to accommodate fittings. The working electrode was 9 × 0.6-mm nickel wire with nominal area of 0.18 cm^2. A platinum auxiliary and a saturated-calomel reference electrode were 1—2 cm downstream in a reservoir positioned for overflow to waste. In the high-temperature experiment, the detector cell was immersed in stone or glass beads. Temperature was maintained to within ±1°C. The temperature of the carrier electrolyte reservoir was also raised to about 60°C, mainly to degas the electrolyte. The operational amplifier-based voltage controller and current-to-voltage converter with current offset were of conventional design. Analytical signals were monitored as peak currents on a potentiometric strip-chart recorder. Experiments with the rotating-disk electrode were done with Pine Instrument Model RDE 3 equipment.

Results and discussion

Optimal applied potential at the nickel electrode was found by operating the detector at various potentials in the flow-injection mode. The optimal applied potential was defined as that producing the largest peak current above baseline. Baseline current noise was relatively independent of baseline current magnitude. At applied potentials more positive than the optimum, increases in background current caused by the increased rate of solvent oxidation were observed. Apparently, analyte oxidation is competitively attenuated by the increased rate of electrolysis of the solvent.

When the potential was applied to a fresh nickel electrode, the instantaneous carrier-electrolyte current was more than 15 μA, which decayed exponentially as the nickel(III) oxide surface was formed. Steady-state currents of about 0.6 μA at 25°C and 6 μA at 105°C are obtained at optimal potentials in about 20 min. Electrodes previously exposed to carrier electrolyte yield steady background current in less than 5 min. With cytosine as a representative substrate, the optimal applied potential was 0.48 V (vs. SCE) at 25°C and 0.43 V at 105°C (Fig. 1A).

The quantitative characteristics for the five common nucleobases (guanine, adenine, cytosine, uracil, and thymine) plus other representative organic molecules were determined at 25 and 105°C (Table 1). Linear responses of peak current vs. concentration were found at both temperatures. Enhancement factors listed are ratios of quantitative sensitivity, i.e., calibration slope, at 105°C to those at 25°C. Typical values of standard error of the estimate were 0.05 and 0.10 μA at 25°C and 105°C, respectively. The relative standard deviations for six or seven repetitive measurements of 0.50 mM cytosine were 1.2% and 3.2% at 25°C and 105°C, respectively. The peak-to-peak baseline noise was 1 nA and 3 nA, respectively, at the two temperatures. The decrease in precision at the higher temperature was attributed to residual temperature instability and effects of gas formation. This temperature enhancement of the noise tends to decrease the advantage of lower detection limits. Unless the high temperature noise can be decreased, further improvement in detection limits will not be achieved. In general, upper limits of

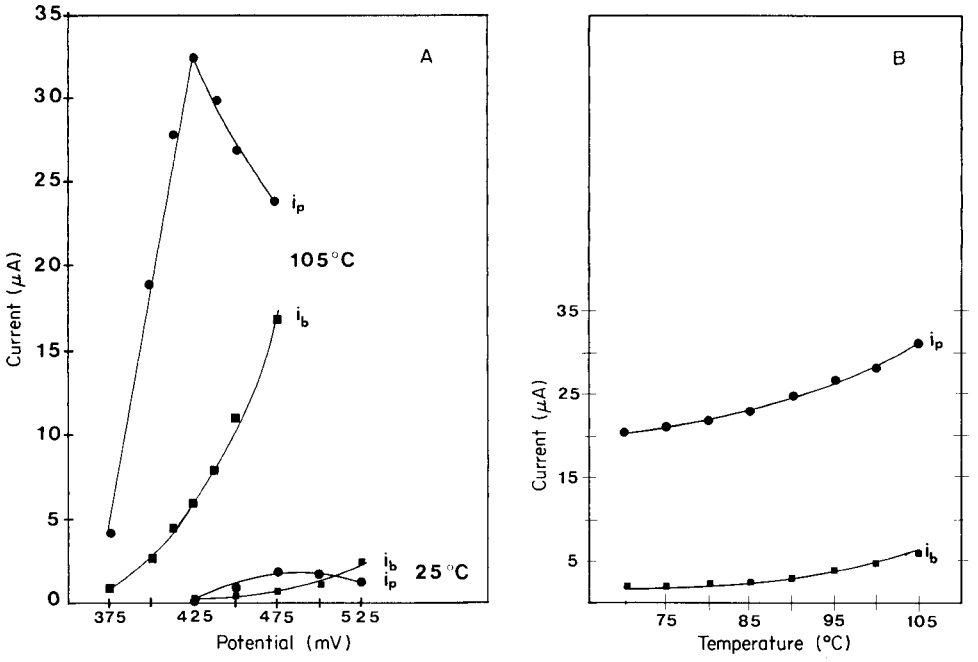

Fig. 1. (A) Potentiostatic response of the nickel electrode to 0.50 mM cytosine. (B) Their temperature dependence. (•) Peak current; (▪) background current.

TABLE 1

Detection characteristics for selected compounds

Compound	Sensitivity[a] (mA cm^{-2} mM^{-1})	Enhancement factor[b]	Detection limit[c] (ng)
Guanine	0.56	4.7	72
Glycine	0.43	4.6	36
Ethylene glycol	0.62	7.5	34
Salicylic acid	0.33	4.5	69
Butylamine	0.23	3.4	55
Ribose	0.32	5.7	41
Caffeine	0.15	5.0	92
Hydroxyproline	0.30	10.0	102
Cytosine	0.36	19.0	163
Proline	0.18	12	163
Adenine	0.38	29	15
Ethanol	0.067	13	18
Uracil	0.040	42	31
Ethyl acetate	0.019	36	264
Thymine	0.014	40	20
Formate	0.0085	35	22
Acetone	0.0004	13	77

[a]At 105°C for the peak area current. [b]At 105°C relative to 25°C. [c]At 105°C.

linearity were about 0.5 mM. The lower limits of detection were calculated from 3 times the standard error of the estimate for an injected volume of 25 μl.

In agreement with data reported earlier for amino acids, the data in Table 1 show that molecular features of the analytes which decrease oxidation rate include steric effects on adsorption (thymine vs. uracil), electron-withdrawing induction effects (proline vs. glycine), and decreasing number of oxidizable sites, i.e., stoichiometry (caffeine vs. guanine, proline vs. hydroxyproline, uracil vs. cytosine). The high oxidation rate for guanine among the purines correlates with work reported by Yao and Musha [5] who examined purine oxidations at glassy-carbon electrodes, and by Pullman and Pullman [6] who predicted by HOMO calculations that the ease of electron removal from purines increases with the number of ring-substituted hydroxy or amino groups in the molecule. There was no response at either temperature to diethyl ether or hexene.

One reason for doing the oxidation at higher temperature was to achieve diffusion-controlled current. Background and cytosine currents were measured at 425 mV from 70°C to 105°C. Figure 1B shows that the cytosine peak current increased from 20.5 μA to 31 μA, a 1.5%/°C increase of signal typical of diffusion rate control. Experiments with a rotating-disk nickel electrode at the same temperatures showed a linear relationship of current to square root of rotation rate. Computations showed that the radial velocity of solution near the electrode surface at the rotating disk was similar to that at the electrode surface when the flow-injection technique was used. The current sensitivity of 0.35 mA cm^{-2} mM^{-1} for cytosine at 105°C is similar to those for diffusion-controlled currents at a glassy carbon electrode reported recently [7]. It was concluded that at the higher temperature, the large currents obtained for some species were diffusion-controlled.

Activation energies. Current/temperature data obtained by using the rotating nickel disk electrode were used to obtain the heterogeneous rate constants ($i/nFAC$) for the oxidations of cytosine, ribose, adenine, and uracil. The currents were measured at the kinetic-controlled region of the rotating disk experiment at a series of temperatures between 24 and 44°C. A roughness factor of unity was assumed for the electrode surface. The values of n were evaluated from coulometry data. Plots of reciprocal temperature vs. rate constants yielded the activation energies shown in Table 2. These values of activation energy are similar to those observed for oxidation of alcohol at a gold electrode under similar conditions [8].

Saponification of ethyl acetate. Ethyl acetate saponifies in alkaline solution to produce electroactive ethanol and unreactive acetate. When saponification was allowed to go to completion before the sample was injected the currents obtained corresponded to those for equal concentrations of ethanol. When ester-containing samples were injected 11% of the ester was saponified at 25°C and 29% was saponified at 105°C. The enhancement of saponification rate together with the enhancement of the electrochemical

TABLE 2

Activation energies (E_a) of selected substrates

Substrate	n	E_a (kcal mol^{-1})
Uracil	2.0	96
Adenine	6.2	71
Cytosine	5.9	42
Ribose	12.0	34

reaction rate explains the 36-fold overall increase. The saponification could be further increased by using a larger length of tubing between the injector and detector. These data illustrate that for some analytes, temperature enhancement of on-line conversion to electroactive species combined with increases in electrode reaction rates can extend detection capability.

Acetone oxidation. It has been assumed that acetone is not electroactive at nickel oxide electrodes because it was found to be the major product of isopropanol oxidation [1]. However, results of this study indicate that the sensitivity for acetone is 0.028 μA cm^{-2} mM^{-1} and 0.39 μA cm^{-2} mM^{-1} at 25° and 105°C, respectively. An electroactive *gem*-diol can be formed between acetone and hydroxide:

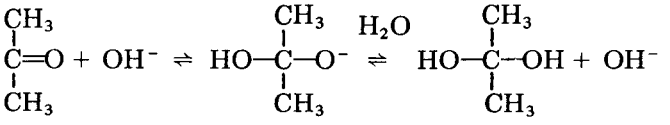

The equilibrium constant for the *gem*-diol formation is about 10^{-3} [9]. Interestingly, the signal obtained for acetone was about three orders of magnitude lower than that for a similar concentration of ethylene glycol. It was observed that acetone in hydroxide solution could be detected at 1.0 mM concentration at 25°C while acetone in distilled water could only be detected at a concentration of 10 mM. The hydroxide reaction with acetone should be much faster than that for water. The enhanced signal at 105°C can thus be attributed to the temperature effect on both the diol equilibrium and the electron-transfer rate.

REFERENCES

1 M. Fleischmann, K. Korinek and D. Pletcher, J. Chem. Soc., Perkin Trans., 2 (1972) 1396.
2 B. Hui and C. O. Huber, Anal. Chim. Acta, 134 (1982) 211.
3 C. J. Yuan and C. O. Huber, Anal. Chem., 57 (1985) 180.
4 H. Gomez, J. R. Vilche and A. J. Arvia, J. Appl. Electrochem., 10 (1980) 611.
5 T. Yao and S. Musha, Bull. Chem. Soc. Jpn., 52 (1979) 2307.
6 B. Pullman and A. Pullman, Quantum Biochemistry, Interscience, New York, 1963, p. 216.
7 J. Wang and P. Tuzkhi, Anal. Chem., 58 (1986) 1787.
8 P. O. Alonso, R. Celdran and J. G. Velasco, J. Electroanal. Chem., 206 (1986) 179.
9 A. Streitwieser and C. H. Heathcock, Introduction to Organic Chemistry, 2nd edn., Macmillan, New York, 1981, p. 381.

Analytica Chimica Acta, 197 (1987) 367—372
Elsevier Science Publishers B.V., Amsterdam — Printed in The Netherlands

Short Communication

STRIPPING VOLTAMMETRY OF TRACE METALS IN RESISTIVE SOLUTIONS WITH MERCURY MICROELECTRODES

JOSEPH WANG* and PENG TUZHI[a]

Department of Chemistry, New Mexico State University, Las Cruces, NM 88003 (U.S.A.)

(Received 21st January 1987)

Summary. Mercury-coated microcylindrical carbon-fiber electrodes (7-μm diameter) are suitable for anodic-stripping voltammetric quantitation of trace metals in non-aqueous solvents. The stripping voltammograms show no distortion resulting from uncompensated ohmic drops when traces of lead, cadmium, and zinc are quantified in acetonitrile, methanol or ethylene glycol. In contrast, analogous measurements at macro-sized electrodes exhibit severe ohmic effects. Organic solutions containing extremely dilute electrolyte (or no deliberately added electrolyte) can be assayed. A two-electrode configuration yields virtually undistorted stripping voltammograms in methanol and acetonitrile. High sensitivity and good precision are obtained by using quiescent solutions.

Because of its inherent sensitivity, anodic stripping voltammetry (ASV) has been widely used for measuring trace metals in numerous matrices [1]. Traditionally, stripping experiments have involved high concentrations of supporting electrolyte. Copeland et al. [2] demonstrated that the stripping peaks are greatly diminished, shifted, and broadened, at lower supporting-electrolyte concentrations (i.e., in the presence of larger uncompensated resistance). Apart from severe peak distortions (expected with any voltammetric technique), large ohmic (iR) drops can affect the "true" plating potential in stripping measurements, and hence may affect the efficiency of the preconcentration step. The ohmic-drop problem becomes extremely severe when stripping experiments in resistive media are attempted, because the potentials applied during the deposition and stripping steps are largely lost in the bulk solution. A deliberately added electrolyte may create some complications when such nonaqueous and aqueous solutions are analyzed for trace and ultratrace metals. For example, risks of contamination from heavy-metal impurities in the added chemicals (even high-purity reagents) are large. Addition of an electrolyte alters the kinetic and thermodynamic properties, thereby invalidating important data (such as speciation information in low-ionic strength natural waters). For various nonpolar solvents, finding a suitable electrolyte may be a problem For these reasons, stripping measurements in solvents/media of high resistance have been largely neglected. A few exceptions are the use of large-volume wall-jet flow cells (where

[a]Present address: Department of Chemistry, Hangzhou University, Hangzhou, People's Republic of China.

0003-2670/87/$03.50

a conductive medium is maintained in the detector compartment [3]), and new adsorptive stripping procedures that are less susceptible to ohmic-drop effects [4]. Unlike voltammetric versions of stripping analysis, potentiometric stripping analysis [5] is free from errors caused by ohmic losses during the stripping step, but requires a conductive medium during the potentiostatic deposition step. (Such measurements are commonly done in the presence of dissolved oxygen, which contributes considerably to the current, and hence to the ohmic drop during deposition.) Nevertheless, the utility of the potentiometric version in various organic solvents has been demonstrated [6].

The low-resistance polarization of the recently introduced ultramicroelectrodes seems to hold great promise for voltammetric measurements in highly resistive media. Because electrode currents are small, ohmic losses can be negligible even for poorly conductive media. Indeed, recent studies have reported the use of microelectrodes to achieve undistorted cyclic voltammograms in acetonitrile [7, 8] and reliable amperometric detection in flowing solutions of dilute supporting electrolyte [9]. Several papers have demonstrated recently that sensitive ASV measurements can be obtained at mercury ultramicroelectrodes [10—13]. These studies have emphasized that the steady-state diffusional flux of microelectrodes obviates the need for convective hydrodynamics during the deposition period, thus simplifying the operation and instrumentation for ASV work. However, to date the possibility of using mercury ultramicroelectrodes to do ASV measurements of trace metals in nonaqueous media has not been explored. In this communication, the feasibility of such measurements is demonstrated.

Experimental

Apparatus. Voltammograms were obtained with a EG+G Princeton Applied Research (PAR) Model 264A voltammetric analyzer, in conjunction with an EG+G PAR Model 0073 *X-Y* recorder. A Bioanalytical Systems Model VC-2 electrochemical cell was used in most experiments. The working electrode, reference electrode (Ag/AgCl, Model RE-1, Bioanalytical Systems), platinum-wire auxiliary electrode, and the nitrogen delivery tube were inserted into the cell through holes in its teflon cover. The working electrode was a mercury-coated carbon-fiber cylinder. Carbon fibers of 7-μm diameter were obtained from Union Carbide Corp. (Thornell 300 grade XYP-90 1/0 fibers). The fibers were soaked and washed in acetone, and dried thoroughly at room temperature. A single fiber was then inserted into a 1.0-mm i.d. tip of borosilicate glass pipet (14673-043, VWR) and sealed with epoxy resin; microcylinders of 2-mm length were used in most experiments. The pipet was back-filled with mercury, and electrical contact was established with a copper wire. A "fresh" fiber was used for each experiment. Conventional mercury electrodes, a mercury-coated glassy-carbon rotating-disk electrode of 3-mm diameter (Model MF2012, Bioanalytical Systems) and a hanging mercury drop electrode (EG+G PAR Model 303) were used for comparison purposes.

Reagents. Stock solutions (10^{-3} M) of the metal ions were prepared by dissolving the pure metal or its salt in nitric acid and diluting to volume with water. The water was double-distilled. Tetraethylammonium perchlorate (TEAP; Fluka), acetonitrile (HPLC-grade, Aldrich), methanol (Baker) and ethylene glycol (reagent-grade, Baker) were used as received.

Procedure. A 9.9-ml aliquot of the sample and 0.1 ml of the 5×10^{-3} M mercury(II) nitrate solution were introduced to the cell (final mercury(II) concentration, 5×10^{-5} M). The solution was purged with nitrogen for 8 min and was kept under a nitrogen atmosphere throughout the measurement step. In-situ plating of the mercury film was accomplished by applying a potential of −0.9 V in quiescent solution. After 20 min, the potential was switched to +0.1 V and kept there for 2 min. Background and sample measurements were done successively as follows. The deposition potential was imposed on the mercury-coated carbon-fiber electrode in the quiescent solution. Following the deposition period, the metals were stripped from the mercury film by applying a differential-pulse anodic-potential ramp. The scan was stopped at +0.1 V, and after 60 s the system was ready for the next deposition/stripping cycle. All data reported refer to freshly prepared fiber electrodes. Analogous measurements at conventional-size mercury electrodes involved stirred solutions during deposition.

Results

Figure 1 compares stripping voltammograms for some common trace metals in acetonitrile and methanol, recorded at conventional-size hanging-mercury-drop and mercury-coated glassy-carbon electrodes, as well as at a mercury microelectrode. In both solvents, the conventional electrodes exhibited severe peak distortion that does not permit convenient trace quantitation. In contrast, well-defined and sharp peaks with good peak resolution were observed at the microelectrode, despite the presence of little or no deliberately added electrolyte. Coupled with the low background current and the high hydrogen overvoltage, submicromolar levels of the metals can be easily measured following short deposition periods. Measurements of the peak width at half-height ($b_{1/2}$) can provide a useful estimate of the degree of ohmic distortion. For example, $b_{1/2}$ values of 58 and 86 mV were obtained for the lead peak at the micro- and macro-sized mercury film electrodes, respectively, in the methanol solution (Fig. 1B). Similarly, $b_{1/2}$ values of 70 and 124 mV were observed at the same electrodes for similar lead measurements using the acetonitrile solution (Fig. 1A). When an acetonitrile solution containing no deliberately added electrolyte was tested, an ohmic distortion of the lead peak was observed at both electrodes, with $b_{1/2}$ of 97 (micro) and 127 (macro) mV (not shown).

The minimization of ohmic losses associated with solution resistance can be coupled with two-electrode operation, hence offering further advantages. For example, stripping voltammograms are compared in Fig. 2 for a methanolic solution containing 5×10^{-7} M cadmium(II) and lead(II) (and no

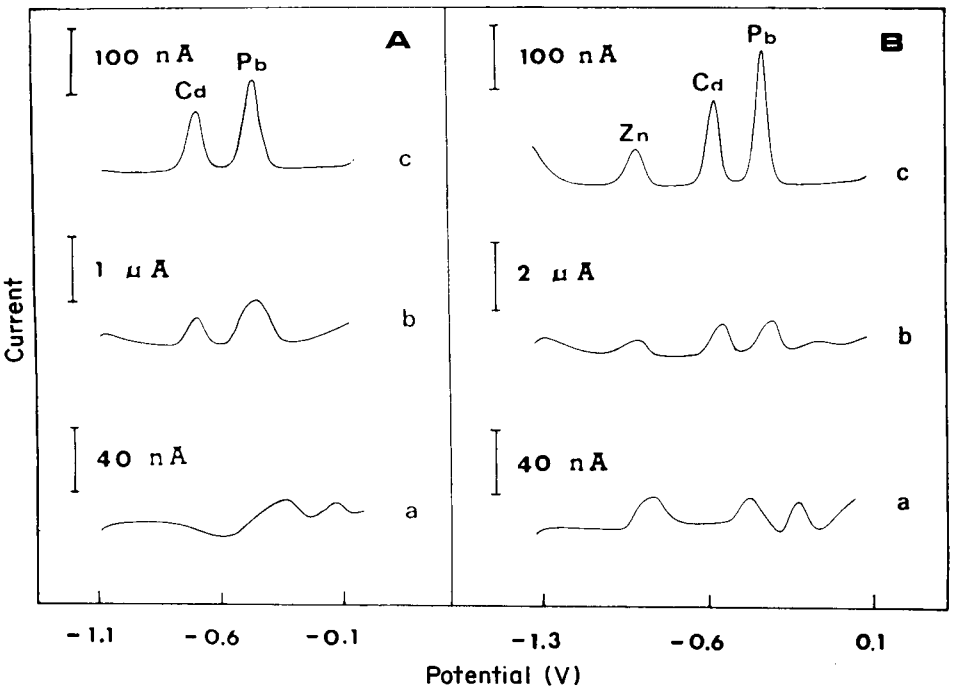

Fig. 1. Stripping voltammograms of trace metals. Medium: (A) acetonitrile; (B) methanol. Electrode: (a) hanging mercury drop; (b) mercury-coated glassy carbon; (c) carbon fiber. Electrolyte: (A) 10^{-5} M TEAP; (B) none. Analyte: (A) 5×10^{-7} M cadmium and lead; (B) 1×10^{-4} M zinc and 4×10^{-7} M cadmium and lead. Deposition time: (A) 3; (B) 2 min. Deposition potential: (A) —1.1 V; (B) —1.35 V. Stirring rate during deposition, 400 (a, b) and 0 (c) rpm. Differential-pulse waveform with 10 mV s^{-1} scan rate, 50 mV amplitude, and 0.2-s pulse repetition.

deliberately added electrolyte), recorded at the micro and conventional mercury electrodes, using three- and two-electrode systems. The two-electrode operation causes further distortion of the macroelectrode voltammogram (B, b), but at the microelectrode, identical well-defined voltammograms are obtained with the two- and three-electrode configurations (compare A, a and b). Analogous measurements in an acetonitrile solution containing 10^{-4} M TEAP exhibited similar behavior. When the microelectrode was used, the ratio of the cadmium and lead peak currents (two vs. three electrodes) remained essentially the same, indicating no effect on the potential control during the deposition step.

Methanolic solutions (containing no added electrolyte) of increasing lead concentration ($1.0—7.0 \times 10^{-7}$ M) were used to evaluate the linearity. Heights of the well-defined sharp peaks varied linearly with concentration. A least-squares fit of this plot yielded a slope of 65.7 ± 2.7 nA per 10^{-7} M, intercept of 14.8 ± 12.4 nA and a correlation coefficient of 0.997. In con-

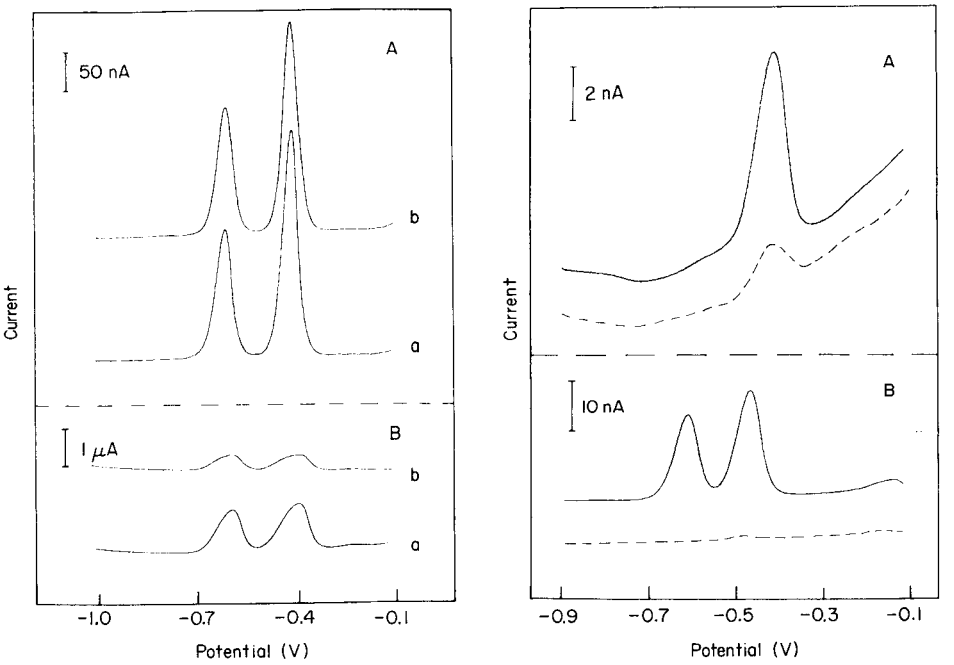

Fig. 2. Stripping measurements of 5×10^{-7} M cadmium and lead in pure methanol, recorded at mercury-coated carbon-fiber (A) and glassy-carbon (B) electrodes, using three- (a) and two- (b) electrode systems. Added electrolyte, none; deposition for 3 min at −1.1 V with 0 (A) and 400 (B) rpm stirring. Other conditions as in Fig. 1.

Fig. 3 Stripping voltammograms for samples of "regular" gasoline (A) and ethylene glycol (B), containing no added electrolyte, spiked with 1×10^{-6} M lead (A) and 1×10^{-6} M lead and cadmium (B). Dotted lines represent the unspiked samples. Deposition for 3 min at −1.1 V in quiescent solution. Other conditions as in Fig. 1.

trast, broad peaks that did not exhibit a linear increase with concentration were observed in analogous measurements at the conventional electrode. The well-defined peak observed at the microelectrode for the 1×10^{-7} M level following a short deposition period indicates that subnanomolar detectability can be easily achieved by using longer deposition times. Reliable calibration data were obtained with the microelectrode for similar additions of lead to an acetonitrile solution containing 10^{-4} M TEAP (slope, 30.5 ± 0.5 nA per 10^{-7} M; intercept, −1.8 ± 2.2 nA; correlation coefficient, 0.999 (conditions as in Fig. 2)). The reproducibility of the data was estimated from ten successive measurements of 4×10^{-7} M lead in acetonitrile (10^{-4} M TEAP), for a 90-s deposition at −1.0 V. The mean peak current found was 230.5 nA, with a range of 228—235 nA, and a relative standard deviation of 1.0%. This relative standard deviation compares favorably with those common in aqueous media of high ionic strength. These precision data indicate no short-term electrode fouling by the organic solvent.

Figure 3 illustrates the practical utility of using microelectrodes for

stripping analysis in resistive media. For lead in gasoline, a well-defined lead peak was observed for the original sample; the lead can be easily quantified by using standard addition. Ethylene glycol is commonly used as the principal ingredient in permanent antifreeze. Cadmium and lead added to ethylene glycol (10^{-6} M) yielded well-defined and sharp stripping peaks even without any added electrolyte. The relatively large stripping peaks indicate enhanced diffusional flux during the deposition step, despite the high viscosity of the solvent. Analogous measurements at the mercury-coated glassy-carbon macroelectrode yielded broad and distorted peaks (not shown).

Discussion

Because there were several sources of electrolyte in these studies (e.g., mercury(II) nitrate used in the preparation of the mercury-film electrode [14], acid added to stabilize the mercury(II) solution, impurities in solvents [15], and contributions from reference electrodes, the full capabilities of the microelectrodes to handle highly resistive solutions were not evaluated. Even so, ultramicroelectrodes offer substantial improvements in response relative to conventional electrodes, as indicated from various comparative experiments. Extension to organic solvents of low dielectric constant will require identification of a suitable supporting electrolyte and/or use of shorter electrodes of smaller radius. The ability to do trace metal measurements in media of high resistance provides the prospect for a wide range of new applications of ASV such as analysis of petroleum and oils. The use of ASV in the absence of added electrolyte may extend the useful voltage range.

This work was supported in part by the National Institutes of Health (Grant GM30913-04).

REFERENCES

1 J. Wang, Stripping Analysis: Principles, Instrumentation and Applications, VCH, Deerfield Beach, FL, 1985.
2 T. R. Copeland, H. H. Christie, R. K. Skogerboe and R. A Osteryoung, Anal. Chem., 45 (1973) 995.
3 J. Wang and B. A. Freiha, Anal. Chem., 57 (1985) 1776.
4 J. Wang and P. A. M. Farias, J. Electroanal. Chem., 182 (1985) 211.
5 D. Jagner, Analyst, 107 (1982) 593.
6 J. F. Coetzee, A. Hussam and T. P. Petrick, Anal. Chem., 55 (1983) 120.
7 J. O. Howell and R. M. Wightman, Anal. Chem., 56 (1984) 524.
8 A. M. Bond and P. A. Lay, J. Electroanal. Chem., 199 (1986) 285.
9 J. W. Bixler and A. M. Bond, Anal. Chem., 58 (1986) 2859.
10 K. R. Wehmeyer and R. M. Wightman, Anal. Chem., 57 (1985) 1989.
11 A. S. Baranski and H. Quon, Anal. Chem., 58 (1986) 407.
12 G. Schulze and W. Frenzel, Anal. Chim. Acta, 159 (1984) 95.
13 J. Wang, P. Tuzhi and J. Zadeii, Anal. Chem., (1987) in press.
14 T. M. Florence, J. Electroanal. Chem., 27 (1970) 273.
15 J. F. Coetzee, Pure Appl. Chem., 58 (1986) 1091.

Analytica Chimica Acta, 197 (1987) 373—375
Elsevier Science Publishers B.V., Amsterdam — Printed in The Netherlands

Short Communication

A SIMPLE AUTOMATIC TITRATOR BASED ON A DIGITAL BALANCE

JOHN R. CHIPPERFIELD* and DAVID E. WEBSTER
Department of Chemistry, University of Hull, Hull HU6 7RX (Great Britain)
(Received 27th October 1986)

Summary. A computer-controlled automatic titrator incorporating a weight burette is described. The titration vessel is mounted on the pan of a zero-displacement digital balance which records the weight of added sample as well as the weight of titrant added during the titration.

Most automatic titrators use syringe-type burettes which dispense measured volumes of titrant into the titration vessel. Automatic weight-burettes which dispense given weights of titrant have been described [1], but have been used infrequently, and automatic titrators incorporating them have used conventional titration vessels (Fig. 1A) [2, 3]. Here, an alternative approach to automatic titrations is described; the titration vessel, together with its stirrer and electrodes, are all placed on the pan of a top-loading zero-displacement digital balance (Fig. 1B).

A big advantage of having the titration vessel on the balance is that the sample size as well as the weights of added titrant are easily measured. The operator is entirely freed from manipulation of pipettes and other volume measurements. A second advantage follows if titrations are done to a fixed end-point, when further sample can be added and titrated without emptying the titration vessel.

Kratochvil and Maitra [1] have summarized the advantages of weight titrations over volume titrations; no calibration of volumetric glassware is required, and drainage problems associated with viscous or highly coloured materials are eliminated. Generally, the precision and accuracy of weighing is higher than that of measuring volumes, and balances now often have a computer interface which facilitates computer control.

Experimental

A Sartorius Model L2200P top-loading zero-displacement balance, which weighs to 0.01 g on weights up to 400 g after taring, is connected via the RS232 interface to a microcomputer (Acorn BBC B+). Electrodes are interfaced via a buffer amplifier [4] to the built-in 10-bit ADC of the microcomputer. Titrant is added from a gravity-feed burette, and is controlled by a Radiometer solenoid valve (Type MNV1c) in the feed line. The 8-channel

0003-2670/87/$03.50

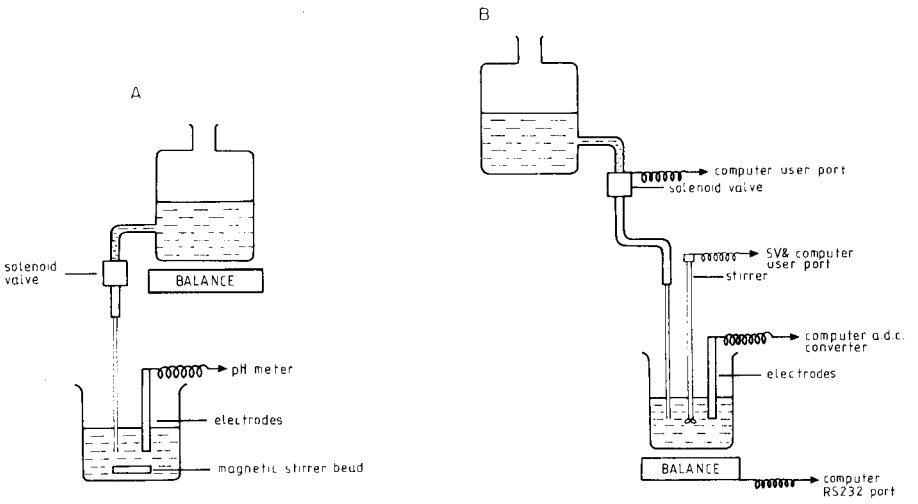

Fig. 1. (A) Arrangement of automatic titrator using a weight burette [2]. (B) Automatic titrator with a zero-displacement balance to weigh both the sample and added titrant.

user port is used to control this solenoid valve, and to switch the stirrer on and off. The stirrer was constructed around a 5-V motor (from a cassette recorder) and is mounted on the electrode holder. Thin PTFE-coated wires are used to connect the stirrer and electrodes (mounted on the balance pan) to the computer. Precision of weighing is unaffected by these leads, or by the silicone rubber titrant tube. It may, however, be desirable to build a draught shield around the equipment if it is used in a laboratory with substantial air movement.

Increments of titrant as small as 0.01 g can be added by rapidly switching the solenoid valve on and off with the computer. After each addition of titrant the solution is stirred for 4 s, and the electrode potential and the weight are measured after a further 4-s settling time. The size of the next titrant increment is then calculated so as to approach the end-point efficiently. The internal program of the balance can be set so that output is provided only if the reading is steady.

A computer program was written to control and record the titration. It provides the usual facilities of displaying the titration curve, detection of inflection points and variation of size of titrant increment dependent on the rate of change of electrode potential.

The titration vessel can be conveniently emptied and washed without removing it from the balance. At the end of a titration, an optional emptying cycle can be initiated. The solution is removed through a tube which is manually inserted; a 12-V car windscreen washer pump is used.

A second such pump can be used for adding the titrant (instead of the solenoid valve and gravity feed), and a version of the automatic titrator has been

made that does this. Rapid switching of the pump on and off allows increments of ca. 0.01 g to be added.

Results and discussion

In a typical trial, ca. 0.05 M sodium borate was titrated with 0.05 M sulphuric acid. Samples of 7—10 g of the borate solution were poured into the titration vessel and titrated to about pH 3.5. The end-points were located in three ways: by the point of inflection of the curve of "pH" against "weight of sulphuric acid added", at pH 5 (the expected end-point for this titration), and with a Gran plot [5, 6]. All three methods gave end-points within 0.02 g. The r.s.d. of the concentration of borate determined was 0.3% (six determinations). This is entirely due to the 0.01 g precision of the balance. If w_1 g of borate gives an end-point at a balance reading of w_2 then the concentration of borate is $c_{acid}(w_2 - w_1)/w_1$.

The only potential drawback of weight titrations is a possible error introduced by evaporation from the solution being weighed, in the reservoir in Fig. 1A and the titration vessel (a small beaker) in Fig. 1B. At normal British laboratory temperatures (15—20°C) evaporation of liquid from the open titration vessel caused an error of less than 0.01 g in the end-point for titrations completed in less than 10 min.

We thank Paul Edmondson for help with the programming of an early version of this equipment.

REFERENCES

1 See, e.g., B. Kratochvil and C. Maitra, Int. Lab., 13(3) (1983) 24.
2 B. Kratochvil and J. E. Nolan, Anal. Chem., 56 (1984) 586.
3 L. Luft, Talanta, 27 (1980) 221.
4 Scottish Schools Service Equipment Research Centre, Bulletin 143, (1984) 8.
5 L. Pehrsson, F. Ingman and A. Johansson, Talanta, 23 (1976) 769.
6 S. L. Burden and D. E. Euler, Anal. Chem., 47 (1975) 793.

ANALYTICA CHIMICA ACTA, VOL 197 (1987)

AUTHOR INDEX

ACA announcements

ANNOUNCEMENTS OF MEETINGS

1988 WINTER CONFERENCE ON PLASMA SPECTROCHEMISTRY, SAN DIEGO, CA, U.S.A., JANUARY 3–9, 1988

The 1988 Winter Conference on Plasma Spectrochemistry, fifth in a series of biennial meetings sponsored by the ICP Information Newsletter, will feature developments in plasma spectrochemical analysis by inductively coupled plasma (ICP), d.c. plasma (DCP), microwave (MIP), and glow and hollow-cathode discharge (GDL, HCL) sources. The meeting will convene Monday, January 4 through Saturday, January 9, 1988 at the San Diego Princess Resort and Convention Center in San Diego, CA, U.S.A. Expert short courses at introductory and advanced levels and an exhibition of spectroscopic instrumentation also will be included.

Further information: 1988 Winter Conference on Plasma Spectrochemistry, ICP Information Newsletter, Department of Chemistry, GRC Towers, University of Massachusetts, Amherst, MA 01003-0035, U.S.A.

39th PITTSBURGH CONFERENCE AND EXPOSITION ON ANALYTICAL CHEMISTRY AND APPLIED SPECTROSCOPY, NEW ORLEANS, LA, U.S.A., FEBRUARY 22–26, 1988

As in previous years, the program committee of the 1988 Pittsburgh Conference is planning a high caliber technical program. The committee's goals are to improve the quality of the program, maximize its educational values, and make it reflect not only the latest state-of-the-art in the field, but also new concepts which are being expressed for the first time. To attain these goals, the committee is planning about 30 symposia, over 900 contributed papers, short courses, mini-courses, and workshops. Further information on the planned topics will appear in the October Update.

The Pittsburgh Conference has become the greatest international spectro-analytical event, and scientists from all around the globe are invited to participate in this enormous scientific interface and exchange.

Contributed papers are vital for a successful program. We encourage you to participate by submitting an abstract of a paper in some phase of analytical chemistry, spectroscopy, and related fields. The program committee will carefully review each abstract. Contributed papers may take the form of either posters, or formal, oral presentations.

Four (4) copies of a 500-word abstract must be submitted for review; the deadline for receipt of Abstracts is August 3, 1987. All abstracts will be carefully evaluated. The abstract should clearly state (a) the objective of the work, (b) equipment and procedures used and (c) results and conclusions. Abstracts must include sufficient content for adequate evaluation by the conference program committee. The Pittsburgh Conference reserves the right to reject any paper. The designated speaker will be notified of acceptance or rejection of the paper in November, 1987. Specific references to vendor products in the titles of papers are not permitted and will be automatically eliminated. No conference proceedings will be published. Authors may publish their papers after the Conference. A second abstract will be required for reproduction in book form for distribution to the conferees. Forms and instructions concerning this second abstract will be sent to the designated speaker with the notification of acceptance of the paper. The second abstract will be due December 11, 1987. The title of the paper and the author information originally submitted cannot be changed for the second abstract; therefore, bé sure you have the desired title and author information on the original abstracts.

Authors wishing to present papers in the 1988 Pittsburgh Conference and Exposition Technical Program should submit four (4) copies of a 500-word abstract by August 3, 1987 to: Mrs. Alma Johnson, Program Secretary, 12 Federal Drive, Suite 332, Pittsburgh, PA 15235, U.S.A.

BIOCHEMISCHE ANALYTIK 88, 11th INTERNATIONAL CONFERENCE ON BIOCHEMICAL ANALYSIS, MUNICH, F.R.G., APRIL 19–22, 1988

The 11th conference Biochemische Analytik 88 will as usual, be held in the Munich Trade-Fair Centre. The main topics will be environmental water analysis, environmental biotechnology and modern methods of molecular biology and genetic engineering. Once again the poster exhibition is to reflect the entire spectrum of analytics within the scope of biosciences. A special exhibition will be dedicated to current problems of environmental analytics and to problems of radioactivity measurement in biomaterials and in the environment.

As has been the case in previous years, the "Analytica-Forum München" will offer to representatives of the industry the opportunity to present and discuss new apparatus and analytical methods in addition to the trade exhibition.

For further information contact: Ulrike Arnold or Anneli Höhnke, Nymphenburger Straße 70, D-8000 München 2, F.R.G. Tel.: (080) 1 23 45 00, telex: 5 216 018 dgkc d.

ELECTROFINNANALYSIS, AN INTERNATIONAL CONFERENCE ON ELECTROANALYTICAL CHEMISTRY, TURKU (ÅBO), FINLAND, JUNE 6–9, 1988

The conference will be mainly devoted to application of modern electrochemical methods of analysis. The scientific programme will consist of invited plenary lectures, keynote lectures, submitted research papers and posters. The programme will be divided into sessions concerned with: instrumentation, industrial applications, pharmaceutical applications, clinical applications, electrochemical sensors and electrochemical flow analysis. An exhibition of electroanalytical instruments will be held in conjunction with the conference. The official language of the conference is English. The conference will be held at the Åbo Akademi campus located in the older part of Turku (Åbo), half a kilometer from the town centre.

Participants wishing to present a paper should submit an abstract, in English, of about 250 words before December 31, 1987.

For further information contact: ElectroFinnAnalysis, Dr. Ari Ivaska, Laboratory of Analytical Chemistry, Åbo Akademi, SF-20500 Turku (Åbo), Finland.

J. HEYROVSKÝ CENTENNIAL CONGRESS ON POLAROGRAPHY, PRAGUE, CZECHOSLOVAKIA, AUGUST 20–25, 1990

The Congress is organized to commemorate the 100th anniversary of birthday of Professor J. Heyrovský (born December 20, 1890) by the Czechoslovak Academy of Sciences and the International Society of Electrochemistry. New developments of polarography and ter electrochemical methods and their applications in various fields will be covered. Major topics of the Congress will be: polarography and other electroanalytical methods in industrial, biomedical and environmental applications; theory of charge transfer; molecular electrochemistry; non-metallic electrodes; and conversion and energy storage.

For further information contact: Secretariat J. Heyrovský, Centennial Congress on Polarography, J. Heyrovský Institute of Physical Chemistry and Electrochemistry, Czechoslovak Academy of Sciences, Vlašská 9, 118 40 Prague 1, Czechoslovakia.

CALENDAR OF FORTHCOMING MEETINGS

Sept. 28–30, 1987
Barcelona, Spain

International Symposium on Applied Mass Spectrometry in the Health Sciences
Contact: Dr. Emilio Gelpí, Symposium Secretariat, International Symposium on Applied Mass Spectrometry in the Health Sciences, Palau de Congressos, Dept. de Convencions, Avgda. Reina Maria Cristina s/n, 08004 Barcelona, Spain. Tel.: (325) 30 00-223 99 40, telex: 53.117 foimb-e. (Further details published in Vol. 187.)

Sept. 28–Oct. 1, 1987
Gaithersburgh, MD, U.S.A.

Accuracy in Trace Analysis – Accomplishments, Goals, Challenges
Contact: Harry Hetz, A309 Chemistry Building, National Bureau of Standards, Gaithersburg, MD 20899, U.S.A. Tel.: (301) 921 2851. (Further details published in Vol. 181.)

Sept. 28–Oct. 2, 1987
Amsterdam, The Netherlands

2nd Amsterdam HPLC Summercourse
Contact: Dr. J.C. Kraak, Laboratory for Analytical Chemistry, University of Amsterdam, Nieuwe Achtergracht 166, 1018 WV Amsterdam, The Netherlands.

Oct. 4–9, 1987
Detroit, MI, U.S.A.

FACSS XIV, Federation of Analytical Chemistry and Spectroscopy Societies
Contact: Dr. Steve Swarin, Publicity Chairman, Analytical Chemistry Department, General Motors Research Laboratories, Warren, MI 48090-9055, U.S.A. Tel.: (313) 986-0806. (Further details published in Vol. 190, No. 2.)

Oct. 12–17, 1987
Varna, Bulgaria

6th Danube Symposium on Chromatography
Contact: 6th Danube Symposium on Chromatography, Scientific Council on Chromatography of the Bulgarian Academy of Sciences, Centre of Chemistry, BU-1040 Sofia, Bulgaria. Tel.: 7131 (3591), telex: 22729 ech ban bg.

Oct. 19–23, 1987
Fellbach, F.R.G.

ECASIA '87, European Conference on Applications of Surface and Interface Analysis
Contact: U. Nagorny, Max-Planck-Institut für Metallforschung, Institut für Werkstoffwissenschaften, Seestrasse 92, D-7000 Stuttgart 1, F.R.G.

Nov. 4–6, 1987
Atlantic City, NJ, U.S.A.

Scientific Computing and Automation, Conference and Exposition
Contact: Expocon Management Associates, 3695 Post Road, Southport, CT 06490, U.S.A. Tel.: (203) 259–5734.

Nov. 18–20, 1987
Paris, France

2nd International Conference on Passive Components: Materials, Technologies, Processing
Contact: Secrétariat Général du Colloque International, sur les Composants Passifs, 11 rue Hamelin, F-75783 Paris Cedex 16, France.

Nov. 24–27, 1987
Bordeaux, France

EXPERMAT '87, An International Symposium on Materials with Exceptional Properties
Contact: Bordeaux-Congrès, 33300 Bordeaux-Lac, France. Tel.: (33) 56 50 84 49, telex: 540 519 F.

Nov. 26–28, 1987
Milan, Italy

ATB '87, Advanced Technology for the Clinical Laboratory and Biotechnology; 3rd European Edition of the Oak Ridge Conference
Contact: ATB '87 Conference, Via C. Farini 70, 20159 Milan, Italy. Tel.: 39 2 6070074 (international), 02 6070074 (national).

Jan. 3–9, 1988 San Diego, CA, U.S.A.	**1988 Winter Conference on Plasma Spectrochemistry** Contact: 1988 Winter Conference on Plasma Spectrochemistry, ICP Information Newsletter, Department of Chemistry, GRC Towers, University of Massachusetts, Amherst, MA 01003-0035, U.S.A.
Jan. 19–21, 1988 Ft. Lauderdale, FL, U.S.A.	**Separation Science and Biotechnology Seminar** Contact: Mrs. Janet Cunningham, Barr Enterprises, P.O. Box 279, Walkersville, MD 21793, U.S.A. Tel.: (301) 898-3773.
Feb. 22–26, 1988 New Orleans, LA, U.S.A.	**39th Pittsburgh Conference and Exposition on Analytical Chemistry and Applied Spectroscopy** Contact: Mrs. Alma Johnson, Program Secretary, 12 Federal Drive, Suite 322, Pittsburgh, PA 15235, U.S.A.
March 15–18, 1988 Avoriaz, France	**Selenium in Medicine and Biology, 2nd Congress on Trace Elements in Medicine and Biology** Contact: Congrès Oligoéléments: Sélénium, Laboratore de Biochimie C, C.H.R.U.G., BP 217 X, 38043 Grenoble Cedex, France.
March 29–31, 1988 Noordwijkerhout, The Netherlands	**ANABIOTEC '88, 2nd International Symposium on Analytical Methods and Problems in Biotechnology** Contact: Symposium Secretariat ANABIOTEC '88, c/o QLT Convention Services, Keizersgracht 792, 1017 EC Amsterdam, The Netherlands. Tel.: (20) 261372, telex 31578 INTER NL attn. QLT. (Further details published i Vol. 190, No. 2.)
April 15–18, 1988 Neuherberg, F.R.G.	**5th International Workshop on Trace Element Analytical Chemistry in Medicine and Biology** Contact: Gesellschaft für Strahlen- und Umweltforschung mbH, Institut für Ökologische Chemie, AG "Spurenelementanalytik", Dr. P. Schramel, Ingolstädter Landstrasse 1, D-8042 Neuherberg, F.R.G. (Further details publishe in Vol. 190, No. 2.)
April 18–21, 1988 Las Vegas, NV, U.S.A.	**Flow Analysis IV, An International Conference on Flow Analysis** Contact: Dr. Gilbert E. Pacey, Department of Chemistry, Miami Universit Oxford, OH 45056, U.S.A. (Further details published in Vol. 181.)
April 19–22, 1988 Munich, F.R.G.	**Biochemische Analytik 88, 11th International Conference on Biochemical Analysis** Contact: Biochemische Analytik 88, Nymphenburger Strasse 70, D-8000 Munich, F.R.G.
April 27–29, 1988 Basle, Switzerland	**4th Symposium on Handling of Environmental and Biological Samples in Chromatography** Contact: Professor R.W. Frei, Department of Analytical Chemistry, Free University, De Boelelaan 1083, 1081 HV Amsterdam, The Netherlands. Te (020) 5485379. (Further details published in Vol. 190, No. 2.)
May 4–6, 1988 Stockholm, Sweden	**International Symposium on Biomolecules — Analytical Options** Contact: The Swedish Academy of Pharmaceutical Sciences, P.O. Box 1136 S-111 81 Stockholm, Sweden.

May 18–20, 1988 Amsterdam, The Netherlands	**CAC–88, 4th International Conference on Chemometrics in Analytical Chemistry** Contact: CAC–88, Laboratory for Analytical Chemistry, University of Amsterdam, Nieuwe Achtergracht 166, 1018 WV Amsterdam, The Netherlands. Tel.: (020)-5223541 (Dr. Smit). (Further details published in Vol. 190, No. 2.)
June 5–11, 1988 Frankfurt am Main, F.R.G.	**ACHEMA 88. International Meeting or Chemical Engineering and Biotechnology, 22nd Exhibition-Congress** Contact: DECHEMA, Organisation ACHEMA, Postfach 97 01 46, D-6000 Frankfurt am Main 97, F.R.G.
June 19–24, 1988 Washington, DC, U.S.A.	**HPLC '88, 12th International Symposium on Column Liquid Chromatography** Contact: Symposium Manager, Barr Enterprises, P.O. Box 279, Walkersville, MD 21793, U.S.A. Tel.: (301) 898 3772.
June 19–26, 1988 Trieste, Italy	**EUCHEM Conference on Chemometrics in Organic and Bioorganic Chemistry** Contact: Professor Paolo Linda, EUCHEM Conference on Chemometrics, c/o Istituto di Chimica Farmaceutica, Università degli Studi, Piazzale Europa 1, 34128 Trieste, Italy. Tel.: (040) 574181, telex: 460865 univts i.
June 20–23, 1988 Gaithersburg, MD, U.S.A.	**10th Symposium on Thermophysical Properties** Contact: A. Cezairliyan, Room 124, Hazards Building, National Bureau of Standards, Gaithersburg, MD 20899, U.S.A., tel.: (301) 975-5931, or J.V. Sengers, Institute for Physical Science and Technology, University of Maryland, College Park, MD 20742, U.S.A., tel.: (301) 454-4117.
June 27–July 2, 1988 Moscow, U.S.S.R.	**ISEC '88, International Solvent Extraction Conference** Contact: Dr. B. Spivakov, Vernadsky Institute of Geochemistry and Analytical Chemistry of the U.S.S.R., Academy of Sciences, 117975 GSP-1, Kosygin Str. 19, Moscow V-334, U.S.S.R. (Further details published in Vol. 190, No. 2.)
July 24–29, 1988 Compiegne, France	**1st International Conference on Modern Aspects of Protein Dye Interaction — Role in Downstream Processing** Contact: Secrétariat, C. Lacroix, Université de Technologie de Compiegne, BP 233, 60206 Compiegne Cédex, France
Sept. 5–8, 1988 Jena, G.D.R.	**COMPANA '88, 4th Conference on Computer Application in Analytical Chemistry** Contact: Professor Dr. K. Danzer, c/o Friedrich Schiller University Jena, Department of Chemistry, Steiger 3, 6900 Jena, G.D.R. Tel.: Jena 82 25028, telex: 05886134 uni dd. (Further details published in Vol. 190, No. 2.)
Sept. 21–23, 1988 Gothenburg, Sweden	**Biological Determinants of Drug Response in Man** Contact: The Swedish Academy of Pharmaceutical Sciences, P.O. Box 1136, S-111 81 Stockholm, Sweden.
Oct. 17–19, 1988 Nice, France	**International Symposium on Supercritical Fluids: Properties and Applications** Contact: M. Perut, E.N.S.I.C., 1 rue Grandville, F-54042 Nancy Cédex, France.

Nov. 2–4, 1988 Freiburg, G.D.R.	**5th (Montreux) Symposium on Liquid Chromatography–Mass Spectroscopy** Contact: Professor R.W. Frei, Department of Analytical Chemistry, De Boelelaan 1083, Vrije Universiteit, 1081 HV Amsterdam, The Netherlands. (Further details published in Vol. 190, No. 2.)
July 30–August 5, 1989 Cambridge, U.K.	**SAC 89, International Conference on Analytical Chemistry** Contact: SAC 89, Royal Society of Chemistry, Analytical Division, Burlington House, London W1V 0BN, U.K. Tel.: (01) 437-8656.
Aug. 28–Sept. 1, 1989 Wiesbaden, F.R.G.	**11th International Symposium on Microchemical Techniques** Contact: Gesellschaft Deutscher Chemiker, Abt. Tagungen, P.O. Box 900440, D-6000 Frankfurt/Main 90, F.R.G. Tel.: (069) 79 17-366/360, telex: 4170497 gdch d.
Aug. 20–25, 1990 Prague, Czechoslovakia	**J. Heyrovský Centennial Congress on Polarography** Contact: Secretariat, J. Heyrovský Centennial Congress on Polarography, J. Heyrovský Institute of Physical Chemistry and Electrochemistry, Czechoslovak Academy of Sciences, Vlašská 9, 118 40 Prague 1, Czechoslovakia.

Experimental Design: A Chemometric Approach

by **S. N. Deming,** *University of Houston, Houston TX, and* **S. L. Morgan,** *University of South Carolina, Columbia, SC, USA*

(Data Handling in Science and Technology, 3)

One of the greatest needs in all areas of competitive research and development is an efficient approach to experimentation. To be effective scientists, engineers or managers, individuals today require a clear understanding of the principles of experimental design. This book – unlike most current textbooks – approaches experimental design from the point of view of the experimenter, rather than that of the statistician. It provides a *practical* approach to experimental design and allows the reader to obtain the required information in the minimum number of experiments.

The book introduces the reader to the fundamentals of experimental design. Systems theory, response surface concepts, and basic statistics serve as a basis for the further development of matrix least squares and hypothesis testing. The effects of different experimental designs and different models on the variance-covariance matrix and on the analysis of variance (ANOVA) are extensively discussed. Applications and advanced topics (such as confidence bands, rotatability, and confounding) complete the text. Numerous worked examples are presented.

The clear and practical approach adopted by the authors makes the book applicable to a wide audience. It will appeal particularly to those with a practical need (scientists, engineers, managers, research workers) who have completed their formal education but who still need to know efficient ways of carrying out experiments. It will also be an ideal text for advanced undergraduate and graduate students following courses in chemometrics, data acquisition and treatment, and design of experiments.

1987 about 294 pages; US $ 109.75 / Dfl. 225.00;
ISBN 0-444-42734-1

ELSEVIER THE SCIENCE PUBLISHER
P. O. BOX 211 • 1000 AE AMSTERDAM • THE NETHERLANDS
P. O. BOX 1663 • GRAND CENTRAL STATION • NEW YORK • NY 10163

INFORMATION FOR AUTHORS

Detailed "Information for Authors" was published in Vol. 190, No. 2, pp. 375–378. A free reprint is available from the Editors or from:

Elsevier Editorial Services Ltd., Mayfield House, 256 Banbury Road, Oxford OX2 7DH (Great Britain)

Types of contribution. The journal welcomes original research papers, short communications and reviews. Reviews are written by invitation of the editors, who welcome suggestions for subjects. Short communications are usually complete descriptions of limited investigations, and should generally not exceed six printed pages. Preliminary communications of important urgent work can be printed within four months of submission, if the authors are prepared to forgo proofs.

Manuscripts. The preferred language of the journal is English, but French and German manuscripts are also acceptable. For authors whose first language is not English, French or German, linguistic improvement is provided as part of the normal editorial processing. Authors should submit three copies of the manuscript in double-spaced typing on one side of the paper only, with a margin of 4 cm, on pages of uniform size. If any variety of machine copying is used (e.g. xerox), authors should ensure that all copies are easily legible and that the paper used can be written on with both ink and pencil. Authors are advised to retain at least one copy of the manuscript. Manuscripts should be preceded by a sheet of paper carrying (a) the title of the paper, (b) the name and full postal address of the person to whom proofs are to be sent, (c) the number of pages, tables and figures.

Information on the *submission of papers* is given on the inside front cover.

Summary. Research papers and reviews begin with a Summary (50–250 words) which should comprise a brief factual account of the contents of the paper, with emphasis on new information. Short communications and preliminary communications require summaries, which should not exceed 50 words. Uncommon abbreviations, jargon and reference numbers must not be used. The Summary should be suitable for use by abstracting services without rewriting. Papers in French or German require a Résumé or Zusammenfassung preceded by a Title and Summary in English; authors are encouraged to provide translations where necessary.

Introduction. The first paragraphs of the paper should contain an account of the reasons for the work, any essential historical background (as briefly as possible and with key references only) and preliminary experimental work.

Figures. Figures should be prepared in black waterproof drawing ink on drawing or tracing paper of the same size as that on which the manuscript is typed. One original (or sharp glossy print) and two photostat (or other) copies are required. Attention should be given to line thickness, lettering (which should be kept to a minimum) and spacing on axes of graphs, to ensure suitability for reduction during printing. Axes of a graph should be clearly labelled, along the axes, and outside the graph itself.

All figures should be numbered with Arabic numerals, and require descriptive legends. Explanatory information should be placed not in the figure, but in the legend, which should be typed on a separate sheet of paper. Simple straight-line graphs are not acceptable, because they can readily be described in the text by means of an equation or a sentence. Claims of linearity should be supported by regression data that include slope, intercept, standard deviations of the slope and intercept, standard error, and the number of data points; correlation coefficients are optional.

Photographs should be glossy prints and be as rich in contrast as possible; colour photographs cannot be accepted. In general, line diagrams are more informative and less liable to dating than photographs of equipment, which are therefore not usually acceptable.

Computer outputs for reproduction as figures must be good quality on blank paper, and should preferably be submitted as glossy prints.

Nomenclature, abbreviations and symbols. In general, the recommendations of the International Union of Pure and Applied Chemistry (IUPAC) should be followed, and attention should be given to the recommendations of the Analytical Chemistry Division in the journal *Pure and Applied Chemistry* (see also *IUPAC Compendium of Analytical Nomenclature*, 1978).

References. The references should be collected at the end of the paper, numbered in the order of their appearance in the text (*not* arranged alphabetically), and typed on a separate sheet.

In the list of references, the following forms should be adopted.

Journals

1 W. Lund and M. Salberg, Anal. Chim. Acta, 76 (1975) 131.

2 M. McDaniel, A. D. Shendrikar, K. D. Reizneir and P. W. West, Anal. Chem., 48 (1976) 2240.

The title of the journal must be abbreviated as in the Bibliographic Guide for Editors and Authors.

Books

1 D. D. Perrin, Masking and Demasking of Chemical Reactions, Interscience–Wiley, New York, 1970, p. 188.

2 S. Hofmann, in G. Svehla (Ed.), Wilson and Wilson's Comprehensive Analytical Chemistry, Vol. 9, Elsevier, Amsterdam, 1979, p. 89.

Titles of papers are unnecessary. Citations of reports which are not widely available (e.g., reports from government research centres) should be avoided if possible. Authors' initials should not be used in the text, unless real confusion could be caused by their omission. If the reference cited contains three or more names, only the first author's name followed by et al. (e.g., McDaniel et al.) should be used in the text; but the reference list must contain the initials and names of *all* authors.

ANABIOTEC '88

2nd INTERNATIONAL SYMPOSIUM ON ANALYTICAL METHODS AND PROBLEMS IN BIOTECHNOLOGY

Noordwijkerhout, The Netherlands, 29–31 March, 1988

FIRST ANNOUNCEMENT AND CALL FOR PAPERS

Organized under the auspices of the Royal Netherlands Chemical Society (KNCV), Section for Analytical Chemistry, and the Netherlands Biotechnological Society (NBV)

ANABIOTEC '88

Analytical methods and systems for biotechnological applications are becoming increasingly important. The development of these methods and systems therefore calls for an interdisciplinary approach.

The use of analytical methods in daily practice in biotechnological research, development and industrial production is coming to be seen as essential for progress in biotechnology in general.

Close cooperation is needed between experts in analytical methodology, system development, and biotechnology.

The purpose of this second ANABIOTEC Symposium is to outline the progress already made through interdisciplinary discussion and cooperation and to deal with the rapid developments taking place.

The Symposium is intended for analytical chemists and both industrial and academic biotechnologists.

Topics

Topics covered will include:

- State-of-the-art analytical techniques already successfully applied in biotechnology.
- Strategies for the selection of analytical procedures with regard to optimum process control in industrial biotechnology, for environmental biotechnology and for fundamental and developmental research.
- Development of new analytical techniques for the above-mentioned areas.

Sessions are planned on: Sampling strategies, biosensors, mass spectrometry in process control, application of computers in analysis and process control, prospects for practical application of new analytical techniques, analytical problems in biotechnology.

The programme will consist of invited plenary lectures, invited and submitted papers (both oral and poster presentations) and discussion sessions.

Organizing Committee

Ir. B. te Nijenhuis
(Gist-brocades N.V.)
Dr. Ir. C. van Dijk
(TNO-Biotechnology)
Ir. W. A. Scheffers
(Delft University of Technology)
Dr. J. Kragten
(University of Amsterdam)

Call for Papers

Participants wishing to present a paper should submit an abstract, in English, of about 250 words before 15 October 1987 to the Symposium Secretariat.

In conjunction with the Symposium, an exhibition of instruments within its scope will be held.

For further information contact:

Symposium Secretariat
ANABIOTEC '88
c/o QLT Convention Services
Keizersgracht 792
1017 EC Amsterdam,
The Netherlands
Telephone: (31-20) 261372
Telefax: (31-20) 259574
Telex: 31578 inter nl attn. qlt

ELSEVIER THE SCIENCE PUBLISHER
P O BOX 211 • 1000 AE AMSTERDAM • THE NETHERLANDS
P O BOX 1663 • GRAND CENTRAL STATION • NEW YORK • NY 10163